JAERI-M
84-107

JAPANESE CONTRIBUTIONS TO THE JAPAN-US WORKSHOP ON FER/ETR DESIGN

(EXCHANGE Q-16 IN THE JAPAN-US FUSION COOPERATION PROGRAM, MARCH 26~30, 1984)

June 1984

Tatsuzo TONE, Hiromasa IIDA, Masayoshi SUGIHARA
Tatsuo KASAHARA*1, Masana NISHIKAWA*2, Kazunori KITAMURA*3
Toshimasa KURODA*4

日本原子力研究所
Japan Atomic Energy Research Institute

JAERI-Mレポートは，日本原子力研究所が不定期に公刊している研究報告書です。
入手の問合わせは，日本原子力研究所技術情報部情報資料課（〒319-11茨城県那珂郡東海村）あて，お申しこしください。なお，このほかに財団法人原子力弘済会資料センター（〒319-11 茨城県那珂郡東海村日本原子力研究所内）で複写による実費頒布をおこなっております。

JAERI-M reports are issued irregularly.
Inquiries about availability of the reports should be addressed to Information Section, Division of Technical Information, Japan Atomic Energy Research Institute, Tokai-mura, Naka-gun, Ibaraki-ken 319-11, Japan.

編集兼発行　日本原子力研究所
印　　刷　いばらき印刷㈱

JAERI-M 84-107

Japanese Contributions to the Japan-US Workshop on FER/ETR Design

(Exchange Q-16 in the Japan-US Fusion Cooperation Program, March 26-30, 1984)

Tatsuzo TONE, Hiromasa IIDA, Masayoshi SUGIHARA, Tatsuo KASAHARA*1, Masana NISHIKAWA*2, Kazunori KITAMURA*3 and Toshimasa KURODA*4

Department of Large Tokamak Development
Tokai Research Establishment, JAERI

(Received May 18, 1984)

This reports describes Japanese presentations at the Japan-US Workshop on FER/ETR Design which was held at Fusion Engineering Design Center, Oak Ridge National Laboratory, March 26-30, 1984. The presentations cover the overview of Fusion Experimental Reactor (FER) design and major outcomes obtained from the FER design work in FY1983 on the three topics for the Workshop which are (1) RF heating and current drive, (2) impurity control and divertor/pumped limiter design, and (3) design integration and maintenance.

Keywords: Nuclear Fusion, Japan-US Fusion Cooperation, Exchange Program, Tokamak, Fusion Experimental Reactor, RF Heating, Current Drive, Impurity Control, Reactor Design.

*1 Hitachi Ltd.

*2 Mitsubishi Atomic Power Industries, Inc.

*3 Toshiba Corporation

*4 Kawasaki Heavy Industries, Ltd.

FER／ETR設計に関する日米ワークショップにおける日本側発表論文

（日米核融合研究協力・交流計画Q－16）

日本原子力研究所東海研究所大型トカマク開発部
東稔達三・飯田浩正・杉原正芳・笠原達雄[*1]
西川正名[*2]・喜多村和憲[*3]・黒田敏公[*4]

（1984年5月18日受理）

本報告書は，1984年3月26日～30日に米国のオークリッジ国立研究所FEDCにおいて開催された，「FER／ETR設計」に関する日米ワークショップにおいて日本側（原研）が発表したものをとりまとめたものである。内容は，核融合実験炉（FER）の概要とワークショップの3つのテーマに対するFERの58年度の主要設計成果で構成されている。3つのテーマは，(1)高周波加熱と電流駆動，(2)不純物制御とダイバータ／ポンプリミタ設計，及び(3)炉本体設計と保守である。

＊1　（株）日立製作所
＊2　三菱原子力工業（株）
＊3　（株）東芝
＊4　川崎重工業（株）

Contents

目　　次

はじめに

本報告書は，“FER／ETR設計”に関する日米ワークショップ（昭和58年度日米交流計画Q－16）において日本側（原研）が核融合実験炉（FER）の設計について発表したものをとりまとめたものである。前回のワークショップ（第1回）は原研の那珂サイトで開催され（58年3月28～31日），今回（59年3月26～30日）はオークリッジ研究所のFEDC（Fusion Enginering Design Center）で行われた。

今回のワークショップの主要テーマは

(1) RF Heating and Current Prive

(2) Impurity Control／Limiter and Divertor Design

(3) Design Integration and Maintenance

である。これらは，プラズマ保持法と運転シナリオ選定のための物理・工学設計，及び炉本体構造設計における主要課題であり，炉概念を選定するのに極めて重要なものである。参考のために巻末の付録にワークショップのAgendaを記す。ワークショップの参加者は原研から3名（東稔，飯田，杉原），発注契約によってFERの設計に従事しているメーカから各社1名（笠原：日立，西川：三菱原子力，喜多村：東芝，黒田：川重）の計7名である。

本報告書の内容は58年度の設計成果に基づいている。工学設計については58年度に4社（日立，東芝，三菱，川重）に設計外注して得た成果をとりまとめた。まだ最終報告書の納入前であったが，設計作業はほぼ実質的に終了している段階であり，従って本報告書の内容は58年度の最終設計成果とみなしてよい。具体的内容については参加者の合議によって詰め，各とりまとめの主たる責任者は目次に記している。内容は，FERの設計の現状と今後の設計の方向について述べると共に，炉概念，システム，シナリオといったマクロなFERのイメージが理解されるように努めた。従って上記のテーマ(1)と(2)については，それぞれ個々の物理・技術上の議論のみならず，運転シナリオの広範囲な検討，電流駆動を取り入れた炉システムの設計例，ダイバータ／ポンプリミタの炉システムの相互評価を提示している。FERとしては当然のことであるが，物理設計と工学設計の整合性をできるだけ図っている。

(3)のテーマについても，仕様，設計指針及び炉本体構造設計例のみならず，高非円形プラズマで重要な垂直位置不安定性の制御と耐ディスラプション構造に関する電磁気設計のシステム的検討を提示している。さらに電磁気設計上及びトーラス構成上インパクトの大きい増殖ブランケットの総合的検討も提示している。

59年度からFERの基本炉概念を固める作業が始められる。これまでのFERの広範囲な物理・工学設計検討の成果は，今後のFERの基本構想固めと設計作業のデータベースとして大いに資するものと考えられる。これまで広く進めてきた設計検討の主要成果の詳細のとりまとめは，別途報告書を出す予定であるが，本報告書は58年度のFERの炉本体関連の設計の主要成果の速報的性格をもつものである。ワークショップにおける発表は全てOHP－viewgraphを用いて行ったが，本報告書では概要と図表の説明文をつけて理解を得やすくしてある。

本ワークショップの参加・準備に当っては，礒　康彦核融合研究センター所長，苫来地　顕部長（センター付），吉川允二大型トカマク開発部長には多くの支援と激励を得たことを感謝します。なお本報告書の作成に理解と激励を載いた飯島勉次長及びコメントを載いた炉設計研究室の諸氏に感謝します。

1. Status of FER Design

1.1 Scope of FER design activities

Conceptual design studies of the Fusion experimental Reactor (FER) have been performed at JAERI in line with a long-range plan for fusion reactor development laid out in the new long-term program of the Atomic Energy Commission issued in June 1982. The FER is an experimental tokamak reactor succeeding the large tokamak device JT-60 with a major mission of realizing ignited DT plasma and demonstrating engineering feasibility of fusion reactors including tritium breeding. The objectives and characteristics of the FER have been identified by the Review Subcommittee of Long-Term Strategy established under the Nuclear Fusion Council of the Atomic Energy Commission. The design of FER is conducted under the following guidelines: (1) to reach a DT ignition with a rather moderate neutron wall loading, (2) to obtain a breeding ratio larger than unity and (3) to be designed with cost/benefit considerations.

The FER design activities have been extended to many design options which are realistic or potential candidates for FER concept in terms of the present data base or its anticipated evolution in the near future. We selected a reference FER concept and set up its physics and engineering design specifications in mid-FY 1982 after reviewing the previous specifications and design works. In parallel with the reference design studies have been initiated to evaluate advanced reactor concepts such as RF current drive and pumped limiter, and comparative studies for double-null divertor/single-null divertor/pumped limiter. The detailed engineering design works have been conducted with the cooperation of industry under contract with JAERI.

The reference design of the FER is based on a D-shaped tokamak plasma with a double-null divertor and on an inductive current drive operation. The major design parameters are listed in Table 1.1.1. The heating is provided by neutral beam injection (NBI) and radio-frequency (RF) heating. The superconducting coil system with the poloidal coils placed external to the toroidal coils is enclosed in

a semipermanent common cryostat vacuum chamber (belljar type). Plasma parameters were determined by optimization studies with plausible plasma-physics and engineering restrictions such as confinement scaling, beta limit, divertor configuration and maximum magnetic fields on superconducting magnet. Priority is given to the divertor concept for impurity control and ash exhaust in view of its credible physics data base. A double-null divertor configuration is employed to reduce the major reactor radius and also to improve the coupling between OH coils and the plasma, since it will have a thinner scrape-off layer at the inboard plasma surface than a single-null divertor. Tritium breeding blanket, with Li_2O as breeding material, is installed all around the plasma and at the back side of divertor chambers to enhance breeding ratio.

During FY 1982 and 1983 the reference design has been extensively developed, in particular for torus structure concepts and individual nuclear components since these have the crucial key to establish the engineering feasibility of FER. Several torus structure design options have been developed to evaluate their configuration and design impacts when considering requirements of shield structure, space reduction, vacuum topology for plasma and SCM cryostat, and assembly/disassembly. The elevation and perspective views of the reference-FER are shown in Figs. 1.1.1 and 1.1.2, respectively.

Plasma operation scenario has been investigated based on various schemes of plasma current drive. The reference-FER as of FY 1983 has adopted a conventional startup scheme based on inductive current drive as shown in Fig. 1.1.3.

A quasi-steady state operation scenario of driving the plasma current by lower hybrid waves during both periods of startup and power-dwell as shown in Fig. 1.1.4 has been developed. This scenario is under review to adopt as a reference operation concept in FY 1984.

As the most advanced concept a FER design (RFS-FER) based on steady state burn operation scenario has been developed. The plasma current in all operation phases is noninductively driven by RF waves only as shown Fig. 1.1.5. The candidate wave drivers are CAW

(compressional Alfvén wave), HSMS (high speed magnetosonic wave) and LHW (lower hybrid wave). The elevation and perspective views of the RFS-FER are shown in Figs. 1.1.6 and 1.1.7, respectively. The major design parameters are listed in Table 1.1.2. The RFS-FER is markedly small in size in comparison with the reference-FER, for instance, the major radius is decreased to 4 m.

A work of reviewing extensive design concepts developed so far is in progress to select an optimal FER concept with considerations of physics, engineering, cost and the perspective to DEMO. Among most important issues in the present review work are the plasma operation scenario mainly consisting of startup and shutdown schemes, current drive methods and burn time, the neutron fluence, the required breeding ratio, and the staged operation schedule including engineering test programme.

OBJECTIVES OF THE FER

1. Self-ignition.
2. D-T burning for about one hundred seconds.*
3. Definitive demonstration of essential fusion technologies such as system integration, plasma heating technology, plasma control technology, superconducting magnet technology, and tritium technology, etc.
4. Integral test of technologies concerned with future fusion reactors in the areas of materials, tritium production technology, remote maintenance technology, safety, reliability and durability, and availability improvement.

* : under review

ADDITIONAL REQUIREMENTS FOR THE FER DESIGN

1. Tritium breeding ratio of about unity.*
2. Moderate neutron wall loading of approximately 1 MW/m^2.
3. Staged operation scenarios, for example, of installing the breeding blanket in the second stage, should be evaluated.

* : under review

FER DESIGN ORGANIZATION

(as of FY 1983)

JAERI

- Project Management
- System Definition
- Reactor Concept and Design Specifications
- Guidelines for Detailed Engineering Design of Industry
- Physics Design
- Design Integration
- System Analysis
- Research and Development Program

INDUSTRIAL FIRMS

Detailed Engineering Designs under contract with JAERI

- Hitachi Ltd.: Reactor Components and Systems
- Toshiba Corp.: Reactor Components and Systems
- Mitsubishi Group: Reactor Components and Systems
- Kawasaki Heavy Industries: Blanket and Tritium System
- Sumitomo Heavy Industries: Tritium System (as of FY 1982)

JAERI－M 84－107

FER Design Concepts (JFY 1982 ~ 1983)

Reference

Based on Double-Null Divertor:

- ○ Credible physics data base
- ○ Thinner width of the inboard scrape-off layer in comparison with Single-Null Divertor

Alternatives

1. Single-Null Divertor
   - ○ Reduction of TF coil height
   - ○ Favorableness in installation, repair and maintenance in comparison with Double-Null Divertor

2. Advanced Concepts

(1) RF Current Drive

(a) Application to start-up phase
   - ○ Elimination or substantical reduction of OH-coil magnetic flux supply for start-up

(b) Steady state operation
   - ○ Great advantages in FER itself and commercialization of tokamak

(2) Pumped Limiter
   - ○ Reduction of power supply
   - ○ Reduction of TF coil height
   - ○ Small n-index value
     Favorableness in vertical position control

MAIN DESIGN FEATURES OF THE REFERENCE-FER

- D-shape plasma with the elongation of 1.5:
  (a compromise of high beta values and vertical stability control
- Impurity control: double-null divertor
- Heating: NBI and RF
- Cryostat of SCM: semi-belljar type
  common chamber for TF and PF coil systems
- PFC(NbTi): external to TFC(Nb_3Sn/NbTi)
- Number of TFC: 14 (a compromise of reactor size and toroidal field ripple ≤ 0.75 %)
- Tritium breeding ratio: > 1.0
- Personnel accessibility for maintenance within 24 hours after reactor shutdown: ≤ 2.5 mrem/h

JAERI — M 84 — 107

MAJOR FEATURES OF PHYSICS DESIGN

(1) Plasma Parameters

- Energy confinement
  Alcator scaling law
- Beta-limit
  ballooning instability mode

(2) Impurity Control

- Divertor for reference-FER
  high-density and low-temperature divertor plasma
  → reduction of the required pumping speed and
  mitigation of heat load and erosion
- Pumped limiter for advanced FER

(3) Vertical Position Control

- Passive control by conducting shells
- Active control by PF coils external to TF coils

(4) Plasma Current Drive

- Inductive current drive
  (reference concept as of FY 1983)
- RF-assisted current startup
  (under review to adopt as a reference concept in FY 1984)
- Steady state plasma operation for advanced FER

MAJOR FEATURES OF ENGINEERING DESIGN

(1) Reactor Strucutre

- Vacuum topology
  common in the inboard, top and bottom areas for plasma vacuum and cryostat chambers
- Cryostat of SCM
  common chamber (semi-belljar type) for TF and PF coil systems
- Support structure
  bucking cylinder supporting the total centering force on TF coils
  earthquake-proof
- Tritium breeding blanket
- Double-null divertor chambers
- Maintenance
  - removal torus modules
    blanket/shield and divertor
  - inboard shield
    semi-permanent or removal
  - multiple torus module arrangement for each TF window
  - single and double straight-line motion, (rotation)

JAERI－M 84－107

(2) First Wall/Breeding Blanket

- Structural material

  type 316 stainless steel ($\lesssim$ 300 °C)

- Tritium breeding material

  Li_2O (400 ~ 1000 °C)

- Coolant

  H_2O ($\lesssim$ 100 °C)

- Tritium recovery

  continuous recovery by helium purge gas

  (1 atm, 200 Nm^3/hr)

- Candidate neutron multiplier materials

  Be, Pb

- Candidate conducting shell materials

  Cu, Be, Pb

- Armor on first wall

  under review

(3) Divertor

- Candidate materials

  Armor : W, Mo (alloy)

  Heat sink : Cu

- Coolant

  H_2O ($\lesssim$ 100 °C)

Table 1.1.1

MAJOR DESIGN PARAMETERS (Ref-FER)

POWER	
Fusion power (MW)	440
Neutron wall loading (MW/m^2)	1.0
OPERATION	
Burn time (s)	100
Duty factor/Availability (%)	50–70/25–50
PLASMA	
Major/Plasma radius (m)	5.5/1.1
Plasma elongation	1.5
Burn average beta (total) (%)	4
Plasma current (MA)	5.3
Toroidal field on axis (T)	5.7
HEATING	
NBI/RF power (MW)	30/30
IMPURITY CONTROL	
Poloidal divertor	double null
Power to divertor plate (MW)	45
BREEDING BLANKET	
Structural material	Type 316 SS
Breeding material	Li_2O
Breeder temperature (°C)	400–1000
Tritium breeding ratio	1.05
Coolant	H_2O
TOROIDAL FIELD COILS	
Number	14
Conductor	Nb_3Sn, NbTi
Maximum field (T)	12
POLOIDAL FIELD COILS	
Conductor	NbTi
Maximum field (T)	8

Table 1.1.2 Major design parameters of RFS-FER

RF Driver	CAW	HSMS	LHW
1. Plasma parameters			
Temperature (keV)	13	19	14.5
Density ($\times 10^{19}$ m^{-3})	9	6.2	8.1
Fusion power (MW)	250	210	250
Wall loading (MW/m^2)	0.9	0.76	0.9
Q value	14	4.2	10
RF power (MW)	18	50	25
2. Device parameters			
Major radius (m)	4.0		
Minor radius (m)	1.1		
Noncircularity	1.5		
Toroidal field (T)	4.5		
Plasma current (MA)	6.4		

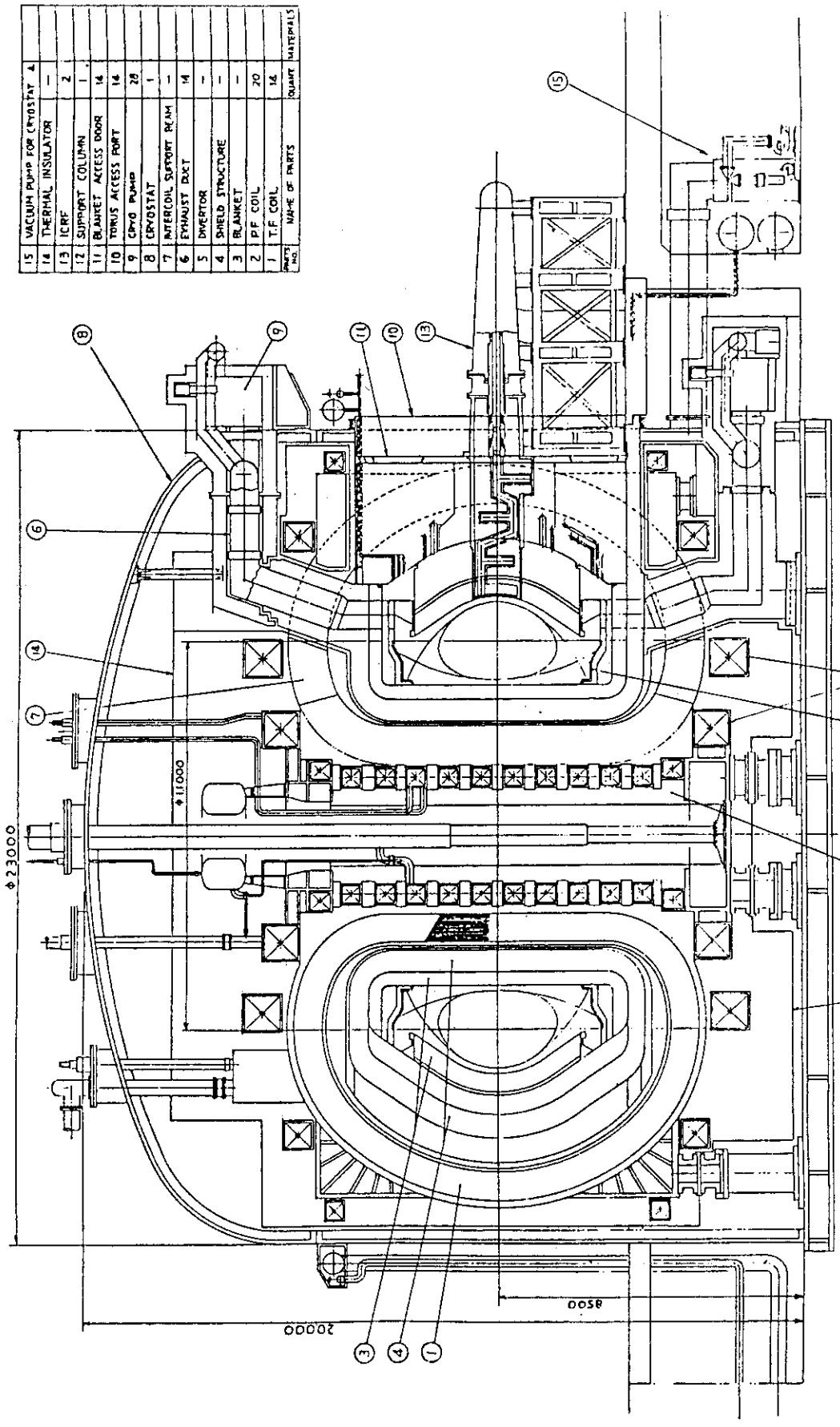

Fig. 1.1.1 Elevation view of Ref- FER

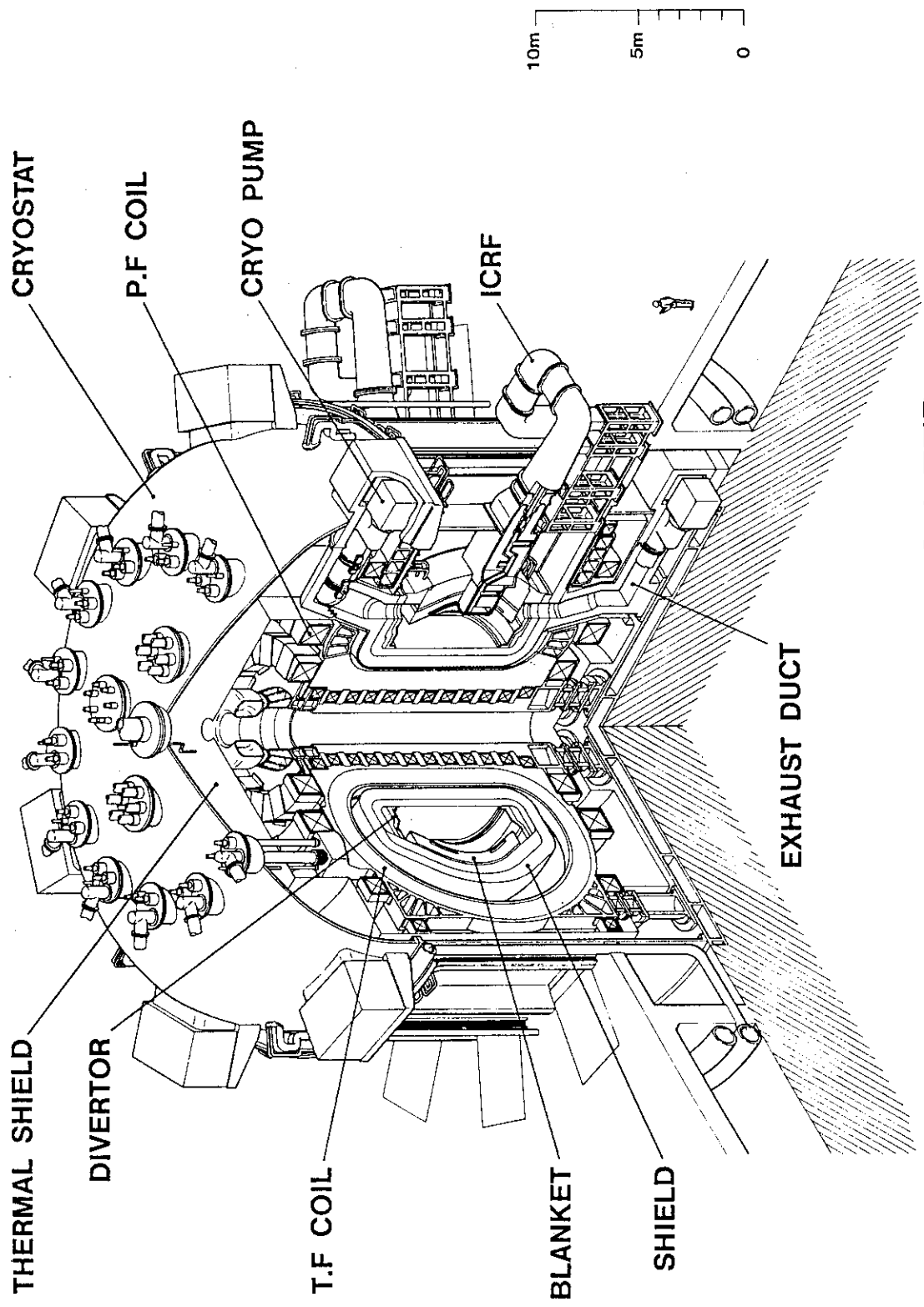

Fig. 1.1.2 PERSPECTIVE VIEW OF FER

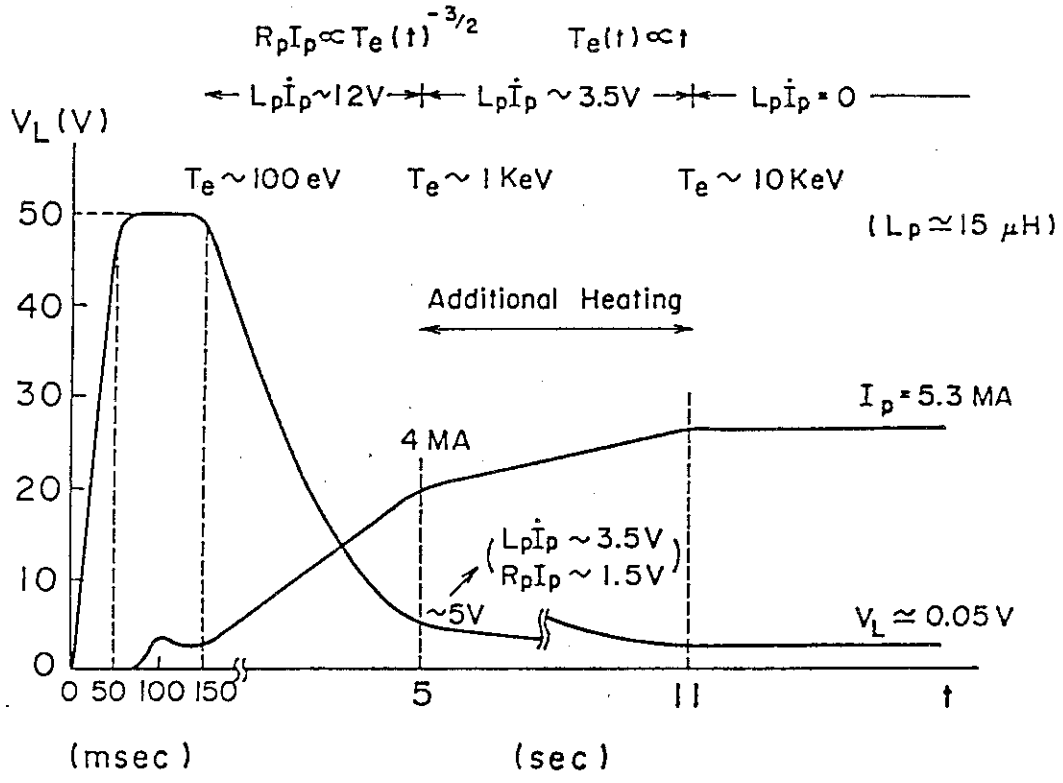

Fig. 1.1.3 Startup scheme for Ref-FER

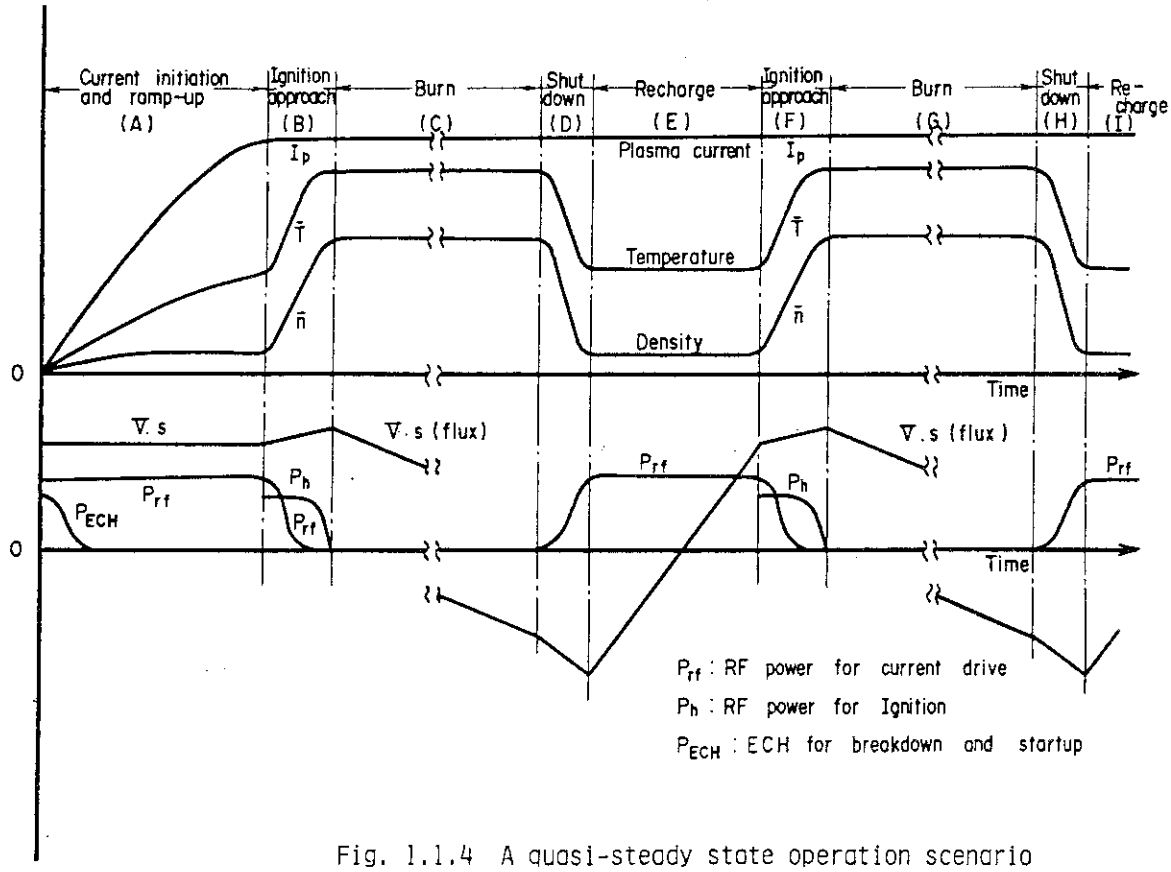

Fig. 1.1.4 A quasi-steady state operation scenario

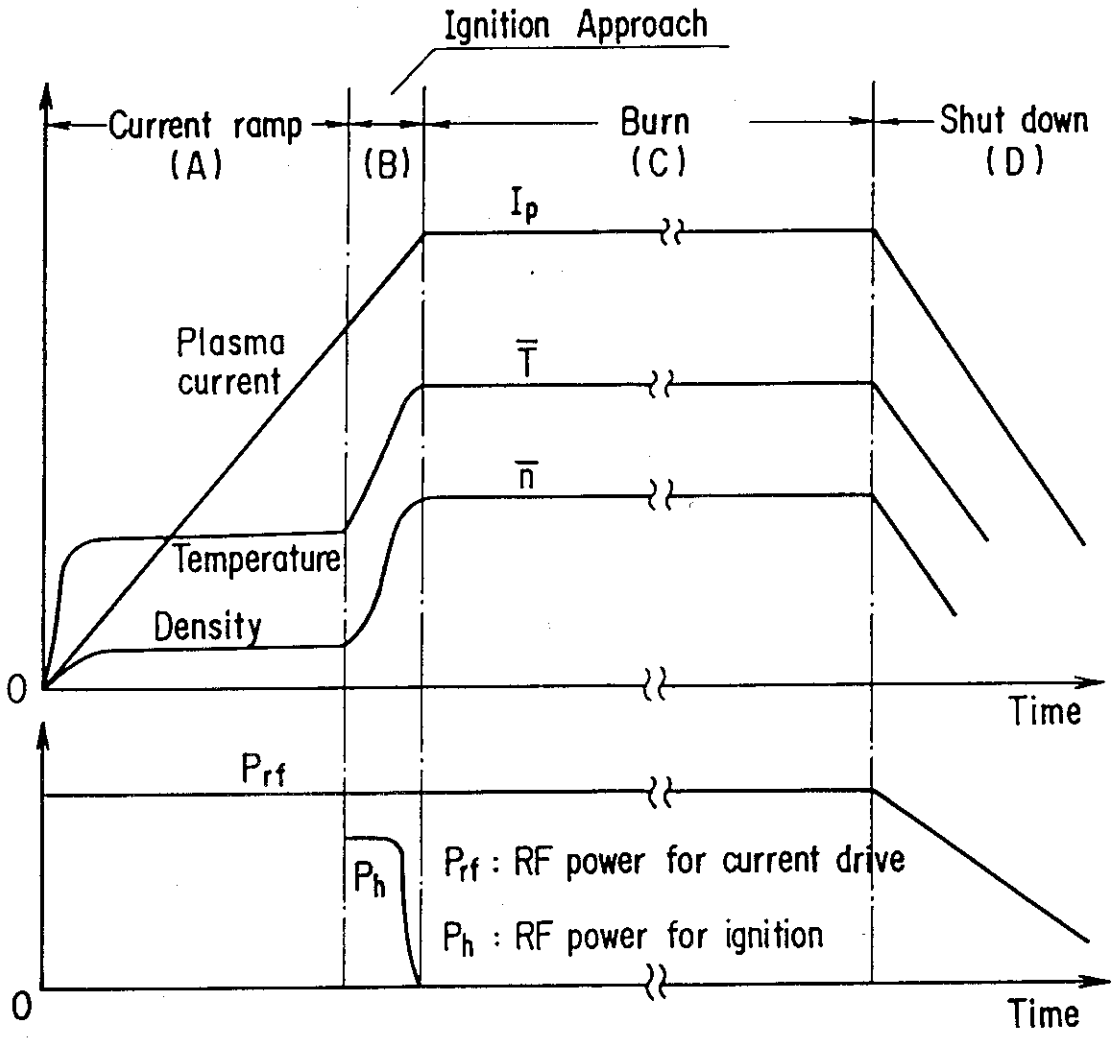

Fig. 1.1.5 A steady state operation scenario(RFS-FER)

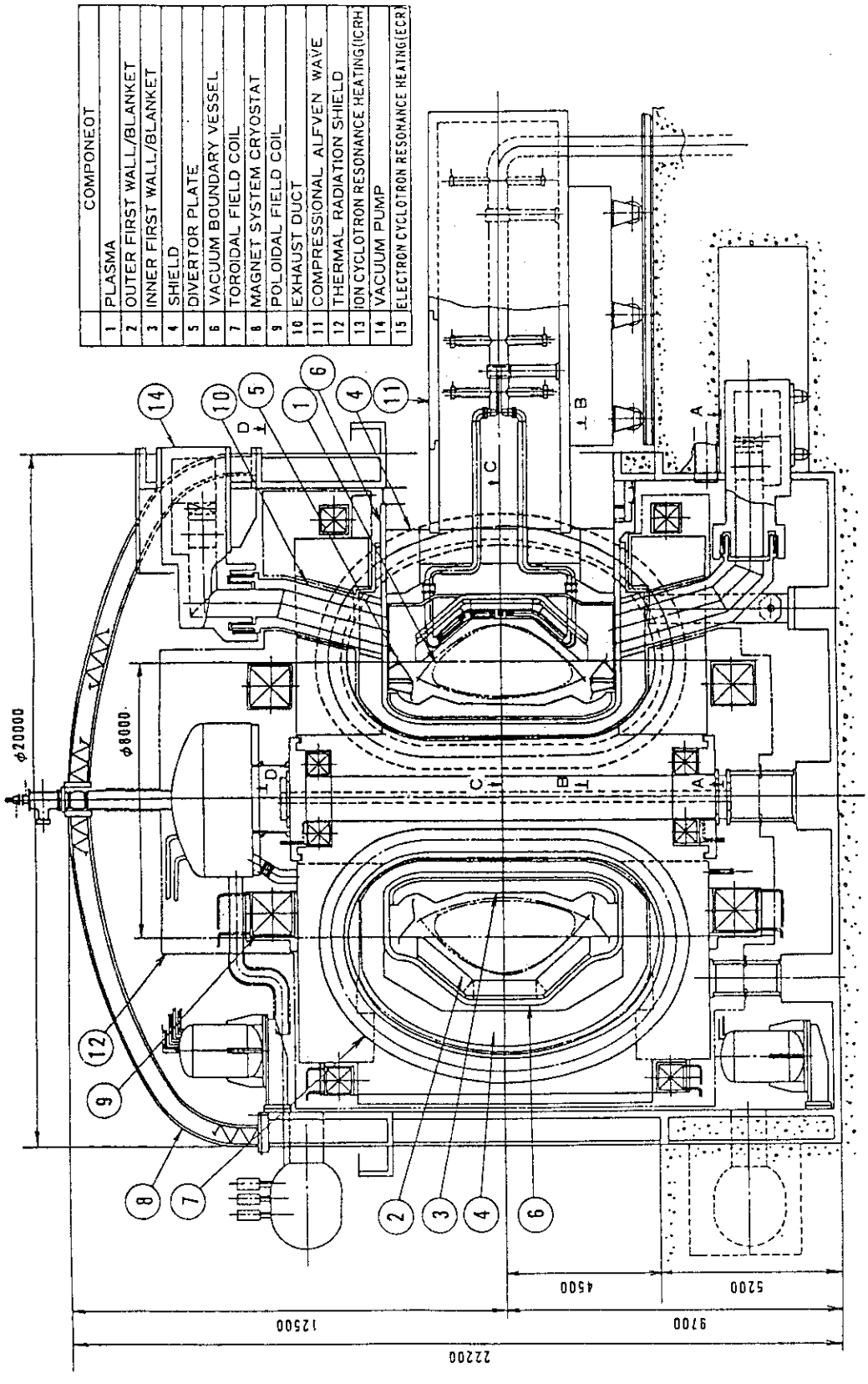

Fig. 1.1.6 Elevation view of RFS-FER

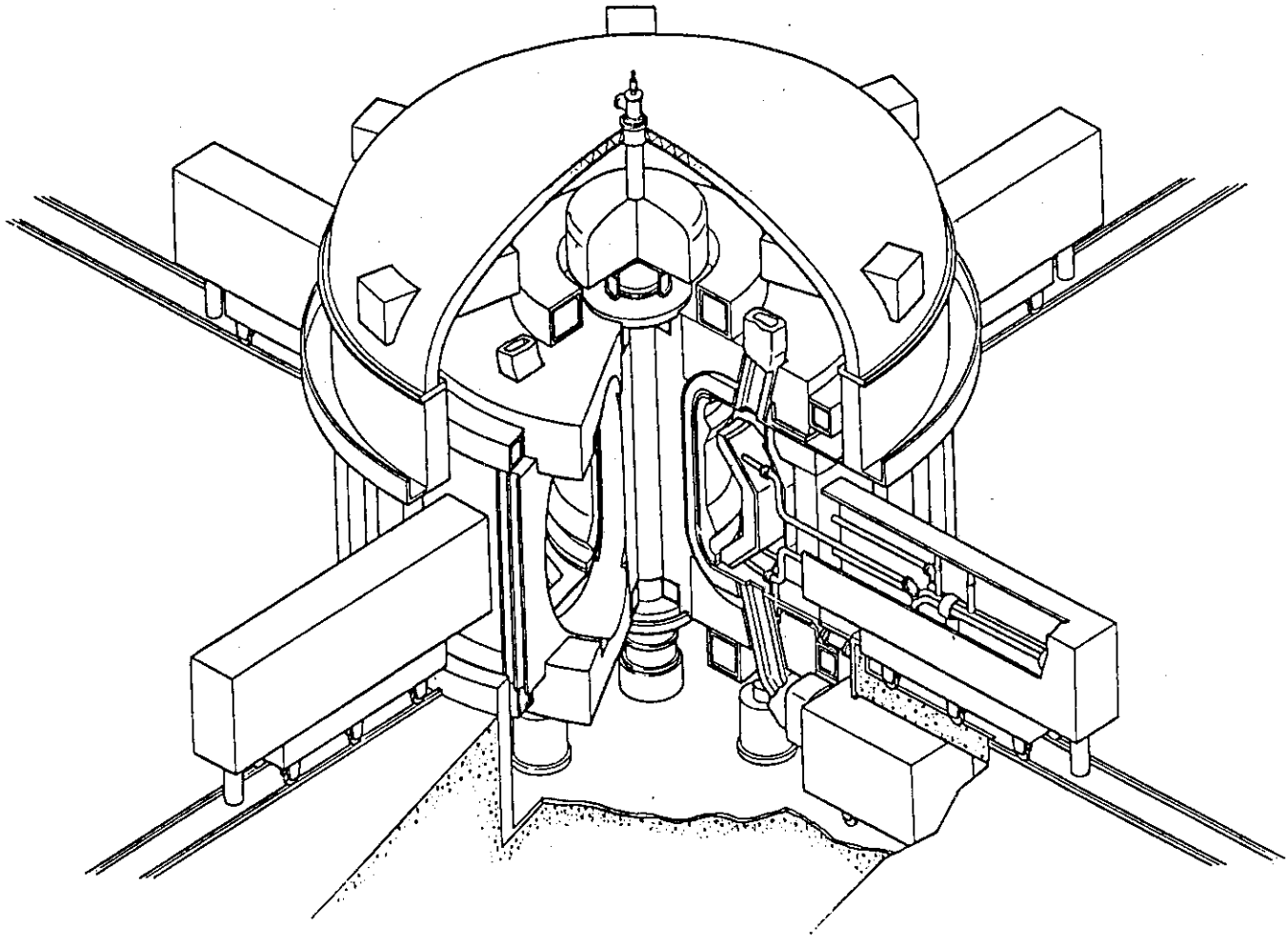

Fig. 1.1.7 Perspective view of RFS-FER

1.2 Overview of FER physics design

Data base for the determination of plasma and device parameters of reference FER are summarized in Table 1.2.1. They are almost the same as those of INTOR data base. Figure 1.2.1 shows the fundamental philosophy to realize the stable core plasma. Most stringent instabilities are disruption and ballooning instability, so that the safety factor at the plasma surface and the toroidal beta value are set to 2.5 and 4%, respectively, to avoid these instabilities. Figures 1.2.2-1.2.4 show the optimization of device parameters. Emphases of the optimization are placed on the device size and power supply capacity for the PF coils. By these optimization, the aspect ratio of FER is set to 5, which is slightly larger than INTOR. As a result of this optimization, the capacity of power supply for PF coils is reduced by a factor of 2, and the narrow space of the inboard region can be greatly mitigated compared with INTOR. Figure 1.2.5 shows the operation scenario of reference FER. By this operation, control scenarios for the stable burning and helium ash exhaust will be established, while that for current diffusion may be difficult to be established. The latter feature of the operation means that data base for OH long pulse operation of the commercial reactor cannot be provided by the present operation scenario. This deficiency is now under review. Table 1.2.2-1.2.8 summarize the critical issues for seven major items in physics design; they are 1) particle and energy confinement, 2) beta value, 3) impurity control, 4) additional heating, 5) equilibrium and stability, 6) disruption and 7) operation scenario.

Two operation scenarios with RF assistance are considered for alternative and advanced FER. One is the current ramp-up in low density plasma by lower hybrid wave current drive (LHCD), experimental data base of which has already been established. Quasi-steady operation is included in this scenario. The other is completely steady-state operation scenario by RF current drive. For long pulse operation by lower hybrid wave current ramp-up, the following items are important; optimization of current ramp-up scenario, optimization of PF coils for long burn, characteristics of quasi-steady operation. Minimization of current ramp-up time is studied by quasi-linear theory of current drive coupled with

power balance. It is most essential for inner most PF coils to be freed from equilibrium for long burning or decreasing the device size, and it is shown possible for all range of beta poloidal values by the equilibrium code calculation. Characteristics of quasi-steady state operation must be studied from various view points shown in Table 1.2.9. Conclusions for long pulse operation scenario by LHW current ramp-up are summarized in Table 1.2.10. For the completely steady-state operation scenario, three candidate waves for current driver are examined. They are compresional Alfv́en wave (CAW), high speed magneto-sonic wave (HSMS) and lower hybrid wave (LHW). Advanced and disadvanced feature of each wave are summarized in Table 1.2.11. Relations between each wave in ω-$k_{/\!/}$ plane are shown in Fig. 1.2.6. CAW is chosen as a primary candidate wave, since it has the highest potential advantage for commercial reactor. Table 1.2.12 shows plasma and device parameters for each candidate wave. Emphases are placed on how much the major radius can be reduced without aggravating the plasma performance. Based on the parameters of CAW for current drivers, the design studies on the completely steady-state FER are made.

A primary candidate for the impurity control of the present reference FER is the poloidal divertor. To optimize the divertor configuration, two-dimensional numerical calculation code for divertor plasma has been developed. They consist of the fluid portion, which describes the plasma behavior in divertor chamber, and the Monte-Carlo portion, which describes the neutral particle behavior in the chamber and the evacuating duct. Based on the numerical analyses by this code, low temperature and high density plasma near the divertor plate can be formed even for rather open divertor. Figure 1.2.7 shows the two-dimensional views of the electron temperature (a) and the electron density (b) in the divertor chamber. These features of the divertor plasma can mitigate the heat load, erosion of the plate and the pumping requirement. Preliminary calculation of the pumped-limiter is made by one-dimensional transport code. Various transport coefficients in the scrape-off layer are fitted to reproduce ASDEX limiter experiments. These coefficients are used to predict the performance of FER. Figure 1.2.8 shows the ion particle flux, heat flux and erosion of the limiter plate. Applicability of the pumped-limiter to FER is examined by this

calculation. It is found that the radiation cooling is less expectable than divertor and there should be large heat load and erosion in any transport coefficients. It is then concluded that cold boundary layer should be considered for application of pumped-limiter to FER. Design study is made for advanced FER with pumped-limiter, whose plasma minor radius is enlarged by about 20 cm for cold boundary layer. Plasma and device parameters for the design study are tabulated in Table 1.2.13.

1. Outline of Reference FER Physics Design
   - ○ Data base
   - ○ Stable core plasma
   - ○ Plasma/device parameter
   - ○ Operation scenario
   - ○ Critical issues

2. Outline of Advanced and Alternative FER physics Design

   (1) RF assisted operation scenario
   - ○ Current ramp-up by LHCD (Long pulse/ Quasi-steady)
   - ○ Steady operation by CAW, HSMS, LHW CD

   (2) Pumped-limiter
   - ○ Applicability to FER→ cold boundary plasma

Table 1.2.1 Data base for reference FER.

Data Base for FER Physics Design

Major items	Data base
1. Energy and Particle Confinement	$x_e = (4\sim5)\times10^{19}/n_e$ $x_i = (2\sim3)x_{ineo}$
2. Beta value	4 ~ 5 %
3. Non-circularity	1.5 ~ 1.6
4. Cold boundary layer	Divertor chamber 20 ~ 30 cm(pumped-limiter)
5. Impurity control method	Poloidal divertor
6. Additional heating	NBI former period RF latter period
7. Toroidal field ripple	± 0.75 %
8. Burn time	≳ 100 sec

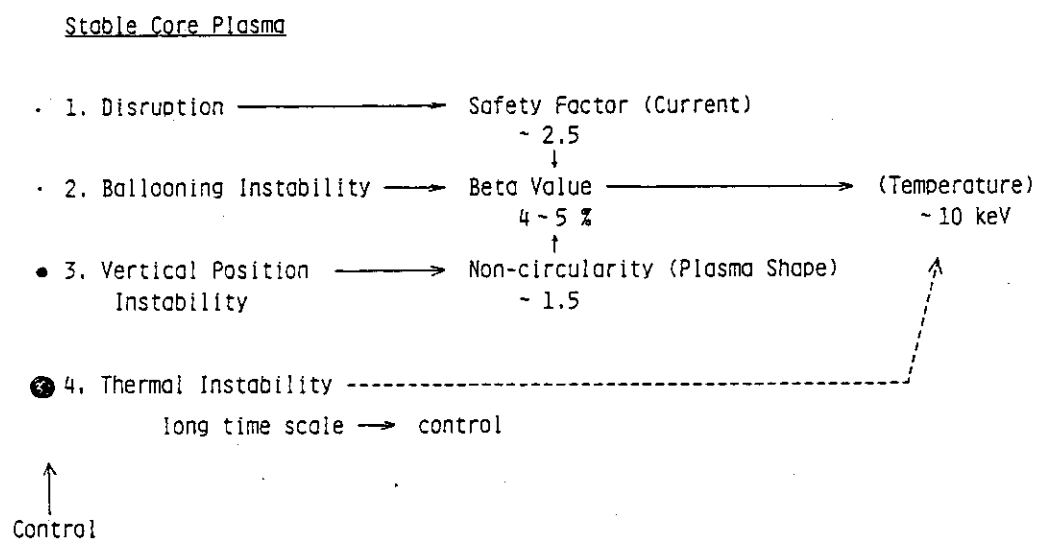

Fig. 1.2.1 Four major instablities and the parameters to avoid or control them. Radius of the closed circle before the item number denotes the weight of control.

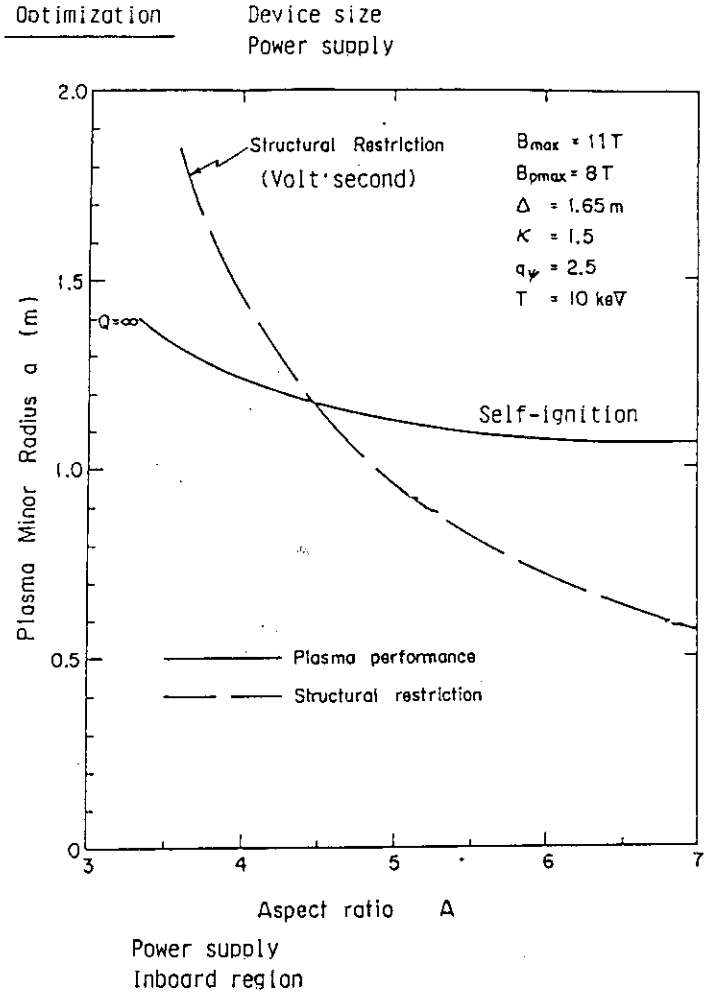

Fig. 1.2.2 Optimization of the device size. Solid line shows the self-ignition and long brokn line shows the structural restriction due to volt·second requirement.

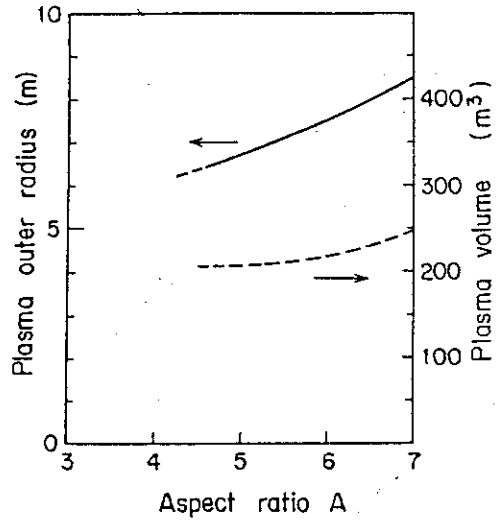

Fig. 1.2.3
Plasma outer radius and plasma volume as a function of aspect ratio along the ignition line of Fig. 1.2.2.

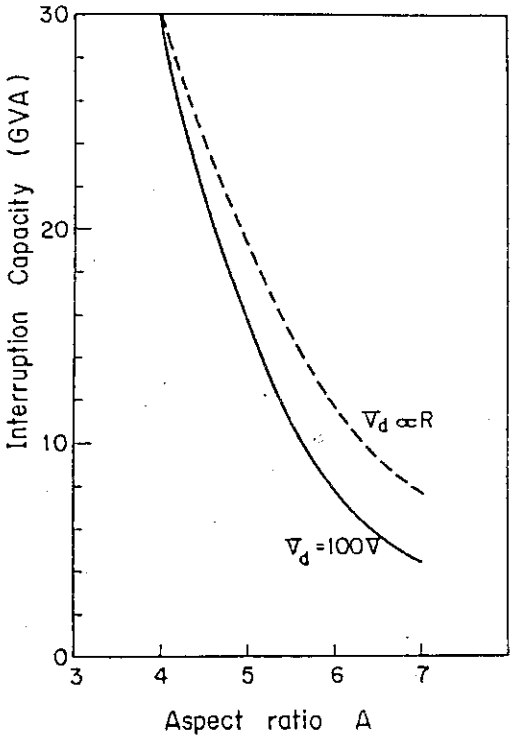

Fig. 1.2.4
Interruption capacity as a measure of capacity of PF coils power supply along the ignition line of Fig. 1.2.2. Solid line shows the case with constant one-turn voltage of 100 V, while dotted line shows the case, in which one-turn voltage is assumed proportional to major radius.

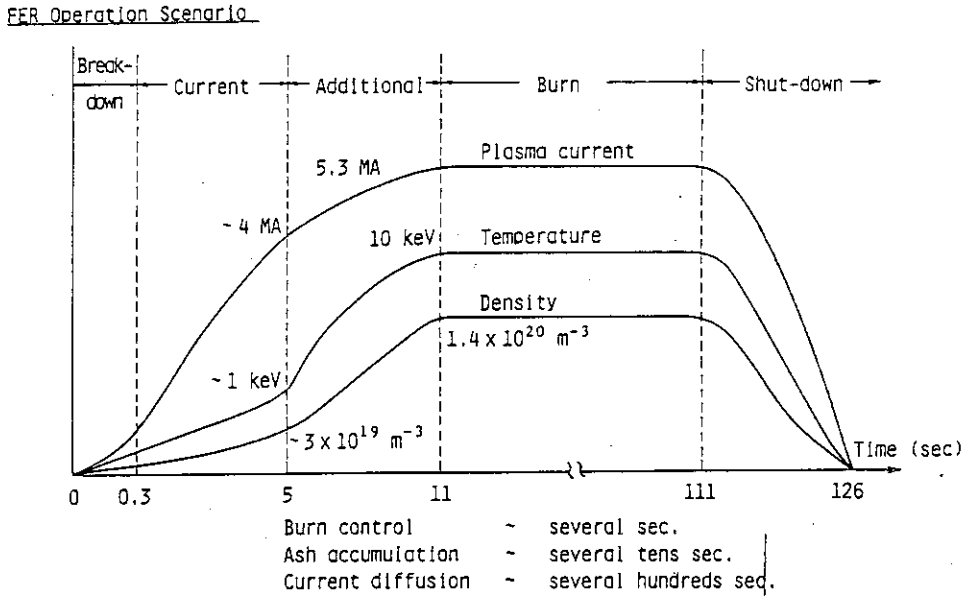

Fig. 1.2.5 Schematic drawing of operation scenario of reference FER. By this scenario, burn control and helium ash exhaust can be demonstrated, while current diffusion for OH long burning cannot be examined.

Critical Issues

1. Energy and Particle Confinement
2. Beta Value
3. Impurity Control
4. Additional Heating
5. Equilibrium and Stability
6. Disruption
7. Operation Scenario
   - ○ Design value and data base for reference FER
   - ○ Major problems in design
   - ○ Future direction for alternative or advanced FER

Table 1.2.2 Critical issues of FER for energy and particle confinement.

1. Energy and Particle Confinement

Design value and data base for reference FER	Major problems in design	Future direction for alternative or advanced concept
• $\tau_E \sim 1.5$ sec (a = 1.1 m, B = 5.7 T) (Empirical scaling)	• Large device size a = 1.1 m, b = 1.65 m • High heat load (400 MW fusion power) • Large additional heating power (~60 MW)	• Improvement of energy confinement ○ small, circular shape ○ small fusion output, additional heating power ○ divertor-less
• Toroidal field ripple (analysis of α-loss)	• Toroidal field coils size 6.3 × 9.4 m number 14	Heating profile control ○ small size, number
• $\tau_{He} \sim 0.5$ sec no helium enrichment	• Pumping speed $\sim 2 \times 10^5$ ℓ/s • Pumped-out fuels $\sim 3 \times 10^{21}$ s^{-1}	• Reduced τ_{He} (divertor) • Helium selective pumping

Table 1.2.3 Critical issues of FER for beta value.

2. Beta Value

Design value and data base for reference FER	Major problems in design	Future direction for alternative or advanced concept
• $\beta \sim 4\%$ (5.7 T) Circular 3% JFT-2 Non-circular 4.6% D-III Ballooning mode theory ~2.7%	• Large device size • High toroidal field	• Higher beta value 6~7% Noncircular 4~5% Circular ○ Small, circular shape ○ Low toroidal field ○ Wide operation region high T, low n (Thermally stable, Long burn, Current drive low T, high n (Low erosion of first wall, limiter

Table 1.2.4 Critical issues of FER for impurity control.

3. Impurity Control

Design value and data base for reference FER	Major problems in design	Future direction for alternative or advanced concept
• Poloidal divertor Experiments DIVA, D-III PDX, ASDEX Numercial analysis	• High heat load, erosion • Large power supply (5 GJ, 1500 MVA) • Complicated remote maintenance	• Low temperature, high density divertor plasma • Low temperature boundary plasma ○ Pumped-limiter small-power supply, Small non-circular shape ○ Long life of first wall ○ Variety choice of wall material

Table 1.2.5 Critical issues of FER for additional heating.

4. Additional Heating

Design value and data base for reference FER	Major problems in design	Future direction for alternative or advanced concept
• Former period NBI (150 keV, 30 MW) Later period RF (30 MW) Burn period RF (DC 10 MW) • Breakdown assist ECH (10 MW)	• Adjustment, maintenance of NBI	• RF heating only ○ simplification of reactor periphery ○ mitigation of D,T isotope separation • Unification of RF system including current drive ○ simplification of RF system

Table 1.2.6 Critical issues of FER for equilibrium and stability.

5. Equilibrium and Stability

Design value and data base for reference FER	Major problems in design	Future direction for alternative or advanced concept
• D shape, $\kappa \sim 1.5$ (D-III $\kappa \sim 1.8$)	• Installation of passive shell complicated structure of first wall decline of T.B.R.	• Small non-circularity • Pumped-limiter
• Double null configuration (divertor configuration)	• Large power supply	

Table 1.2.7 Critical issues of FER for disruption.

6. Disruption

Design value and data base for reference FER	Major problems in design	Future direction for alternative or advanced concept
• Frequency 10^3	• Electromagnetic force	• Decay of frequency
• Time 15 ms current 5 ms heat	• High heat flux	• Control for softening
• Energy 180 MJ		

Table 1.2.8 Critical issues of FER for operation scenario.

7. Operation Scenario

Design value and data base for reference FER	Major problems in design	Future direction for alternative or advanced concept
• Pulse operation (10^6/life)	• Thermal, mechanical stress fatigue of first wall, T coil	• Steady/Long pulse (quasi-steady) operation by RFCD
• Breakdown 30 V 0.2 mΩ	• Current interuption capacity • Bellows structure	• Preionization by ECH
• Start-up/Shut-down (~ 10 sec)	• Large power supply • Large AC loss (~ 70 MW)	• Additional heating • Current ramp-up by RFCD

1. Long pulse operation scenario (Alternative FER)
   - ○ Operation scenario by using LHW current drive in low density plasma
     - • Optimization of current ramp-up scenario
     - • Optimization of PF coils for long burn
     - • Characteristics of quasi-steady operation
2. Steady state operation (Advanced RFS-FER)
   - ○ Physics design consideration for candidate wave drivers

     CAW, HSMS, LHW
   - ○ Plasma and device parameters for design study

Table 1.2.9
Important items to be examined for long pulse or quasi-steady operation scenario.

Important Items

1. Duty cycle
   - ○ Current ramp-up time
   - ○ OH coil recharging time
   - ○ Burn time
   - ○ Pumping time
2. Energy transfer of PF coils
3. Over-turning moment of TF coils
4. Device size

Table 1.2.10 Conclusions of the optimization of long pulse operation scenario.

Conclusions for long pulse operation scenario

1. Static equilibrium control is possible over whole range of beta-p and I_D. The inner-most PF coils can be free from equilibrium.
2. Long burning can be realized when plasma current is ramped-up to 4 MA by LHW.
3. Ramp-up to 4 MA is favorable from view point of total energy consumption per fusion output energy.
4. Recharging time will be 200～300 sec for 100 v.s. The time can be shortened effectively by impurity.
5. Recharging at $I_D = 4$ MA is also favorable to reduce the variation of over-turning force.
6. Reduction of magnetic energy transfer will be difficult for non-circular plasma.

Table 1.2.11
Advantage and disadvantage of candidate waves for current driver. CAW is chosen as a primary candidate wave for current driver due to its potential advantage for commercial reactor.

Candidate Waves for Current Driver

(1) Fast wave ----- Good accessibility

Compressional Alfvén Wave (CAW)

Theoretically best efficiency

Difficulties --- Antenna design
trapped electrons effect

High Speed Magnetosonic Wave
Low efficiency
No difficulties in CAW

(2) Lower Hybrid Wave
Experimentally proven
Density limit, Accessibility

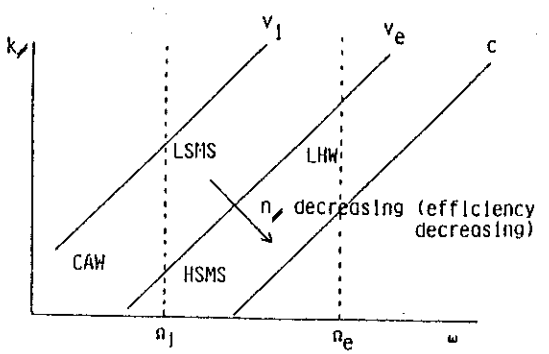

Fig. 1.2.6

Relations between three kinds of fast waves of ICRF in ω-$k_{//}$ plane. v_i, v_e and C denote ion and electron thermal velocity and the velocity of light, respectively. Lower hybrid wave is also shown by LHW.

Table 1.2.12
Plasma and device parameters for completely steady-state advanced FER. Major radius is decreased as long as possible without aggravating the plasma performance.

Plasma and device Parameters for RFS-FER

RF Driver		CAW	HSMS	LHW
1. Plasma parameters				
Temperature	(keV)	13	19	14.5
Density	($\times 10^{19}$ m^{-3})	9	6.2	8.1
Fusion power	(MW)	250	210	250
Wall loading	(MW/m^2)	0.9	0.76	0.9
Q value		14	4.2	10
RF power	(MW)	18	50	25
2. Device parameters				
Major radius	(m)	4.0		
Minor radius	(m)	1.1		
Noncircularity		1.5		
Toroidal field	(T)	4.5		
Plasma current	(MA)	6.4		

I. Reference: Poloidal divertor

- Optimization of FER divertor

  (2D (z,r) numerical analyses)

  - He pumping requirement
  - Remote radiation cooling
  - Dense/cold plasma formation

II. Advanced: Pumped-limiter

- Applicability for FER impurity control system (1D (r) transport analyses)
  - He exhaust
  - Heat load
  - Erosion

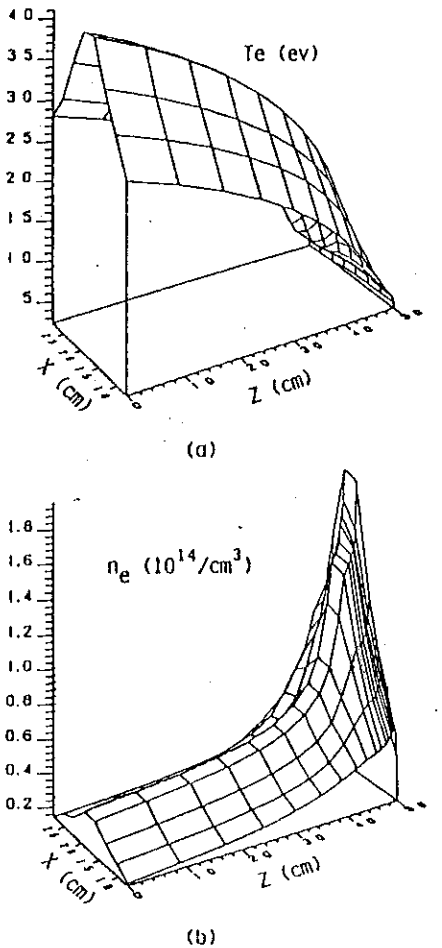

Fig. 1.2.7
Two-dimensional view of electron temperature and electron density in the divertor chamber calculated by self-consistent numerical code of divertor plasma. Electron temperature decreases below 10 eV at the divertor plate.

I. Poloidal Divertor

(1) Guideline of divertor design (conclusion by numerical analyses)

- low pumping requirement for He exhaust
  ($S \leq 10^5$ ℓ/s)
- low plasma temperature near divertor plate
  ($T_e \leq 30$ eV)
- moderate heat load on divertor plate
  ($P \leq 20$ MW/d.p)

(2) Criteria for the formation of dense/cool divertor plasma

II. Pumped-Limiter

- Limiter chamer: 2D calculation as in divertor
- Limiter surface: scrape-off analyses including main plasma are essential

↓ Preliminary Calculation

1D (r) calculation with convection model

[impact of transport coefficients on performance of limiter]

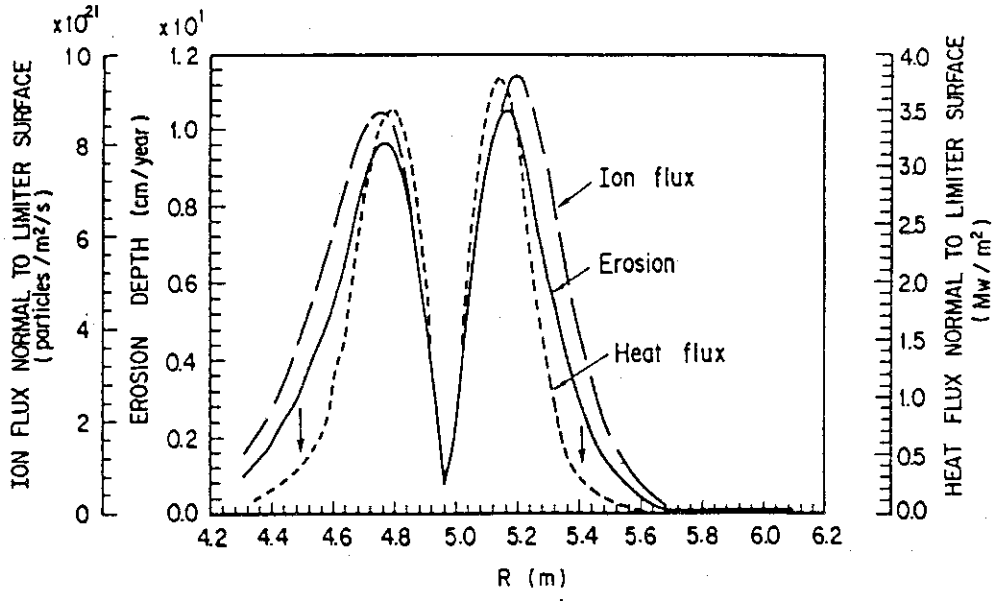

Fig. 1.2.8 Ion particle and heat flux to the limiter and erosion depth of the limiter surface calculated by one-dimensional transport code, in which the transport coefficients are fitted to reproduce ASDEX limiter experiments.

Applicability of Pumped-Limiter

- ○ Large uncertainty in transport coefficients
- ○ Plasma parameters greatly depend on the coefficients
- ○ Large heat load/erosion in any case
- ○ convective model is insufficient?
  - { radiative cooling is less expectable than divertor
    2D calculation is necessary?
- ○ Cold boundary layer should be considered for application of pumped-limiter
  ⟶ larger plasma size

Table 1.2.13 Plasma and device parameters for comparative design studies of pumped-limiter. In Case L2, cold boundary layer of 20 cm is considered.

Plasma and Device Parameters for Design Study of Pumped-Limiter

	Case L1	Case L2
1. Cold boundary layer	None	Yes ~ 0.2 m
2. Temp. of scrape-off layer	≳ 100 eV	~ several tens eV
3. Major radius (m)	5.7	6.0
4. Minor radius (m)	1.17	1.46*
5. Average ion temp. (keV)	10	10
6. Average ion density (10^{20} m^{-3})	1.28	1.2
7. Toroidal field (T)	5.5	5.2
8. Plasma current (MA)	5.5	5.8*
9. Safety factor	2.5	2.5*
10. Fusion power (MW)	460	480*

* Same plasma performance within the cold boundary layer

Conclusions

	Divertor	Pumped-Limiter
Advantage	○ Cold/dense plasma in divertor region	○ Applicability to less elongated plasma
Critical point	○ Vertical position control	○ Formation of cold boundary layer⟶ larger plasma size, potential advantage in heat removal in commercial reactor
Suitable for	FER	Commercial Reactor

1.3 Overview of FER engineering design

Specifications and Guidelines for
the Reference-FER Engineering Design

1. Reactor Configuration and Maintenance
2. First Wall/Blanket
3. Divertor
4. Electromagnetics
   (Control of Plasma Positional Instability)
5. Shield
6. TF/PF Coils
7. Plasma Heating System
8. Power Supply System
9. Cooling System
10. Tritium System
11. Safety
12. Plant Layout

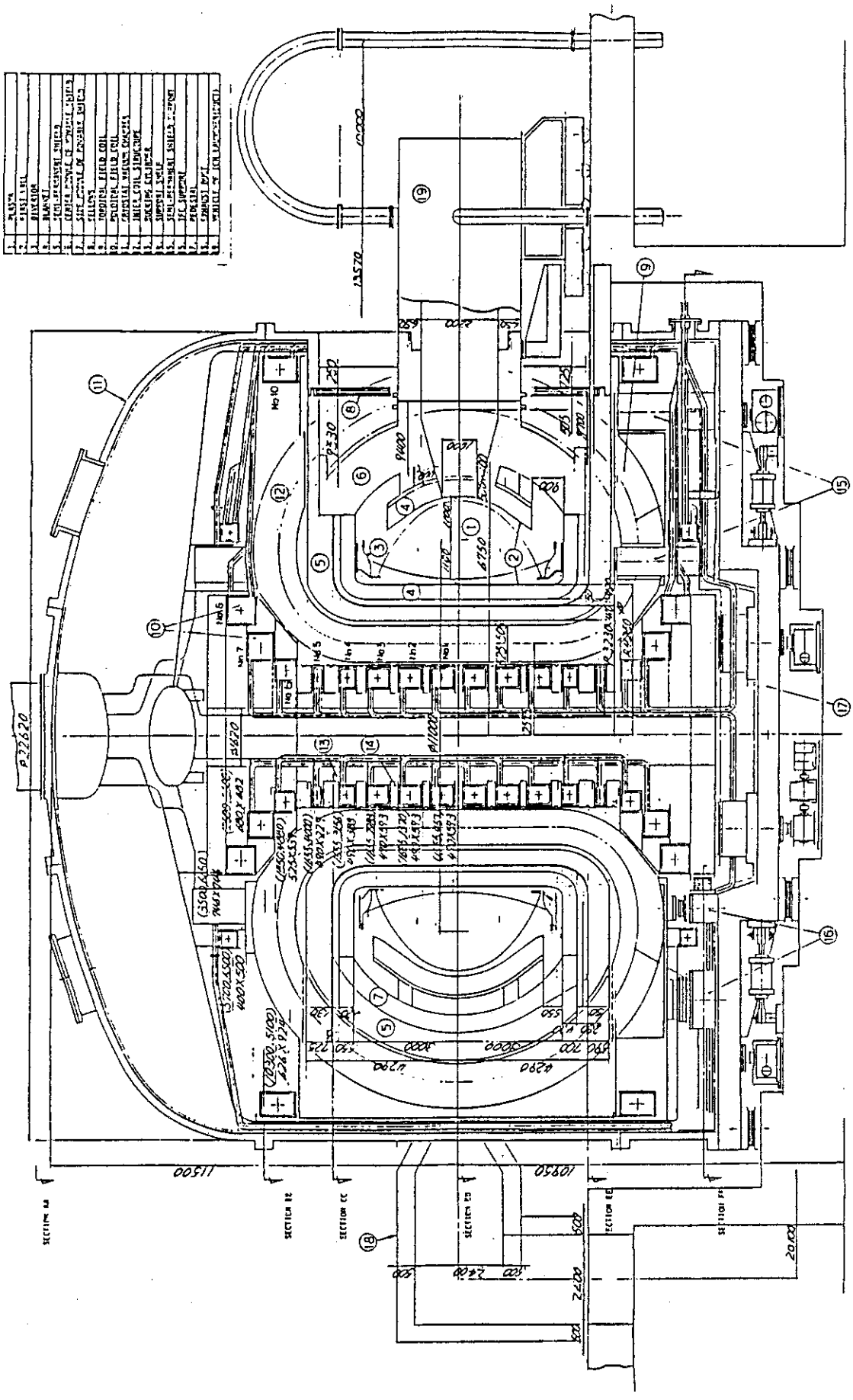

REACTOR CONFIGURATION

Case	Shield Post	Vacuum Port Location	Segmentation of Torus
A	no	Top & Bottom	42 (3/port)
B	yes	Top & Bottom	28 (2/port)
C	yes	Midplane	28 (2/port)
D	yes	Top & Bottom	42 (3/port)

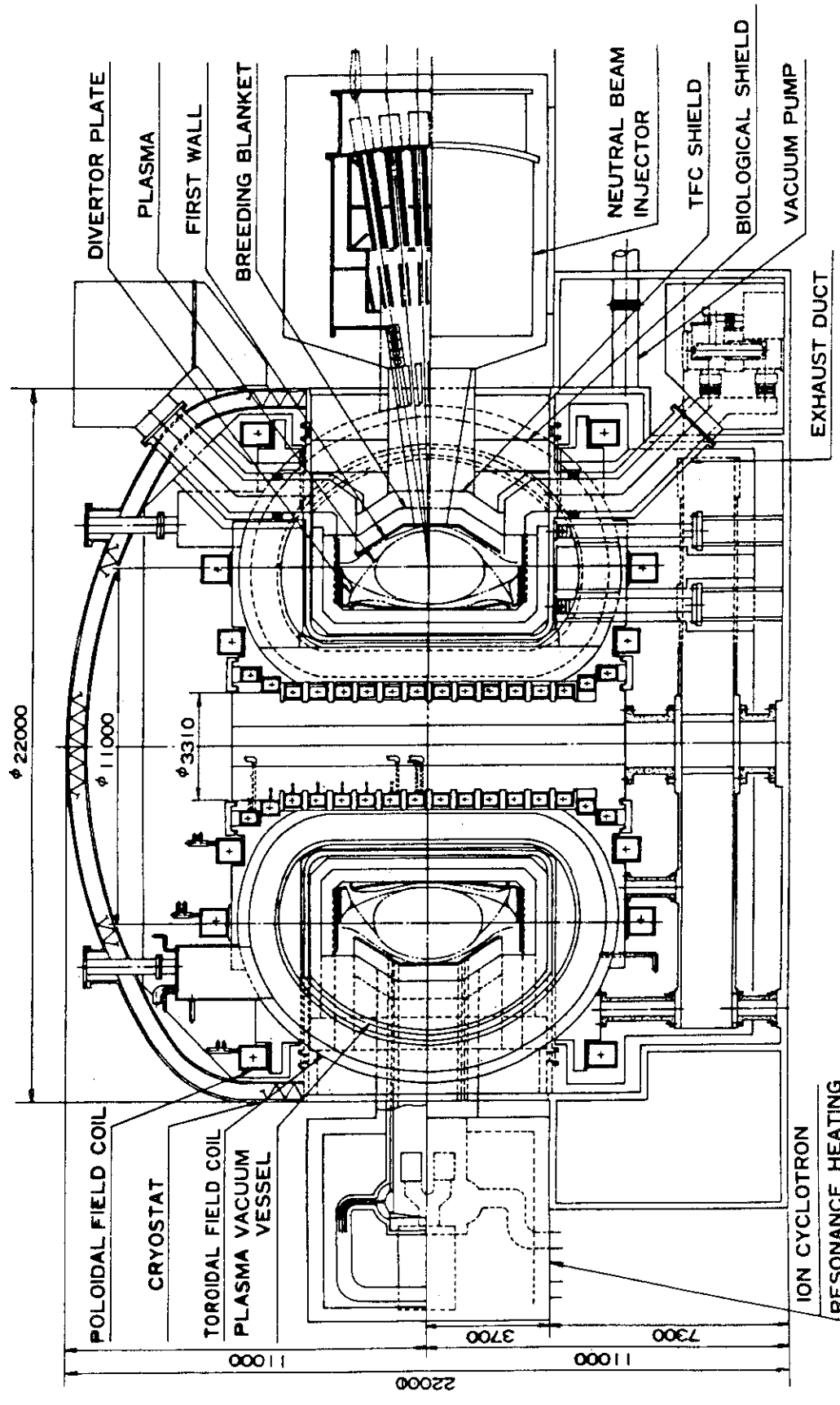

FUSION EXPERIMENTAL REACTOR
(DOUBLE NULL DIVERTOR)

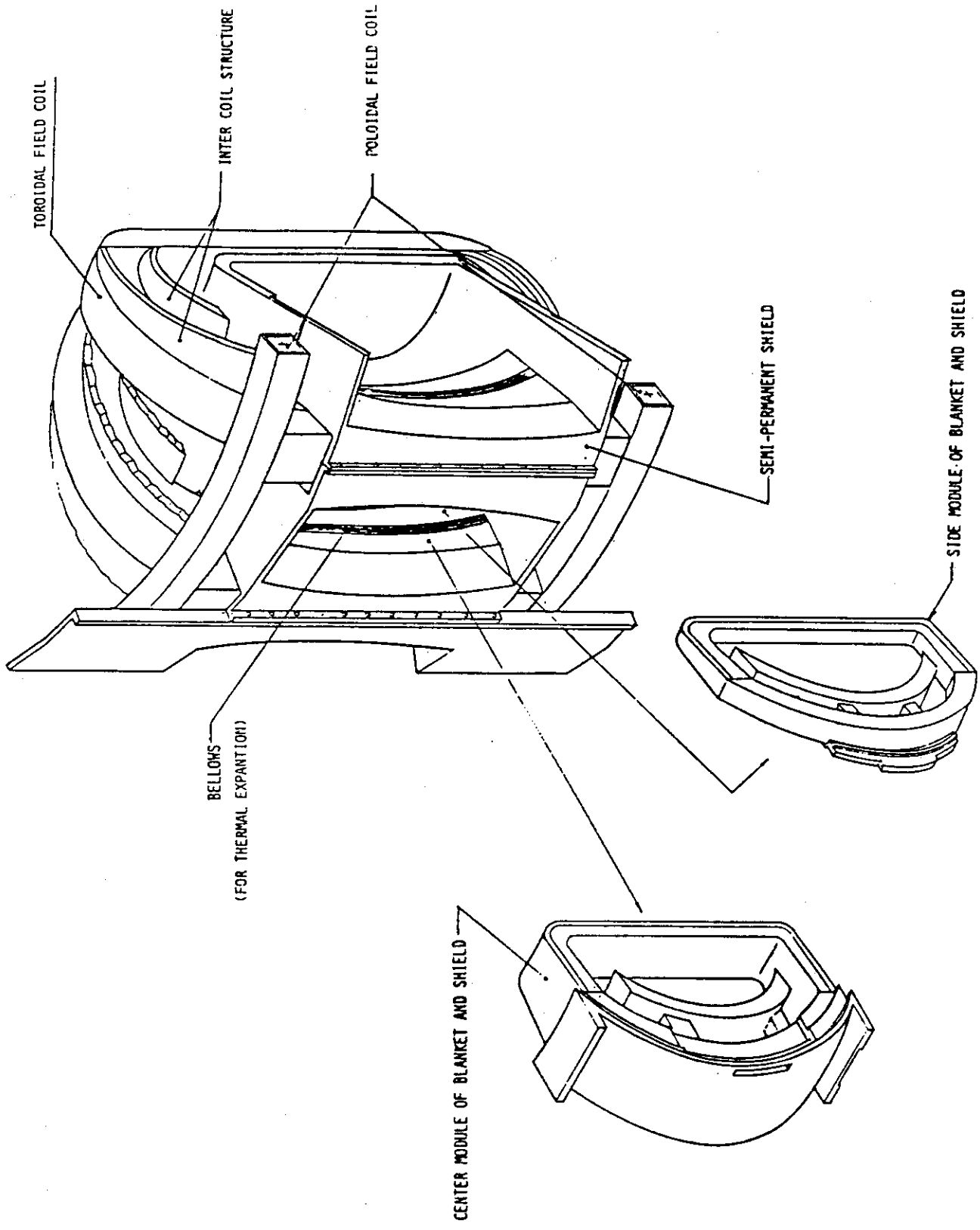
TOROIDAL FIELD COIL
INTER COIL STRUCTURE
POLOIDAL FIELD COIL
SEMI-PERMANENT SHIELD
SIDE MODULE OF BLANKET AND SHIELD
BELLOWS
(FOR THERMAL EXPANTION)
CENTER MODULE OF BLANKET AND SHIELD

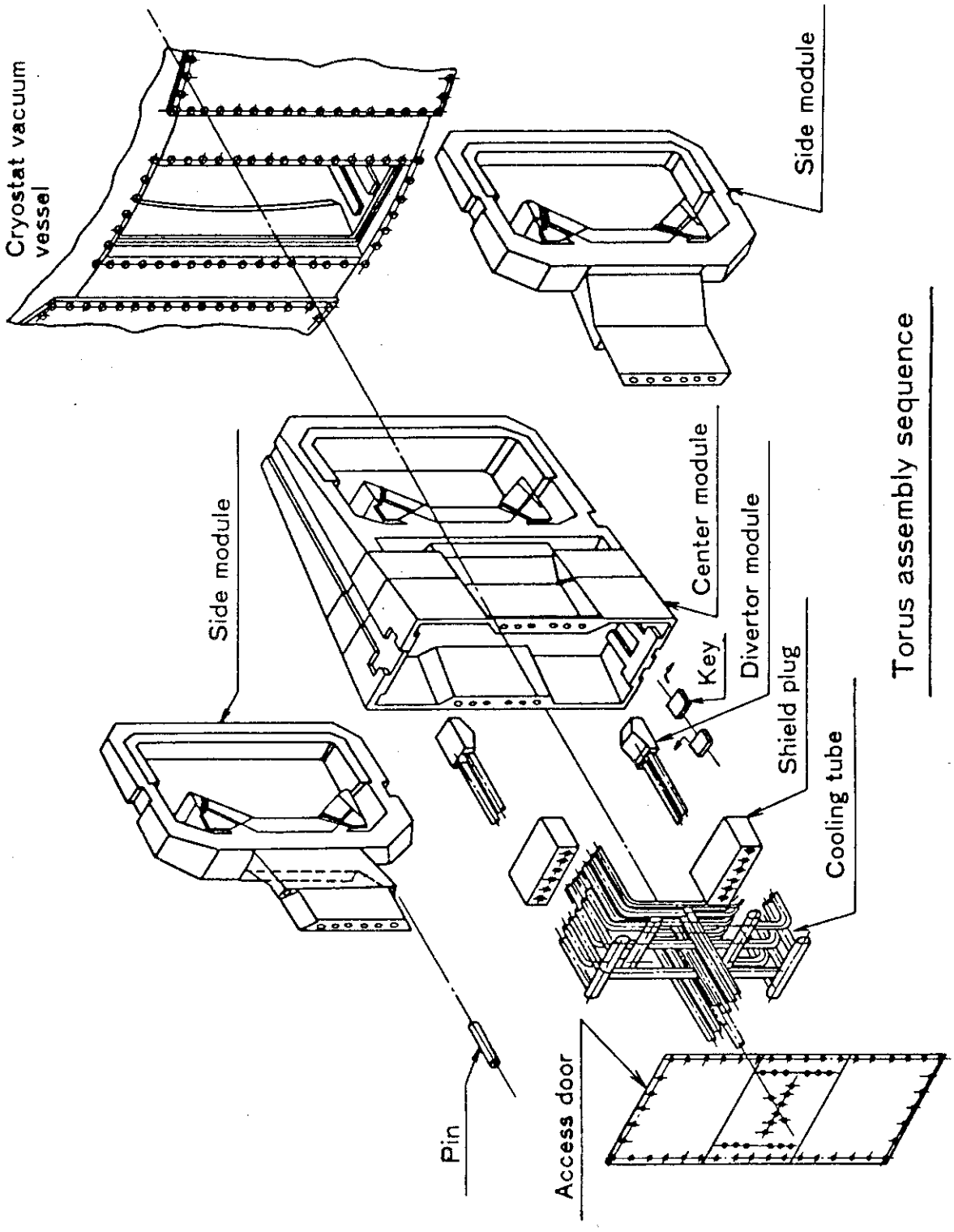
Cryostat vacuum vessel
Side module
Side module
Center module
Key
Divertor module
Shield plug
Cooling tube
Pin
Access door
Torus assembly sequence

First Wall

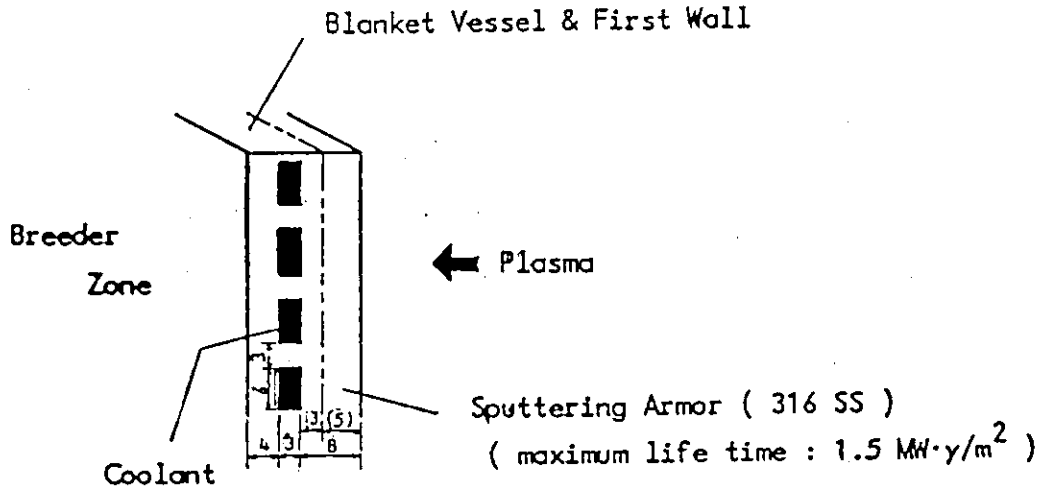

Bare 316 SS First Wall

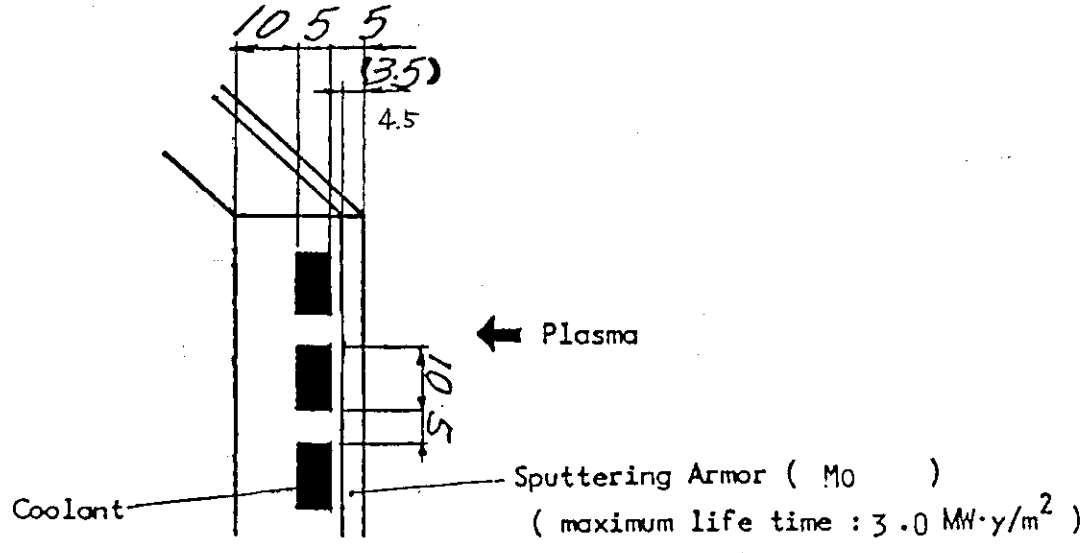

First Wall with Mo Armor

FIRST WALL

1. Bare Stainless Steel

   - ○ Simple
   - ○ Short Life Time (1.5 MWY/m²)
   - ○ Large Thermal Stress during Plasma Disruption.

2. Stainless Steel with Mo Armor

   - ○ Longer Life Time (3 MWY/m²)
   - ○ Acceptable from the View Point of Impurity Control?
   - ○ Fabricability?

Impurity Control

1. Comparative Study of Engineering Features for Divertor and Pumped Limiter Reactor Concept

   Reference Design ---- Double Null Divertor

   Alternative Designs
   - (1) Single Null Divertor
   - (2) Pumped Limiter, L1
   - (3) Pumped Limiter, L2

   Effects on the following items are studied

   (a) Reactor Size

   Reference Design is the smallest

   (b) Mainteance

   Alternative Designs have adantage over the Reference Design

   (c) Magnet System

   Mechanical Stress and AC loss are smaller in the alternative designs

   (d) Required Capacity for the PF power Supply

   The required capacity for pumped limiter design is about half of those for divertor design

Main plasma parameters for the Reference and Alternative designs

	Double Null Divertor	Single Null Divertor	Single Pumped Limiter, L1	Single Pumped Limiter, L2
Plasma major radius (m)	5.5	5.72		6.01
Plasma minor radius (m)	1.1	1.17		1.46+
Plasma elongation	1.5	1.5		1.5
First wall radius (m)	1.25	1.395		1.685
Average ion temperature (keV)	10	10	Same as	10
Average ion density (10^{22} m^{-3})	1.36	1.28	single null	1.19
Toroidal field on plasma axis (T)	5.7	5.48	divertor	5.22
Peak thermonuclear power (MW)	440	458		480
Plasma current (MA)	5.3	5.54		5.8*
Safety factor	2.5	2.5		2.5*
Toroidal β (%)	4.0	4.1		4.1

Note : Parameters are determined for equality of plasma confinement performance.

*) Plasma scrape off layer is excluded
Current in plasma cold layer in neglected

+) Plasma sheath (0.2 m) is included.
Plasma confinement performance is evaluated for plasma minor radisu of 1.26 m

Conclusion

	DND	SND	L1	L2
Reactor size	○	△	△	X
TF Coil Stress	X	△	○	○
PF Coil Stress	X	～	↗	△
Plasma Control	X	△	○	X
Power Supply Capacity for PF Coil	X	X	○	○
TF Coil AC loss	X	X	△	△
PF Coil AC loss	○ (X)	○ (X)	○ (△)	○ (△)
Maintenance	X	○	○	○

○ ---- good

△ ---- medium

X ---- bad

2. Engineering Design of Divertor and Pumped Limiter Plates

a) Thermal-hydraulic design

b) Thermal stress Analysis

c) Electrical Insulation design

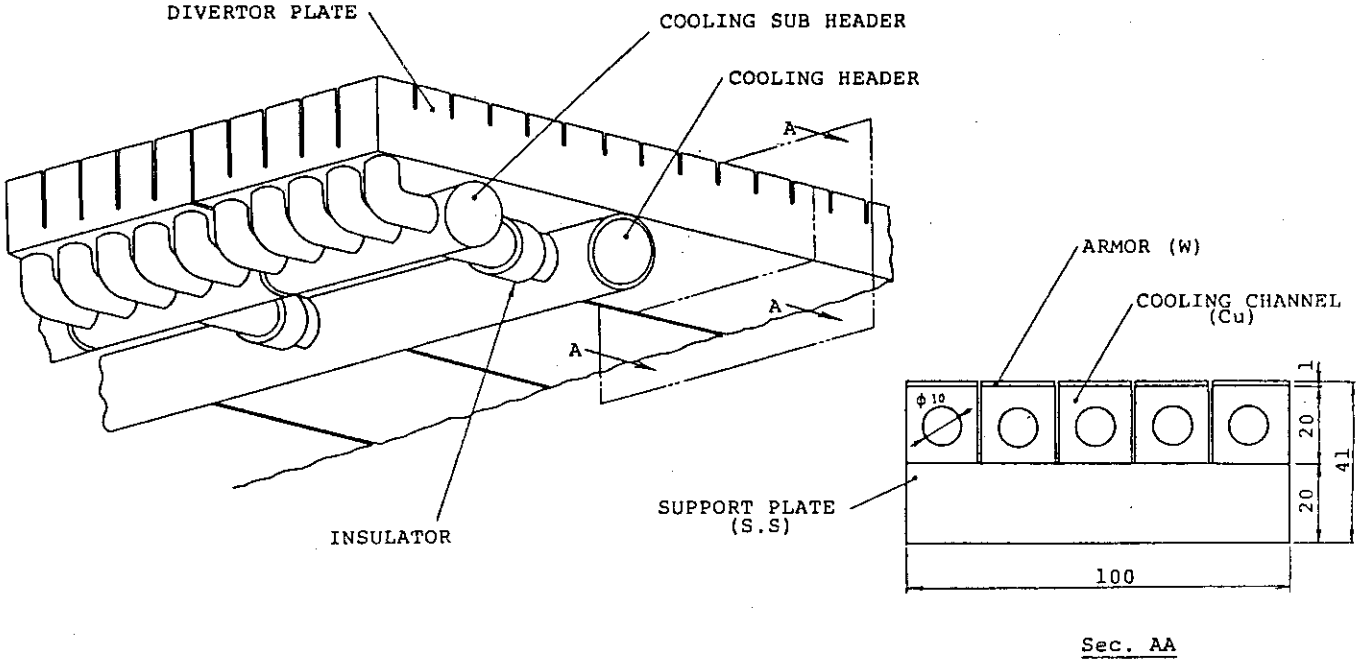

Divertor plate

Tritium Breeding Blanket

Main Specification and Guideline

1. Tube-in-Shell Type
2. Li_2O for Breeding Matenial
3. Temperature range of Li_2O 400°C ~ 1000°C
4. 316 ss for Structural Material
5. H_2O for Coolant
6. Tritium Breeding Ratio (TBR) > 1.0

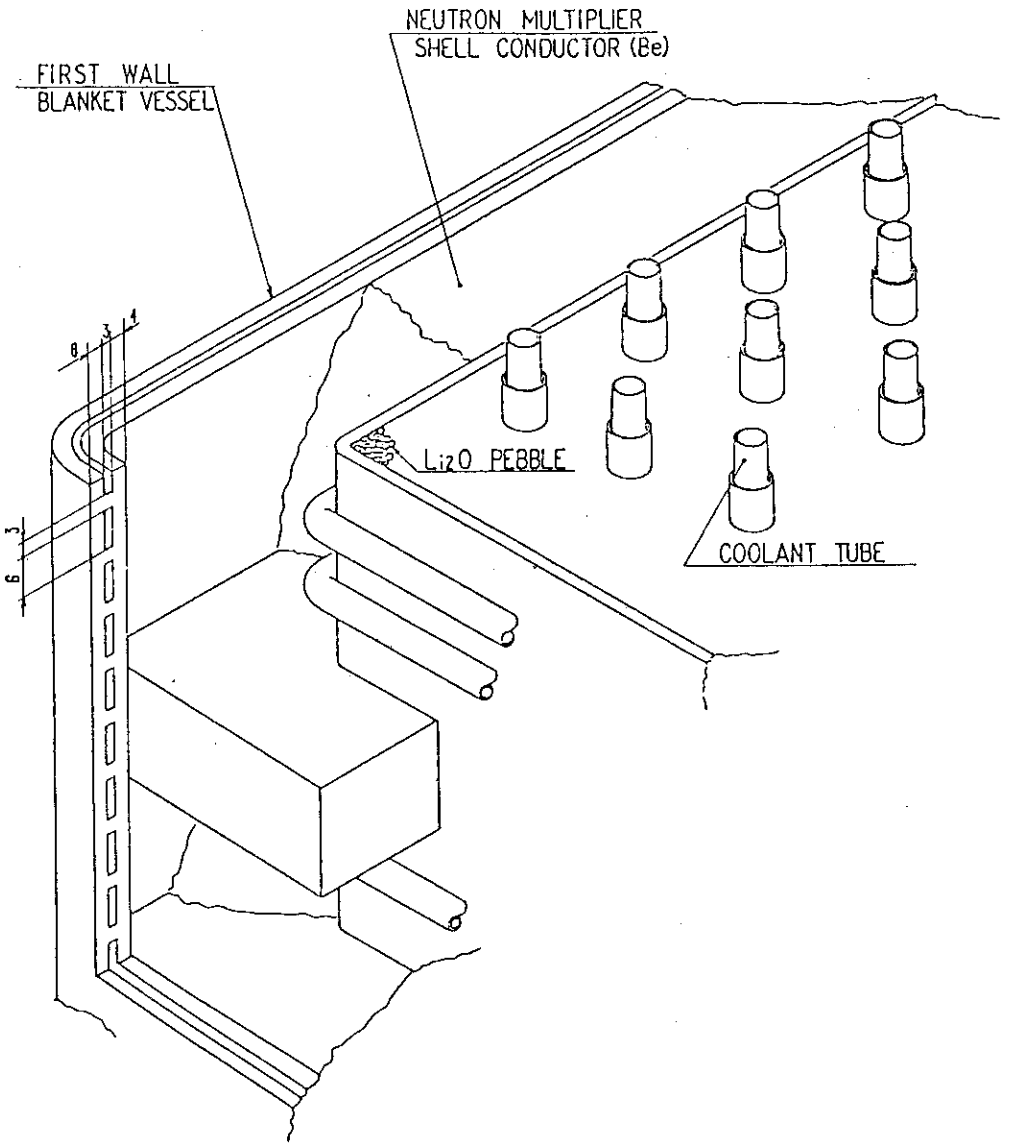

Concept of Blanket

Items Studied

1. Neutronics Analysis
2. Tritium Recovery Study
3. Structural Analysis
4. Temperature Control Analysis
5. Fabrication Procedure Study

Electromagnetic Design

1. Parametric Study of the Shell Effects
   - Number of Shell Segmentation
   - Shell Location (Inbord and/or Outboard)
   - Thickness of Front-Shell
   - Thickness of Side-Shell
   - Conductive End Wall
2. Electromagnetic Force and Stress Analysis
3. Plasma Position Control Simulation

   (Evaluation of Required power supply capacity for active control coil)

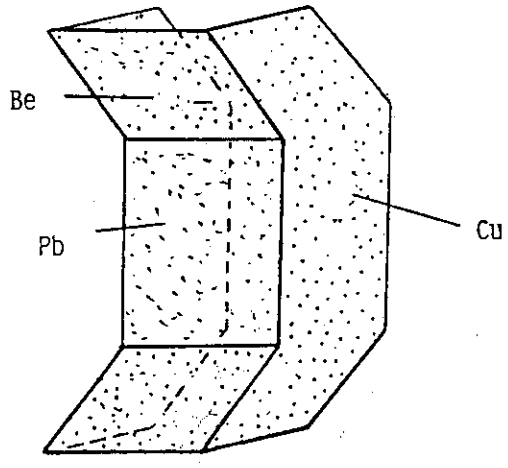

Shell Configuration

REFERENCE SHELL MODEL

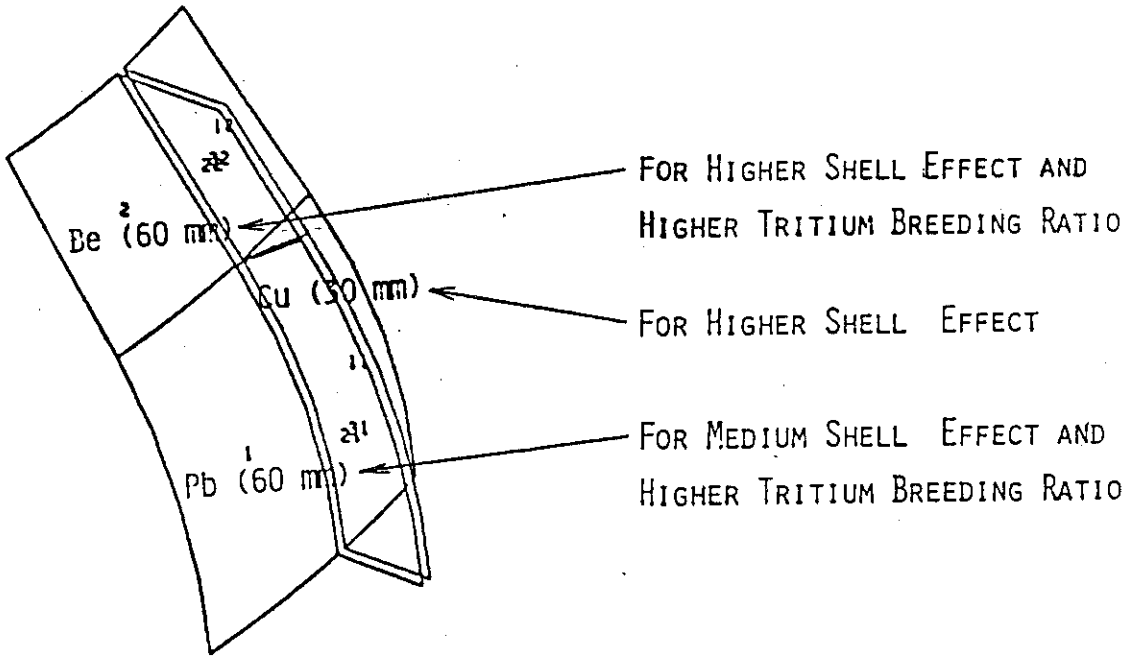

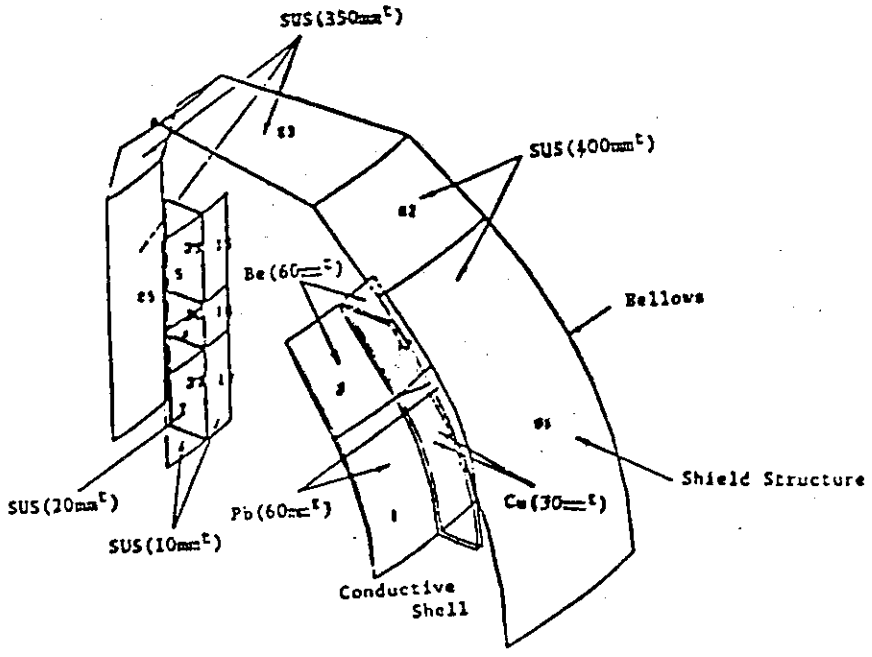

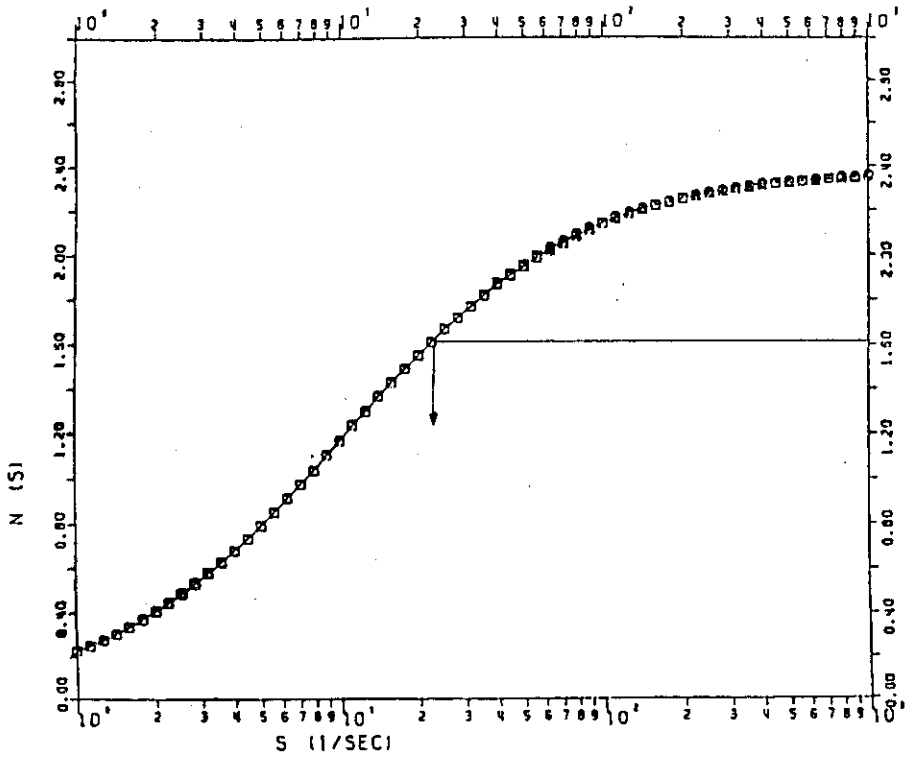

GROWTH TIME τ_g = 44 MSEC

N-FUNCTION OF BLANKET SHELL AND BELLJAR, REFERENCE MODEL

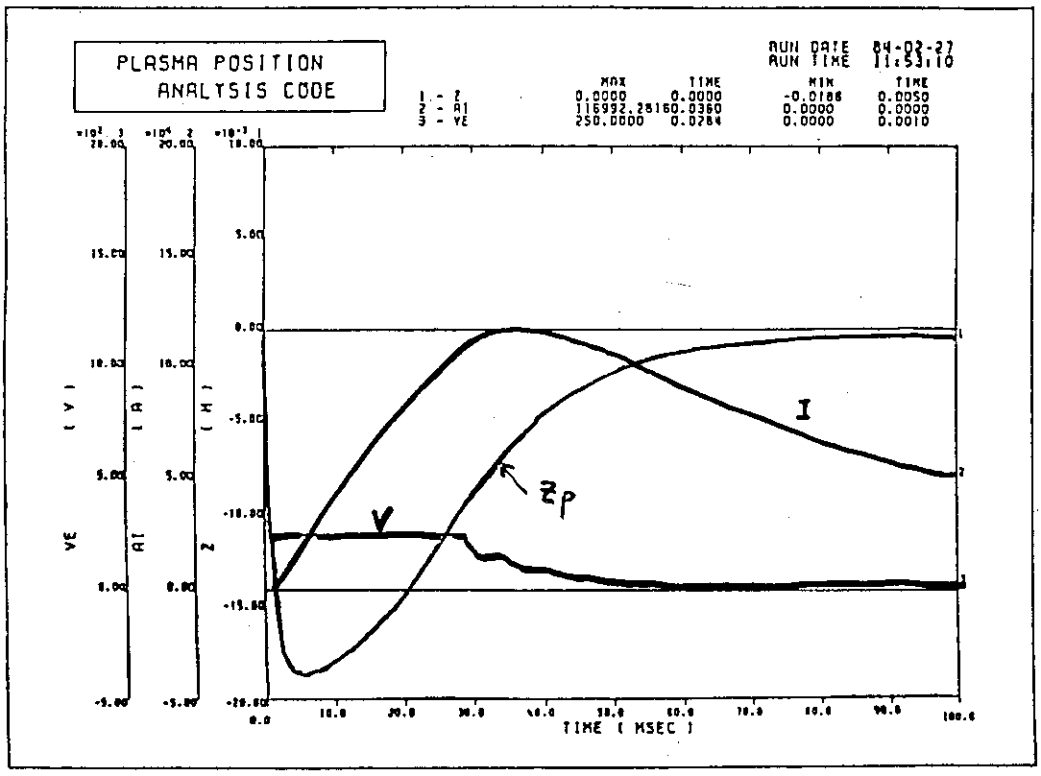

PD-CONTROL, T_D = 10 MSEC, G = 50,000, V_L = 250 V

(REFERENCE MODEL, CONTROL COIL - B)

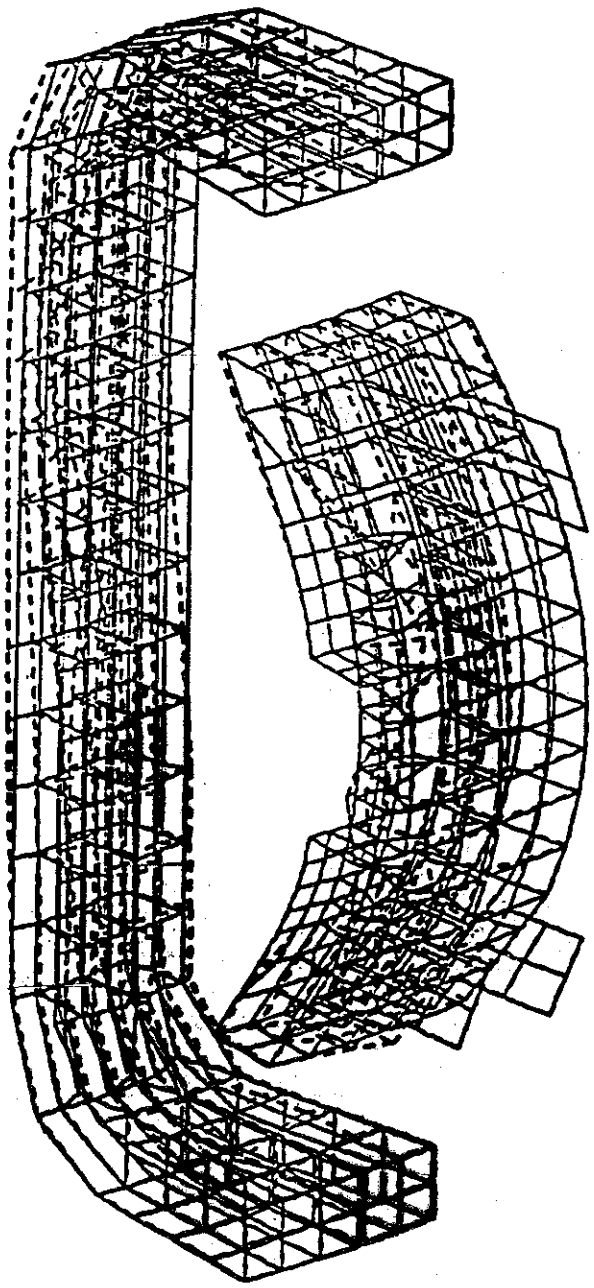

DEFORMATION OF BLANKET
ELECTROMAGNETIC FORCE (REFERENCE)

Conductive Shell

Case	Location	Number of Saddle Coils
A	Outside of Blanket	2
B	Outside of Blanket	14 (1/port)
C	Inside of Blanket	28 (2/port)
D	Inside of Blanket	42 (3/port)

RF Launcher Design for FER

1. ICRF

Specifications

items	model 1	model 2
Frequency (MHz)	88	
Total input power (MW)	15	5
Pulse width (Sec)	10	100
Port number	2	

Items Studied

- RF Power Loss of the Faraday Shield
- Electromagnetic Force and Mechanical Stress
- Replacement Procedure

2. LHRF

Specifications

Items	model 1	model 2
Frequency (GHz)	2	
Total input power (MW)	15	5
Pulse width (Sec)	10	100
Port number	1	

Items Studied

- Structural Design of Waveguides
- Replacement Procedure

3. ECRF

Specifications

Frequency (GHz)	160
Input power (MW)	10
Pulse width (Sec)	10
R.F. wave mode	0
injection	Low Field Side
Transport and launch of RF wave	Quasi Optical

Items Studies

- Optical System Design
- Replacement Procedure

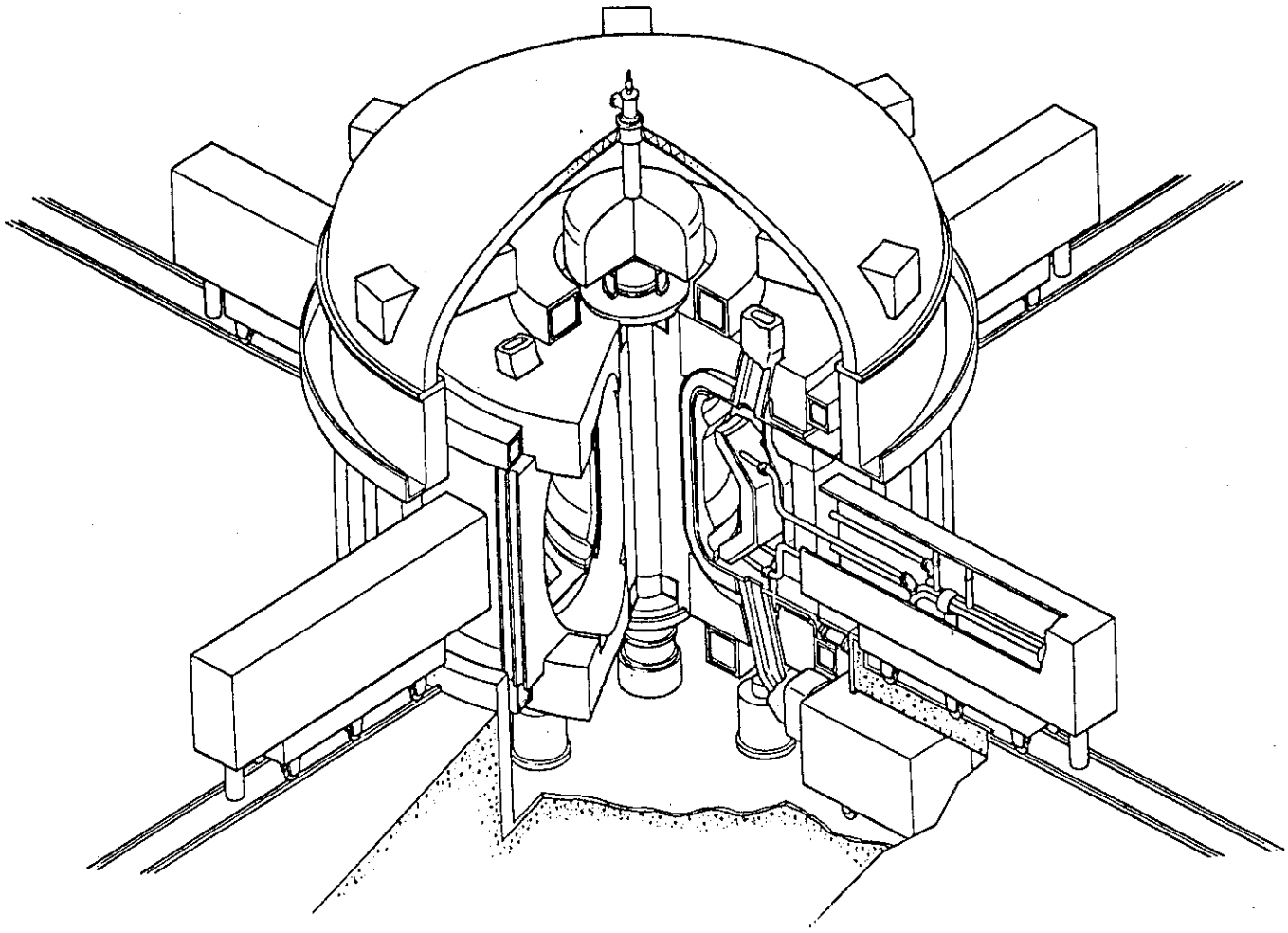

Bird's-eye View of the RFS-FER

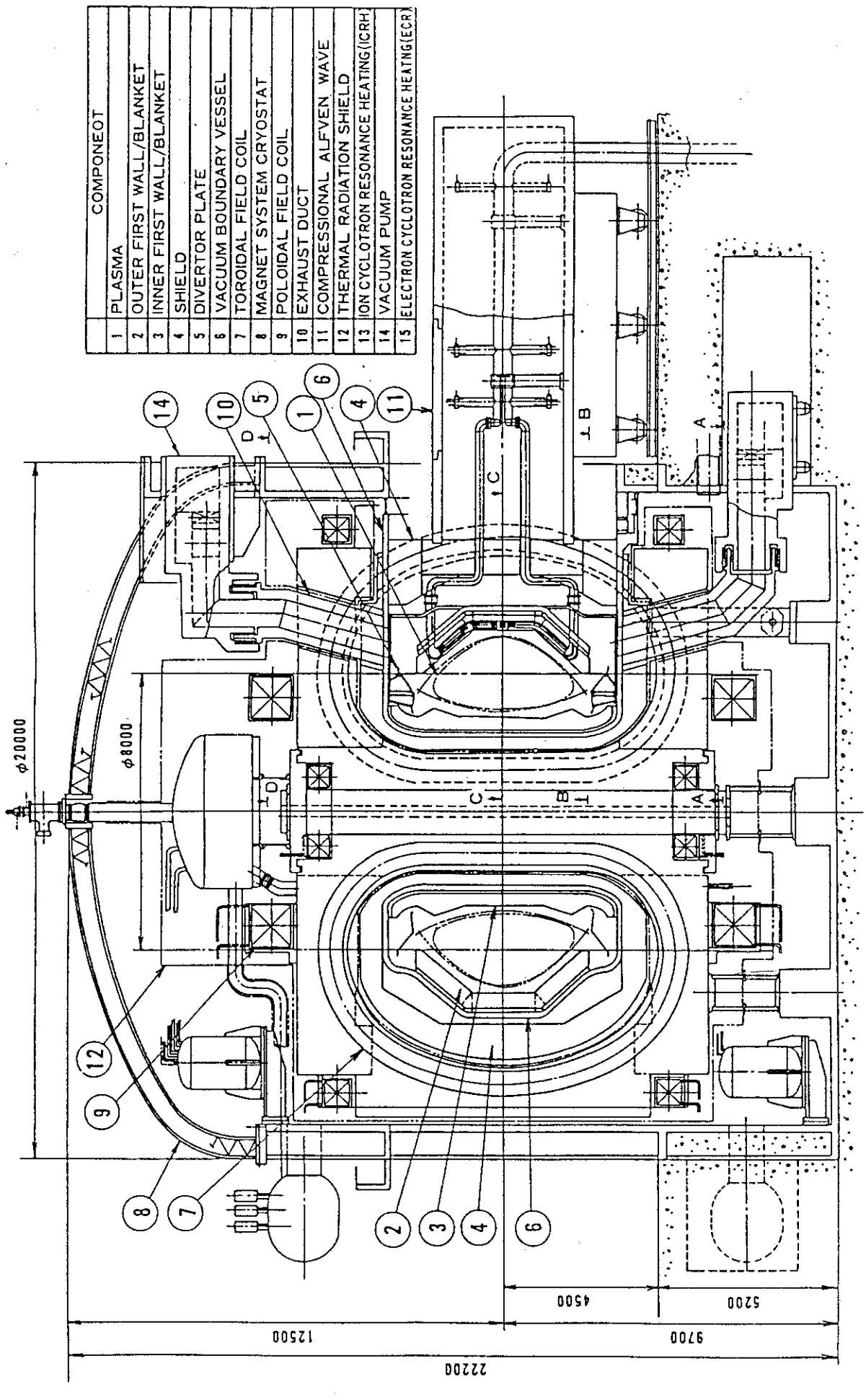

Cross Sectional View of the RFS-FER

2. RF Heating and Current Drive

2.1 RF Assisted Plasma Operation Scenario for FER

Two operation scenarios using RF wave current drive have been investigated for alternative and advanced FER. The first one is long pulse operation scenario for alternative FER using lower hybrid wave (LHW) current drive in low density plasma, which is based on the present-day experimental data base. In this operation scenario, the plasma current is ramped-up by LHW in low density plasma, so that the inductive volt·sec can be used for burning. Quasi-steady operation, in which the plasma current is sustained by LHW even during the recharging phase of OH coils, will be natural extention of the long pulse operation scenario. Long burning and high duty cycle will be essential factors, so that optimization of current ramp-up and flux supply by PF coils are most important. Characteristics of quasi-steady operation is also investigated.

The second one is completely steady-state operation for advanced FER. For the design study, plasma and device parameters by considering three candidate wave drivers; compressional Alfvén wave (CAW), high speed magneto-sonic wave (HSMS) and lower hybrid wave (LHW).

Figure 2.1.1 shows schematic drawing of long pulse (quasi-steady) operation. Table 2.1.1 summarizes potential (dis)advantages for quasi-steady operation. Those for completely steady-state operation are also summarized for comparison. For the long pulse (quasi-steady operation, important items to be investigated are duty cycle, energy transfer of PF coils, over-turning moment of TF coils and device size. To improve the duty cycle, the optimization of current ramp-up time, OH coil recharging time, burn time and pumping time is essential. Optimization of current ramp-up time and recharging time is done by using a simple physical model based on quasi-linear theory of current drive coupled with power balance equation. The results of the optimization are shown in Figs. 2.1.2-2.1.9. From these results, it is concluded that both current ramp-up time and OH coil recharging time are rather long (~100 sec and ~200 - 300 sec, respectively), so that some measure to reduce this time will be necessary. Impurity contamination will be a promising

method for this. To prolong the burn time by OH coils, the key point is whether or not the inner-most solenoid coils can be freed from the function of equilibrium. This point is also essential to remove completely the inner-most PF coils in completely steady state reactor. Strong restrictions, however, exist for this; total ampere turn and the position of magnetic null point. It is concluded by the static equilibrium calculation that the inner-most PF coils can be freed from the equilibrium for various beta poloidal values without increasing total AT so much and changing the null point so much. To realize long pulse operation, current ramp-up scenario is very important. Figure 2.1.10 shows various ramp-up scenarios and their burn time. To investigate the characteristics of the quasi-steady operation, it is very important to examine the variation of the over-turning moment of TF coils, the amount of magnetic energy transfer and total energy consumption for various current ramp-up and ramp-down scenarios. The results are shown in Figs. 2.1.11-2.1.15. From these investigations, we conclude that current ramp-up and the current sustaining in recharging phase by LHW at the level of 4 MA will be most favorable.

For the design studies of completely steady-state operation reactor, three candidate wave drivers are examined (CAW, HSMS, LHW). Advanced and disadvanced features of each wave are summarized in Table 2.1.2. Relations between each wave in ω-$k_{/\!/}$ plane are shown in Fig. 2.1.16. Current drive efficiency, frequency for fast wave (CAW, HSMS) are shown in Figs. 2.1.17-2.1.19. A key point for the steady-state reactor design is the reduction of the major radius due to the removal of the inner-most PF coils. RF power injection compensates the aggravation of the plasma performance due to the reduction of the toroidal magnetic field on axis through the reduction of the major radius. The parameter for the risk of the performance is introduced, and the plasma temperatures are chosen so as to retain the same plasma performance for each candidate wave driver with different driving efficiency (Figs. 2.1.20, 2.1.21). Table 2.1.3 summarizes the plasma and device parameters for steady-state FER by three candidate wave drivers. CAW is chosen as a primary candidate for driver, since it has highest potential advantages for commercial reactor (highest efficiency and good accessibility). However, these candidate waves can easily be replaced by others in design study by changing operation temperature when data base is clarified.

1. Long pulse operation scenario (Alternative FER)

   ○ Operation scenario by using LHW current drive in low density plasma

      • Optimization of current ramp-up scenario

      • Optimization of PF coils for long burn

      • Characteristics of quasi-steady operation

2. Steady state operation (Advanced RFS-FER)

   ○ Physics design consideration for candidate wave drivers

      CAW, HSMS, LHW

   ○ Plasma and device parameters for design study

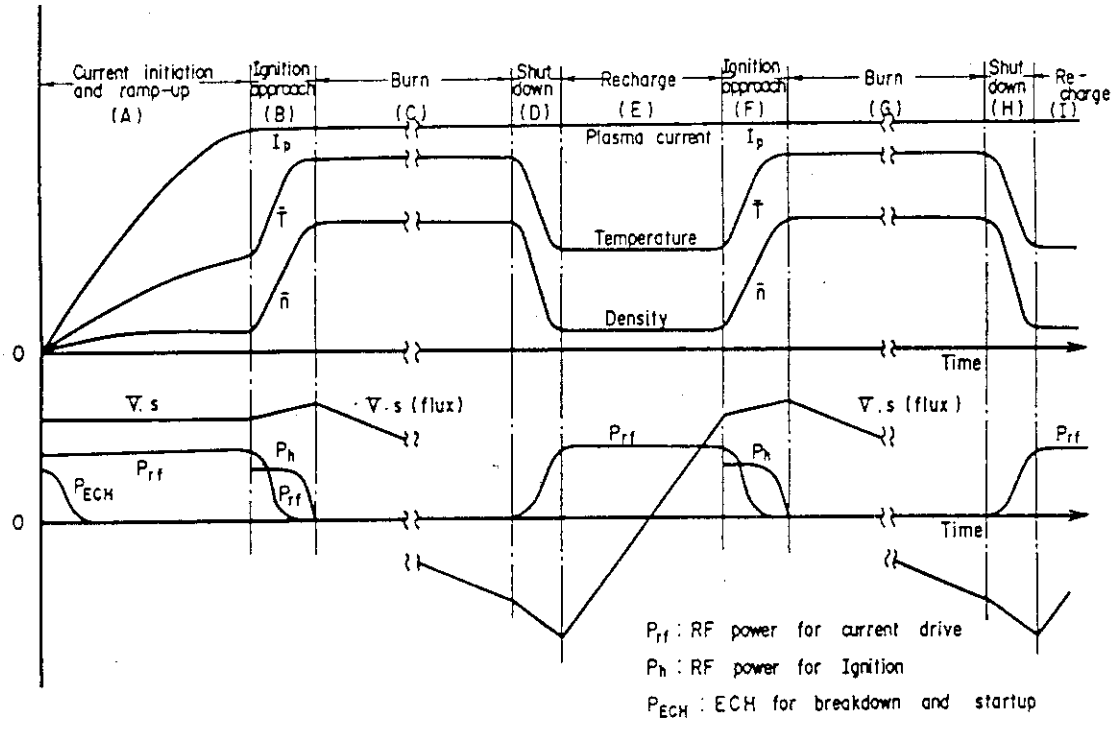

Fig. 2.1.1 Schematic drawing of long pulse or quasi-steady operation by lower hybrid wave current drive. Current ramp-up and sustainment in recharging phase is performed by LHCD.

Table 2.1.1 Possible advantage and disadvantage of quasi-steady operation and completely steady-state operation compared with the conventional OH pulse operation. Open circle denotes advantage and closed circle disadvantage. Size of the circle denotes degree of (dis)advantage. Hyphen denotes no (dis)advantage.

Possible advantage	Major impact	Quasi-steady operation	Completely steady-state operation
1. Increase of duty cycle	• Capacity of energy reservoir	(●)	○
2. Reduction of number of thermal and mechanical stress cycle	• Thermal stress of 1st wall/divertor/ blancket	–	○
	• Mechanical stress of TF coils by overturning moment	–	○
3. Reduction of variation of thermal and mechanical stress	• Heat load on 1st wall and divertor plate	○	○
	• Mechanical stress of TF coils by overturning moment	○	○
4. Reduction of magnetic energy loss of PF coils during energy transfer	• Total required energy for operation	○	○
5. Reduction of peak power in start-up phase	• Capacity of power supply	○	○
6. Reduction of AC loss in PF and TF coils in start-up/shut-down phase	• Capacity of cooling system	○	○
	• Total required energy for operation	○	○
7. RF system	• Capital cost	●	●
	• Total required energy for operation	●	●
8. Reduction of device size	• Construction cost	○	○
9. Reduction of plasma disruption	• Life of 1st wall	–	○
	• Support system for electro-magnetic force	–	○

JAERI – M 84 – 107

Important Items

1. Duty cycle
   - ○ Current ramp-up time
   - ○ OH coil recharging time
   - ○ Burn time
   - ○ Pumping time
2. Energy transfer of PF coils
3. Over-turning moment of TF coils
4. Device size

Simple Model Equations

○ Driven current, deposited power: Quasi-linear theory

$$j_{rf}(r) = 6.64 \times 10^{-9} \frac{n_e(r)}{\sqrt{T_e(r)}} \exp\left[-\frac{2.56 \times 10^5}{n_{Z1}^2 T_e(r)}\right]\left(\frac{1}{n_{Z2}^2} - \frac{1}{n_{Z1}^2}\right) \quad (A/m^2)$$

$$P_{rf}(r) = 3.79 \times 10^{-29} K \frac{n_e^2(r)}{\sqrt{T_e(r)}} \exp\left[-\frac{2.56 \times 10^5}{n_{Z1}^2 T_e(r)}\right] \ln\frac{n_{Z1}}{n_{Z2}} \quad (W/m^3) \ ,$$

Saturated value ⟶ avoid hollow current profile

○ n_{Z2} ← Accessibility condition

○ $\omega = 2\,\omega_{LH}(0)$ ← Avoid parametric instability

○ Power balance

$$G_e P_\alpha + P_{rf} + P_J + P_{xe} - P_{sy} - P_{br} - P_{ei} - P_{imp} = 0 \ : \ \text{electron}$$

$$(1 - G_e)P_\alpha + P_{ei} - P_{xi} = 0 \ : \ \text{ion}$$

○ Equivalent circuit equations

$$\text{OH coil} : \ L_1 \frac{dI_1}{dt} + M_{12} \frac{dI_p}{dt} + M_{13} \frac{dI_3}{dt} = V_1 \ ,$$

$$\text{Plasma} : \ M_{12} \frac{dI_1}{dt} + L_p \frac{dI_{OH}}{dt} + M_{23} \frac{dI_3}{dt} + (R_p + \frac{dL_p}{dt}) I_{OH}$$

$$= - L_p \frac{dI_{rf}}{dt} - \frac{dL_p}{dt} I_{rf} \ ,$$

$$\text{Vertical coil:} \ M_{13} \frac{dI_1}{dt} + M_{23} \frac{dI_p}{dt} + L_3 \frac{dI_3}{dt} = V_3 \ .$$

Accessibility condition for lower hybrid wave

$$n_z > n_{LC} = \left(1 - \frac{\omega^2}{\Omega_e \Omega_i}\right)^{-\frac{1}{2}} \qquad \omega \leq \omega_c \quad ,$$

$$n_z > n_{LC} = \frac{\omega_{pe}}{\Omega_e} + \left[1 + \left(\frac{\omega_{pe}}{\Omega_e}\right)^2 \left(1 - \frac{\Omega_e \Omega_i}{\omega^2}\right)\right]^{\frac{1}{2}} \qquad \omega \geq \omega_c \quad ,$$

where

$$\omega_c^2 \equiv \frac{\omega_{pe}^2 \Omega_i}{2\Omega_e}\left[\left(1 + \frac{4\Omega_e^2}{\omega_{pe}^2}\right)^{\frac{1}{2}} - 1\right] \quad .$$

○ Current ramp-up time

$$\tau_s = -\tau \ell n \left(1 - \frac{I_p}{I_{rf}}\right) \qquad \text{(sec)}$$

where $\tau = (L_p + \psi/I_p)R_p$

○ OH coil recharging time

$$\tau_r = \frac{1}{R_p(I_{rf} - I_p)} \qquad \text{(sec/V·s)}$$

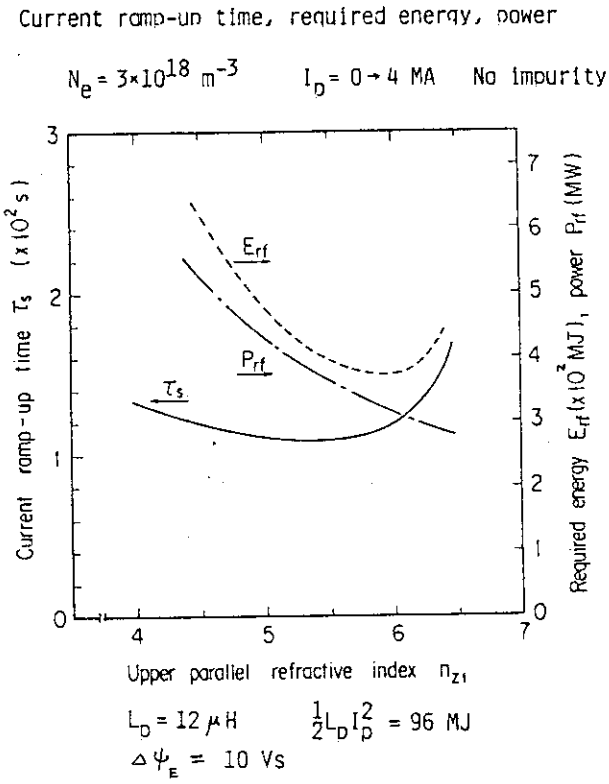

Fig. 2.1.2
Current ramp-up time, required energy and power by LHCD as a function of upper parallel refractive index. Plasma current is ramped-up to 4 MA. Electron density is 3×10^{18} m^{-3} and no impurity contamination. Efficiency of ramp-up (stored magnetic energy/injected RF energy) is ∿25% at its maximum, which is roughly consistent with PLT results.

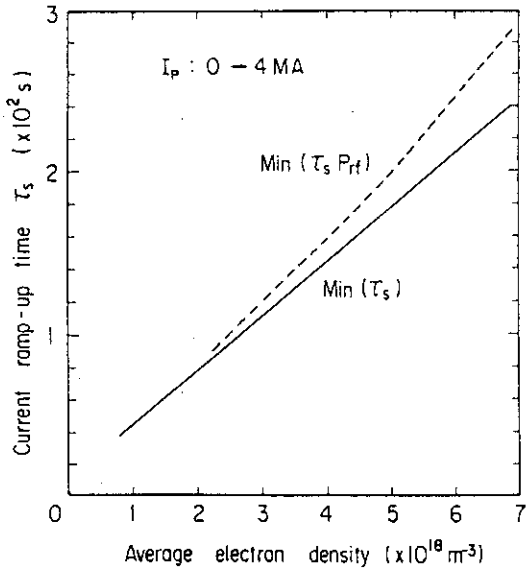

Fig. 2.1.3
Minimum current ramp-up time (solid line) and the ramp-up time when the injected energy is minimum (dotted line) for various electron density.

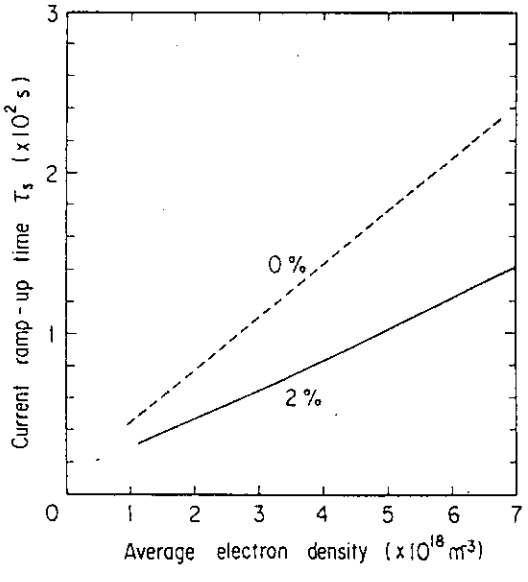

Fig. 2.1.4
Minimum current ramp-up time for impurity contaminated plasma as a function of electron density. Oxygen impurity is assumed.

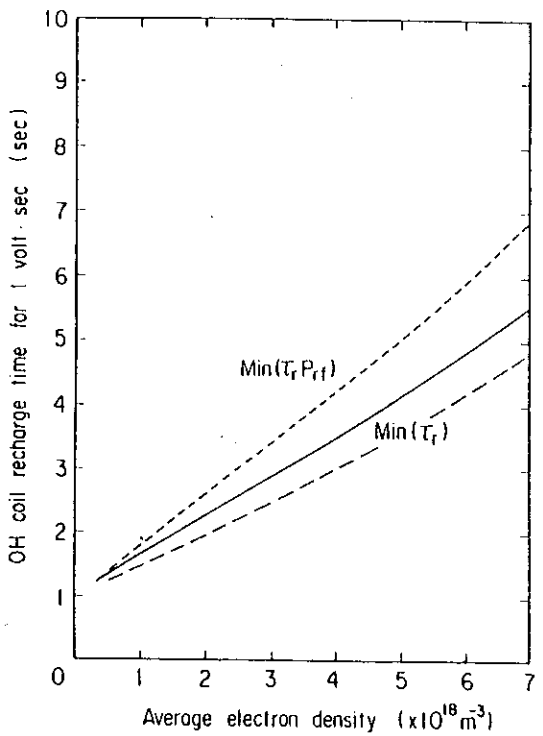

Fig. 2.1.5
OH coil recharging time for 1 volt·sec as a function of electron density. Solid and long broken lines show the minimum recharging times for $I_p = 5.3$ MA and 2.65 MA, respectively. Short broken line shows the recharging time when the injected energy is minimum.

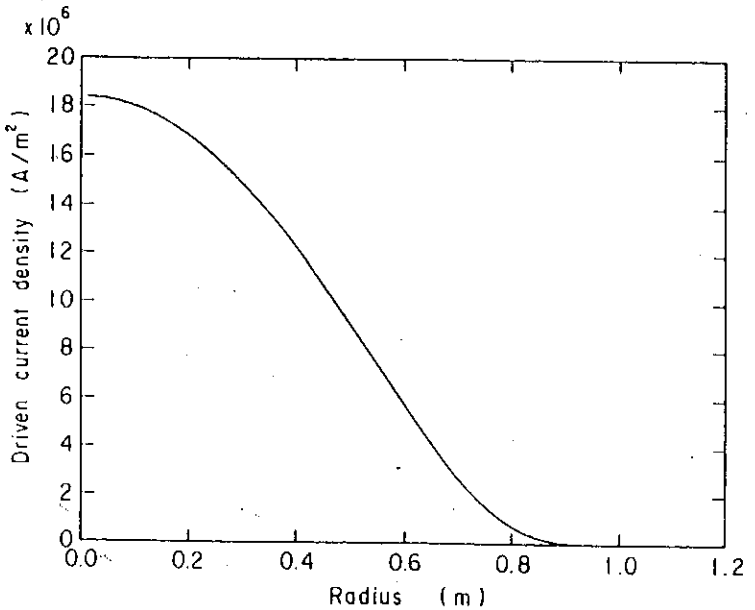

$$\frac{\partial F}{\partial X} = - \frac{X}{1 + X^3 \bar{D}_{rf}(\tilde{P}_{rf})} F \quad ,$$

$$\frac{\partial \tilde{P}_{rf}}{\partial r} = - 4\pi^2 R\, r\, P_{ab}(n_z, r) \quad ,$$

$$P_{ab}(n_z, r) = - m_e\, v_z\, \bar{D}_{rf} \frac{\partial F}{\partial v_z} \quad .$$

$$j_{rf}(r) = - e \int_{-\infty}^{\infty} v_z\, F\, dv_z \quad .$$

Fig. 2.1.6 Current density profile driven by lower hybrid wave calculated by quasi-linear theory.

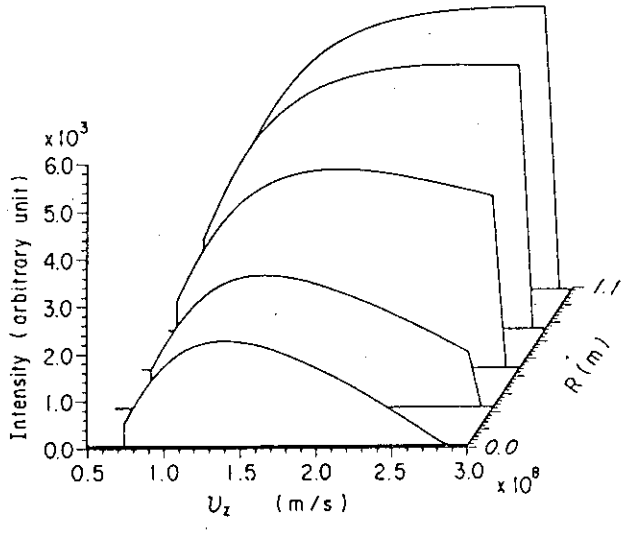

Fig. 2.1.7

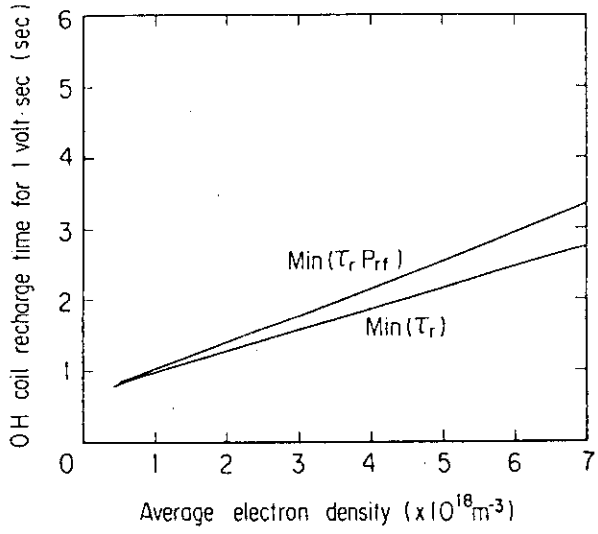

Fig. 2.1.8

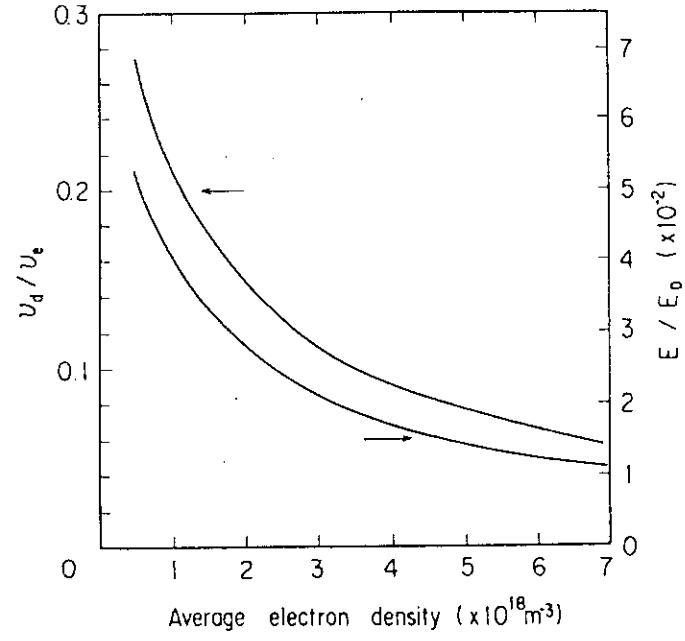

Fig. 2.1.9 Drift velocity normalized by electron thermal velocity and electric field normalized by Dreicer field as a function of electron density for the minimum recharging time.

Burn Time

- Inner-most solenoid coils can be freed from function of equilibrium?: Key point
  → This possibility leads to complete removal of inner-most PF coils in complete steady state reactor

  Restriction
  - Static equilibrium must be realized without increasing total AT too much
  - Position of magnetic null point must not be moved too much
- Optimization of flux supply by OH and EF coils
  Optimum operation scenario for current ramp-up by RF and OH, increase of β_p

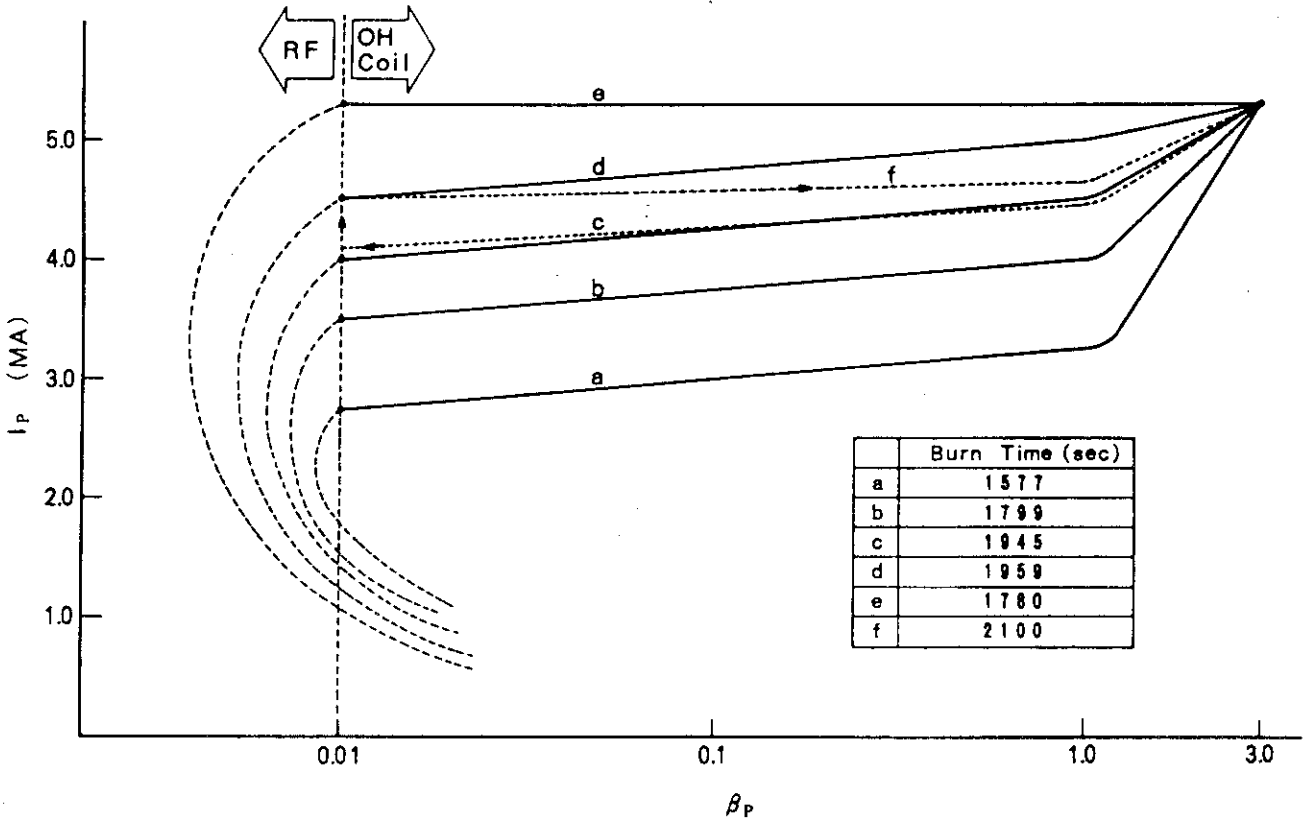

Fig. 2.1.10 Burn time for various scenarios of current ramp-up by LHCD. Resistive volt·sec in the OH phase is assumed 3 V.s for all cases.

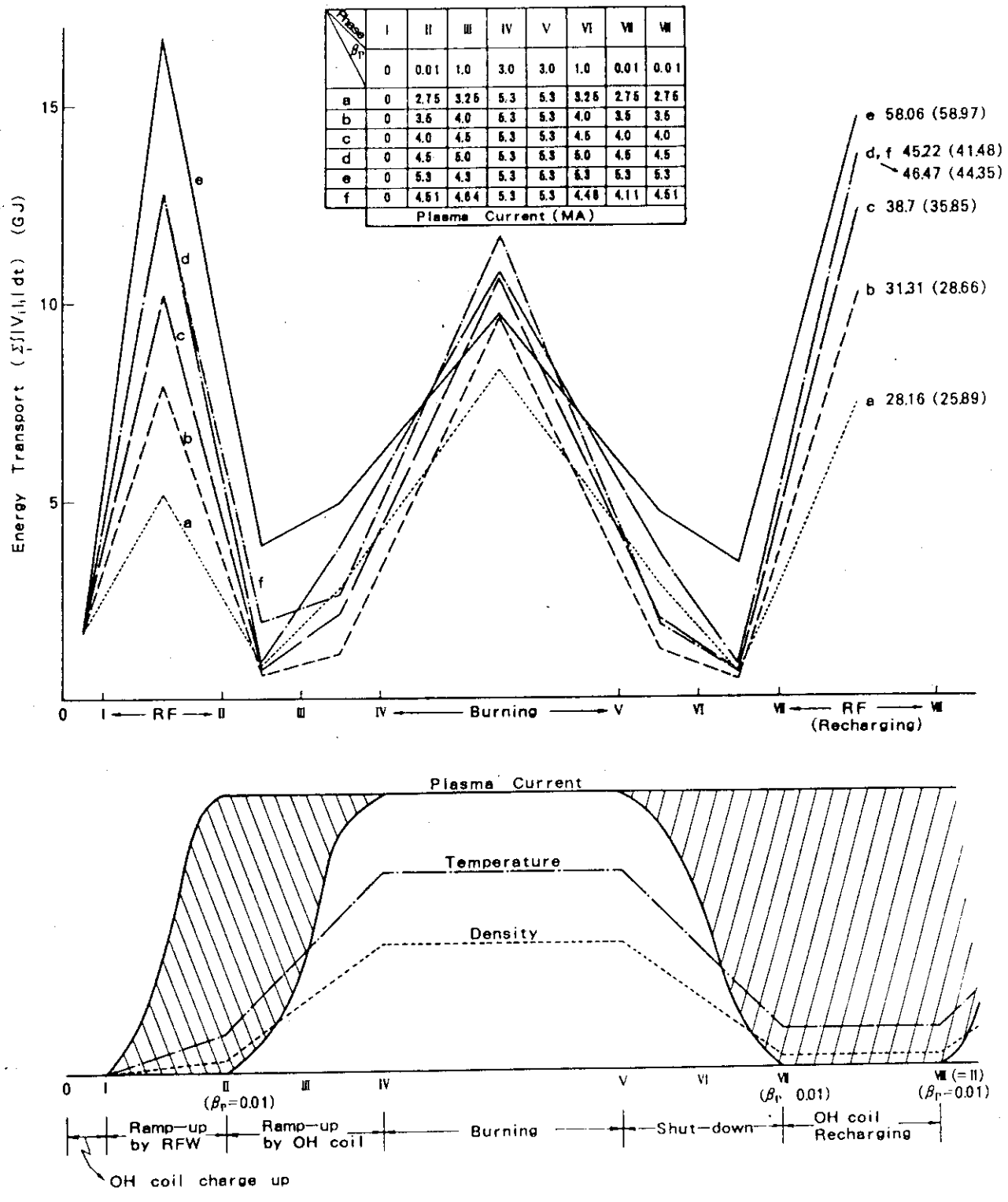

Fig. 2.1.11 Magnetic energy transfer in various phases of quasi-steady operation scenarios given in Fig. 2.1.10.

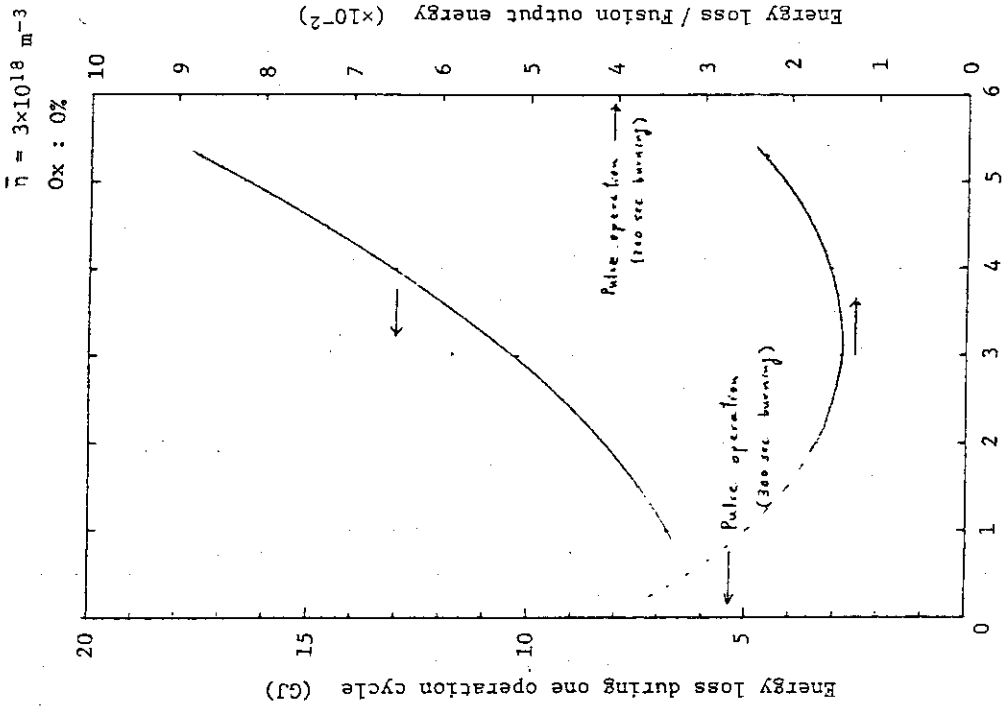

Fig. 2.1.13

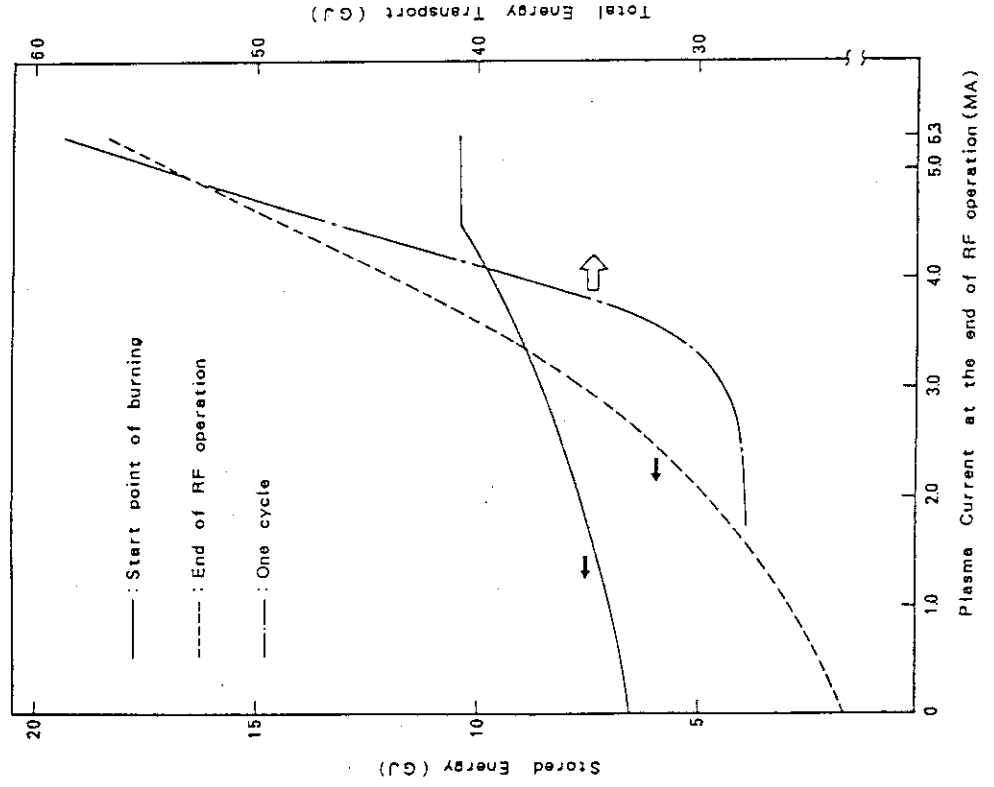

Fig. 2.1.12

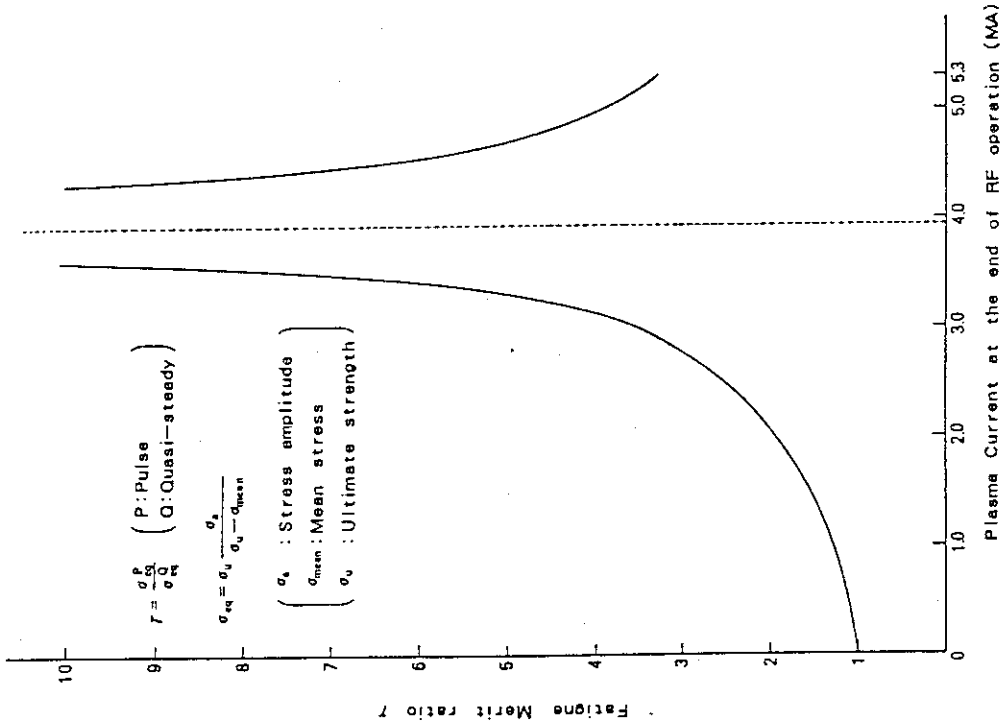

Fig. 2.1.15

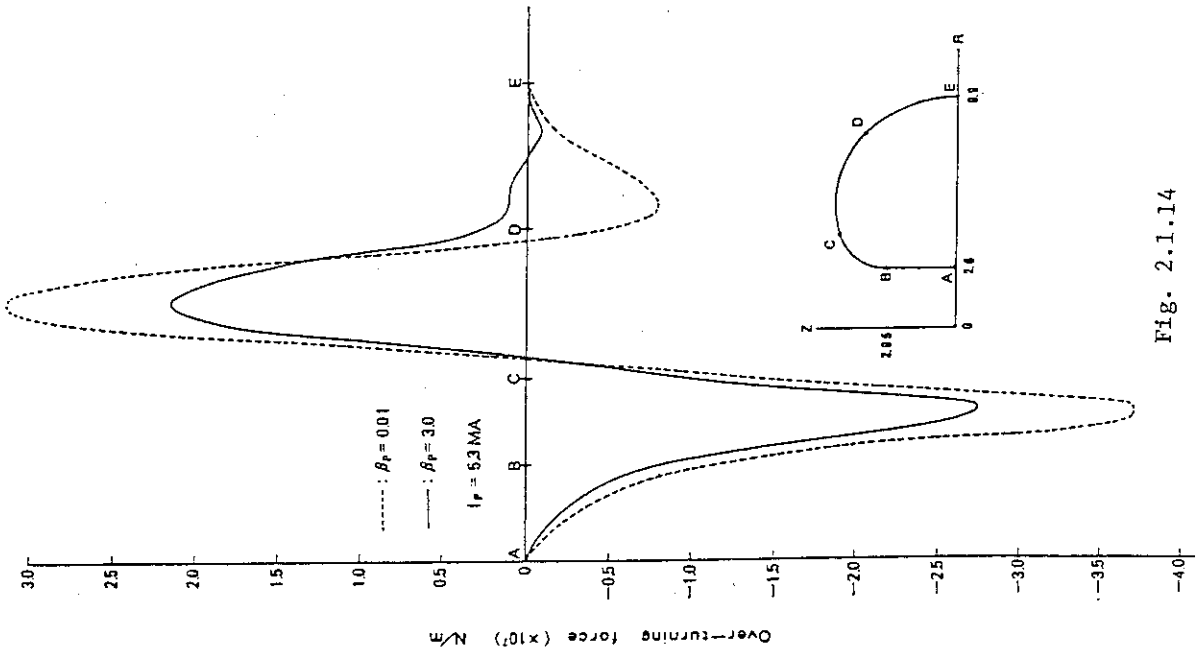

Fig. 2.1.14

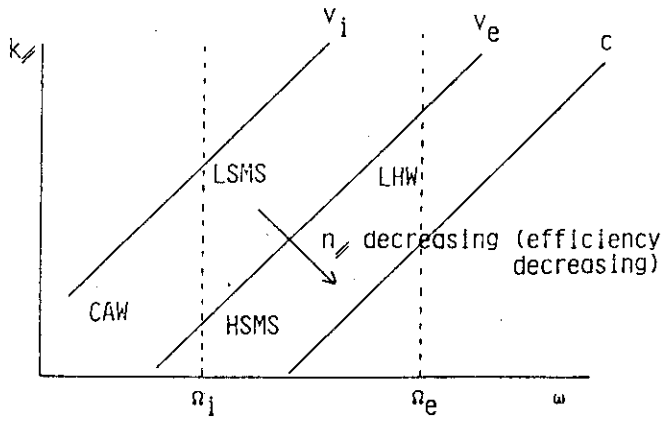

Fig. 2.1.16 Relations between three candidate wave drivers of fast waves of ICRF in ω-$k_{//}$ plane. v_i, v_e, and C denote ion and electron thermal velocity and the velocity of light, respectively. Lower hybrid wave is also shown by LHW. Current drive efficiency is decreasing as the parallel refractive index $n_{//}$ is decreasing.

Table 2.1.2 Advantage and disadvantage of candidate waves for current driver. CAW is chosen as a primary candidate wave for current driver due to its potential advantage for commercial reactor.

Candidate Waves for Current Driver

(1) Fast wave ----- Good accessibility

Comppressional Alfvén Wave (CAW)

Theoretically best efficiency

Difficulties --- Antenna design
trapped electrons effect

High Speed Magnetosonic Wave
Low efficiency
No difficulties in CAW

(2) Lower Hybrid Wave
Experimentally proven
Density limit, Accessibility

Conclusions for long pulse operation scenario

1. Static equilibrium control is possible over whole range of beta-p and I_D. The inner-most PF coils can be free from equilibrium.

2. Long burning can be realized when plasma current is ramped-up to 4 MA by LHW.

3. Ramp-up to 4 MA is favorable from view point of total energy consumption per fusion output energy.

4. Recharging time will be 200～300 sec for 100 v.s. The time can be shortened effectively by impurity.

5. Recharging at I_D = 4 MA is also favorable to reduce the variation of over-turning force.

6. Reduction of magnetic energy transfer will be difficult for non-circular plasma.

Current Driver Efficiency of CAW, HSMS

$$\frac{p}{j} \propto \frac{n_e}{n_{/\!/}\, T_e^{3/2}}$$

Dispersion relation $k^2 V_A^{\,2} = \omega^2$

$$\frac{I_p}{P_{rf}} = 7.14 \frac{\sqrt{B}}{R\sqrt{1+\alpha^2 \lambda_{/\!/}^2}} \frac{T_4}{n_{20}} \quad (A/W)$$

$$\equiv \gamma \frac{T_4}{n_{20}}$$

where $\alpha = \frac{\ell}{2a} \equiv \frac{1}{\lambda_\perp}$

$$\omega = 7.78 \times 10^4 \sqrt{\frac{T}{\beta}} \frac{1}{\lambda_{/\!/}} \sqrt{1 + \alpha^2 \lambda_{/\!/}^2}$$

β : Theoretical ballooning limit

$$7.8\, q_\psi^{-0.54} (A-1)^{-0.76} \kappa^{1+0.14(q_\psi - 1)} \quad (\%)$$

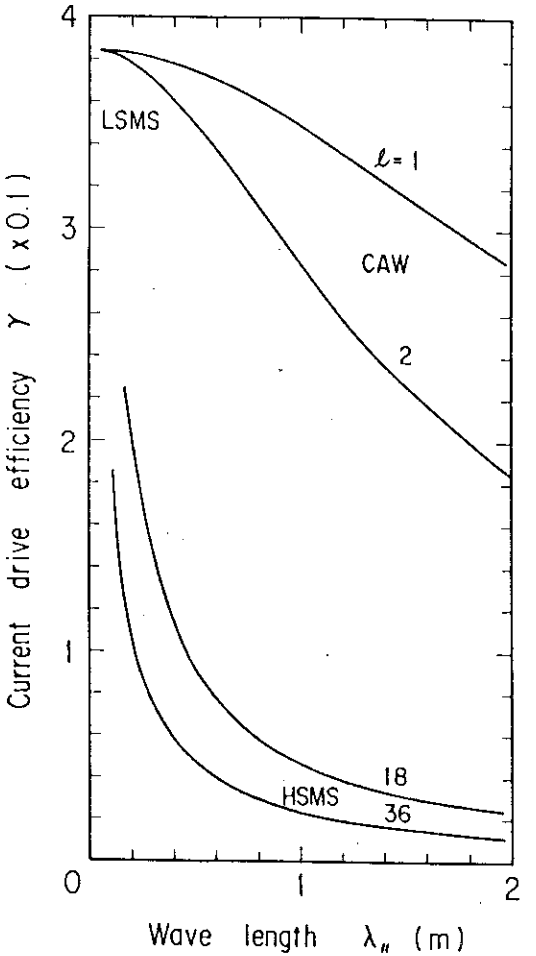

Fig. 2.1.17

Current drive efficiency of CAW, HSMS and LSMS (low speed magneto-sonic wave) as a function of the parallel wave length. Wave number in radial direction is denoted by ℓ.

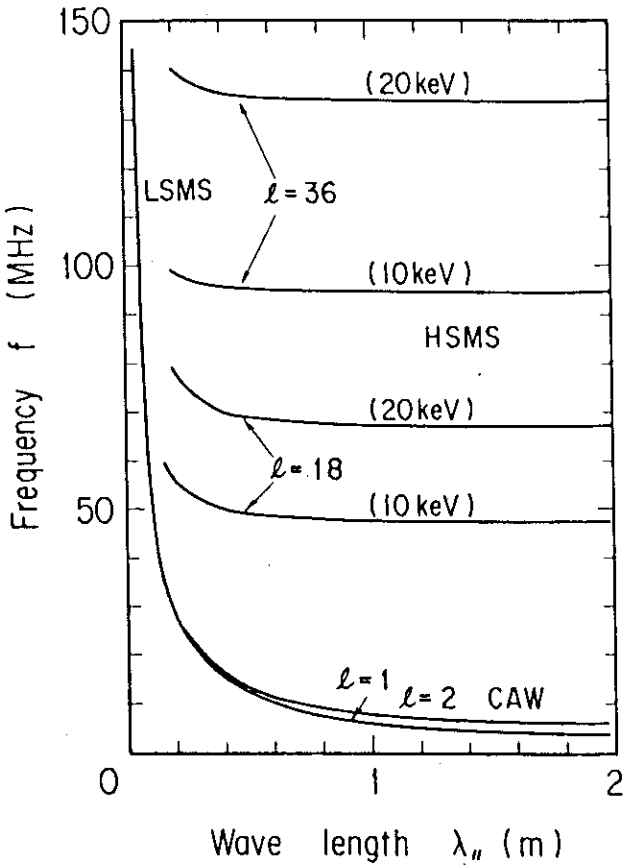

Fig. 2.1.18 Various ion cyclotron harmonic resonance frequencies inside the plasma region of steady-state FER. Major radius is 4 m and the toroidal field on axis is 4.5 T.

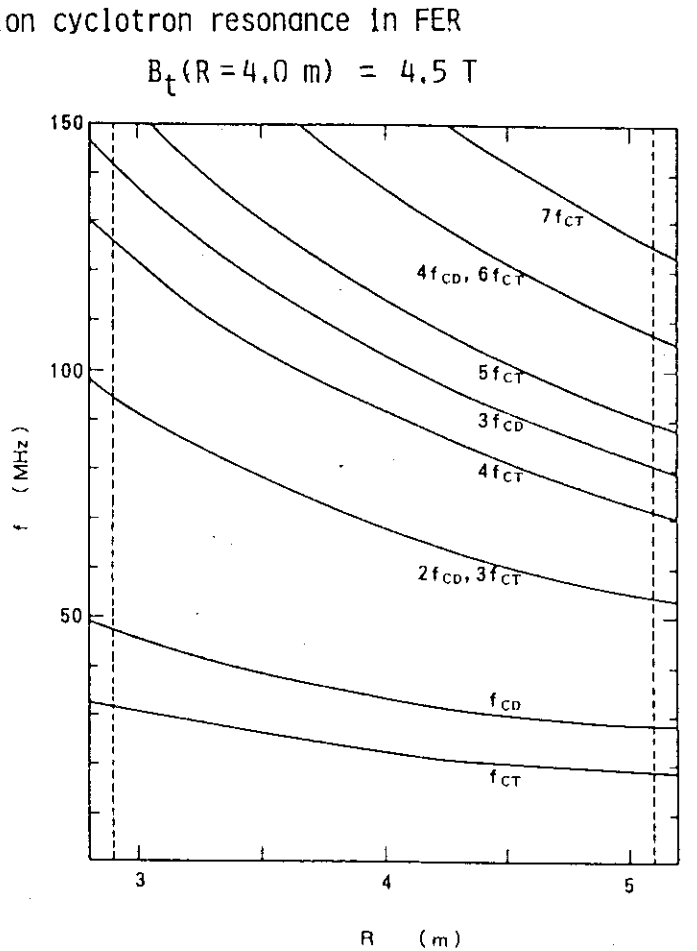

Fig. 2.1.19 Dispersion relation of fast wave of ICRF.

Major Radius

Compactness ⟷ Plasma performance

Measure of plasma performance

$$C_R = \frac{3n\,T/\tau_E}{P_\alpha + P_{rf} - P_b}$$

$C_R \sim 0.6$ for reference FER

Minor radius is not changed　　a = 1.1 m

Major radius is decreased

- R ~ 4 m may be limiting value for engineering
  Removal of inner-most EF coils
  Increase of area of conductor
  Installation of center cylinder

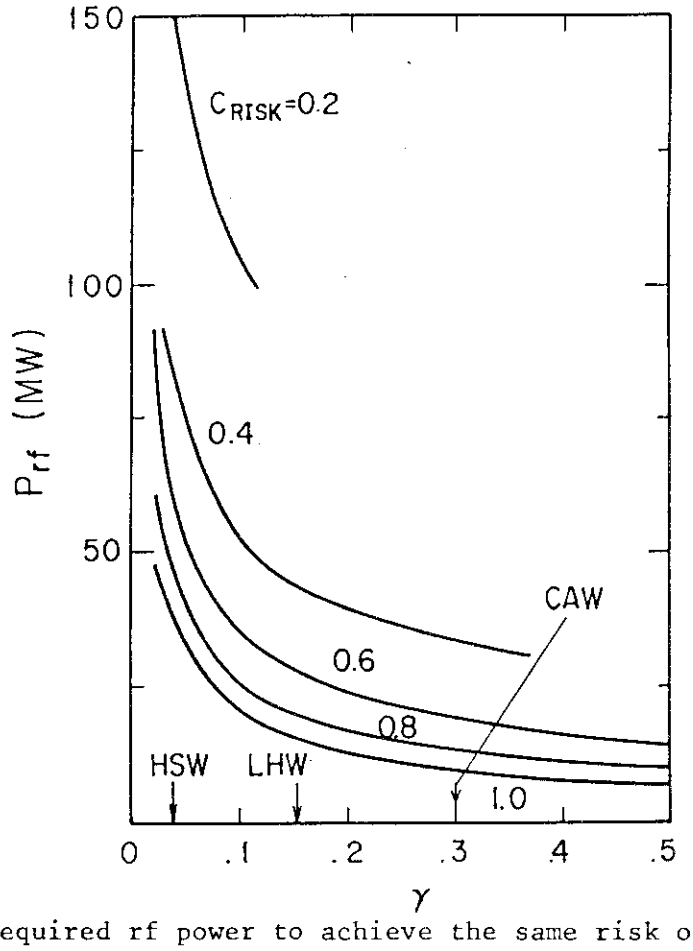

Fig. 2.1.20　Required rf power to achieve the same risk of plasma performance as a function of the current dirve efficiency γ. The efficiencies of CAW, HSMS and LHW are shown on the horizontal axis. Major radius is 4 m and minor radius is 1.1 m.

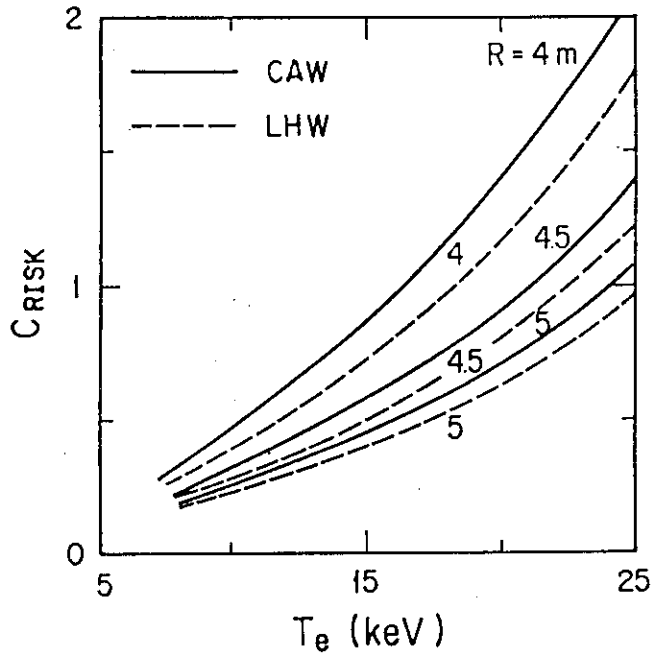

Fig. 2.1.21 The risk of plasma performance for various major radii as a function of average electron temperature. Solid line shows the case of CAW and the dotted line the case of LHW.

Table 2.1.3 Plasma and device parameters for completely steady-state advanced FER. Major radius is decreased as long as possible without aggravating the plasma performance.

Plasma and device Parameters for RFS-FER

RF Driver	CAW	HSMS	LHW
1. Plasma parameters			
Temperature (keV)	13	19	14.5
Density ($\times 10^{19}$ m^{-3})	9	6.2	8.1
Fusion power (MW)	250	210	250
Wall loading (MW/m^2)	0.9	0.76	0.9
Q value	14	4.2	10
RF power (MW)	18	50	25
2. Device parameters			
Major radius (m)	4.0		
Minor radius (m)	1.1		
Noncircularity	1.5		
Toroidal field (T)	4.5		
Plasma current (MA)	6.4		

RF Parameters

1. CAW (current drive)

power	20 MW
frequency	8 MHz
wave length in z direction	1.26 m

2. ICRF (additional heating)

power	30 MW
frequency	69 MHz
mode	D 2nd harmonics

3. ECH (preionization, control)

power	10 MW
frequency	126 GHz
mode	0 mode

Summary and Conclusions

1. CAW is chosen as primary candidate for driver
   - ○ Efficiency (potential advantage for commercial reactor)
   - ○ Accessibility
2. Major radius is decreased to 4 m
   - ○ Compactness of reactor
   - ○ Equilibrium without inner-most EF coils
3. Almost same plasma performance
   - ○ No degradation of confinement
   - ○ Adjustable by lowering plasma temperature and increasing RF power
4. Candidate waves can easily be replaced by others in design study by changing operation temperature when data base is clarified

2.2 Engineering Design of an advanced FER Based on Steady State Plasma Operation Scenario

Part 1. Engineering Design

(1) Introduction

Engineering design study of a RF driven steady-state advanced FER (RFS-FER) with a double-null poloidal divertor is presented.

CAW (Compressed Alfven Wave) is adopted as the RF for plasma current driving.

Taking the advantage of continuous operation, the engineering design of the reactor is simplified on the basis of the concept for eliminating OH coil and taking structual advantage of rigid vacuum boundry vessel.

(2) Specification

Specification of the RF driven steady-state advanced FER is shown in Tables 2.2.1, 2.2.2, 2.2.3 and 2.2.4.

(3) Design Concept

(3.1) Basic Assumption

The concept of the RF (CAW driven steady-state advanced FER with double null poloidal divertor has been assumed as follows:

(1) OH coils are eliminated by the use of CAW current drive.

(2) All magnetic field coils are superconducting coil.
All EF coils are set outside the TF coil to minimize the size of the TF coils.

(3) The number of EF coil is minimized as far as the plasma equilibrium is permited.

(4) Shell effect for stabilizing vertical positional instability of non-circular plasma is given by simple members.

(5) A maintenance system is full remote handling and adapted for the life of components. In-vessel components, that is, divertors, blankets and RF antennas require replacement for maintenance every fixed period. On the other hand, vacuum vessel, shield, and magnets are expected to last long and fix during plant life under normal operating condition, however provisions are placed for their replacement.

(6) Stainless steel is mainly used as the structural material.

(3.2) Reactor Configuration

Major design parameters are listed in Table. 2.2.1 and bird's-eye view of the reactor is shown in Fig. 2.2.1.

The reactor cross-section is shown in Fig. 2.2.2 and the top view is shown in Fig. 2.2.3.

(1) The reactor has two vacuum region, that is, plasma vacuum region and cryostat vacuum region. These two vacuum regions are separated by a commOn vacuum boundary which is located behind blanket except the access port.

The concept of vacuum boundary is shown in Fig. 2.2.4.

(2) Bellows of a vacuum vessel for sustaining one-turn electric resistance along toroidal direction are also eliminated by adopting RF current drive.

(3) Construction has been emphasized that in-vessel components can be removed and replaced in a simple and practical manner dividing into small and easy handling modules.

(4) Torus is divided into 12 sectors and access ports are provided in every sector.
The divertor is divided into 3 modules in one sector and 36 modules in a whole. Its concept is shown in Fig. 2.2.5.
In each sector, one module called the center module is placed in the middle of the sector and the other two called the side module are placed both side of the center module.
The blanket is divided into outer blankets and inner blankets.
Outer blanket is divided into three modules, and inner blanket is divided into two modules in every sector, as shown in Fig. 2.2.6.

(5) The vaccum boundary vessel is designed to give the shell effect.
Emphasis is put on the construction which permits the removal of in-vessel components without breaking the seal of cooling pipe for maintenance.
As shown in Fig. 2.2.7, it has removable part in access ports between TF coils.
The removable part is composed of two pieces.
One is a shell piece which play a roll of shell effect member connected with a fixed part and the other is a seal plate to take

a roll of sealing. The concept of shell structure is shown in Fig. 2.2.8.

(6) The shield consists of two parts. A part of the shield is located in the cryostat vacuum region, however the removal part for maintenance is put in the access ports. Fig. 2.2.9 shows concept of the shield.

(7) The magnets coils are all incorporated in the cryostat which provides vacuum insulation.
They are also surrounded with thermal radiation shield that is cooled by liquid N_2 to minimize the heat leak.
TF coils are joined with shear panels to withstand the out-of-plane forces rigidly in upper and lower sides. The space near the midplane between TF coils is made use of maintenance as access ports.
Number of EF coil is three for each half plane. They are located in the same cryostat vacuum region with TF coils and supported by the structure for TF coil.

(8) Cryostat incorporates the whole magnet system.
Cryostat is connected with vacuum boundary vessel at access ports. So the cryostat vacuum is kept independently during maintenance without any interference.

(9) The vacuum pumps are located at the top and bottom of the reactor to pump out the exhaust gas arround the poloidal double null divertor.

(10) Five access ports are used for RF antennas of three kinds, that is, two ports for CAW, two ports for ICRF and one port for ECH.

(11) As the results of the configuration of above mentioned, the removable methods of in-vessel components such as divertor and blanket, for maintenance, are shown in Fig. 2.2.10 and 2.2.11 respectively.

(12) Radial build of reactor compositions in the midplane of reactor core is Fig. 2.2.12.

(4) Results of analysis

(4.1) Equilibrium configuration

Fig. 2.2.13 Equilibrium poloidal field configuration

Fig. 2.2.14 Current patern of PFC

(4.2) Divertor

Fig. 2.2.15 Divertor structure

Fig. 2.2.16 Thermal stress analysis of divertor plate

(4.3) First wall/Blanket

Fig. 2.2.17 First wall/Blanket structure concept

Fig. 2.2.18 Integrated trtium breeding ratio in blanket region.

Fig. 2.2.19 Nuclear heating distribution in blanket region.

Fig. 2.2.20 Temperature distribution in blanket region

Fig. 2.2.21 Thermal stress analysis of first wall

(4.12) Site plan

Fig. 2.2.35 Site plan

(5) Conclusion

RF driven steady state reactor can be possibly simple in a view point of engineering design requirement and feasible in expectation of development of technology with R & D.

Part 2. Comparison of RFS-FER with Reference FER.

Comparison of the design parameters of RFS-FER with that of FER is shown in Table 2.2.8 (consists of 15 sheets)

Table 2.2.1 Specifications of RFS-FER

Plasma Parameters		
Average plasma temperature	(KeV)	13
Average plasma density	(m^{-3})	9×10^{19}
Effective mean charge		$\leqq 1.5$
Toroidal beta	(%)	4.7
Safety factor		2.5
Thermonuclear power	(MW)	250
Neutron wall load	(MW/m^2)	0.9
Current Drive RF＝CAW		
Injection power	(MW)	20
Frequency	(MHz)	8
Wave length of Z direction	(m)	1.26
Additional heating＝ICRF		
Injection power	(MW)	30
Frequency	(MHz)	69
Mode		2 nd Harmonics (D)
Pre-ionization＝ECRF		
Injection power	(MW)	10
Frequency	(GHz)	126
Mode		Ordinary

Table 2.2.2 Torus Parameter

Plasma major radius (m)	4.0
Plasma half-width (m)	1.1
Plasma elongation	1.5
Toroidal field on chamber axis (T)	4.5
Toroidal ripple (%)	≤ 1.0
Plasma current (MA)	6.4
Impurity control	Double NuLL Poloidal Divertor
Number of toroidal field coils	12

Table 2.2.3 Plasma Operation Scenario

Description	Value
Start up (sec)	500
Shut down (sec)	100
Burn time (sec)	continuous
Number of burn	1000／life

Table 2.2.4 Plasma Disruption Parameter

Major disruption		
Number of disruption		10
Time constant		
Plasma current	(ms)	15
Thermal energy	(ms)	5
Energy		
Thermal energy	(MJ)	80.5
Magnetic energy	(MJ)	30
Distribution		
Phase II (thermal energy)		
40%		Divertor
Phase III (thermal energy+magnetic energy)		
50%		30% on inboard (Peaking factor 2)
50%		Uniformally by radiation

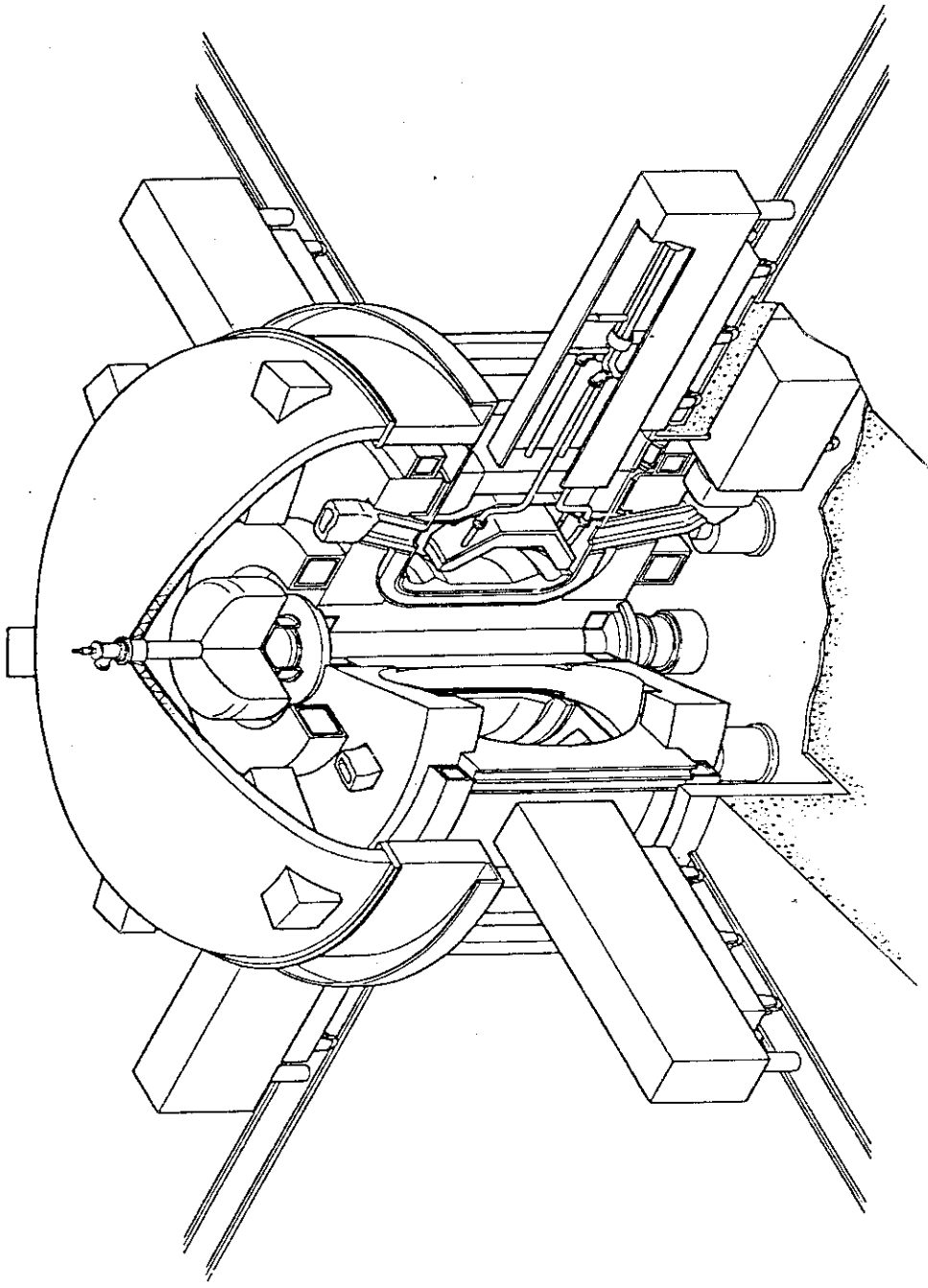

Fig. 2.2.1 Bird's-eye View of the RFS-FER

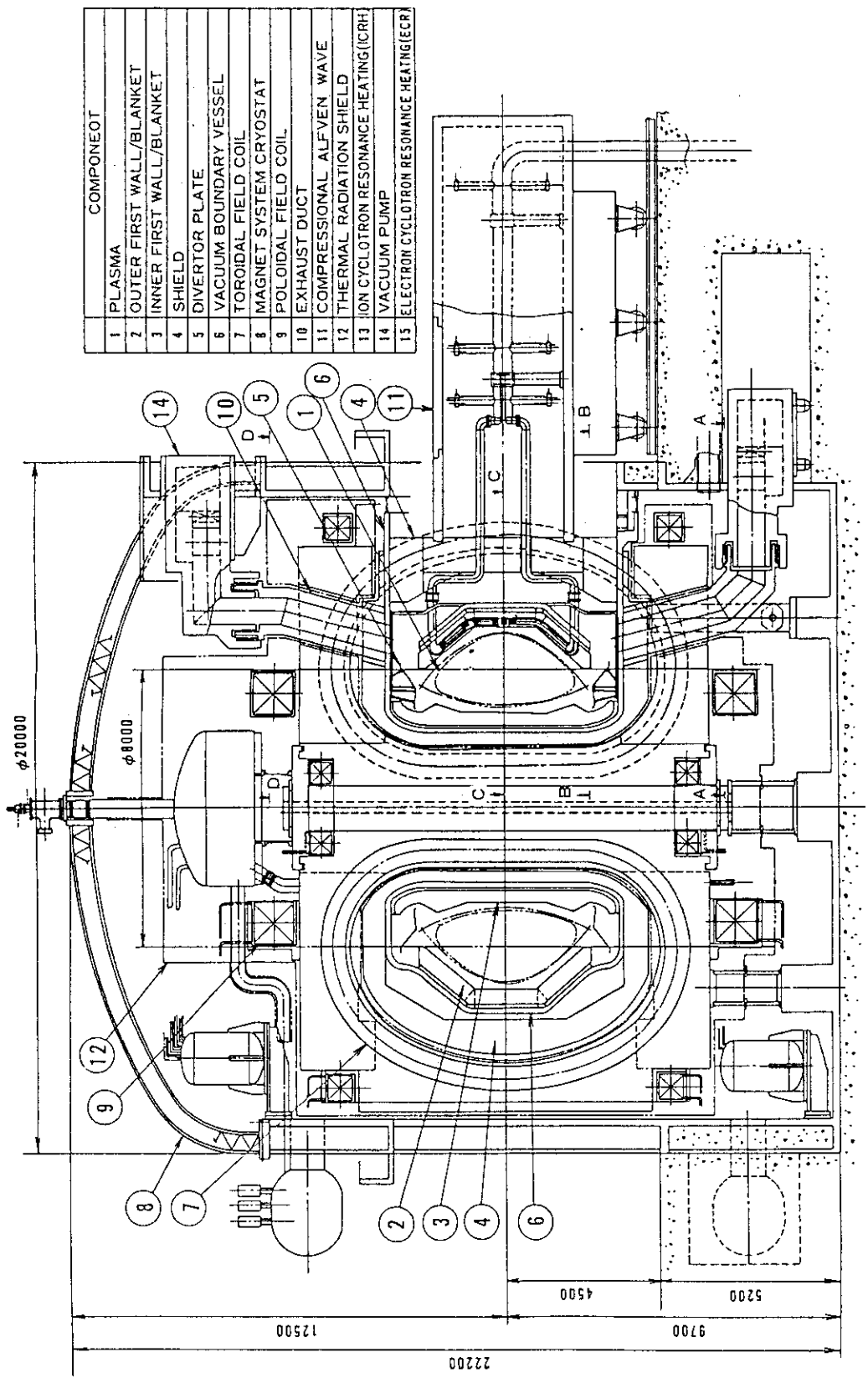

Fig. 2.2.2 Cross Sectional View of the RFS-FER

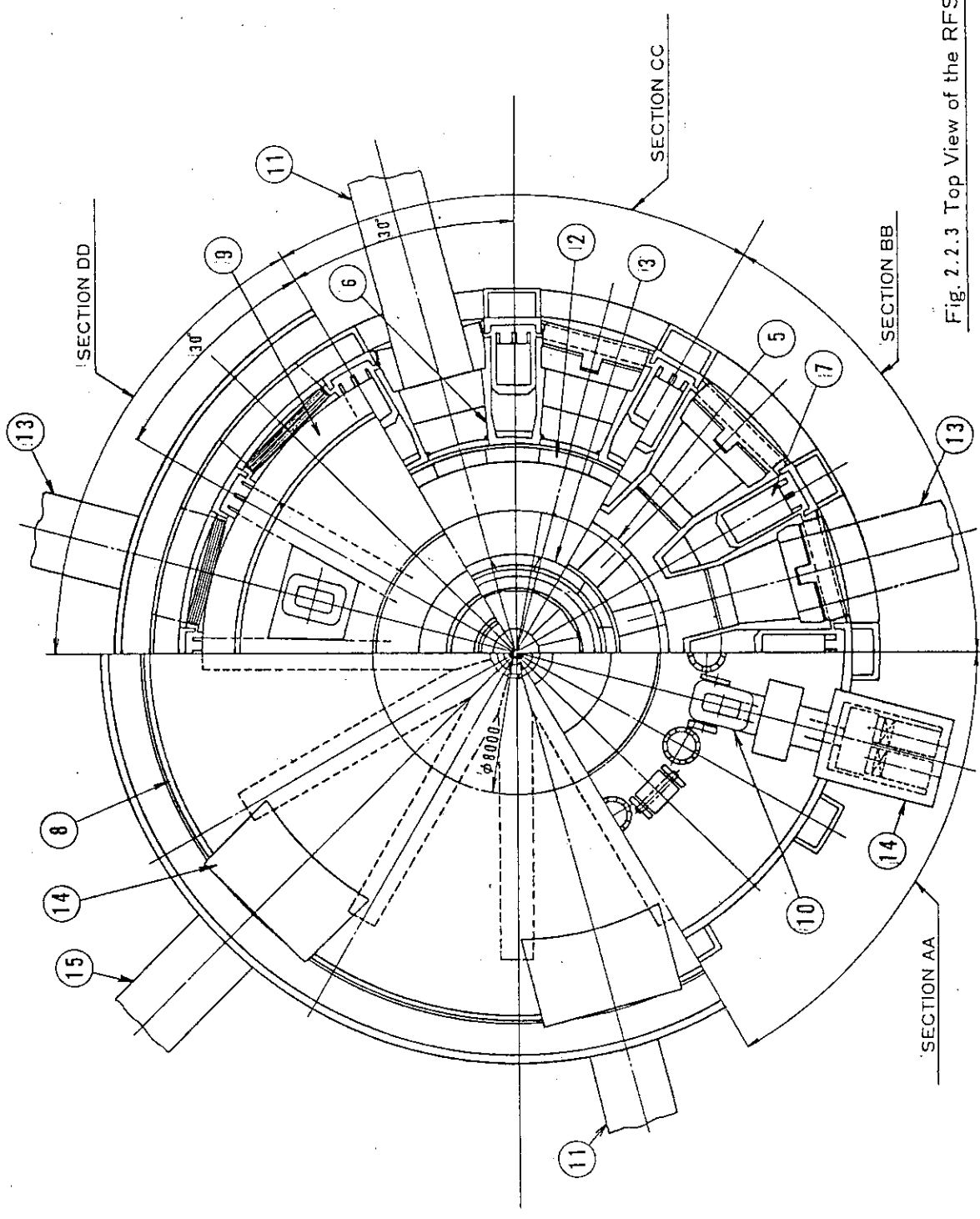

Fig. 2.2.3 Top View of the RFS-FER

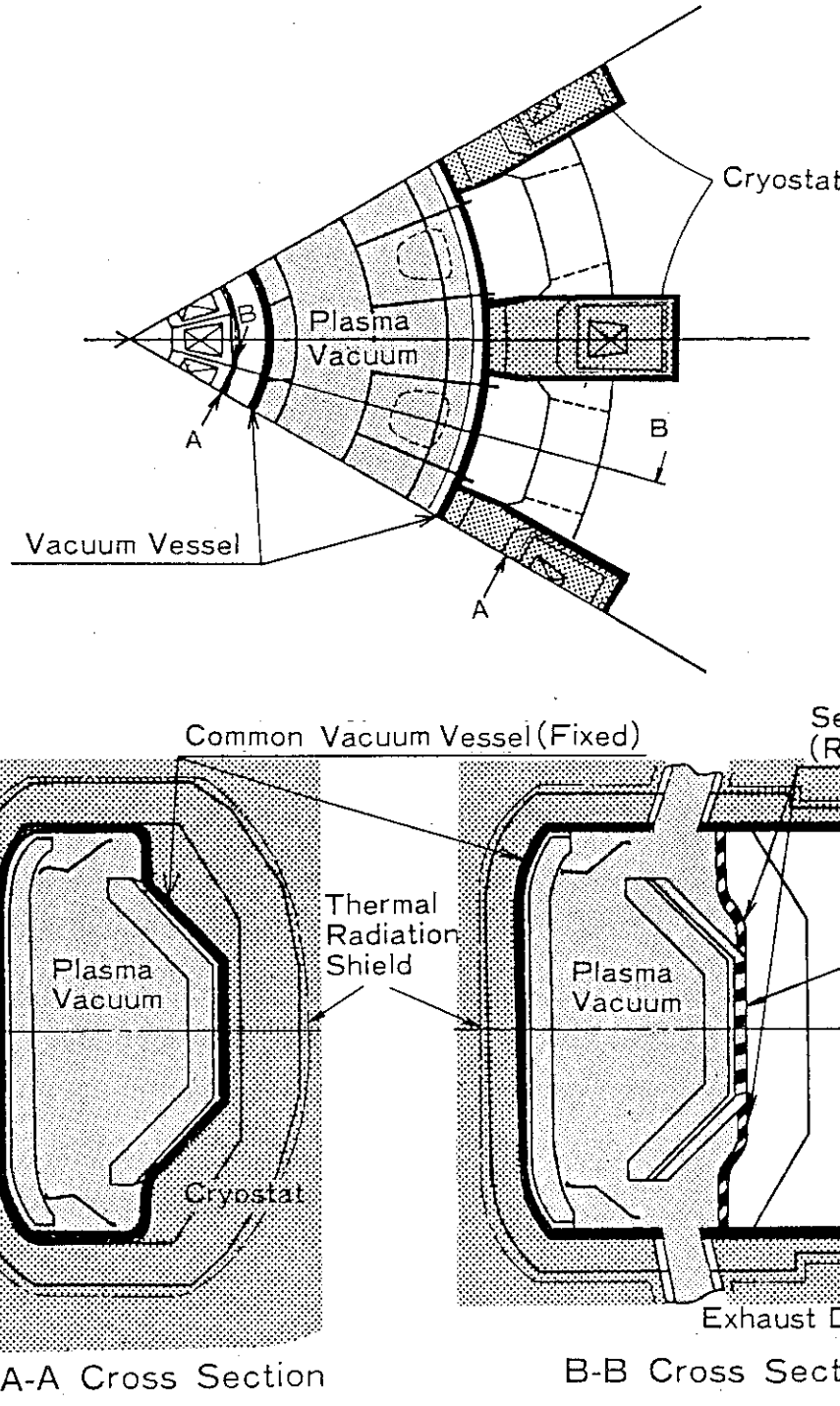

Fig.2.2.4 Concept of Vacuum Boundary

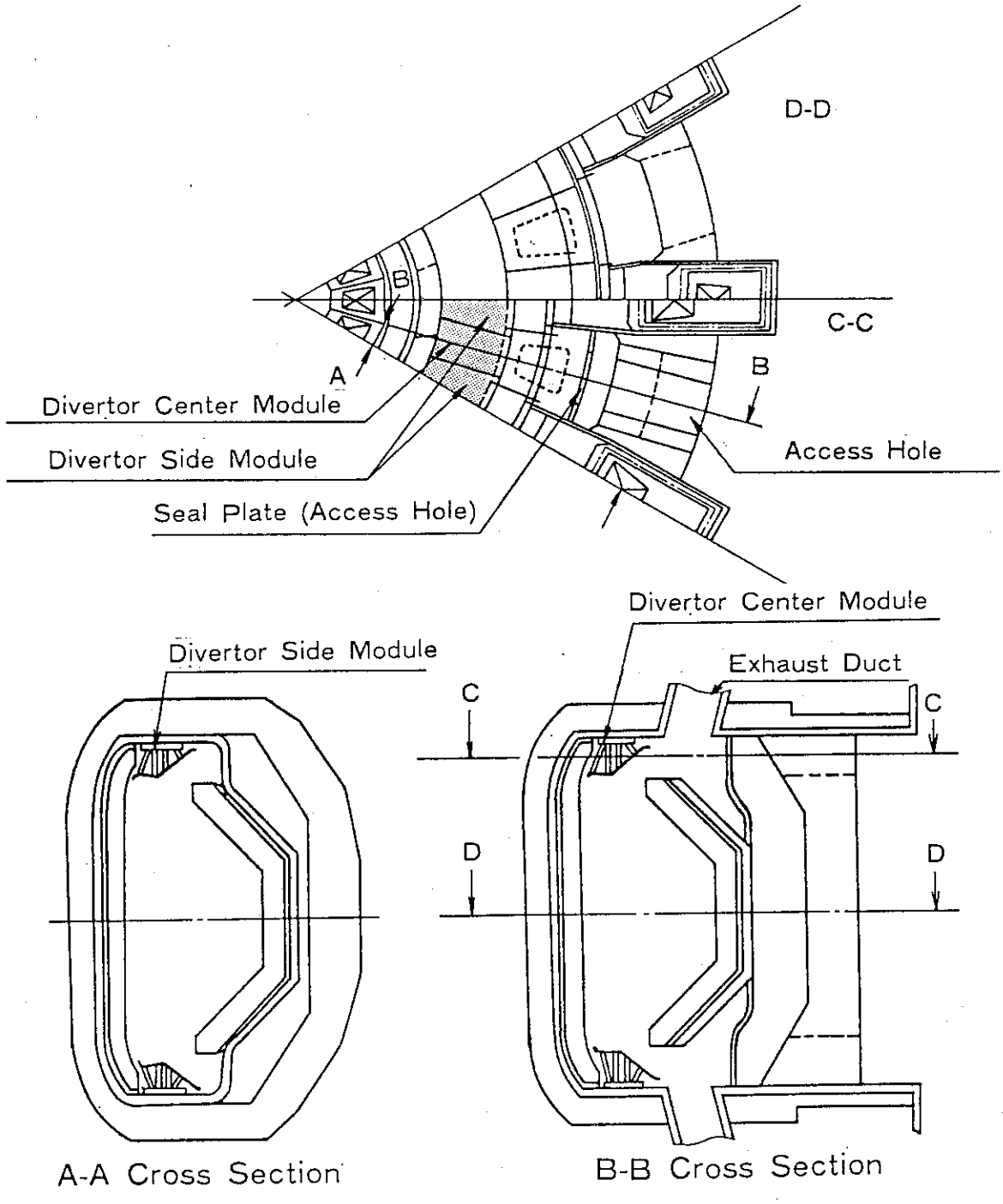

Fig. 2.2.5 Concept of Divertor

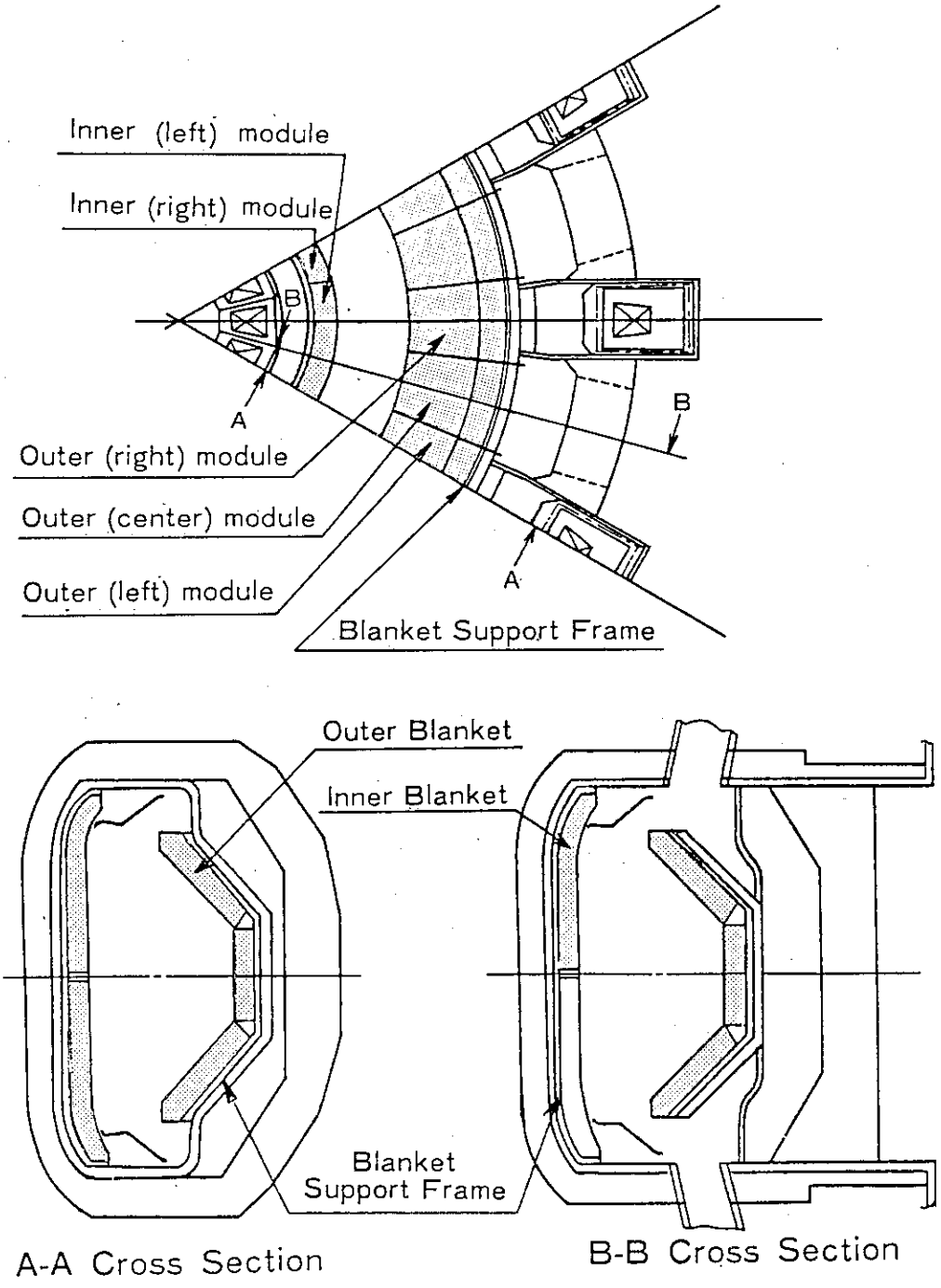

Fig. 2.2.6 Concept of Blanket

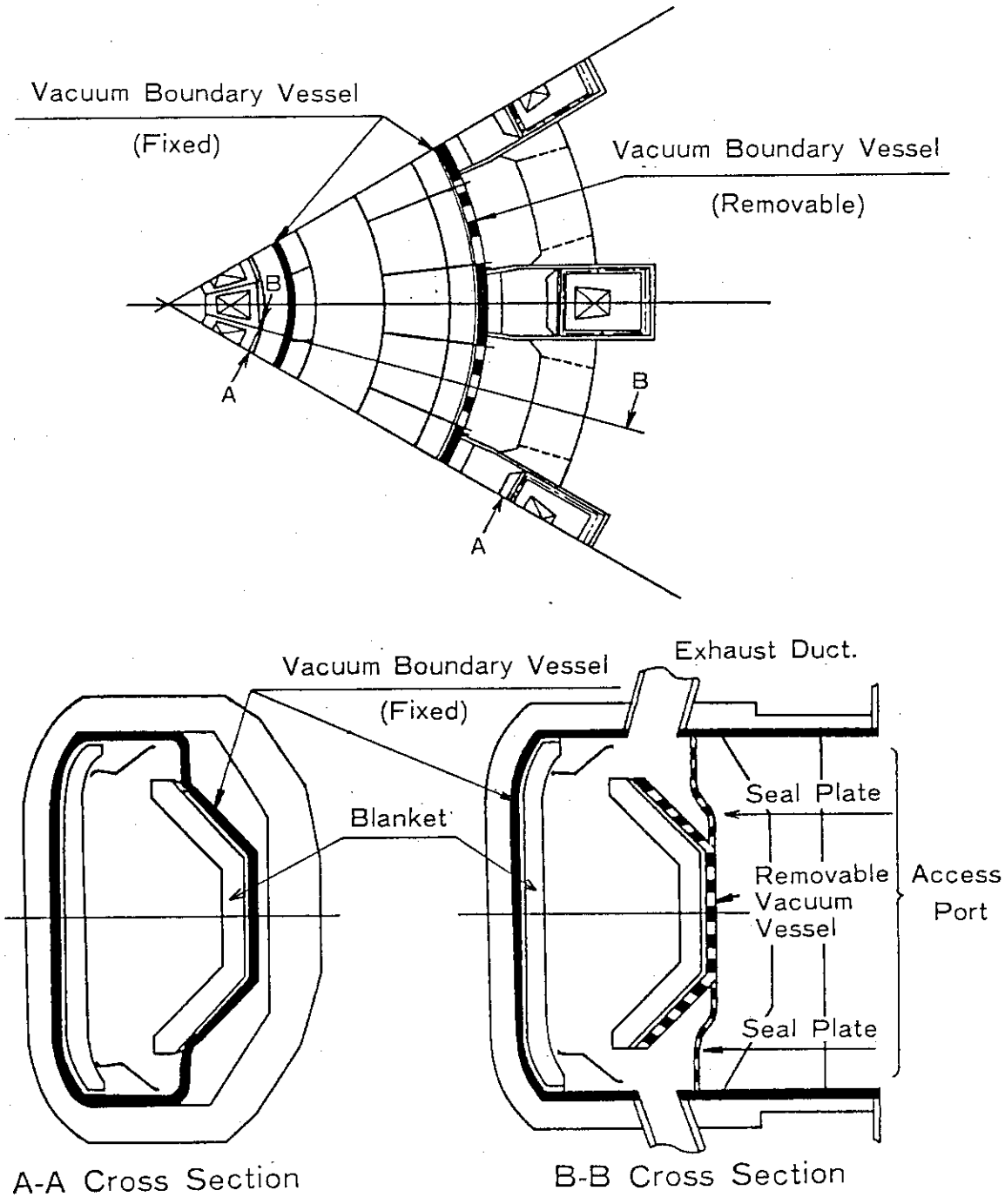

Fig. 2.2.7 Vacuum Boundary Vessel

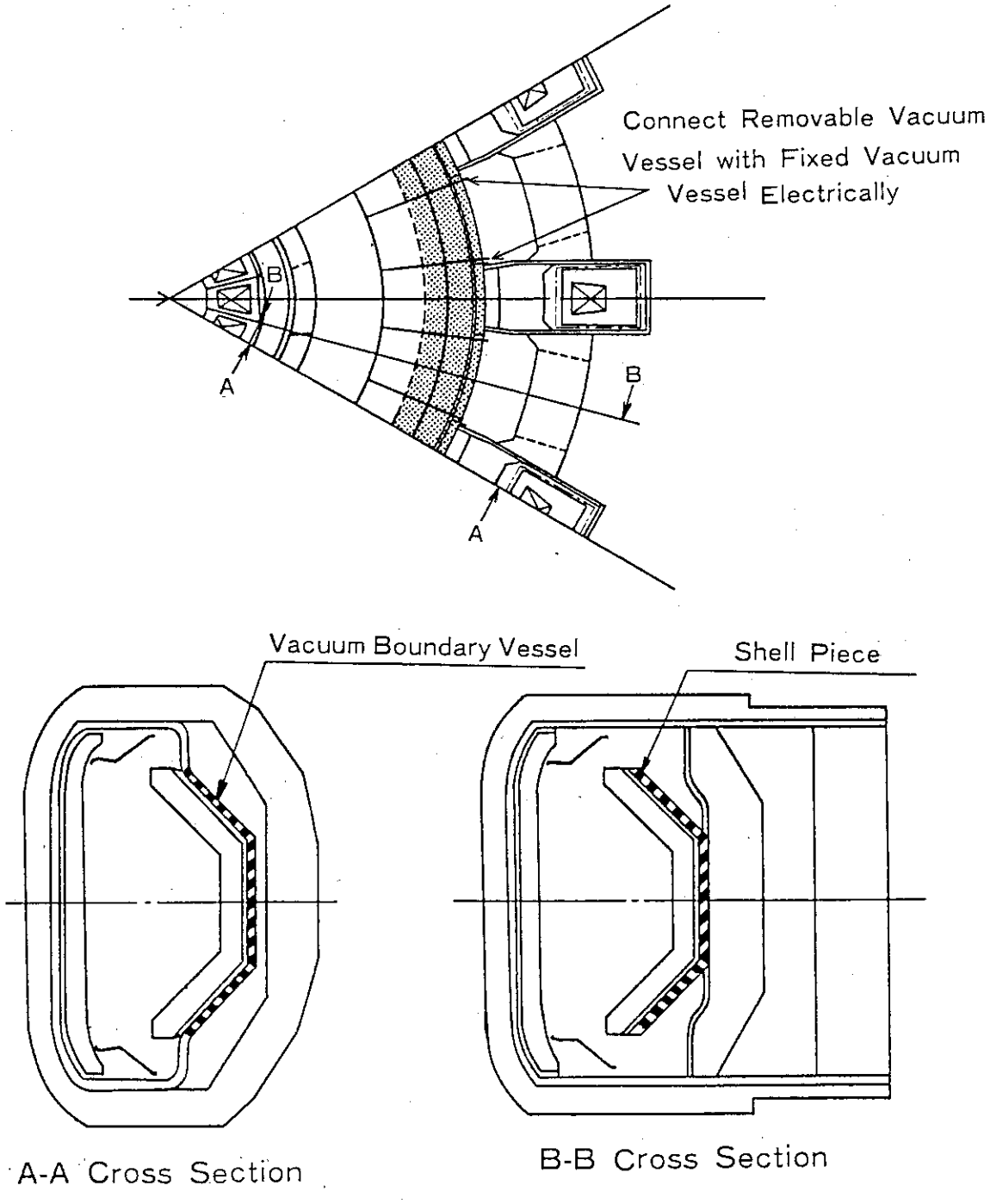

Fig. 2.2.8 Concept of Shell Structure

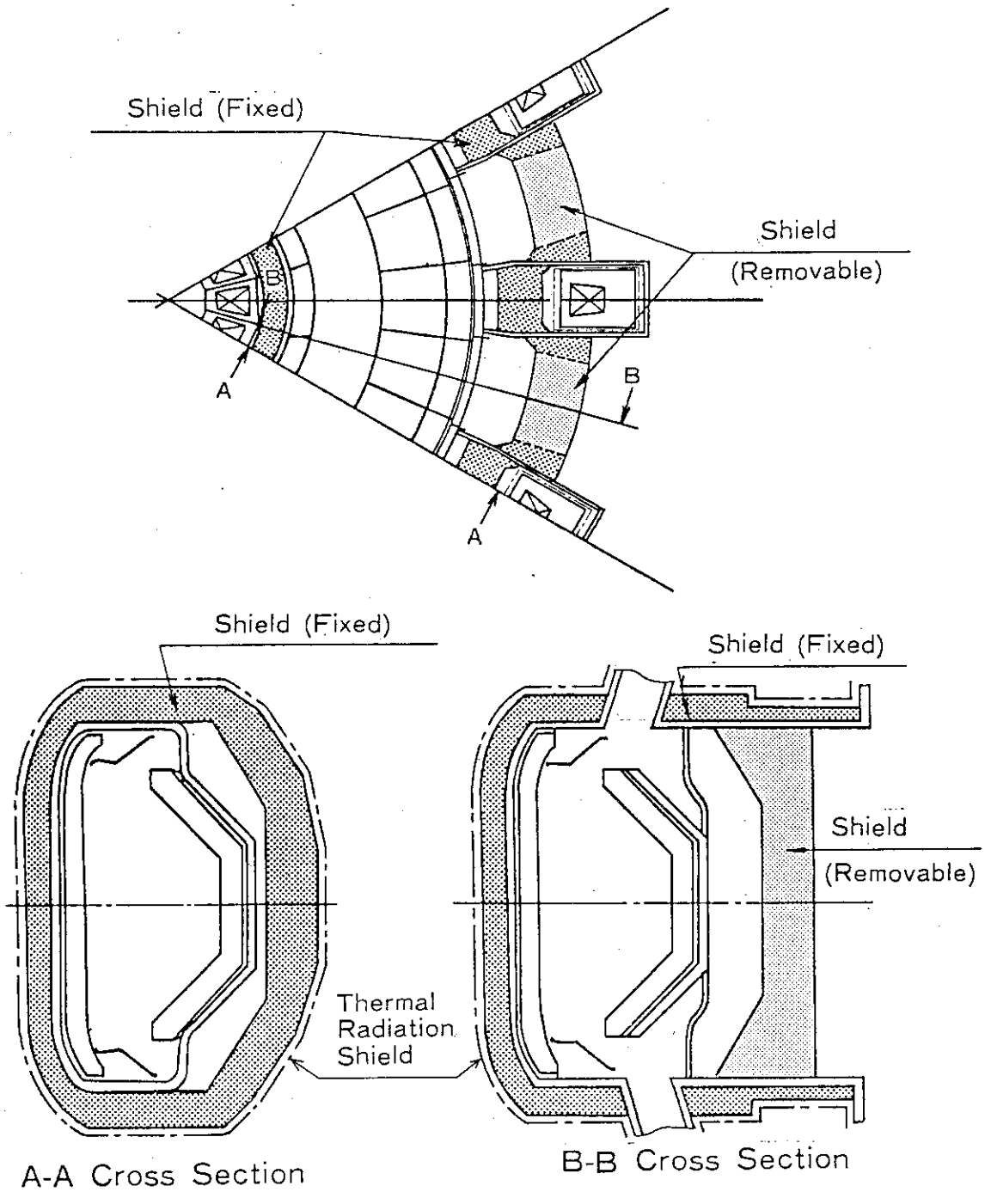

Fig. 2.2.9 Concept of Shield

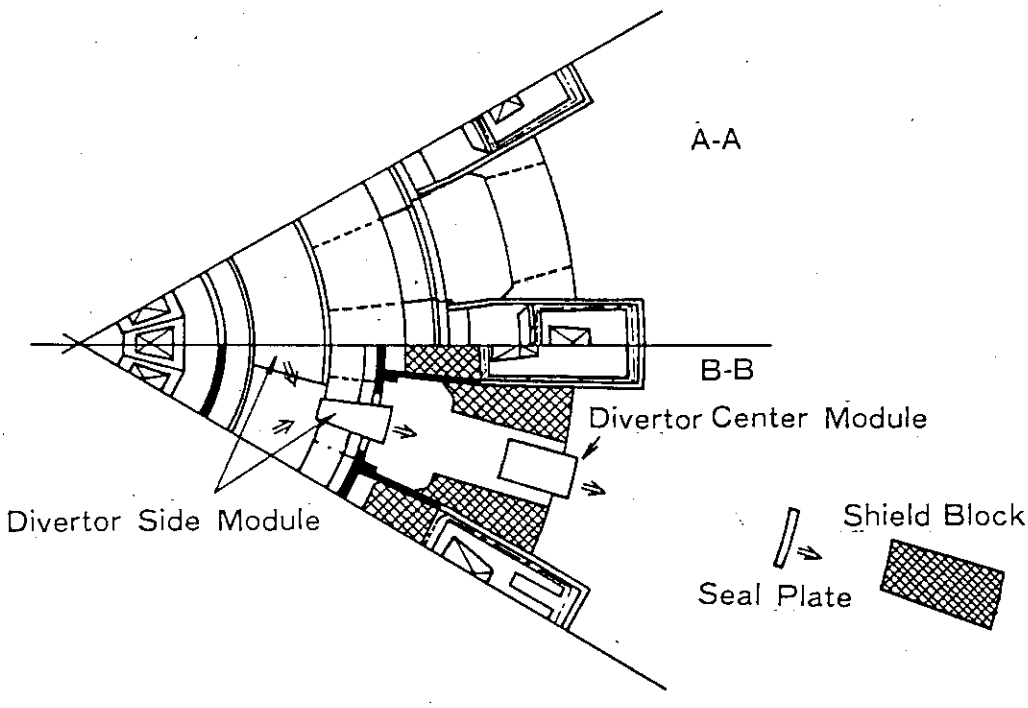

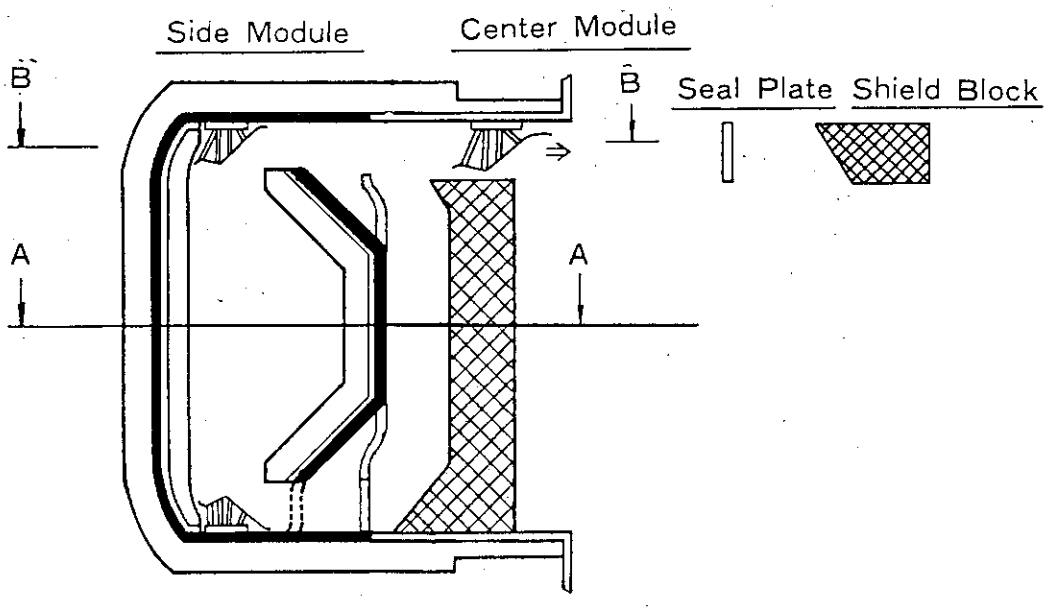

Fig. 2.2.10 Divertor Module Removal

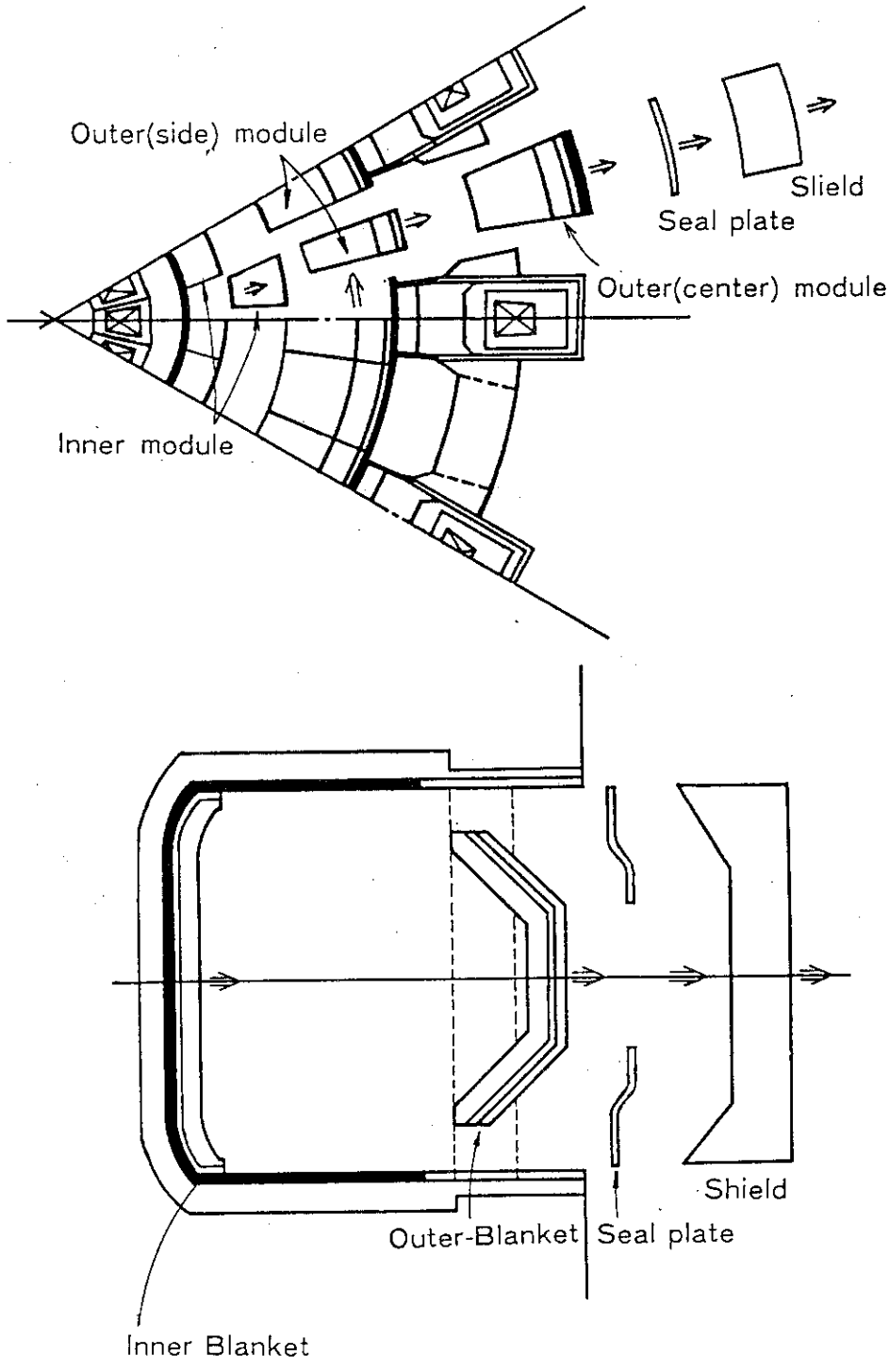

Fig. 2.2.11 Blanket Module Removal

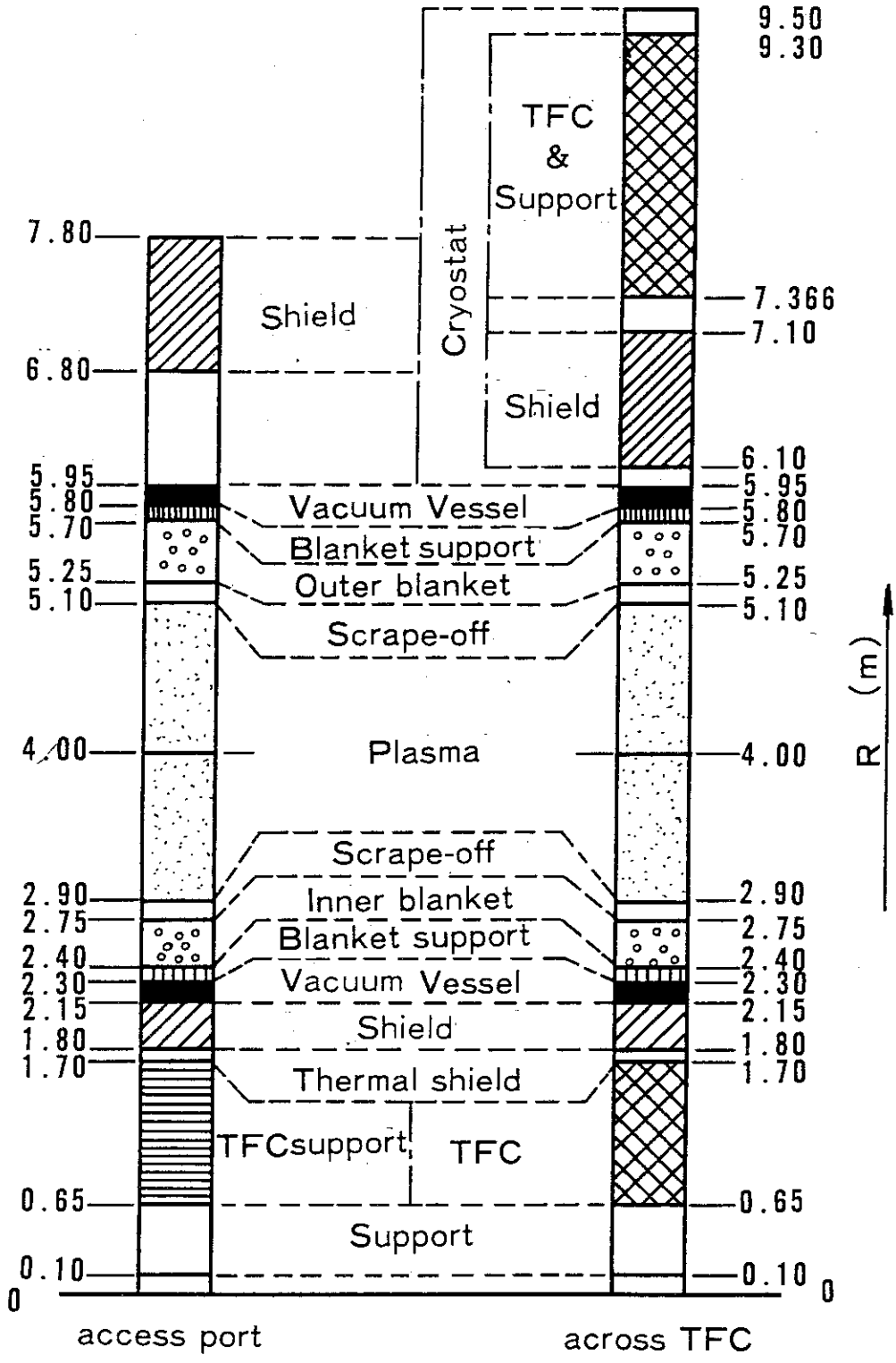

Fig. 2.2.12 RFS-FER radial build

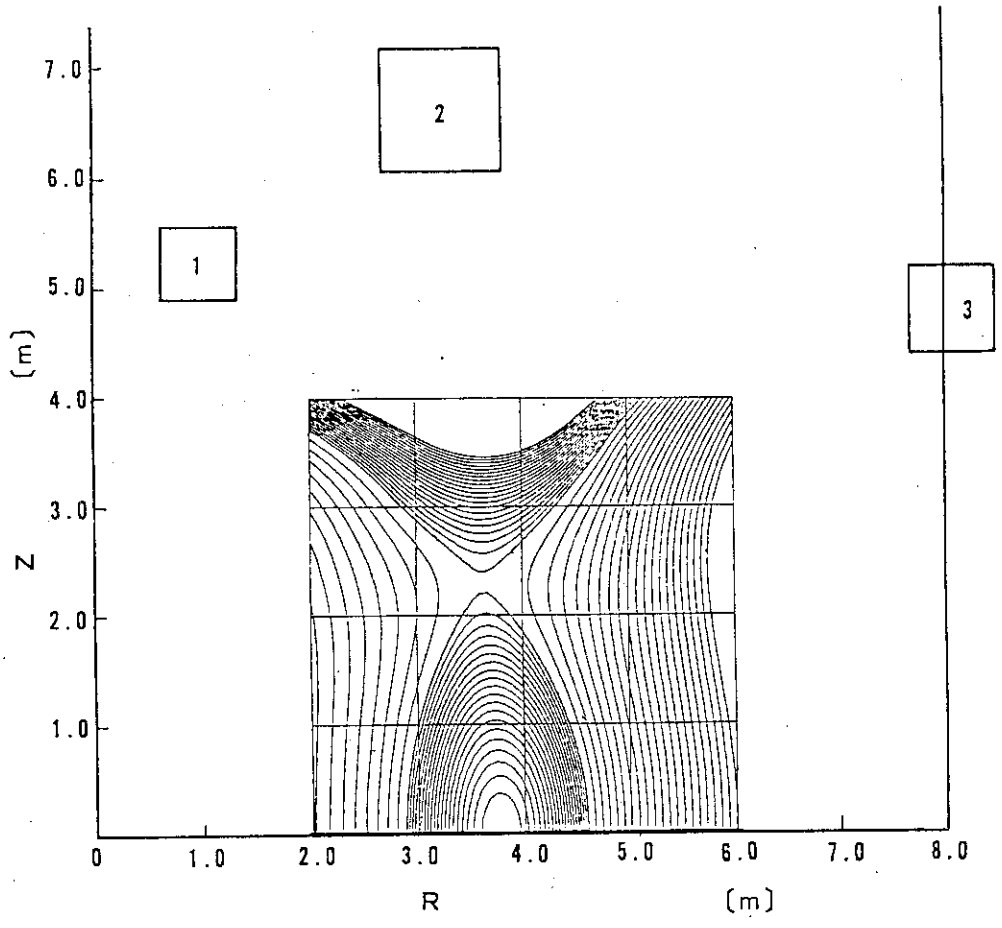

EQUILIBRIUM-FIELD COIL CONFIGURATION

Coil No.	Coil configuration R(m)	Coil configuration Z(m)	Equilibrium-field coil current at start-up current (MAT)
1	1.0	5.3	$I_1 = -2.0$
2	3.3	6.7	$I_2 = 20.0$
3	8.1	4.8	$I_3 = -5.9$
Plasma current			$I_p = 3.2$ (MA)
Poloidal beta			$\beta_p = 0.1$

Fig.2.2.13(1) Equilibrium Poloidal Field Configuration

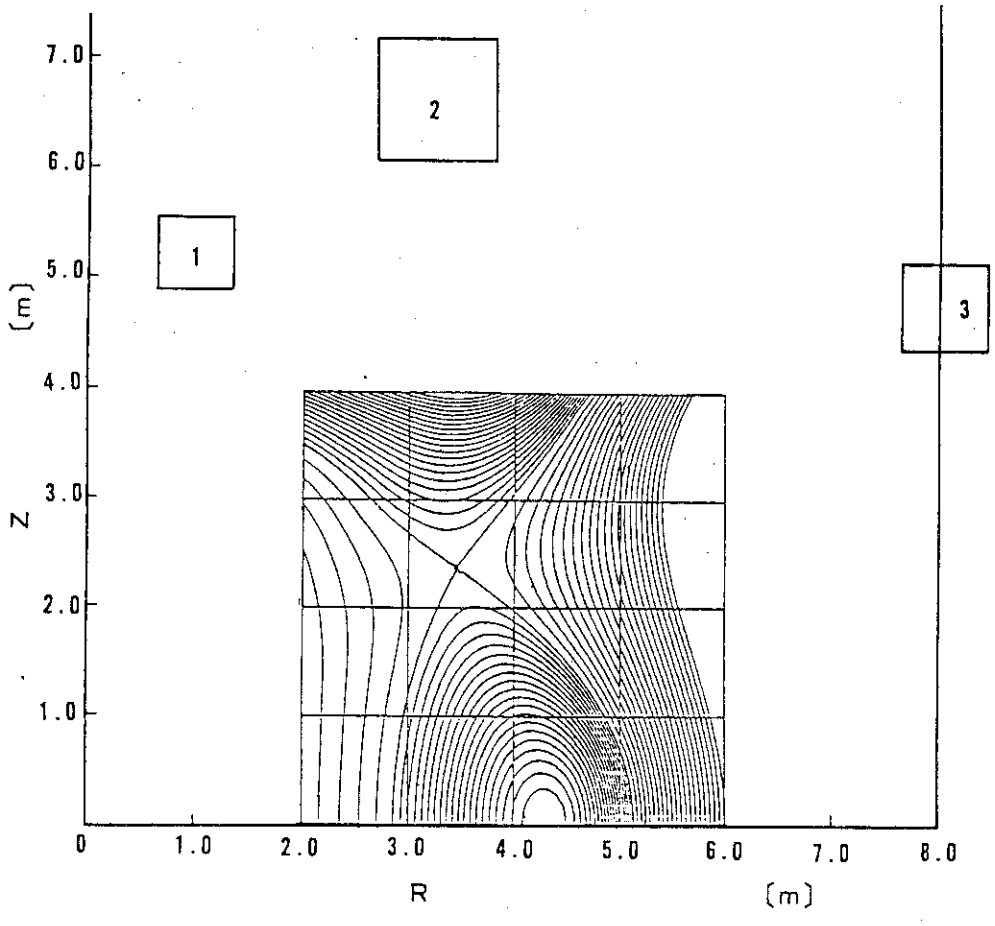

EQUILIBRIUM-FIELD COIL CONFIGURATION

Coil No.	Coil contiguration R(m)	Coil contiguration Z(m)	Equilibrium-field coil current at flat-top current (MAT)
1	1.0	5.3	I_1 =-10.0
2	3.3	6.7	I_2 = 33.8
3	8.1	4.8	I_3 =-13.0
Plasma current			I_p = 6.4 (MA)
Poloidal beta			β_p= 2.5

Fig. 2.2.13(2) Equilibrium Poloidal Field Configuration

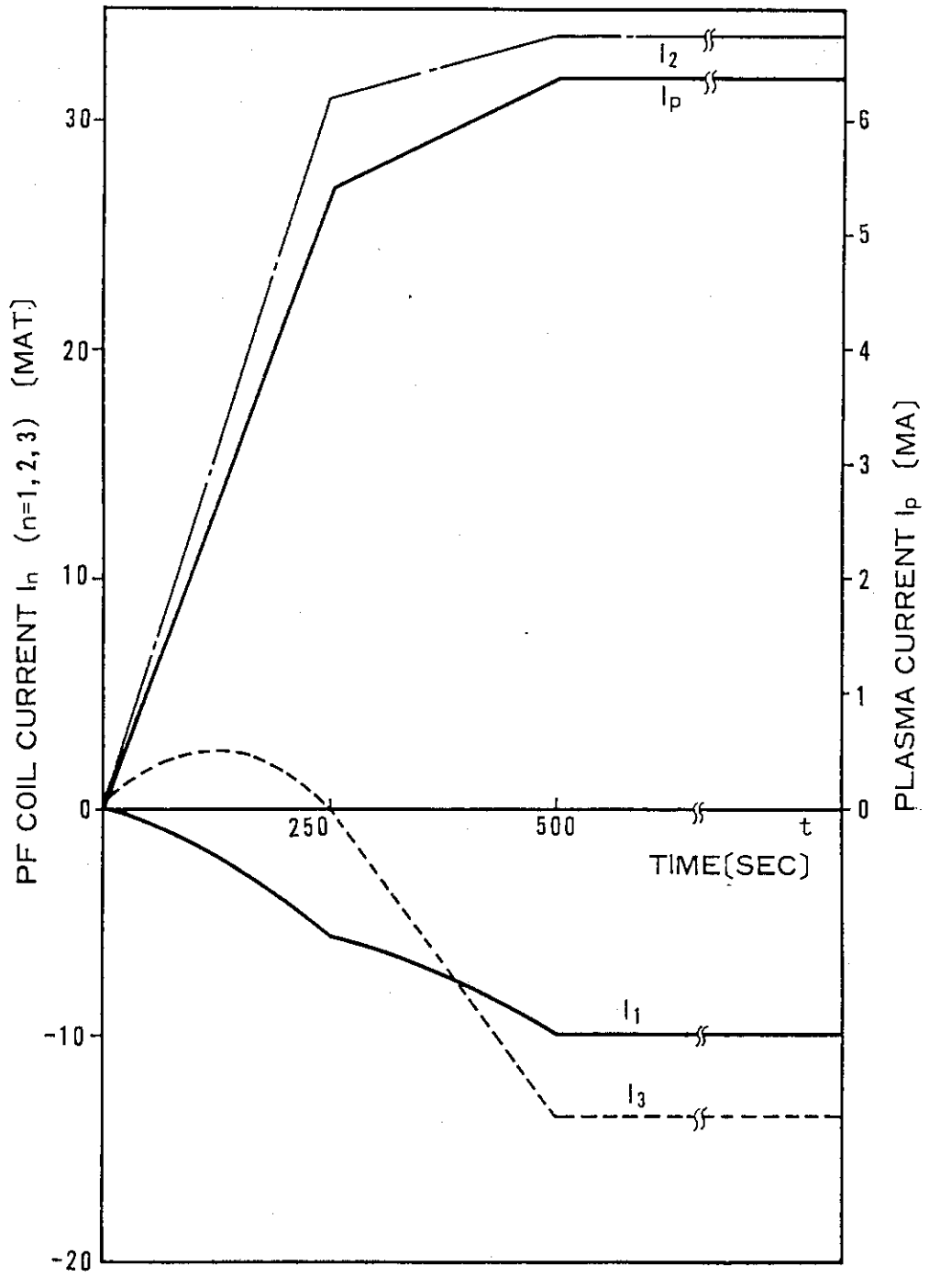

Fig.2.2.14 Current Pattern of PFC

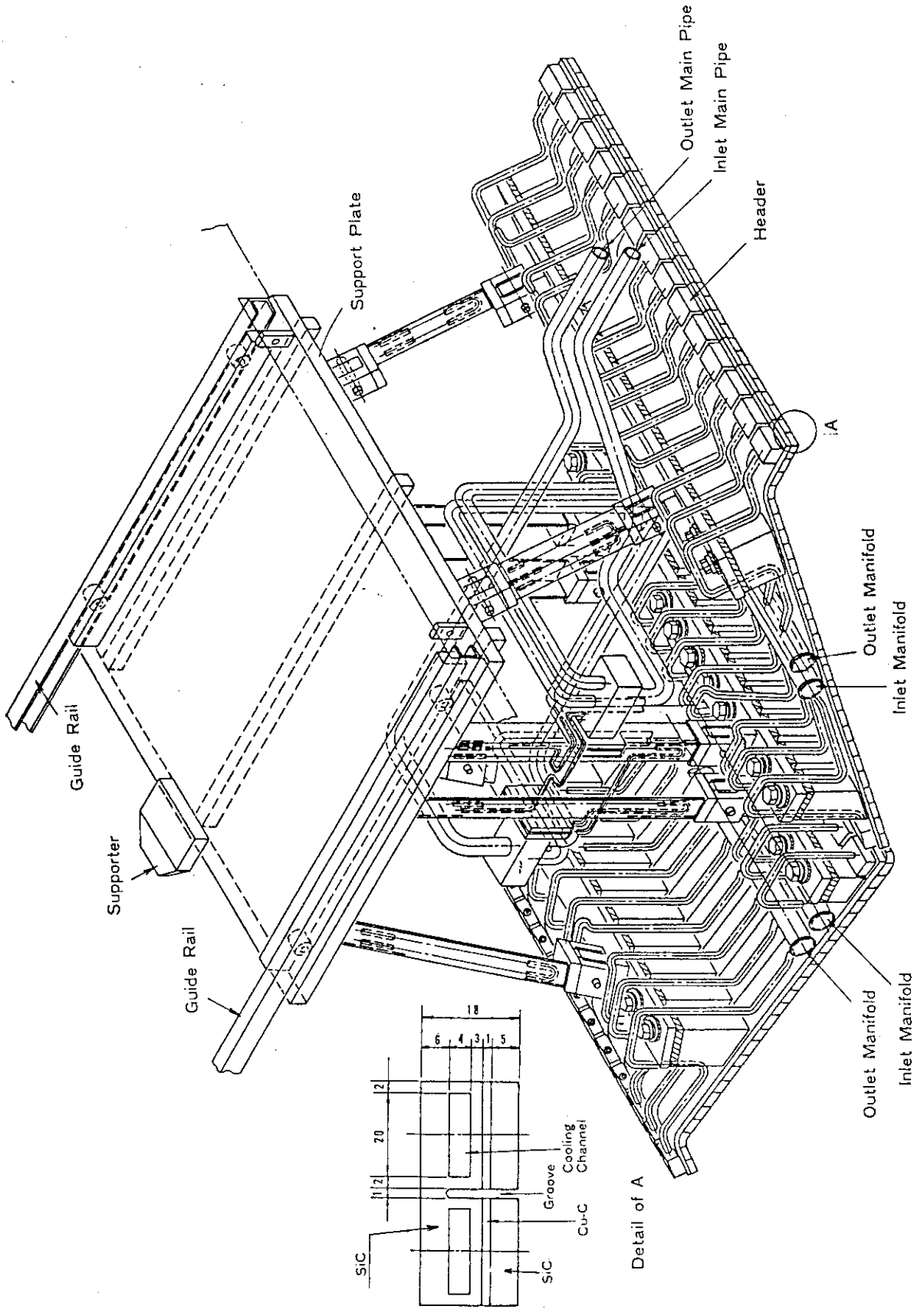

Fig.2.2.15 Divertor Structure

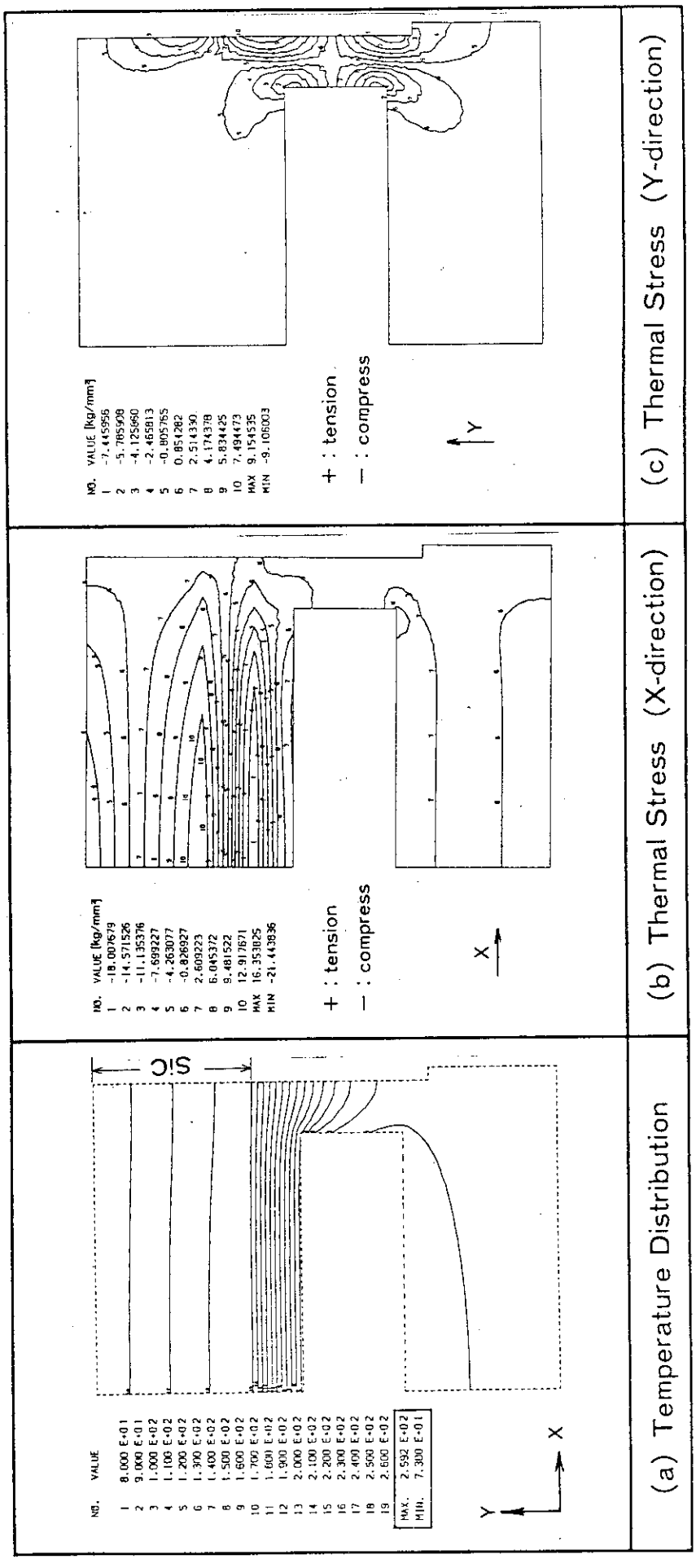

(a) Temperature Distribution　(b) Thermal Stress (X-direction)　(c) Thermal Stress (Y-direction)

at Normal operation

Fig. 2.2.16 Thermal stress analysis of the Divertor plate

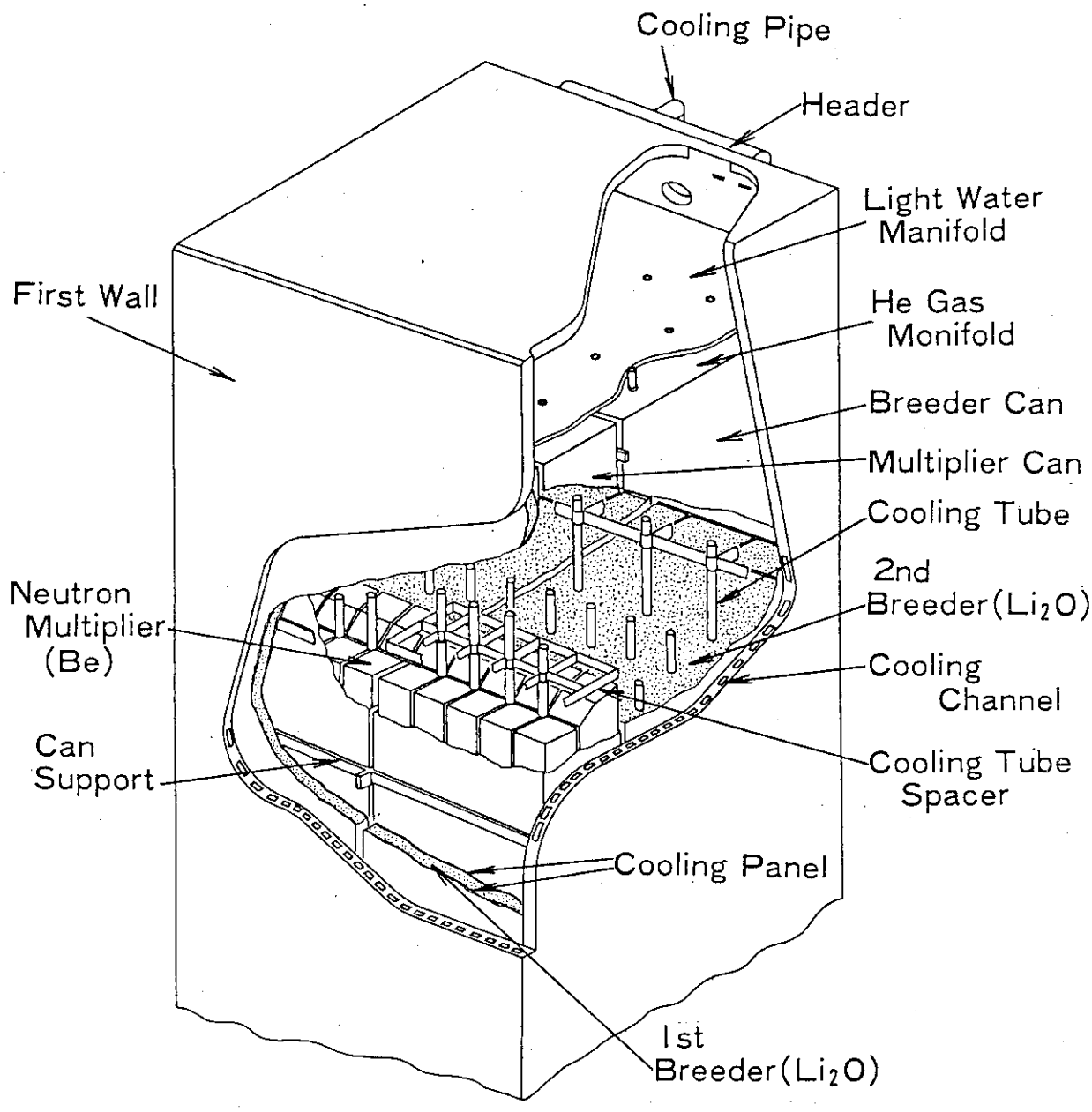

Fig.2.2.17 First Wall/Blanket structure concept

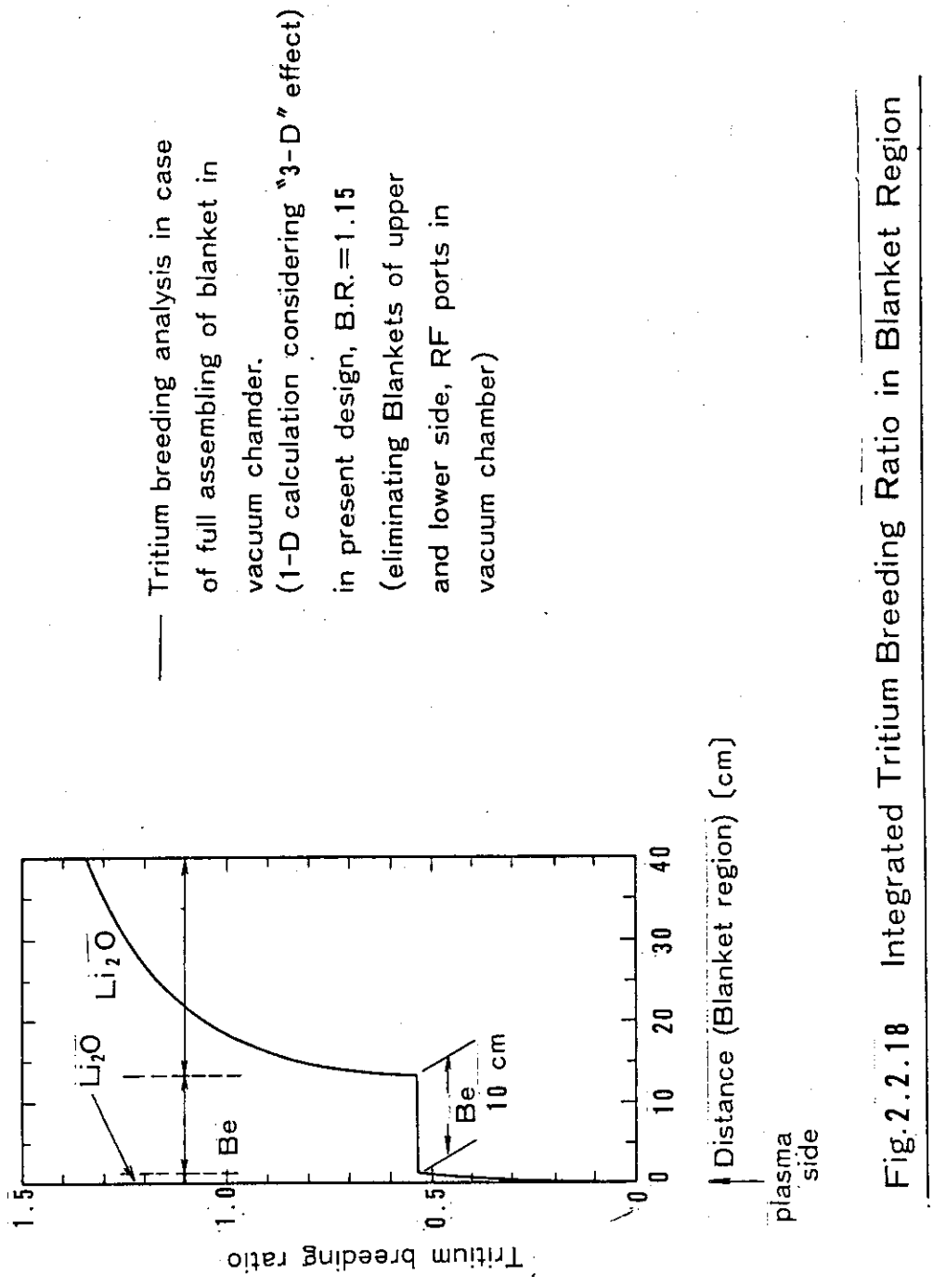

Fig. 2.2.18 Integrated Tritium Breeding Ratio in Blanket Region

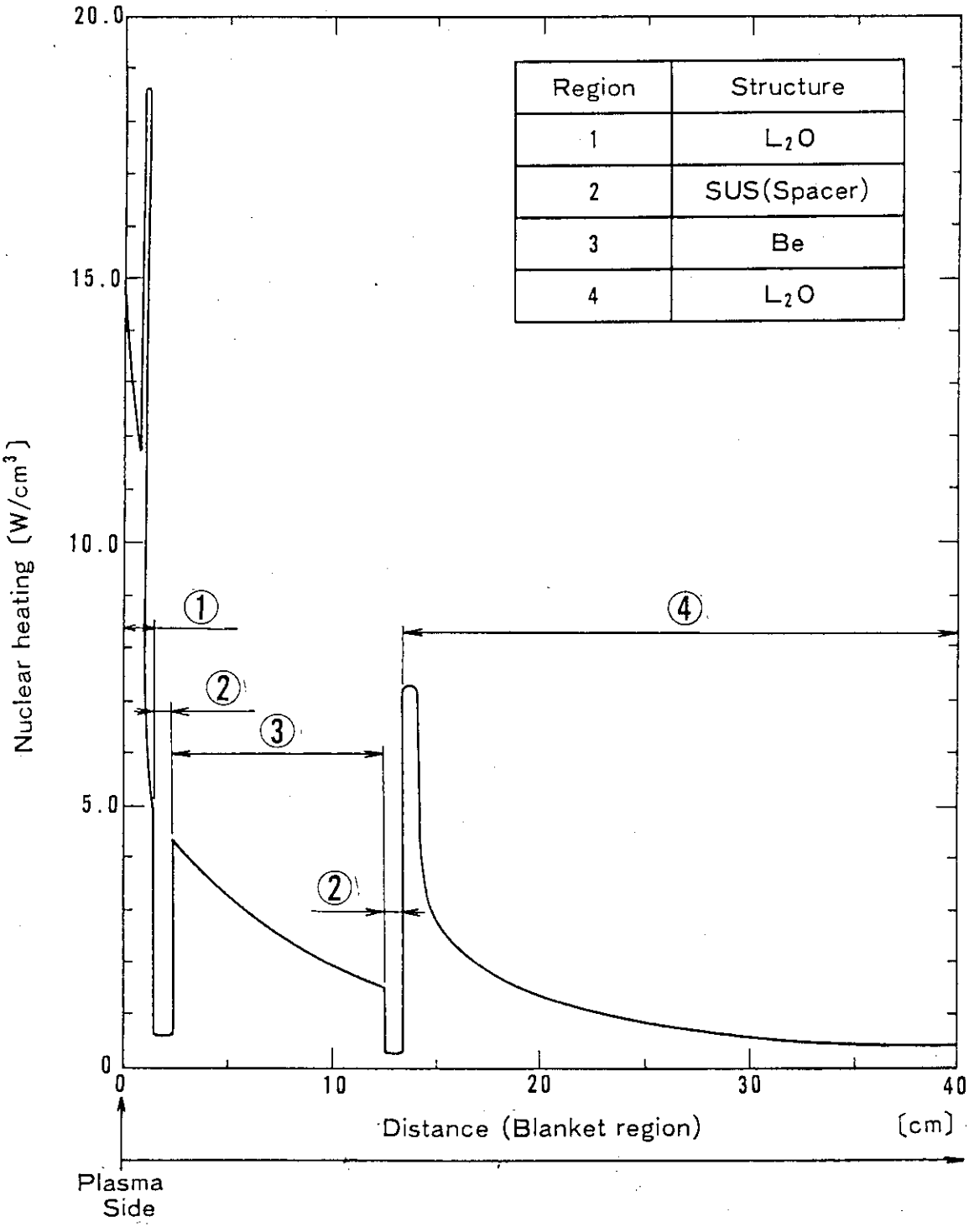

Fig.2.2.19 Nuclear heating distribution in blanket region

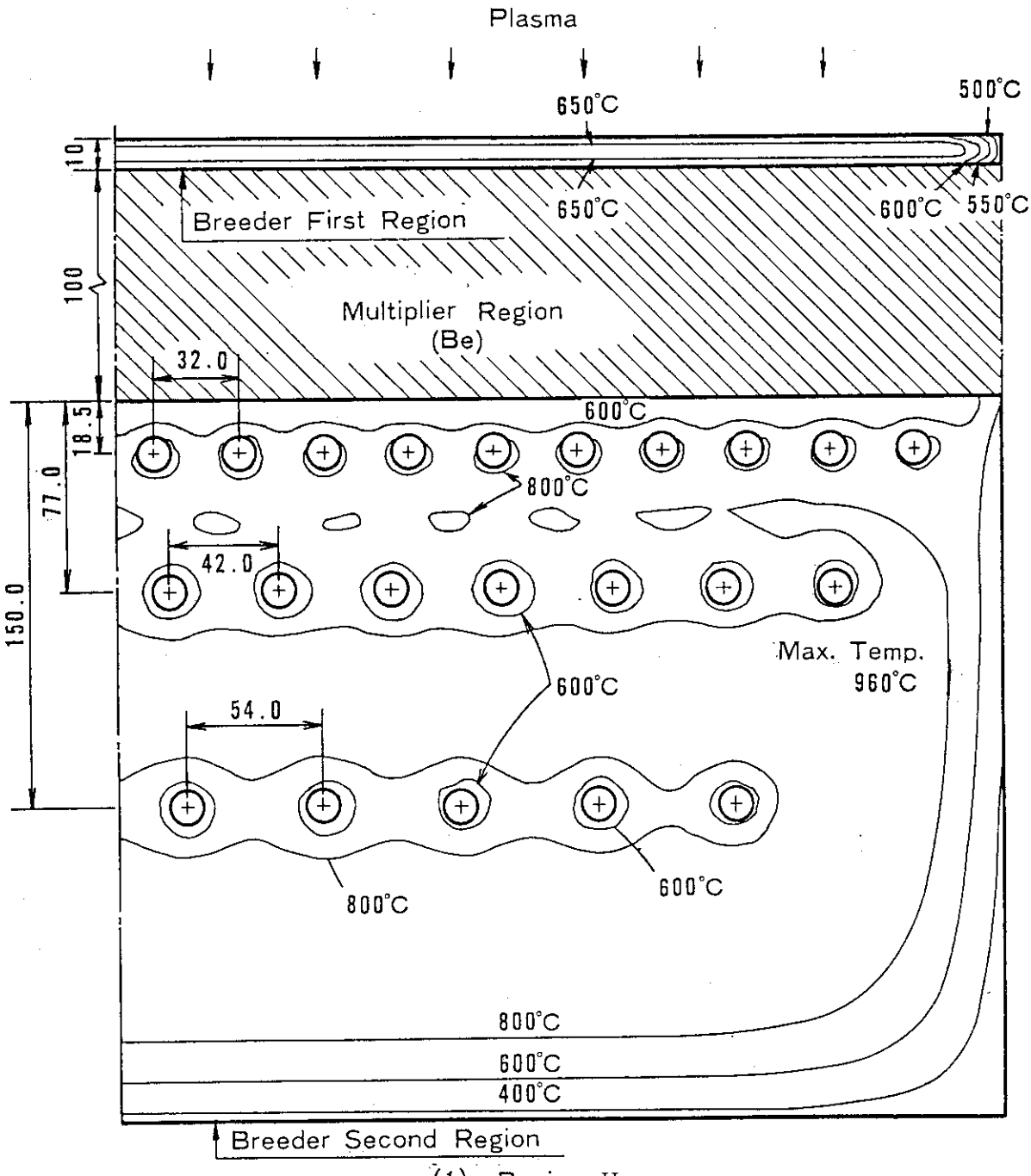

(1) Region II

Fig.2.2.20 (a) Temperature distribution in Li_2O Regions of the Blanket

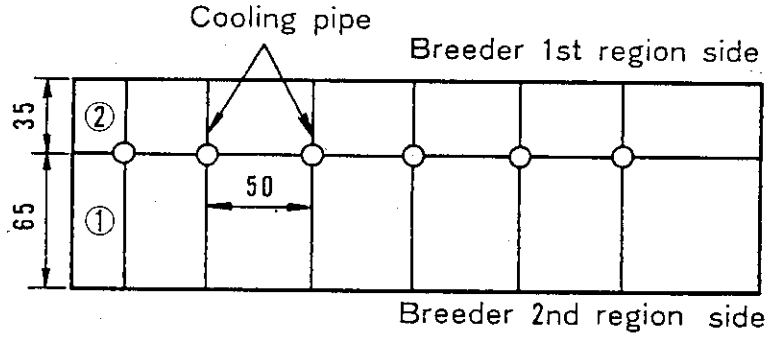

(a) Cooling pipe position in Be multiplier

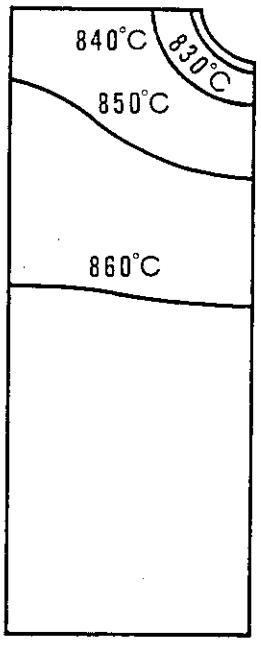

(b) Result of the region ①

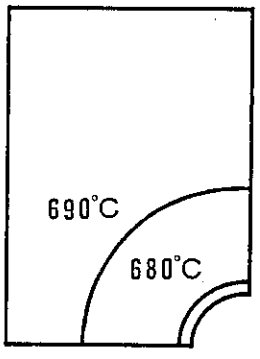

(c) Result of the region ②

Fig.2.2.20(b)Temperature Distribution in Be Multiplier Region of the Blanket

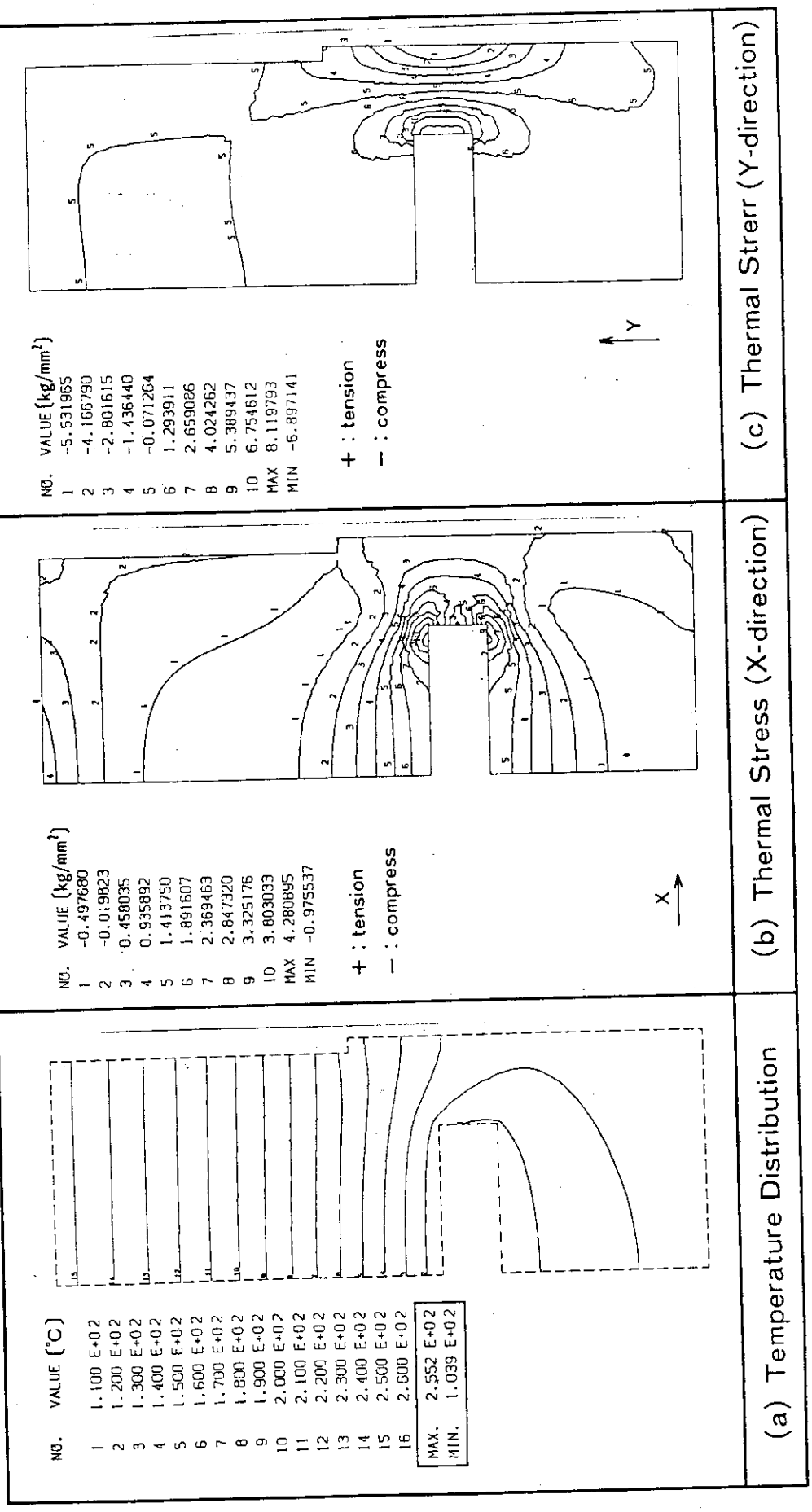

Fig. 2.2.21 Thermal stress analysis of the First Wall

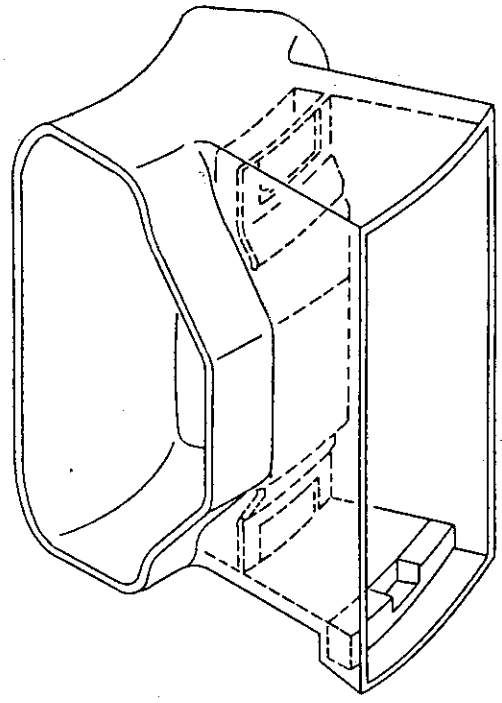

Fig.2.2.22(a) Concept of Vacuum Boundary Vessel

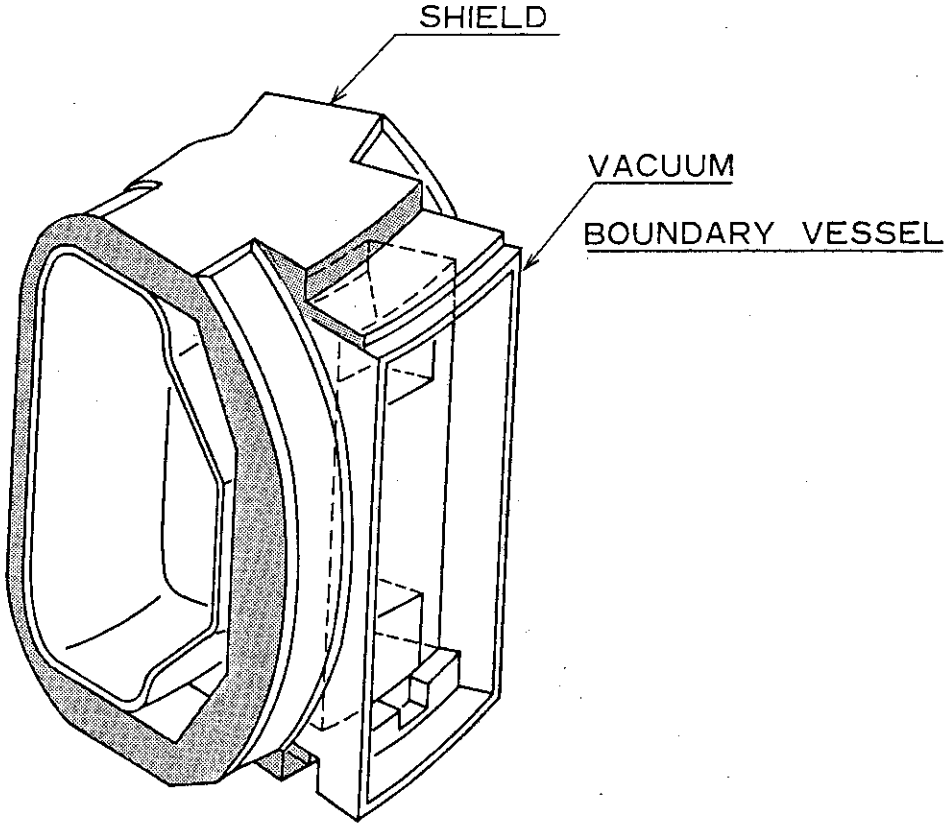

Fig. 2.2.22(b) Concept of Vacuum Boundary Vessel and Shield

Fig. 2.2.23 (a) Main Parameters of TF Coils

1. Bore radius	9.0m/5.7m
2. Number of coils	12
3. Total ampere-turns	90 MAT
4. Ampere-turns per coil	7.5 MAT
5. Winding dimension	(Max 538mm, Min 270)×697mm
6. Winding	double pancake winding
7. Average current density	26.8 A/mm^2
8. Number of turns/1coil	360 turns
9. Operating current	20.8 KA
10. Conductor 12T, 10T 8T, 5T	4 grades Nb_3Sn NbTi
11. Maximum magnetic field of winding	12.6 T
12. Inductance	56 H (total)
13. Stored energy	12 GJ
14. Cooling	Pool boiling

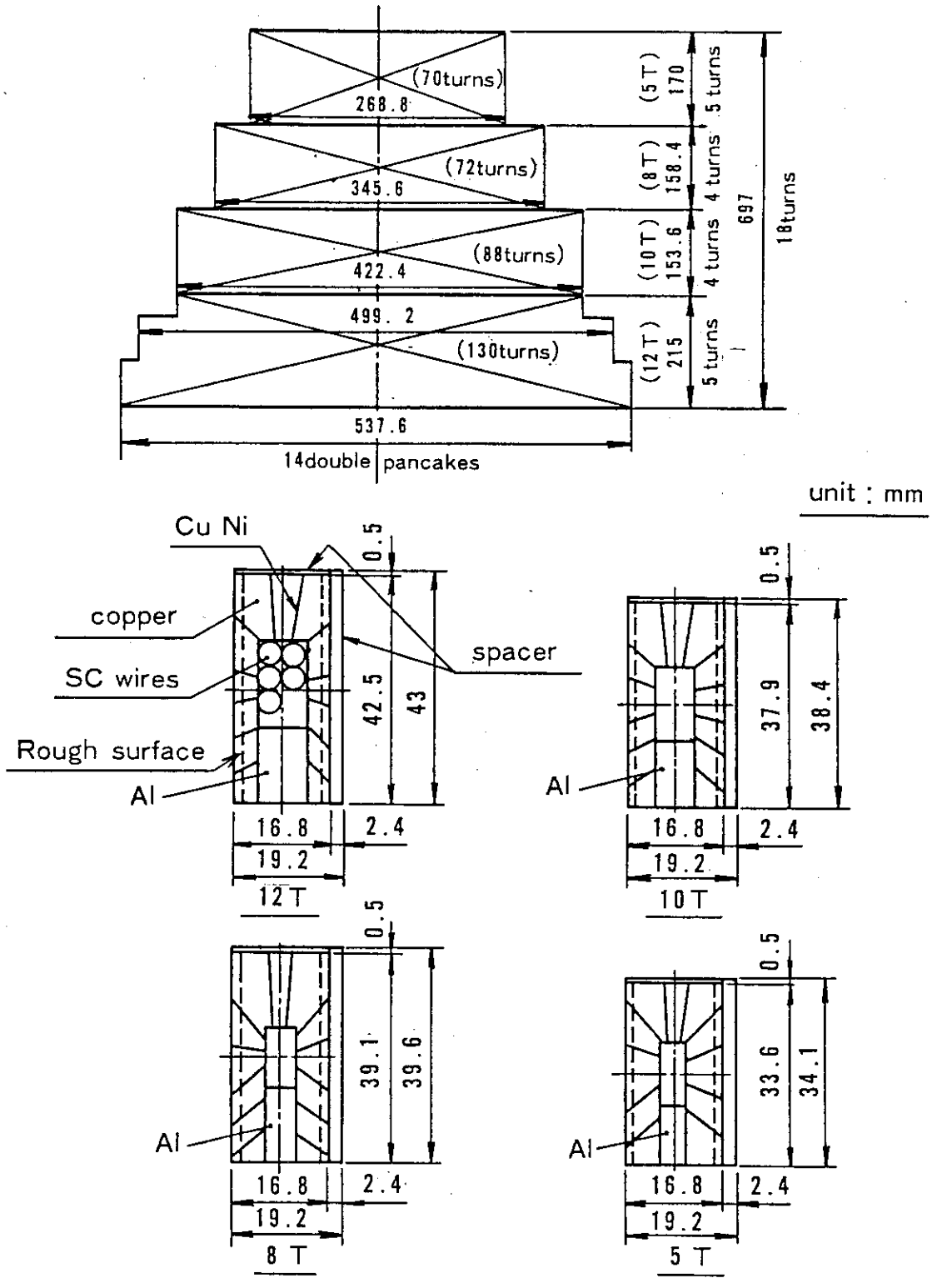

Fig.2.2.23(b) Dimensions of winding & conductors

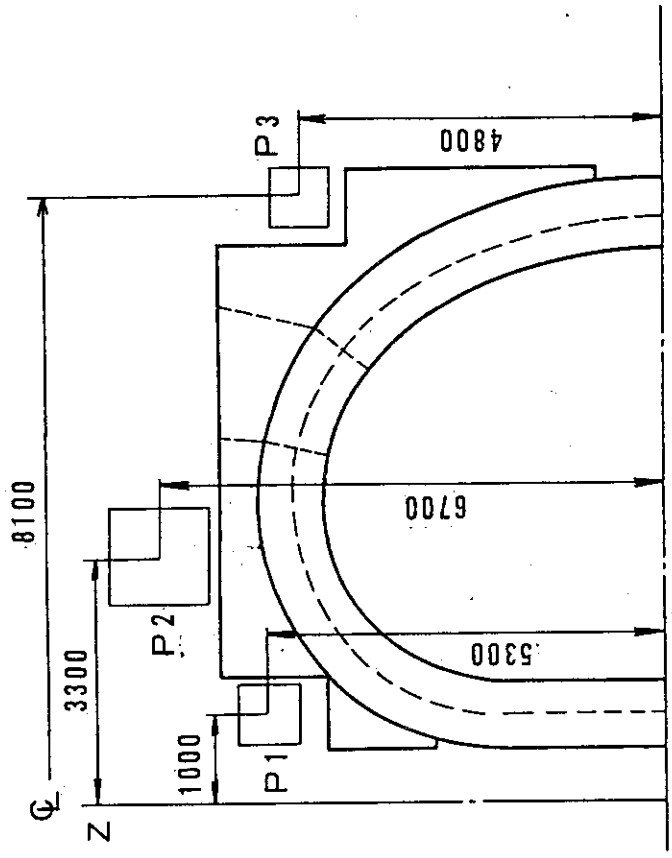

Coil No.	Position R(m)	Position Z(m)	Max. AT (MAX)	Number of torus	Max. Current (kA)	dimension WR	dimension Wz	Current Density (A/mm²)	Cooling	Components of Coil
P1	1.0	5.3	12.0	400	30	780	780	20.0	Forced Flow	Shaping
P2	3.3	6.7	34.0	1156	〃	1320	1320	20.0	Forced Flow	Shaping
P3	8.1	4.8	13.0	441	30	810	810	20.0	Forced Flow	Shaping

Fig. 2.2.24(a) PF Coils arrangement and parameters

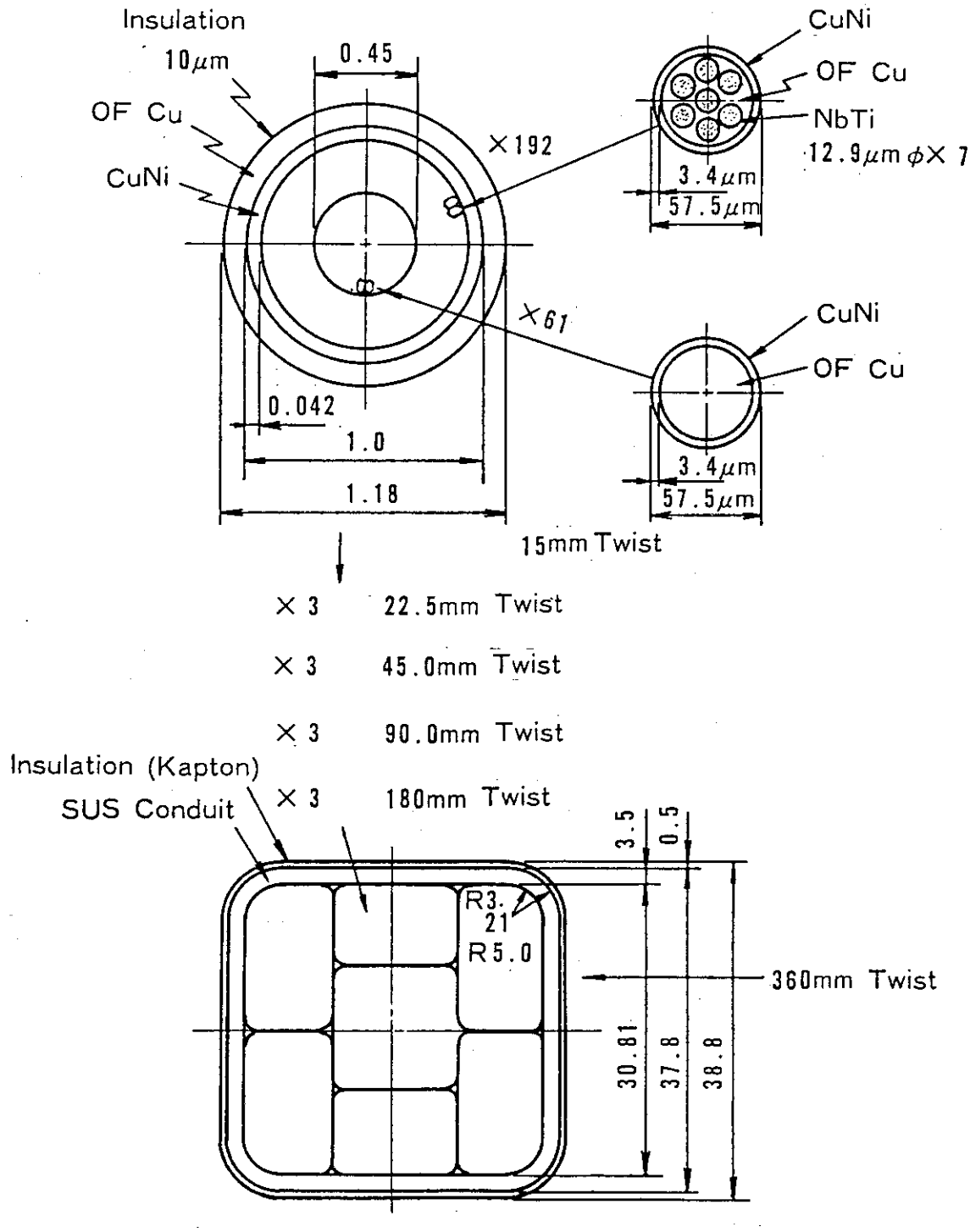

Fig.2.2.24(b) Cross section of a Conductor for PFC

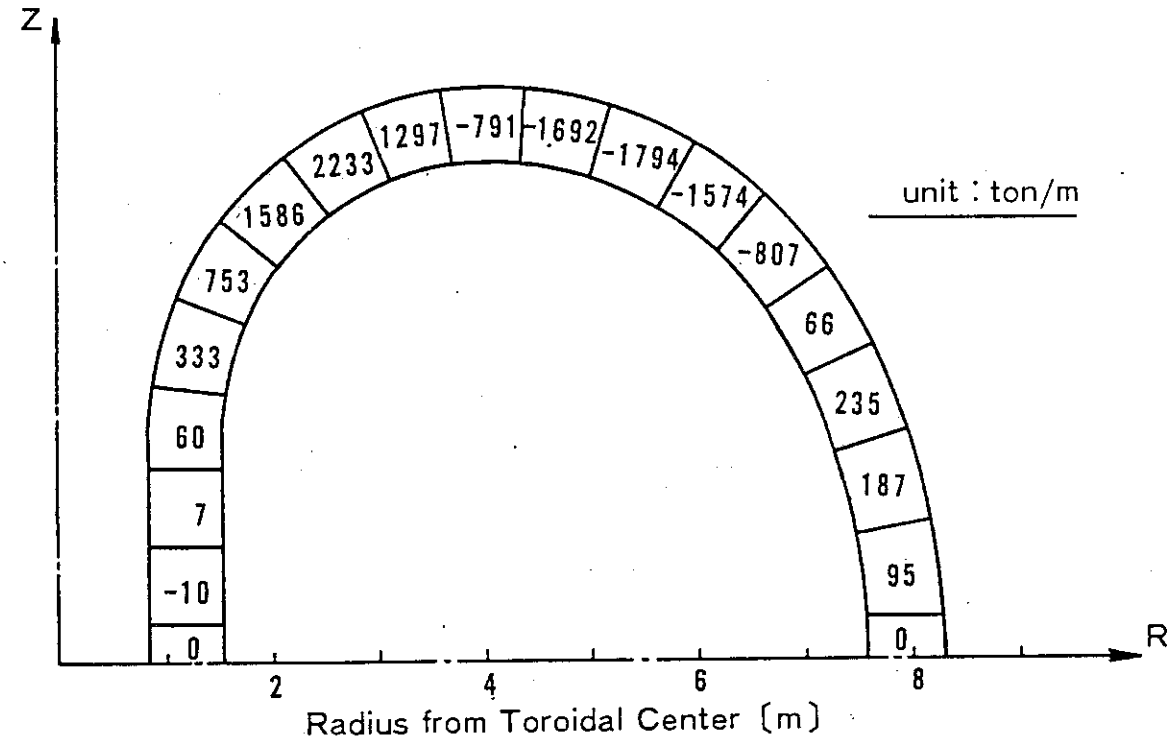

(a) Distribution of Overturning Force of Each Block on TF Coil

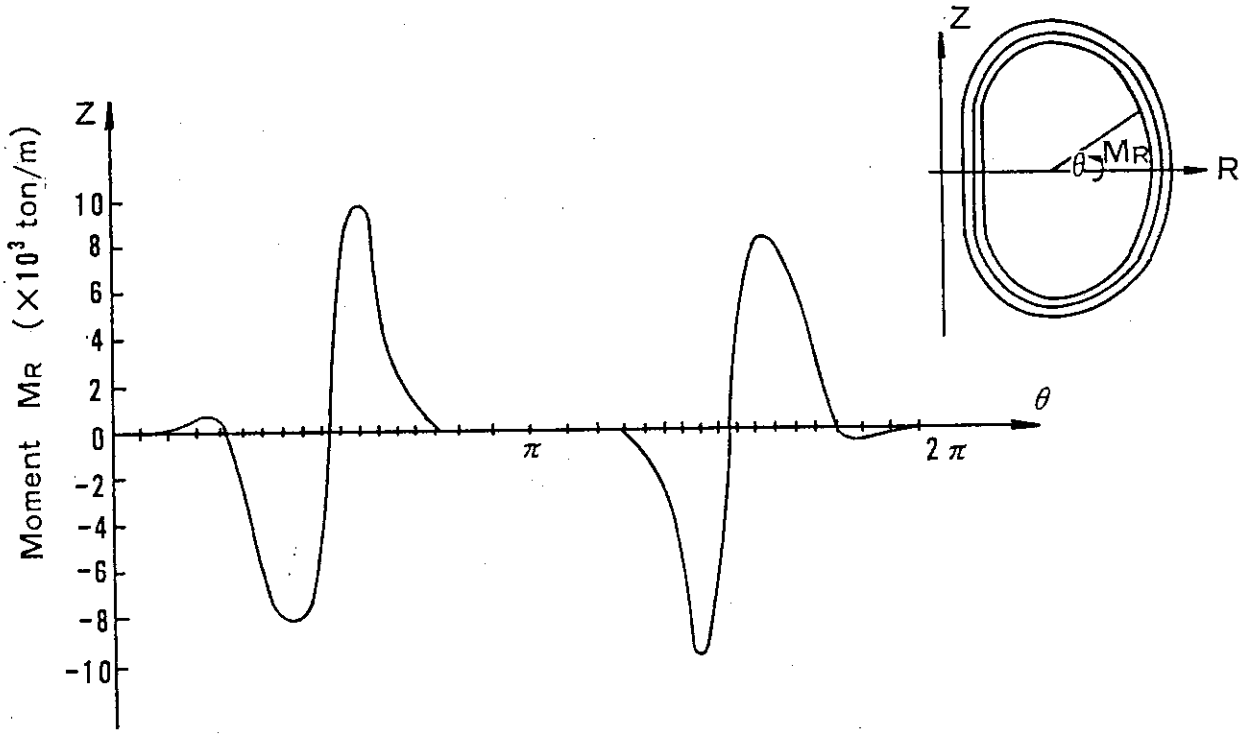

(b) Distribution of Overturning Moment per Unit Length Along the Coil Perimeter (Steady State)

Fig. 2.2.25 Overturning moments distributions of TFC

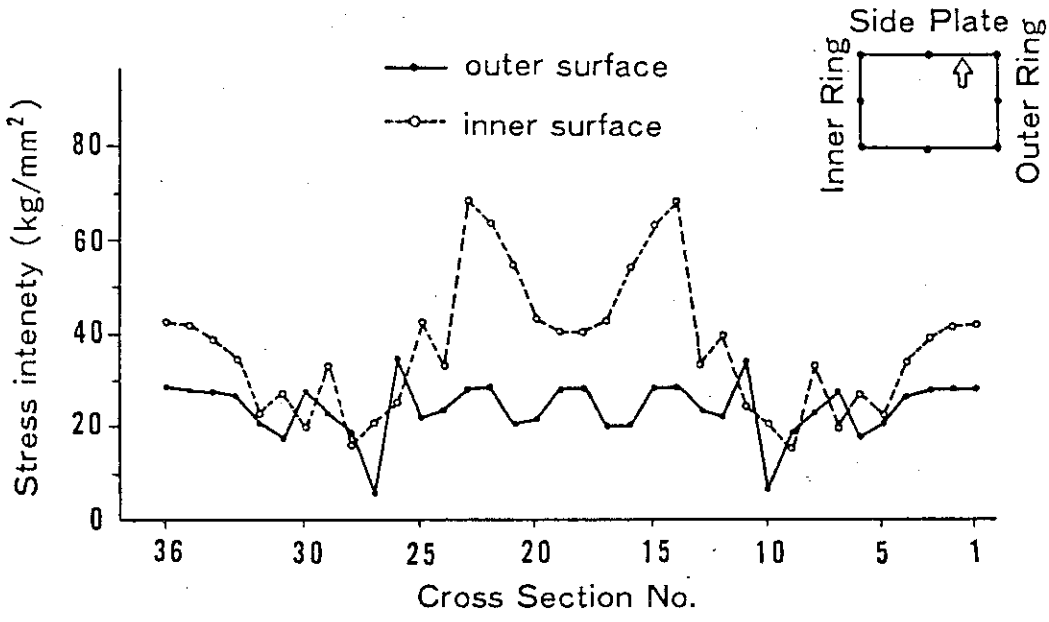

(a) Stress distribution of Side Plate
(by hoop froce and overturning force)

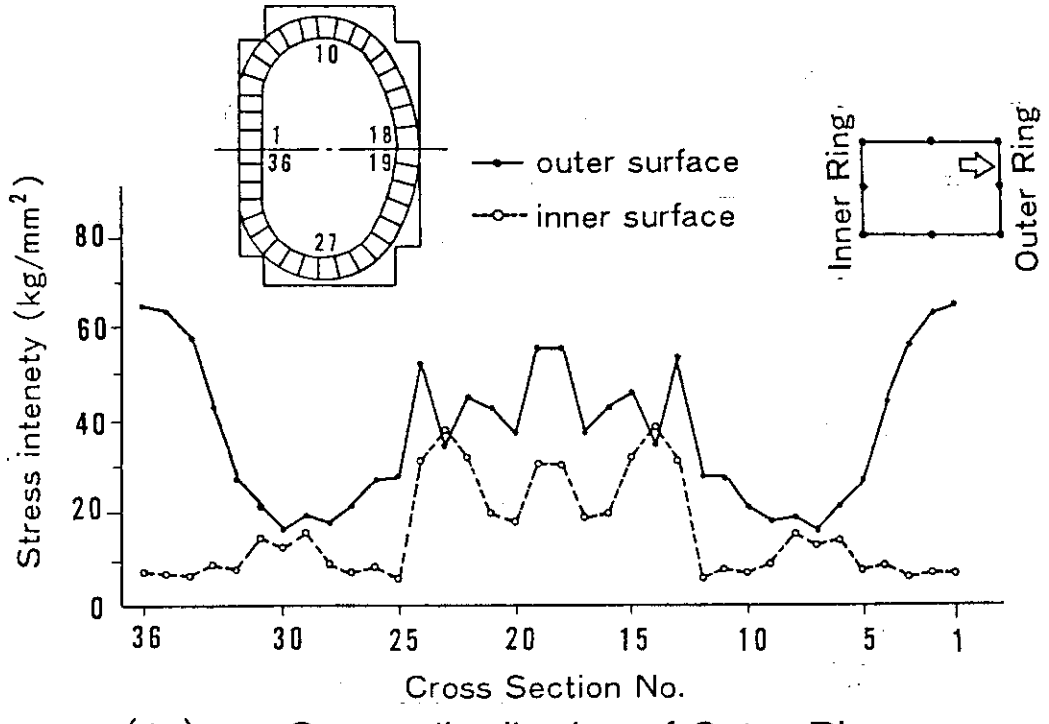

(b) Stress distribution of Outer Ring
(by hoop force and overturning force)

Fig. 2.2.26 Stress distributions of TFC He Case

Allowable Stress Intensity

Unit kg/mm^2

	Sm	1.5Sm
OFHC (Winding)	22.7	34
SUS 316LN (He Container / Shear Pannel)	53.3	80

Maximum Stress Intensity

		Pm	Sm	Pm+Pb	1.5Sm
Winding		9.0	22.7	14.5	34
He Container	Inner Ring	38.3	53.3	53.6	80
	Side Plate	39.3		69.2	
	Outer Ring	20.0		64.5	
Shear Pannel		28.7		60.2	

Table. 2.2.5 Evaluation of Stress Intensity

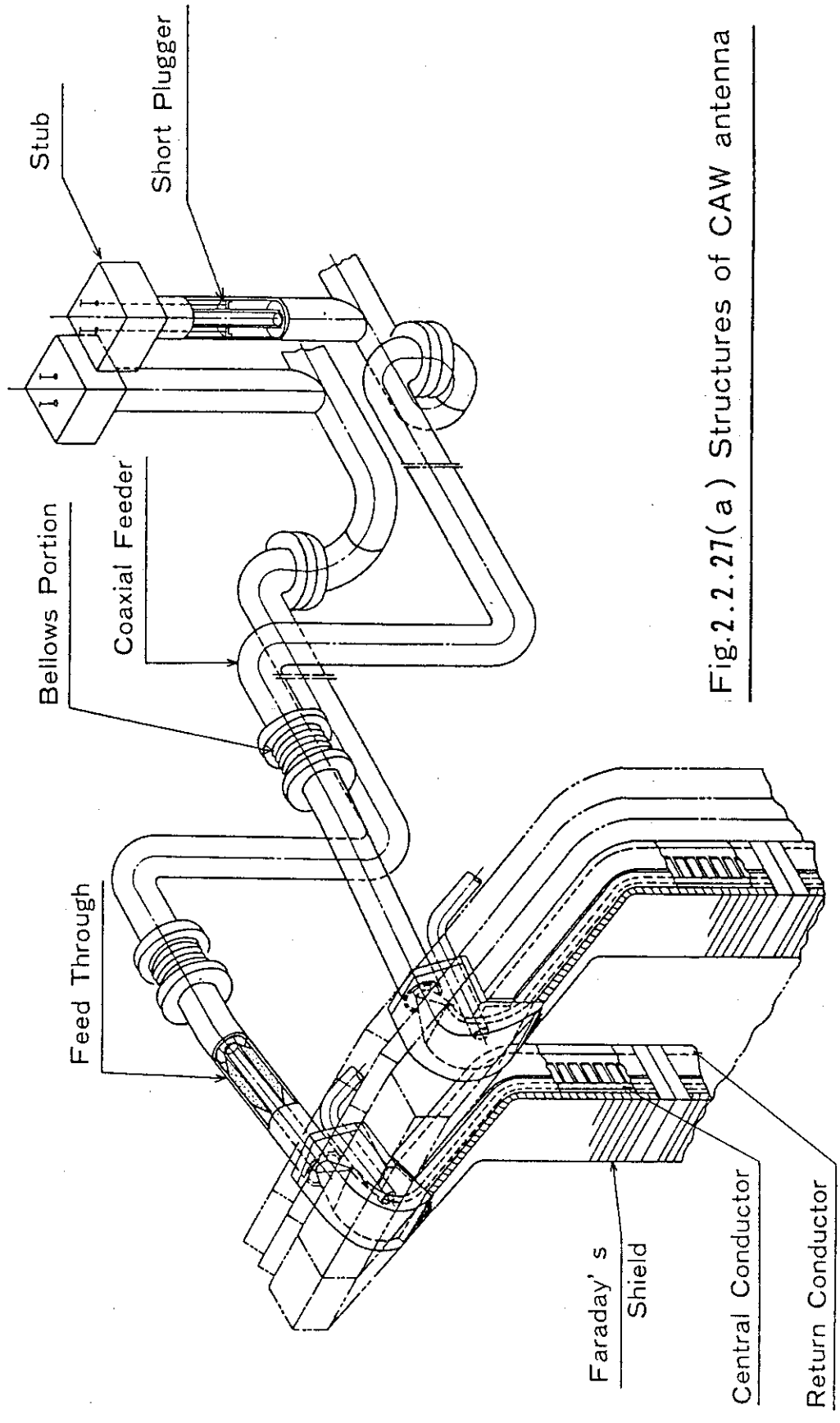

Fig.2.2.27(a) Structures of CAW antenna

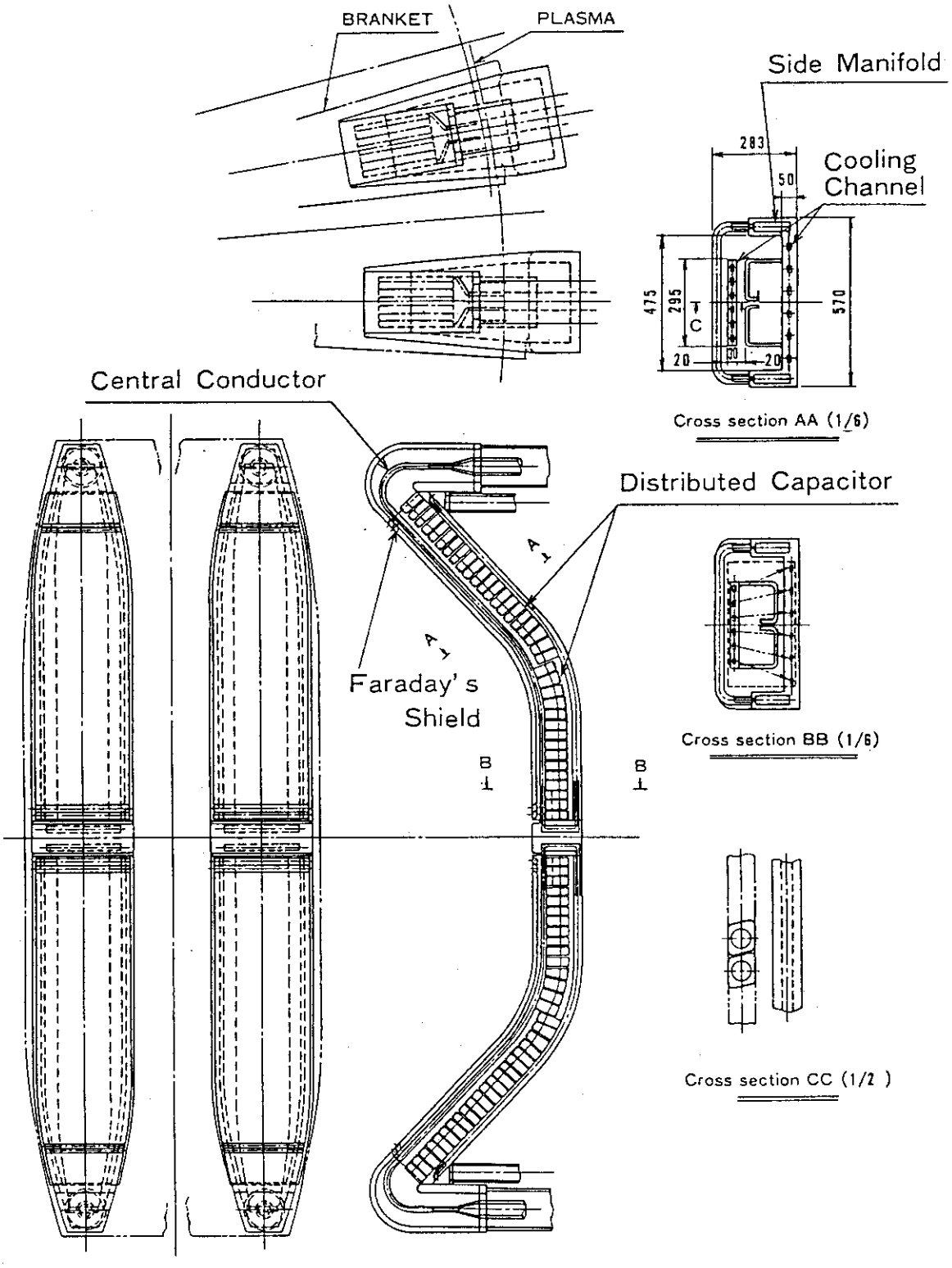

Fig. 2.2.27 (b) Strucfures of CAW antenna

Fig.2.2.27(c) Some Characteristics of Ion Cyclotron Wave Launchers for RFS-FER

	Specification of RF System			Antenna type		Power per antenna	Antenna		electrical length of antenna	distance central conductor -retern conductor (=wall) (mm)	distance central conductor Faradays Shield (mm)	toroidal distance between midpoints of antenna (m)	resistance of coaxial feeder (Ω)	characte-ristic Impead-ance (Ω)	maximum voltage on antenna (kV)
	Name	Frequency (MHz)	Injection Power (MW)	Antenna Array	Antenna port	(MW)	Length (m)	Width (mm)							
1	CAW	8	20	2×2	2	2.5	2.3	295	$\simeq \lambda s/4$	153	20	1.0	50	50	$\simeq$ 33
2	ICRF	69	30	4×2	2	1.88	1.09	400	$\simeq 3\,\lambda s/4$	150	20	1.0	50	50	$\simeq$ 33

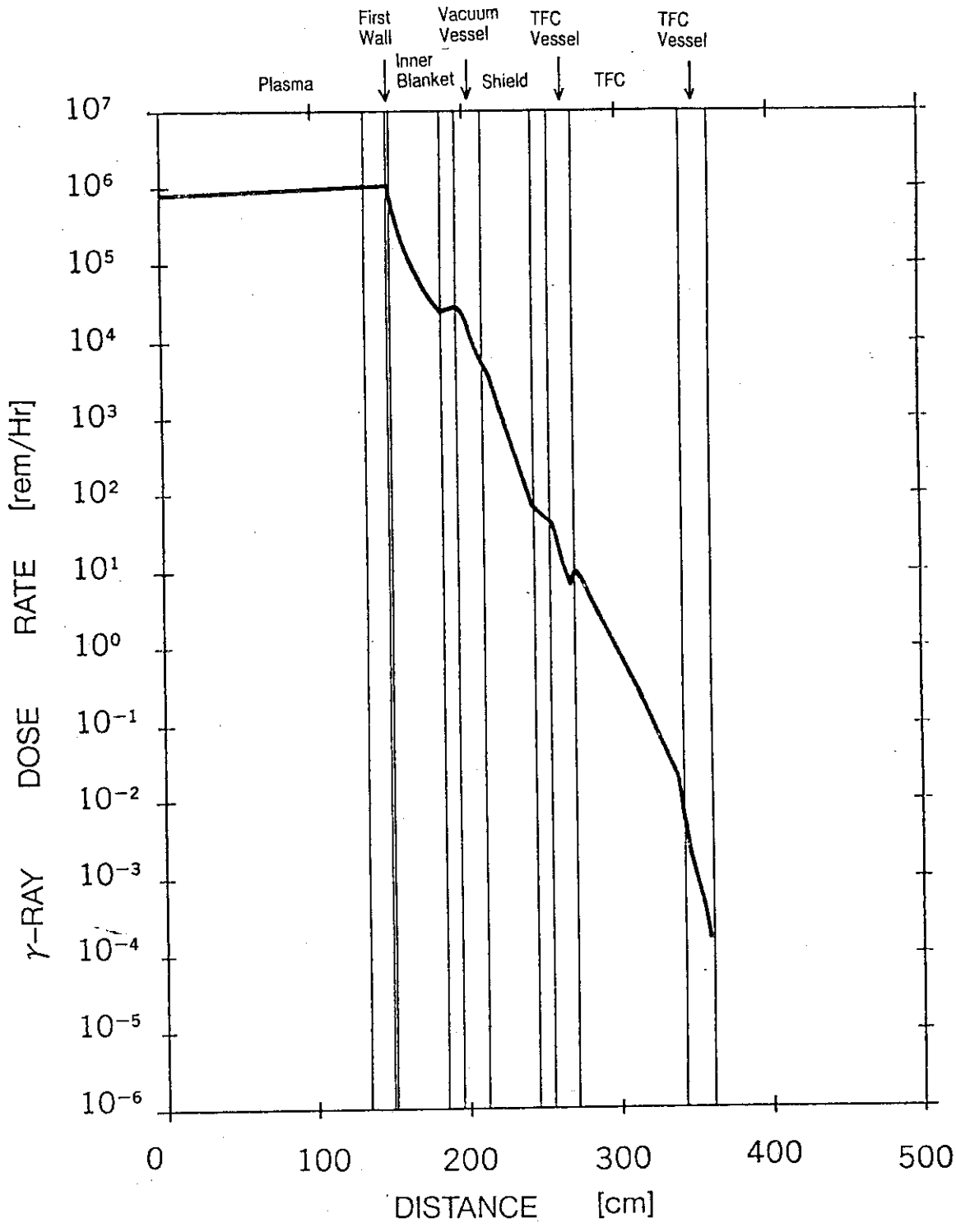

Fig. 2.2.28 Dose rate distributions in reacter core at 24hrs after reacter

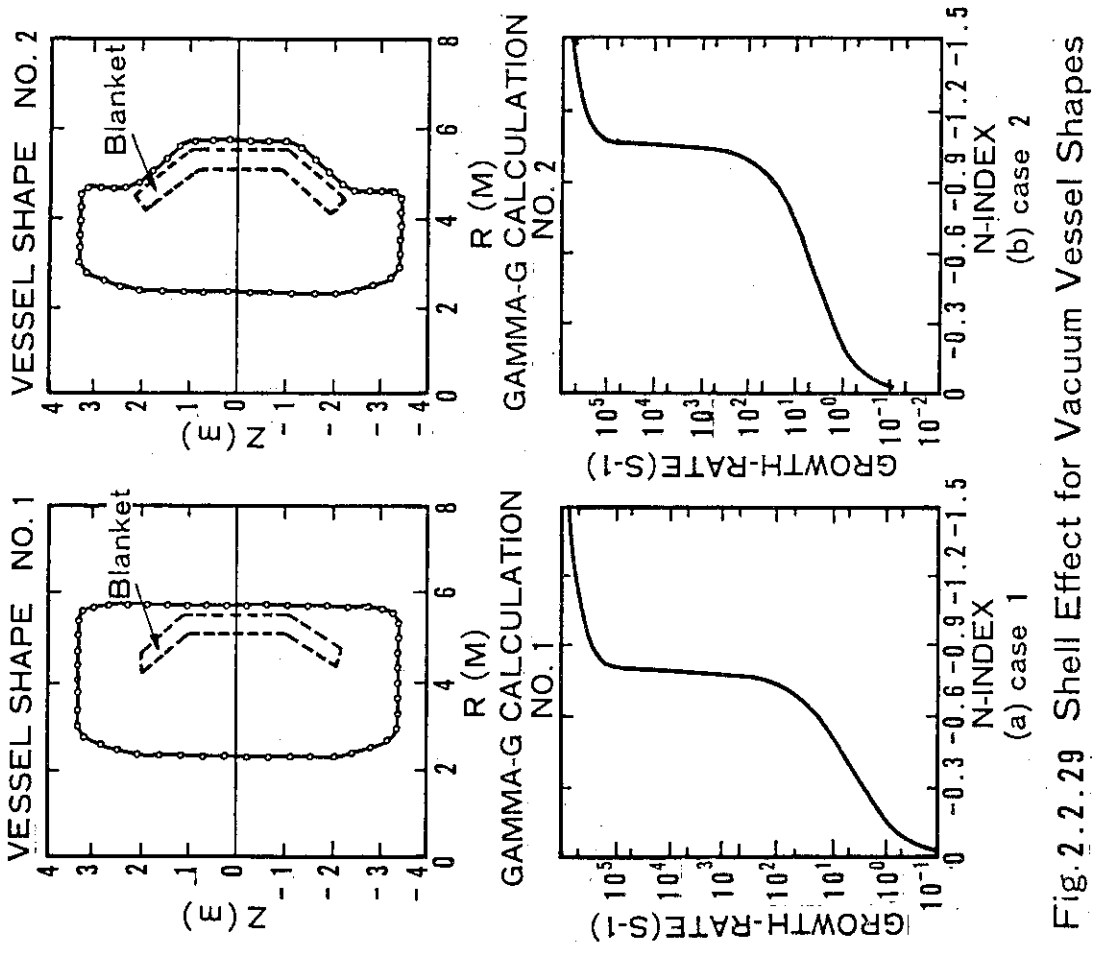

Table n_s & r_g^{-1}

case		1	2
n_s		0.780	1.042
r_g^{-1}	n=-0.6	56.5ms	155.3ms
	-0.7	20.2ms	99.9ms
	-0.8	7.8 μs	59.8ms
	-0.9	3.2 μs	30.0ms

r_g : Vertical Positional Instability Growth Rate

Vacuum Vessel :

- NO Bellows
- Vessel Thickness : 150mm
- Material : SUS

Fig. 2.2.29 Shell Effect for Vacuum Vessel Shapes

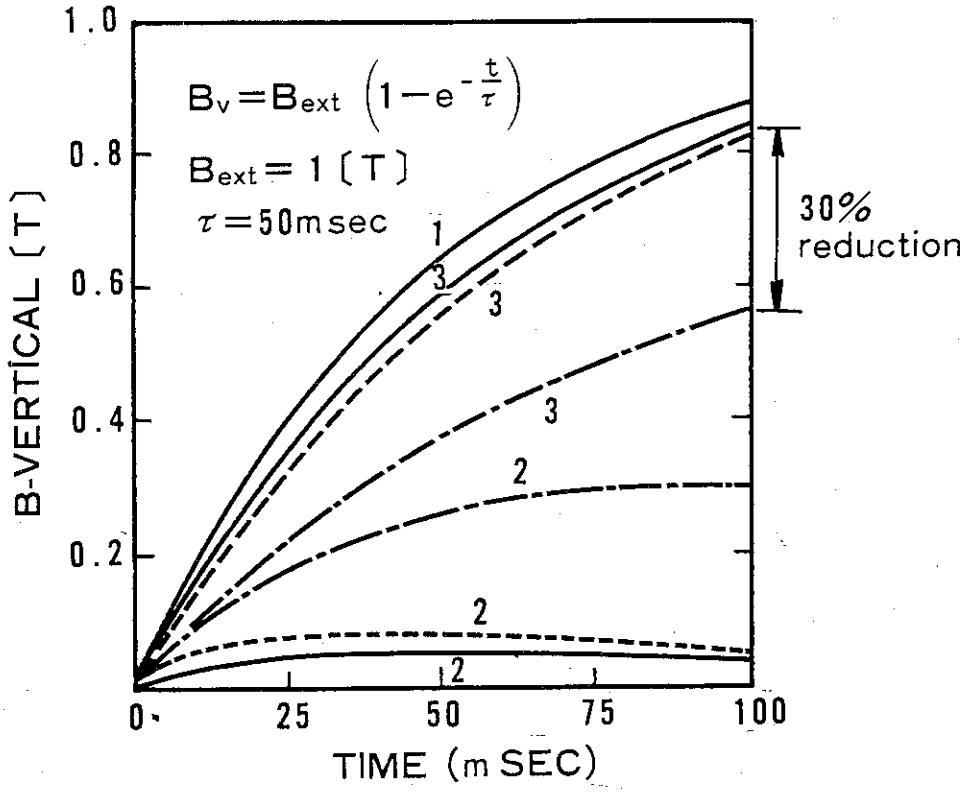

1.	External field
2.	Field of eddy current on vaccum vessel
3.	Field at the center of plasma

———	12 of electrical breaks
- - - - -	12 of Bellows
—·—	Neither break nor bellow

A thickness of vaccum vessel is 150mm.

Fig.2.2.30 Vertical Field Penetration (1)

Table 2.2.6 Weight of Reactor Components

(unit : ₹)

Item	Weight	Remarks
Blanket	410	inner module : 6 outer module : Center 10 Side 6
Divertor	10	Center module : 0.25 Side module : 0.2
Vacuum boundary vessel	700	
Shield	4000	
TF coil	4440	one of TF coil : 370
PF coil	750	
Supports (Duct support, Backing post et.)	820	
Bell-jar	3000	
Total	14,130	

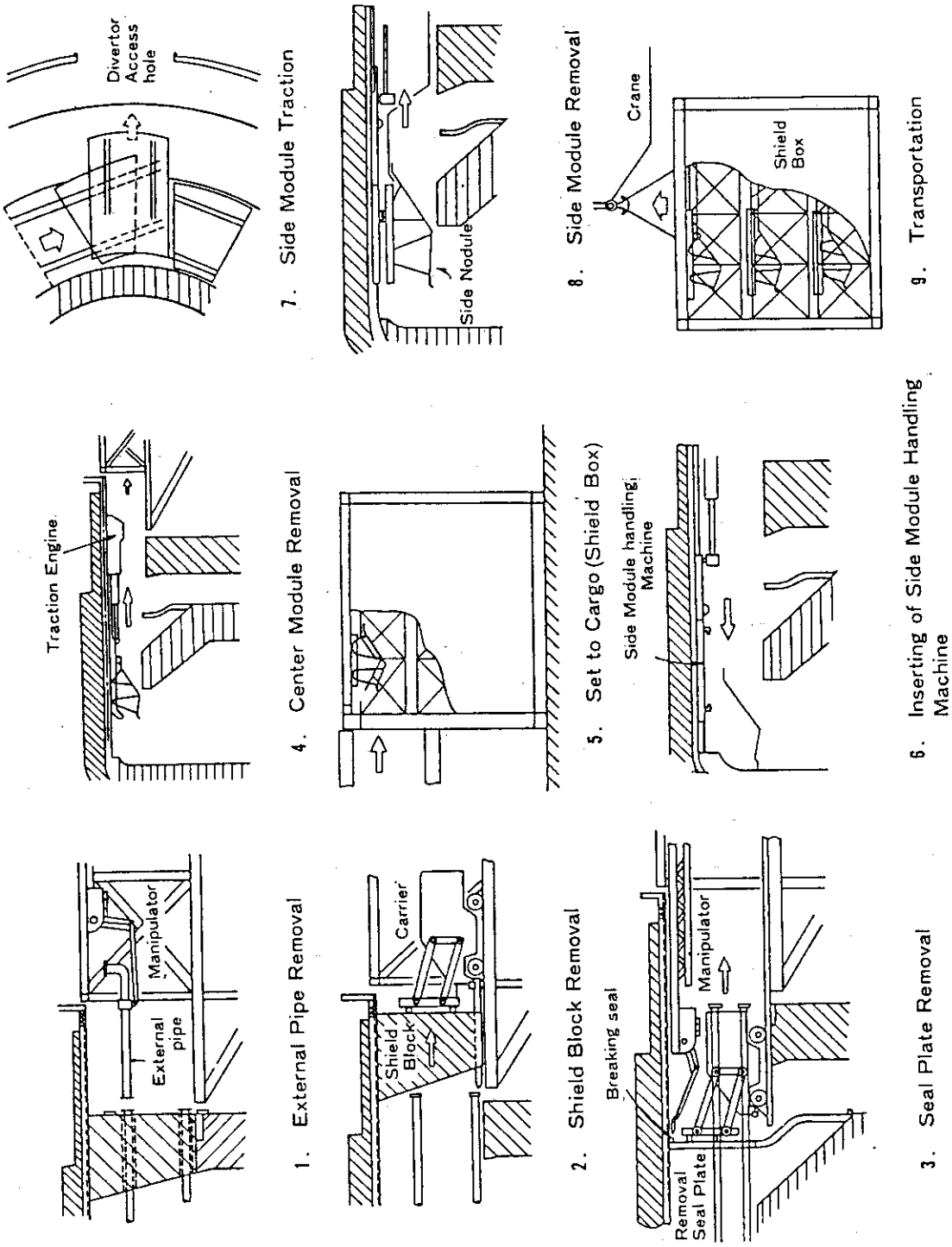

Fig. 2.2.31 Divertor Model Replacement Process

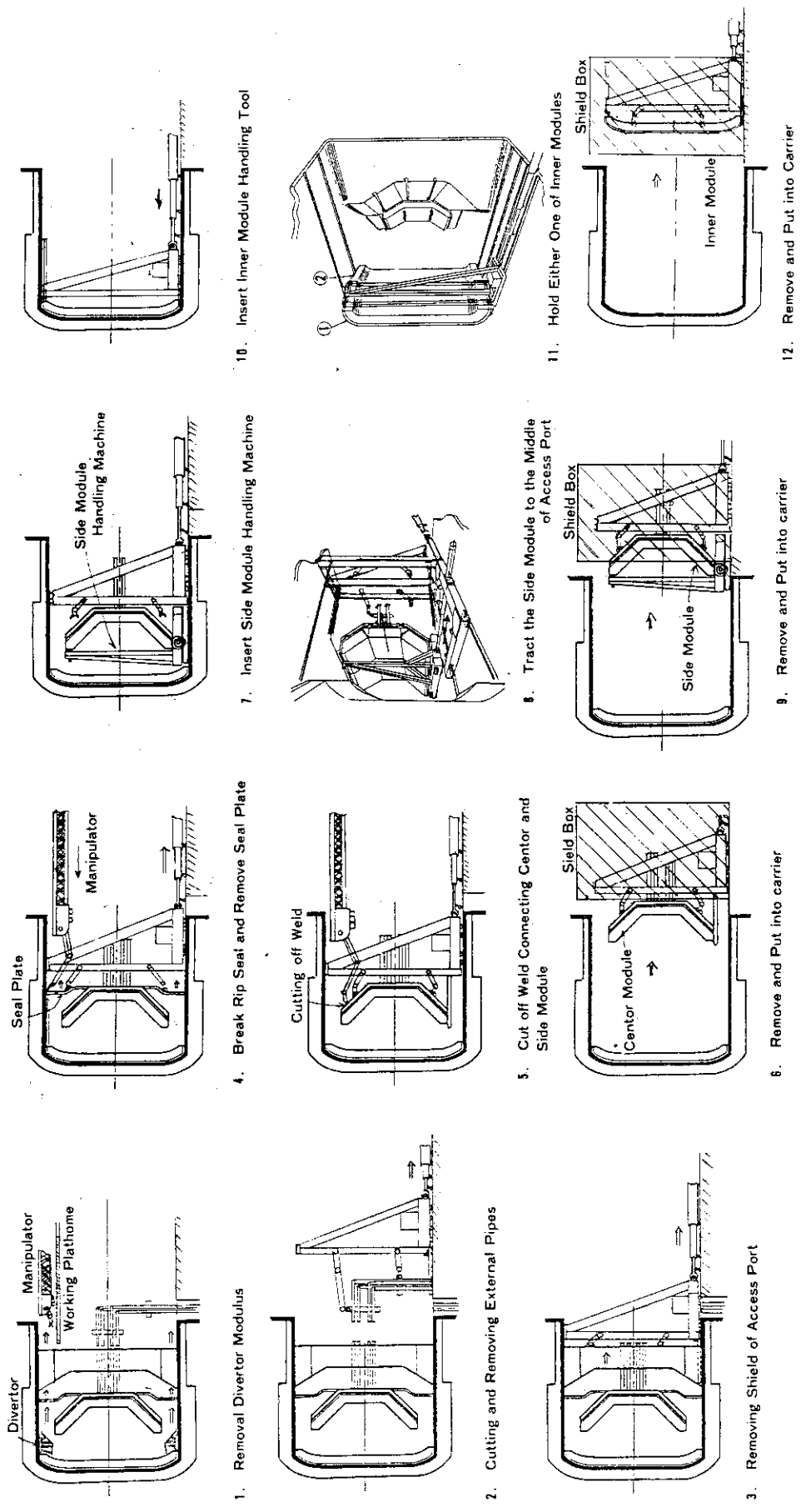

Fig. 2.2.32 Blanket Module Replacement Process

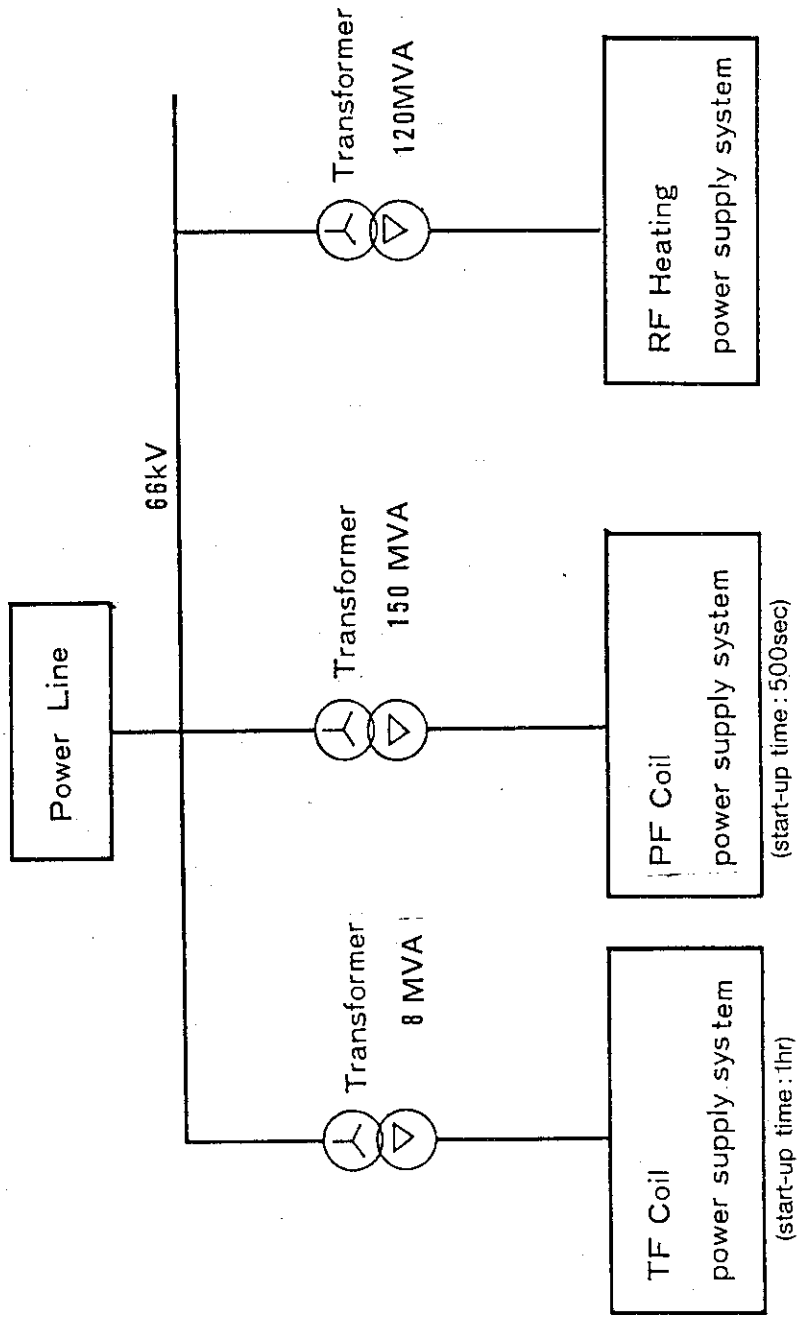

Fig. 2.2.33 System concept of the power supply system

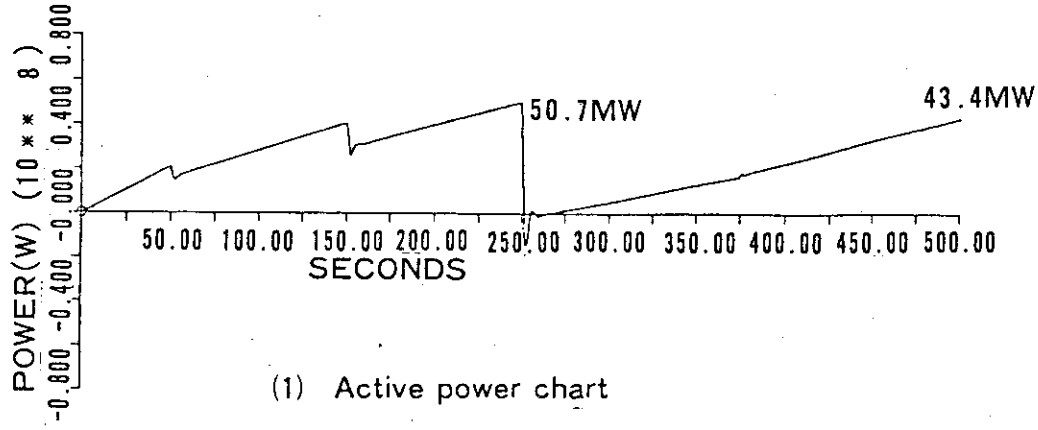

(1) Active power chart

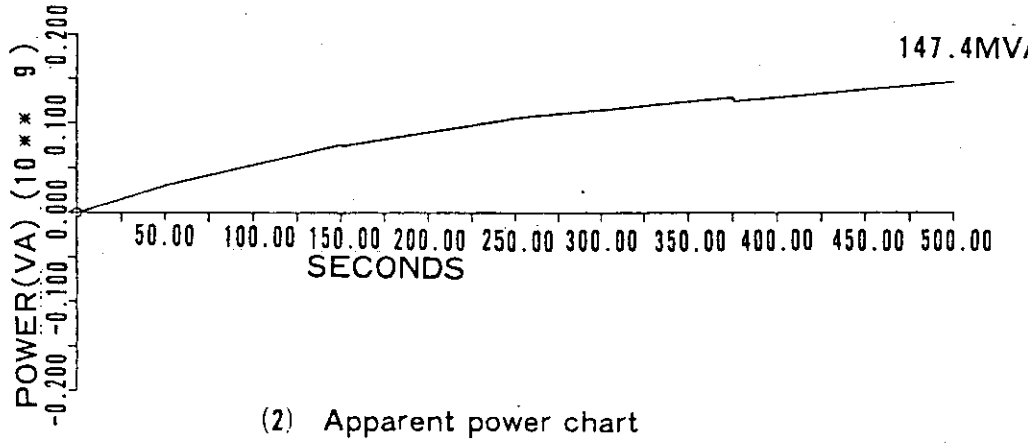

(2) Apparent power chart

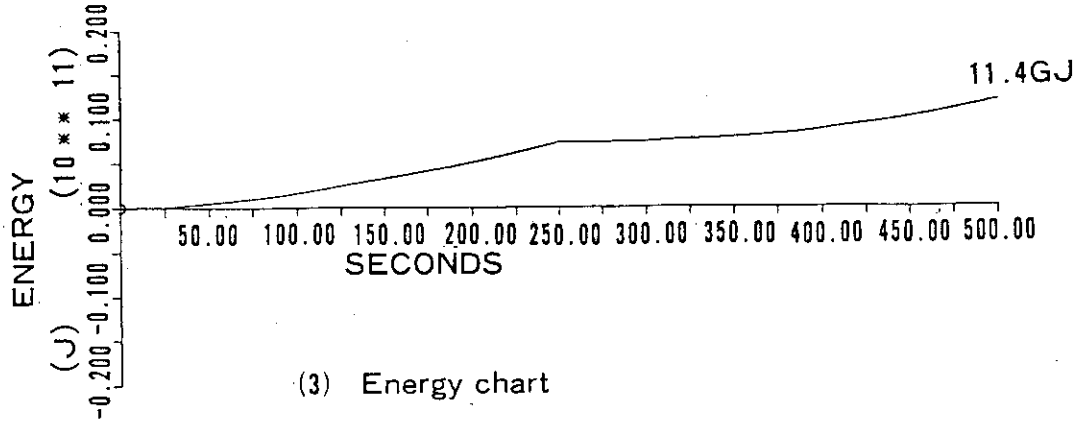

(3) Energy chart

Fig. 2.2.34 Power chart of PF Coil power supply

Table 2.2.7 Peak power and energy of power supply

Power supply systems	Kind of power supply		Start-up time	Peak power	Energy
TF Coil Power supply	Supplied directly from the power line		1 hr.	17 MVA	~20 GJ
PF Coil Power supply	Case I	Motor generator fly wheel	100 SEC	750 MVA	~12 GJ
	Case II	Motor generator fly wheel	300 SEC	245 MVA	~12 GJ
	Case III	Supplied directly from the power line	500 SEC	150 MVA (50.7MW)	~12 GJ
RF Heating Power supply	Supplied directly from the power line		500 SEC	120 MVA (60 MW)	~25 GJ
RF Current Drive Power Supply	Supplied directly from the power line		Normal operation at flat top		

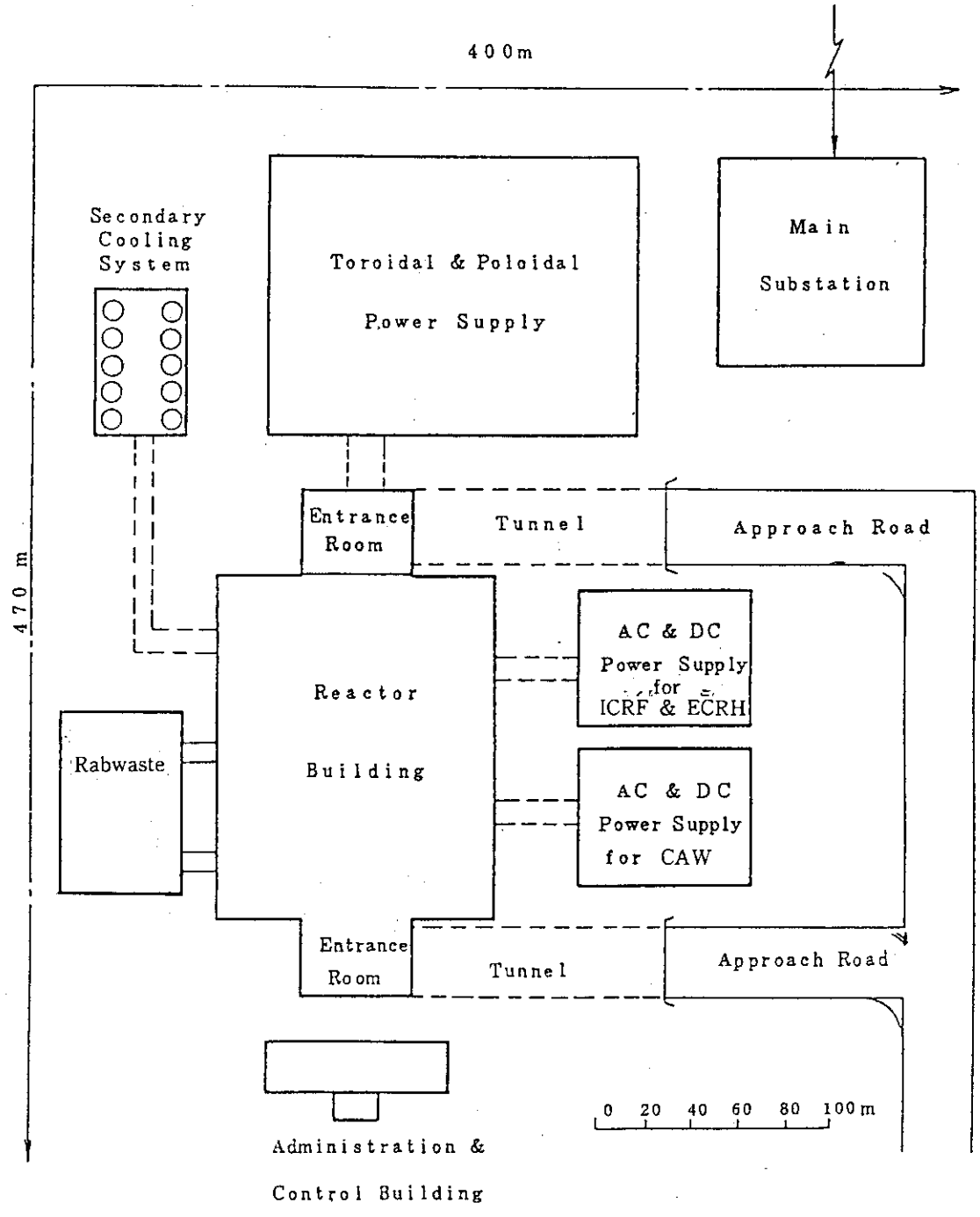

Fig. 2.2.35(a) Site Plan

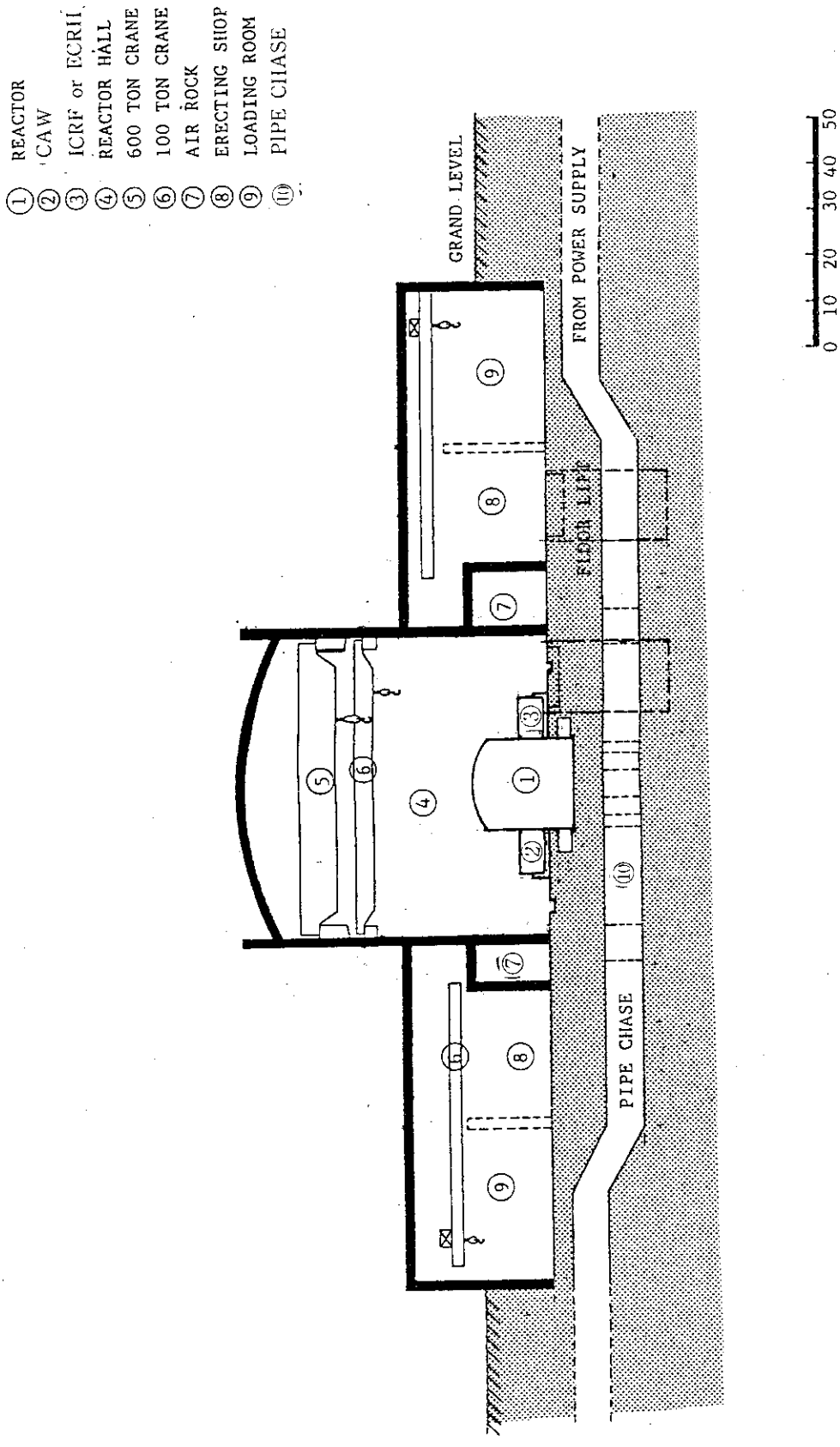

Fig. 2.2.35(b) Reactor Building

Part 2 Comparison of RFS-FER with Reference-FER

Introduction

(1) Specification (Basic Items for Comparison)

No.	Item	Comparison	RFS-FER	Reference-FER
1	Plasma cross section	Equal	1.1m×1.65m	1.1m×1.65m
2	Aspect ratio	Possibly small in RFS-FER	3.6 (R = 4m)	5.0 (R=5.5m)
3	Max magnatic field on TF coil	Equal	12T (Bo=4.5T)	12T (Bo=5.7T)
4	Operation	Different	Steady state	Pulse

Table 2.2.8 Comparison of RFS-FER with Reference FER (15 sheets)

JAERI — M 84 — 107

Introduction (continued)

(2) Design Concept (Basic Items for Comparison)

	RFS-FER	Reference FER
OH Coil	none	with
Bellows for oneturn resistance	none	with
Vacuum Boundary Vessel	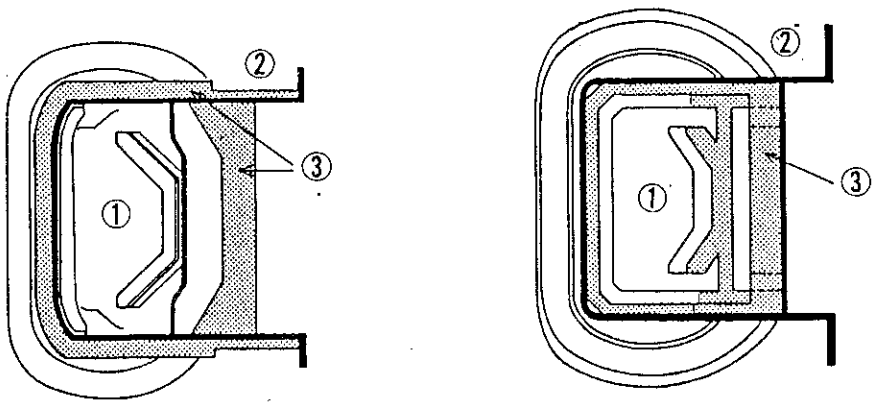	

①Plasma vacuum region ③Shield

②Cryostat region

	Items	unit	RFS-FER	Refererence-FER	Remarks
1	Specification				
1.2	Plasma Parameter				
(1)	Average plasma temperature	keV	13	10	
(2)	Average plasma density	m^{-3}	9×10^{19}	1.36×10^{20}	
(3)	Effective mean charge	—	<1.5	<1.5	
(4)	Toroidal beta	%	4.7	4.0	
(5)	Safety factor	—	2.5	2.5	
(6)	Thermonuclear Power	MW	250	440	
(7)	Neutron Wall load(average)	MW/m^2	0.9	1.0	
1.2	Current Drive				
(1)	Method	—	CAW	———	
(2)	Injection Power	MW	20	———	
(3)	Frequency	MHz	8	———	
(4)	Wave length(Z direction)	m	1.0	———	
1.3	Additional heating				
	Method	—	ICRF	ICRF	
	Injection power	MW	30	15	
	Frequency	MHz	69	88	
	Mode	—	2nd Harmonics(D)	2nd Harmonics(D)	

	Items	Unit	RFS-FER	Reference-FER	Remarks
1.4	Preionization				
	Method	—	ECRF	ECRF	
	Injection power	MW	10	10	
	Frequency	GHz	126	160	
	Mode	—	Ordinary	Ordinary	
1.5	Tokamak System				
	Major Radius	m	4.0	5.5	
	Minor Radius	m	1.1	1.1	
	Elongation	—	1.5	1.5	
	Toroidal field on axis	T	4.5	5.7	
	Toroidal ripple	%	$\leqq$1.0	$\leqq$0.75	
	Plasma current	MA	6.4	5.3	
	Impurity control	—	double null poloidal divertor	double null poloidal divertor	
	No. of TFC	—	12	14	
	Aspect ratio	—	3.6	5	
	Volume of Plasma	m^3	143	200	
1.6	Operation Scinario				
	Start up	s	500	~10	
	Shut down	s	100	~15	
	Burning cycle	times/life	1000	$\sim 10^5$	

	Items	Unit	RFS-FER	Reference-FER	Remarks
2	Design Concept				
2.1	Basic Assumption				
	OH coil	—	none ※	with	※in advantage of steady state operation
2.2	Configuration				
2.2.1	Vacuum Boundary Vessel				※to minimize vacuum volume of plasma vacuum vessel
	Type	—	Common	Common	
	Location		between blanket & shield※	behind shield	
	Structure		thick plate without bellows	thick plate and bellows	
2.2.2	Divertor	—			
	Type		separate from blanket	separate from blanket	
2.2.3	First Wall/Blanket	—			
	Type		Integrated※	Separate	※due to reduction plasma disruption

	Items	Unit	RFS-FER	Reference-FER	Remarks
2.2.4	Shell	—	making use of vacuum boundary vessel※	passive shell coils of Al located in front of blanket	※due to elimination of bellows out of vacuum boundary vessel
2.2.5	Shield				
	Composition	—	single	double (core + biological shield)	
	Location	—	outside the plasma vacuum region	inside the plasma vacuum region	
2.2.6	Magnet Coil				
	TF Coil				
	number	—	12	14	
	cooling	—	pool cooling	pool cooling	
	PF Coil				
	system	—	hybrid system without OH coil 3coils for half plain	hybrid system with OH coil 12coils for half plain	
	cooling	—	forced cooling	forced cooling	

	Items	Unit	RFS-FER	Reference-FER	Remarks
2.2.1	Cryostat				※due to elimination of OH coil
	Type	—	bell-jar	bell-jar	
	Breaks for one turn resistance		none ※	with	
3	Result				
3.1	Vacuum Boundary Vessel				
	(1)chamber surface area	m^2	270	350	
	(2)chamber volume of vacuum	m^3	290	470	
	(3)material	—	SUS	SUS	
	(4)one turn resistance	Ω	$\sim 10^{-6}$	2×10^{-4}	
	(5)nuclear heating	W/cm^3	0.36 ※	0.02	※inside shield
	(6)max. temperature	℃	~room temp	room temp	

	Items	Unit	RFS-FER	Reference-FER	Remarks
3.2	Divertor				
	(1) neutrization plate	—	SiC	SiC	
	(2) structure material	—	SUS	SUS	
	(3) coolant	—	Water	Water	※normal operation
	(4) heat load ※	W/m²	88	100	
	(5) coolant temp. inlet/outlet	°c	60/80	60/80	
	(6) max. temp.	°c	260	285	
	(7) erosion	mm/yr	～2	～2	control average energy of incident ion＜5eV
3.3	First Wall/Blanket				
	First Wall	—	Integrated※ Stainless steel with groove	Separate SiC ceramic bonded with coolant tube	※decrease of number of plasma disruption
	Blanket	—	double breeder	double breeder	
	Tritium breeder	—	Li_2O	Li_2O	
	Neutron multiplier	—	Be	Be	
	Structure material	—	SUS	SUS	
	Thickness (FW+Blanket)	m	0.35～0.45	0.4	
	Coolant	—	Water	Water	

	Items	Unit	RFS-FER	Reference-FER	Remarks
	Tritium purge gas	—	He	He	
	Breeding ratio	—	1.15	1.05	
	Nuclear heating in structure material	W/cm³	1st region 19 2nd region 1.5	1st region 22.7 2nd region 1.7	
	Temp. coolant inlet/outlet	℃	50/100	50/100	
	Max. Temp. of first wall※	℃	1060	410	※ at disruption (RFS. ……SUS, R. ……SiC)
	Max. Temp. of breeder	℃	~960	960	
	Max. Temp of structure	℃	260※※	150	※※at ordinary operation in first wall integrated type, SUS)
	Volume of breeder	m³	57	99	
3.4	Shield			(core) | (bio)	
	(1) material	—	SUS	SUS | SUS	
	(2) thickhess				
	inner	m	0.35	0.4 | —	
	outer	m	1.0	0.7 | 1.0	
	(3) coolant	—	Water	Water Water	
	(4) nuclear heating	W/cm³	6.4×10^{-2} (Max)	0.1 (Max)	
	(5) Temp. of coolant inlet/outlet	℃	60/80	60/80	
	(6) Max. temp.	℃	R.T.	R.T.	
	(7) Temp. of outer surface	℃	R.T	R.T	

	Items	Unit	RFS-FER	Reference-FER	Remarks
3.5	Magnet Coil				
3.5.1	TF Coil				
	(1) No. of coils	—	12	14	
	(2) Bore diameter	m	9/5.7	9.1/6.1	
	(3) Magnetic Field on Axis	T	4.5	5.7	
	(4) Max. Magnetic Field	T	12	12	
	(5) Conductor	—	Nb_3Sn+NbTi	Nb_3Sn+NbTi	
	(6) Current	kA	20.8	18.7	
	(7) Total AT	MAT	90	157	
	(8) Stored Magnetic Energy	GJ	12	30	
	(9) Electromagnetic Force(Hoop)	₹	6.96×10^4	1.31×10^5	
	(10) Cooling	—	pool cooling	pool cooling	
3.5.2	PF Coil				
	(1) Function	—	EF	EF, OH	
	(2) No. of coils	—	3 × 2	12 × 2	
	(3) largest diameter	m	16.2	19.2	
	(4) Conductor	—	NbTi	NbTi	
	(5) Max. Current	kA	30	30	

	Items	Unit	RFS-FER	Reference-FER	Remarks
	(6) Max induce voltage	V			
	(7) Total AT	MA	113.6	83.6	
	(8) Stored Magnetic Emergy	GJ	15.5	6.3	
	(9) Electro-Magnetic Force (Hoop)※	₹	2.3×10^5	5.1×10^4	※Max. value
	(10) Cooling		forced flow	forced flow	
3.6	Cryostat				
	(1) Type	m	Bell-jar	Bell-jar	
	(2) Outer Dimention				
	Diameter	m	20	23	
	Height	m	22	23	
	(3) Volume	m^3	6900	9100	
	(4) Material	—	SUS	SUS	

	Items	Unit	RFS-FER	Reference-FER	Remarks
3.7	RF • NBI				
3.7.1	C A W				
	usage		current drive		
	injection power	MW	20		
	operating time	Sec	continuous	none	
	no. of unit	—	2		
	antenna	—	loop type		
3.7.2	ICRH				
	usage		additional heating	additional heating	
	injection power	MW	20	15	
	operating time	Sec	100～500	10	
	no. of unit	—	2	1	
	antenna	—	loop type	loop type	
3.7.3	ECRH				
	usage		primary heating	primary heating	
	injection power	MW	10	10	
	operating time	Sec	10	10	
	no. of system	—	1	1	
	antenna	—			

No.	Items	Unit	RFS-FER	Reference-FER	Remarks
3.7.4	NBI				
	usage		none	additional heating	
	injection power	MW		30	
	no. of unit.			3	
3.8	Radioactiviey (Shield)				
	TF coil (operating)	mr/hr	$\sim 10^8$ ※	$\sim 10^9$ ※※	※1-D calculation
	reactor room (operating)	〃	$\sim 10^6$	$\sim 10^5$	※※2-D calculation
	(24Hr after shut down)	〃	< 2.5	< 2.5	
3.9	Electro-magnetics				※Vertical positional instabi-lity growth rate
	Shell effect※	ms	~ 50	~ 100	
	Bv penetration	%	70	100 ※※	※※with 14 bellows
3.10	Reactor Component Weight				
	Blanket	$	410	500	
	Divertor	〃	10	13	
	Vacuum boundary vessel	〃	700	1100	
	Shield	〃	4000	4800	
	TF coil (include shear pannel)	〃	4440	5040	
	PF coil	〃	750	1370	
	Supports (duct, Backing post et.)	〃	820	1850	
	Bell-jar	〃	3000	4000	
	Total	〃	$\sim 14,000$	$\sim 19,000$	

No.	Items	Unit	RFS-FER	Reference-FER	Remarks
3.11	Maintenance				
3.11.1	Divertor				
	(i) No. of module/sector		3	3	
	(ii) Max. Weight of one module	$	0.25	0.3	
	(iii) Removal way for side module		double straight line	double straight line	
3.11.2	Blanket				
	(1) Outer Blanket				
	(i) No. of Module/sector		3	3	
	(ii) Max. Weight of one module	$	10	12	
	(iii) Removal way for side module		rotation/straight line	rotation/straight line	
	(2) Inner Blanket				
	(i) No. of Module/sector		2	3	
	(ii) Max. Weight of one module	$	6	9	
	(iii) Removal way for side module		straight line	straight line	

No.	Items	Unit	RFS-FER	Reference-FER	Remarks
3.12	Power Supply				
3.12.1	Magnet System				
	(1) Peak·Power				
	TF Coil	MVA	8 ※	17※	
	PF Coil	MVA	147 ※※	2000※※※	rise time ※ 1 hr ※※500 s ※※※ 11 s
	(2) Energy				
	TF Coil	GJ	13※	20※	
	PF Coil	GJ	12※※	10※※※	
3.12.2	RF. NBI System				
	(1) Peak Power				
	RF	MVA	200	130	
	NBI	MVA	——	400	
	(2) Energy				
	RF	GJ	25	7	
	NBI	GJ	——	7	

2.3 RF Launcher Design for FER

RF plasma heating of FER is composed of three heating systems according to frequency ranges, that is ICRF, LHRF and ECRF.
The general restriction of this design is the aperture height limitation (±75 cm from the mid-plane) of r.f injection because of the attachment of plasma stabilization shell to the first wall.

In ICRF heating, the frequency is 88 MHz, the input power launched by 4 loop antennae is 15 MW for the first 10 sec and 5 MW for the following 100 sec as shown in Table 2.3.1. Specifications of antenna are shown in Table 2.3.2. The power supply is about 30 MVA as shown in Fig. 2.3.11. The typical voltage and current distribution along a line are shown in Fig. 2.3.1. The bird's eye view of a standard all metal type antenna is shown in Fig. 2.3.2. The lateral cross sectional view is shown in Fig. 2.3.3. The heat load of the antenna is shown in Table 2.3.3. The electromagnetic forces at plasma disruption and mechanical stress are shown in Figs. 2.3.4, 2.3.5 and Table 2.3.4. The outer frame structure of Faraday shield shown in Fig. 2.3.4 is adopted to reduce the electromagnetic force. The most important problem of this design is not only the electromagnetic force but also the larger r.f power loss of the Faraday shield as shown in Table 2.3.5. It cannot be helped that the gaps of Faraday shield are more separated to reduce the r.f power loss as shown

in Fig. 2.3.6, so that the heat flux from plasma is deposited on the conductor surface. The cross sectional view of ICRF launcher is shown in Fig. 2.3.7. The choke type coaxial cable connector shown in Fig. 2.3.8 is used to make the launcher replacement procedure simple. Two feed throughs are located for safety and SF_6 gass between then can cool the ceramic heat due to tanδ loss. The installation and replacement of ICRF launcher are illustrated by Figs. 2.3.9, 2.3.10 and Table 2.3.6.

In LHRF heating, the frequency is 2 GHz, the input power launched by 4 Grill launchers is 15 MW for the first 10 sec and 5 MW for the following 100 sec. The specifications of LHRF heating are shown in Tables 2.3.7 and 2.3.8. The power supply is about 70 MVA as shown in Fig. 2.3.18. The launcher front view is shown in Fig. 2.3.12. There are two special features of this design. The one is the grooves on the launcher front surface as shown in Fig. 2.3.13. These grooves can reduce the thermal stress of the surface. The heat loads of launcher result from the nuclear heat (8 W/cm^3), the plasma radiation (17 W/cm^2) and R.F power loss are shown in Table 2.3.9. The electromagnetic forces shown in Fig. 2.3.14 are not problem. The forces and the mechanical stress are shown in Table 2.3.10. The other feature is the multi waveguide connector using choke circuit as shown in Fig. 2.3.15. The low resistive contact can be gained by the choke. The installation and replacement of LHRF launcher are shown in Figs. 2.3.16, 2.3.17 and Table

2.3.11. The connecting part is composed of the multi waveguide connector.

In ECRF heating, the frequency is 160 GHz, the input power launched by 2 metal mirrors is 10 MW for 10 sec. The specifications are shown in Table 2.3.12. The power supply is about 80 MVA as the preliminary result as shown in Fig. 2.3.22. RF wave beam is injected from low field side in O-mode. RF wave beam is transported by quasi-optical system consists of some metal mirror as shown in Fig. 2.3.19, which have negligible conduction loss on their surfaces. The heat loads of the metal mirror for r.f beam injection are shown in Table 2.3.13. The electromagnetic force at the plasma disruption is not problem. The ECRF heating system is shown in Fig. 2.3.20. The ceramic window is composed of two ceramic plates for safety. They are cooled by circulating SF_6 or N_2 gass. RF beams are deflected to change the injection angle by the deflector consists of a metal mirror and a motor. The replacement of ECRF launcher is illustrated by Fig. 2.3.21 and Table 2.3.14. ECRF heating system maintenance is easiest from the point of view of the disassembly and assembly.

In future, the material consideration is the most important.

Table 2.3.1 Specifications of RF Parameters

items	mode 1	mode 2
Frequency (MHz)	88	
Total input power (MW)	15	5
Pulse width (sec)	10	100
Port number	2	

Heating scenario

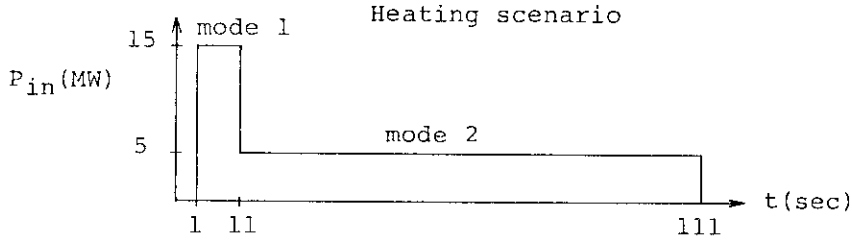

,where Pin is the input power and t is the time from tokamak start.

Table 2.3.2 Specifications of Antenna Parameters

Number of antenna ---------- 2 /port

Distance between plasma surface (including scrape off layer 2 cm) and central conductor ---------- 18 cm

Distance between central conductor and return conductor ---------- 30 cm

Central conductor length ---------- 1 m

Central conductor width ---------- 40 cm

Central conductor thickness ---------- 3 cm

Gap between Faraday shield and central conductor ---------- 1.5 cm

Load impedance R = 5.3 Ω/m ,

X = 140 Ω/m ,

where plasma center density is 2×10^{20} m^{-3}

Characteristic impedance of coaxial cable --- 30 Ω

Table 2.3.3 Heat load of ICRF antenna, where the nuclear heat density is 8 w/cm^3, plasma radiation density is 17 w/cm^2 and conductors and Faraday shield have no copper coating.

Element	R.F power loss	Nuclear heat	Plasma radiation
Central conductor	∿10 kW	50 kW	70 kW
Return conductor	∿10 kW	50 kW	70 kW
Faraday shield	∿20 kW	10 kW	30 kW

Table 2.3.4 Electromagnetic force and mechanical stress of ICRF antenna, where $f_1 \sim f_4$ are shown in Figs.1.4 and 1.5.

(1) Faraday shield (header)

force		σ (kg/mm^2)
f_1	8 kg/mm	4
f_2	2 kg/mm	2

(2) Center conductor

force		σ (kg/mm^2)
f_3	2×10^{-3} kg/mm^2	2×10^{-3}
f_4	1 kg/mm	5

Table 2.3.5 RF loss of Faraday shield, where v is the vertical width of the shield bar, $R_\perp$ is the antenna resistance due to the dissipation of $B_{rf\perp}$ field, $R_{//}$ is the antenna resistance due to the dissipation of $B_{rf//}$ field, P_f is the r.f power loss of Faraday shield, $\Delta P_\perp$ is the r.f loss density for $B_{rf\perp}$ and $\Delta P_{//}$ is the r.f loss density for $B_{rf//}$. $B_{rf\perp}$ is the r.f magnetic field perpendicular to the shield bar and $B_{r.f//}$ is the r.f magnetic field parallel to the shield bar.

(a) No coating case, where the resistivity of SS (∿20°C) is 7.2×10^{-7} Ω-m and the setting pitch of shield bar is 4 cm.

v(cm)	$R_\perp$(Ω/m)	$R_{//}$ (Ω/m)	P_f(kW)	$\Delta P_\perp$ (W/cm^2)	$\Delta P_{//}$ (W/cm^2)
2	0.13	0.011	100	23	1.0
2.5	0.24	0.013	170	40	1.0
3	0.53	0.014	350	85	1.0
3.5	2.1	0.015	1100	270	1.0

(b) Copper coating case, where the resistivity of Cu (∿200°C) is 3.44×10^{-8} Ω-m and the setting pitch of shield bar is 4 cm.

v(cm)	$R_\perp$(Ω/m)	$R_{//}$ (Ω/m)	P_f(kW)	$\Delta P_\perp$ (W/cm^2)	$\Delta P_{//}$ (W/cm^2)
2	0.029	0.0025	22	5	0.2
2.5	0.051	0.0028	38	9	0.2
3	0.12	0.0031	82	20	0.2
3.1	0.14	0.0031	100	25	0.2
3.5	0.46	0.0034	300	75	0.2

(c) No coating case, where the resistivity of SS (∿200°C) is about 9×10^{-7} Ω-m and the setting pitch of shield bar is 10 cm.

v(cm)	$R_\perp$(Ω/m)	$R_{//}$ (Ω/m)	P_f(kW)	$\Delta P_\perp$ (W/cm^2)	$\Delta P_{//}$ (W/cm^2)
2	0.011	0.0037	22	10	1
3	0.015	0.0020	38	13	1

Table 2.3.6 Replacement procedure of ICRF antenna

- Disassembly -

(1) Shutdown.

(2) (Bake and evacuate for tritium removal)

(3) Cool for the removal of decay heat.

(4) Disconnect the bolts of connecting part-A.

(5) Cut the lip seal of connecting part-A.

(6) Install the sub-support structure.

(7) Cut the vacuum seal between the access door and the antenna.

(8) Cut the cooling pipes.

(9) Remove the antenna.

- Assembly-

(1) Install the antenna.

(2) Connect (weld) the cooling pipes and NDT.

(3) Weld the vacuum seal between the access door and the antenna, and NDT.

(4) Remove the sub-support structure.

(5) Weld the lip seal of connecting part-A and NDT.

(6) Connect the bolts of connecting part-A.

(7) Bake and evacuate.

Table 2.3.7 Specifications of RF parameters

items	mode 1	mode 2
Frequency (GHz)	2	
Total input power (MW)	15	5
Pulse width (sec)	10	100
Port number	1	

Table 2.3.8 Spcecifications of Grill antenna

Waveguide size ---------- 125 mm^H × 28 mm^W

Distance between lateraly adjacent two waveguides centers ---------- 36 mm

Total waveguide number --------- 128

λ/4 short waveguide ---------- 32

Launcher size ---------- 330 mm^H × 770 mm^W

Number of launcher ---------- 4

Table 2.3.9 Heat load of launcher, where the launcher length is 2 m.

	Heat load (kW)
Nuclear heat	1500
Plasma radiation	30
R.F loss	10
Total heat load	1540

Table 2.3.10 Electromagnetic force and stress at disruption, where σ_S is the shering stresses due to f_{10} and f_{11}.

	Force and stress
f_{10} (kg/mm)	52
f_{11} (kg/mm)	13
σ_S (kg/mm^2)	0.2

Table 2.3.11 Replacement procedure of LHRF launcher

- Disassembly -

(1) Shutdown.

(2) (Bake and evacuate for tritium removal)

(3) Cool for the removal of decay heat.

(4) Disconnect the bolts of connecting part-A.

(5) Cut the lip seal of connecting part-A.

(6) Install the sub-support structure.

(7) Cut the vacuum seal between the access door and the antenna.

(8) Cut the cooling pipes.

(9) Remove LHRF launcher.

- Assembly -

(1) Install LHRF launcher.

(2) Connect (weld) the cooling pipes and NDT.

(3) Weld the vacuum seal between the access door and the antenna, and NDT.

(4) Remove the sub-support structure.

(5) Weld the lip seal of the connecting part-A, and NDT.

(6) Connect the bolts of the connecting part-A.

(7) Bake and evacuate.

Table 2.3.12 Specifications

Frequency (GHz)	160
Input power (MW)	10
Pulse width (sec)	10
R.F wave mode	O mode
Injection	Low Field Side
Transport and launch of RF wave	Quasi Optical

Table 2.3.13 Heat load of launching mirror, where heat flux from plasma is 12 W/cm^2, nuclear heat density is 7 W/cm^3 and the mirror surface is not coated by copper.

Plasma radiation	60 kW
Nuclear heat	90 kW
RF power loss	∿4 kW

Table 2.3.14 Replacement procedure of ECRF

- Disassembly -

(1) Shutdown

(2) (Bake and evacuate for tritium removal)

(3) Cool for the removal of decay heat

(4) Remove the module-b with the overhead crane

(5) Cut the vacuum seal between the access door and the module-a

(6) Cut the cooling pipes

(7) Withdraw and remove the module-a

- Assembly -

(1) Install the module-a

(2) Weld the cooling pipes and NDT

(3) Weld the vacuum seal between the access door and the module-a and NDT

(4) Install the module-b

(5) Bake and evacuate

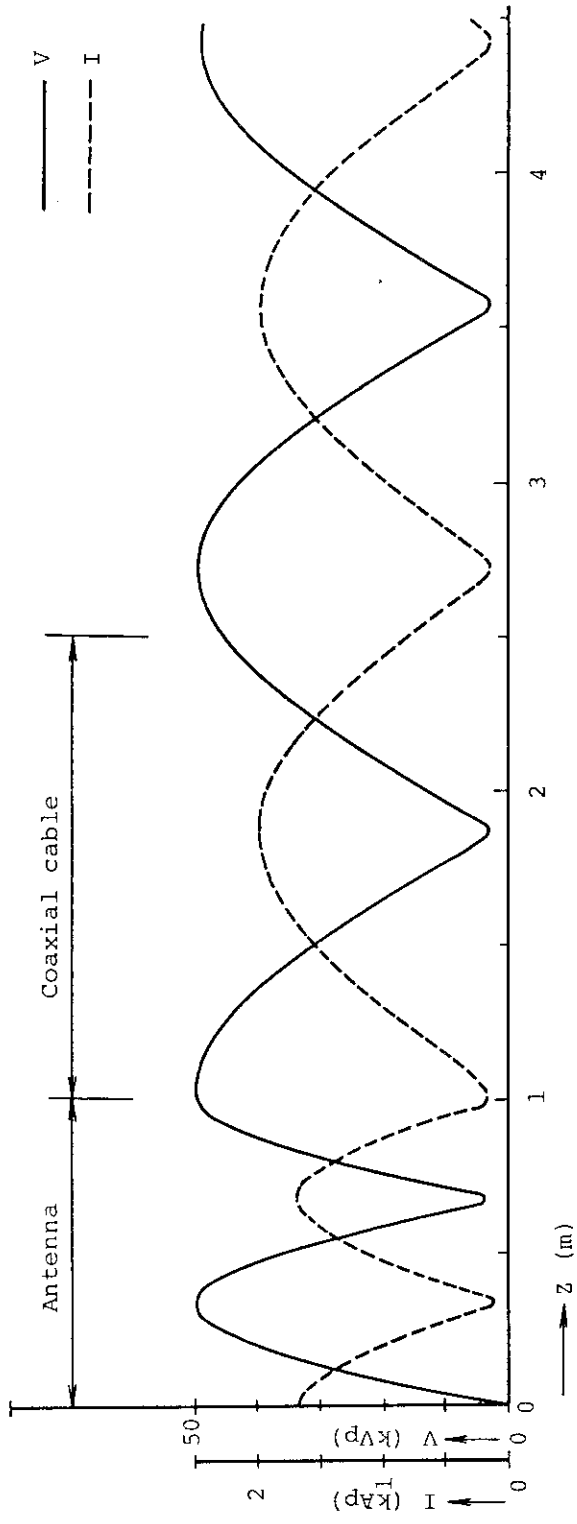

Fig.2.3.1 V,I distribution along the antenna and coaxial cable for R=5.3 Ω/m, X=140 Ω/m, CF=2.4×10^{-10} F/m and Z_0=30 Ω, where CF is the capacitance between Faraday shield and central conductor and Z_0 is the characteristic impedance of coaxial cable.

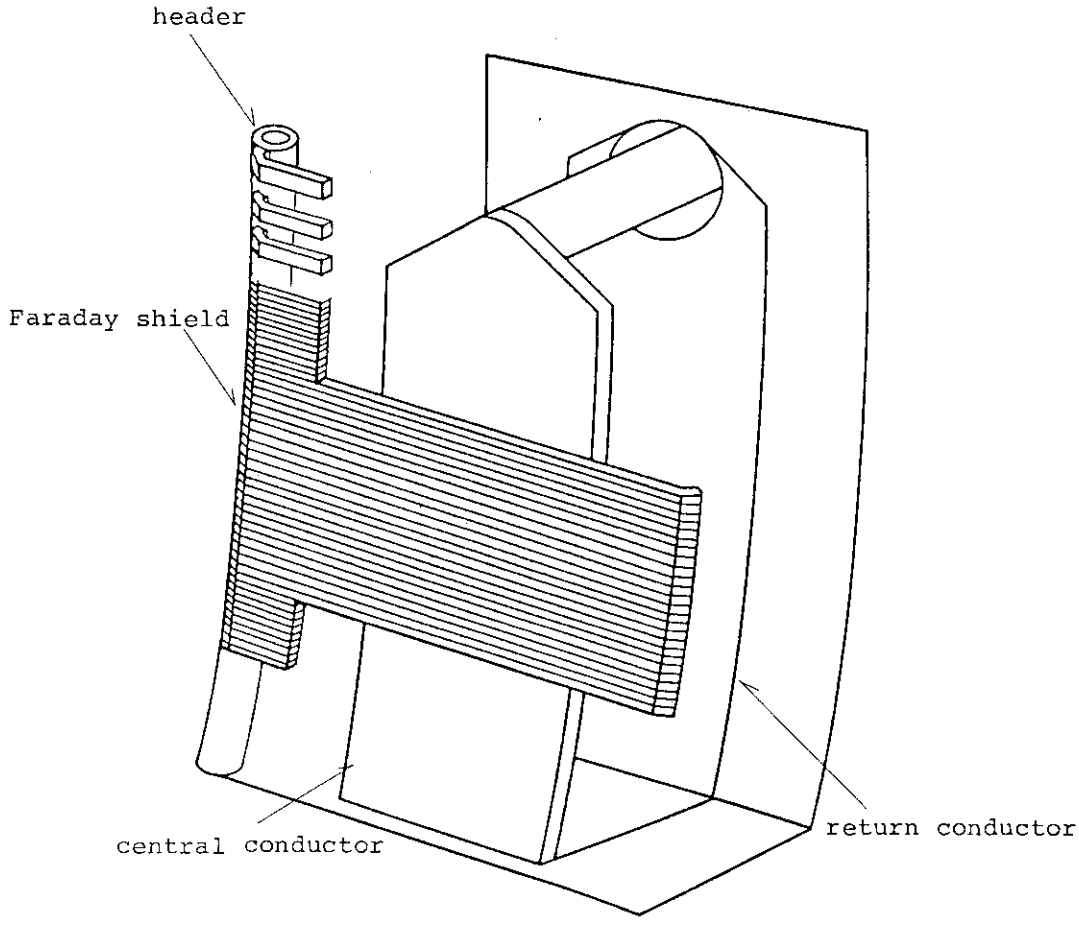

Fig.2.3.2 Bird's-eye view of standard metal type antenna composed of central conductor, return conductor and Faraday shield. They are all made of SS without copper coating.

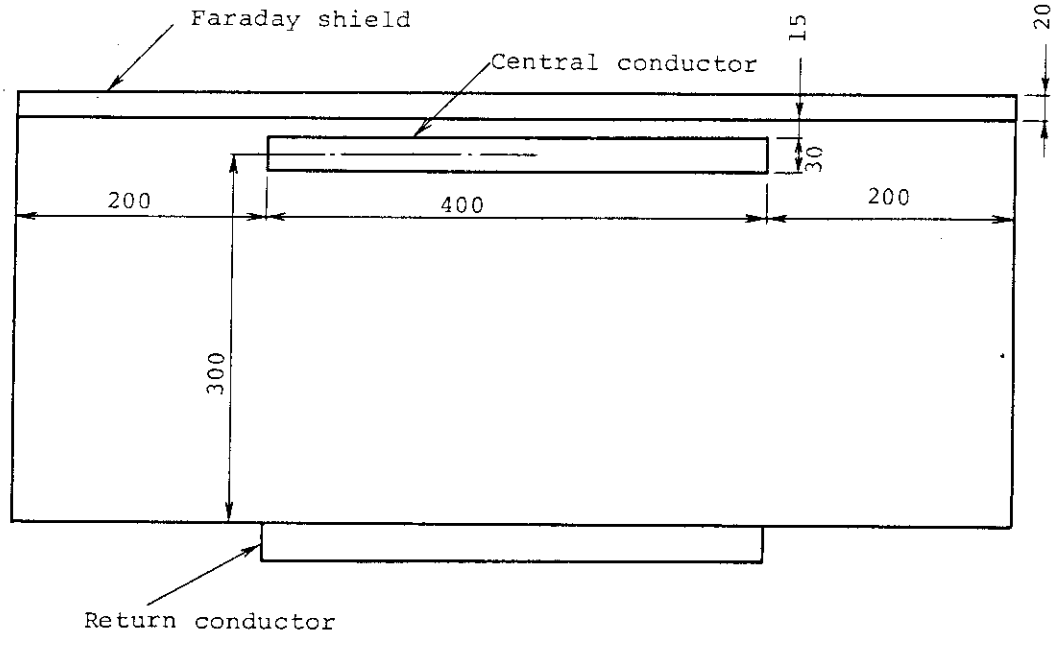

Fig.2.3.3 Latelal cross sectional view of ICRF antenna.
unit : mm

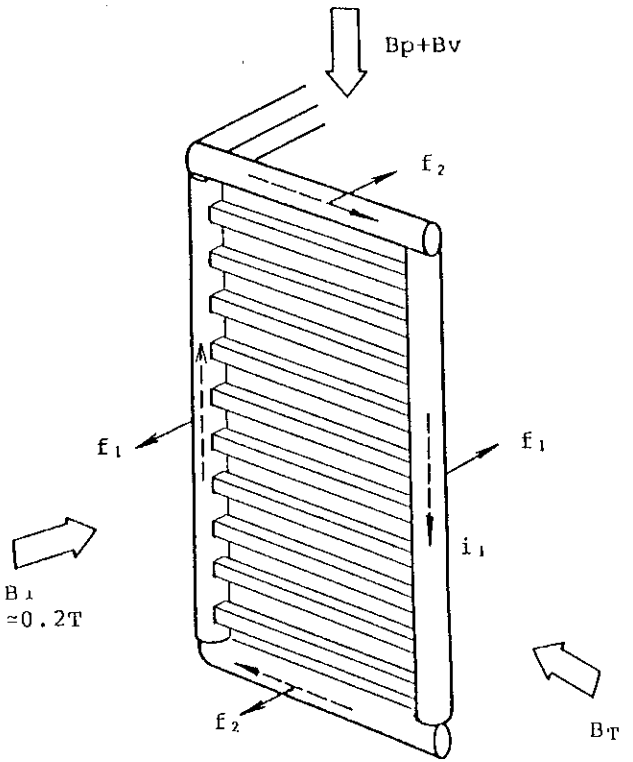

Fig.2.3.4 Electromagnetic force of Faraday shield for the plasma current decay time is 15 ms, f_1 arises from $i_1 \times B_T$, f_2 arises from $i_1 \times (B_P+B_V)$, where i_1 is induced current at the plasma disruption, B_T is the toroidal field, B_P is the poloidal field, B_V is the vertical field and $B_\perp$ is the magnetic field normal to the Faraday shield.

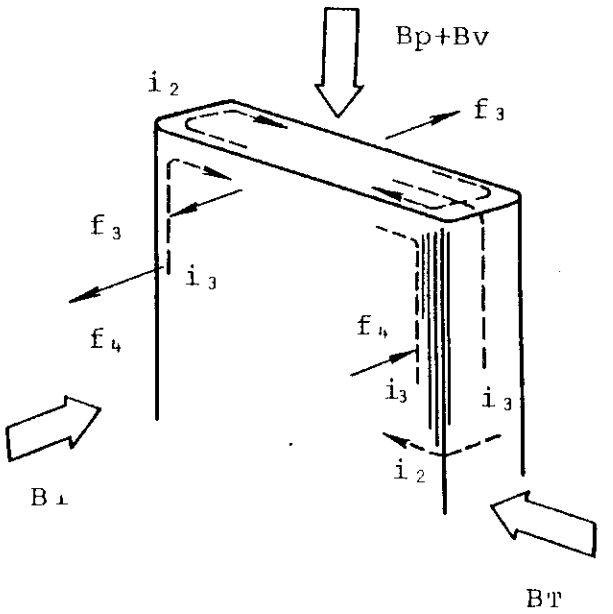

Fig.2.3.5 Electromagnetic force of center conductor for the plasma current decay time is 15 ms, f_3 arises from $i_2 \times (B_P+B_V)$, f_4 arises from $i_3 \times B_T$.

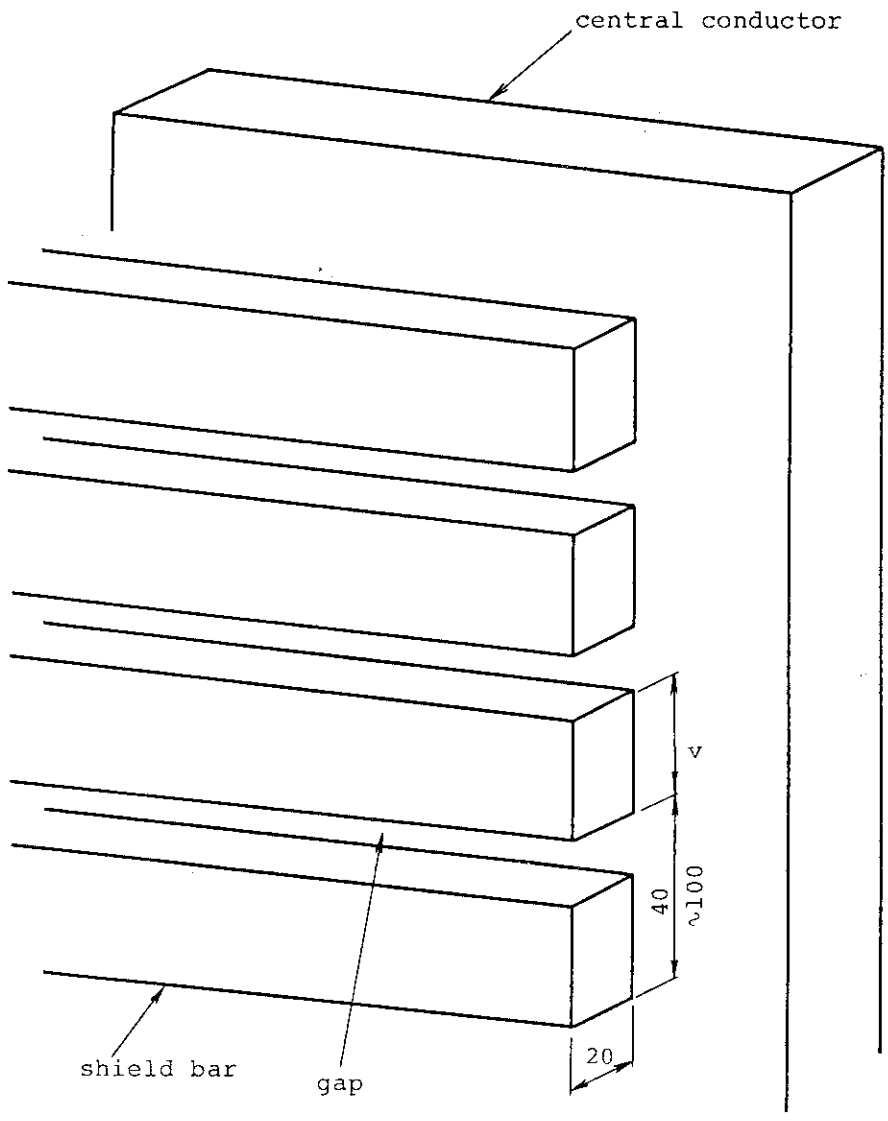

Fig.2.3.6 Schematic view of Farady shield unit: mm , where V is the height of the shield bar.

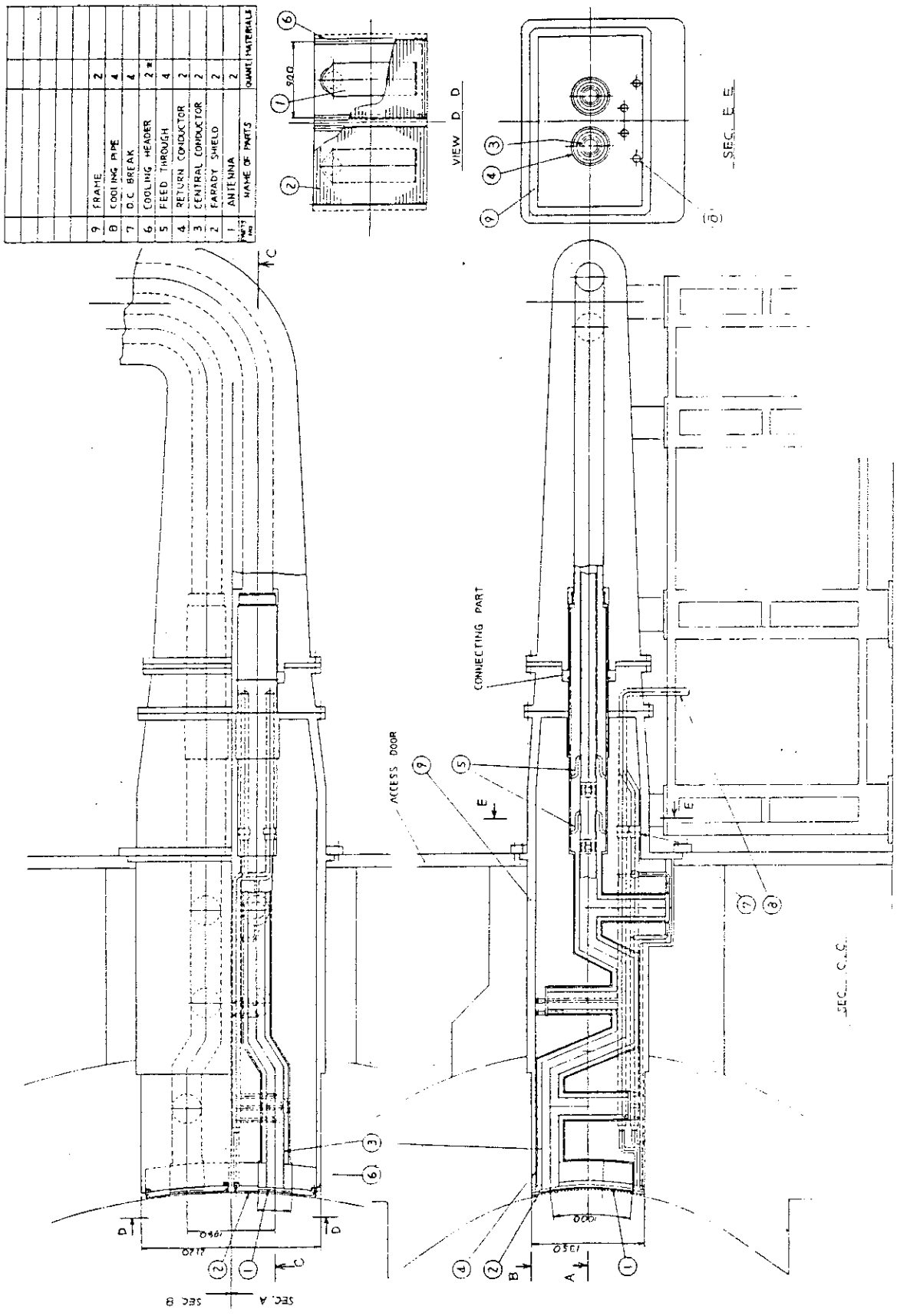

Fig.2.3.7 The cross sectional view of ICRF launcher. The inner conductor of the coaxial cable in vacuum is supported by λ/4 short terminated stub, where λ is the wave length.

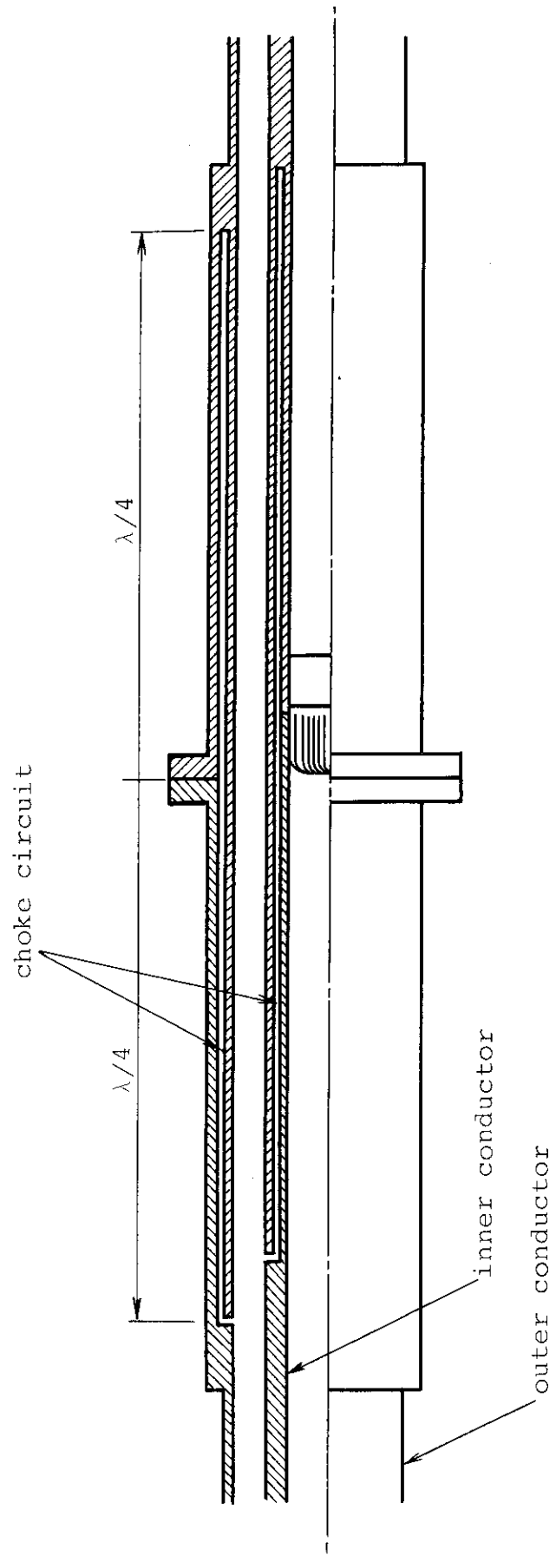

Fig.2.3.8 Coaxial cable connector using choke circuit, where λ is the wave length.

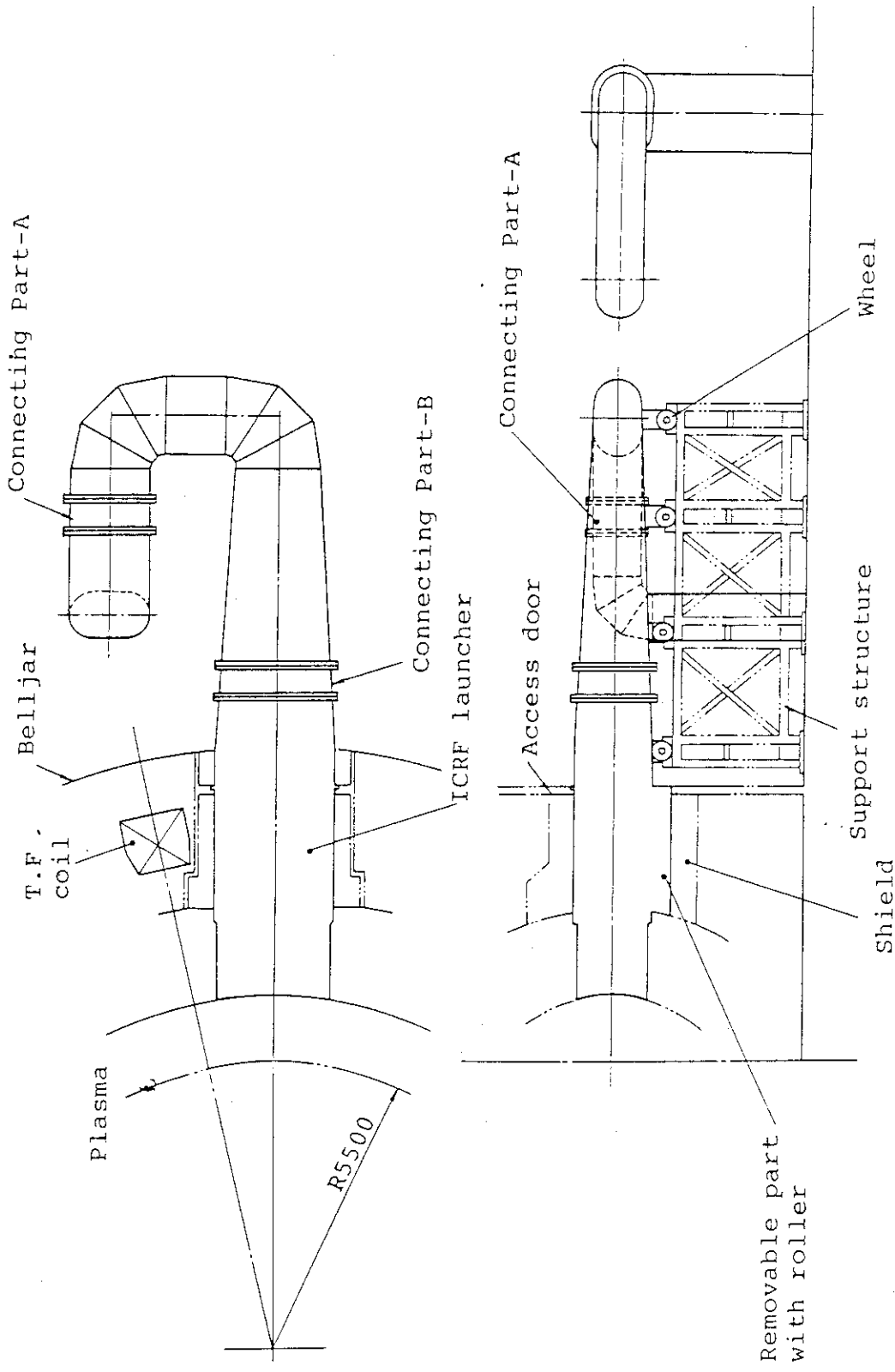

Fig.2.3.9 Installation of ICRF launcher, where connecting part is constructed by choke type coaxial cable connector.

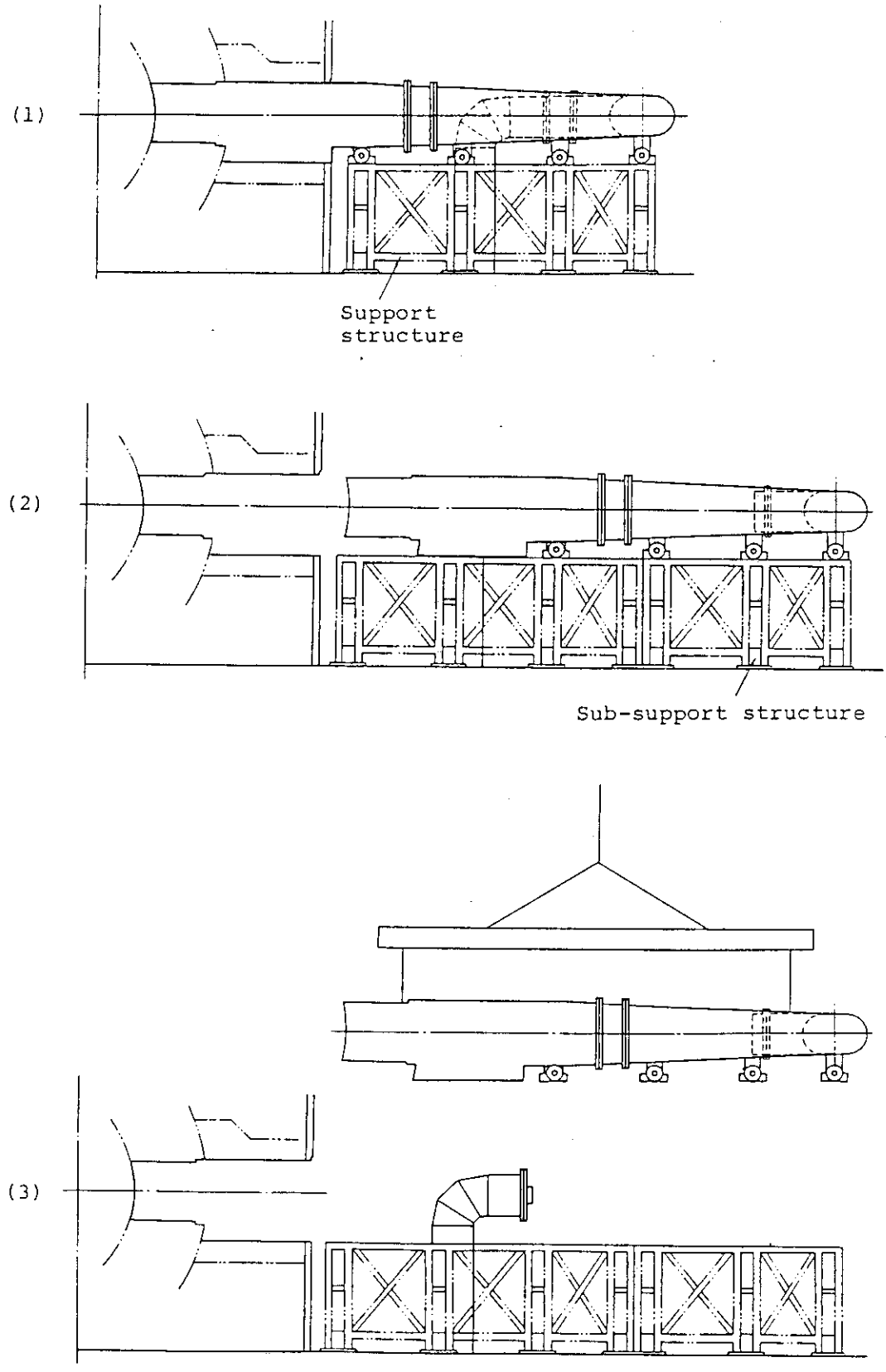

Fig.2.3.10 Replacement of ICRF launcher.

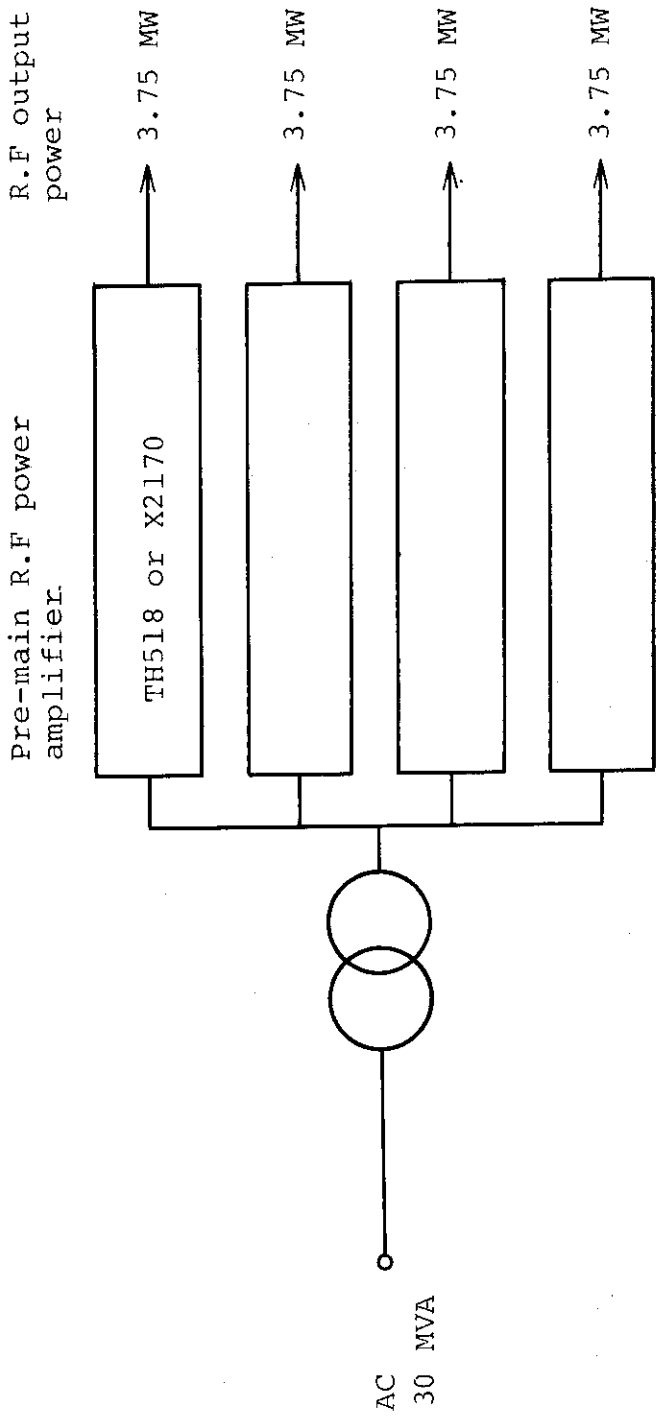

Fig.2.3.11 Schematic diagram of power supply of ICRF heating system, where r.f transport efficiency is 90%, r.f amplification efficiency is 65% and power factor of D.C supply is 85%.

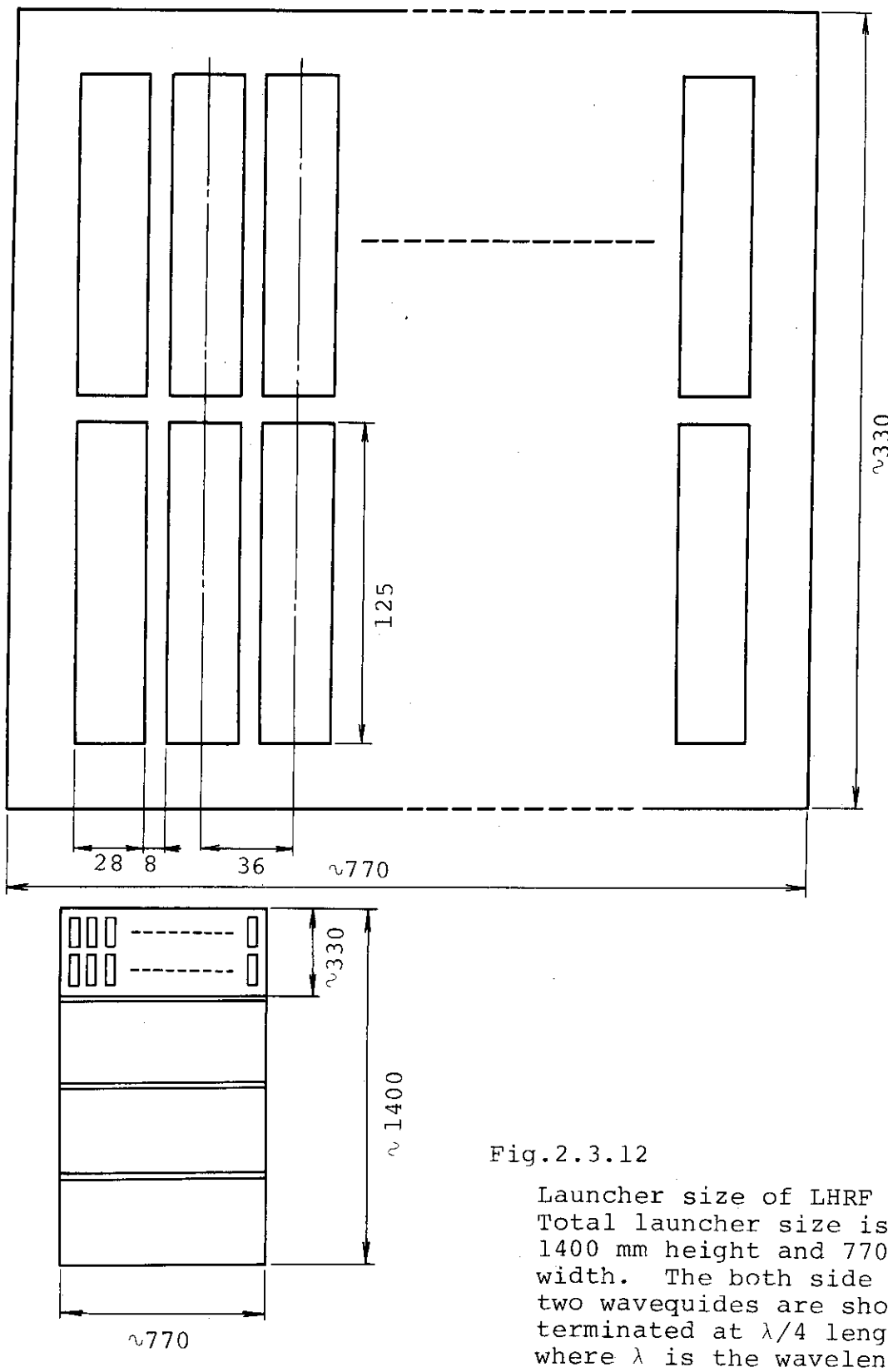

Fig.2.3.12

Launcher size of LHRF heating. Total launcher size is about 1400 mm height and 770 mm width. The both side each two wavequides are short terminated at λ/4 length, where λ is the wavelength.

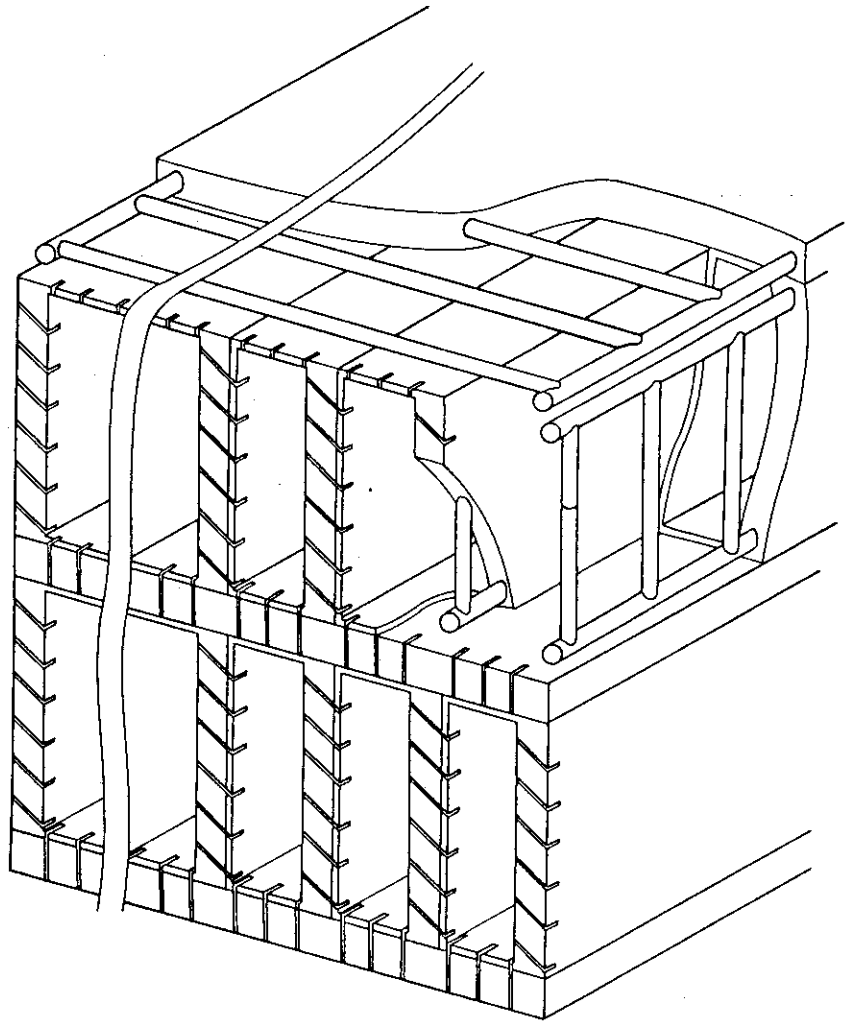

Fig.2.3.13 Grill launcher of LHRF heating. The groove can reduce the thermal stress of the front surface.

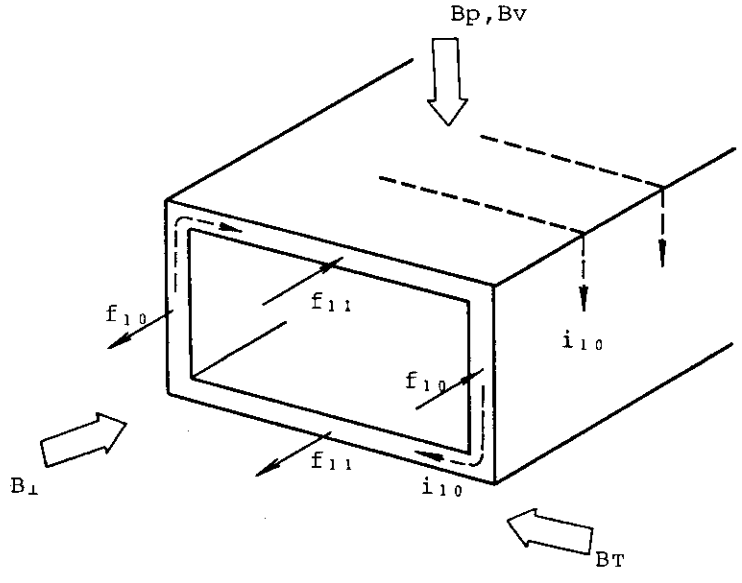

Fig.2.3.14 Induced current and electromagnetic force of LHRF launcher, where f_{10} arises from $i_{10} \times B_T$, f_{11} arises from $i_{10} \times (B_P + B_V)$, and the current i_{10} is induced by $B_\perp (\sim 0.2T)$.

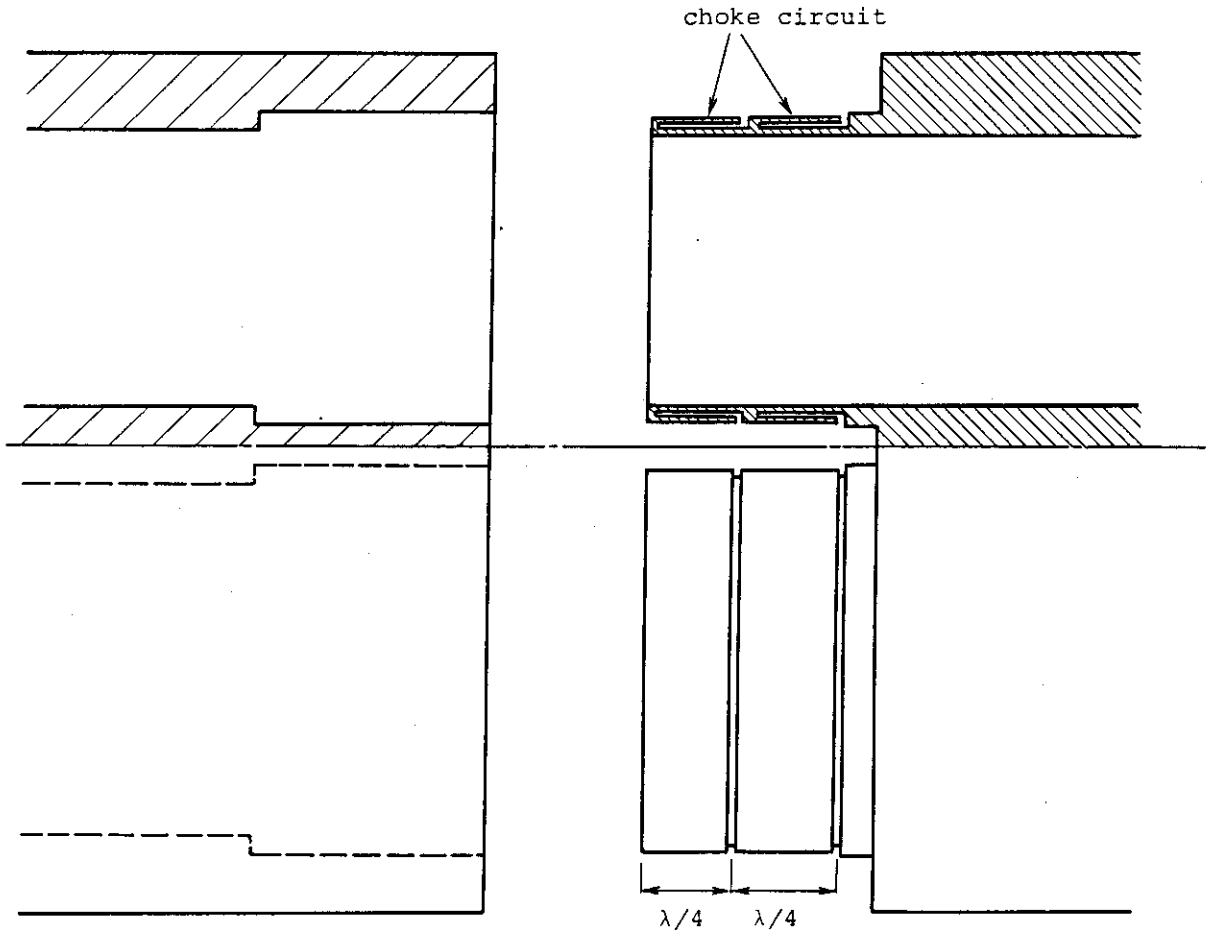

Fig.2.3.15 Multi-waveguide connector using choke circuit. This connector is the example of double choke. λ is the wave length.

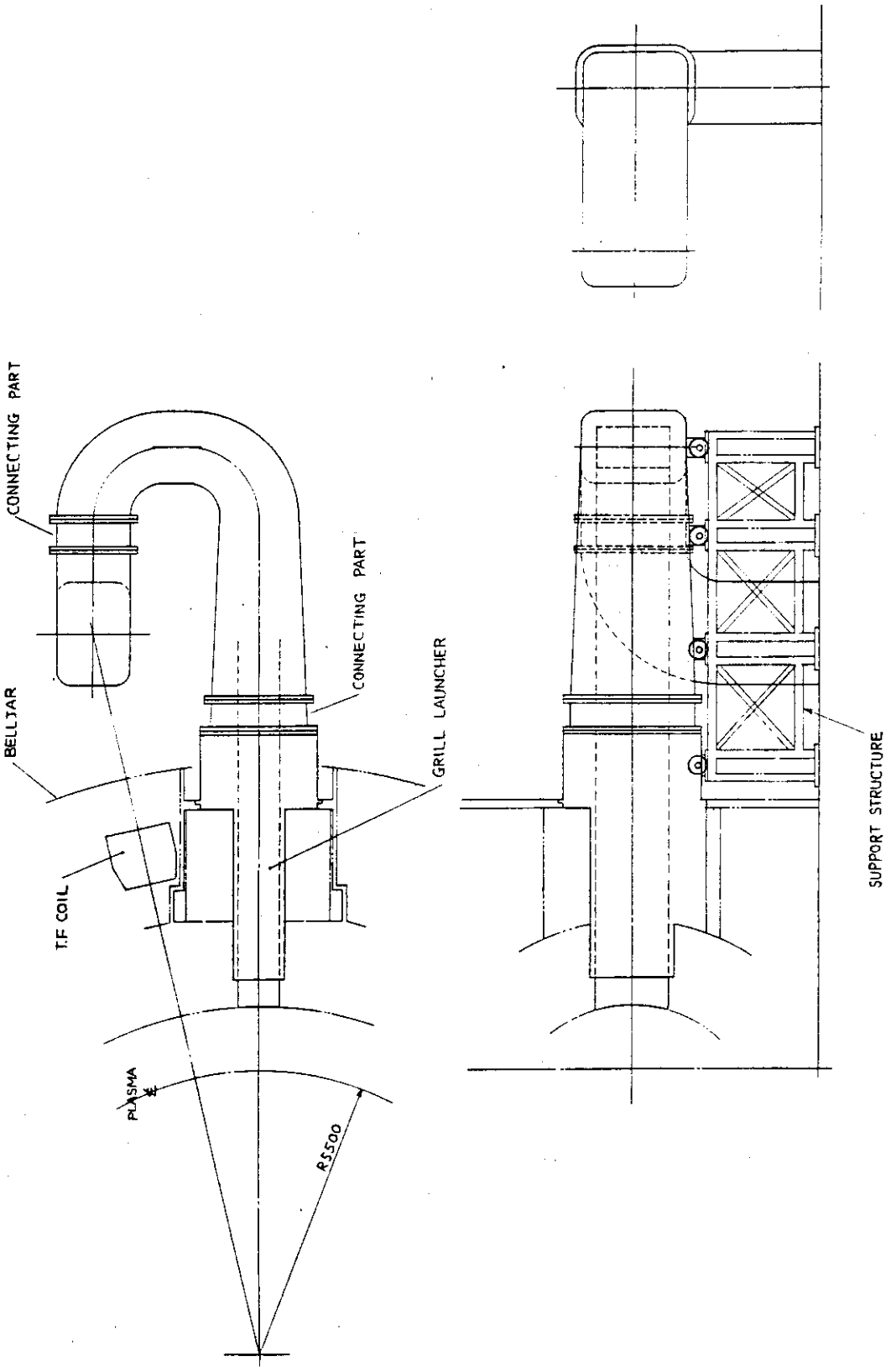

Fig.2.3.16 Installation of LHRF. The connecting part is composed of the multi waveguide connector.

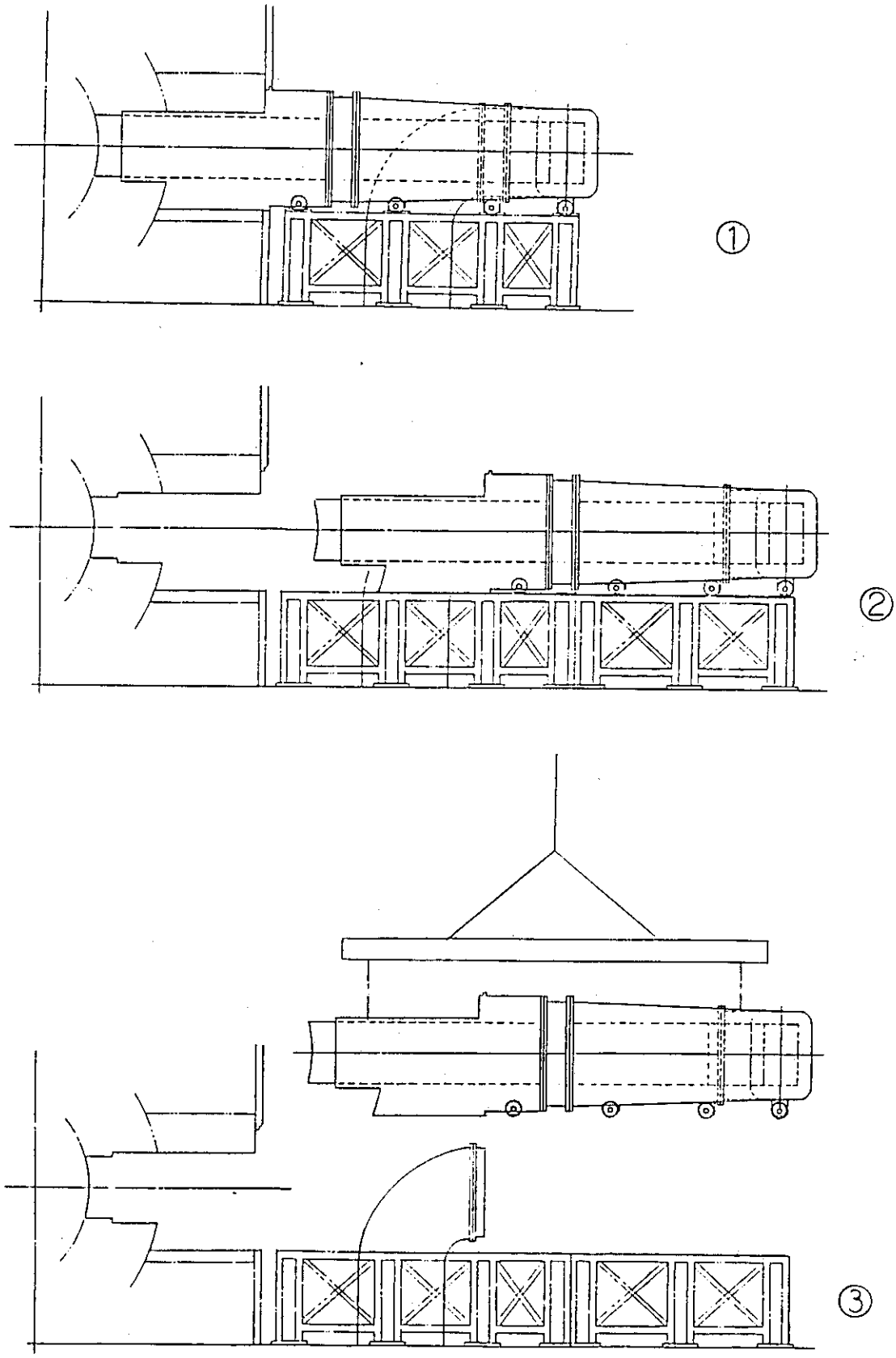

Fig.2.3.17 Replacement of LHRF launcher.

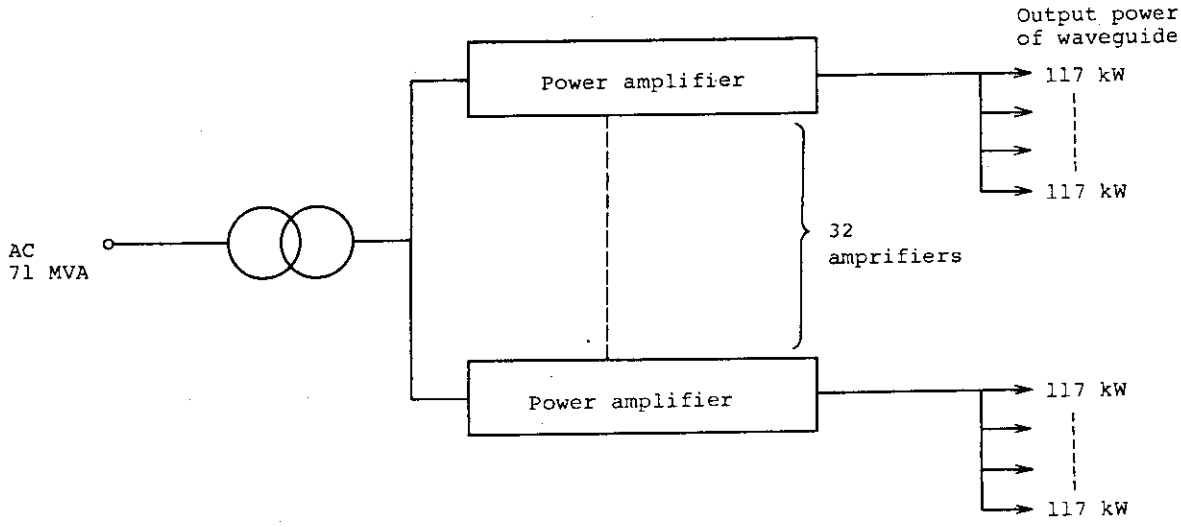

Fig.2.3.18 Schematic diagram of power supply, where the transport efficiency is about 50%, the r.f amplification efficiency is about 50% and the power factor of D.C supply is about 85%.

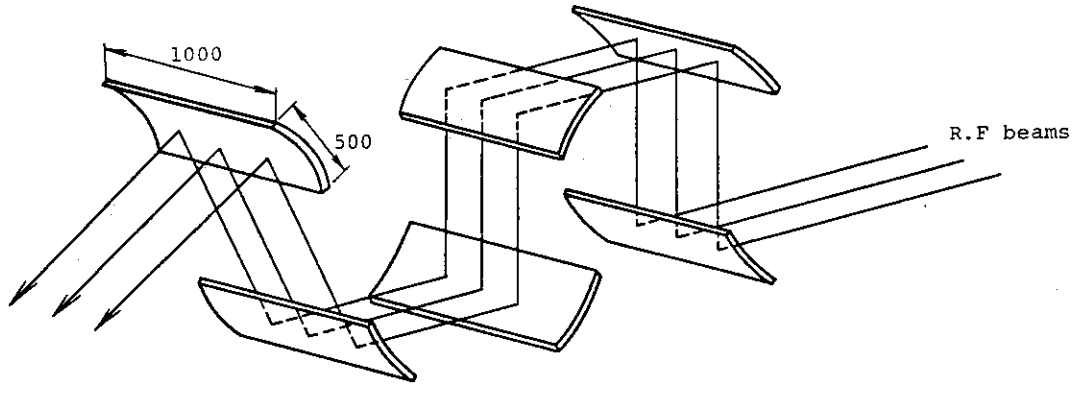

Fig.2.3.19 Mirror system of ECRF heating unit : mm. RF beams are reflected at the mirror and injected into plasma. The mirror surface is curved to focus the beams perpendiculary.

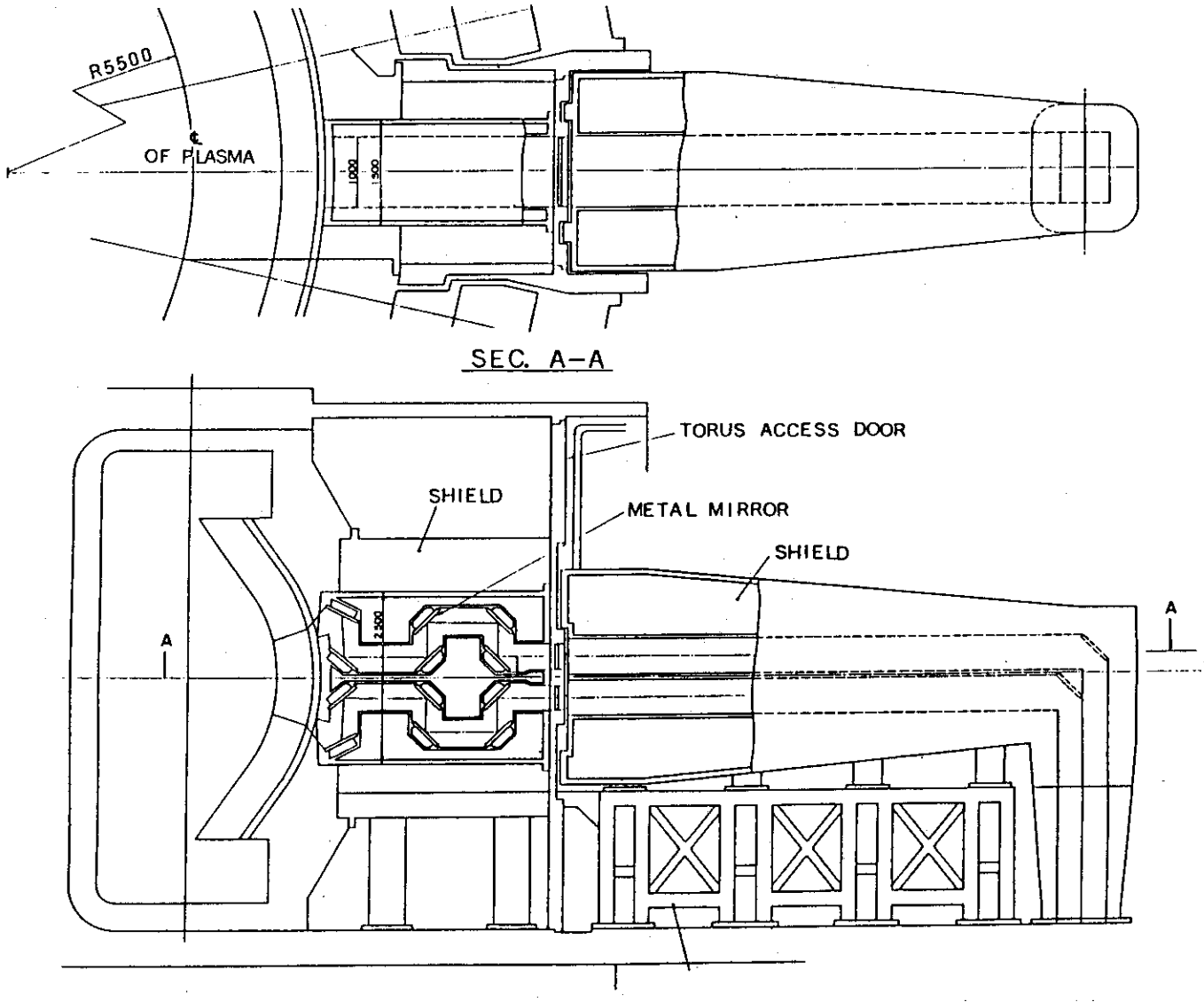

Fig.2.3.20 Schematic cross sectional view of ECRF heating system. The ceramic window is composed of two ceramic plates for safety. SF_6 gass is circulated between the two plates to cool the tanδ loss heat.

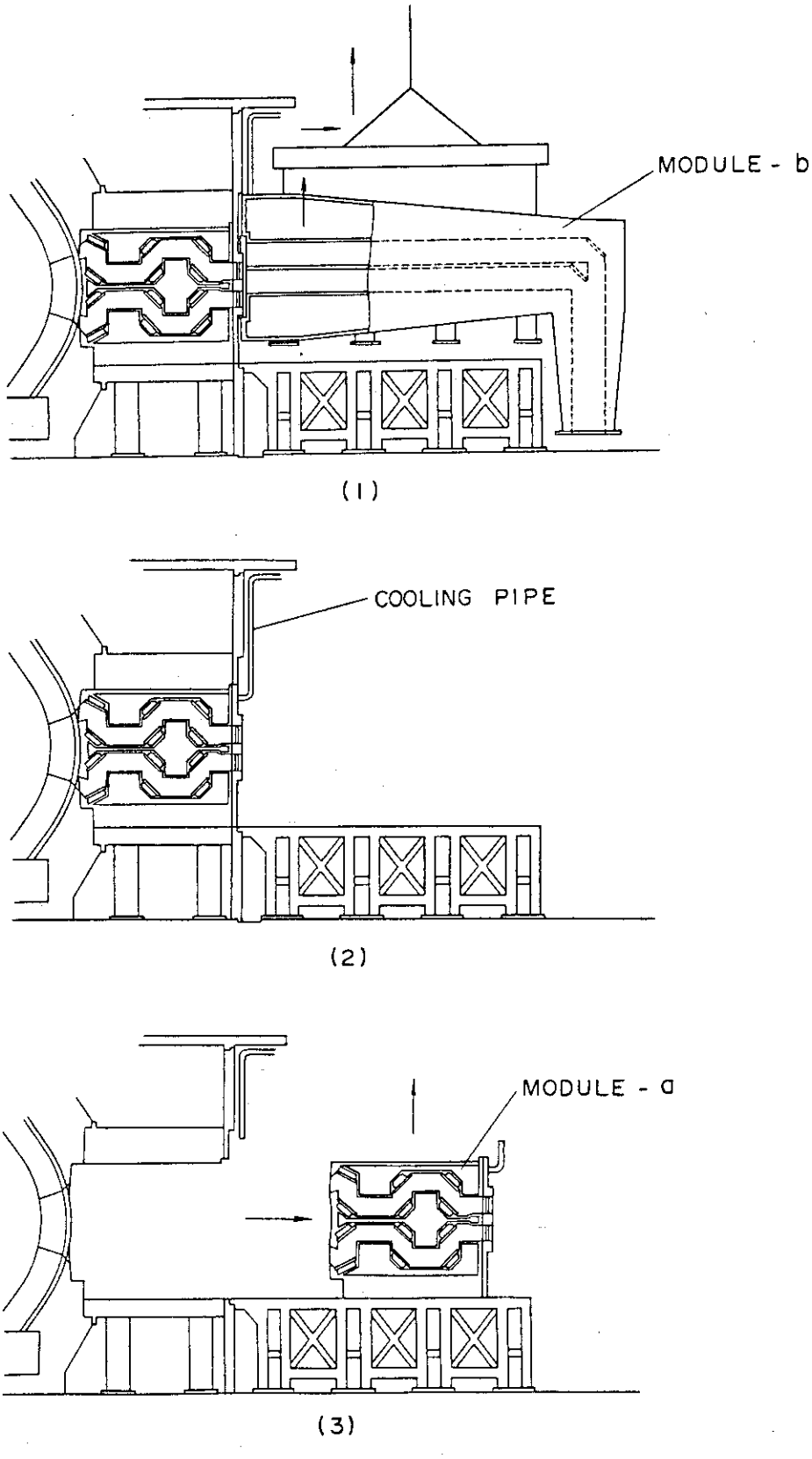

FIG.2.3.21 REPLACEMENT OF ECRF LAUNCHER.

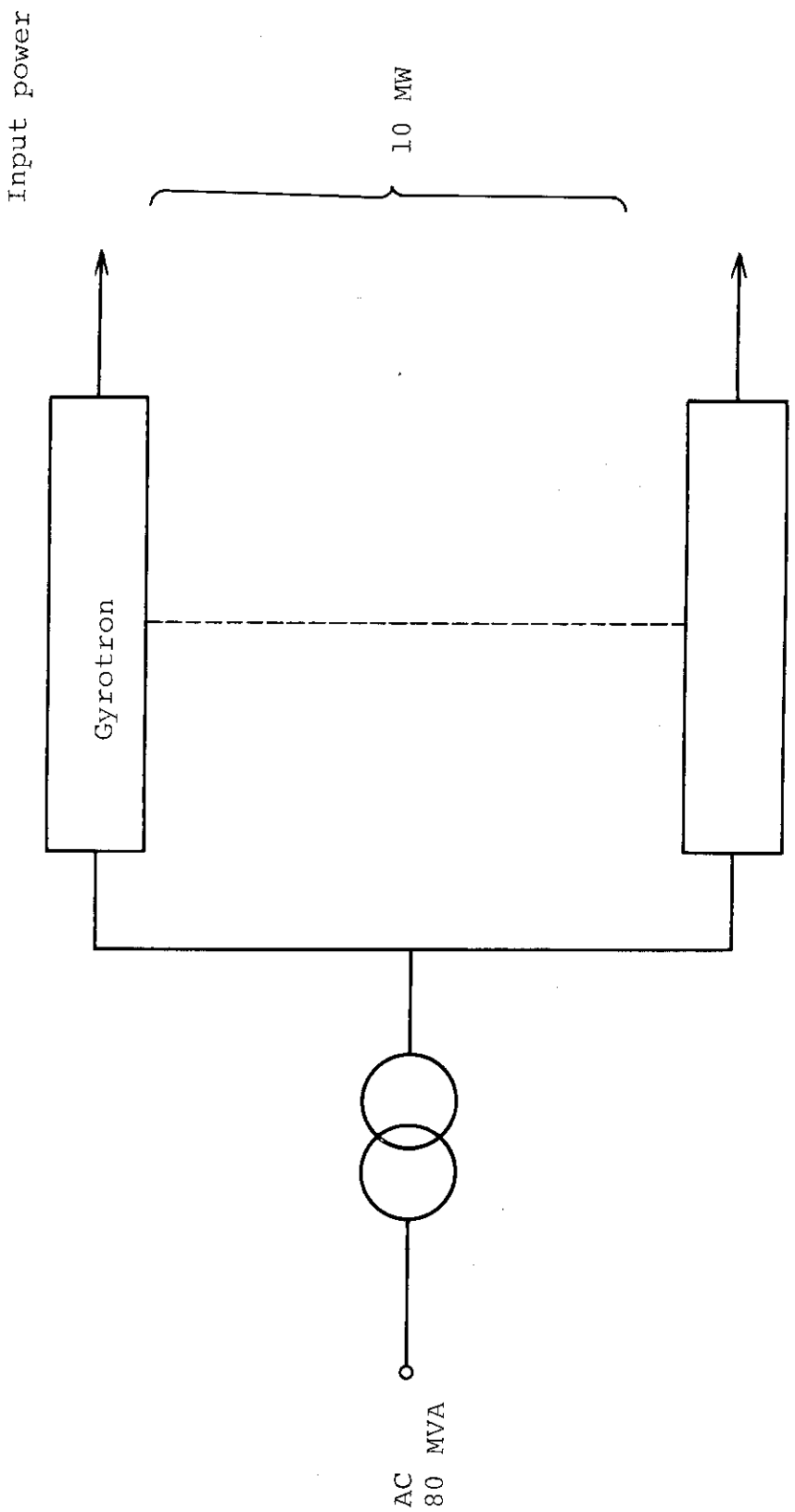

Fig.2.3.22 Power supply of ECRF system, where r.f transport efficiency is about 50%, r.f generation efficiency is about 30% and power factor of D.C supply is 85%.

3. Impurity Control and Divertor/Pumped-Limiter Design

3.1 Physics design considerations for impurity control by divertor and pumped-limiter

Poloidal divertor is a primary candidate for impurity control of reference FER, while pumped-limiter is also considered for advanced FER. In the poloidal divertor, the optimization of the divertor configuration is studied by two-dimensional self-consistent numerical analyses of divertor plasma. Emphases are placed on the helium pumping requirement, remote radiation cooling in the divertor chamber and dense/cold plasma formation near the divertor plate. Based on these analyses, guidelines of divertor design are given as follows; low pumping requirement for helium exhaust ($S \lesssim 10^5$ ℓ/s), low plasma temperature near divertor plate ($T_e \lesssim 30$ eV) and moderate heat load on divertor plate ($P \lesssim 20$ MW/d.p). It is most important to clarify the criteria for the formation of dense/cold divertor plasma and this study is now under way. Figures 3.1.1. and 3.1.2 show simplified model geometry of the numerical calculation. Behavior of the plasma in the divertor chamber is described by fluid equations, which consist of the conservation equations of particle, momentum and electron and ion energy. The source terms from the neutral particles for these conservation equations are calculated by the Monte-Carlo neutral particle transport code. They are solved self-consistently by iteration. Figures 3.1.3－3.1.5 show the results of the numerical calculations. It is shown that dense and cold divertor plasma can be formed even for rather low incoming ion flux to divertor. Since it has not yet been fully clarified that these dense and cold divertor plasma can be formed in any divertor configuration such as open divertor, some geometrical restrictions are imposed on the design study of the divertor shown as in Fig. 3.1.6. Another factor, which is not identified at present, is the incoming particle flux to the divertor. Thus, the required pumping speed is set to 10^5 ℓ/s, which is rather larger than the calculated value.

In the pumped-limiter for advanced FER, it is most important to examine the applicability to FER impurity control system. Since the limiter surface contacts with the main plasma directly, it is essential

to solve the main plasma and scrape-off plasma simultaneously. At least, two-dimensional (one-dimensional in minor radius direction for main plasma and one-dimensional in magnetic field direction for scrape-off plasma) treatment is necessary. However, these numerical calculation code has not yet been fully developed, so that one-dimensional calculation both for main and scrape-off plasma is made as a preliminary calculation for the design study. Emphases are placed on the impact of the variation of transport coefficient in scrape-off plasma on helium exhaust, heat load and erosion of the limiter. Convection models are incorporated into the scrape-off layer transport model and the transport coefficients are adjusted to reproduce the ASDEX limiter experiments. Figure 3.1.7 shows the schematic drawing of the numerical calculation. Two examples of the numerical calculations are shown in Figs. 3.1.8－3.1.10: one is the conventional sheath model case and the other is the best fitting case to the ASDEX experiments. Transport coefficients of both cases are summarized in Table 3.1.1. From these preliminary calculations, it is concluded that the erosion and heat load on the limiter surface will be untolerably large for any transport case. Although the convection model is not sufficient, radiative cooling and flux amplification is less expectable than divertor. Even when a more precise two-dimensional calculation of limiter scrape-off plasma is done, these situations will not be changed so much. Thus, we conclude that cold boundary layer should be considered for the application of pumped-limiter to FER. This leads to a larger minor radius of the plasma. For the comparative design study, we determine two sets of plasma and device parameters, which are summarized in Table 3.1.2. In determining the parameters of Case L2, in which about 20 cm of the cold boundary layer is considered, they are set so as to realize the same plasma performance within the cold boundary layer. Conclusions for the choice of divertor and limiter are summarized in Table 3.1.3. In divertor, the advantageous point is the substantial reduction of heat load and erosion due to the cold and dense plasma formation near the plate. Critical point is the control of the vertical position instability. In pumped-limiter, the advantageous point is the applicability to less elongated plasma. The critical point is the formation of stable cold boundary layer compatible to the hot core plasma. This leads to a larger plasma size. while has the potential advantage in heat removal in commercial reactor.

I. Reference: Poloidal divertor
- ○ Optimization of FER divertor
  (2D (z,r) numerical analyses)
  - ○ He pumping requirement
  - ○ Remote radiation cooling
  - ○ Dense/cold plasma formation

II. Advanced: Pumped-limiter
- ○ Applicability for FER impurity control system (1D (r) transport analyses)
  - ○ He exhaust
  - ○ Heat load
  - ○ Erosion

I. Poloidal Divertor

(1) Guideline of divertor design (conclusion by numerical analyses)
- ○ low pumping requirement for He exhaust
  ($S \lesssim 10^5$ ℓ/s)
- ○ low plasma temperature near divertor plate
  ($T_e \lesssim 30$ eV)
- ○ moderate heat load on divertor plate
  ($P \lesssim 20$ MW/d.p)

(2) Criteria for the formation of dense/cool divertor plasma

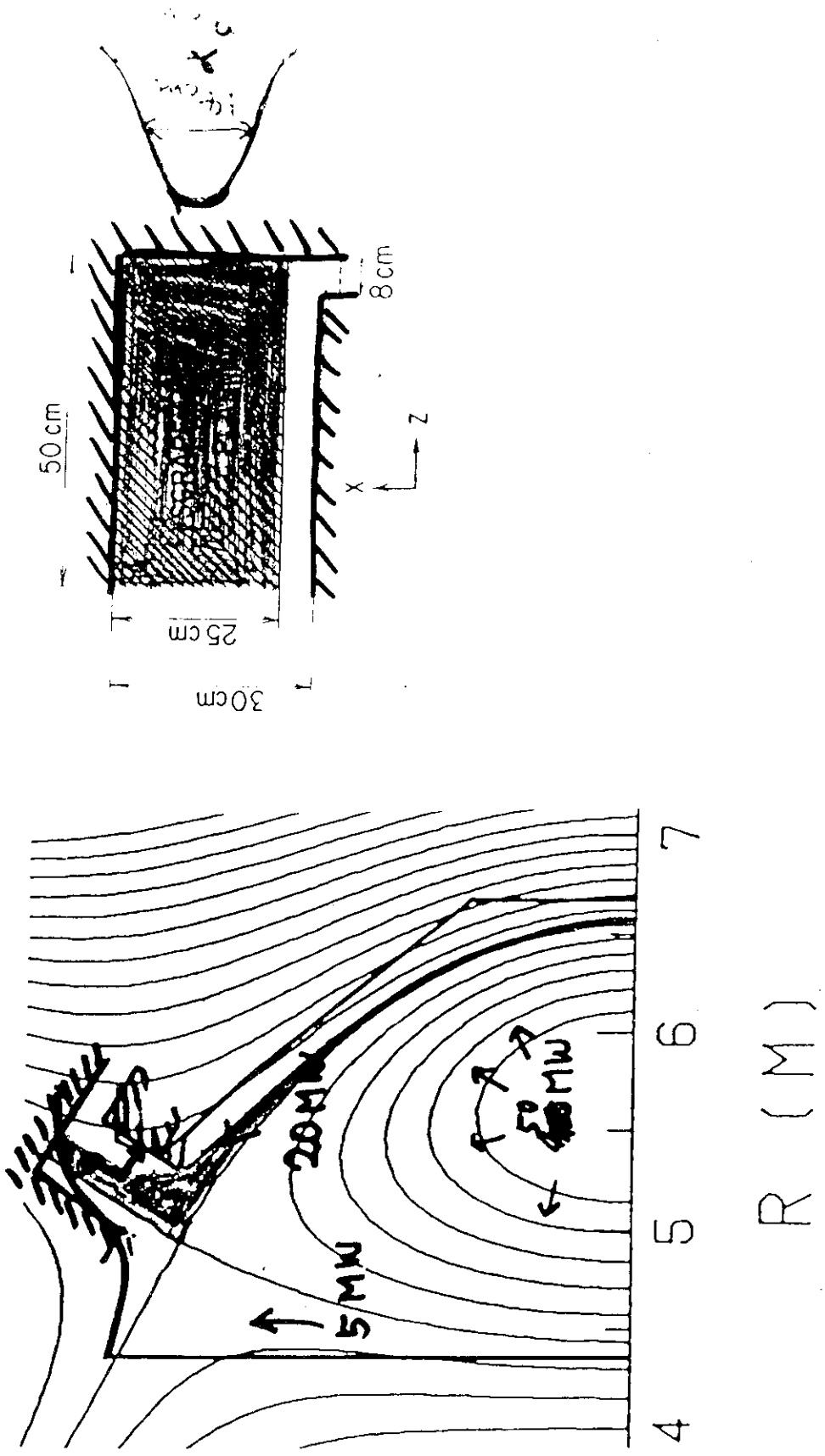

Fig. 3.1.1 Equilibrium magnetic field configuration of FER poloidal divertor and model geometry of numerical code.

Skeleton of numerical model

CONSISTENCY BETWEEN PLASMA AND NEUTRAL PARTICLE

(1) SCRAPE-OFF PLASMA — FLUID MODEL

- particle, momentum & energy conservation eq.
- ionization, charge exchange & radiation
- perpendicular diffusion

(2) NEUTRAL PARTICLES — MONTE CARLO MODEL

(ITELATION)

Geometry for fluid model

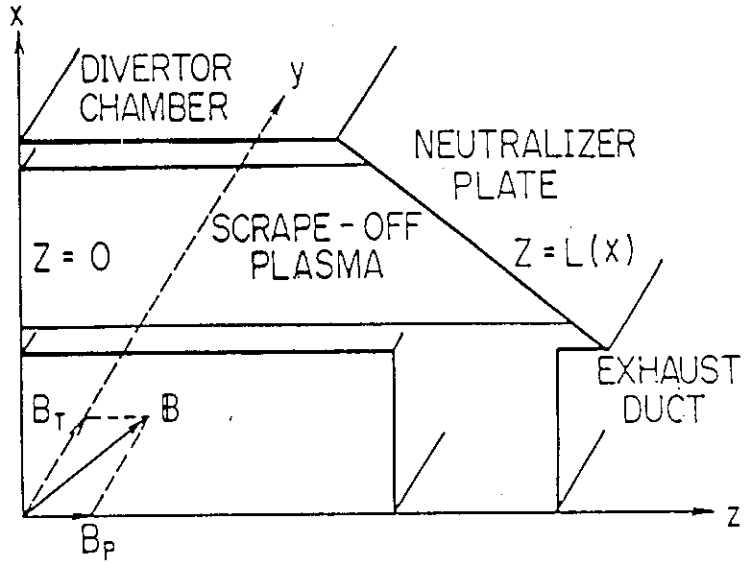

Fig. 3.1.2 Model geometry of fluid model of divertor plasma. Z = 0 is divertor throat entrance and Z = L is divertor plate.

Fluid Equations for Divertor Plasma

• Particle $$\frac{\partial}{\partial z} f_{k,z}(x,z) = S_{K,N}(x,z) + \frac{\partial}{\partial x}\left(D_{\perp} \frac{\partial n_k(x,z)}{\partial x}\right) , \quad k = D,T,\alpha$$

• Momentum $$\frac{\partial}{\partial z}\left[n_p(x,z)\{2U(x,z) + Z_p T_e(x,z) + T_i(x,z)\}\right]$$

$$= \frac{B_T}{B_p}\left[S_p(x;z) + \frac{\partial}{\partial x}\left\{\frac{2U(x,z)}{V_{/\!/}(x,z)} D_{\perp} \frac{\partial n_p(x,z)}{\partial x}\right\}\right]$$

$$U = \frac{1}{2} m_p V_{/\!/}^2(x,z)$$

• Electron energy $$\frac{\partial}{\partial z}\left\{\frac{5}{2} T_e(x,z) f_z(x,z) + q_{ez}(x,z)\right\}$$

$$= V_z(x,z) \frac{\partial P_e(x,z)}{\partial z} - P_{ei}(x,z) + P_R(x,z) + S_{Ee}(x,z)$$

$$+ \frac{\partial}{\partial x}\left\{\frac{3}{2} T_e(x,z) D_{\perp} \frac{\partial n_e(x,z)}{\partial x}\right\} + \frac{\partial}{\partial x}\left\{K_{e\perp} \frac{\partial T_e(x,z)}{\partial x}\right\}$$

• Ion energy $$\frac{\partial}{\partial z}\left[\left\{U(x,z) + \frac{5}{2} T_i(x,z)\right\} f_z(x,z) + q_{iz}(x,z)\right]$$

$$= - V_z(x,z) \frac{\partial P_e(x,z)}{\partial z} + P_{ei}(x,z) + S_{Ei}(x,z)$$

$$+ \frac{\partial}{\partial x}\left[\left\{U(x,z) + \frac{3}{2} T_i(x,z)\right\} D_{\perp} \frac{\partial n_p(x,z)}{\partial x}\right] + \frac{\partial}{\partial x}\left\{K_{i\perp} \frac{\partial T_i(x,z)}{\partial x}\right\}$$

Independent variables $(f_{k,z}, U, T_e, T_i)$

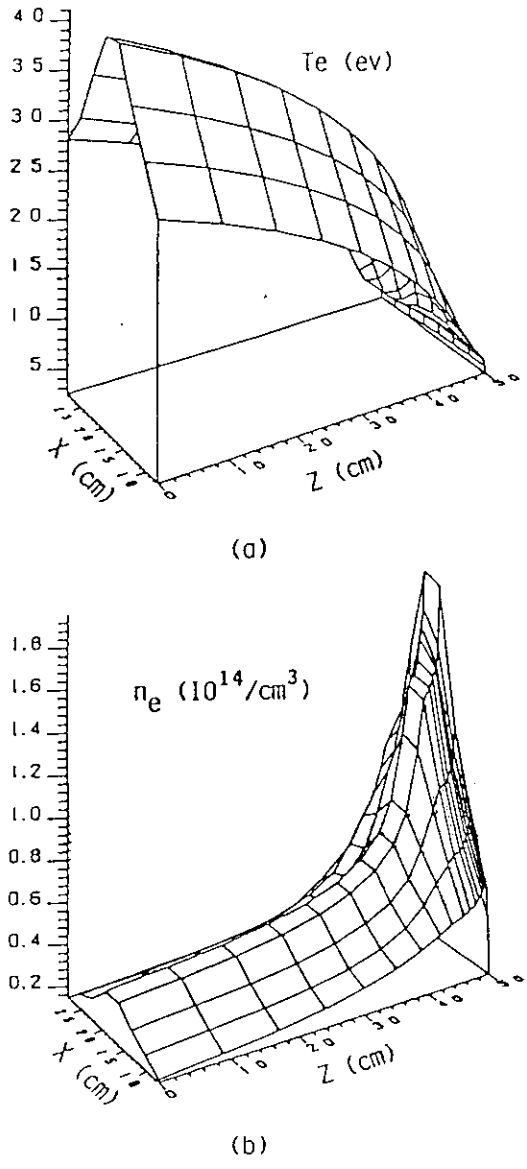

Fig. 3.1.3 Two-dimensional view of electron temperature and electron density in the divertor chamber calculated by self-consistent numerical code of divertor plasma. Electron temperature decreases below 10 eV at the divertor plate.

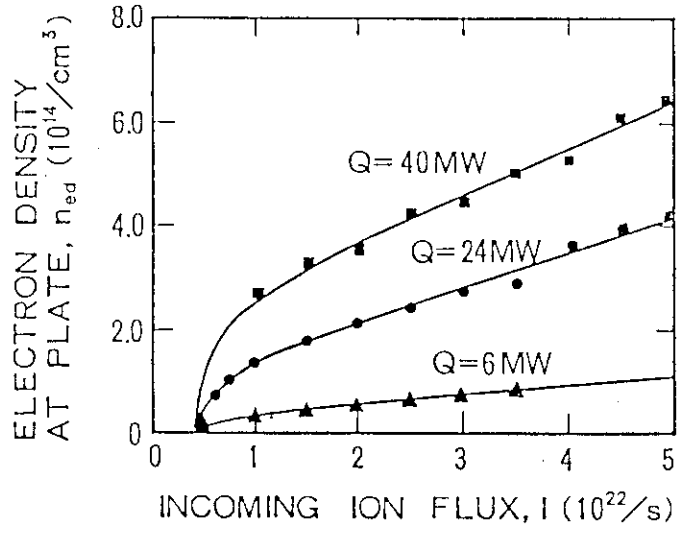

Fig. 3.1.4 Electron density at the divertor plate for various heat flux to divertor chamber as a function of incoming ion flux. Low temperature and high density plasma can be formed even when the incoming flux is rather small.

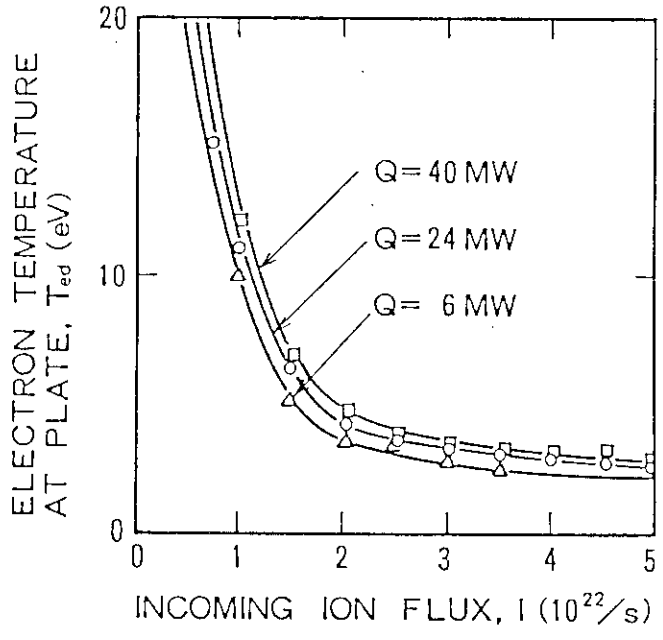

Fig. 3.1.5 Electron temperature at the divertor plate for the case of Fig. 3.1.4.

Conclusions in Divertor analyses

1. Cold and dense divertor plasma formation can well be expected in FER.

2. Geometry of divertor chamber is important to support the cold and dense plasma formation.

3. Low pumping speed ($\leq 10^5$ l/s) will be sufficient for helium ash exhaust.

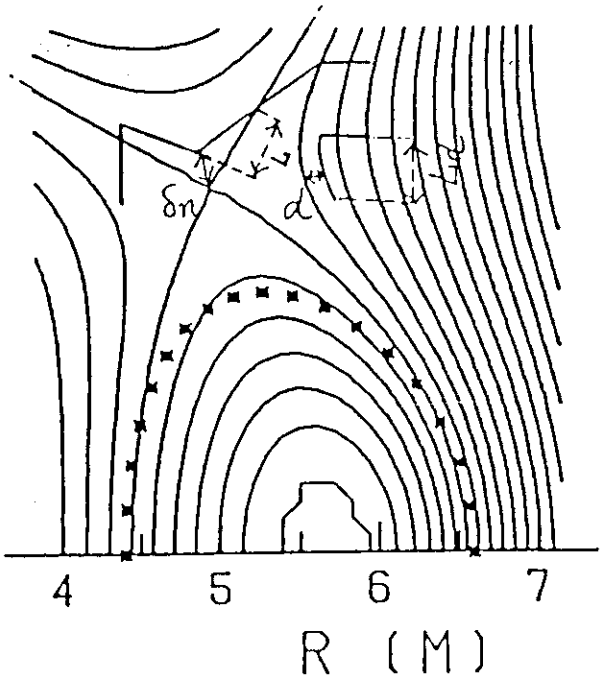

Geometry

L	50 cm
L_d	40 cm
d	5 ~ 10 cm
δ_n	10 cm

Particle flux 2×10^{24} l/s

Electron temperature near divertor plate 30 eV

Heat load

particle	6.4 MW
radiation	7.7 MW

Pumping speed 10^5 l/s

Fig. 3.1.6 Geometrical restriction imposed on the divertor design study.

II. Pumped-Limiter

- Limiter chamer: 2D calculation as in divertor
- Limiter surface: scrape-off analyses including main plasma are essential

↓ Preliminary Calculation

1D (r) calculation with convection model

[impact of transport coefficients on performance of limiter]

Model

(1) Main plasma transport equations

Deuterium:

$$\frac{\partial n_D}{\partial t} = -\frac{1}{r}\frac{\partial}{\partial r} r\,\Gamma_D - n_D n_T \langle\sigma v\rangle_f - \frac{n_D}{\tau_{\parallel}} + S_D \quad ,$$

Tritium:

$$\frac{\partial n_T}{\partial t} = -\frac{1}{r}\frac{\partial}{\partial r} r\,\Gamma_T - n_D n_T \langle\sigma v\rangle_f - \frac{n_T}{\tau_{\parallel}} + S_T \quad ,$$

Singly ionized helium:

$$\frac{\partial n_{He^+}}{\partial t} = -\frac{1}{r}\frac{\partial}{\partial r} r\,\Gamma_{He^+} - \frac{n_{He^+}}{\tau_{\parallel}} + S_{He^+}$$

Fully ionized helium:

$$\frac{\partial n_{He^{++}}}{\partial t} = -\frac{1}{r}\frac{\partial}{\partial r} r\,\Gamma_{He^{++}} + n_D n_T \langle\sigma v\rangle_f - \frac{n_{He^{++}}}{\tau_{\parallel}} + S_{He^{++}} \quad ,$$

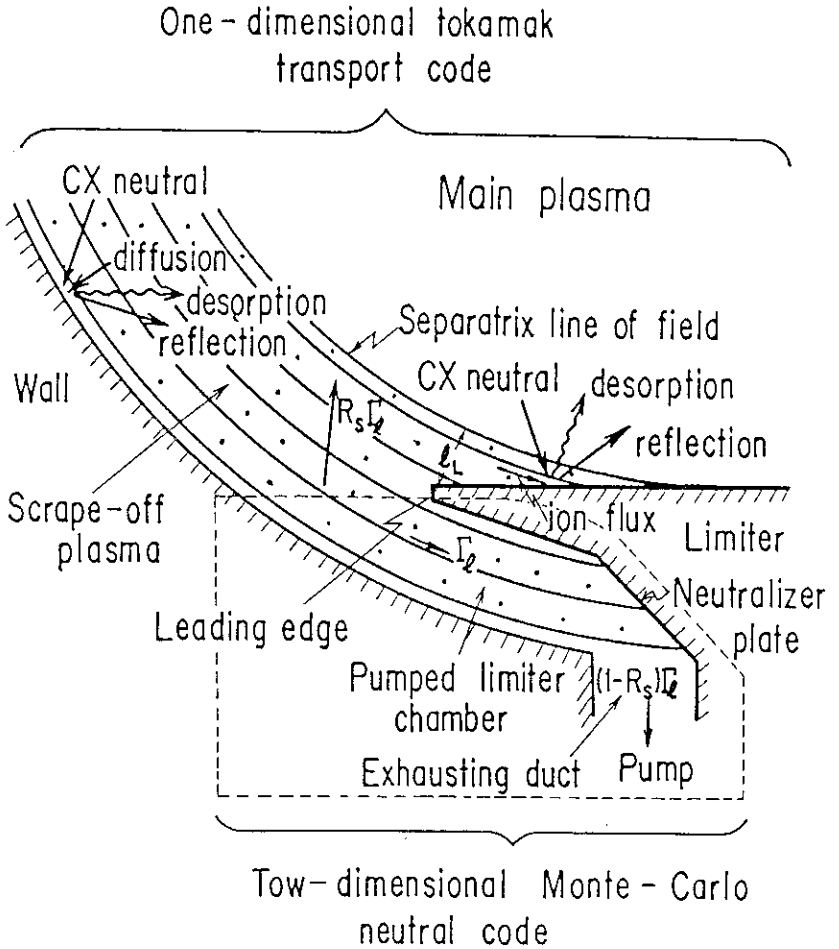

Fig. 3.1.7 Schematic drawing of the model for the calculation of the scrape-off layer plasma by one-dimensional transport code.

(2) Main plasma transport scaling

INTOR Scaling

(3) Neutral transport: 1D Boltzmann eq.

$$N(r) = \int_0^R N(r')\ \tilde{\psi}(r,r')dr' + \psi(r)$$

(4) Transport model in scrape-off layer (convection model)

Particle loss	$\frac{n}{\tau_{/\!/}} = \frac{n}{L/V_f}$
electron energy loss	$\underline{\gamma_i}\ \frac{n_e T_e}{\tau_{/\!/}}$
ion energy loss	$\underline{\gamma_e}\ \frac{n_i T_i}{\tau_{/\!/}}$
radial transport	$D = \chi_e = \chi_i = \underline{C_B}\ D_{Bohm}$
flow velocity	$V_f = \underline{\underline{C_d}} \times C_s$

Table 3.1.1 Two cases of various transport coefficients in the scrape-off layer, conventional simple sheath model case and best fitting case for the simulation of ASDEX limiter experiment by one-dimensional transport code.

Simulation of ASDEX Limiter Experiment

	Conventional Sheath Model	Best Fitting
C_d	0.3	1.0
C_B	0.3	0.5
γ_e	5.8	15.0
γ_i	2.0	2.0

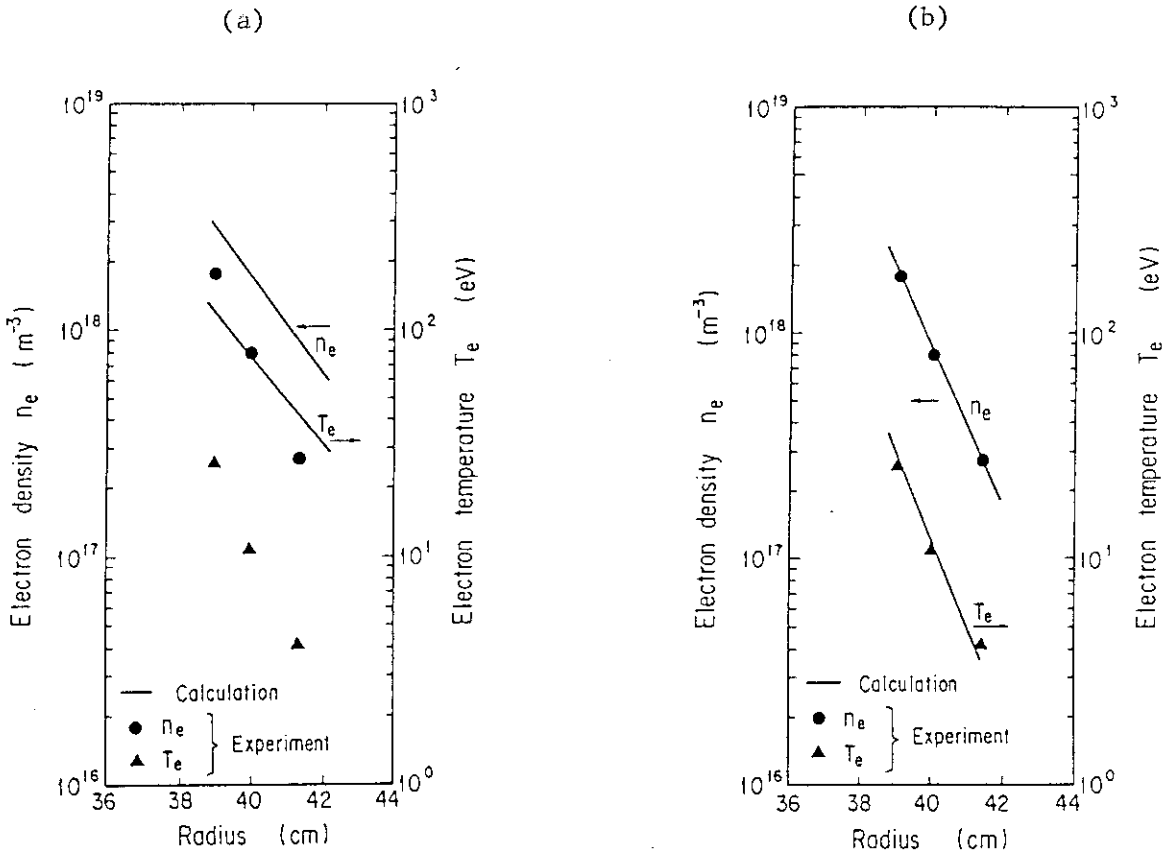

Fig. 3.1.8 Electron density (●) and temperature (▲) profile in the scrape-off layer observed in ASDEX limiter experiments. Solid lines show the results of numerical calculation by using conventional sheath model (a) and best fitting transport coefficients (b).

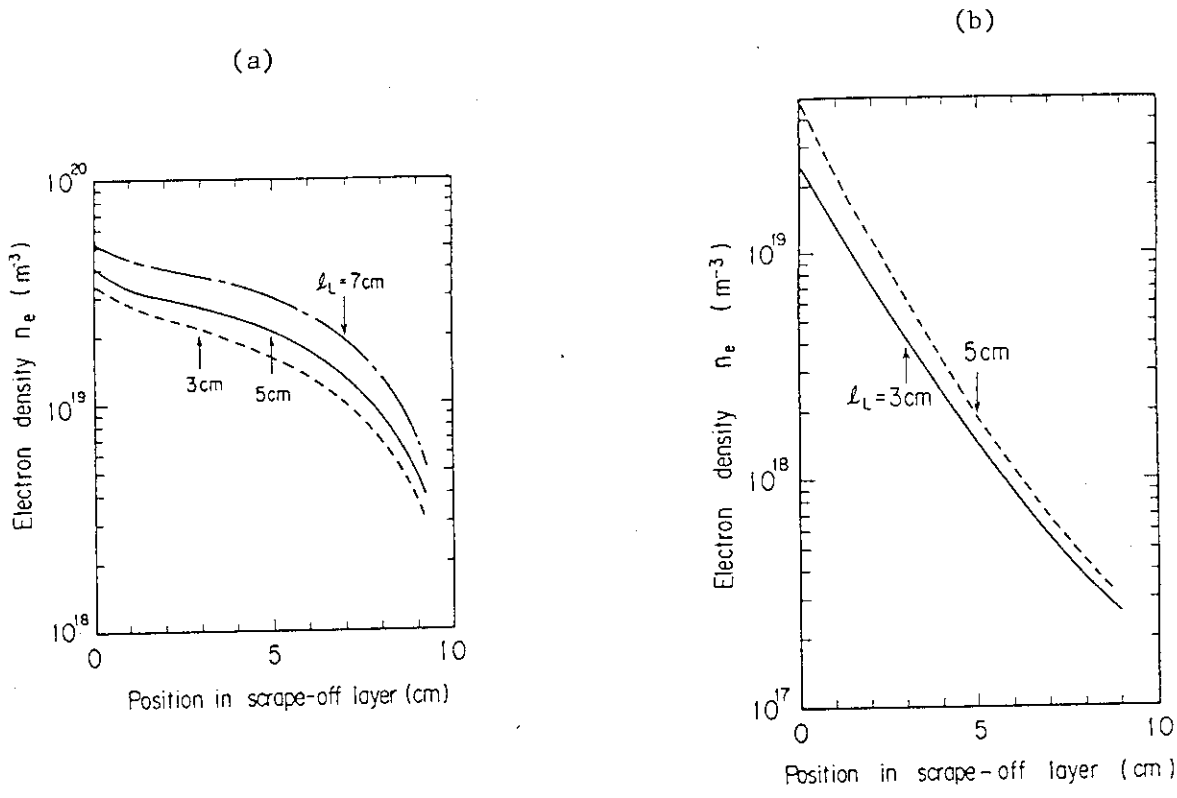

Fig. 3.1.9 Density profile in scrape-off layer of FER with pumped-limiter calculated by numerical code by using simple sheath model (a) and best fitting transport coefficients (b).

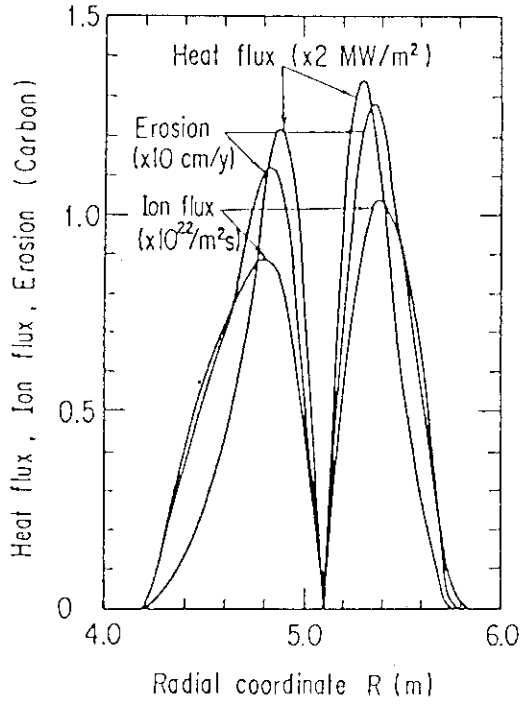

(a)

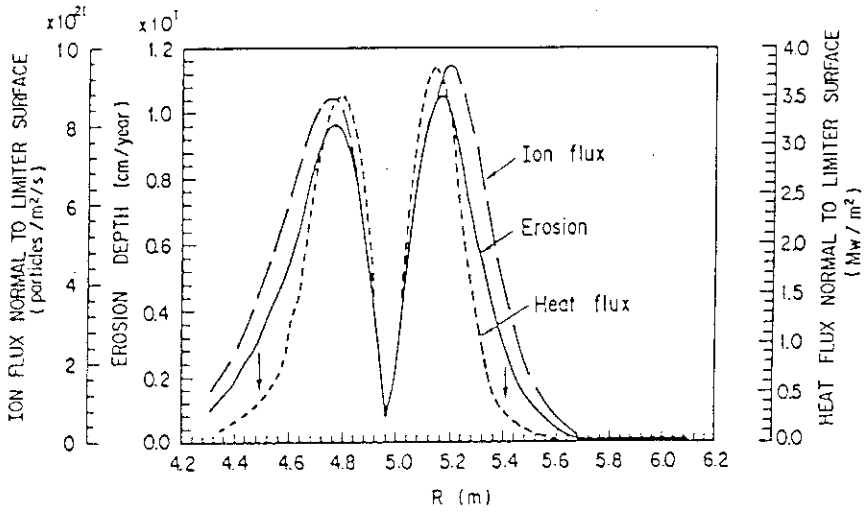

(b)

Fig. 3.1.10 Ion and heat flux and erosion of FER pumped-limiter surface calculated by numerical code by using simple sheath model (a) and best fitting transport coefficients (b).

Applicability of Pumped-Limiter

- Large uncertainty in transport coefficients
- Plasma parameters greatly depend on the coefficients
- Large heat load/erosion in any case
- convective model is insufficient?
  - radiative cooling is less expectable than divertor
  - 2D calculation is necessary?
- Cold boundary layer should be considered for application of pumped-limiter
  ⟶ larger plasma size

Table 3.1.2 Plasma and device parameters for comparative design studies of pumped-limiter. In Case L2, cold boundary layer of 20 cm is considered.

Plasma and Device Parameters for Design Study of Pumped-Limiter

	Case L1	Case L2
1. Cold boundary layer	None	Yes ~ 0.2 m
2. Temp. of scrape-off layer	≳ 100 eV	~ several tens eV
3. Major radius (m)	5.7	6.0
4. Minor radius (m)	1.17	1.46*
5. Average ion temp. (keV)	10	10
6. Average ion density (10^{20} m^{-3})	1.28	1.2
7. Toroidal field (T)	5.5	5.2
8. Plasma current (MA)	5.5	5.8*
9. Safety factor	2.5	2.5*
10. Fusion power (MW)	460	480*

* Same plasma performance within the cold boundary layer

Table 3.1.3 Conclusion of physics design considerations of poloidal divertor and pumped-limiter.

Conclusions

	Divertor	Pumped-Limiter
Advantage	○ Cold/dense plasma in divertor region	○ Applicability to less elongated plasma
Critical point	○ Vertical position control	○ Formation of cold boundary layer⟶ larger plasma size, potential advantage in heat removal in commercial reactor
Suitable for	FER	Commercial Reactor

3.2 Comparative study of engineering features for divertor and pumped limiter reactor concepts

Comparative study of engineering features is carried out for divertor and pumped limiter reactor concepts. These are 4 concepts: double null divertor (DND) as a reference concept of FER, single null divertor (SND), single pumped limiter with medium edge temperature (SPL1) and single pumped limiter with low edge temperature (SPL2). Plasma parameters of these concepts are determined by maintaining equality of plasma confinement performance (confinement time and plasma β). It is found that SND, SPL1 and SPL2 have several merits and demerits relative to the reference conceptsas follows.

(1) Reactor size and maintenance

The single null divertor and pumped limiter concepts have a disadvantage of the increase of TF coil bore, resulting in the increase of magnetic ripple (0.89% in SPL1 to 0.5% in DND) and reactor size. However, divertor and limiter plate replacements for those cases are simpler than that of double null divertor case becase they can be done with single straight motion.

(2) Passive stabilization

Plasma vertical displacement will be stabilized partly by means of saddle coils made of beryllium in the blanket. Since plasma decay index of DND is relatively large, DND is not good selection in comparison with SND and SL1 concepts for passive stabilization. The SL2 concept is also not advantageous because the location of shell must be far from plasma.

(3) Magnet system

In the single null divertor and pumped limiter, case mechanical fatigue strength for both TF and PF coils are reduced considerably. The AC losses in the magnets also decrease considerably, in particular, reduced by half in cases of the pumped limiter concepts.

(4) Capacity of power supply

Stored energies of PF coils in cases of pumped limiter concepts are about half of those of DND. Capacities of power supply for PF coils also are approximately reduced in proportion to the sotred energy.

Table 3.2.1 Main plasma parameters in cases of Reference and Alternative designs

	Double Null Divertor	Single Null Divertor	Single Pumped Limiter, L 1	Single Pumped Limiter, L2
Plasma major radius (m)	5.5	5.72	Same as single null divertor	6.01
Plasma minor radius (m)	1.1	1.17		1.46+
Aspect ratio	5.0	4.89		4.12
Plasma elongation	1.5	1.5		1.5
Plasma triangularity	$\gtrsim$0.2	$\gtrsim$0.2		$\gtrsim$0.2
First wall radius (m)	1.25	1.395		1.685
Average ion temprature (keV)	10	10		10
Average ion density (m)	1.36	1.28		1.19
Toroidal fiels on plasma axis (T)	5.7	5.48		5.22
Peak thermonuclear power (MW)	440	458		480
Plasma current (MA)	5.3	5.54		5.8*
Safety factor	2.5	2.5		2.5*
Toroidal ß (%)	4.0	4.1		4.1
Poloidal ß (%)	2.28	2.18		2.08

Note: Parameters are determined for equality of plasma confinement performance.

*) Plasma cold layer is excluded.
Current in cold layer is neglected.

+) Cold layer (o.2 m) is included.
Plasma confiment performance is evaluated for plasma minor radius of 1.26 m.

Table 3.2.2 Bore size of TF coil and toloidal ripple in Reference and Alternative Designs

	Bore of TF coil (m)	Magnet-motive force (MAT)	Max. Field (T)	Ripple at plasma outer radius (%)
Double Null Divertor (Reference)	6.3×9.42 m	157	11.58	0.50
Single Null Divertor	6.79×8.9	157	11.56	0.53
Single Pumped Limiter, L 1	6.59×8.2	157	11.57	0.73
Single Pumped Limiter, L 2	7.17×8.8	157	11.58	0.71

Table 3.2.3 Electro-magnetic Forces on TF coil in Reference and Alternative Designs

	Double Null Divertor (DND)	Single Null Divertor (SND)	Single Pumped Limiter Case 1 (SPL 1)	Single Pumped Limiter Case 2 (SPL 2)
Hoop Force (ton)	114,500	110,700	104,800	109,900
Centering Force (ton)	-36,960	-35,400	-32,150	-35,160
Vertical Force (ton)	24,610	25,510	25,130	26,230
Overturn Force (ton)	-1,461 (Upper Half)	1,663	590	644
Max. Overturning Force per Unit Length (ton/m)	2,040	1,910	964	1,110
Overturning Moment around R-axis (ton·m)	3,896	9,338	10,800	10,480
Torsional Moment around Z-axis (ton·m)	12,290	17,680	16,960	18,020

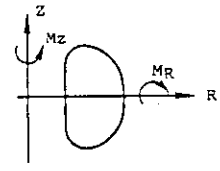

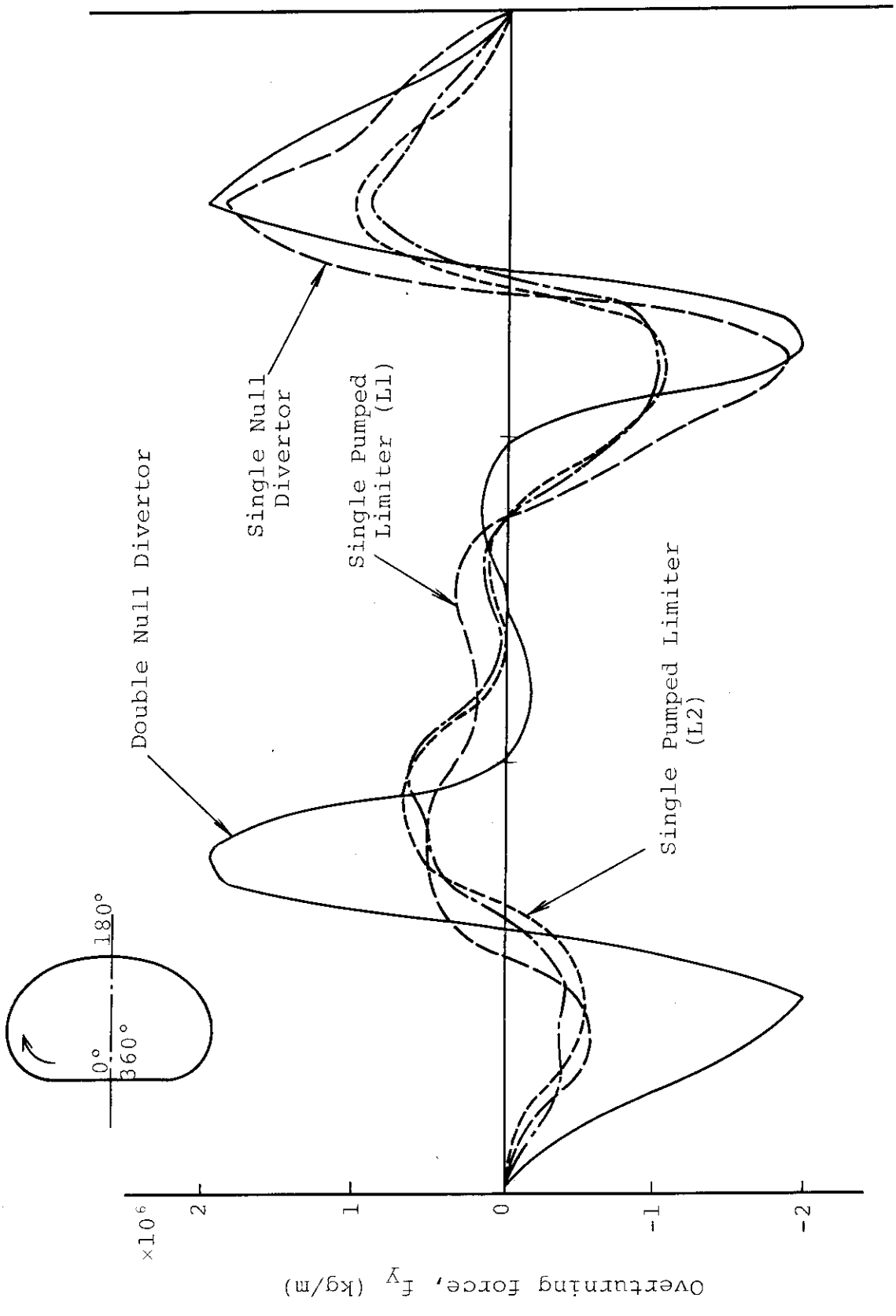

Fig. 3.2.1 Overturning forces distribution along coil perimeter

Table 3.2.4 Stress of inner ring at each position due to overturning force

	A	B	C	D
Double Null Divertor	45.4	12.4	12.4	31.4
Single Null Divertor	16.8	13.6	17.8	36.8
Single Pumped Limiter, L1	16.6	13.5	15.3	16.7
Single Pumped Limiter, L2	18.0	14.0	16.0	15.5

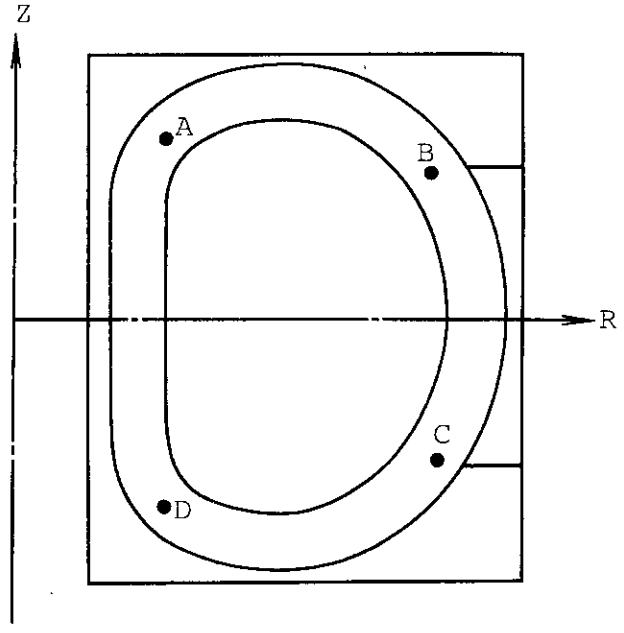

Table 3.2.5 Stress in TF coil due to hoop and overturning forces in Reference and Alternative Designs

		Thickness (mm)	Double Null Divertor	Single Null Divertor	Single Pumped Limiter, L1	Single Pumped Limiter, L2
Helium Vessel	Inner Ring	100	45.8	39.4	27.2	29.0
	Outer Ring	180	59.2	63.7	60.4	62.5
	Side Plate	150	29.0	29.4	27.6	30.0
Support Frame		100	15.8	15.7	16.7	17.6
Shear Panel		100	40.5	32.7	21.2	24.2
Support Ring		300	-37.6	-39.6	-37.7	-38.9
Center Post		600	45.0	41.3	41.0	41.2
Coil Leg		100	8.1	7.8	7.2	9.0
FRP Spacer	Radial	——	-24.1	-22.6	-21.2	-21.5
	Axial	——	-17.1	-15.9	-10.7	-11.7
Conducter		——	28.6	27.6	27.0	27.4

Unit : kg/mm^2

Table 3.2.6 Equivalent cyclic stress amplitude, Seq of support structures on TF coil

	Double Null Divertor	Single Null Divertor	Single Pumped Limiter, L1	Single Pumped Limiter, L2
Inner Ring	29.0	22.9	9.7	10.5
Outer Ring	13.6	13.4	9.0	10.0
Shear Panel	24.9	22.1	12.9	14.9

$$Seq = \frac{Salt}{1 - \frac{Smean}{Su}}$$

Salt: Cyclic stress amplitude
Smean: Modified mean stress
Su : Ultimate strength

Table 3.2.7 Comparison of Electromagnetic characteristics for PF system

	Double Null Divertor	Single Null Divertor	Single Pumped Limiter, L1	Single Pumped Limiter, L2
Max. Ampere turns (MAT)	98.7	71.3	52.6	66.9
Max. Field on coil (T)	7.2	6.9	6.7	6.3
Stored Energy (GJ)	5.96	4.94	2.73	3.47
Induced Voltage (kV)	12	16	8	8.5

Table 3.2.8 Electromagnetic forces of PF coils in Reference and Alternative Designs

	Inboard coil		Outboard coil	
	Hoop force	Out-of- plane force	Hoop force	Out-of-plane force
Double Null Divertor	15,000	6,570	42,600	9,360
Single Null Divertor	13,800	4,070	32,500	7,950
Single Pumped Limiter (L 1)	13,200	5,110	20,600	6,190
Single Pumped Limiter (L 2)	11,500	3,400	22,800	3,260

Unit : ton

Table 3.2.9 Stress of PF coil in Reference and Alternative Designs

	Inboard coil		Outboard coil	
	Hoop stress	Bending stress	Hoop stress	Bending stress
Double Null Divertor	41.5	8.49	20.2	8.18
Single Null Divertor	38.0	8.24	17.8	11.2
Single Pimped Limiter (L 1)	36.3	6.58	9.71	8.20
Single Pumped Limiter (L 2)	31.8	5.96	13.5	8.02

Unit : kg/mm

Table 3.2.10 AC Lesses in Toroidal Coil of Reference and Alternative Designs

		Double Null Divertor	Single Null Divertor	Single Pumped Limiter, L 1	Single Pumped Limiter, L 2
Superconductor	Eddy current loss	4.02	2.97	1.08	1.28
	Coupling loss	7.15	4.50	1.57	1.87
Support Structures	Helium Vessel	49.73	31.75	13.02	15.0
	Shear panel	32.05	24.43	11.22	16.32
	Center post	17.84	18.64	19.15	16.29
Sum		110.8	82.3	46.0	50.8

Unit : kW

Table 3.2.11 AC Losses in Poloidal Field Coils of Reference and Alternative Designs

		Double Null Divertor	Single Null Divertor	Single Pumped Limiter, L1	Single Pumped Limiter, L2
Superconducter	Hysteresis loss	0.56	0.47	0.39	0.39
	Eddy current loss	0.24	0.18	0.12	0.12
	Coupling loss	1.49	1.27	0.80	0.86
Support Structures (Eddy current loss)	S.S reinforcement in conductor	0.04	0.03	0.01	0.02
	S.S support frame for outer coils	2.91	1.50	0.22	0.34
	S.S support rings for inner coils	12.43	13.03	11.19	11.42
Sum		17.7	16.5	12.7	13.2

Unit : kW

Table 3.2.12 Capacity of PF Power Supply

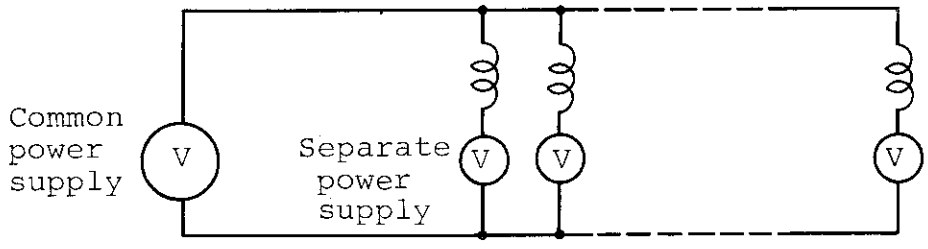

	Effective Power	Reactive Power	Apparent Power
Double Null Divertor	1234 MW	1926 MVA	2566 MW
Single Null Divertor	1208 MW	1864 MVA	2705 MW
Single Pumped Limiter, L1	462 MW	889 MVA	1421 MW
Single Pumped Limiter, L2	637 MW	1133 MVA	1854 MW

Table 3.2.13 Parameters for passive stabilization analysis

	Double-null divertor	Single-null divertor	Single-limiter (1) (L1)	Single-limiter (2) (L2)
Plasma				
Major plasma radius	5.5 m	5.72 m	5.72 m	6.01 m
Plasma current	5.3 MA	5.54 MA	5.54 MA	5.8 MA
Poloidal beta	2.28	2.18	2.18	2.08
<Bz>	-0.37 T	-0.39 T	-0.41 T	-0.39 T
<n>	-1.86	-1.50	-1.33	-1.28
Shell				
Material	Be	Be	Be	Be
Electrical resistivity	7 μΩ·cm	7 μΩ·cm	7 μΩ·cm	7 μΩ·cm
Cross section	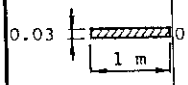	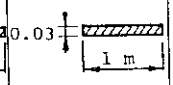	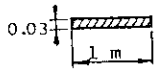	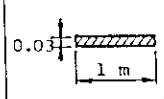
Connector				
Material	Cu	Cu	Cu	Cu
Electrical resistivity	2 μΩ·cm	2 μΩ·cm	2 μΩ·cm	2 μΩ·cm
Cross section	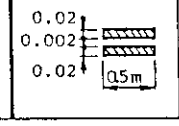	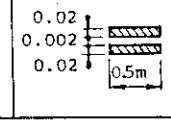	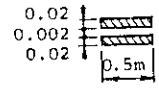	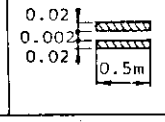

(1) Medium edge temperrature limiter

(2) Low edge temperature limiter

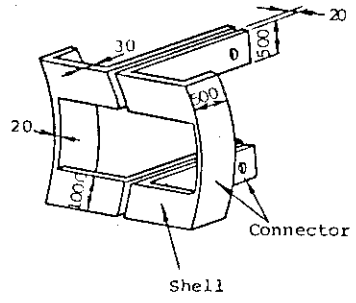

Table 3.2.14 Characteristics of the passive stabilizing coils for divertor/limiter concepts

	Double-null divertor	Single-null divertor	Single limiter (1) (L1)	Single limiter (2) (L2)
Max. decay index of passive coil	2.8	2.6	2.6	1.8
Time constant of passive coil	72ms	74ms	74ms	78ms
Growth rate of plasma vertical instability	36ms	54ms	71ms	32ms

(1) Medium edge temperature limiter

(2) Low edge temperature limiter

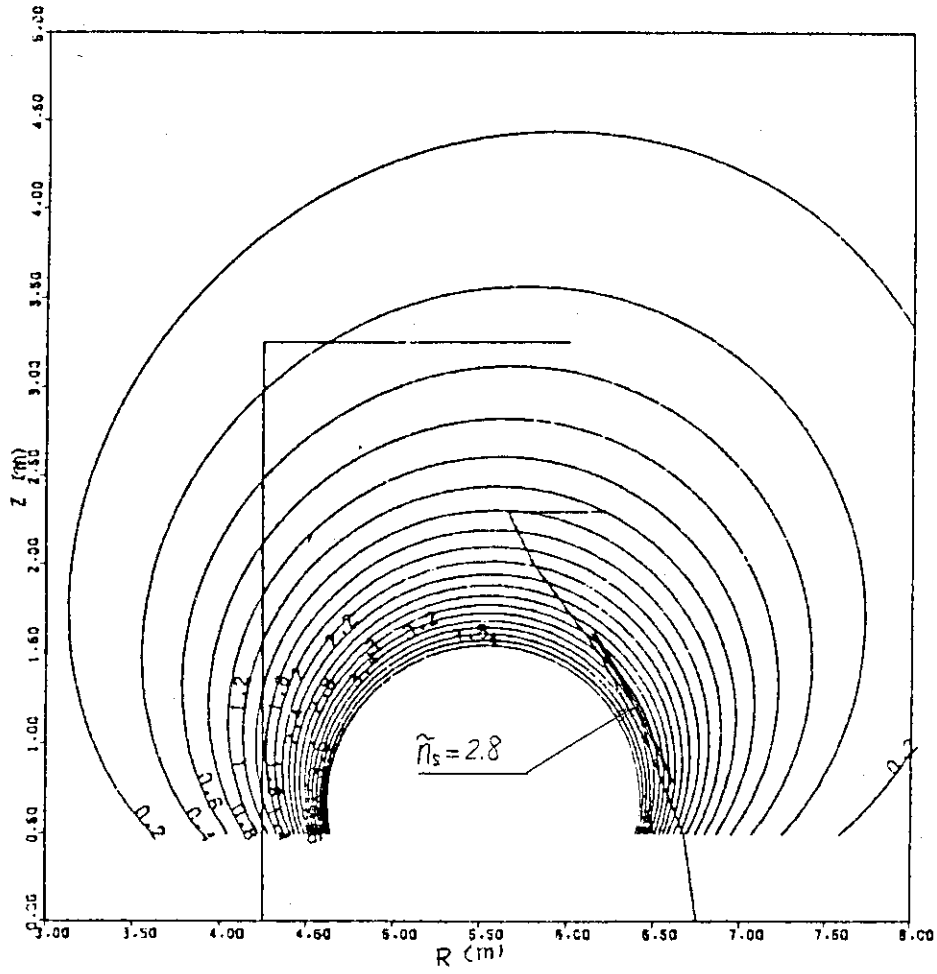

Fig. 3.2.2 Contours of decay index on the plasma due to currents induced in passive stabilizing coils located at (R,Z) as a result of vertical plasma displacement (Double-null divertor)

Table 3.2.15 Conclusion

	DND	SND	L1	L2
Reactor size	○	△	△	X
TF Coil Stress	X	△	○	○
PF Coil Stress	X	～	↗	△
Plasma Control	X	△	○	X
Power Supply Capacity for PF Coil	X	X	○	○
TF Coil AC loss	X	X	△	△
PF Coil AC loss	○ (X)	○ (X)	○ (△)	○ (△)
Maintenance	X	○	○	○

○ ---- good
△ ---- medium
X ---- bad

3.3 Engineering design of divertor and pumped limiter plates

Several concepts have been considered for the FER impurity control system. The purpose of this section is shown in Table 3.3.1. Table 3.3.2 shows the design requirement of plates. The results of the engineering-related consideration for the divertor and limiter plates is presented.

(1) Operating conditions and mechanical configuration

The divertor and limiter operating conditions are given in Table 3.3.3 to Table 3.3.5. The profiles of the divertor and limiter operations are shown in Figure 3.3.1 to Figure 3.3.4. The divertor collector plates are set with an angle which limits the peak heat flux to 2 MW/m^2. The electron temperature on divertor plate is 30 eV.

The limiter plate is a flat shape with two leading edges. Two plasma scrape-off conditions have been considered for the limiter operation. For the medium edge temperature condition (L1), the peak heat flux on the top surface is 3 MW/m^2. The peak electron temperature on plate is 150 eV. The heat flux on the leading edge far from the main plasma is small. For the low edge temperature condition (L2), the peak heat flux is only 0.5 MW/m^2. The peak electron temperature is 25 eV.

The collector plates of divertor and limiter are shown in Figure 3.3.5 to Figure 3.3.7. The divertor/limiter plate is composed of a protective material, heat sink and supporting structure. The protective material in the form of tiles is brazed to the copper heat sink. Reference materials considered for the tiles are tungsten for the divertor plate and the low edge temperature limiter, and beryllium for the medium edge temperature limiter.

(2) Thermal hydraulics and stress analysis

The operating conditions used in the thermal hydraulics and stress analysis are listed in Table 3.3.6. The analysis is conducted by a three-dimensional model as shown in Figure 3.3.8 and Figure 3.3.9. Temperature and stress distributions in the divertor plate are shown in Figure 3.3.10 and Figure 3.3.11. Temperature and stress distributions at the top surface of limiter are shown in Figure 3.3.12 to Figure 3.3.15. Table 3.3.7 summarizes the maximum temperatures and stresses of the collector plate.

For the divertor concepts, the maximum temperature in the tungsten tile is 194°C. The maximum temperatures in a 20 mm thick beryllium tile is 651°C for the limiter with the medium edge temperature condition. The temperature in plate is very low for the limiter with the low edge temperature condition.

The stress intensity in the copper heat sink is quite high (227 MPa) for the divertor concepts. This stress is above the ASME allowable stress of 117 MPa for annealed OFHC copper. The stress intensity in copper is 106 MPa for the medium edge temperature limiter with the 20 mm thick beryllium tile. The stress in plate is quite low for the low edge temperature limiter.

(3) Lifetime of divertor and limiter plates

The lifetime of the divertor/limiter plate has been estimated by the erosion of plasma side material and the fatigue life of copper heat sink. The erosion rate of divertor/limiter plate is shown in Table 3.3.8. The erosions considered for tile materials are the loss during plasma disruption and the physical sputtering. The estimated erosion rate by disruption is the total of vaporized and melt layers assuming the melt layer is lost. The estimated erosion rate by sputtering does not include the effect of the redeposition on the plate of the sputtered impurity ions.

Table 3.3.9 shows the estimated lifetime of plates. The lifetime due to erosion is 1.4 year for the divertor, and 0.9 year for the medium edge temperature limiter with 20 mm thick tile. The effect of the redeposition will extend the lifetime of plates. The lifetime is very long for the low edge temperature limiter.

The fatigue life of the heat sink is 1 year for the divertor concepts, even if the design curve of fatigue with the safety factor of 1.5 on strain range or 20 on life is employed. The limiter concepts have the long lifetime. The summary of engineering design of plates is shown in Table 3.3.10.

TABLE 3.3.1 PURPOSE OF ENGINEERING DESIGN FOR DIVERTOR AND PUMPED LIMITER PLATES

PURPOSE

- TO DEVELOP A FEASIBLE DIVERTOR AND LIMITER PLATES DESIGN
- TO COMPARE DIVERTOR AND LIMITER SOLUTIONS

CONCEPTS FOR IMPURITY CONTROL SYSTEM

- DOUBLE-NULL DIVERTOR
- SINGLE-NULL DIVERTOR
- SINGLE PUMPED LIMITER WITH A MEDIUM EDGE TEMPERATURE CONDITION (L1)
- SINGLE PUMPED LIMITER WITH A LOW EDGE TEMPERATURE CONDITION (L2)

TABLE 3.3.2 DESIGN REQUIREMENT OF DIVERTOR/LIMITER PLATES OPERATING CONDITION

- HEAT AND PARTICLE FLUXES UNDER NORMAL OPERATION
- HEAT FLUX AND ELECTROMAGNETIC FORCE DURING PLASMA DISRUPTION

ENGINEERING DESIGN OF PLATE

- TO HAVE THE SUFFICIENT LIFETIME FOR BOTH THERMAL FATIGUE AND EROSION

Table 3.3.3 Heat fluxes to divertor and limiter

		Divertor		Pumped limiter	
		Double-null (Ref.)	Single-null	Medium T (L1)	Low T (L2)
Peak thermonuclear power	(MW)	437	455	455	480
Neutrons	(MW)	350	364	364	384
Alpha-heating	(MW)	87	91	91	96
First wall					
Radiation (Bremsstrahlung and synchrotron)	(MW)	10	10	10	10
Radiation (Impurity near plasma centre)	(MW)	12	12	12	12
Radiation (Impurity at plasma edge)	(MW)	15	15	15	60
Charge exchange	(MW)	5	5	5	5
Divertor/Limiter					
Conduction and connection into divertor/limiter(1)	(MW)	60	60	60	10
Radiation	(MW)	44	45	-	-
Ions and electrons on plates	(MW)	16	15	60	10

(1) Design value considering the uncertainty of heat loss at plasma edge region

Table 3.3.4 Divertor/limiter operating conditions

	Double-null divertor	Single-null divertor	Single limiter (L1)	Single limiter (L2)
Heat loads (MW/m^2)				
Peak, Middle of collector plate	2 (1)	2	3	0.5
Peak, Leading edge	-	-	0.5	0.1
Particle fluxes ($m^{-2}S^{-1}$)				
Ions, Middle of collector plate	1.1×10^{23}	1.1×10^{23}	1.1×10^{22}	1.1×10^{22}
Ions, Leading edge	-	-	7.3×10^{21}	7.3×10^{21}
Electron temperature (eV)				
Peak, Middle of collector plate	30	30	150	25
Peak, Leading edge	-	-	44	7
Engineering				
Inclination of plate to separatrix				
Outboard	30°	24°	-	-
Inboard	63°	27°	-	-
Plasma side clading				
Material	W	W	Be	W
Thickness (mm)	1	1	10,20	1
Sputtering rate (mm/y) (2)	0.7	0.7	16	0.05
Heat sink	Cu	Cu	Cu	Cu
Supporting structure	SS	SS	SS	SS

(1) Peak heat flux on inboard plate is 1 MW/m^2 in case of the same inclination of plate to separatrix as the single-null divertor operation

(2) Only physical sputtering

Table 3.3.5 Major plasma disruption characteristics

			Double-null divertor	Single-null divertor	Single limiter(1) (L1)	Single limiter(2) (L2)
Frequency		(cycles)	1000	1000	1000	1000
Time	Plasma current	(ms)	15	15	15	15
	Thermal energy	(ms)	5	5	5	5
Energy	Thermal energy	(MJ)	150	166	166	188
	Field energy	(MJ)	30	34	34	50
Divertor/Limiter	Energy(3)	(MJ)	60	66	66	75
	Energy density	(J/cm^2)	200	220	330	380
First Wall	(a) Local wall(4)					
	Energy	(MJ)	60	67	67	81
	Energy density	(J/cm^2)	110	110	110	110
	(b) Uniform wall					
	Energy (Radiation)	(MJ)	60	60	60	60
	Energy density	(J/cm^2)	20	20	20	20

(1) Medium edge temperature limiter

(2) Low edge temperature limiter

(3) 40% of thermal energy with the same spatial distribution as the operating load

(4) On to 30% of wall with an additional peaking factor of 2

Table 3.3.6 Divertor/limiter operating conditions for temperature and stress calculation

			Double-null divertor	Single-null divertor	Single limiter (L1)	Single limiter (L2)
Surface heat flux		(MW/m^2)	2	2	3 (1)	0.5 (1)
Nuclear heating rate						
Plasma side cladding		(MW/m^3)	19	19	8	19
Heat sink	(Cu)	(MW/m^3)	10	10	15	10
Support structure	(SS)	(MW/m^3)	8	8	12	8
Coolant temperature						
Inlet/Outlet		(°C)	50/80	50/80	50/80	50/60
Coolant velocity		(m/s)	7	7	7	7
Heat transfer coefficient		($W/m^2°C$)	3.2×10^4	3.2×10^4	3.4×10^4	3.4×10^4
Plasma side cladding						
Material			W	W	Be	W
Thickness		(mm)	1	1	10,20	1
Heat sink thickness	(Cu)	(mm)	20	20	10	10
Support structure thickness	(SS)	(mm)	20	20	40	40

(1) At the top surface of limiter plate

Table 3.3.7 Temperature and thermal stress of divertor/limiter plate

		Double-null divertor	Single-null divertor	Single limiter (L1)	Single limiter (L2)
Plasma side cladding					
Material		W	W	Be	W
Thickness	(mm)	1	1	10 , 20	1
Heat sink (Cu)					
Thickness	(mm)	20	20	10	10
Maximum temperature					
Plasma side cladding	(°C)	194	194	409 , 651	82
Heat sink	(°C)	178	178	176 , 179	78
Maximum stress intensity					
Plasma side cladding	(MPa)	292	292	200 , 215	41
Heat sink	(MPa)	227	227	97 , 106	35

Table 3.3.8 Erosion rate of divertor/limiter plate

		Double-null divertor	Single-null divertor	Single limiter (L1)	Single limiter (L2)
Operating conditions					
Particle flux on plate	($m^{-2}s^{-1}$)	1.1×10^{23}	1.1×10^{23}	1.1×10^{22}	1.1×10^{22}
Electron temperature on plate	(eV)	30	30	150	25
Duty cycle	(%)	50	50	50	50
Availability	(%)	25	25	25	25
Plasma side cladding					
Reference material		W	W	Be	W
Erosion rate					
W	(mm/yr)	0.7	0.7	∞(1)	0.05
Be	(mm/yr)	64	64	16	5
C	(mm/yr)	97	97	12	8
SiC	(mm/yr)	110	110	21(2)	10

(1) Self-sputtering yield exceeds unity

(2) The DSPUT code predicts self-sputtering yield greater than unity. Then, SiC will have a severe erosion.

JAERI－M 84－107

Table 3.3.9 Life time of divertor/limiter plate

		Double-null divertor	Single-null divertor	Single limiter (L1)	Single limiter (L2)
Normal operating conditions[1]					
Heat flux on plate	(MW/m^2)	2	2	3	0.5
Particle flux on plate	($m^{-2}s^{-1}$)	1.1×10^{23}	1.1×10^{23}	1.1×10^{22}	1.1×10^{22}
Electron temperature on plate	(eV)	30	30	150	25
Number of shots	(/yr)	4×10^4	4×10^4	4×10^4	4×10^4
Tile thickness	(mm)	1(W)	1(W)	10,20 (Be)	1(W)
Heat sink thickness (Cu)	(mm)	20	20	10	10
Plasma disruption conditions[1]					
Peak energy density	(J/cm^2)	200	220	330	380
Life time					
Life due to erosion					
Erosion by sputtering	(mm/yr)	0.7	0.7	16	0.05
Melt/vapor loss by disruption	(mm/yr)	-	-	6	-
Life	(year)	1.4	1.4	0.45,0.9	20
Fatigue life of Cu					
Stress range	(MPa)	227	227	97,106	35
Life[2]	(year)	0.25	0.25	>Reactor life	>Reactor life
Life[3]	(year)	1	1	>Reactor life	>Reactor life

(1) Duty cycle=50%, Availability=25%, Disruption time constant=5ms, Disruption per year=42

(2) Design curve of fatigue with the safety factor of 2 on strain range or 20 on life

(3) Design curve of fatigue with the safety factor of 1.5 on strain range or 20 on life

TABLE 3.3.10 SUMMARY OF ENGINEERING DESIGN OF PLATES

(1) LIMITER CONCEPT L2 HAS A LONG LIFETIME FOR BOTH EROSION AND FATIGUE.

(IT IS DESIRABLE IF THE PHYSICAL CONSIDERATION PERMITS THIS CONDITION.)

(2) DIVERTOR CONCEPT HAS A SHORT FATIGUE LIFETIME. THE PEAK HEAT FLUX IS NEEDED TO BE REDUCED.

(TILES MADE OF LOW Z MATERIALS (BE ETC.) CAN BE USED FOR THE LONG LIFETIME IF THERE IS A EFFECT OF RE-DEPOSITION.)

(3) LIMITER CONCEPT L1 HAS A SHORT LIFETIME DUE TO EROSION. WE HOPE THE LARGE EFFECT OF RE-DEPOSITION ON THE PLATE OF THE SPUTTERED IMPURITY IONS.

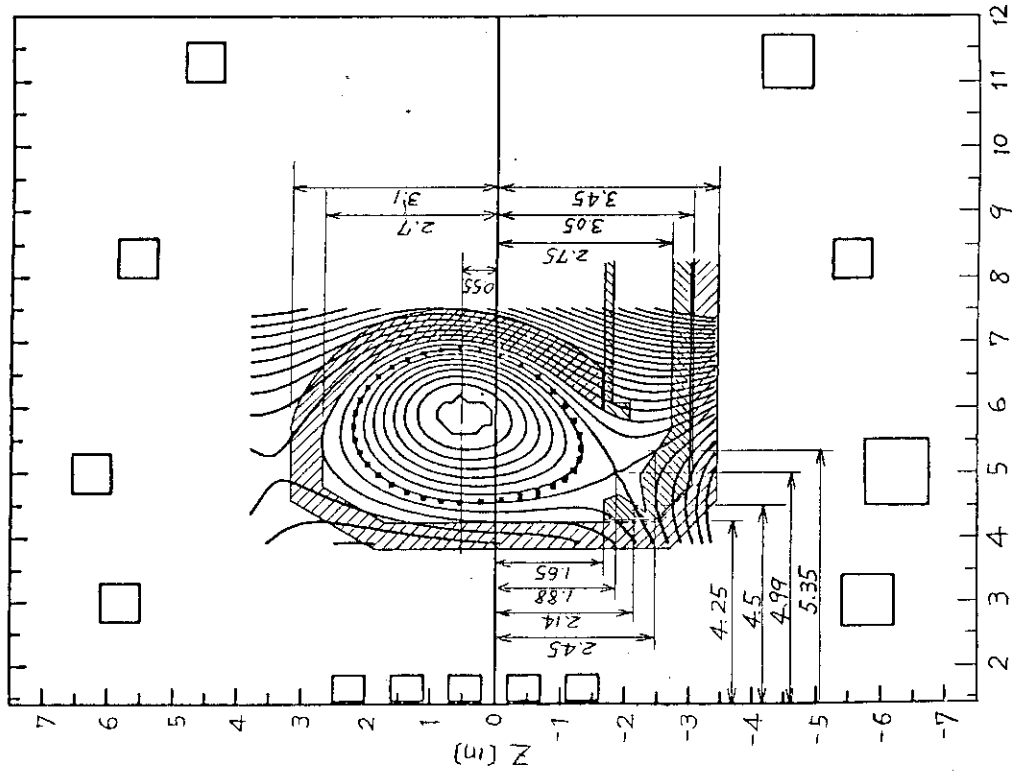

Fig.3.3.2 Profile of single-null divertor

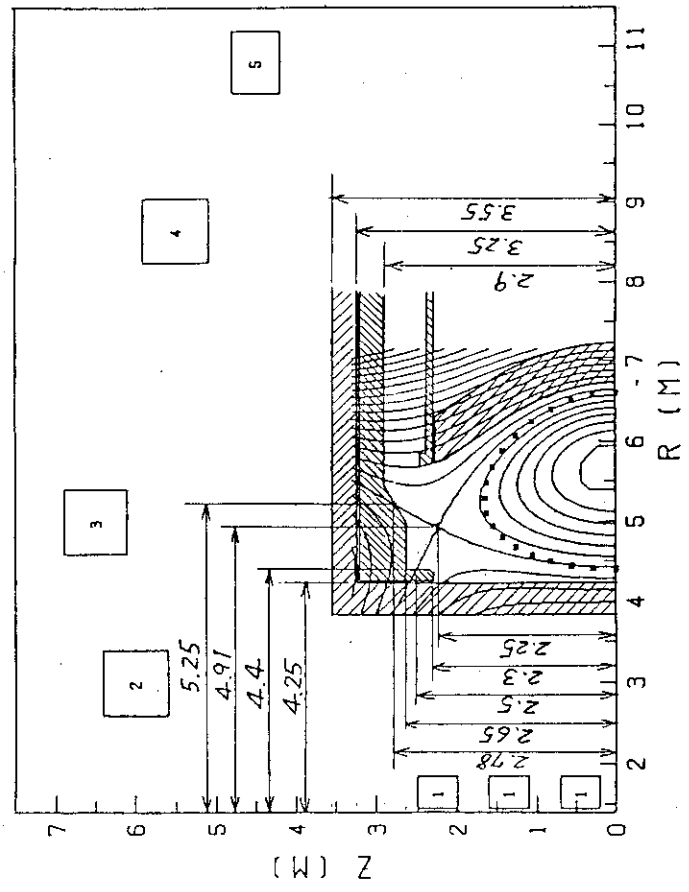

Fig.3.3.1 Profile of double-null divertor

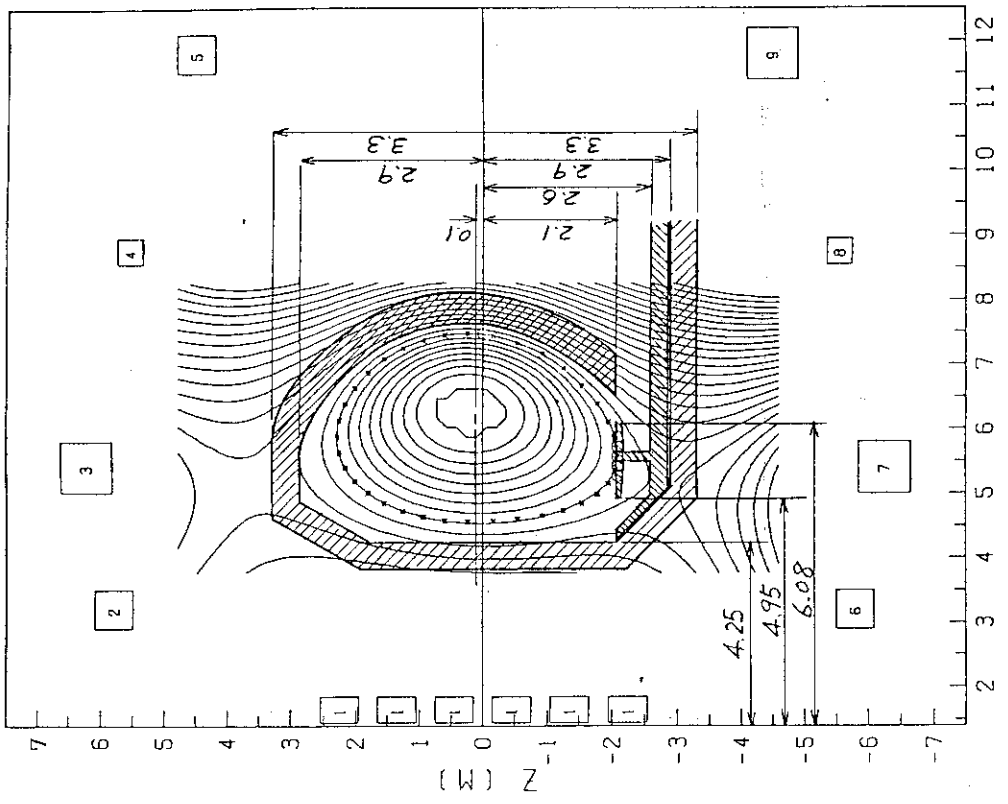

Fig.3.3.4 Profile of single limiter with a low edge temperature condition

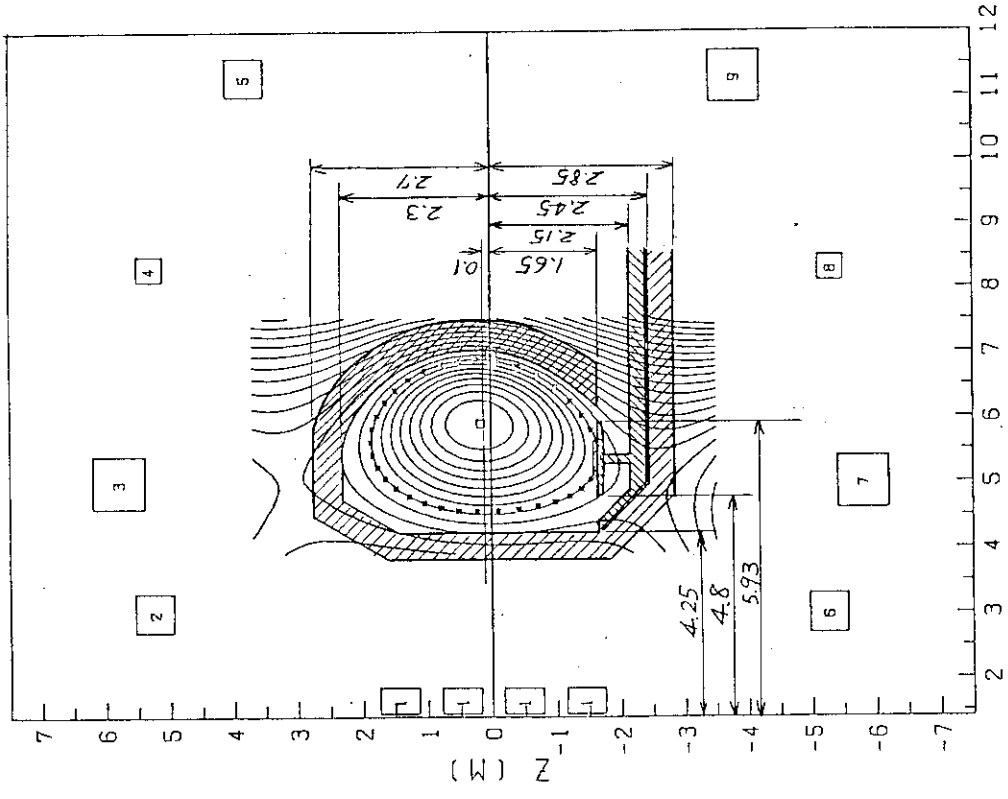

Fig.3.3.3 Profile of single limiter with a medium edge temperature condition

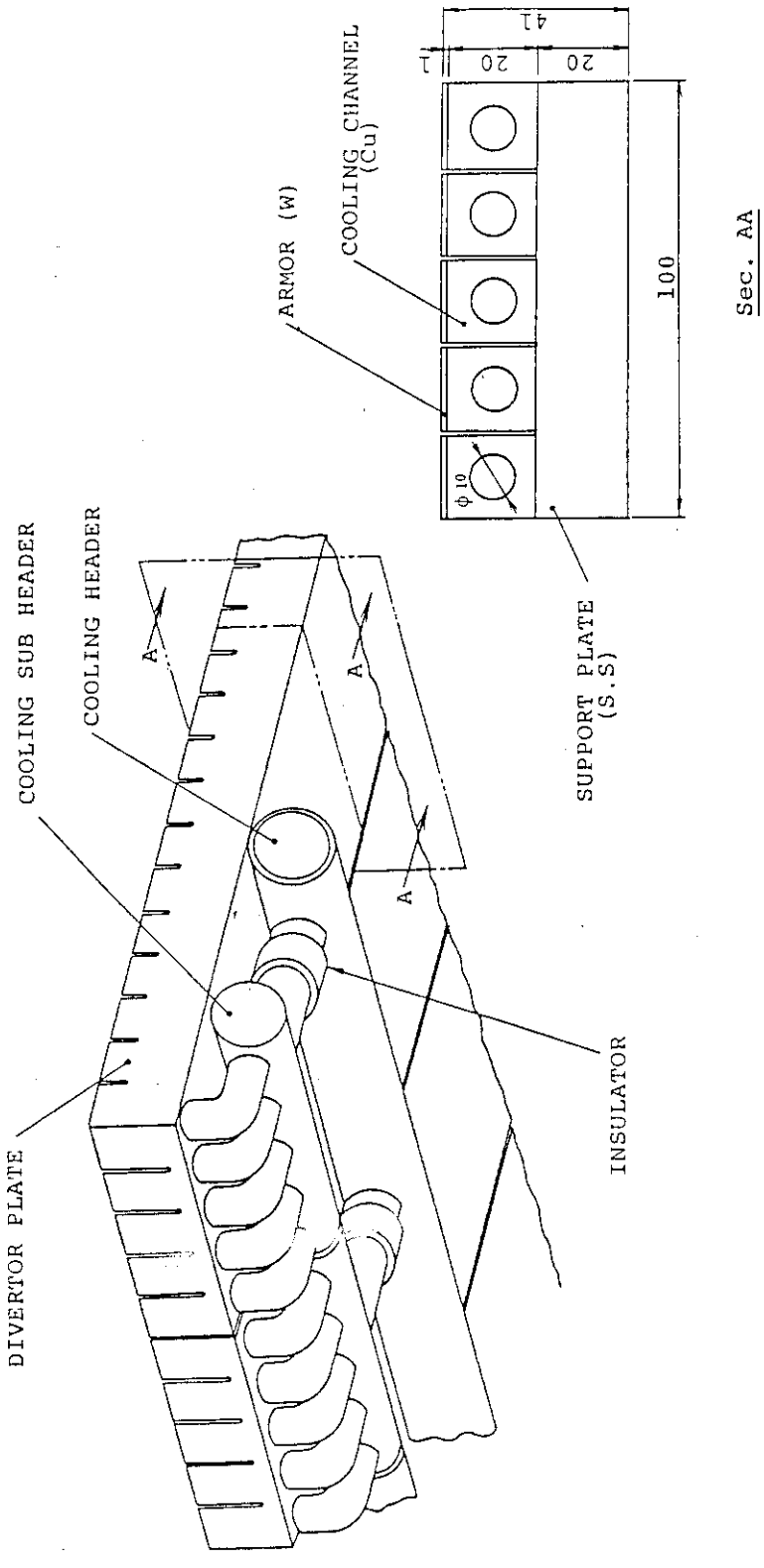

Fig.3.3.5 Divertor plate

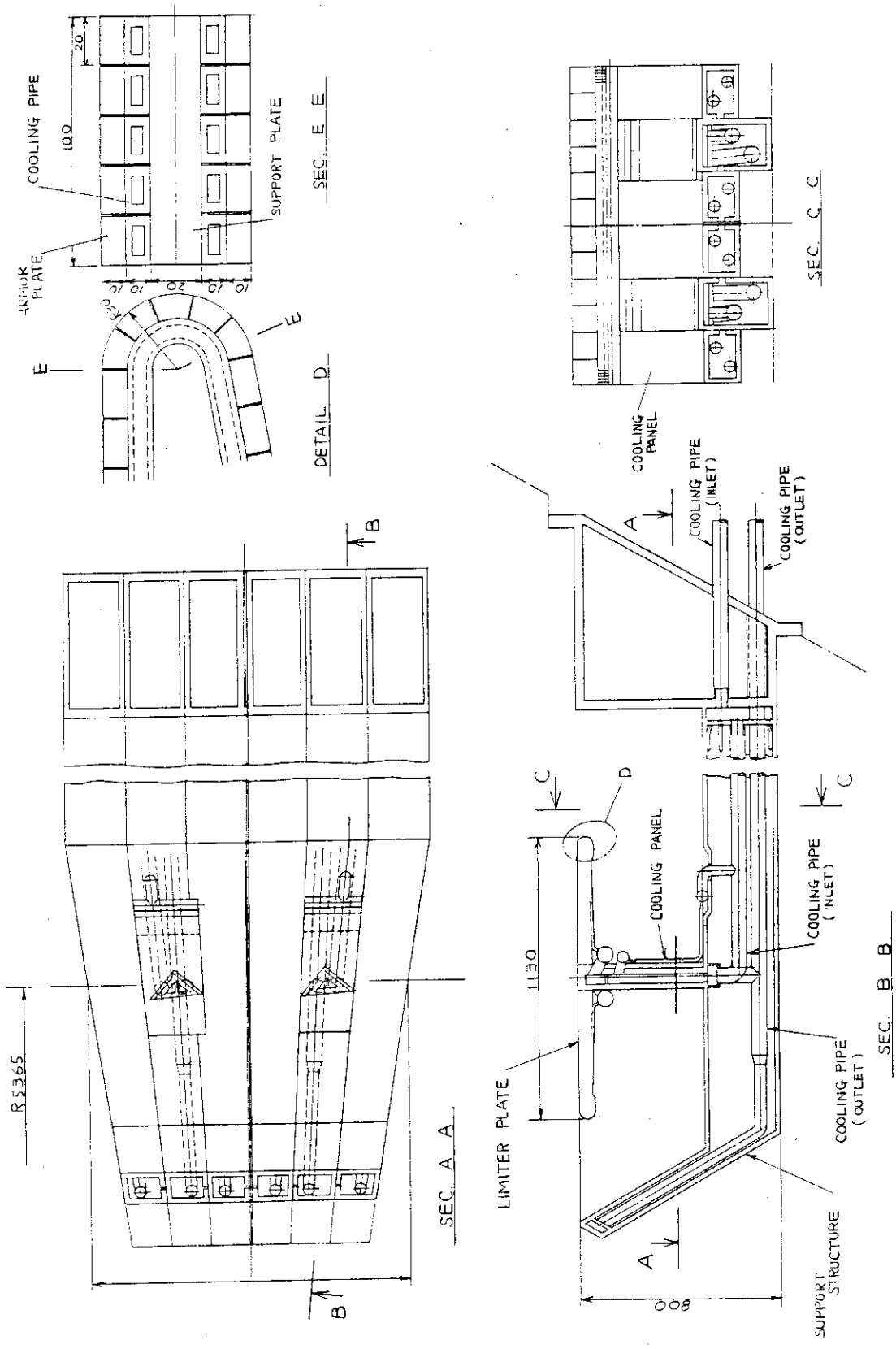

Fig.3.3.6 FER LIMITER (TYPE L1)

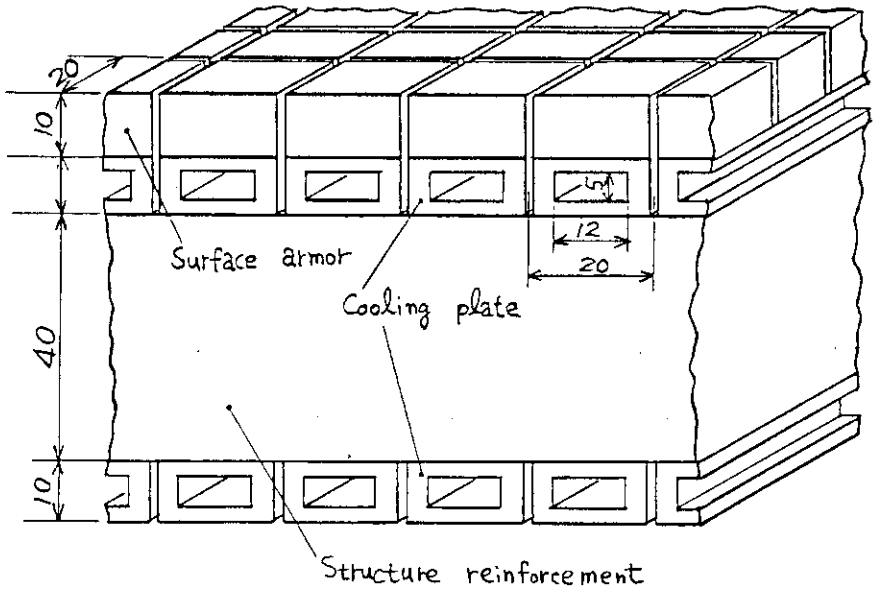

Fig.3.3.7 Cross section at the top surface of limiter plate

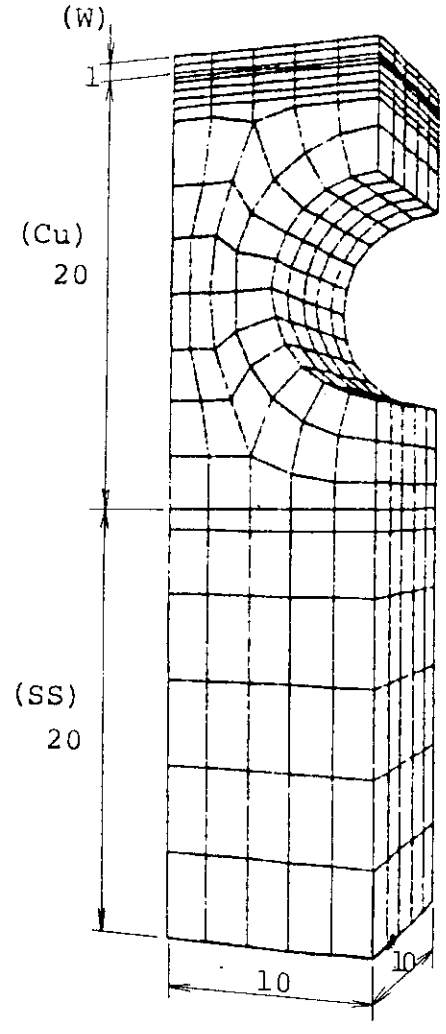

Fig.3.3.8 Divertor plate geometry used for thermal hydraulics and stress analysis

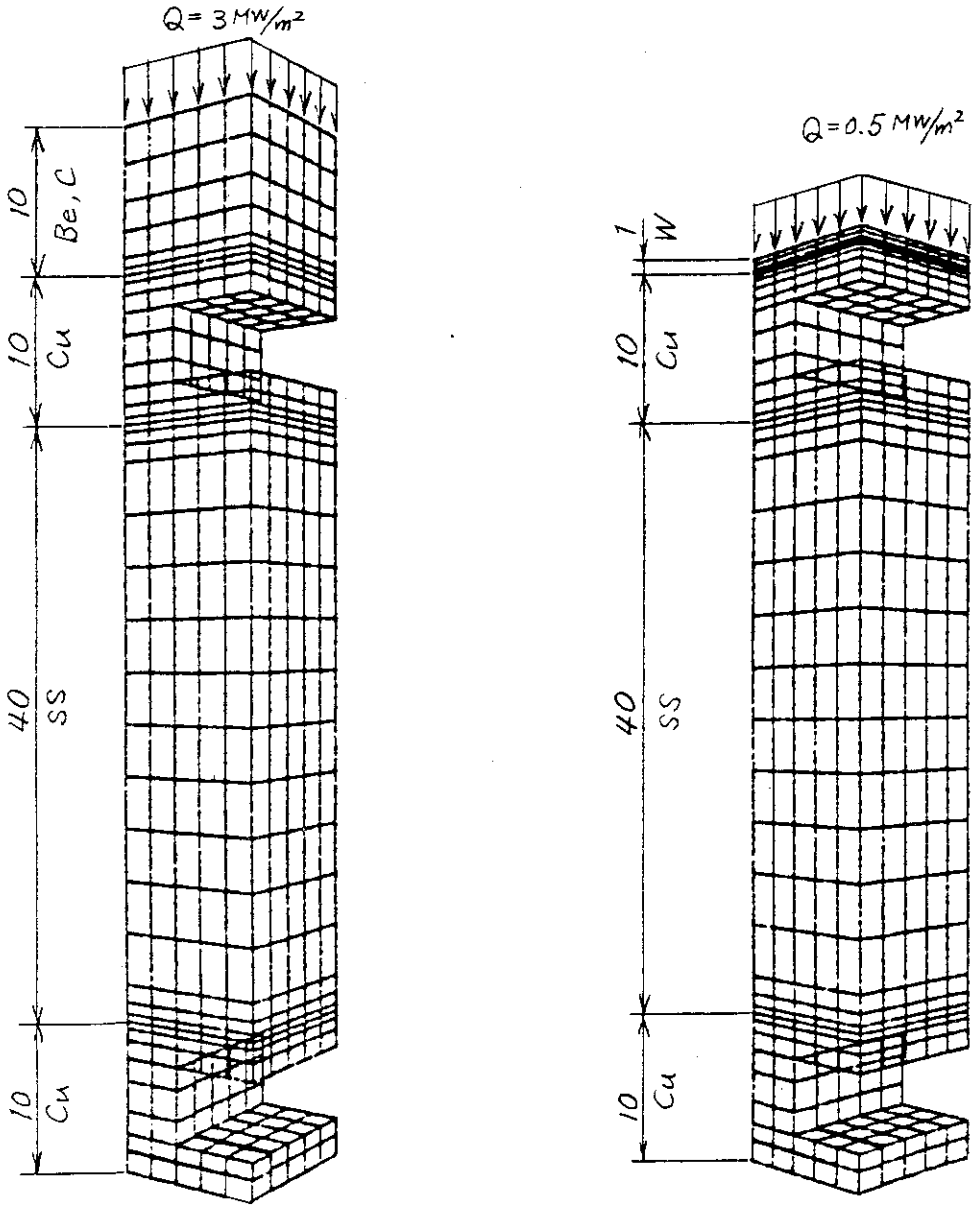

(a) Medium edge temperature limiter

(b) Low edge temperature limiter

Fig.3.3.9 Limiter plate geometry used for thermal hydraulics and stress analysis

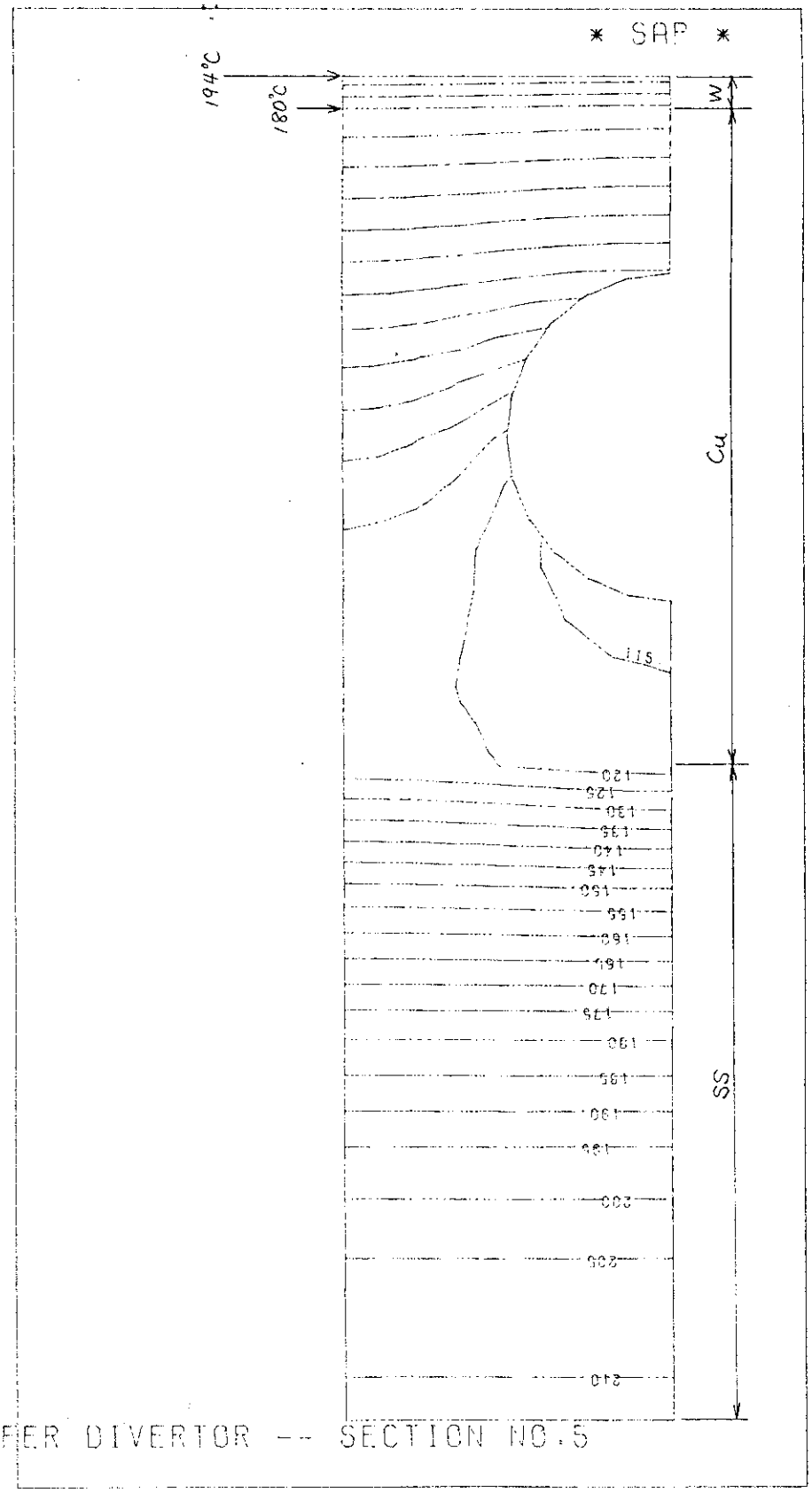

Fig.3.3.10 Temperature distribution of divertor plate with 1 mm thick tungsten tile on copper heat sink (Heat flux = 2 MW/m^2)

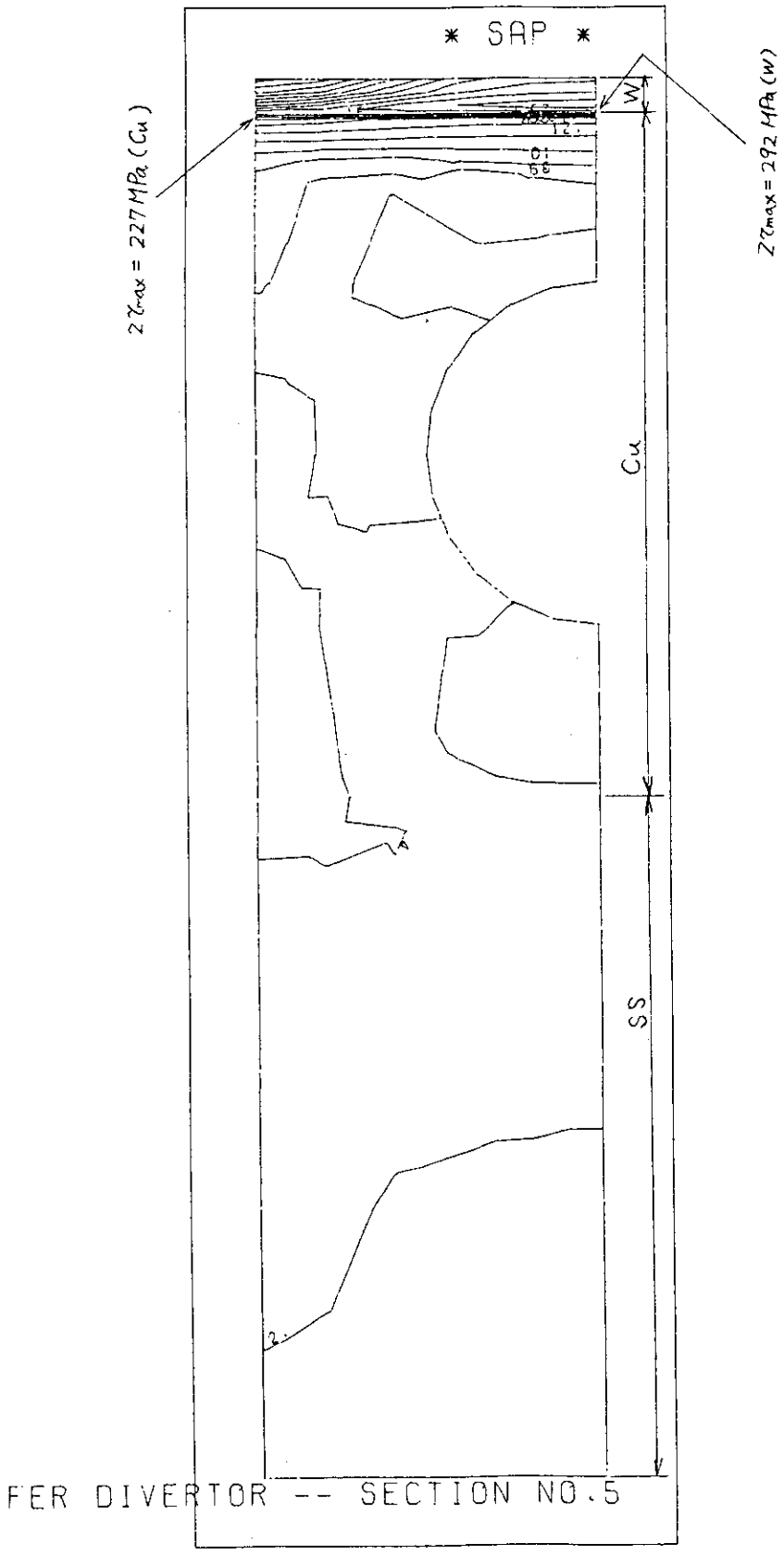

Fig.3.3.11 Stress distribution of divertor plate with 1 mm thick tungsten tile on copper heat sink (Heat flux = 2 MW/m^2)

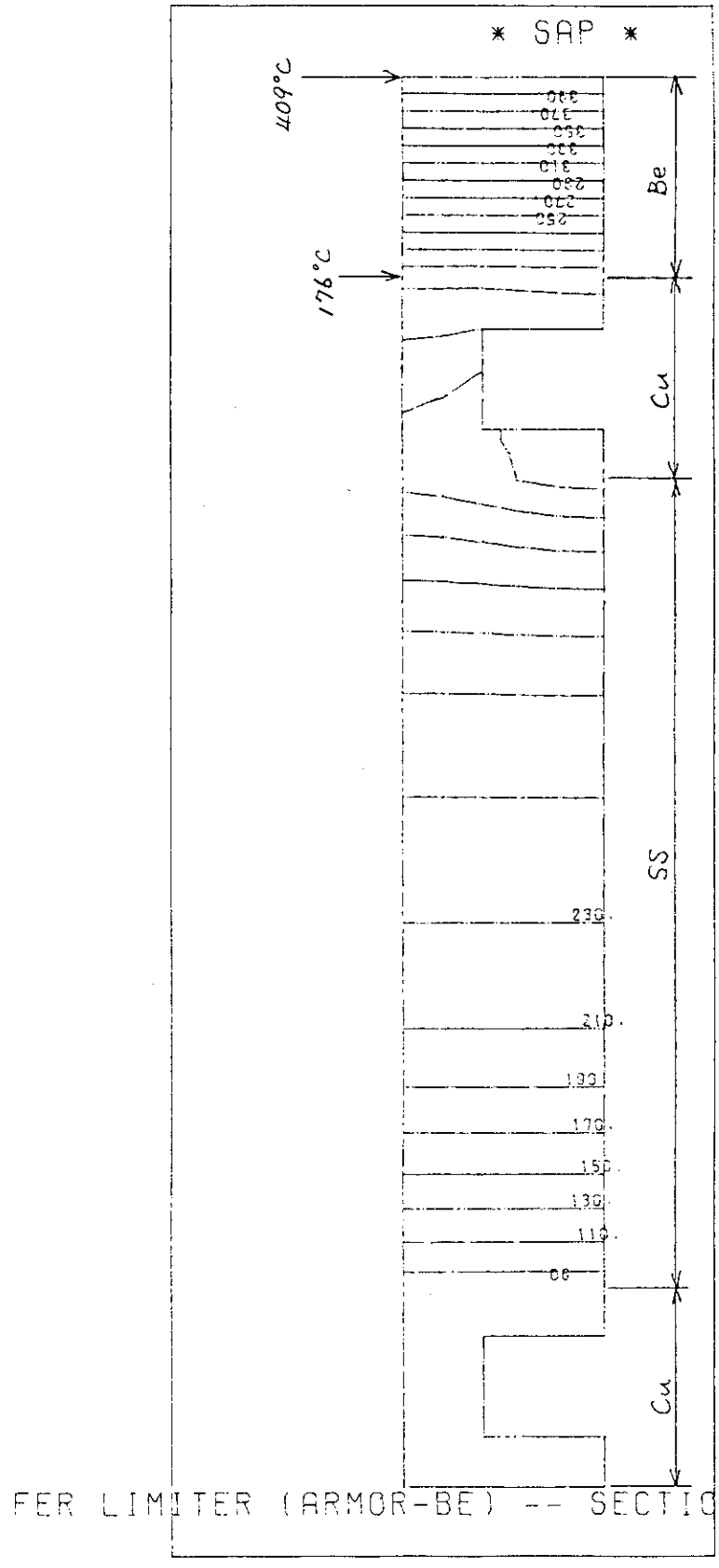

Fig.3.3.12 Temperature distribution at the top surface of a medium edge temperature limiter with 10 mm thick beryllium tile on copper heat sink (Heat flux = 3 MW/m^2)

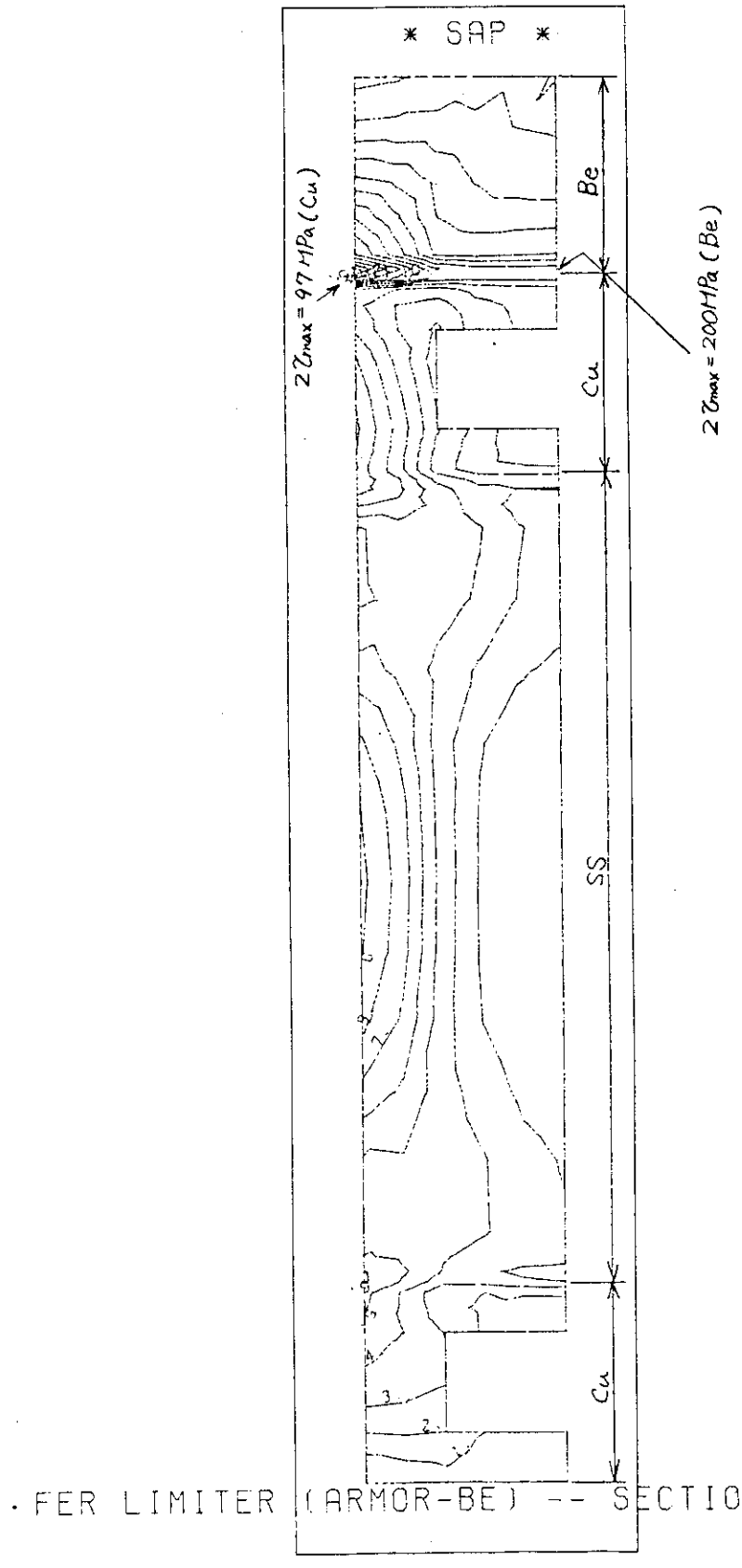

Fig.3.3.13 Stress distribution at the top surface of a medium edge temperature limiter with 10 mm thick beryllium tile on copper heat sink (Heat flux = 3 MW/m^2)

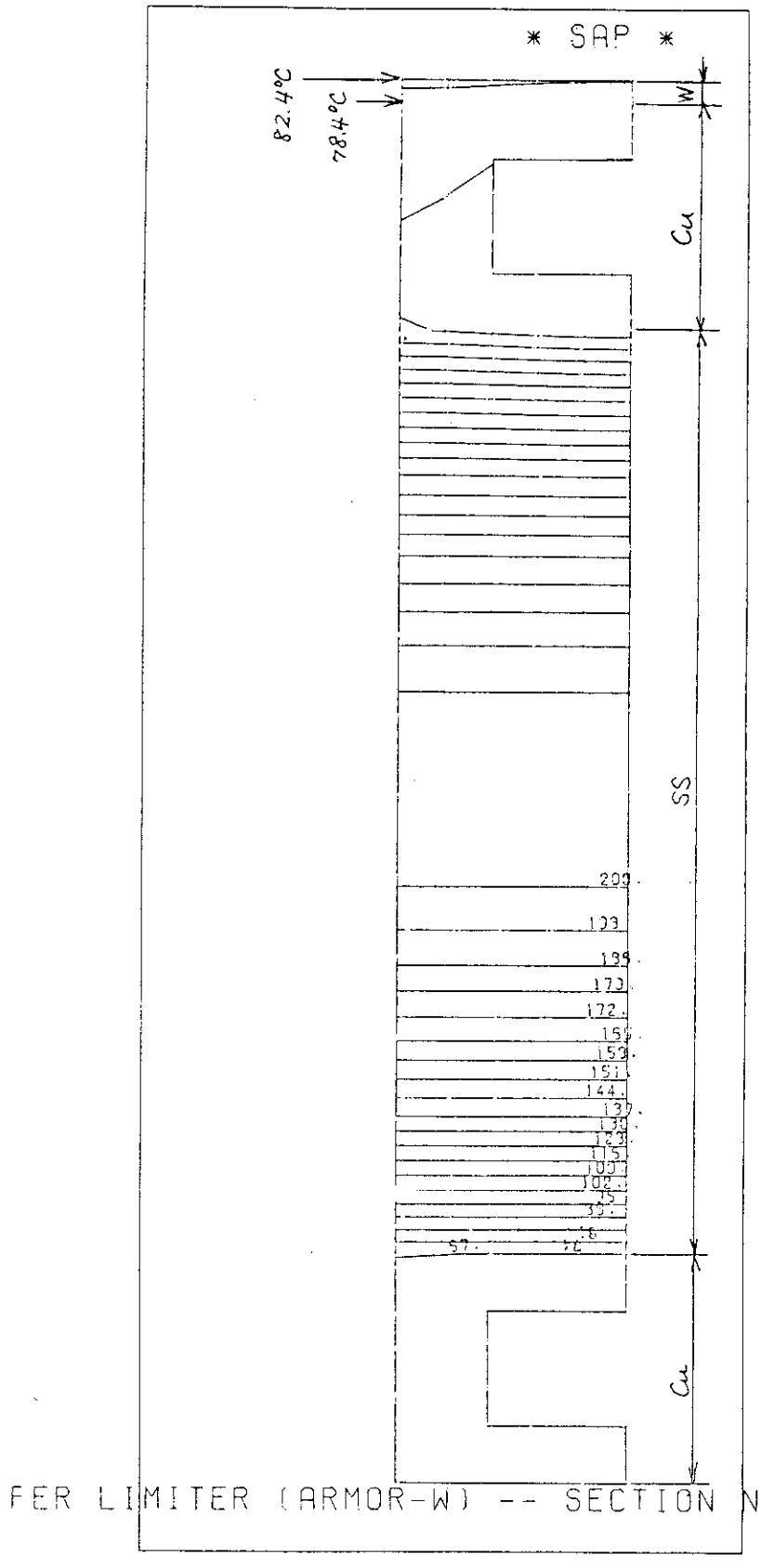

Fig.3.3.14 Temperature distribution at the top surface of a low edge temperature limiter with 1 mm thick tungsten tile on copper heat sink (Heat flux = 0.5 MW/m^2)

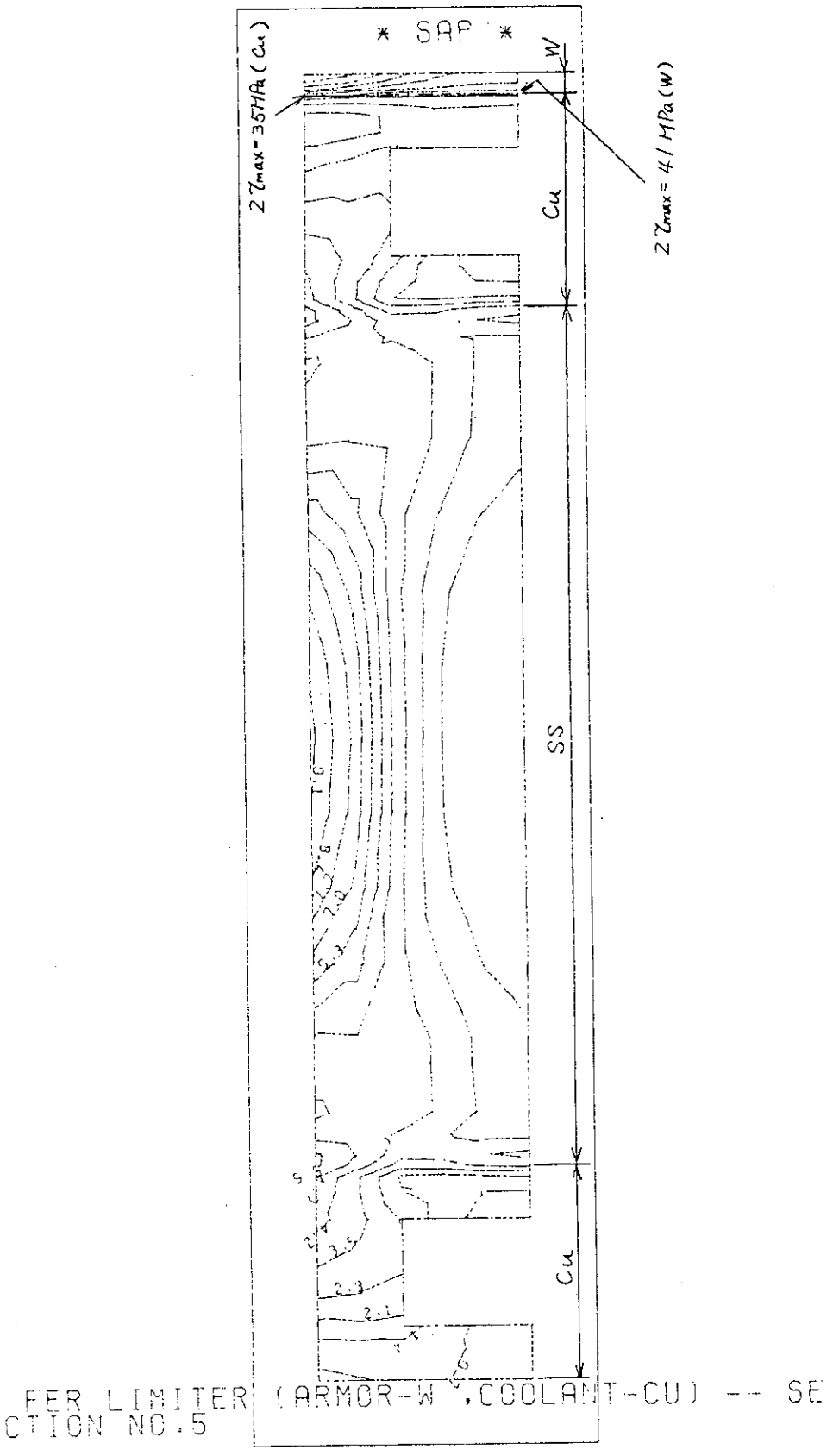

Fig.3.3.15 Stress distribution at the top surface of a low edge temperature limiter with 1 mm thick tungsten tile on copper heat sink (Heat flux = 0.5 MW/m^2)

4. Machine Design Integration and Maintenance

4.1 Specifications and guidelines for the reference-FER engineering design

Specifications and Guidelines for
the Reference-FER Engineering Design

1. Reactor Configuration and Maintenance
2. First Wall/Blanket
3. Divertor
4. Electromagnetics
   (Control of Plasma Positional Instability)
5. Shield
6. TF/PF Coils
7. Plasma Heating System
8. Power Supply System
9. Cooling System
10. Tritium System
11. Safety
12. Plant Layout

1. Reactor Configuration and Maintenance

Guidelines

1) Multisegmentation of torus for obtaining smaller size of TF coil.

2) Compund motion of segments during assembling and disassembling the torus.

3) Double null divertor for impurity control.
   - Thinner width of the inboard scrape-off layer in comparison with Single-Null divertor.
   - Under review from other engineering point of view.
     Effects on TF/PF mangets
     Required power supply capacity for PF Coil
     Control of plasma position instability

4) Common vacuum boundary between plasma and superconducting coils.
   - Reduced size in radial built
     (~ 10 cm)

1. Reactor Configuration and Maintenance
(continued)

5) Support of TF coil centering force by bucking cylinder.
   - Higher reliability for TF coil

6) Tritium breeding blanket on Inboard and outboard sides.
   - Higher tritium breeding ratio

7) Connection and disconnection of the torus segment should be done at the outside of biological shield.

1. Reactor Configuration and Maintenance
(continued)

- Guidelines

8) Plasma Heating Device

	Number of Ports
ECRF	1
LHRF	1
ICRF	1 ~ 2
NBI	2 ~ 3

9) Maintenance classification

Replacement without disassembling torus and removing peripheral components	Divertor Plates
Replacement with disassembling torus and removing peripheral components	First Wall, Blanket, Removable Shield
Principally on replacement after D-T Burnning	TF/PF Coils Shield Posts

2. First Wall/Blanket

2-1 First Wall

1) Combined with blanket vessel
   - ○ Simple
   - ○ Higher tritium breeding ratio

2) 316 ss with or without Mo armor
   Temperature of 316 ss < 300°C

3) H_2O for coolant
   - ○ Low temperature
   - ○ Low pressure
   - ○ Low Pumping Power

2. First Wall/Blanket

2-1 First Wall (continued)

4) Heating Loads
   At normal operation
   Surface heat flux 12 W/cm^2
   Nuclear heating 10 W/cm^3

   At plasma disruption (15 msec)
   Max. energy deposition rate 130 J/cm^2

5) Particle Loads
   Charge exchange neutral 4.6×10^{16}/cm^2·s
   Neutron fluence 3 MW·Y/m^2

2-2 Tritium Breeding Blanket (continued)

Specification

1. Configuration and Dimension
   - ○ Tube-in-Shell Type
   - ○ 50 cm ----- Outboard
     40 cm ----- Inboard

2. Material
   - ○ Breeding Material ----- Li_2O
   - ○ Structural Material ----- 316 ss
   - ○ Neutron Multiplier ----- Be or Pb
   - ○ Coolant ----- H_2O
   - ○ Tritium Purge Gas ----- He

3. Temperature Range
   - ○ 400°C < T_{Li_2O} < 1000°C
   - ○ $T_{structure}$ < 300°C
   - ○ T_{H_2O} < 100°C

4. Tritium Breeding Ratio (TBR)
   - ○ TBR > 1.0

3 Divertor Plate

1. Material

Heat Sink	Cu
Armor	W(W alloy) or Mo
Structure	316 ss
Coolant	Light Water

2. Conditions for Determing Armor Thickness

- Erosion due to Ion Sputtering can be neglected
- Fatigue analysis for
  - a) normal operation 10^6 cycle
  - b) disruption 10^3 cycle

4. Electromagnetic Design

(Control of Plasma Vertical Position Instability)

1. Minimize the Required Power Supply Capacity for the Active Control Coil

P < 100 MVA acceptable

100 MVA < P < 500 MVA Marginal

500 MVA < P not acceptable

2. Assumptions for Electromagnetic Analysis

- Location of Active Coil

  Outside of the TF Coil

- Initial Disturbance

  $B_d(t) = B_{do}\ (1 - e^{t/\tau})$

  τ : 1 msec B_{do} : 10 Gaus

- Shell Effects and Shielding Effects

  Passive Shell, Blanket Vessel, Shield and Cryostat

5. Shield

Guideline

1. Neutronics
   - a. Protection of Superconducting Magnet
   - b. Personal Access to the Reactor after reactor Shutdown
     - Detailed evaluation of radiation Streaming
2. Structural Design
   - a. Consistency with Electromagnetic Design

5. Shield (continued)

Specification

	Criteria
Maximum neutron fluence (E > 0.1 MeV) in the Super-Conductor (n/cm^3/lifetime)*	$< 2 \times 10^{18}$
Maximum atomic displacement in the Copper Stabilizer (dpa/y)	$< 5 \times 10^{-5}$
Maximum dose in the insulator (rad/lifetime)*	$< 3 \times 10^{9}$
Total nuclear heating in the TF-Coils (kW)	< 10

* Lifetime: Wall loading of 3 MWY/m^3

Dose rate in the reactor room after reactor shutdown	< 2.5 mr/h

4.2 Design concepts

4.2.1 FER reactor structure and maintenance

The design of the machine configuration and maintenance for double-null poloidal divertor were presented, stressing five points: (1) magnet system, (2) additional heating system, (3) vacuum boundary, (4) torus segmentation, (5) sector replacement. Table 4.2.1.1 and 4.2.1.2 indicate the design philosophy and the design condition for FER mechanical configuration and maintenance. A whole of reactor is covered with belljar type cryostat of 23 m diameter and 20 m height. Perspective view of FER is given in Fig. 4.2.1.1. Vertical cross sectional view and plane view of the reactor are shown in Fig. 4.2.1.2 and Fig. 4.2.1.3, respectively. In addition, radial build of the reactor is indicated in Fig. 4.2.1.4.

(1) Magnet systems

Toroidal field coil (TF coil) system consists of 14 coils with the bore size of 6.4 m × 9.4 m, providing 5.7T at plasma center (R = 5.5 m) and 0.5% magnetic ripple at plasma outer edge.

Poloidal field coil system is composed of 12 inner solenoid coils and 8 outer ring coils, which are completely located to be external to the bore of TF coil. The coil positions are arranged to provide the clear access through TF coil window. The radius of the solenoid coils are 1.65 m and outermost ring coil of 10.8 m radius.

All the outer ring coils are fixed on the support structures of TF coils. The centering force of TF coil is sustained by center post through the support rings between TF coil and the post, and overturning force primarily by shear panel installed between TF coils. Hoop force is supported by the support structure and conductors for TF coil, and solely supported by interturn reinforcement in conductor for PF coil. Mechanical stresses due to the above-mentioned forced are calculated by 3-D FEM and satisfy the evaluation standard of ASME SEC Ⅲ. Figures 4.2.1.6 and 4.2.1.7 show configuration of toroidal field coil and its support structure. Inboard solenoid coils and the support structure of inboard toroidal coil are illustrated in Fig. 4.2.1.8. Figures 4.2.1.9 and 4.2.1.10 depict the configuration of helium vessel for poloidal coil and the support structure for outer poloidal coils.

(2) Additional heating system

Additional heating system consists of NBI, ICRF, LHRF and ECRF, which are set on 7 TF windows between toroidal field coils, 3 windows for NBI, 2 windows for ICRF and one for each other, as shown in Fig. 4.2.1.3. Seven other windows are used for removal of divertor sectors. Fourteen exhaust ducts are installed at the top and bottom portions of these 7 windows for the divertor replacement. The upper exhaust

duct with enough thickness of shielding is supported from the dome of the cryostat. Figure 4.2.1.4 indicates the support structure for the upper cryopump.

(3) Vacuum boundary

In order to minimize inboard space between TF coil and shield structure, combined vacuum boundary for plasma chamber (shield structure) and coil cryostat is adopted for FER vacuum boundary design, as indicated in Fig. 4.2.1.11. Furthermore, access port attached to outboard shield structure in each TF window for torus sector replacement provides the vacuum boundary. Blanket and divertor sectors are restracted through the access port for disassembly and replacement. Figures 4.2.1.12 and 4.2.1.13 show the concept of combined vacuum boundary and configuration of torus access port.

In order to avoid the T shaped vacuum seal which seems to be less reliable, a blanket access door for the vacuum closure is provided on the blanket access port.

(4) Torus segmentation

Plasma chamber is composed of removable shield sectors and permanent sectors, and divided into 28 sectors. Permanent sectors are located behind outboard TF coils, and form into torus support structure such as spool, as shown in Fig. 4.2.1.14. Bellows are installed in each

permanent sector for electrical break in torus direction. Outer edges of each shield sector are seal-welded. Shield sector is not disassembled except in case of TF coil accident. Torus structures of blanket integrated with first walls is divided into 2 sectors for a TF coil, 28 sectors in total. Each sector of blanket is divided to be symmetrical shape to avoid the unbalanced electromagnetic force induced by plasma disruption, as shown in Fig. 4.2.1.14. Figures 4.2.1.15 to 4.2.1.17 indicate configurations of the blanket sectors and connecting structure of the sectors. Divertor is divided into 3 sectors for 2 TF coils, 21 sectors in total. Segmentation of the divertor is depicted in Figure 4.2.1.18. These are composed of a central sector and 2 side sectors. Figures 4.2.1.19 and 4.2.1.20 show configurations of the divertor sectors.

(5) Replacement procedures of blanket and divertor sectors

As shown in Fig. 4.2.1.21, one of 2 blanket sectors/TF coil (sector A) is withdrawn with a straight radial motion, and then the other (sector B) with a straight oblique motion through each TF window, using the blanket retraction vehicles. For the retraction of sector B, the vehicles are at first inserted into the space which sector A had occupied, and sector B is set on the vehicles after oblique withdrawal of the sector by means of the ball screw. Next it is retract-

ed with a radial motion. The setting of vehicles on the guide rail is conducted by personnel access in advance before the access door is opened. Then, the vehicles are operated with remote handling. The replacement procedure of the blanket sectors using the vehicles is illustrated in Fig. 4.2.1.22 and Table 4.2.1.3. Retraction of the divertor sectors is conducted with a single straight motion (radial) for central sector, and with 2 straight motions (radial and oblique) for side sector.

Withdrawal of side sector is similar with that of blanket sector B. Figures 4.2.1.23 and 4.2.1.24 indicate the concept of the divertor sector replacement. The divertor replacement procedure is shown in Table 4.2.1.4. Figure 4.2.1.25 indicates access door removal and access door carrier which is used after disconnecting bolts between the door and shield structure and the lip seal cutting. Figure 4.2.1.26 shows bolt runner for connecting and disconnecting of the bolts on the access door. The auto lip seal welder and cutter for the access door removal is depicted in Figure 4.2.1.27. Figures 4.2.1.28 to 4.2.1.31 show the concept of in-vessel inspection system and the prototype of multi-joint robbot.

This manipulator can not only inspect the surfaces of the first wall and the divertor plates, but also conduct the welding and cutting

of the cooling pipes by replacement of the attachments at the machine edge.

The initial construction concept of the reactor system is illustrated in Figure 4.2.1.32.

Table 4.2.1.5 shows the summary of mechanical integration and maintenance of FER. The discussion for future design of FER is described in Table 4.2.1.6.

TABLE 4.2.1.1 DESIGN PHILOSOPHY

- DEVELOPMENT OF BALANCED AND COMPACT-SIZED REACTOR SYSTEM DESIGN
- GOOD ACCESSIBILITY TO REACTOR AFTER PLASMA SHUT DOWN
- DEVELOPMENT OF RELIABLE MAINTENANCE DESIGN
- FEASIBLE DESIGN OF COMPONENT STRUCTURES

TABLE 4.2.1.2 DESIGN CONDITIONS FOR MECHANICAL CONFIGURATION AND MAINTENANCE

1. ADOPTION OF DOUBLE NULL DIVERTOR CONCEPT
2. EMPLOYMENT OF COMBINED VACUUM BOUNDARY
3. SYMMETRICAL SEGMENTATION OF BLANKET
4. SUPPORTING OF TFC CENTERING FORCE WITH CENTER POST
5. REPLACEMENT OF DIVERTOR PLATES WITHOUT REMOVAL OF ADDITIONAL HEALING SYSTEM
6. RIPPLE REQUIREMENT OF LESS THAN 0.75% AT PLASMA EDGE

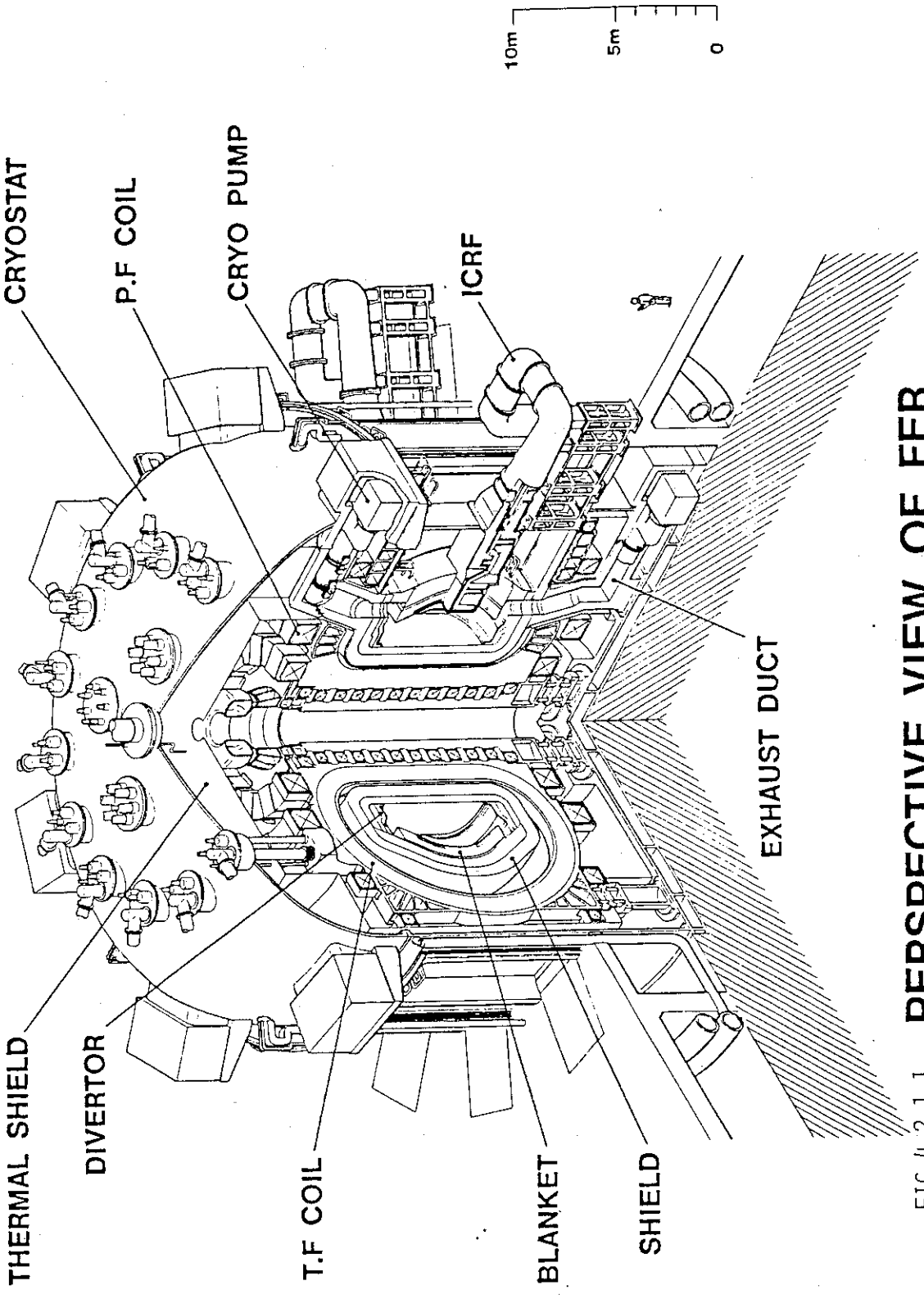

FIG.4.2.1.1 PERSPECTIVE VIEW OF FER

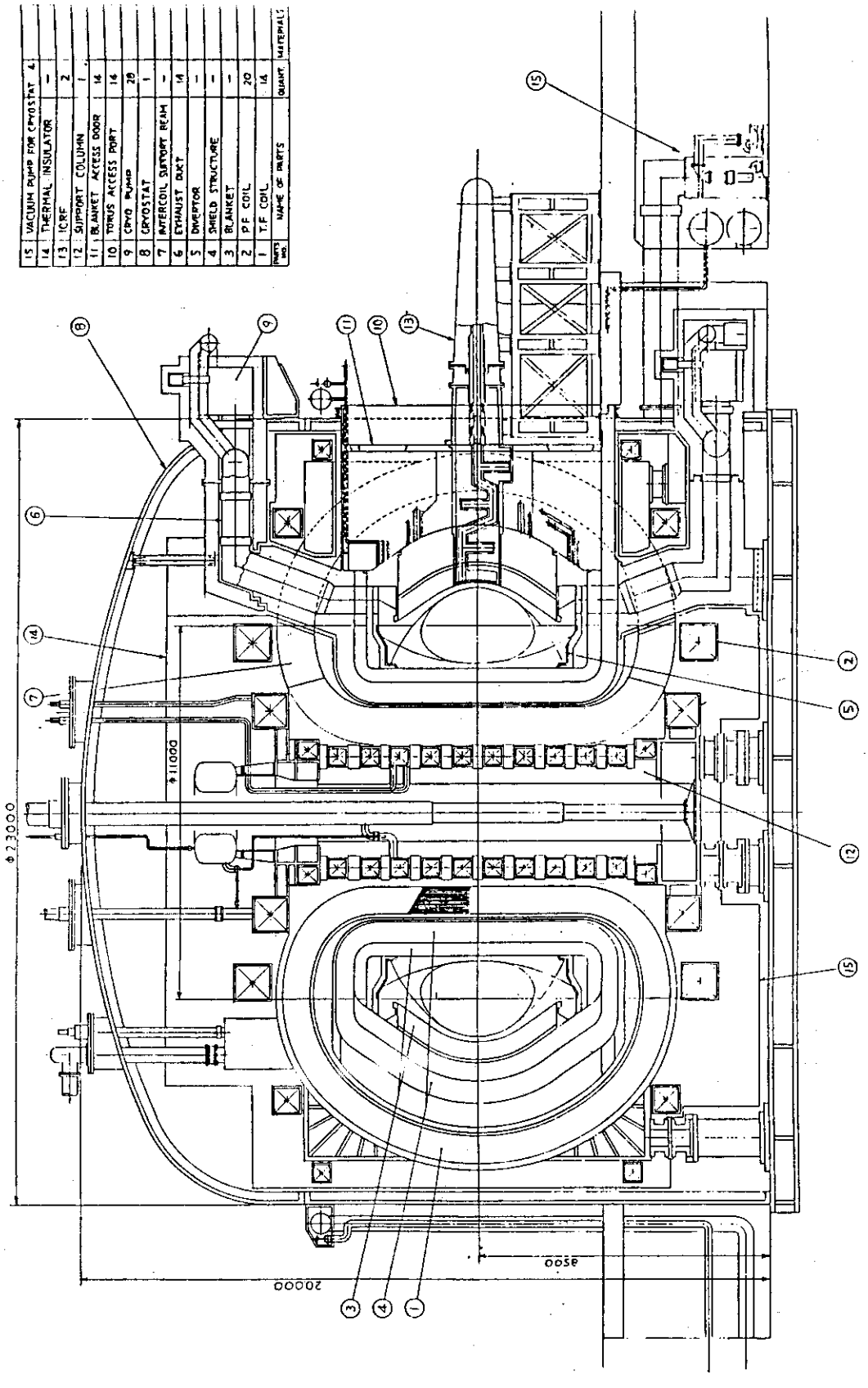

Fig.4.2.1.2 Vertical View of FER

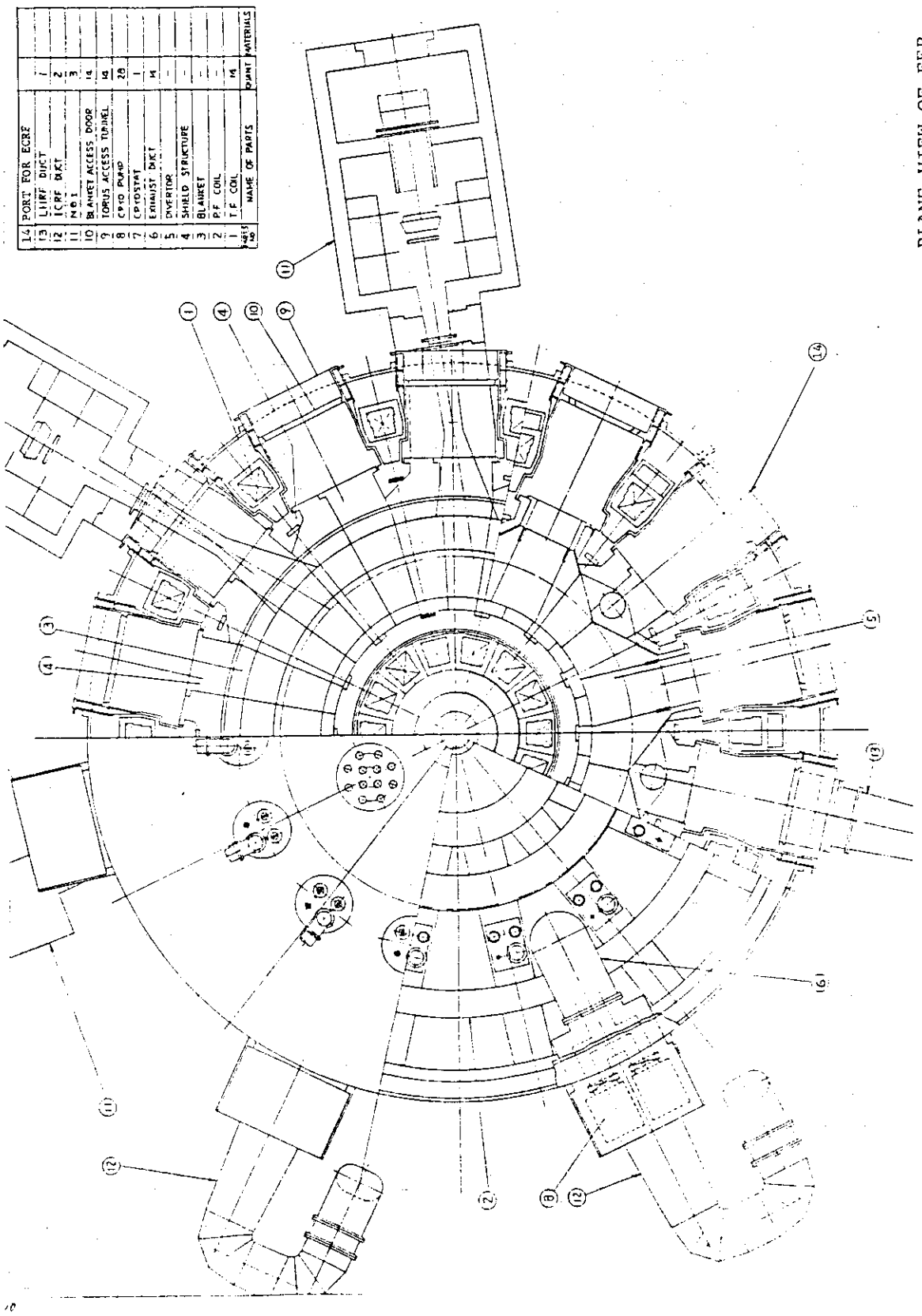

Fig.4.2.1.3 PLANE VIEW OF FER

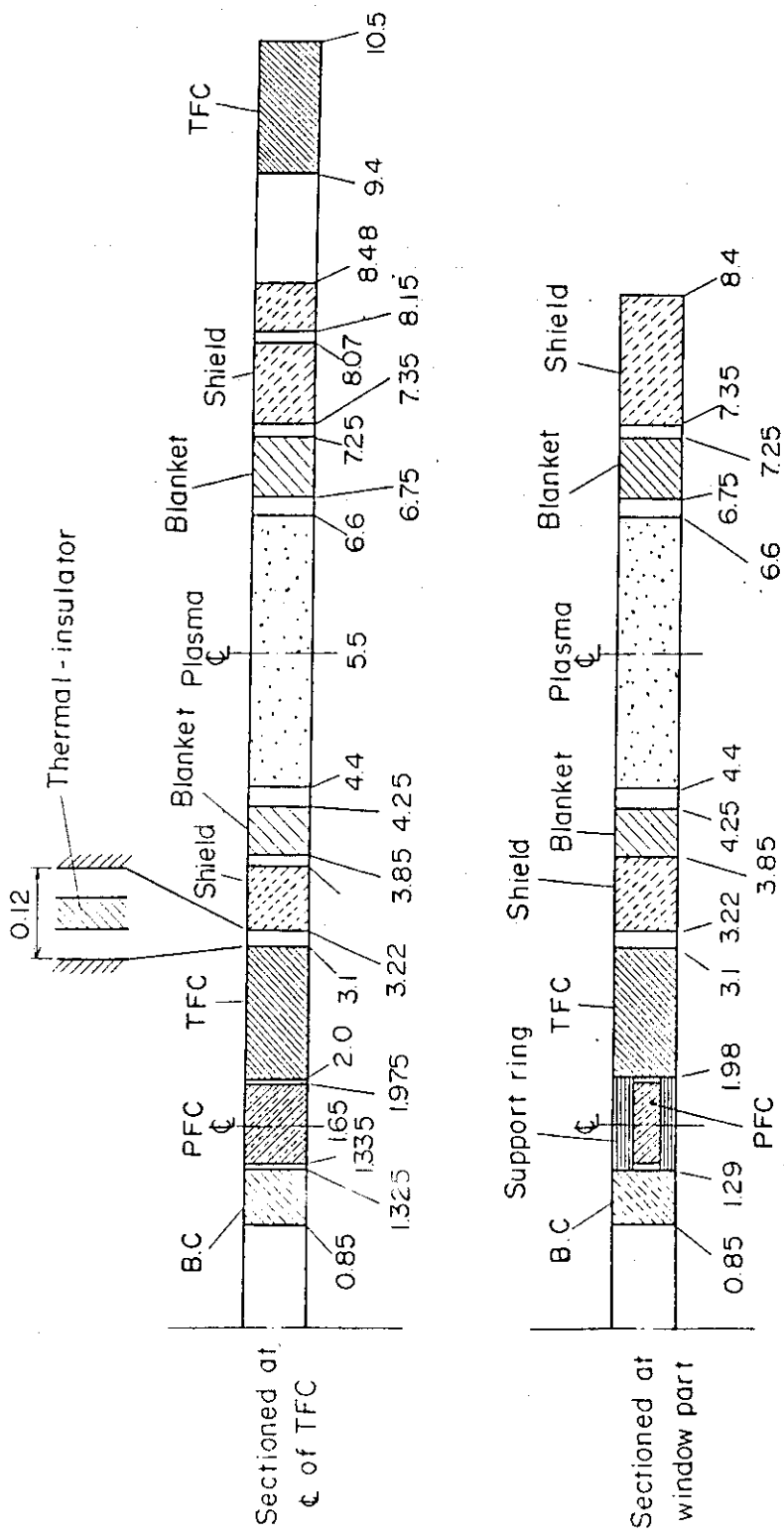

Fig.4.2.1.4 FER Radial build

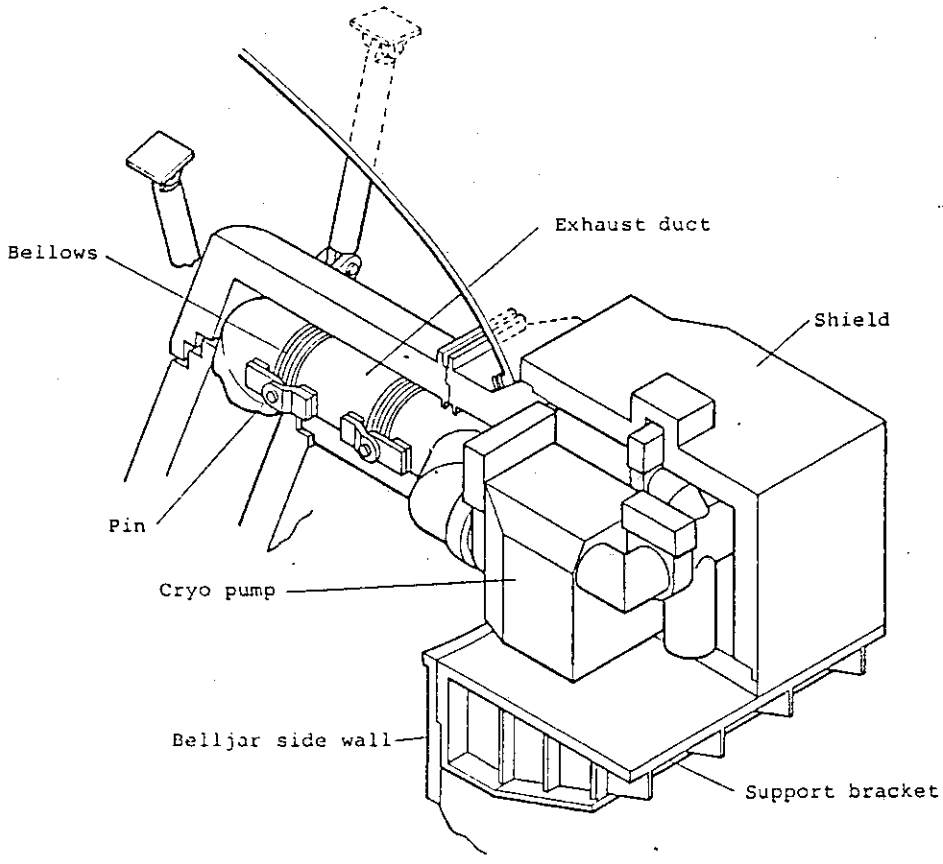

Fig.4.2.1.5 Support structure for upper cryo pump

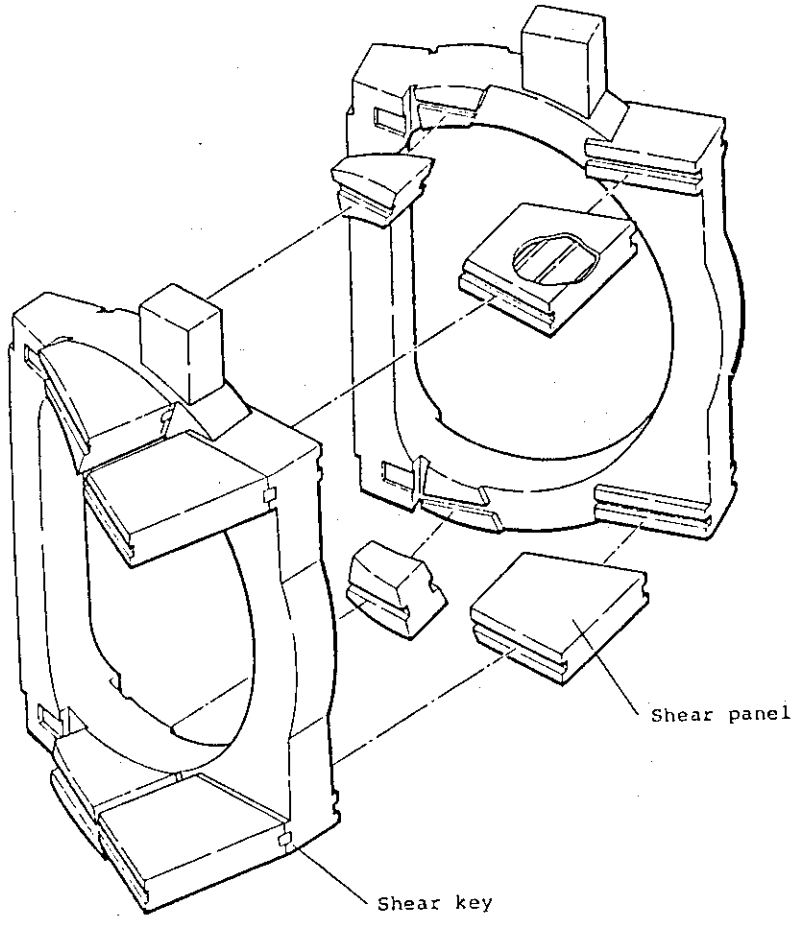

Fig.4.2.1.6 Configuration of toroidal field coil

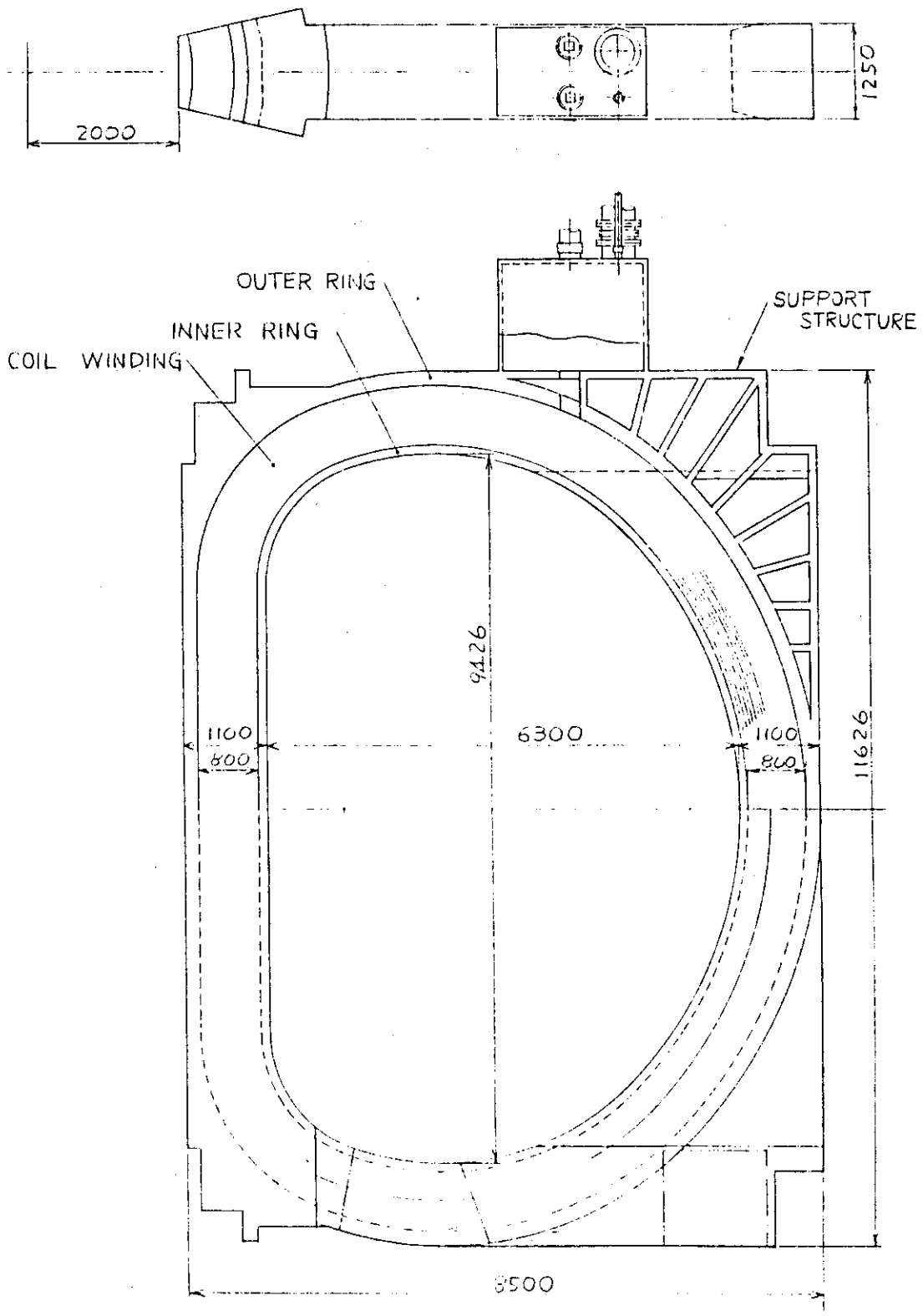

Fig.4.2.1.7 Configuration of Toroidal Field Coil

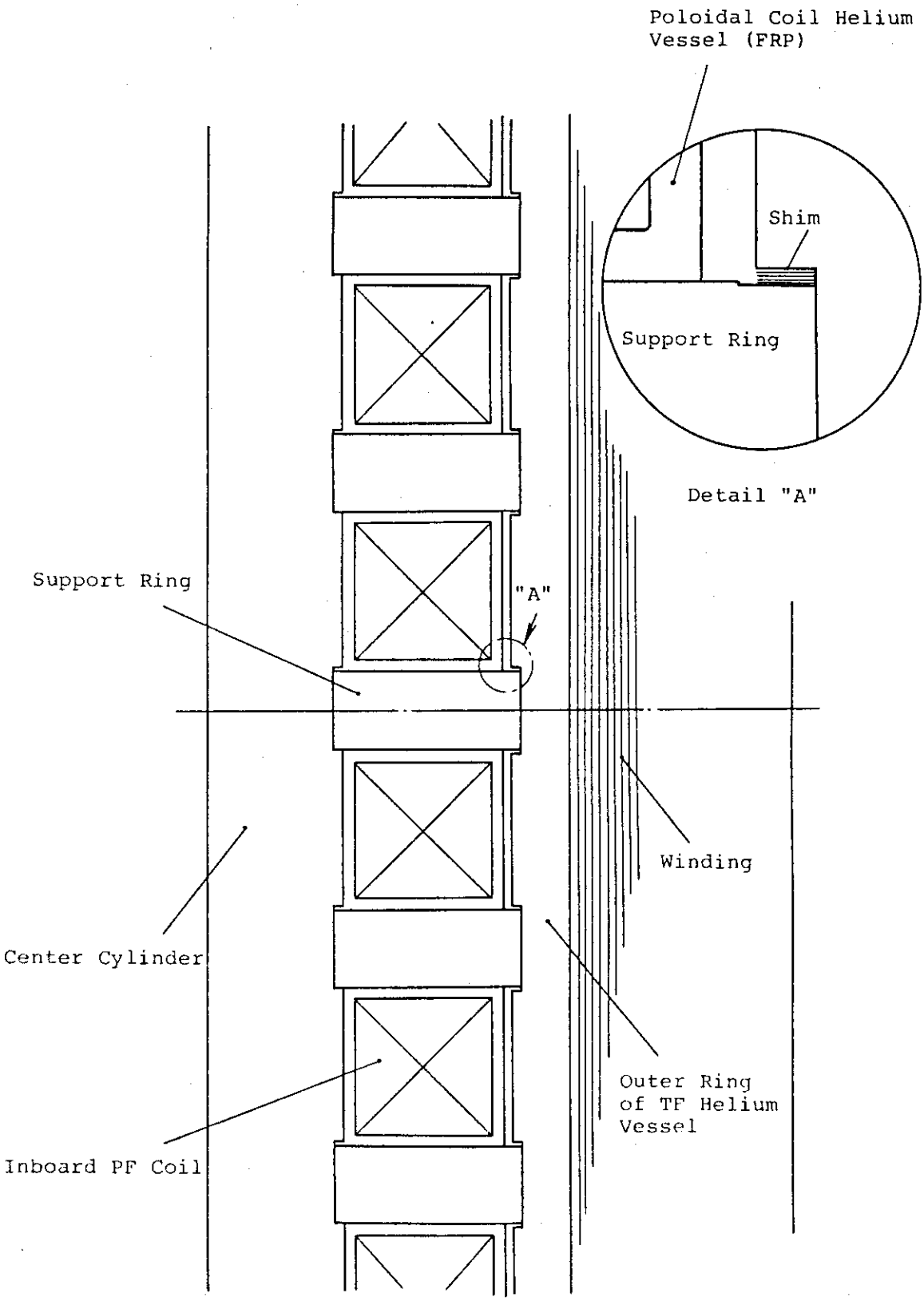

Fig.4.2.1.8 Support Structure of Inboard Toroidal Coil

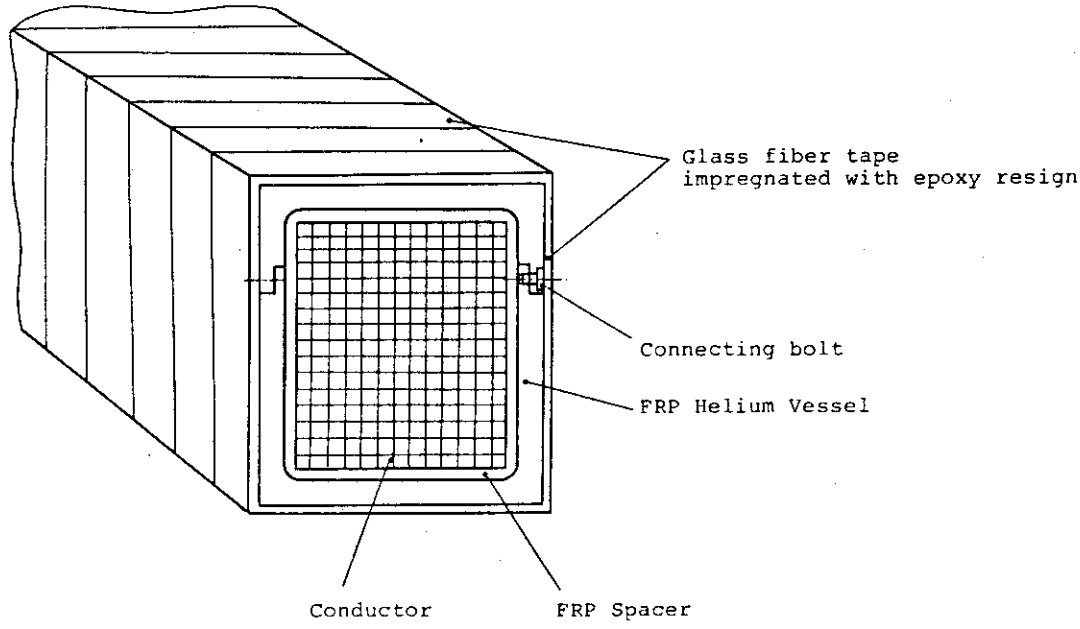

Fig.4.2.1.9 Configuration of FRP helium vessel for poloidal coils

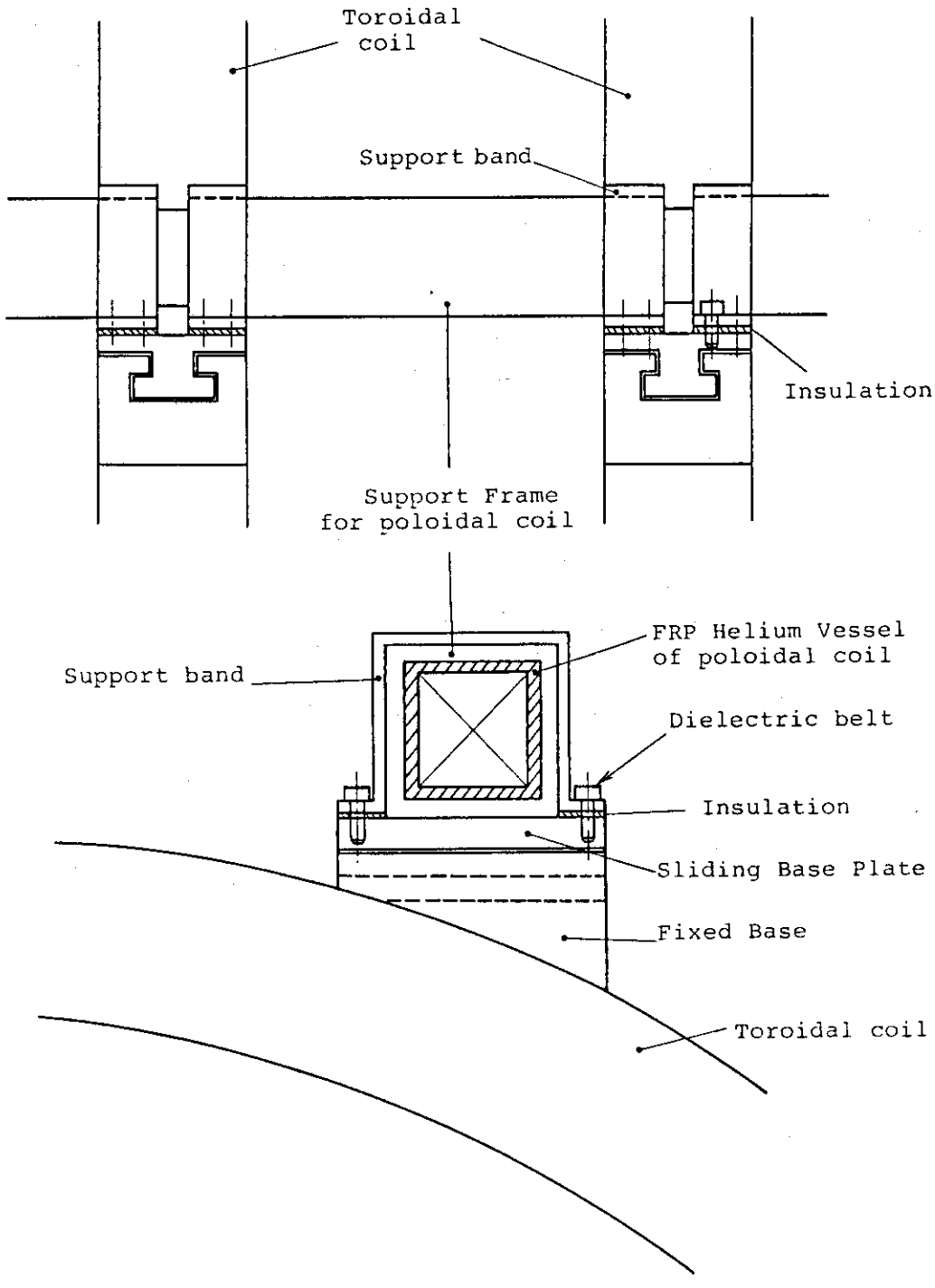

Fig.4.2.1.10 Support structure for outboard poloidal coil

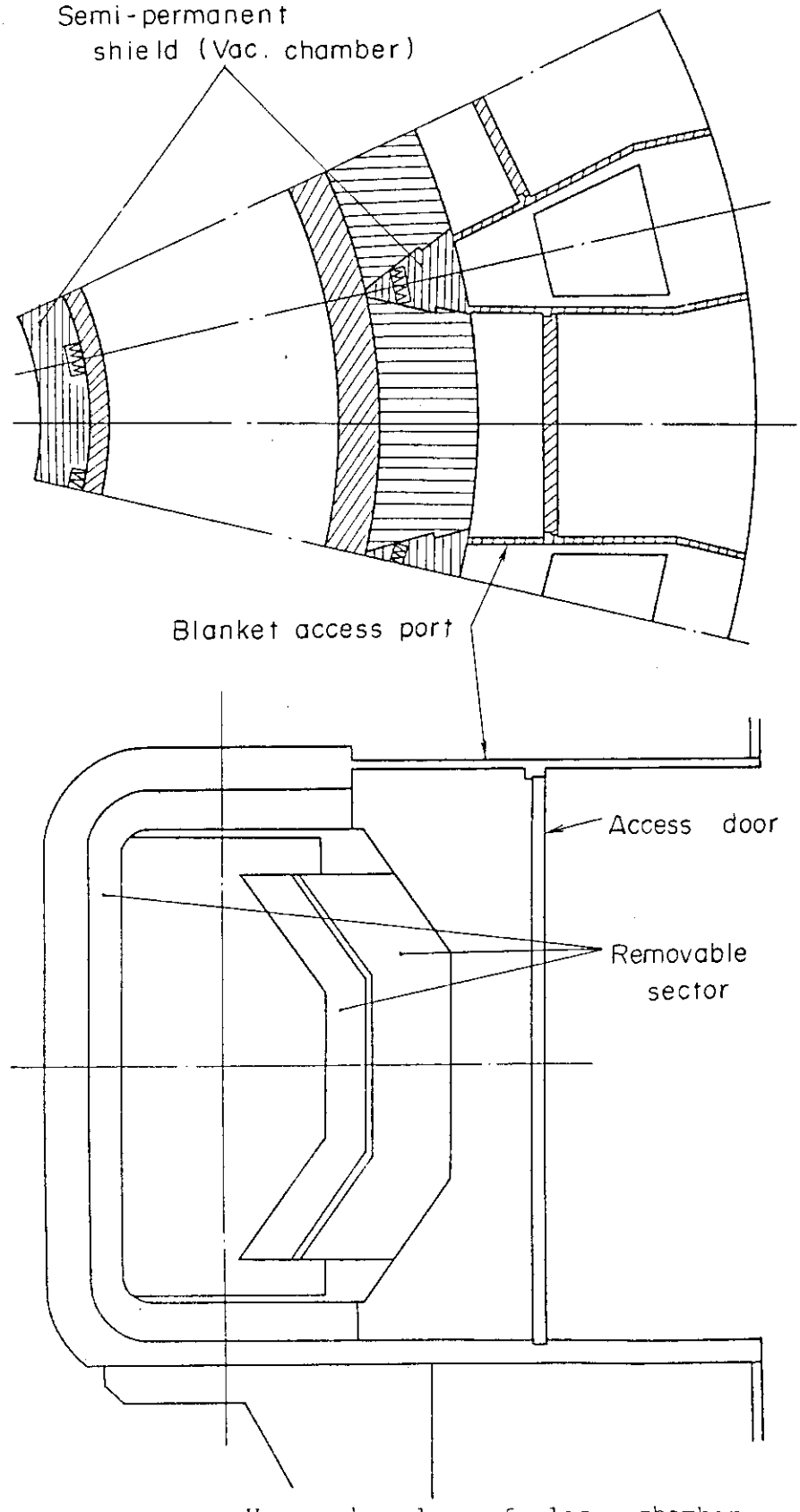

Fig.4.2.1.11 Vacuum boundary of plasma chamber

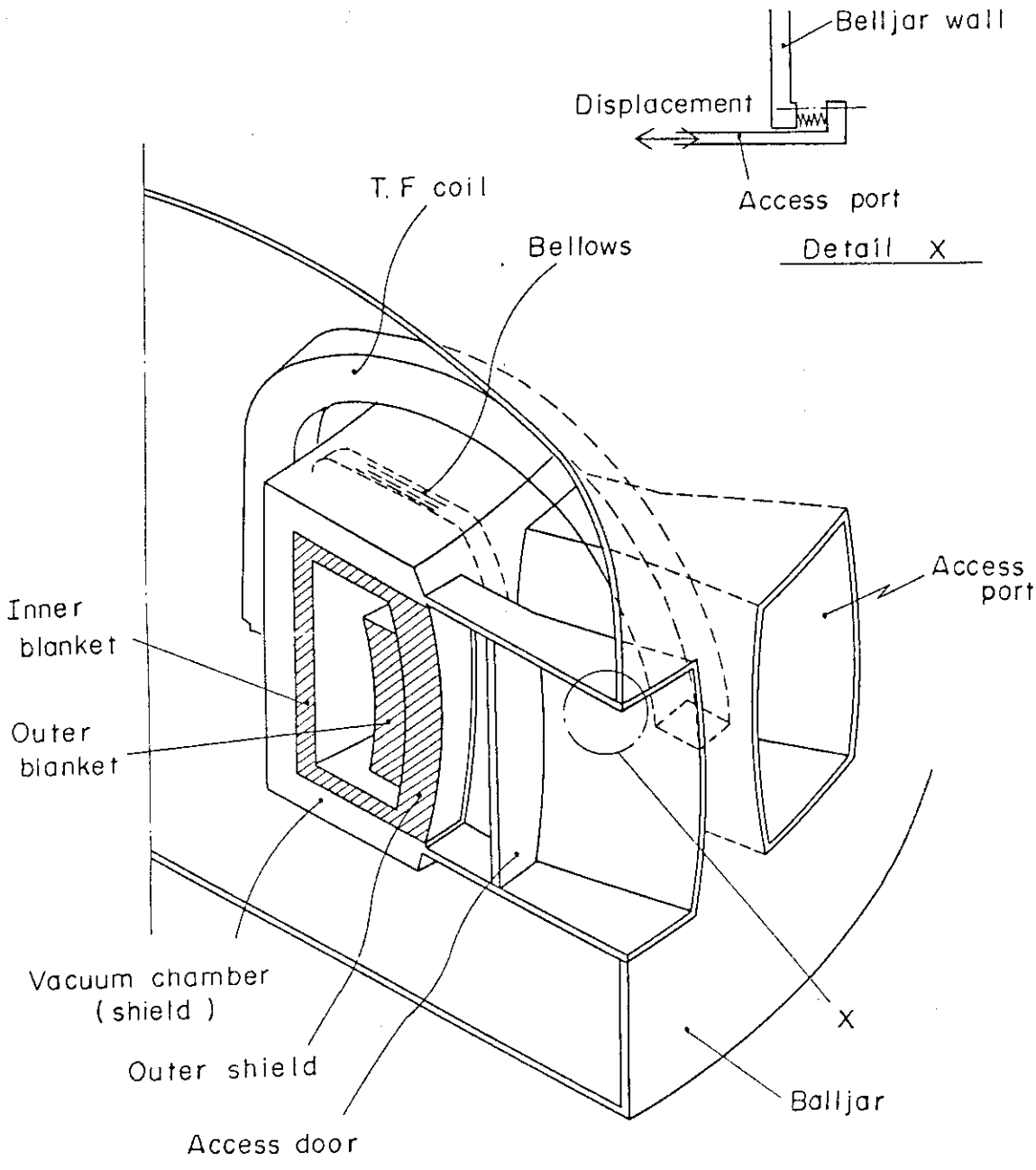

Fig.4.2.1.12 Concept of combined vacuum boundary

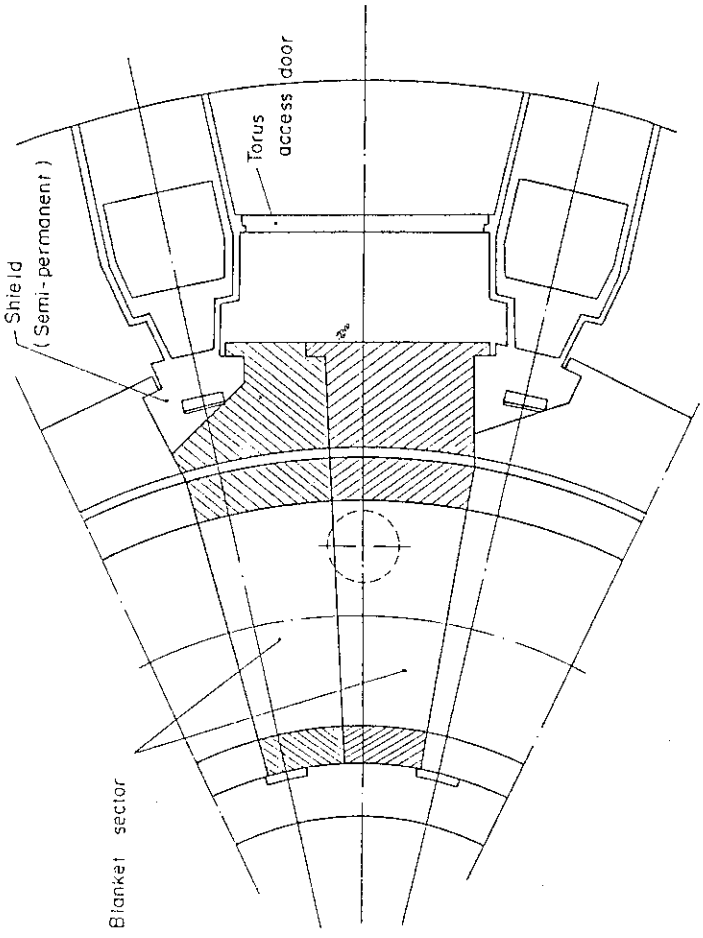

Fig.4.2.1.14 Segmentation of blanket

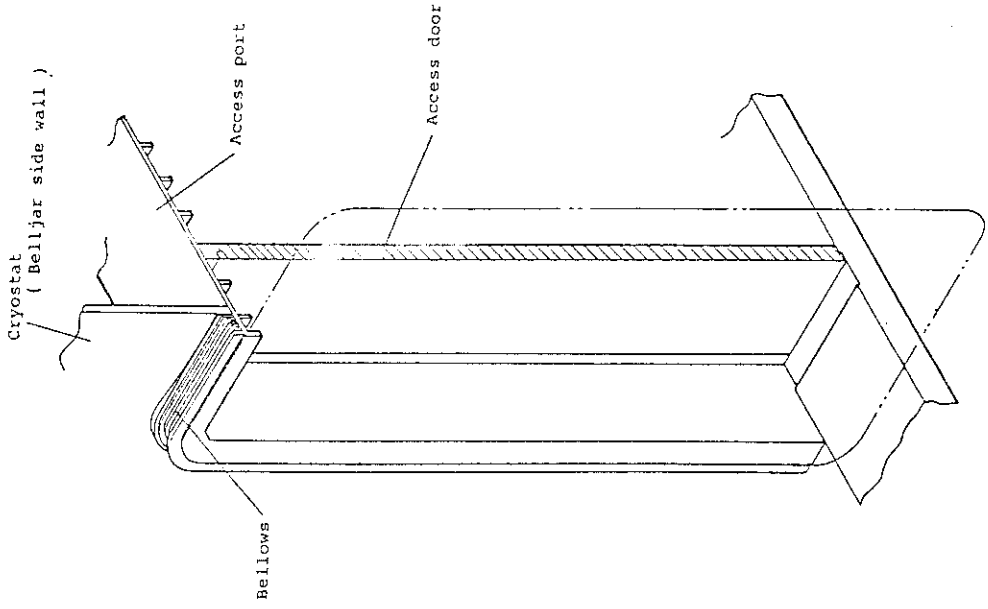

Fig.4.2.1.13 Configuration of torus access port

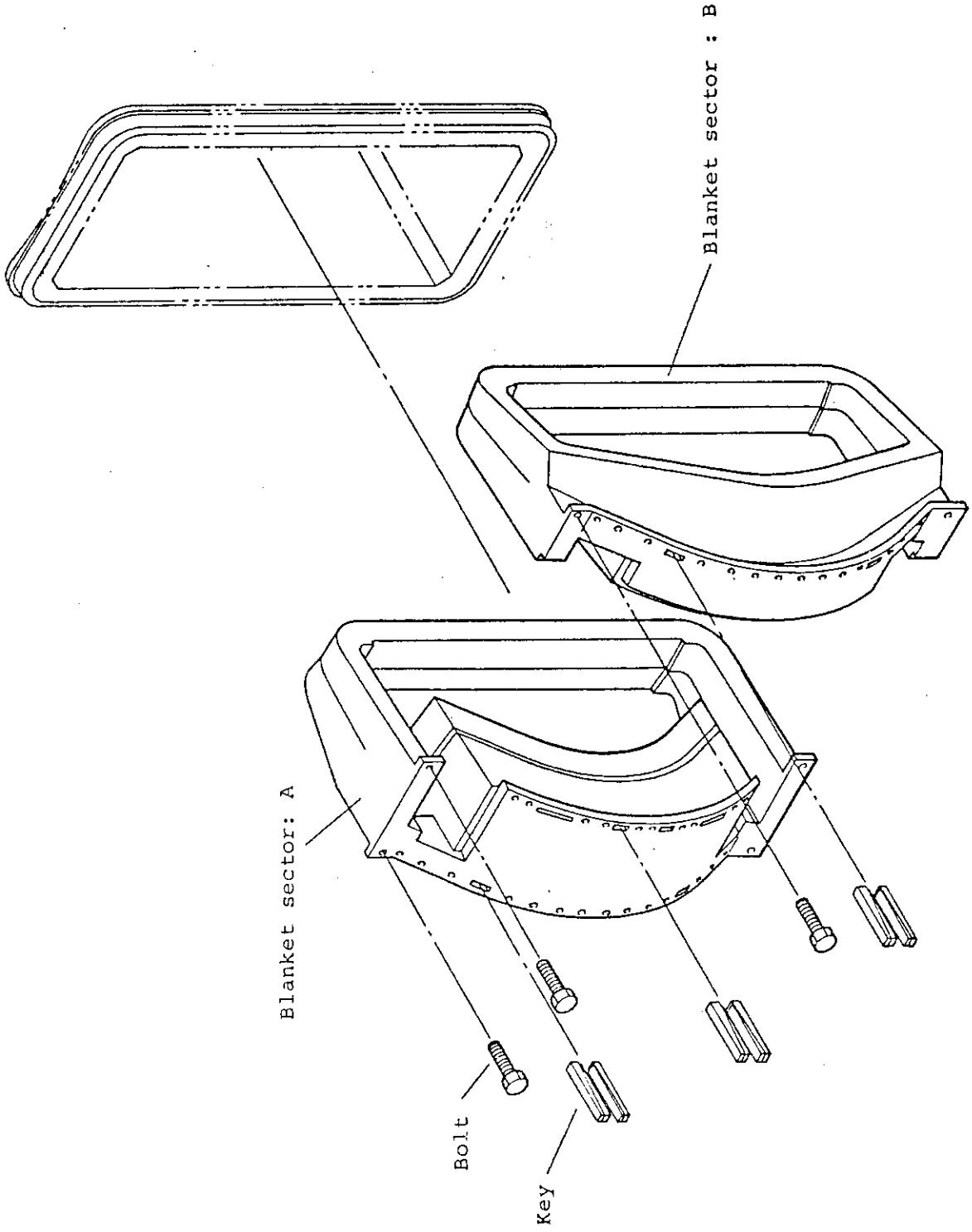

Fig.4.2.1.15 Blanket sectors

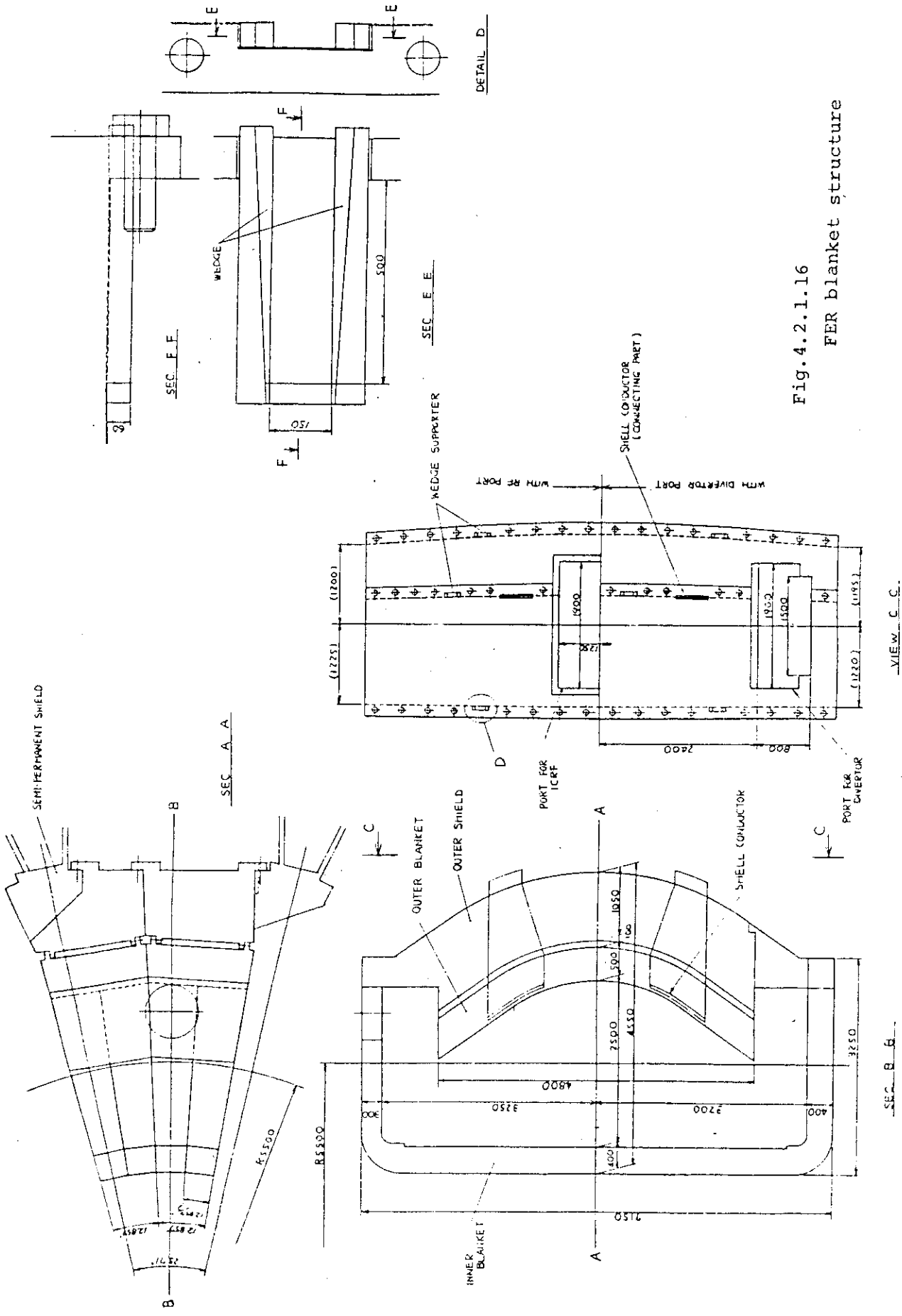

Fig.4.2.1.16 FER blanket structure

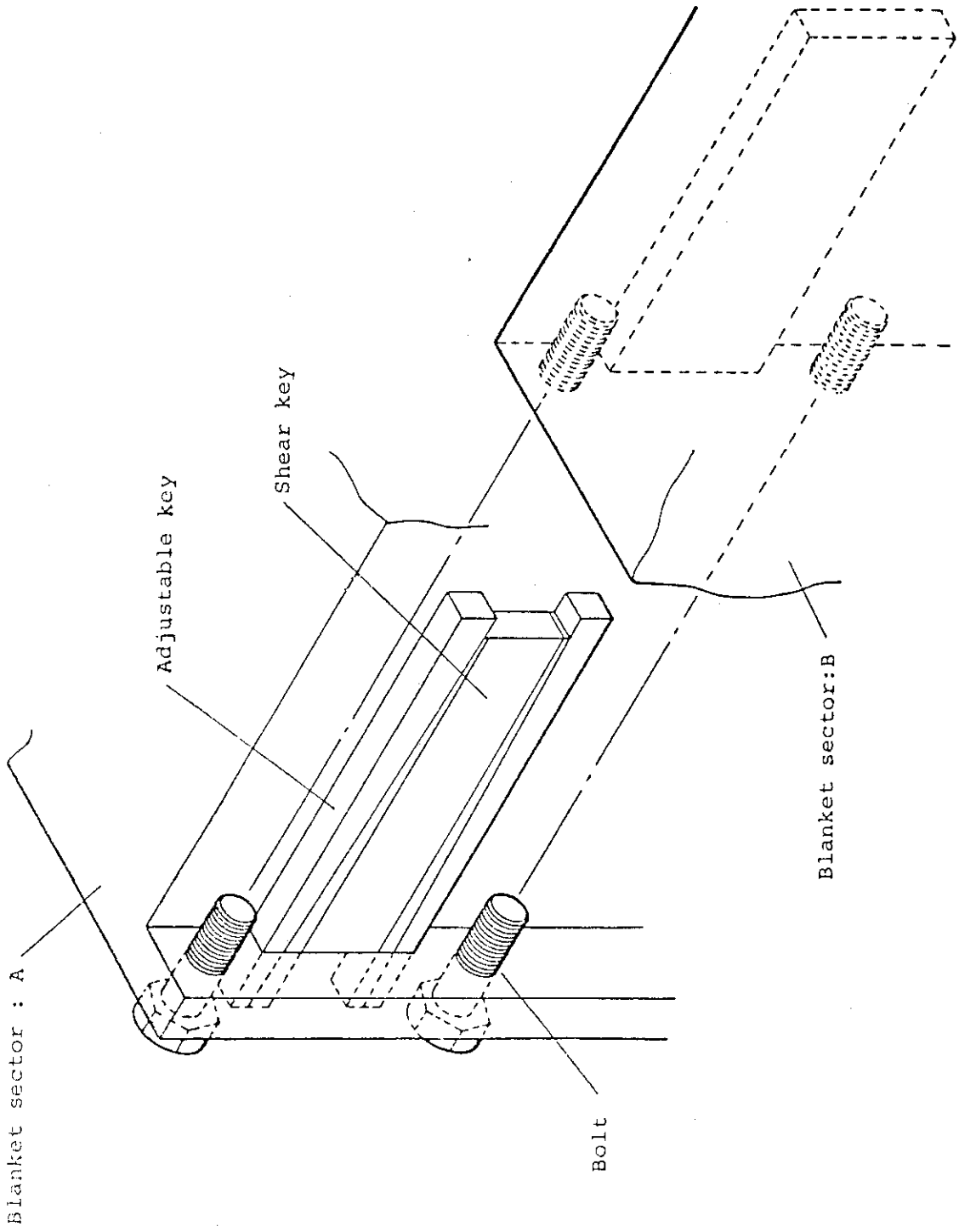

Fig.4.2.1.17 Connecting structure of torus sector

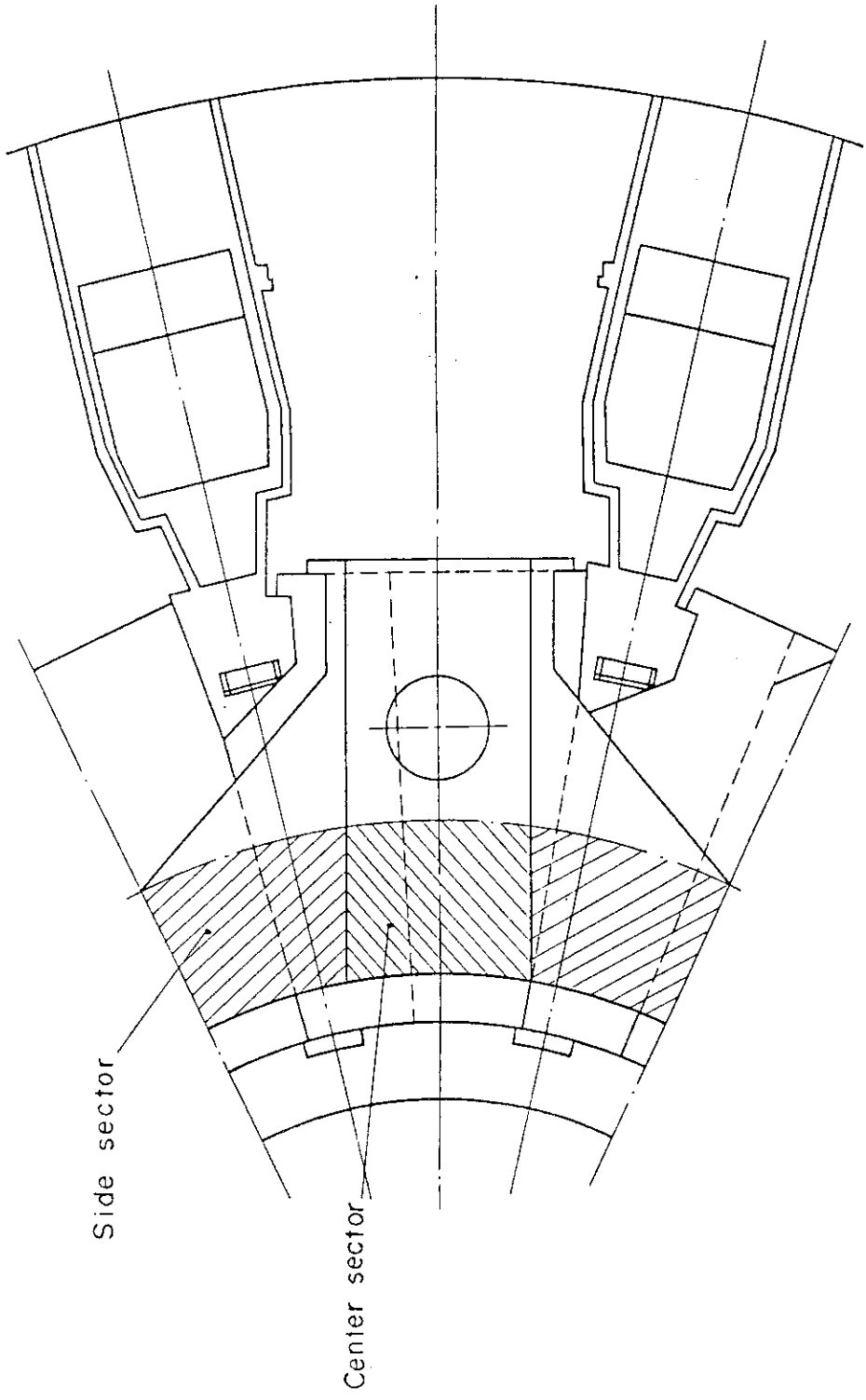

Fig.4.2.1.18 Segmentation of divertor

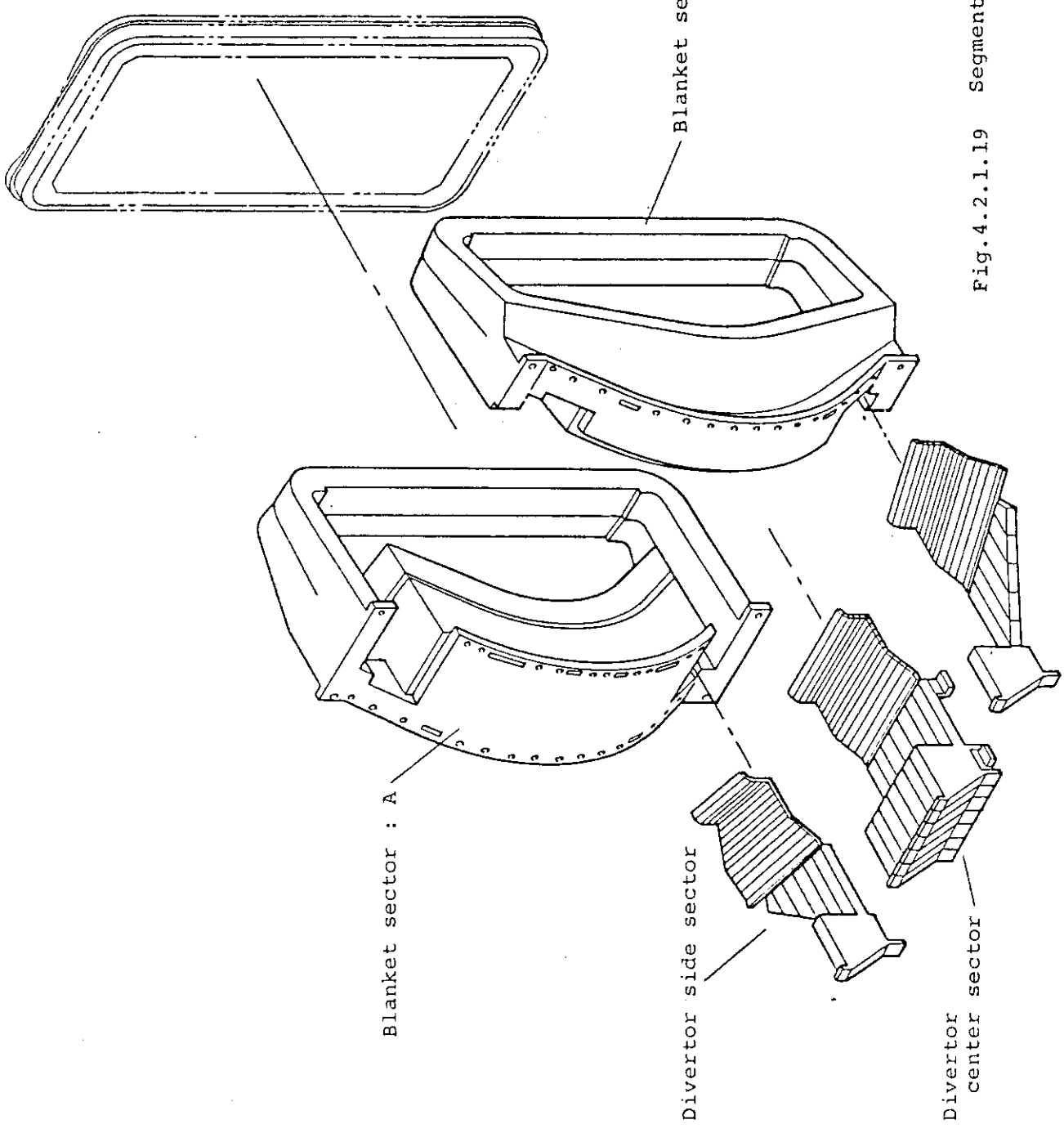

Fig.4.2.1.19 Segmentation of blanket and divertor

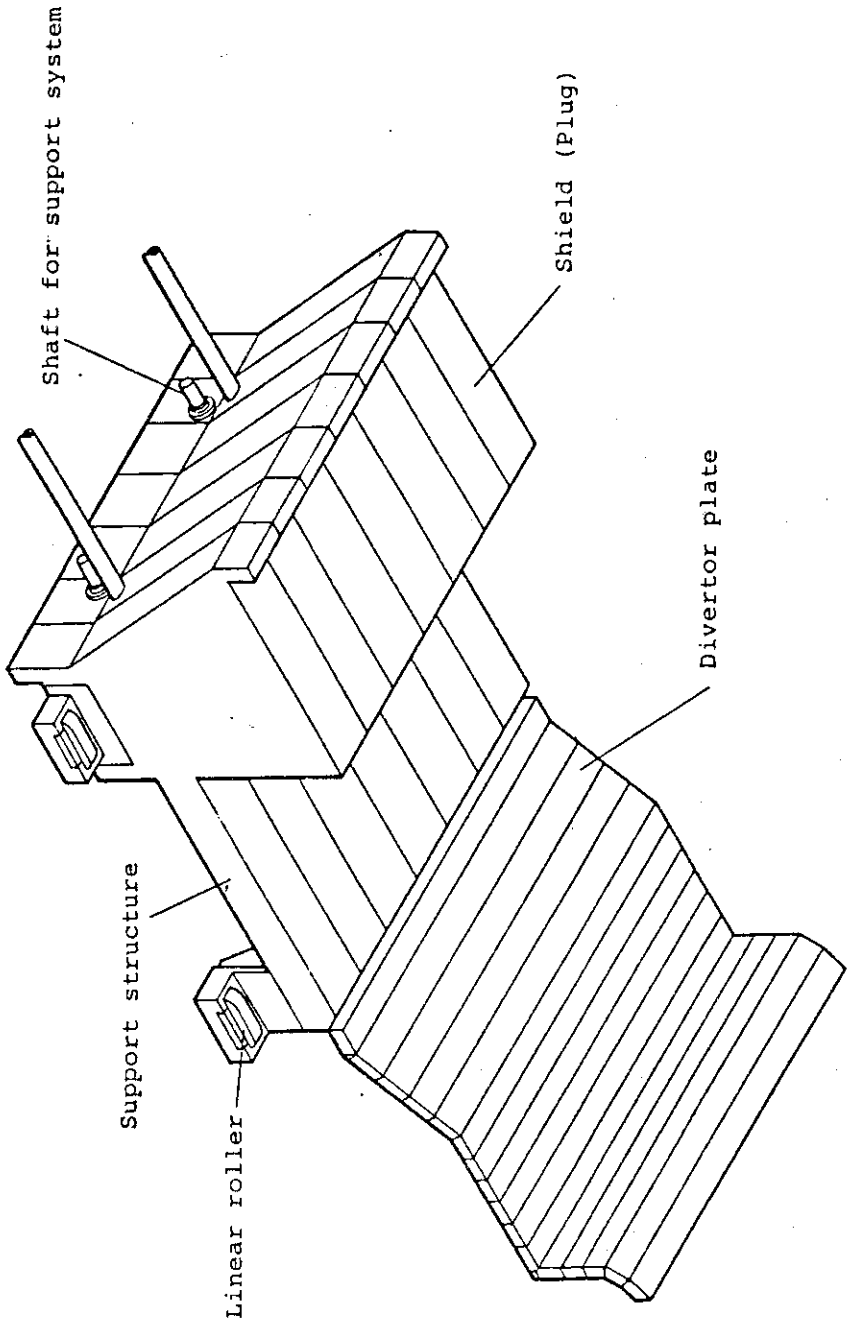

Fig.4.2.1.20 Configuration of divertor (Upper center sector)

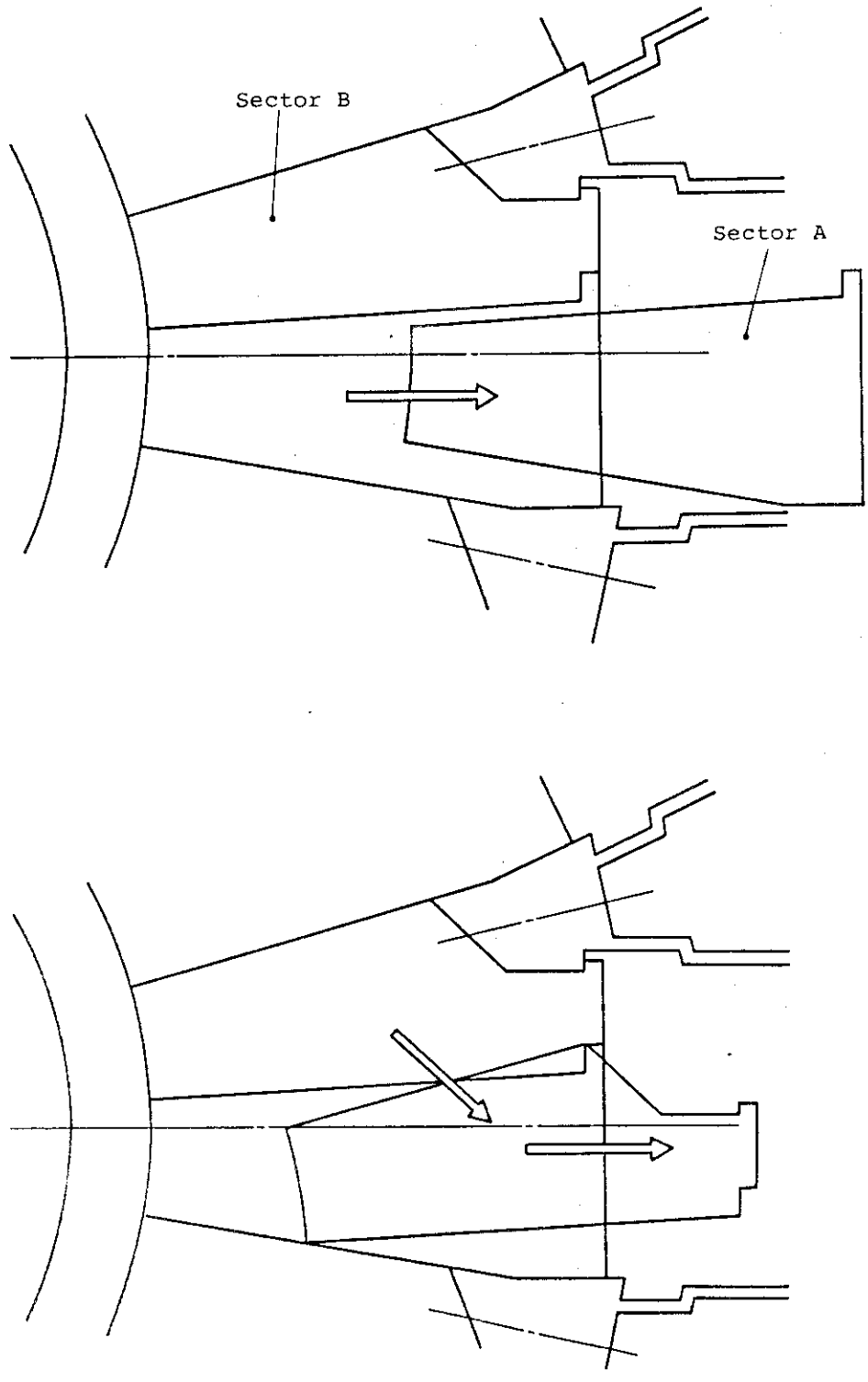

Fig.4.2.1.21 Blanket replacement concept

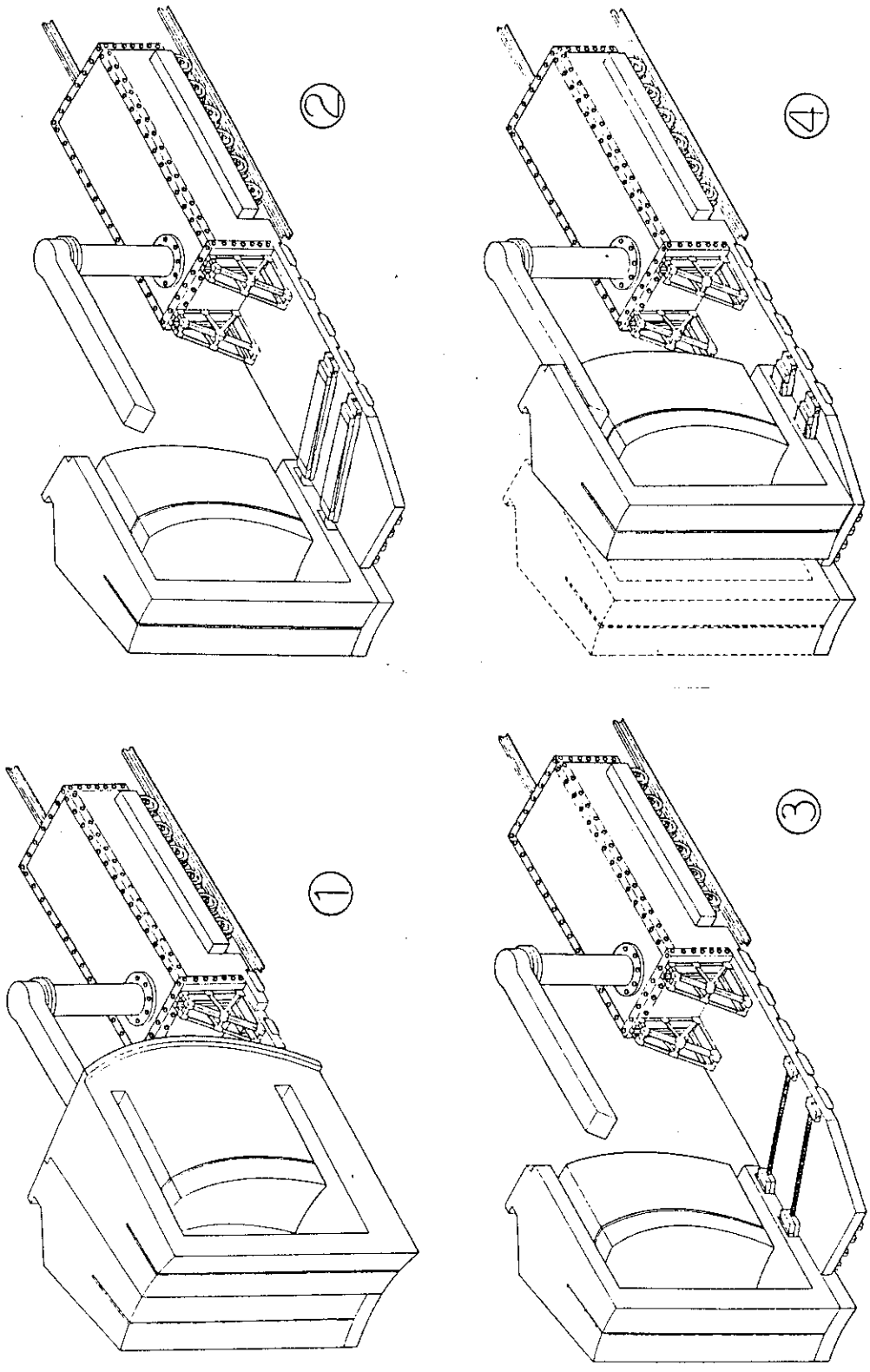

FIG.4.2.1.22 BLANKET REPLACEMENT PROCEDURE

Table 4.2.1.3 Blanket Replacement Procedure

Disassembly

1. Shutdown
2. Start baking, and cooling of decay heat
3. Disconnect the bolts on the access door
   (bolt runner, articulated manipulator)
4. Cut the lip seal on the access door
   (auto seal cutter, articulated manipulator)
5. Remove the access door
   (access door carrier)
6. Disconnect the bolts of the divertor flange and blanket flange
   (articulated manipulator with torque wrench)
7. Cut the cooling pipes of divertors and blankets
   (articulated manipulator with auto pipe cutter)
8. Remove the divertors
   (mechanical stopper handling vehicle, divertor retraction vehicle, support frame)
9. Remove the blanket-A and blanket-B
   (blanket retraction vehicle)

Table 4.2.1.3 Blanket Replacement Procedure (Continued)

Assembly

1. Install the blanket-B and blanket-A
   (blanket retraction vehicle)
2. Install the divertors
   (mechanical stopper handling vehicle, divertor retraction vehicle, support frame)
3. Weld the cooling pipes of divertors and blankets
   (articulated manipulator with auto pipe welder)
   --- at the same time of this work, non-destructive test of the cooling pipes is carried out.---
4. Connect the bolts of the divertor flange and blanket flange
   (articulated manipulator with torque wrench)
5. Install the access door
   (access door carrier)
6. Temporarily connect the several bolts on the access door, and weld the lip seal
7. Connect all bolts on the access door
   (6, 7, bolt runner, auto seal welder, articulated manipulator)
8. Bake, evacuate, and NDT

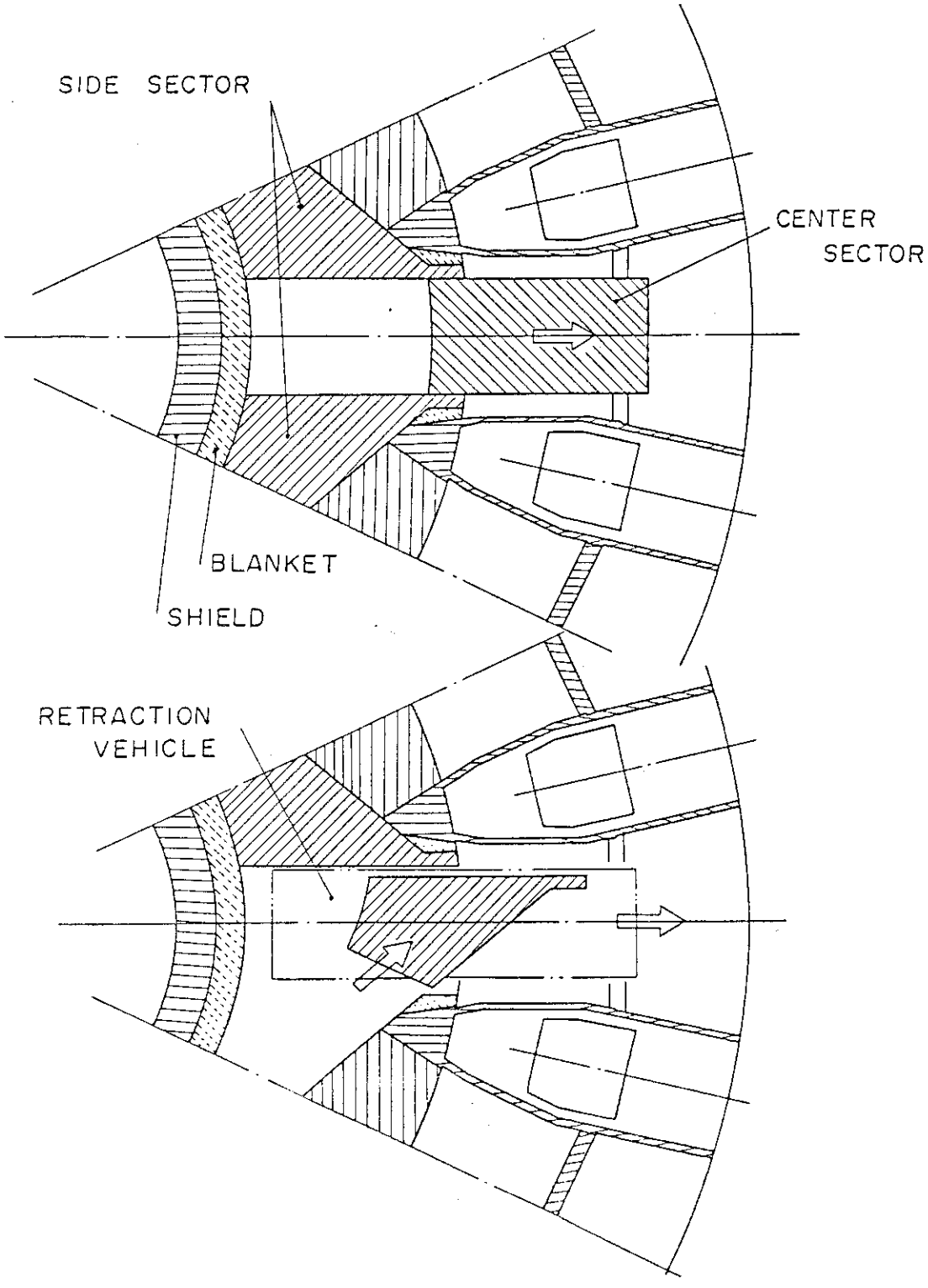

Fig.4.2.1.23 Divertor replacement concept

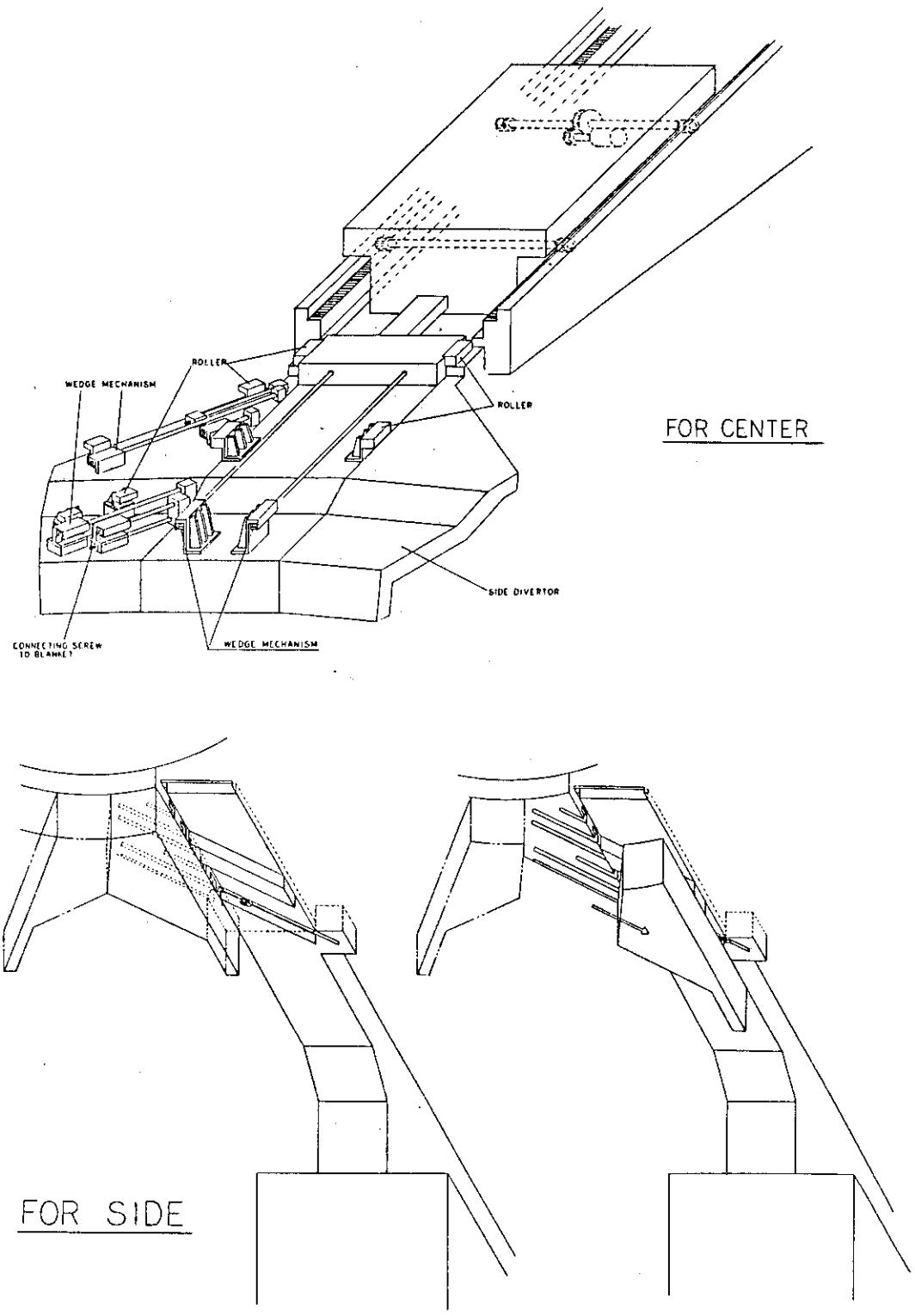

FIG.4.2.1.24 DIVERTOR REPLACEMENT PROCEDURE

Table 4.2.1.4 Divertor Replacement Procedure

Disassembly

1. Shutdown
2. Start baking, and cooling of decay heat
3. Disconnect the bolts on the access door
   (bolt runner, articulated manipulator)
4. Cut the lip seal on the access door
   (auto seal cutter, articulated manipulator)
5. Remove the access door
   (access door carrier)
6. Disconnect the bolts of the divertor flange
   (articulated manipulator with torque wrench)
7. Cut the cooling pipes of divertors
   (articulated manipulator with auto pipe cutter)
8. Loosen the mechanical stoppers (wedge) of center divertor
   (mechanical stopper handling vehicle, support frame)
9. Remove the center divertor
   (center divertor retraction vehicle, support frame)
10. Loosen the mechanical stoppers (wedge) of side divertors
    (mechanical stopper handling vehicle, support frame)
11. Remove the side divertors
    (side divertor retraction vehicle, support frame)

Table 4.2.1.4 Divertor Replacement Procedure (Continued)

Assembly

1. Install the side divertors
   (side divertor retraction vehicle, support frame)
2. Tighten the mechanical stoppers (wedge) of side divertors
   (mechanical stopper handling vehicle, support frame)
3. Install the center divertor
   (center divertor retraction vehicle, support frame)
4. Tighten the mechanical stoppers (wedge) of center divertor
   (mechanical stopper handling vehicle, support frame)
5. Weld the cooling pipes of divertors
   (articulated manipulator with auto pipe welder)
   --- at the same time of this work, non-destructive test of the cooling pipes is carried out.---
6. Connect the bolts of the divertor flange
   (articulated manipulator with torque wrench)
7. Install the access door
   (access door carrier)
8. Temporarily connect the several bolts on the access door, and weld the lip seal
9. Connect all bolts on the access door
   (8, 9, bolt runner, auto seal welder, articulated manipulator)
10. Bake, evacuate, and NDT

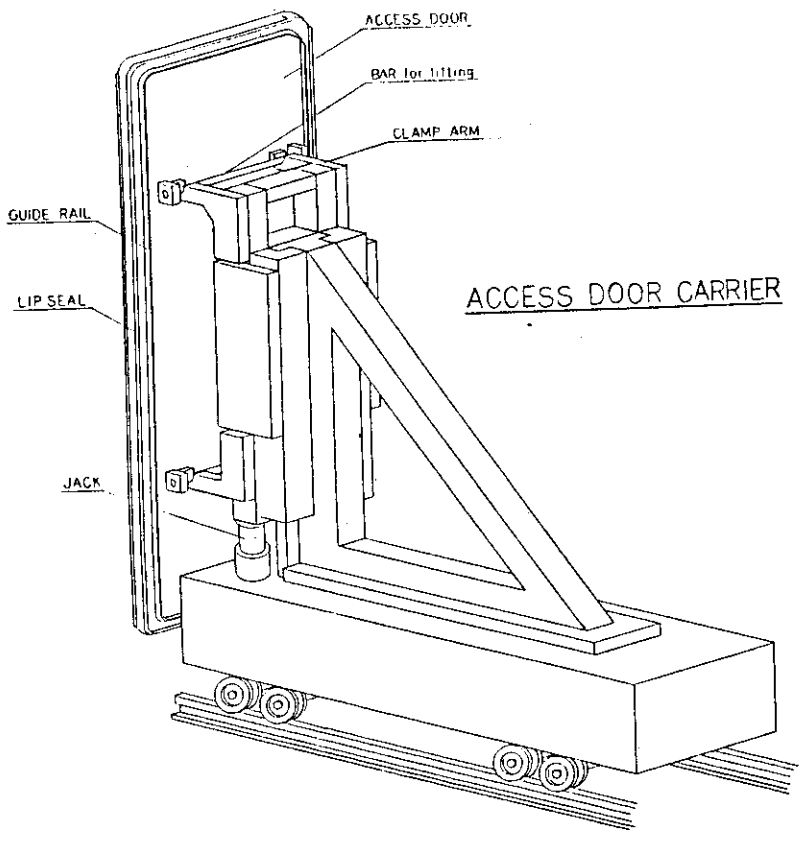

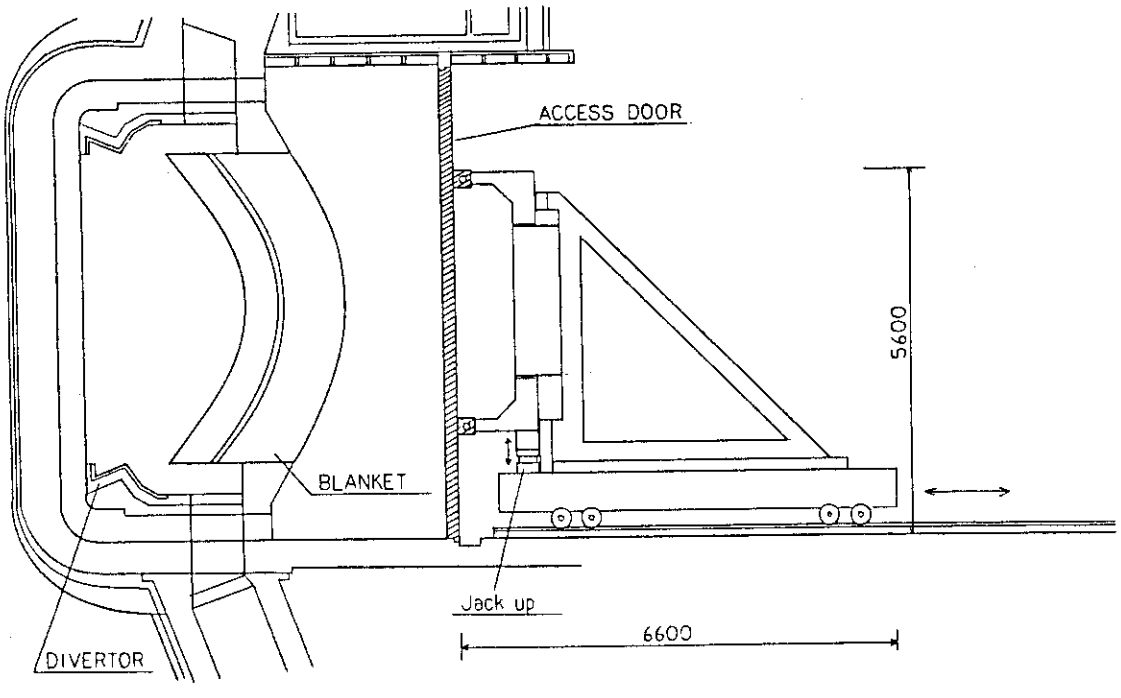

FIG.4.2.1.25 ACCESS DOOR REMOVAL

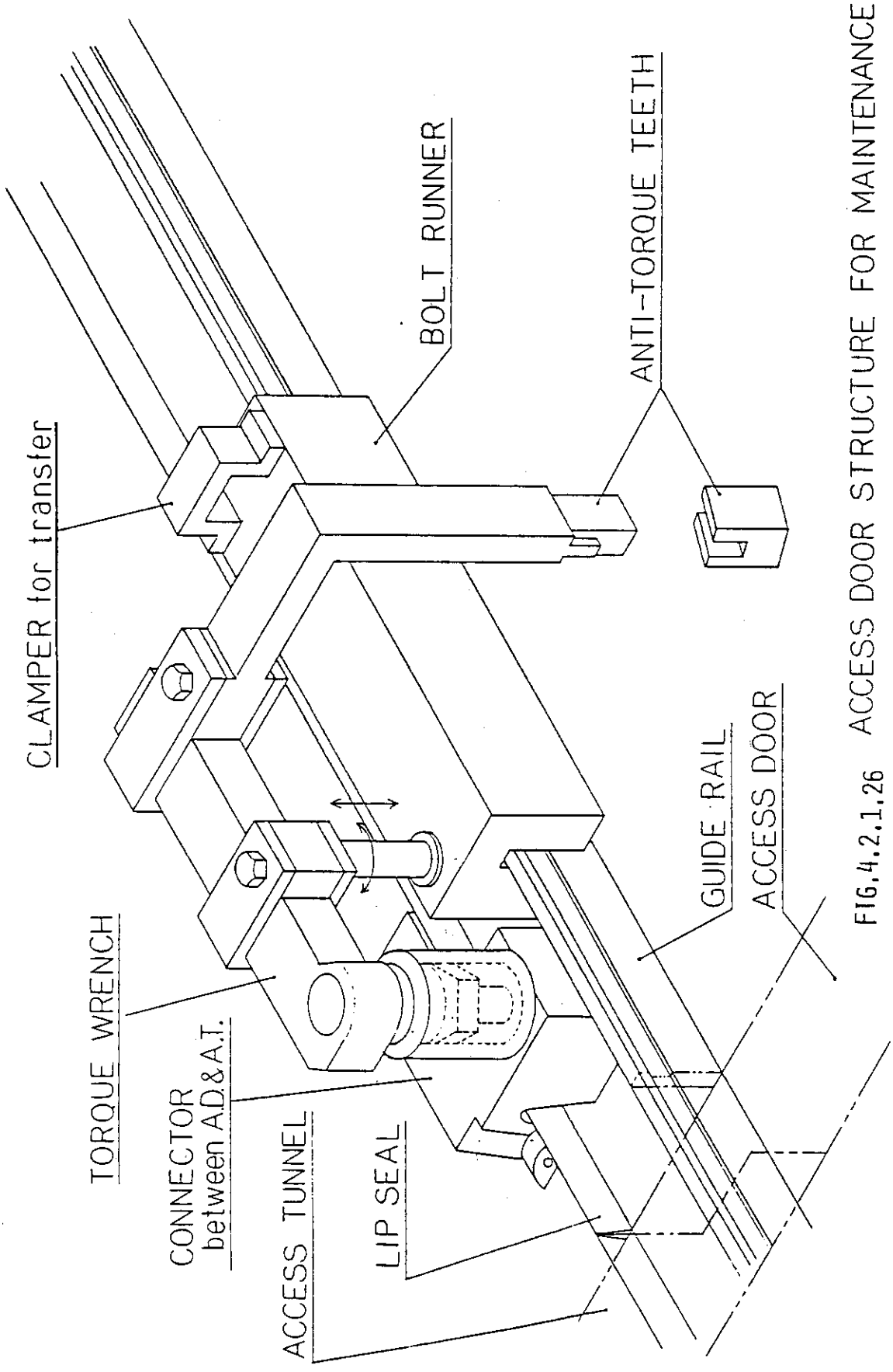

FIG.4.2.1.26 ACCESS DOOR STRUCTURE FOR MAINTENANCE

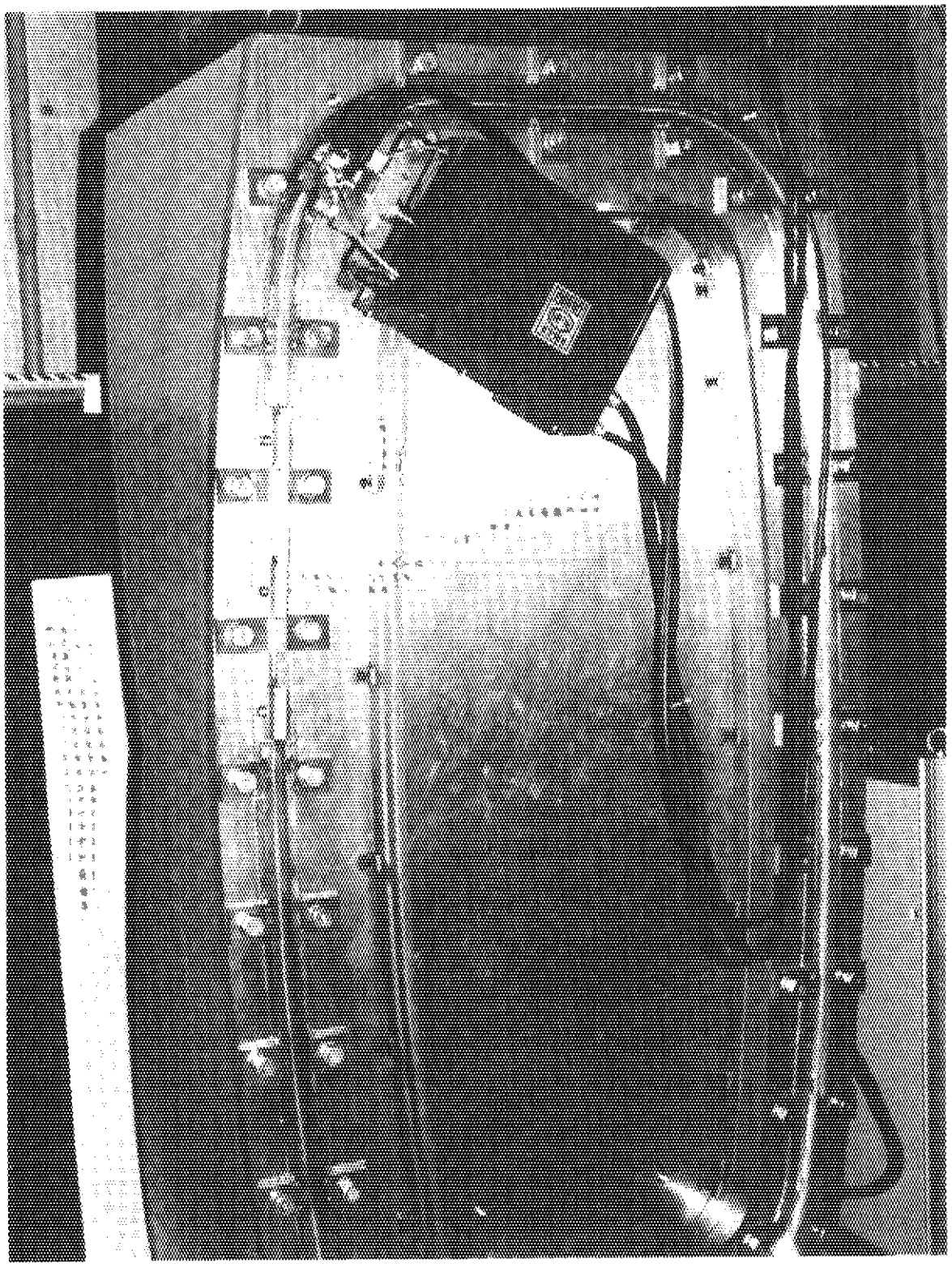

FIG.4.2.1.27 AUTO LIP SEAL WELDER AND CUTTER FOR ACCESS DOOR

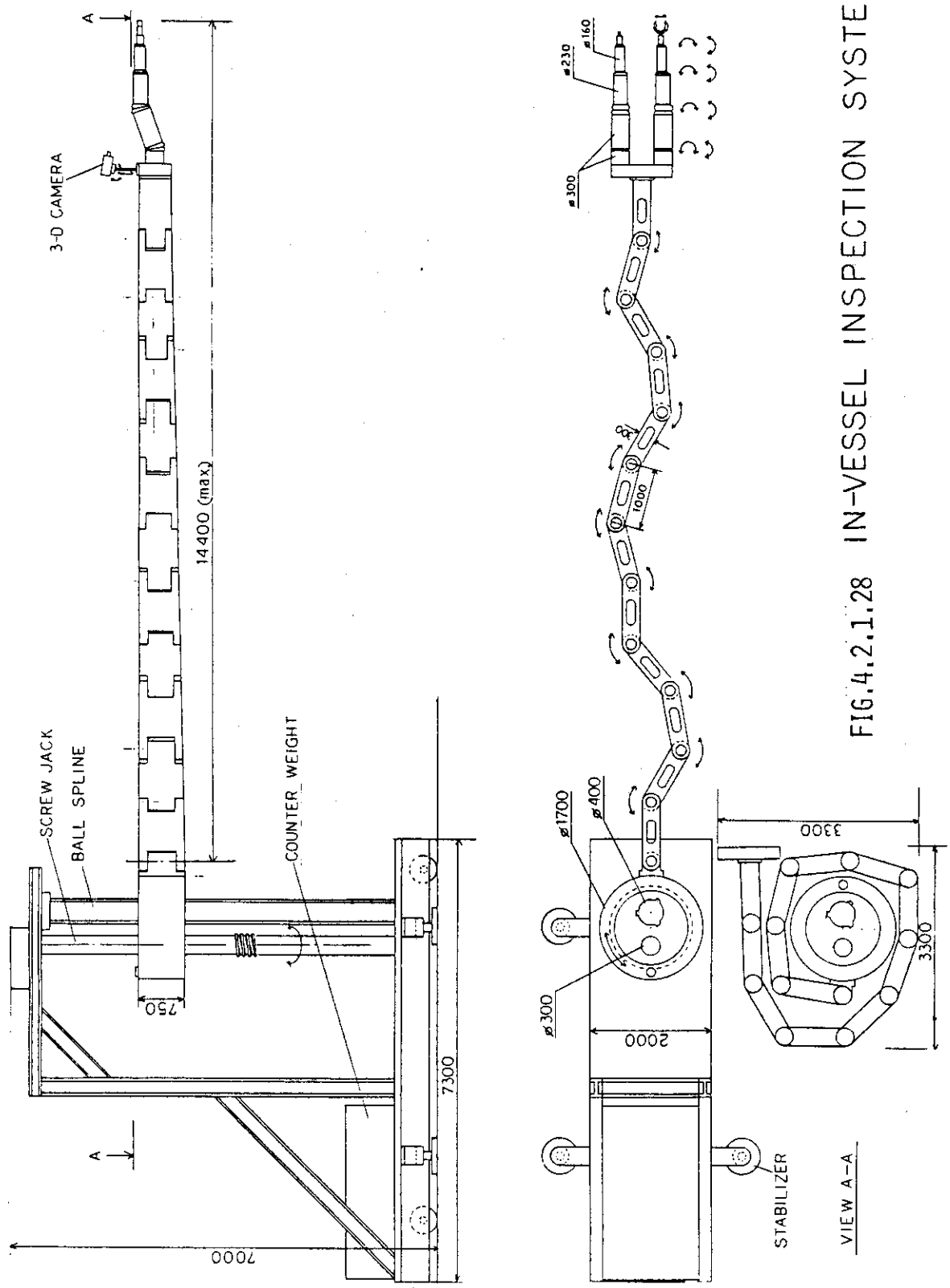

FIG.4.2.1.28 IN-VESSEL INSPECTION SYSTEM (a)

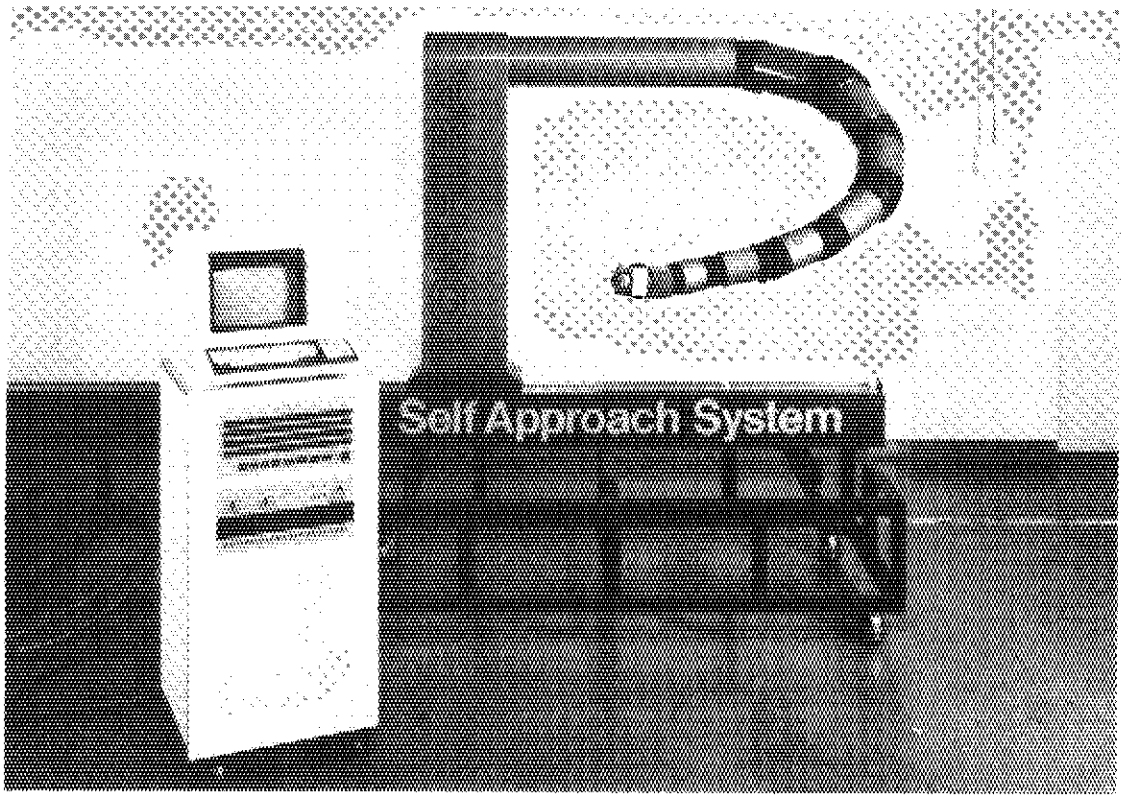

FIG.4.2.1.29 IN-VESSEL INSPECTION SYSTEM (b)

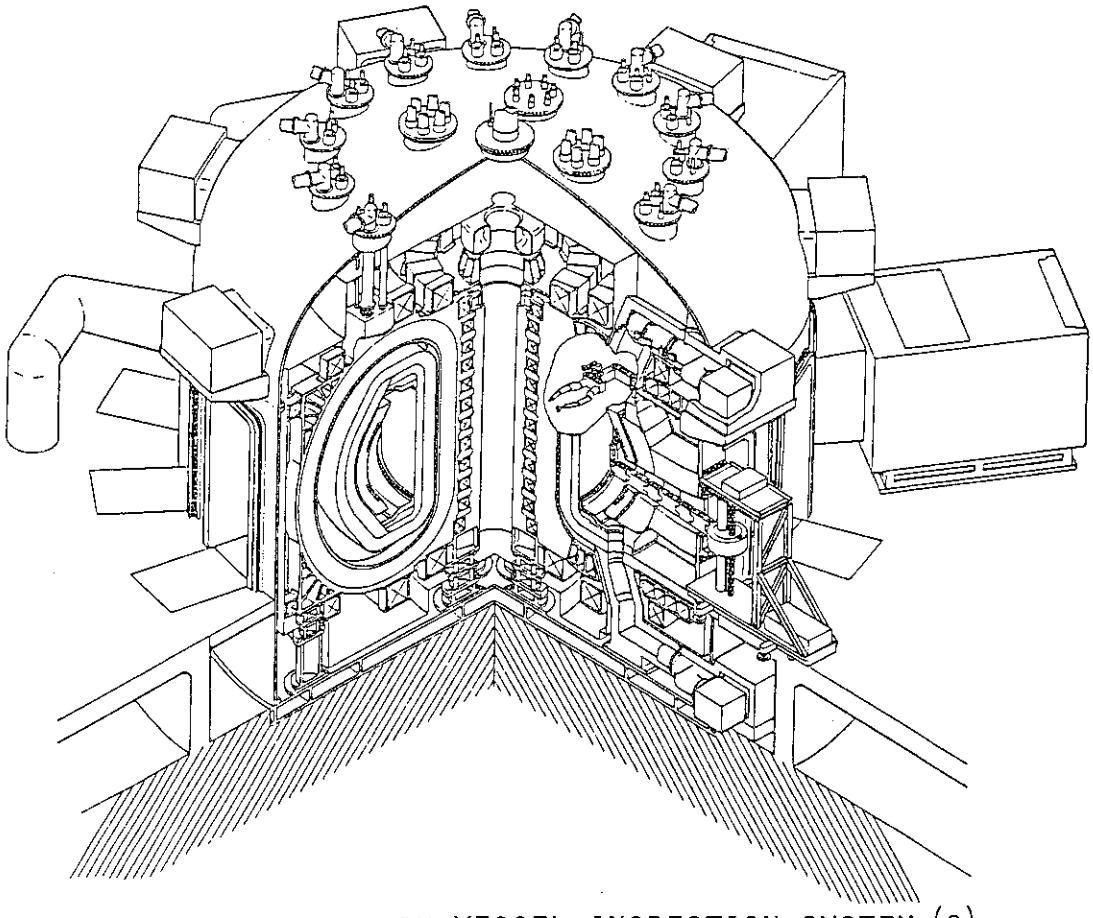

FIG.4.2.1.30 IN-VESSEL INSPECTION SYSTEM (c)

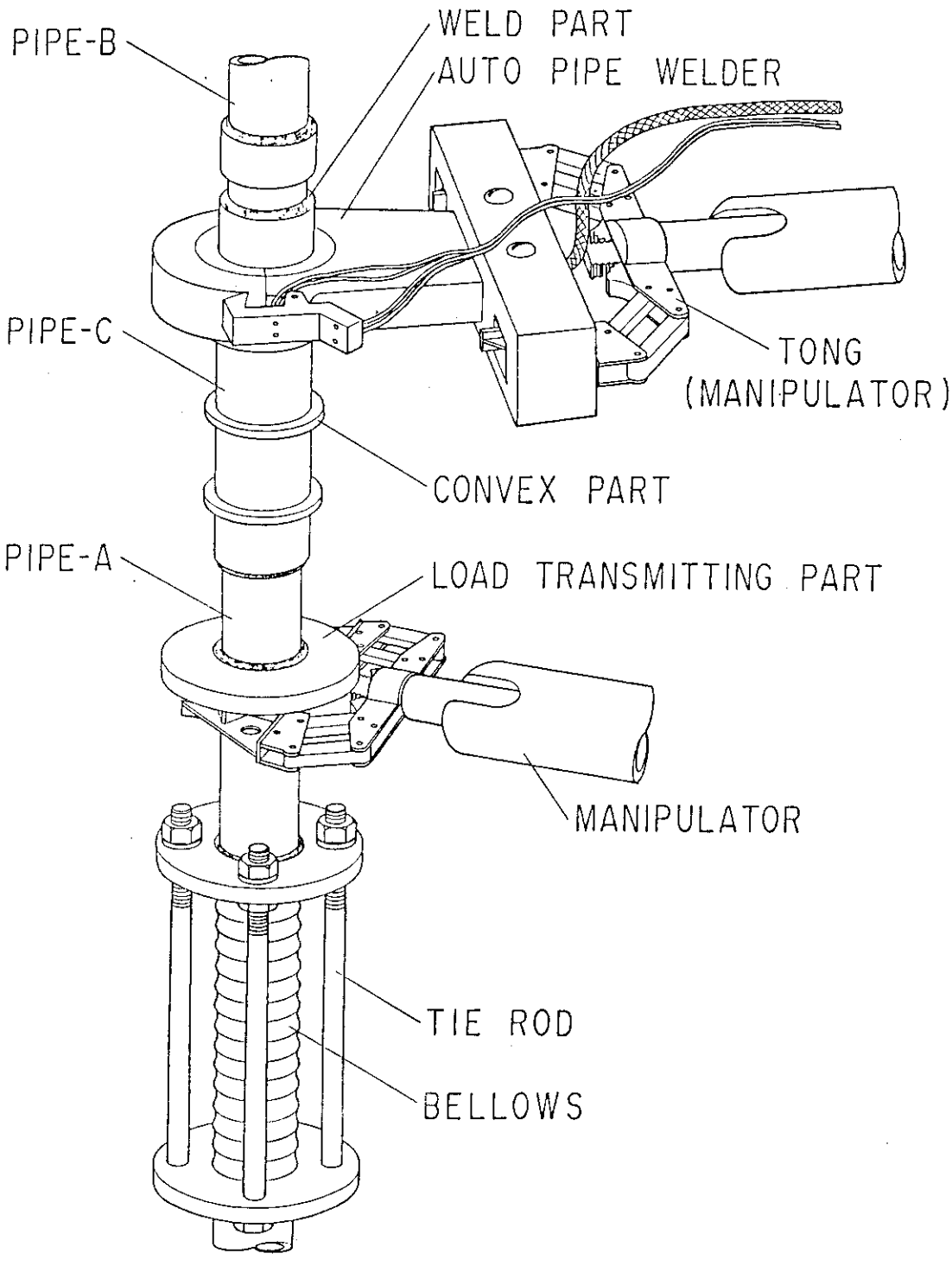

FIG.4.2.1.31 COOLING PIPE WELDING CONCEPT

(1)

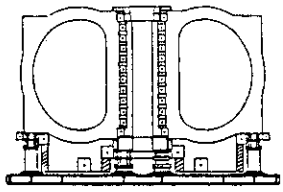

(6)

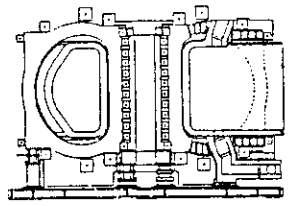

(11)

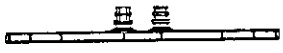

(2)

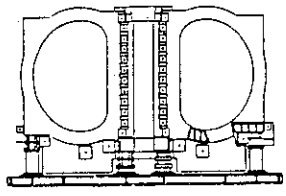

(7)

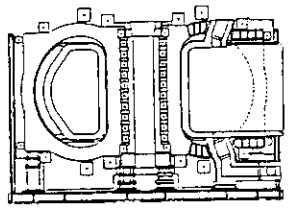

(12)

(3)

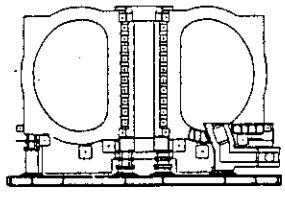

(8)

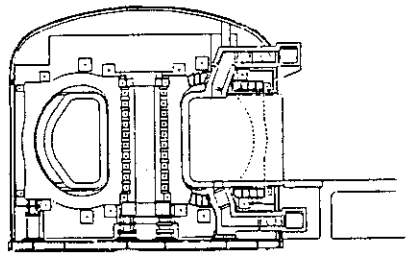

(13)

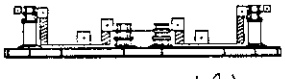

(4)

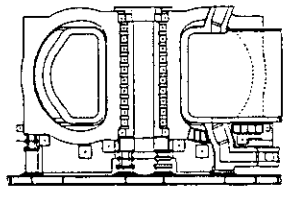

(9)

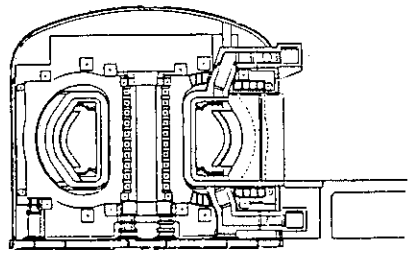

(14)

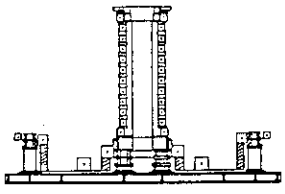

(5)

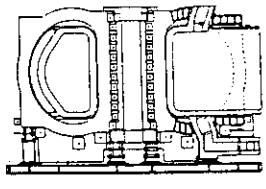

(10)

FIG.4.2.1.32 INITIAL CONSTRUCTION

Table 4.2.1.5 Summary of Mechanical Integration and Maintenance Disign of FER

1) Reactor Concept
   - Double Null Divertor Solution
   - 14 Toroidal Field Coils
   - Hands-on Maintenance before shield open
     and
     Remote Handling after shield open

2) Vacuum Boundary
   - Combined Vacuum Boundary
   - One Turn Resistance
     Thin Wall for Belljar
     Bellows for Plasma Chameer

3) Segmentation
   - Blanket: 2 Symmetrical Sectors/TF Coil
   - Divertor: 1 Center Sector / 2 TF Coils
     2 Side Sectors

4) Replacement
   - Blanket: Single Straight Motion for Sector A
     and
     Double Straight Motions for Sector B through on the TF windows
   - Divertor: Similar with Blanket

5) Magnet
   - TF Coil: Supported centering force with Center Post
     Supported overturning force with Shear Panel
   - PF Coil: Supported with Support Rings for Inboard Coils
     Supported with TFC Structure for Outer Ring Coils

6) Additional Heating System
   - 2 Ports for ICRF
   - 1 Ports for LHRF
   - 1 Ports for ECRF
   - 3 Ports for NBI

Table 4.2.1.6 Discussion For Future Design

1) Reliability for Maintenance
   - Replacement Procedure
   - Feasibility of Torus Structure for Maintenance
   - Remote Handling Machine

2) Fablicability of Component Structure

3) Detailed Analysis for Structural Design

4.2.2 A Scenario of FER electromagnetics design

An attainment of vertical positional stabilization of the elongated plasma with the structural integrity even for the plasma disruption is a main purpose of the electromagnetic design. This field of design has been developing that the method and its application to the FER is described here.

Three issues were discussed in the electromagnetics design: (1) shell effect of blanket/shield, (2) eddy current, electromagnetic force and structural problems, and (3) the plasma position control. Adding to them, the design of the divertor from the viewpoint of electromagnetics design was also presented. The main design/analysis flow and the representative parameters and figures of FER are shown in Figure 4.2.2.1, and Table 4.2.2.1 and Figure 4.2.2.2 ∿ 4, respectively.

For the shell effect, equation of motion of plasma and circuit equation of control coil and eddy current modes are considered as basic equations assuming dipole plasma approximation (Table 4.2.2.2 ∿ 4). Applying the Raplace transformation, we get the block diagram shown in Figure 4.2.2.5. This block diagram shows that the electromagnetic characteristics can be described by three parameters: N(S), M(S), and K(S) (Table 4.2.2.5). Sensitivity analysis of shell effect was carried out for five design parameters: (1) number of division (segmentation), (2) existence of inboard shell, (3) thickness of outboard front-shell, (4) thickness of outboard side-shell, and (5) existence of conductive end-wall (Table 4.2.2.6 ∿ 7, Figure 4.2.2.6 ∿ 10). Based on this sensitivity analysis and considering other design requirements (Table 4.2.2.8 ∿ 9), two shell models were selected: reference shell model and alternative shell model Figure (4.2.2.11 ∿ 12). The former is aiming at higher shell effect and the latter is a model for lower electromagnetic forces. The plasma instability growth time of these models are 44 msec and 32 msec, respectively (Figure 4.2.2.13 ∿ 14). Coupling and shielding functions are also shown in Figure 4.2.2.15 ∿ 18. The design/analysis of the shell effect are summarized in Table 4.2.2.10.

The eddy current, electromagnetic force and structural behavior of the blanket was analysed by the newly developed computer program system: EDDYTRAN (Figure 4.2.2.19). Electromagnetic forces of representative points for reference and alternative models at the plasma disruption are shown in Figure 4.2.2.20 ∿ 21. As shown in the figure, value and occuring position of the maximum electromagnetic force are 32 kg/cm^2 at the side-wall of outboard center module for the reference shell model, and 30 kg/cm^2 at end-wall of inboard center module for the alternative shell model, respectively. The maximum displacement and stress intensities are summarized in Table 4.2.2.11. As shown in the table, the electromagnetic force at the plasma disruption is a dominant load for the blanket and the maximum displacement and stress intensities are 4.6 mm and 17.2 kg/mm^2 (membrene) and 21.8 kg/mm^2 (membrene + bending) for reference model, and 3.7 mm and 17.3 kg/mm^2 (membrene) and 18.1 kg/mm^2 (membrene + bending) for alternative model. The membrene stress intensity seems to be a little larger than the value of ASME but it should be safe when we consider the number of the occurence of the plasma disruption (1,000 for life time).

As the electromagnetic force at the plasma disruption is a impulsive, the natural frequencies of the blanket were also analized (Figure 4.2.2.25 ∿ 27). Comparing Figure 4.2.2.24 and Figure 4.2.2.26, the deformation pattern of eigen mode = 2 is resembling to that by the electromagnetic force. But the natural frequency of igen mode = 2 is 37.9 that the stiffness of the blanket is reasonably high. The summary of the structural analysis is shown in Table 4.2.2.12.

For plasma position control, numerical simulations assuming the passive shell described above and active control coils were carried out. Three control coil positions were assumed: A(R = 3.5 m, Z = 6.15 m), B(R = 5.7 m, Z = 6.5 m), and C(R = 8.0 m, Z = 6.0 m). Gain-phase diagram of open-loop transfer functions of P-, PD- and PID- Control of reference shell model with control coil position - B are shown in Figure 4.2.2.28 ∿ 30. Some examples of plasma position control by reference shell model with control coil position - B are shown in Figure 4.2.2.31 ∿ 35. The gain-phase diagram of open-loop transfer functions and the plasma position control by alternative shell model with control coil

position-B are also shown in Figure 4.2.2.36 ∿ 40. The results for other control coil positions are similar to those shown here. These simulations show that the plasma can be stabilized by P-, PD- and PID-control and that the voltage limiter is effective for reducing the required power supply capacity without losing the plasma controllability. The maximum displacement and required power supply capacity are ∿18 mm and ∿30 MVA for reference shell model and ∿29 mm and ∿35 MVA for alternative one, respectively.

The parametric survey of plasma control by reference shell model with control coil position-B were carried out (Table 4.2.2.13). This survey showed that the plasma displacement and required power supply capacity are not sensitive to the accuracy and delay time of the detector, thyristor dead time and time constant of the applied field disturbance.

Based on these simulations, we conclude that reference shell model is preferable from the viewpoints of smaller plasma displacement and higher tritium breeding (Table 4.2.2.14) and that control coil position-B is preferable because of lower induced voltage. The difference in magnetic configurations for control coil-A, B and C (Figure 4.2.2.41 ∿ 43) are not essential. The plasma position control discussed above is based on the control coil outside TF coil and we got a satisfactory control characteristics with reasonable power supply capacity. Therefore, the control coil inside TF coil is not necessary in FER design (Table 4.2.2.15). The summary of the plasma position control is shown in Table 4.2.2.16.

The divertor is located at near plasma so that high electromagnetic force will be exerted on it at the plasma disruption. On the other hand, divertor accepts high heat flux so that mechanically weak structure is taken to reduce the thermal stress (Table 4.2.2.17). The solution for this dilemma is to break the current loop of the divertor structure to suppress the electromagnetic force. Two concepts of current loop break of the divertor are shown in Figure 4.2.2.44. The divertor structure of FER followed to the "Type-II" in Figure 4.2.2.44 is shown in Figure 4.2.2.45 ∿ 47.

The summary of the electromagnetic design and the discussions for future FER designs are shown in Table 4.2.2.18 ∿ 19.

Table 4.2.2.2 Dipole plasma approximation and n-value definition

1. Reactor Design Features Relating Electromagnetics

(1) R_p = 5.5 m
(2) a_p = 1.1 m
(3) $\kappa \simeq 1.6$
(4) Ip = 5.3 MA
(5) β_p = 2.3
(6) n index = -1.62
(7) B_V = -0.38 V
(8) B_T = 5.7 T
(9) No TF Coils : I4
(10) Blanket / Shield Division No :
14 Center Modules
14 Side Modules

2. Design Requirement

(1) No Remoto Maintenance Within Shield

No Electrical Connection Between Blanket Modules

(2) Reasonable Tritium Breeding Ratio

Table 4.2.2.1 Main parameters and design requirement of FER

Dipole Plasma Approximation

$$R = R_p$$

$$Z = \pm \pi a_p / 4$$

n-Value Is Defined As

$$n = - \frac{1}{I_P B_{VO}} \int_D \frac{\partial B_R^e}{\partial Z} j_P \, Rds$$

Here,

I_P : Toroidal Plasma Current
B_R : Equilibrium Radial Field
j_P : Distributed Toroidal Plasma Current Density

Table 4.2.2.3 Basic equations for plasma stabilization

BASIC EQUATIONS

1. Equation of Motion of Plasma

2. Circuit Equation of Control Coil and Eddycurrent Modes

1. Equation of Motion of Plasma

$$M_P \ddot{Z}_P = -2\pi R_P I_P \left(-\frac{nB_{VQ}}{R_P} Z_P + \nu_C I_C + \sum_I \nu_I I_I + B_d\right)$$

Here,

M_P : Plasma Mass

R_P : Major Radius of Plasma

I_C : Control Coil Current

I_I : Current of I-th Eddy Current

B_d : Disturbance Radial Field

ν_C : Radial Field of Unit Current of Control Coil

ν_I : Average Radial Field of Unit Current of I-th Eddy Current

$$\nu_C = -\frac{M_{PC}}{2\pi R_P} \quad , \quad \nu_I = -\frac{M_{PI}}{2\pi R_P}$$

M_{PC} : Z-Derivative of Mutual Inductance Between Plasma and Control Coil

M_{PI} : Z-Derivative of Mutual Inductance Between Plasma and I-th Eddy Current Mode

Table 4.2.2.4 Basic equations for plasma stabilization (continued)

2. Circuit Equations

2.1 For Control Coil

$$L_C \dot{I}_C + \sum_I M_{CI} \dot{I}_I + I_P M'_{PC} \dot{Z}_P + R_C C_C = V_C$$

Here,

L_C : Self Inductance of Control Coil

R_C : Resistance of Control Coil

V_C : Voltage Applied to Control Coil

M_{CI} : Mutual Inductance Between Control Coil and I-th Eddy Current

2.2 For Eddy Current

$$M_{CI} \dot{I}_C + \tau_I \dot{I}_I + I_P M'_{PI} \dot{Z}_P + I_I = 0, \quad (I=1, \text{----}, N_{mode})$$

Here,

N_{mode}: Number of Eddy Current Modes Taken into Consideration

Table 4.2.2.5 Definition and meaning of N(S), M(S) and K(S)

$$N(s) = \sum_i \frac{n_i s\tau_i}{1+s\tau_i} \quad , \qquad n_i = -\frac{M'^2_{pi} I_p}{2\pi B_{vo} \tau_i}$$

$$M(s) = \sum_i \frac{\mu_i s\tau_i}{1+s\tau_i} \quad , \qquad \mu_i = \frac{M_{ci} M'_{pi}}{M'_{pc} \tau_i}$$

AND

$$K(s) = \sum_i \frac{\kappa_i s\tau_i}{1+s\tau_i} \quad , \qquad \kappa_i = \frac{M_{ci}^2}{L_c \tau_i}$$

N(s) : Represents Stabilizing Effect of Plasma Vertical Motion

M(s) : Represents Shielding Effect to Magnetic Field of Control Coil

K(s) : Represents Coupling Effect Between Control Coil and Eddy Current

Table 4.2.2.6 Design parameters for shell effect survey

PARAMETRIC SURVEY

PARAMETERS

1. Number of Division

   14, 18, 42

2. Inboard Shell

   Exist (P_b, 60)/None

3. Thickness of Outboard Front-Shell

   P_b(100)/P_b(60)

4. Thickness of Outboard Side-Shell

   Cu(22.5)/Cu(15)

5. Conductive End-Wall

   Cu(15)/None

Table 4.2.2.7 Models of shell effect survey

Model No.	No. of Division	Inboard		Outboard			Growth Time: τ_G(ms)
		F/W	S/W	F/W	S/W	E/W	
10	14	Sus (10)	Sus (20)	Pb (60)	Cu (15)	None	32.21
20		Pb (60)	Cu (15)				41.04
30	28	Sus (10)	Sus (20)				17.74
31				Pb (100)			20.62
32				Pb (60)	Cu (22.5)		21.90
33				Pb (100)			26.29
40		Pb (60)	Cu (15)	Pb (60)	Cu (15)		27.62
50		Sus (10)	Sus (20)			Cu (15)	19.73
80	42	Sus (10)	Sus (20)			None	9.27
90		Pb (60)	Cu (15)				17.07

F/W : Front Wall S/W : Side Wall E/W : End Wall

Figures in ( ) is thickness ; mm

Table 4.2.2.8 Results of the shell effect survey and design considerations

EVALUATIONS (1)

No. of Division	Inboard Shell
(1) Smaller Is Better	(1) Inboard Shell is preferable (2) Large Electromagnetic Force
28	No Inboard Shell
(1) No. of TF/C : 14 (2) Electrical Connection By Manuputator Is Impossible	(1) Support of Inboard Blanket Is Difficult
⇩	⇩
Smallest No. : 28	No Shell for Structural Integrity

Table 4.2.2.9 Results of the shell effect survey and design considerations (continued)

EVALUATIONS (2)

Thickness of F/W	Thickness of S/W	End Wall
(1) Thicker Is Better	(1) Thicker Is Better	(1) Not So Sensitive
60 mm	30 mm	No Conductive End-Wall
(1) Thick Pb or Be Is Difficult to Manufacture and to Cool	(1) Cu Eat Neutron	(1) Sus End-Wall Is Preferable for Structure
⇩	⇩	⇩
60mm for Structural Integrity	30mm Cu for Plasma Stability	Sus End-Wall for Structural Integrity

Table 4.2.2.10 Summary of the shell effect

SUMMARY ---- SHELL EFFECT

I. WHAT WAS DONE

(1) DEPENDENCE OF DESIGN FACTORS ON SHELL EFFECT WERE OBTAINED THROUGH PARAMETRIC SURVEY.
(2) REFERENCE AND ALTERNATIVE DESIGNE FOR BLANKET / SHELL WERE DETERMIND BASED ON THE ABOVE AND OTHER DESIGN CONSIDERATIONS
(3) ELECTROMAGNETIC PROPERTIES WERE CALCULATED FOR REFERENCE AND ALTERNATIVE SHELL DESIGN

2. WHAT WAS OBTAINED

(1) NO. OF DIVISION, SIDE WALL THICKNESS, EXISTENCE OF INBOARD SHELL STRUCTURES ARE SENSITIVE

3. WHAT WAS DESIGNED

(1) NO. OF DIVISION IS 28 FOR HIGHER SHELL EFFECT
(2) INBOARD SHELL IS REMOVED FOR STRUCTURAL INTEGRITY AT DISRUPTION
(3) THICK SIDE WALL (CU) IS ADOPTED FOR HIGHER SHELL EFFECT
(4) BE/PB FRONT WALL IS ADOPTED FOR HIGHER TRITIUM BREEDING

Table 4.2.2.11 Computational results of structural analysis

MAXIMUM DISPLACEMENT [mm]

SUBCASE	LOAD	R-DIRECTION	THETA-DIRECTION	Z-DIRECTION	TOTAL
0	ELECTROMAGNETIC FORCE (REFERENCE)[ROUGH MODEL]	2.82(F/W:O/C)	-2.15(F/W:I/C)	1.74(F/W:O/S)	3.52(F/W:O/C)
1	ELECTROMAGNETIC FORCE (REFERENCE)	-3.68(F/W:O/C)	-2.17(F/W:I/C)	-2.74(F/W:O/C)	4.59(F/W:O/C)
2	ELECTROMAGNETIC FORCE (ALTERNATIVE)	-2.97(F/W:O/C)	-2.20(F/W:I/C)	-2.22(F/W:O/C)	3.72(F/W:O/C)
3	HELIUM PRESSURE	-1.05(F/W:O/C)	1.11(S/W:I/C)	-0.72(F/W:I/C)	1.27(F/W:O/C)
4	ELEC.MAG. FORCE (REFERENCE) + HELIUM PRESSURE	-4.66(F/W:O/C)	-2.17(F/W:I/C)	-3.04(F/W:O/C)	5.77(F/W:O/C)
5	ELEC.MAG. FORCE (ALTERNATIVE) + HELIUM PRESSURE	-3.92(F/W:O/C)	-2.20(F/W:I/C)	-2.84(F/W:O/C)	4.84(F/W:O/C)

NOTE) F/W: FIRST WALL O/C: OUTBOARD CENTER
E/W: END WALL O/S: OUTBOARD SIDE
S/W: SIDE WALL I/C: INBOARD CENTER
I/W: INTERNAL WALL I/S: INBOARD SIDE

MAXIMUM STRESS INTENSITY [kgf/mm^2]

SUBCASE	LOAD	MEMBRANE	BENDING	MEMBRANE + BENDING
0	ELECTROMAGNETIC FORCE (REFERENCE)[ROUGH MODEL]	14.91(S/W:I/C)	10.61(F/W:O/C)	14.97 (F/W:I/C)
1	ELECTROMAGNETIC FORCE (REFERENCE)	17.21(S/W:I/C)	21.17(F/W:O/C)	21.79 (F/W:O/C)
2	ELECTROMAGNETIC FORCE (ALTERNATIVE)	17.29(S/W:I/C)	17.44(F/W:O/C)	18.10 (F/W:O/C)
3	HELIUM PRESSURE	2.62(F/W:O/C)	7.41(F/W:O/C)	7.70 (F/W:O/C)
4	ELEC.MAG. FORCE (REFERENCE) + HELIUM PRESSURE	17.21(S/W:I/C)	28.58(F/W:O/C)	29.03 (F/W:O/C)
5	ELEC.MAG. FORCE (ALTERNATIVE) + HELIUM PRESSURE	17.29(S/W:I/C)	24.89(F/W:O/C)	25.10 (F/W:O/C)

NOTE) F/W: FIRST WALL O/C: OUTBOARD CENTER
E/W: END WALL O/S: OUTBOARD SIDE
S/W: SIDE WALL I/C: INBOARD CENTER
I/W: INTERNAL WALL I/S: INBOARD SIDE

Table 4.2.2.12 Summary of the structural analysis

SUMMARY ---- STRUCTURAL ANALYSIS

I. WHAT WAS DONE

(1) EDDY CURRENT, INDUCED ELECTROMAGNETIC FORCES WERE CALCULATED
(2) STRESS AND DEFORMATION WERE CALCULATED
(3) NATURAL FREGUENCIES WERE CALCULATED

2. WHAT WAS OBTAINED

(1) MAX. ELECTROMAGNETIC FORCE:
32Kg/cm^2 FOR REF. DESIGN
30Kg/cm^2 FOR ALT. DESIGN
(2) MAX. DISPLACEMENT:
4.6 mm FOR REF. DESIGN
3.7 mm FOR ALT. DESIGN
(3) MAX. STRESS INTESITY:
17.2Kg/mm^2 (MEMB.),21.8Kg/mm2 (MEMB.+ BEND.) FOR REF. DES.
17.3Kg/mm^2 (MEMB.), 18.10Kg/mm^2 (MEMB. + BEND.) FOR ALT. DES
(4) STIFFNESS OF BLANKET IS REASONABLY HIGH

3. WHAT WAS DESIGNED

REFERENCE MODEL IS PREFERABLE, AND SIDE WALL THICKNESS SHOULD BE INCREASED.

Table 4.2.2.13 Parametric survey of plasma control, reference model with control coil position-B

PARAMETRIC SURVEY OF PLASMA CONTROL
(REFERENCE DESIGN, CONTROL COIL - B)

			MAX. VOLT (V)	MAX. CURRENT (kA)	P/S CAPACITY (MVA)	MAX. DISPLACEMENT (mm)
V_L = ∞	ZGNT (mm)	0.0	612	118.5	72.57	-18.27
		2.0	630	118.5	74.67	-18.24
		5.0	700	120.7	84.50	-18.32
	τ BD (msec)	1.0	612	118.5	72.57	-18.27
		2.5	534	117.1	62.50	-15.59
		5.0	438	112.5	49.21	-12.64
	τ DET (msec)	0.5	615	115.2	70.87	-17.83
		1.0	612	118.5	72.57	-18.27
		2.0	592	125.9	74.49	-18.92
	τ THY (msec)	0.5	588	115.3	67.80	-17.62
		1.0	612	118.5	72.57	-18.27
		2.0	661	126.5	83.69	-19.56
V_L = 250 V	ZGNT (mm)	0.0	250	132.4	33.09	-19.08
		2.0	250	132.0	33.01	-19.05
		5.0	250	133.1	33.28	-19.17
	τ BD (msec)	1.0	250	132.4	33.09	-19.08
		2.5	250	128.3	32.08	-17.47
		5.0	250	121.4	30.35	-14.62
	τ DET (msec)	0.5	250	130.4	32.60	-18.90
		1.0	250	132.4	33.09	-19.08
		2.0	250	135.8	33.95	-19.35
	τ THY (msec)	0.5	250	129.2	32.30	-18.66
		1.0	250	132.4	33.09	-19.08
		2.0	250	138.6	34.66	-19.90

Table 4.2.2.14 Design considerations for the plasma vertical position control

DESIGN

1. Shell Model (Design)

(1) Reference Model Is Preferable for Plasma Control (Displacement, Tritium Breeding)
(2) Stress Intensities of Reference and Alternative Models Are Almost the Same

Reference Model

2. Coil Position

(1) Magnetic Configuration Requires "Position-A"
(2) Induction Voltage in PF Coil Requires "Position-B" (Turns at Postion A and B Are 43 and 20)

Control Coil Position -B

3. Voltage Limiter

(1) Voltage Limiter Reduces Induction Voltage of PF Coil
(2) Voltage Limiter Reduces Power Supply Capacity
(3) Existence of Voltage Limiter on Plasma Control Is Not Essential

200~250 V Voltage Limiter

Table 4.2.2.15 Considerations for the control coil position

CONSIDERATIONS FOR CONTROL COIL POSITION INSIDE TF COIL

1. Inside TF Coil
   (1) Super Conducting Coil Is Imposible To Adopt Because Coil Should Cut Along The Torus
   (2) Normal Conducting Coil Requires High Power And It Should Be Removed By Refregerator
   (3) Finding of Suitable Control Coil Position Is Difficult (Radiation Damage, Error Field, Remoto Maintenace...)
2. Outside TF Coil
   (1) Power Supply Capacity for Control Coil Outside TF Coil Is Not So Severe

⇩

OUTSIDE TF COIL IS PREFERABLE IN FER SYSTEM

Table 4.2.2.16 Summary of the plasma position control

SUMMARY ----PLASMA POSITION CONTROL

I. What Was Done

(1) Simulations of Plasma Position Control By Control Coil-A/B for Reference and Alternative Shell Designs Were Carried Out
(2) Shell Design, Control Coil Position Are Determined and Power Supply Capacity Were Estimated.

2. What Was Obtained

(1) Plasma Vertical Movement Is Controllable with Limited Voltage
(2) Min. Control Power and Max. Plasma Displacedment Are 30 MW and 1.5 (Reference Model) to 3 (alternative Model) cm for 10 Gauss Magnetic Purturbation
(3) Control Power and Plasma Displacement Are Not-Sensitive on Accuracy and Delay Time of Detector, Thyristor Dead Time

3. What Was Designed

(1) Reference Design with Control Coil-B Are Selected
(2) Control Coil Is Separated From PF Coil, Considering Power Supply Capacity

Table 4.2.2.17 The design problem of divertor from the view point of electromagnetics

STATE OF PROBLEM ---- DIVERTOR

1. Divertor Is Located at Near Plasma
⇩
2. High Eddy Current at Plasma Movement and/or Disruption
⇩
3. High Electromagnetic Force

4. Mechanically Weak Structure
⇧
5. Thin Structure for Lower Thermal Stress
⇧
6. Divertor Accept High Heat Flux

Table 4.2.2.18 Summary of electromagnetics design

SUMMARY ---- ELECTROMAGNETICS DESIGN

1. What Was Done

(1) Problems and Method of Electromagnetics Design Were Discussed
(2) Electromagnetics Design Was Carried Out for FER

2. What Was Designed

(1) Blanket/Shield Is Divided into 28 Independent Modules Considering Remoto-Maintenance and Plasma Control
(2) Be/Pb (60 mm) Front Wall and Cu (30 mm) Side Wall Shell Structure Was Built in Outboard Blanket Considering Structural Integrity at Plasma Disruption, Plasma Control and Tritium Breeding
(3) Analysis Shows That Plasma Is Controllable, Electromagnetic Force at Disruption Is Acceptable and Tritium Breeding Ratio Is More Than 1.0
(4) Current Loop of Divertor Structure Is Broken by Insulation As To Suppress Induction Current

Table 4.2.2.19 Discussions of future design from the view point of electromagnetics design

DISCUSSIONS FOR FUTURE DESIGN

1. Limiter Configuration Plasma Is Preferable

2. Disruption Free or Longer Decay Constant of Plasma Current Is Desired

3. Electrical Connection between Modules by Manupulator Is Desred

4. Replace of Be To Other Material Should Be Studied

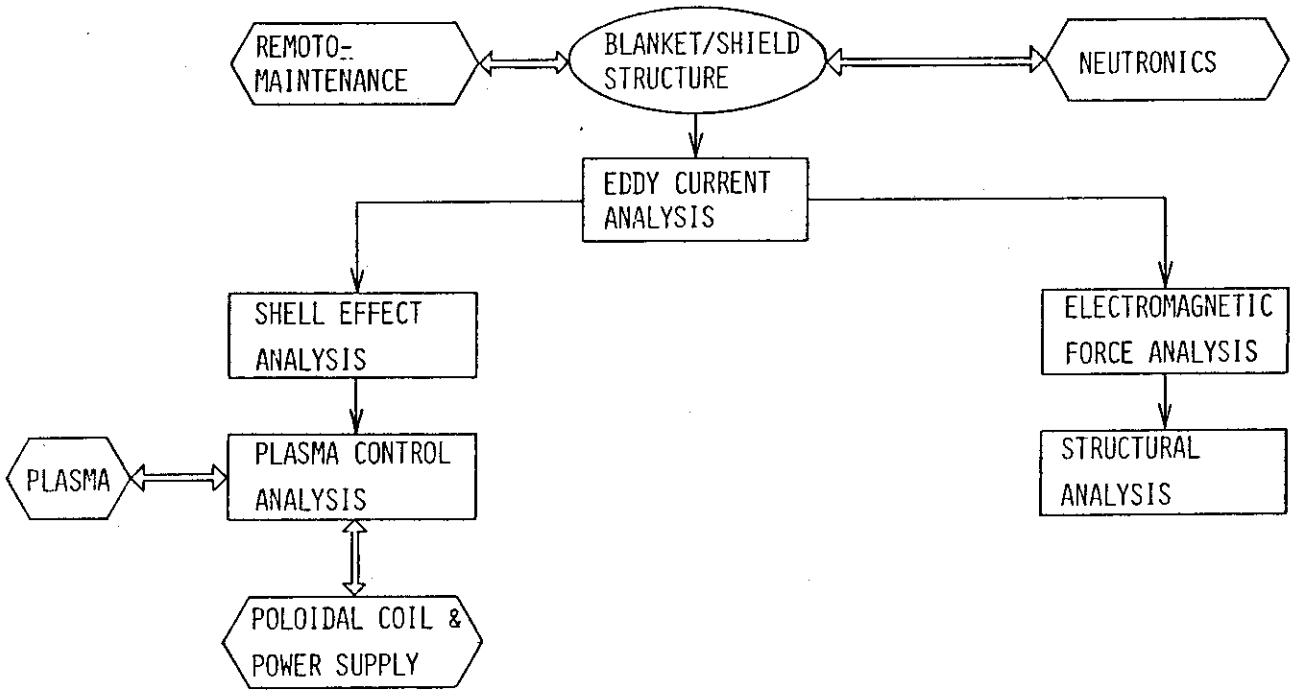

Figure 4.2.2.1 Electromagnetics design/analysis procedure and relations to other design field

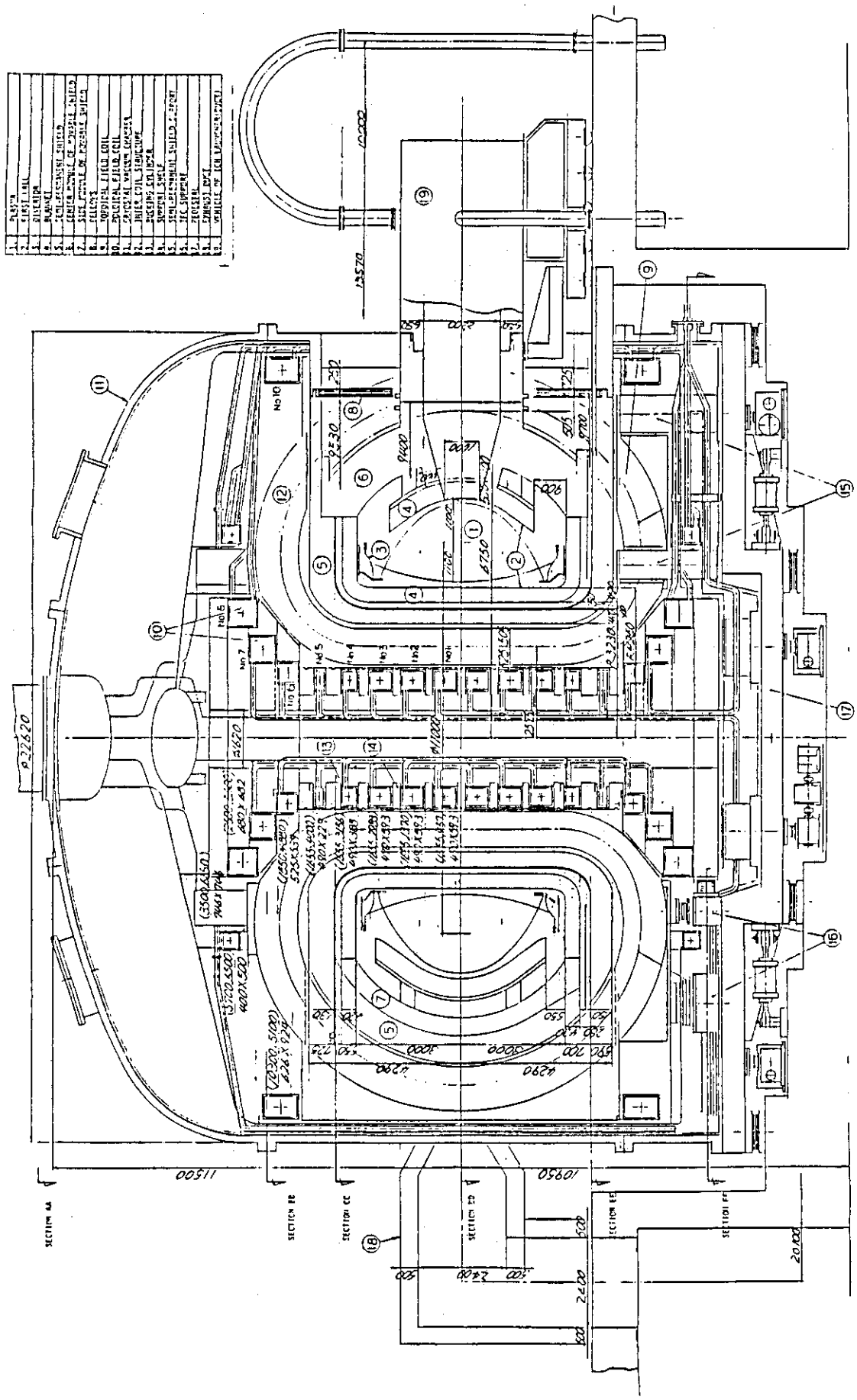

Figure 4.2.2.2 Elevation view of FER design to which electromagnetics design was carried out

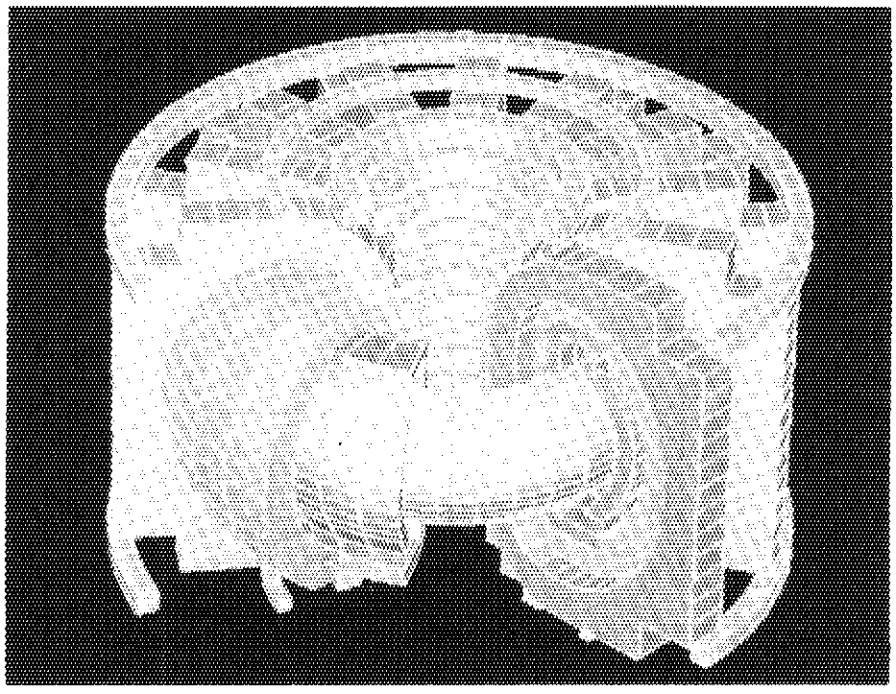

Figure 4.2.2.3 Bird's eye view of FER design

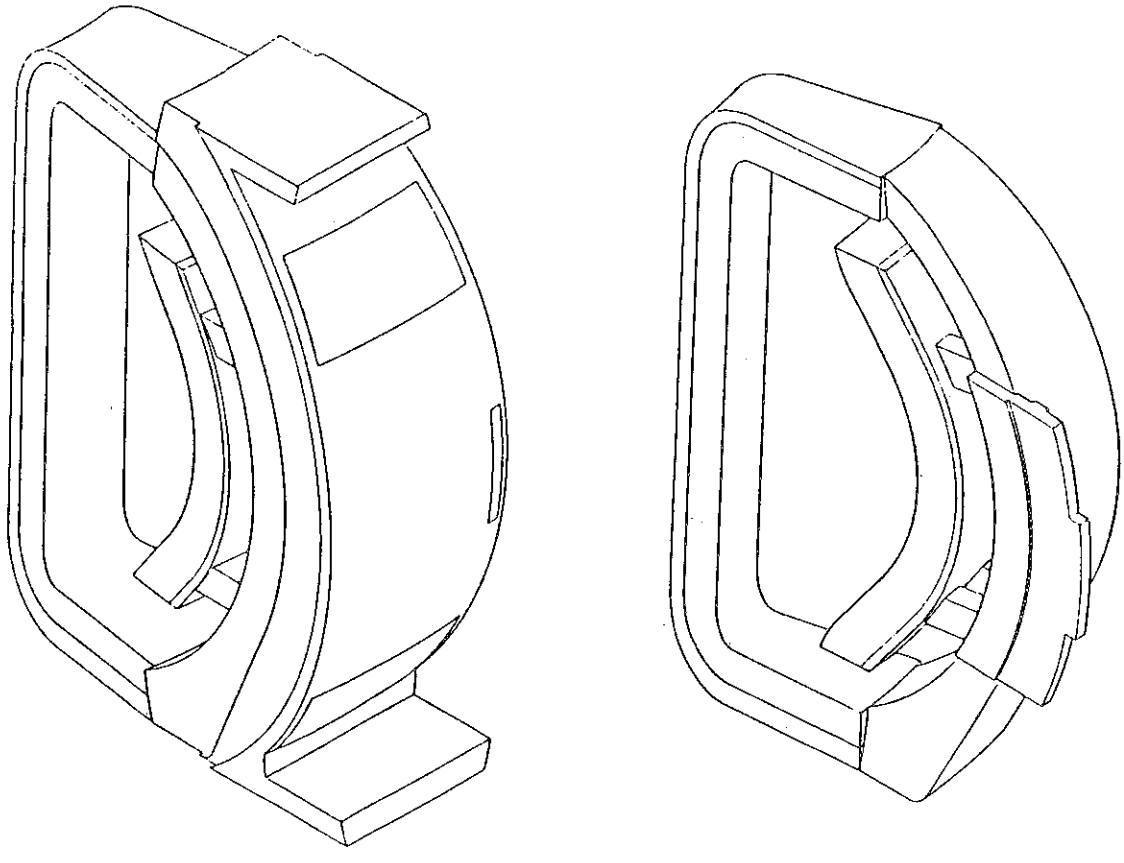

Figure 4.2.2.4 Bird's eye view of movable part of FER blanket and shield (Center module and side module)

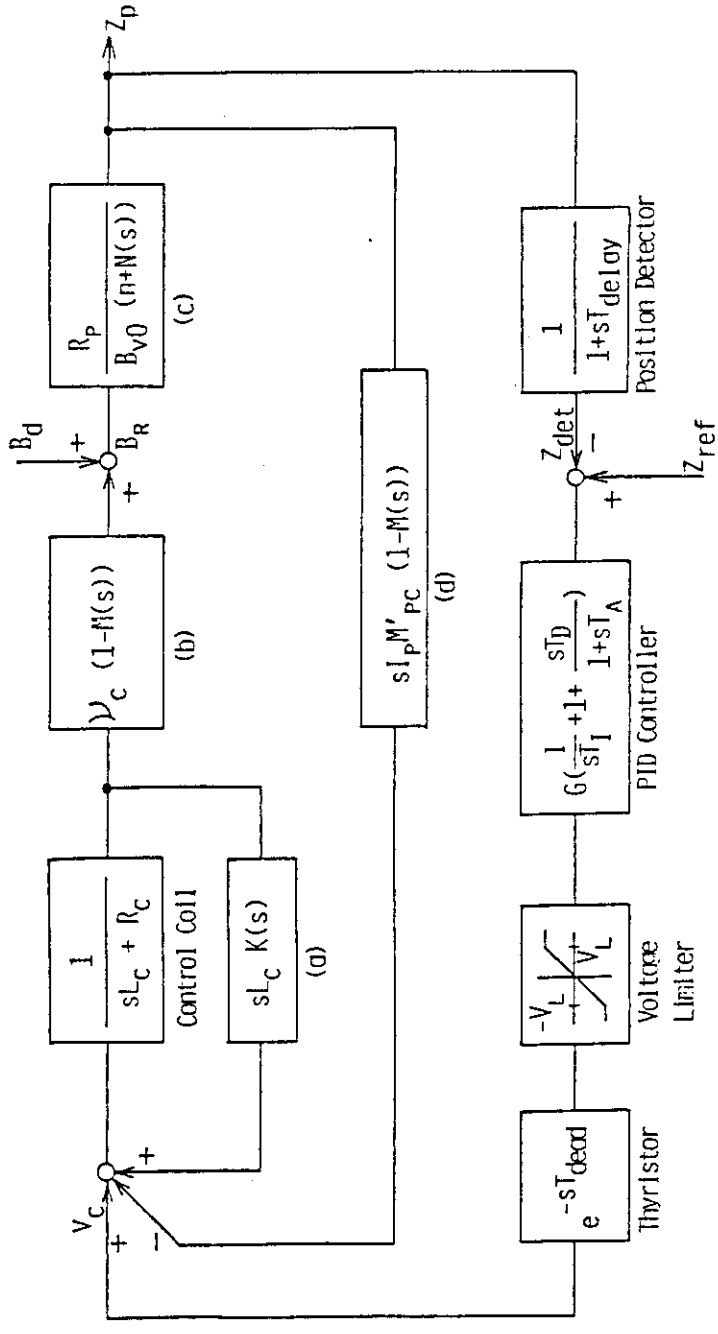

Block Diagram of Plasma Position Control System

Figure 4.2.2.5 Block diagram of plasma position control system

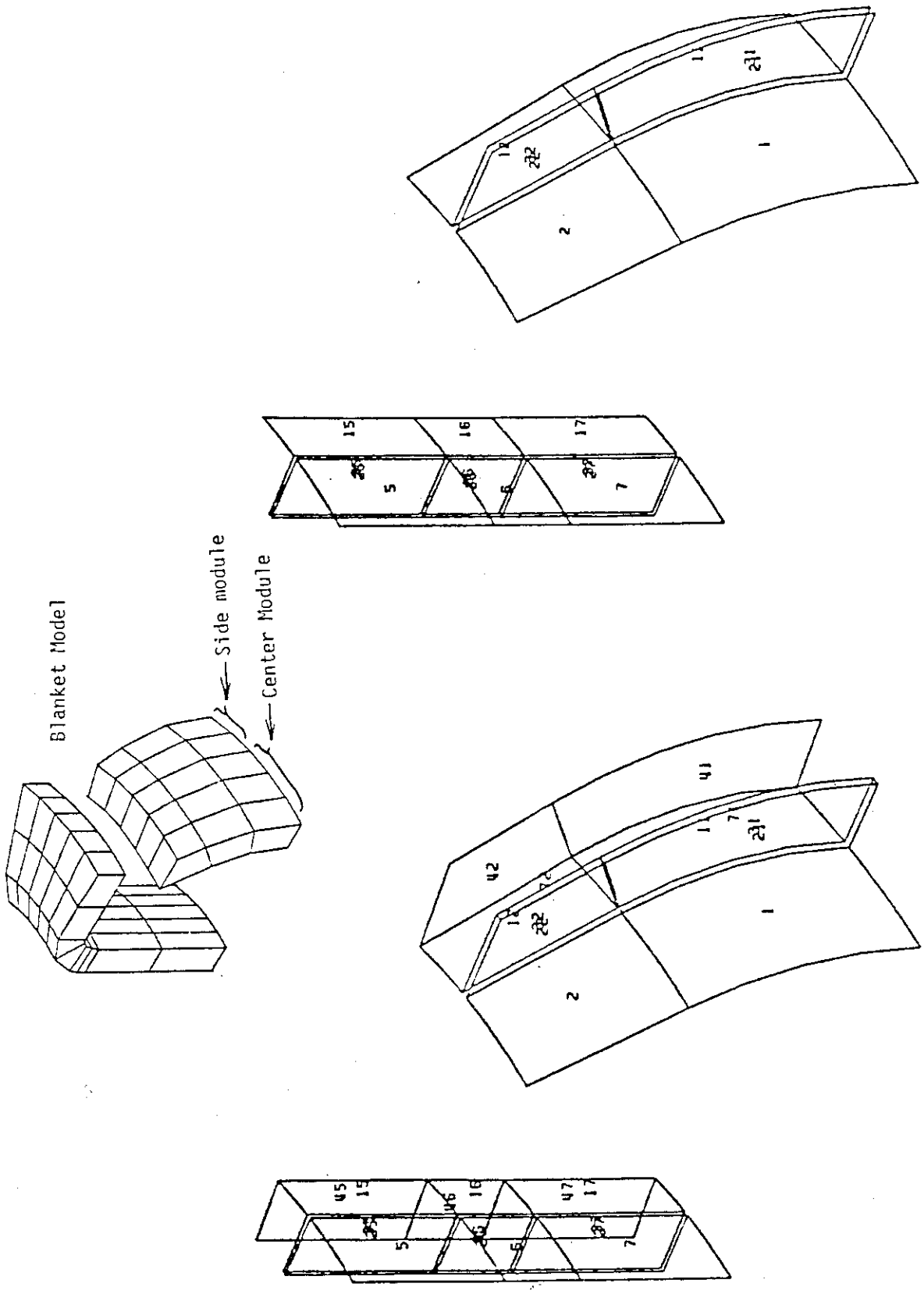

Figure 4.2.2.6 Example of shell effect calculation model

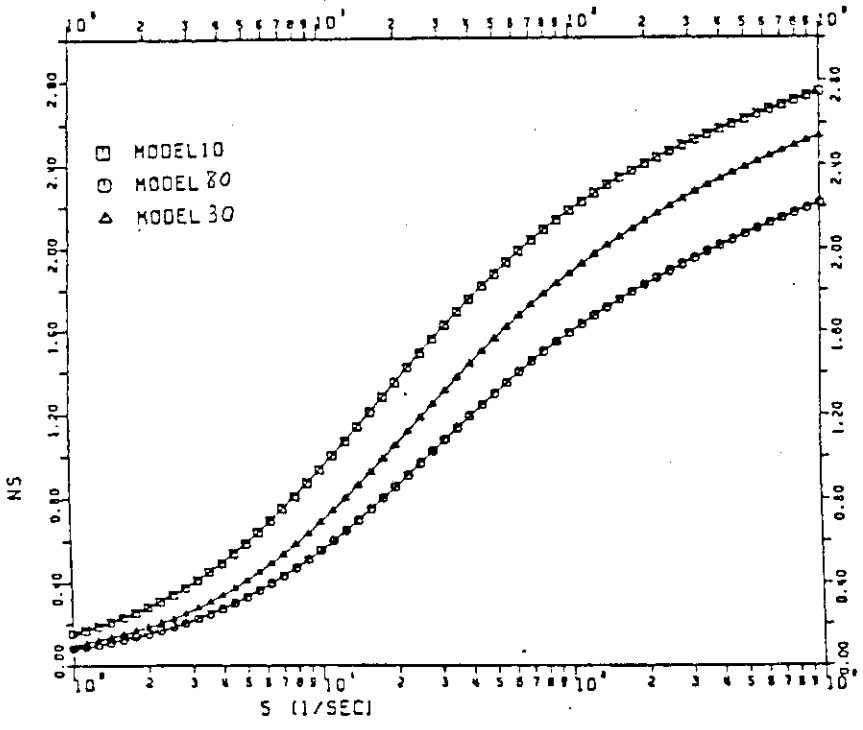

N-FUNCTIONS OF BLANKET SHELL MODELS

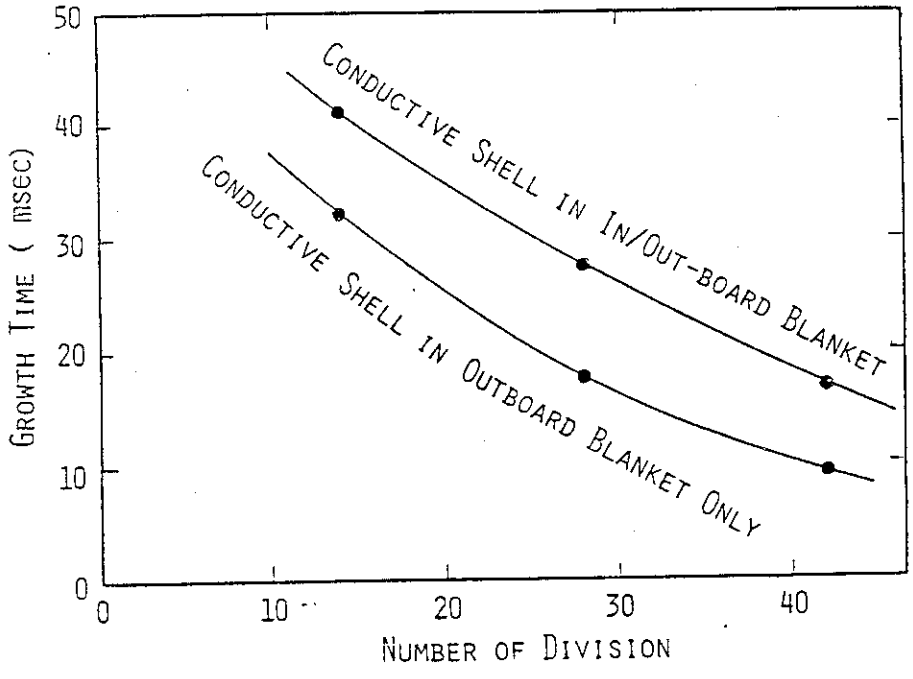

Figure 4.2.2.7 Dependence of N-function on the segmentation number

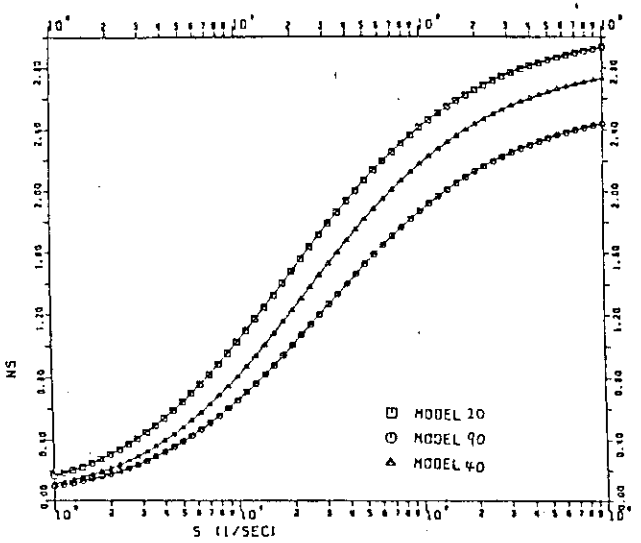

N-FUNCTIONS OF BLANKET SHELL MODELS

1. No. of Division

   (1) Smaller No. is Better

   (2) Sensitive

2. Inboard Shell

   (1) Conductive Shell Is Preferable

   (2) Large Electromagnetic Force

Figure 4.2.2.8
Dependence of N-function on the segmentation number and the effect of the inboard shell existence

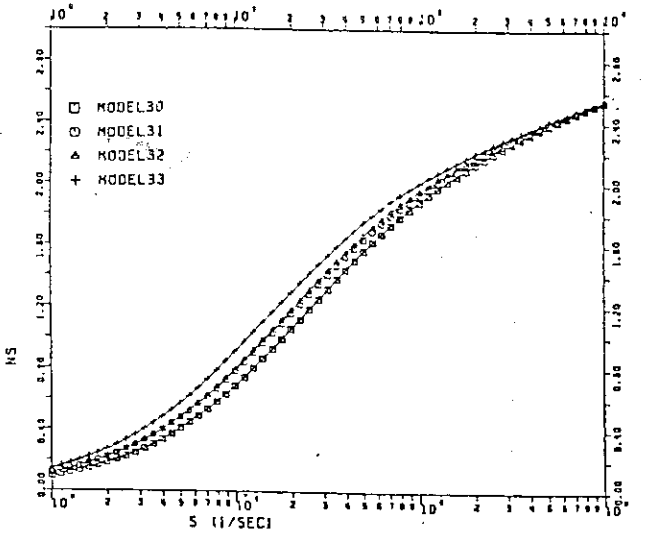

N-FUNCTIONS OF BLANKET SHELL MODELS

3. Thickness of Outboard Front-Shell

   (1) Thicker Is Better

   (2) Not So Sensitive

$$\frac{\partial \tau_G}{\partial t} = \begin{cases} 0.07\ \text{msec}/\text{mm} & \text{(S/W : 15mm)} \\ 0.11\ \text{msec}/\text{mm} & \text{(S/W : 22.5mm)} \end{cases}$$

4. Thickness of Outboard Side-Shell

   (1) Thicker Is Better

   (2) Sensitive

$$\frac{\partial \tau_G}{\partial t} = 0.55\ \text{msec}/\text{mm}$$

Figure 4.2.2.9
Dependence of N-function on the thickness of outboard front- and side- walls

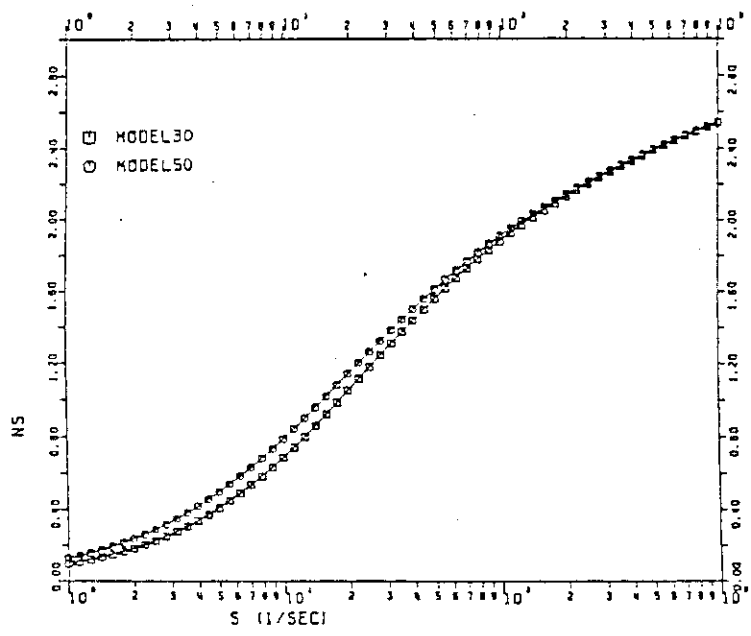

N-FUNCTIONS OF BLANKET SHELL MODELS

5. Conductive End Wall

(1) Not So Sensitive

Figure 4.2.2.10
Dependence of N-function on the existence of conductive end-wall

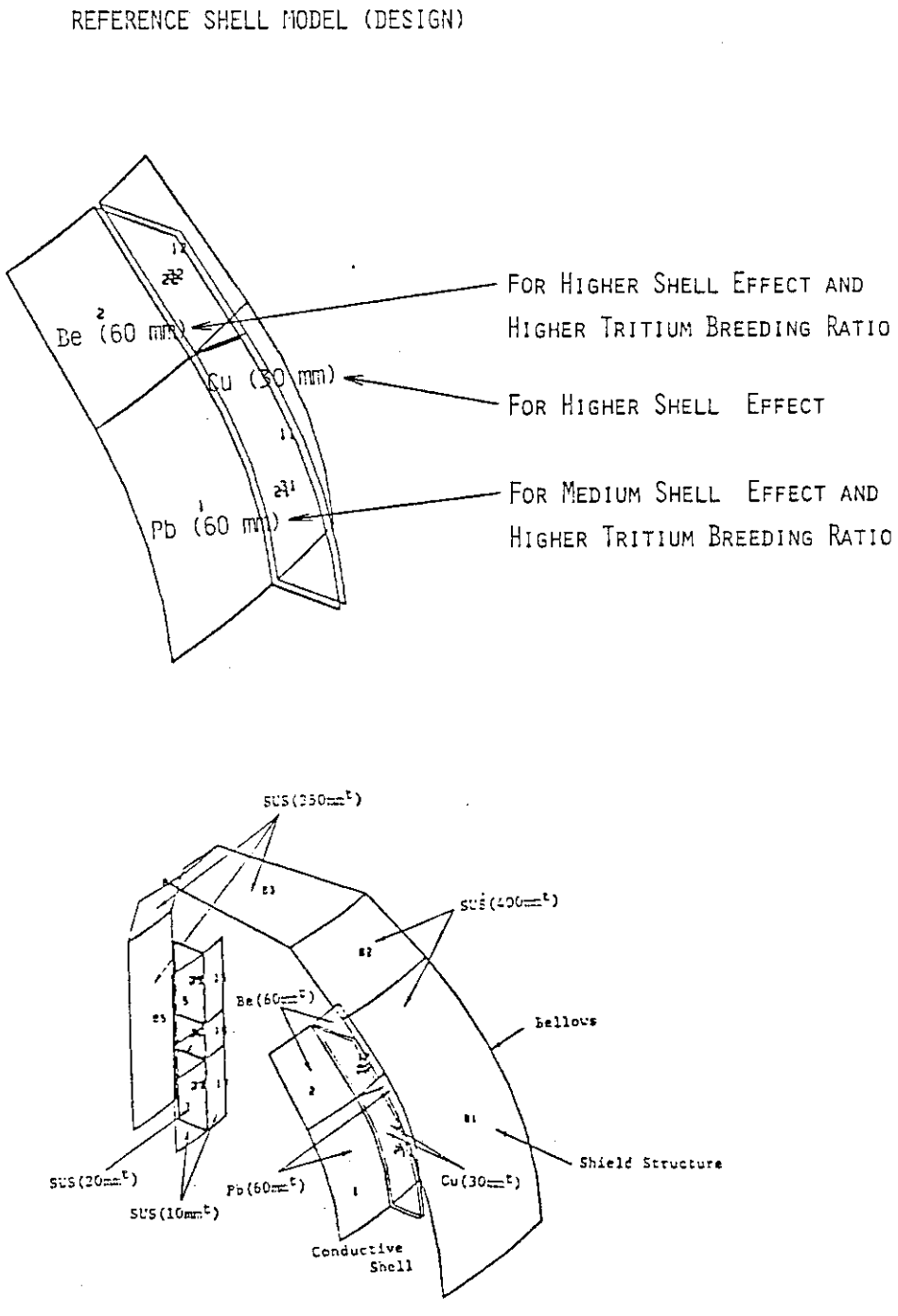

Figure 4.2.2.11 Reference shell model which is aiming for the higher shell effect

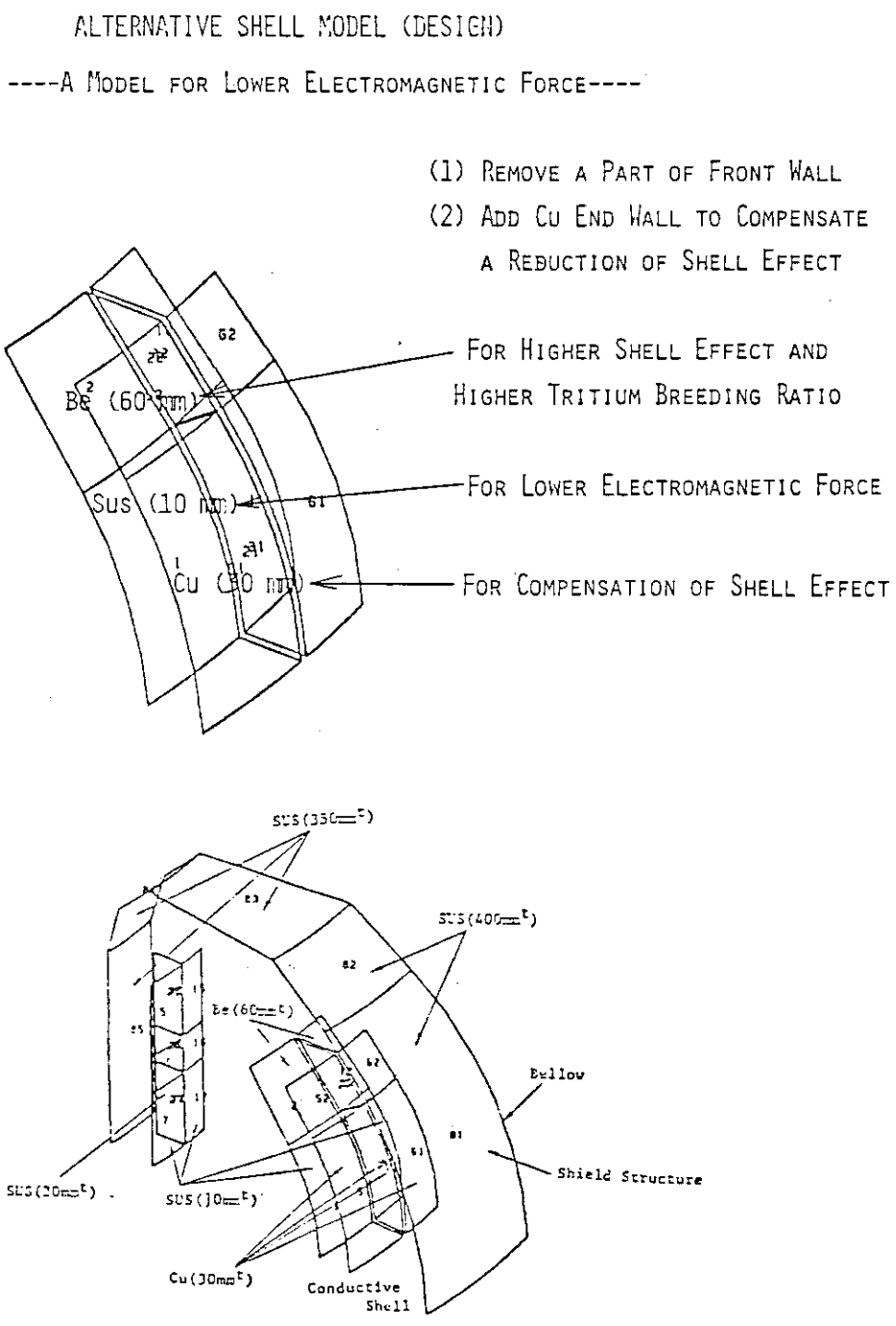

Figure 4.2.2.12 Alternative shell model which is aiming for lower electromagnetic force

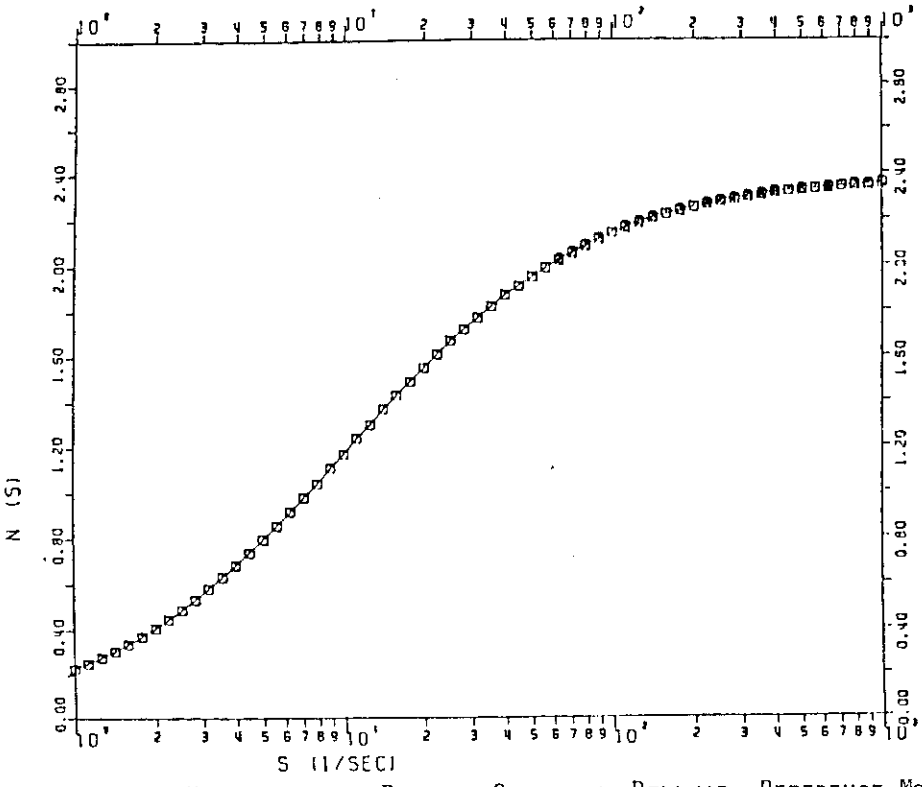

Figure 4.2.2.13 N-function of blanket shell and belljar of the reference model

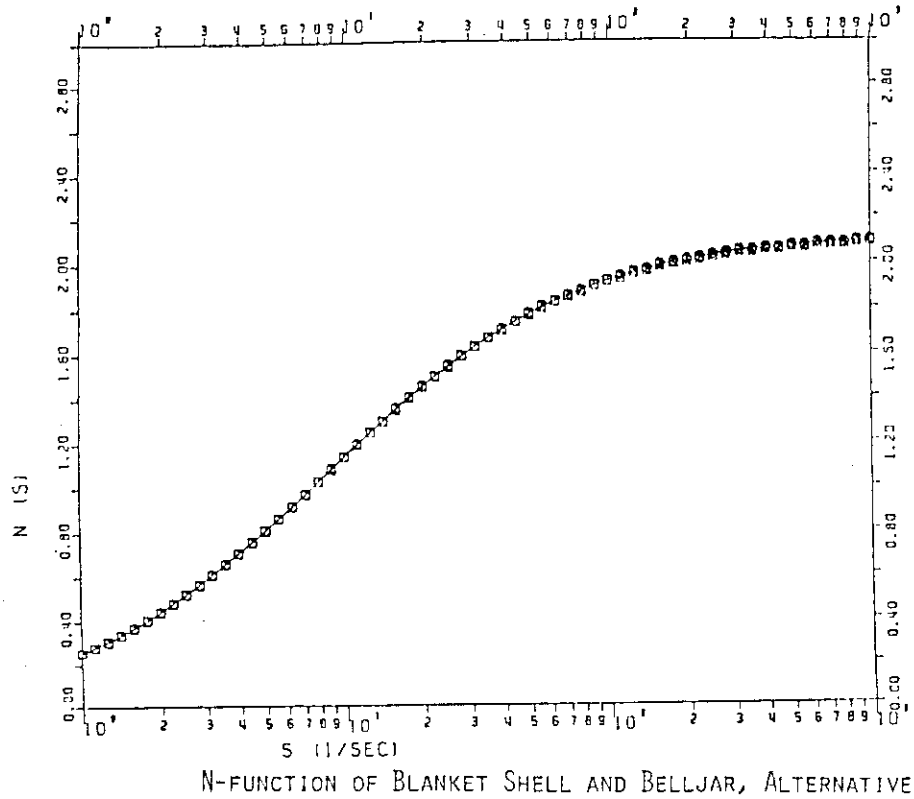

Figure 4.2.2.14 N-fun-tion of blanket shell and belljar of the alternative model

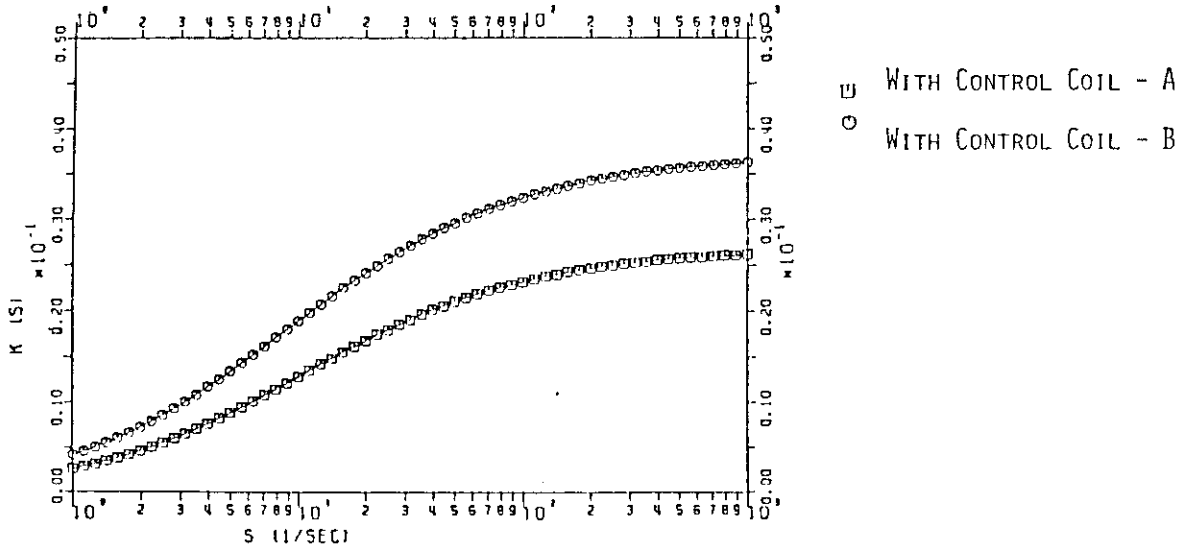

COUPLING FUNCTION OF BLANKET SHELL AND BELLJAR, REFERENCE MODEL

Figure 4.2.2.15 Coupling function of blanket shell and belljar of reference model

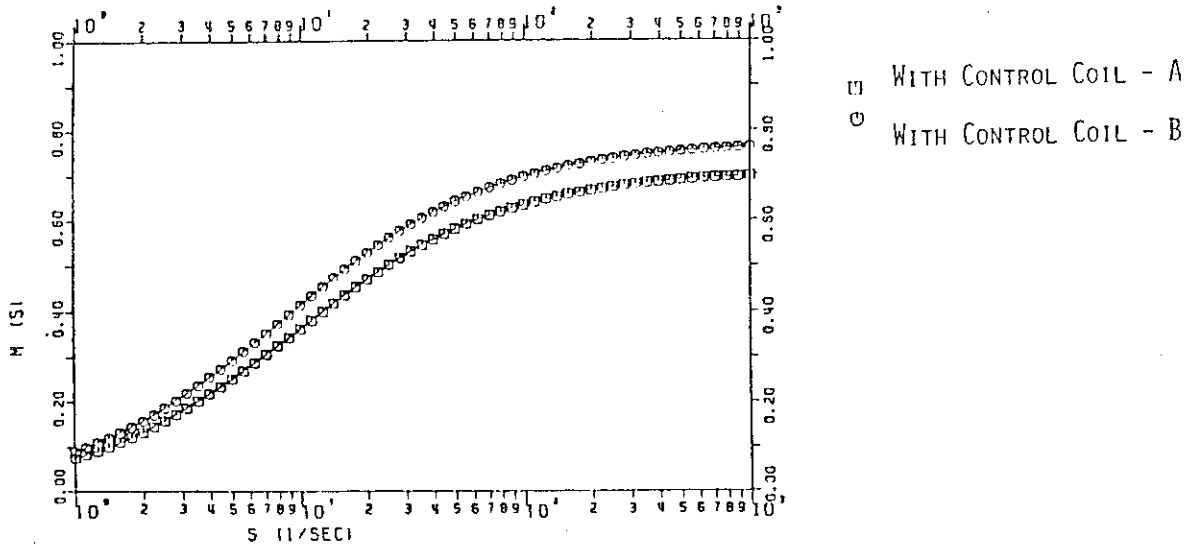

SHIELDING FUNCTION OF BLANKET SHELL AND BELLJAR, REFERENCE MODEL

Figure 4.2.2.16 Shielding function of blanket shell and belljar of reference model

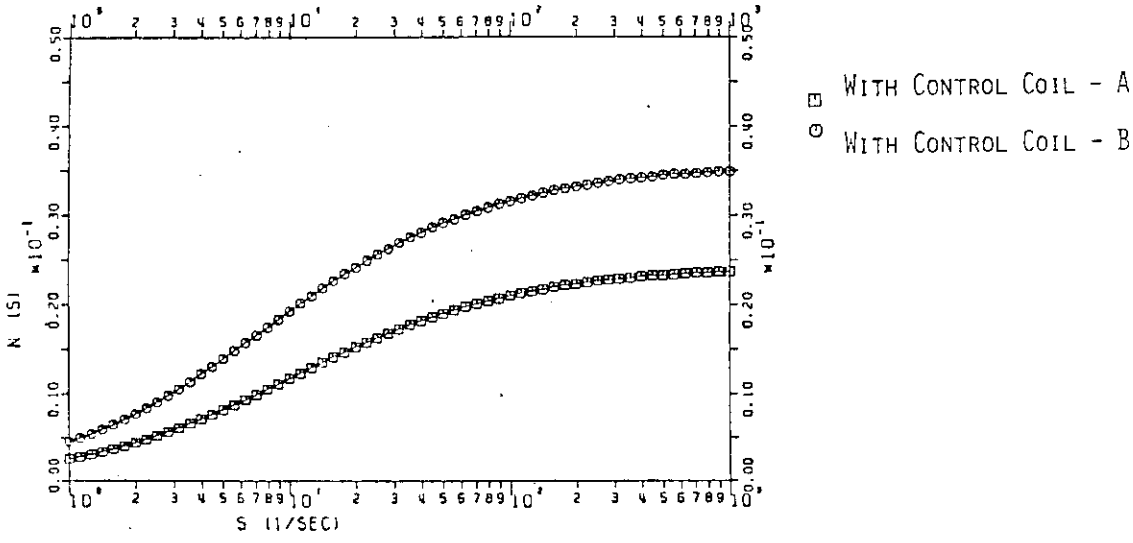

Figure 4.2.2.17 Coupling function of blanket shell and belljar of alternative model

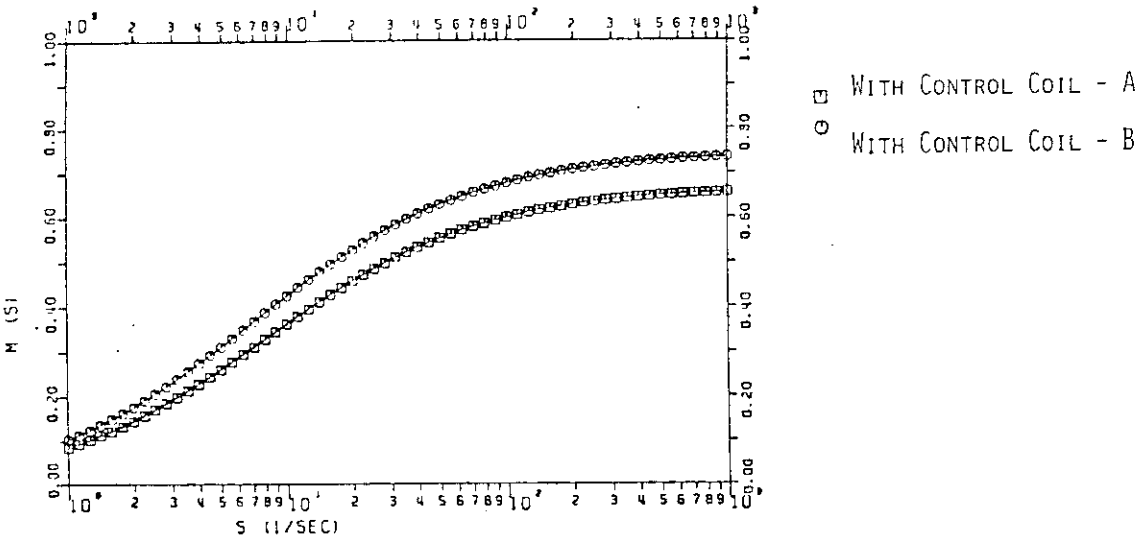

Figure 4.2.2.18 Shielding function of blanket shell and belljar of alternative model

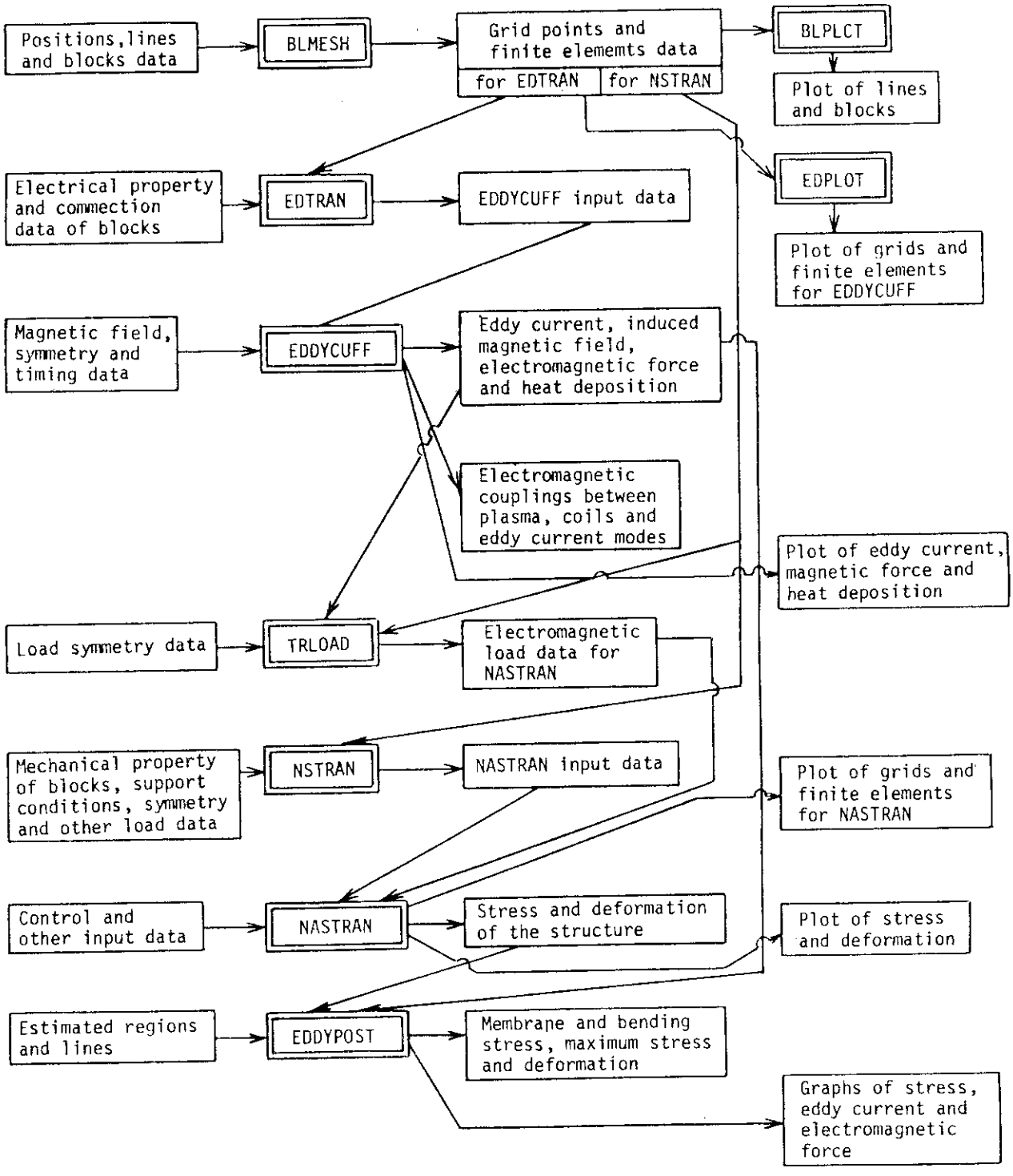

Figure 4.2.2.19 Block diagram of EDDYTRAN program system

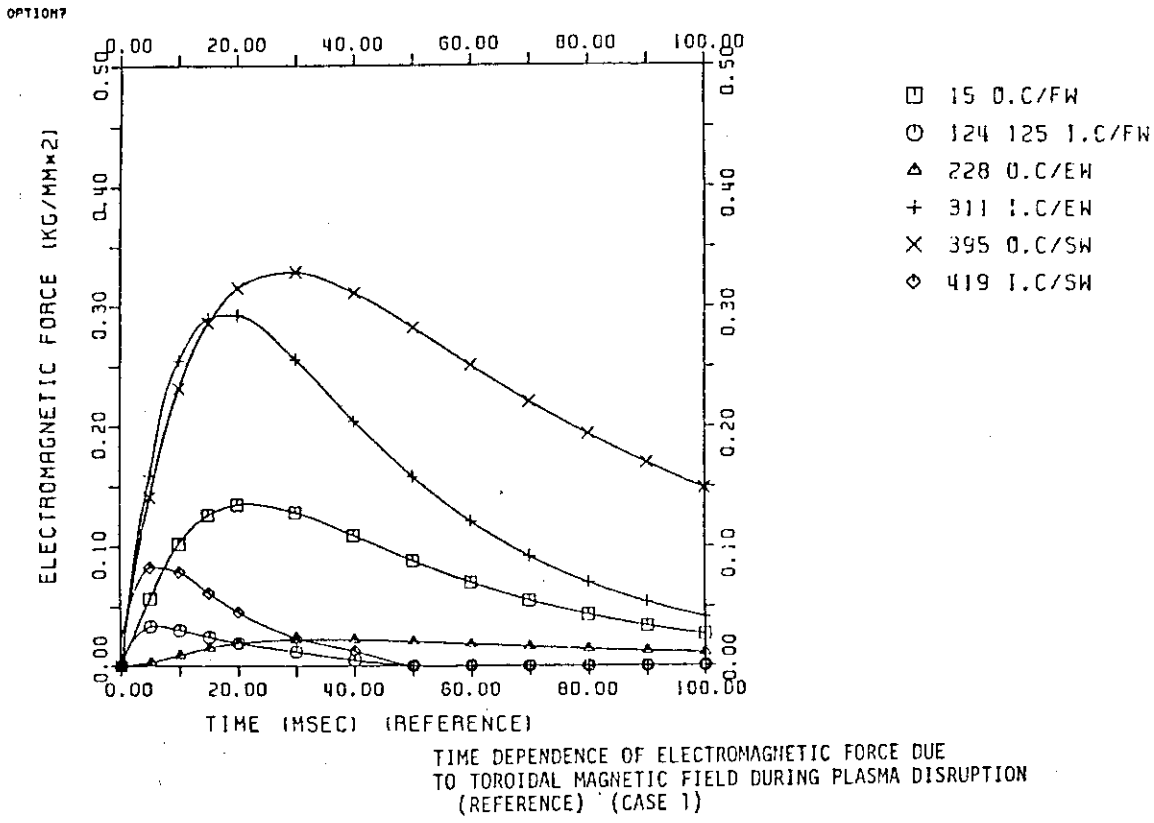

Figure 4.2.2.20 Time dependence of electromagnetic force due to toroidal magnetic field after plasma disruption for reference shell model

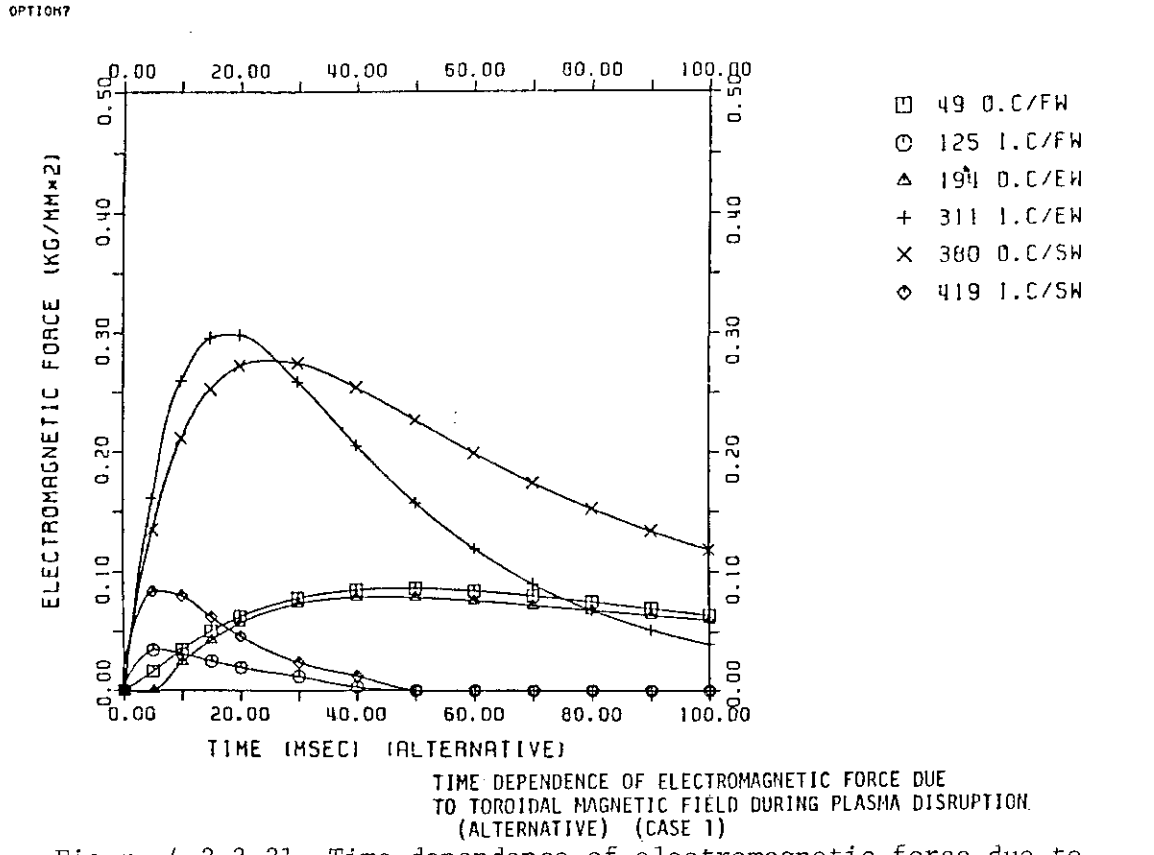

Figure 4.2.2.21 Time dependence of electromagnetic force due to toroidal magnetic field after plasma disruption for alternative shell model

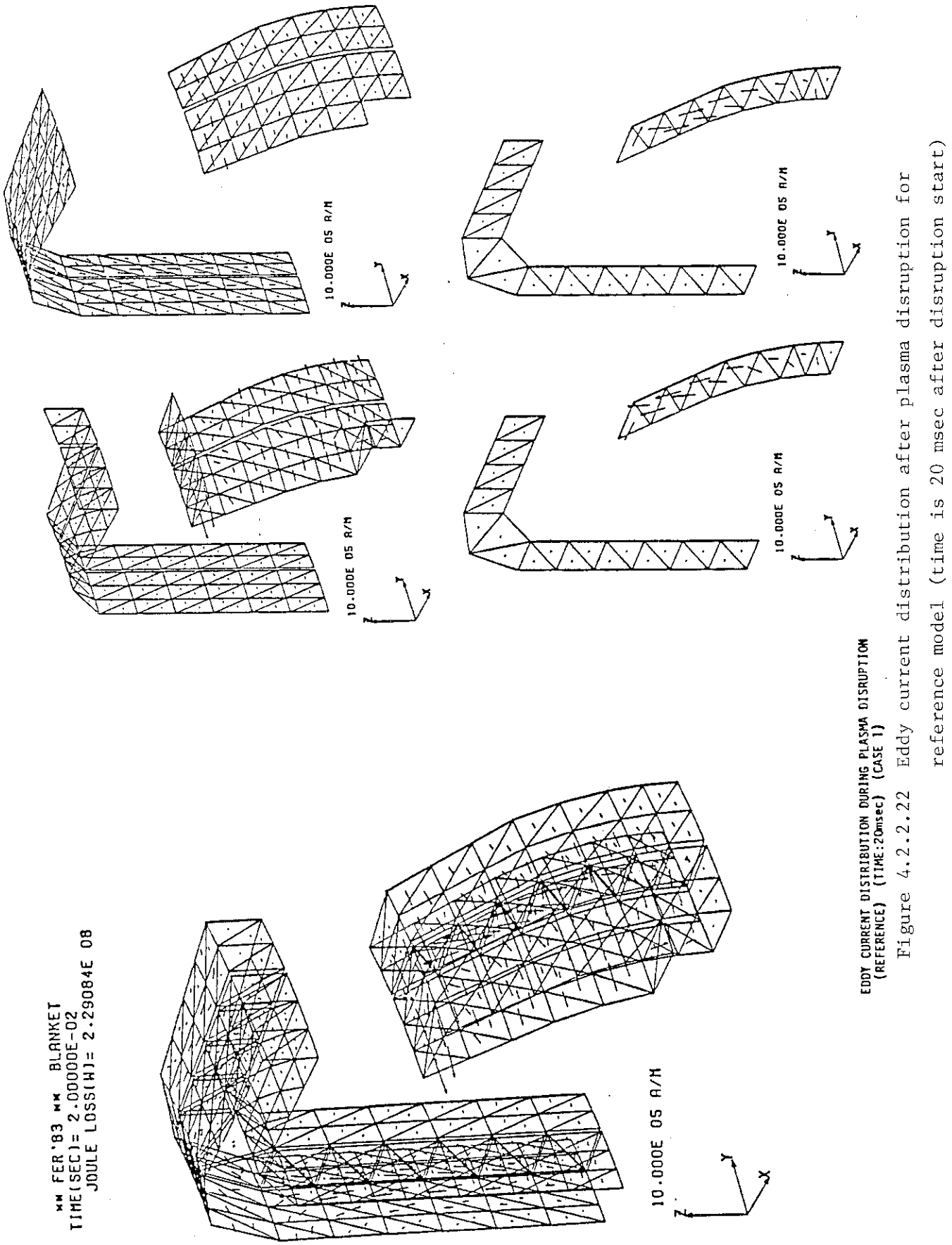

Figure 4.2.2.22 Eddy current distribution after plasma disruption for reference model (time is 20 msec after disruption start)

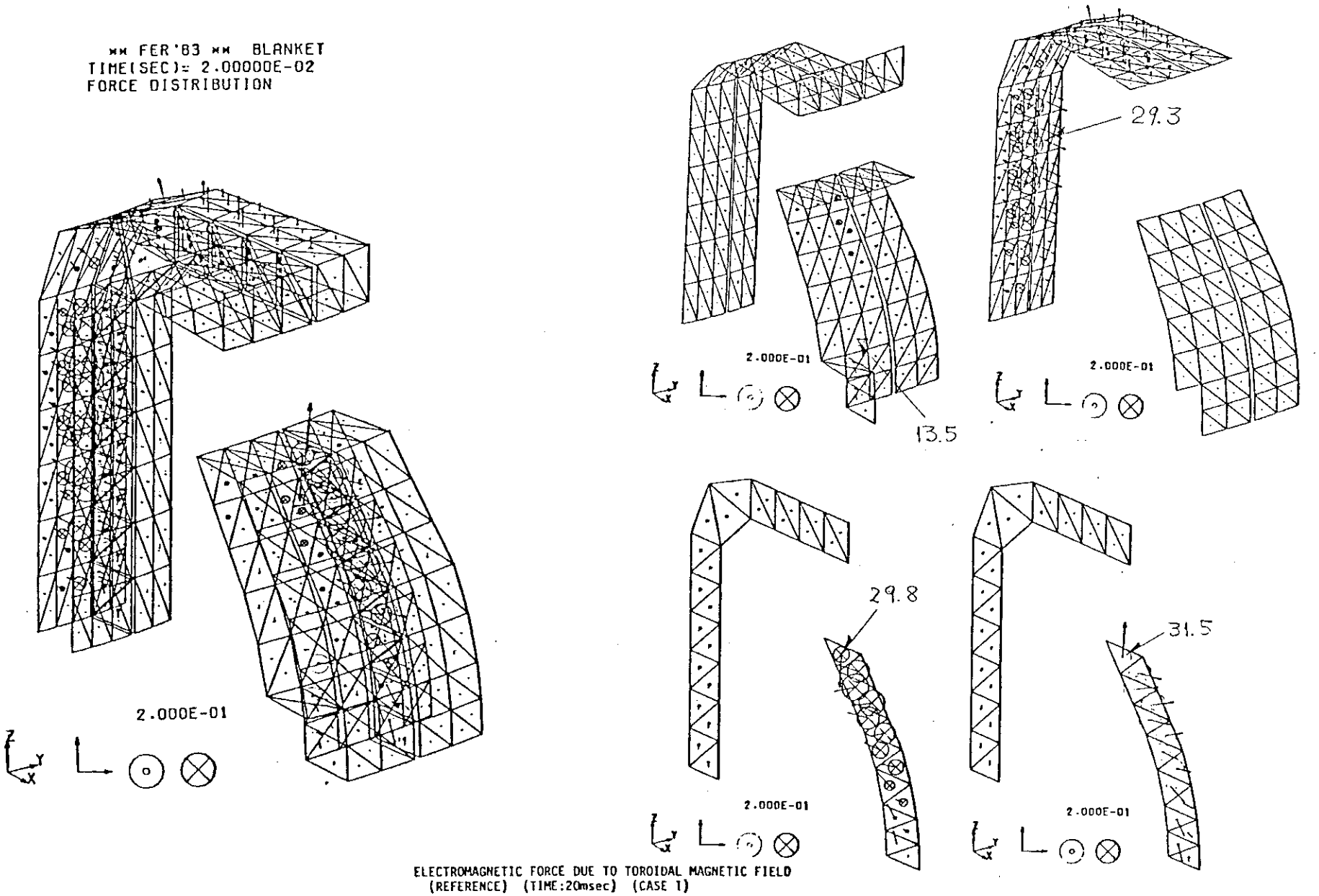

Figure 4.2.2.23 Electromagnetic force due to toroidal magnetic field after plasma disruption for reference model (time is 20 msec after disruption start)

3/ 3/84

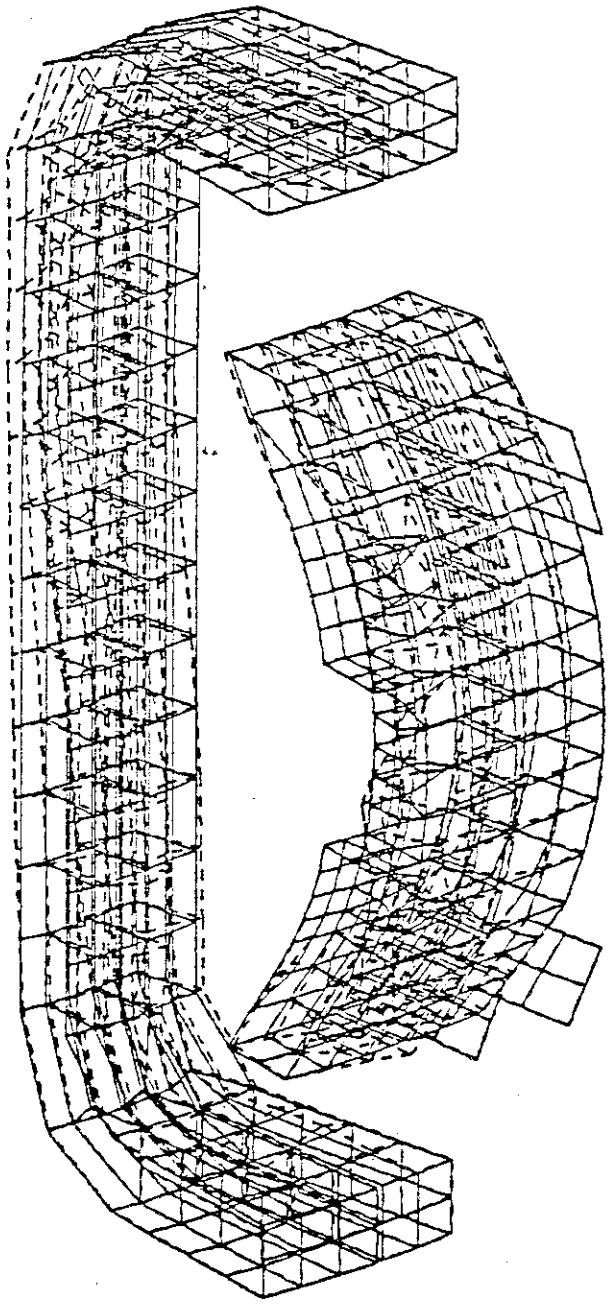

DEFORMATION OF BLANKET
ELECTROMAGNETIC FORCE (REFERENCE)

Figure 4.2.2.24 Deformation of blanket by electromagnetic force at plasma disruption (reference model)

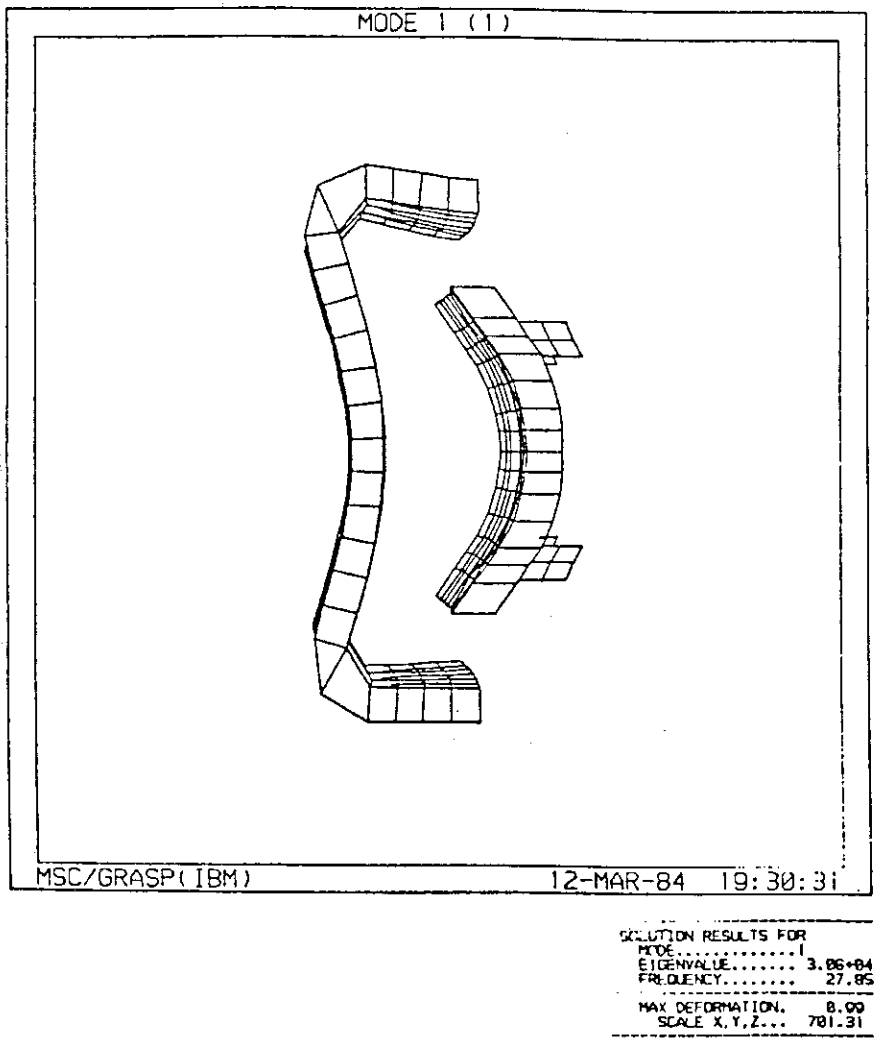

MODE 1 OF BLANKET (1)

Figure 4.2.2.25 Deformation of blanket for natural frequency analysis, mode 1

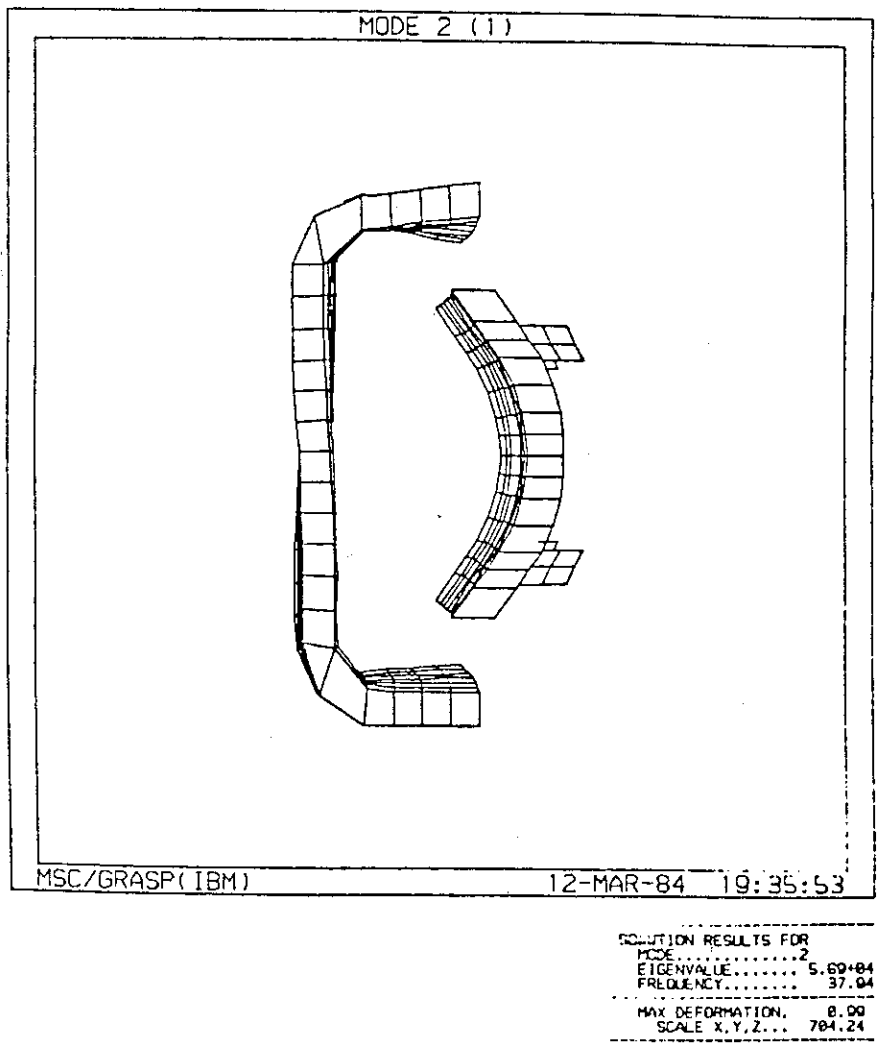

MODE 2 OF BLANKET (1)

Figure 4.2.2.26 Deformation of blanket for natural frequency analysis, mode 2

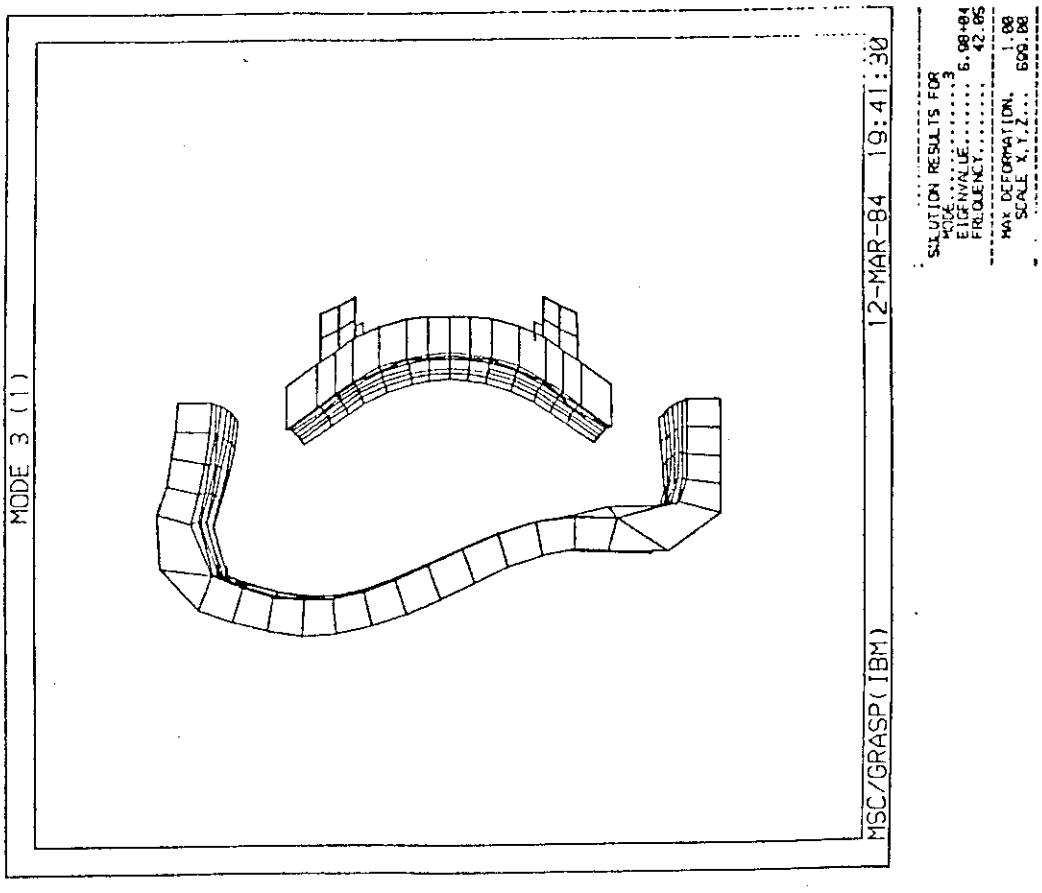

MODE 3 OF BLANKET (1)

Figure 4.2.2.27 Deformation of blanket for natural frequency analysis, mode 3

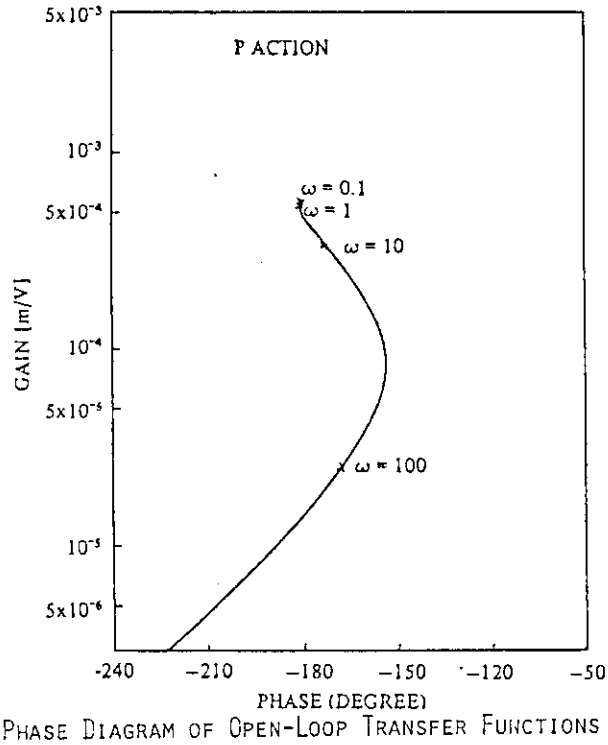

GAIN-PHASE DIAGRAM OF OPEN-LOOP TRANSFER FUNCTIONS
P-CONTROL
(REFERENCE MODEL, CONTROL COIL-B)

Figure 4.2.2.28
Gain-phase diagram of open-loop transfer functions for P-control, reference model with control coil position-B

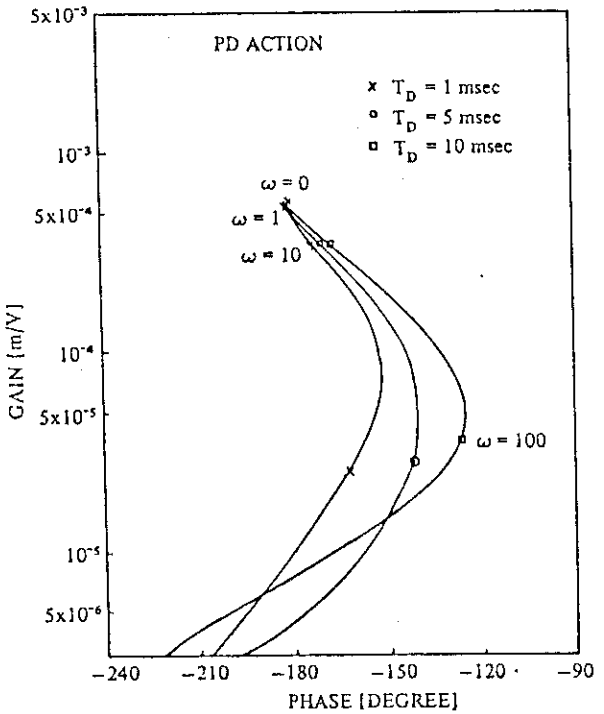

GAIN PHASE DIAGRAM OF OPEN-LOOP TRANSFER FUNCTIONS
PD-CONTROL
(REFERENCE MODEL, CONTROL COIL-B)

Figure 4.2.2.29 Gain-pahse diagram of open-loop transfer functions for PD-control, reference model with control coil position- B

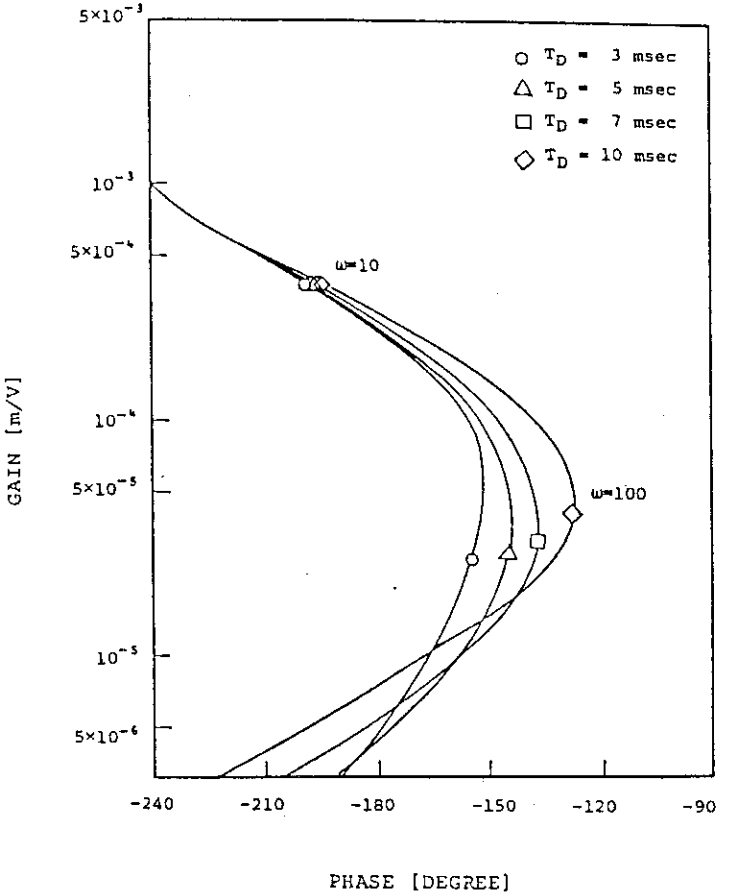

GAIN-PHASE DIAGRAM OF OPEN-LOOP TRANSFER FUNCTIONS
PID-CONTROL, T_I = 200 MSEC
(REFERENCE MODEL, CONTROL COIL-B)

Figure 4.2.2.30 Gain-phase diagram of open-loop transfer functions for PID-control, Ti = 200 msec, reference model with contol coil position-B

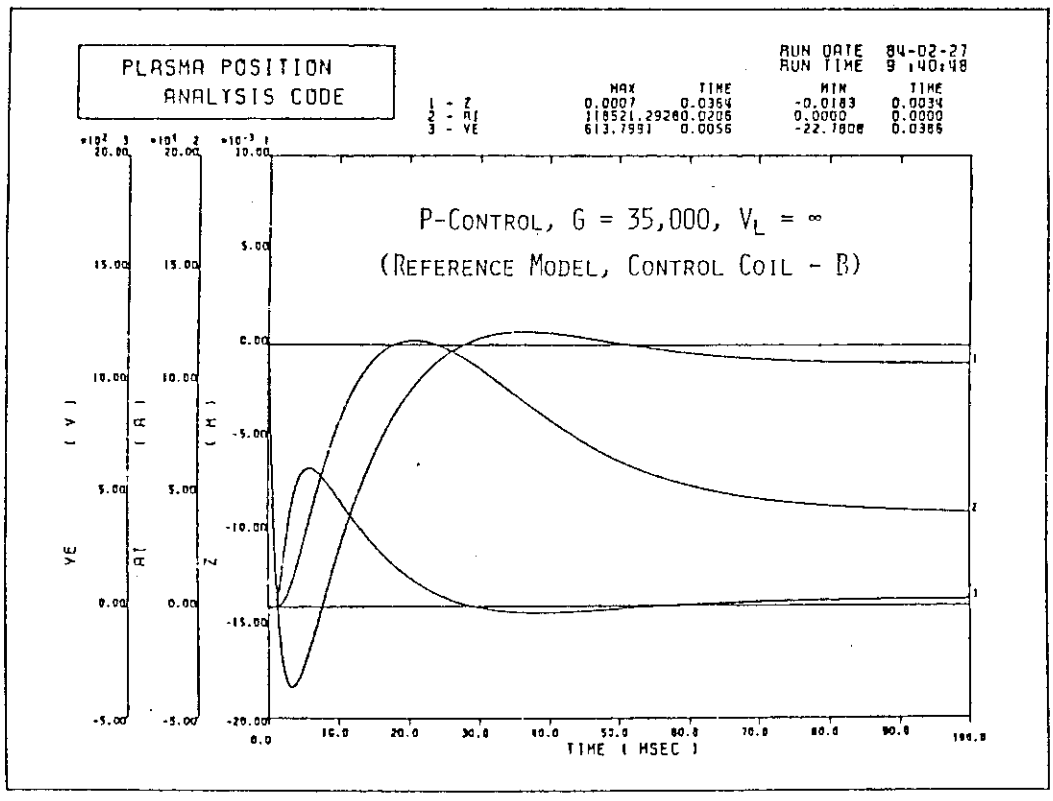

Figure 4.2.2.31 Simulation of plasma vertical stabilization, P-control, G = 35,000, = ∞, reference model with control coil position-B, required power supply capacity = 73 MVA

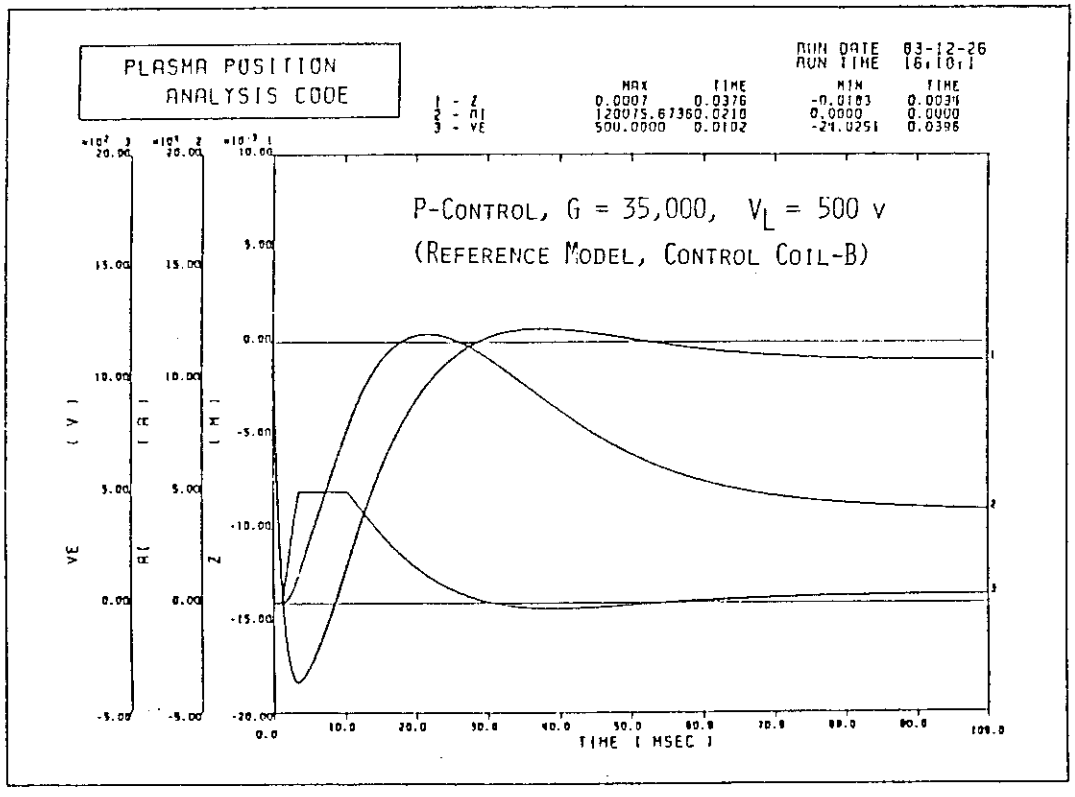

Figure 4.2.2.32 Simulation of plasma vertical stabilization, P-control, G = 35,000, = 500V, reference model with control coil position-B, required power supply capacity = 60 MVA

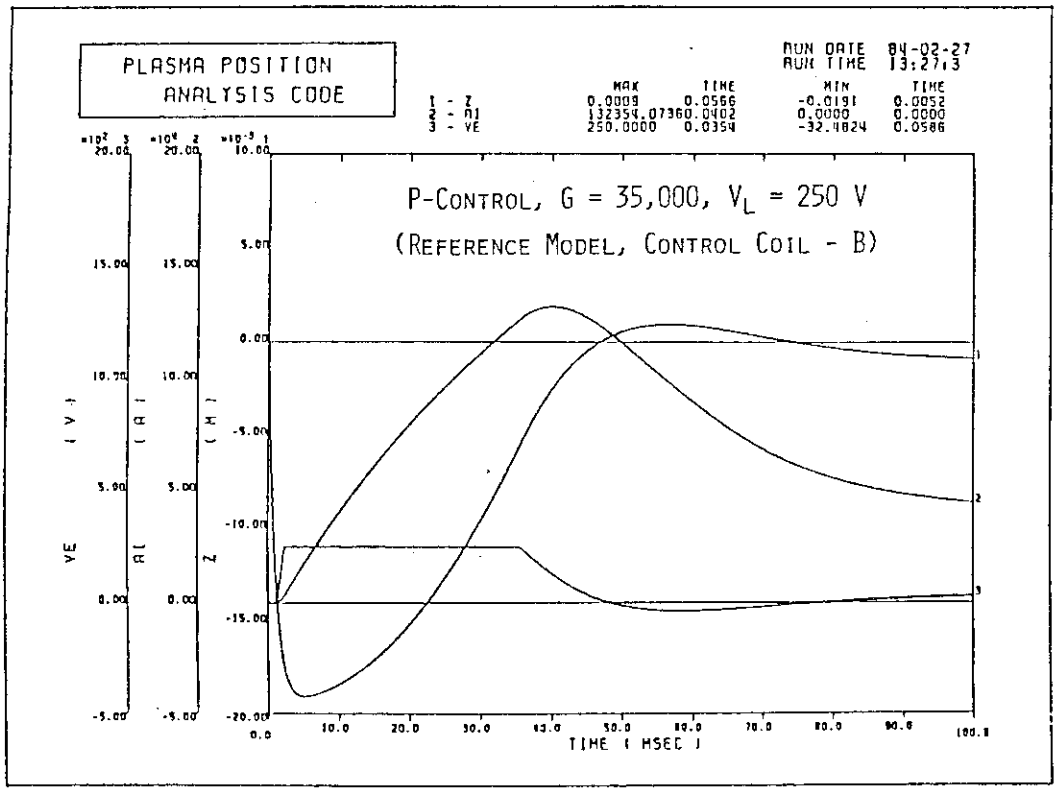

Figure 4.2.2.33 Simulation of plasma vertical stabilization, P-control, G = 35,000, V_l=250V, reference model with control coil position-B, required power supply capacity = 33 MVA

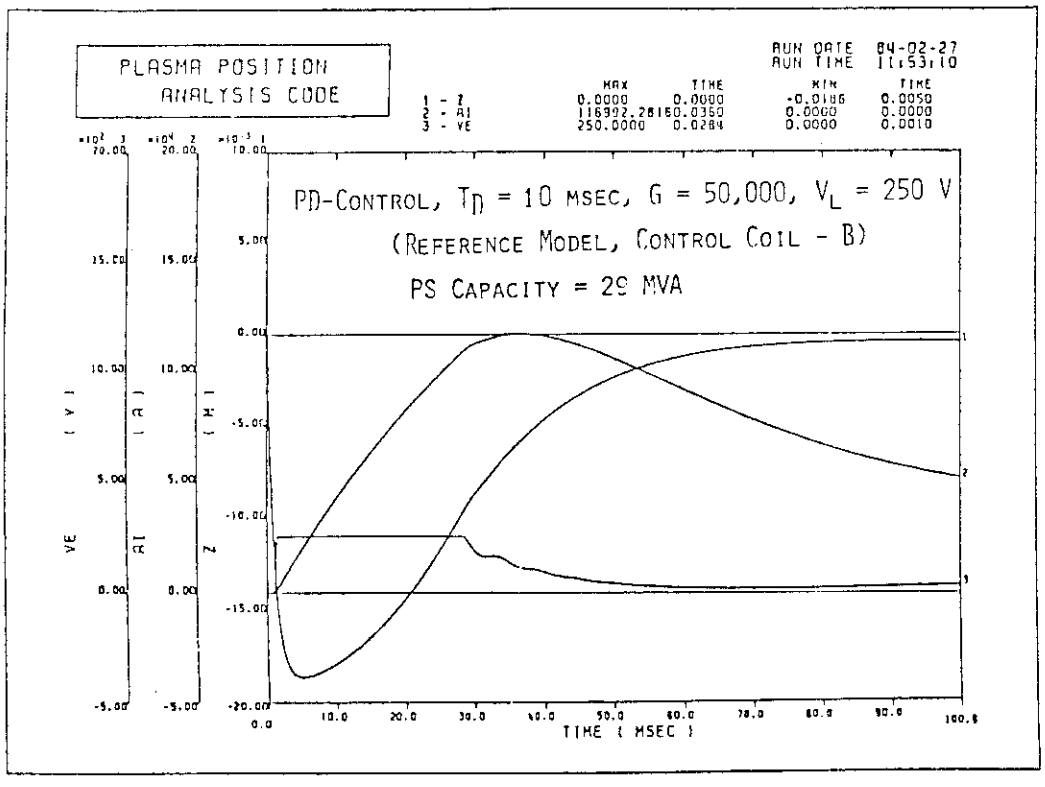

Figure 4.2.2.34 Simulation of plasma vertical stabilization, PD-control, T_d = 10 msec, G = 50,000, V_l = 250V, reference model with control coil position-B, required power supply capacity = 29 MVA

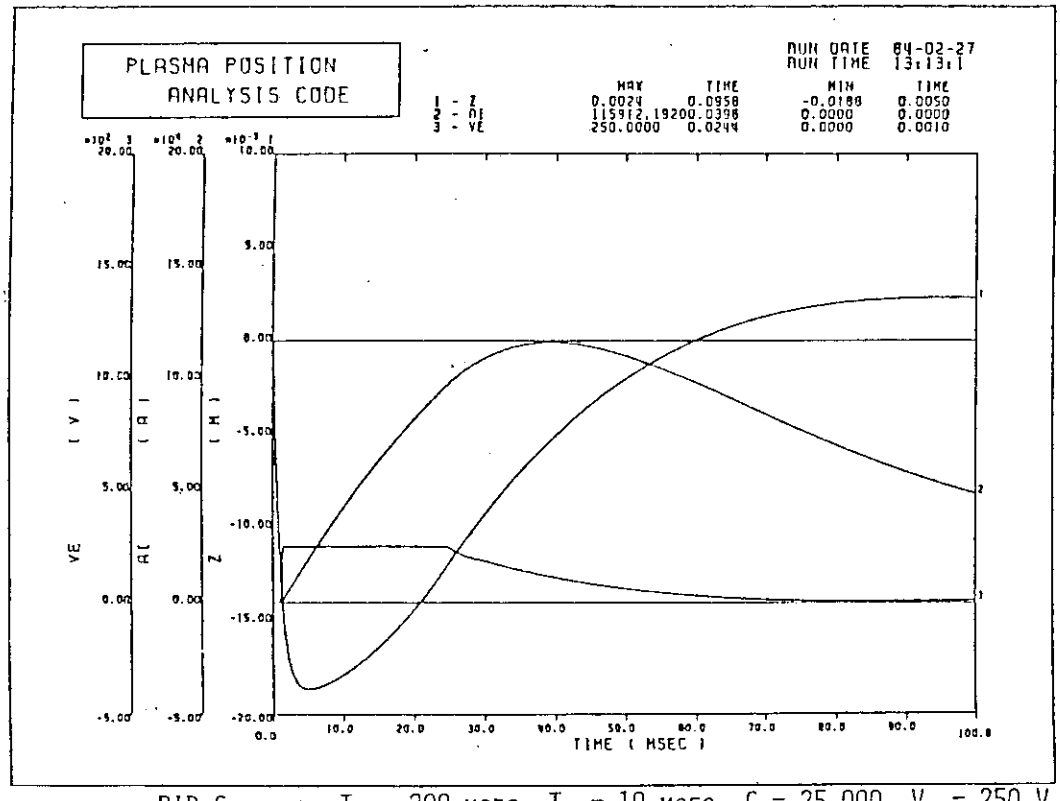

PID CONTROL, T_I = 200 MSEC, T_D = 10 MSEC, G = 25,000, V_L = 250 V
(REFERENCE MODEL, CONTROL COIL - B)

Figure 4.2.2.35 Simulation of plasma vertical stabilization, PID-control, Ti = 200 msec, T_d = 10 msec, G = 25,000, V_1 = 250V, reference model with control coil position-B, required power supply capacity = 29 MVA

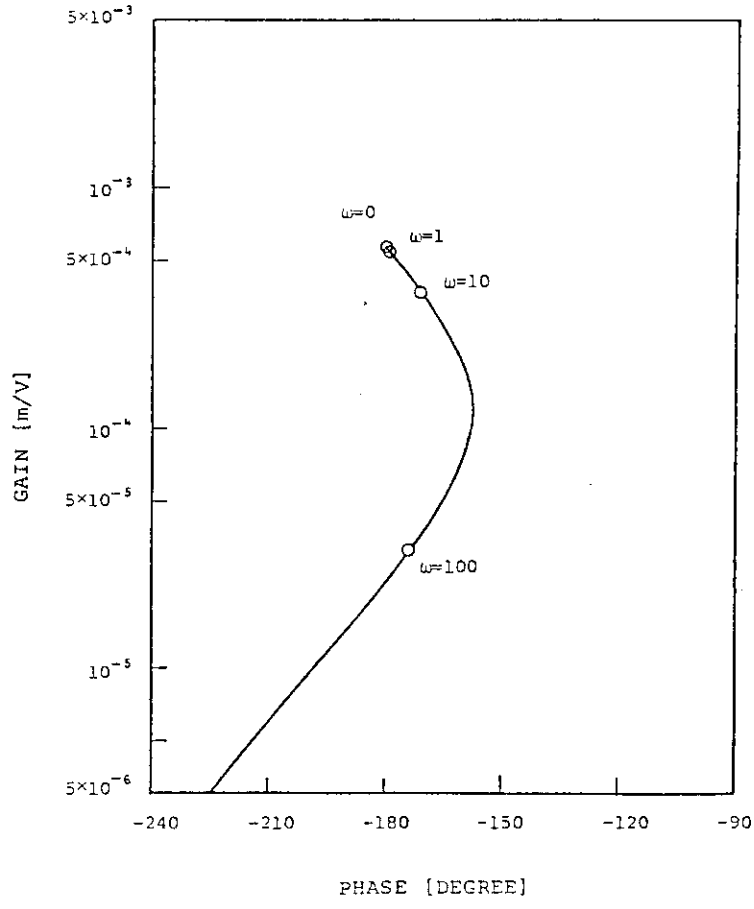

GAIN-PHASE DIAGRAM OF OPEN-LOOP TRANSFER FUNCTIONS
P-CONTROL,
(ALTERNATIVE MODEL, CONTROL COIL-B)

Figure 4.2.2.36 Gain-phase diagram of open-loop transfer functions for P-control, alternative model with control coil position-B

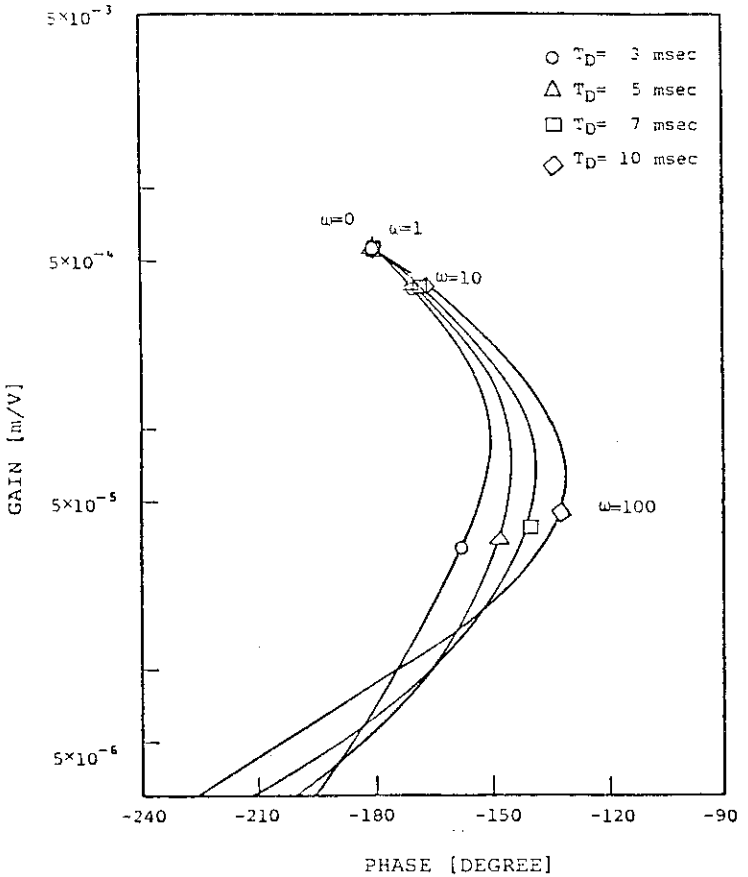

GAIN-PHASE DIAGRAM OF OPEN-LOOP TRANSFER FUNCTIONS
PD-CONTROL
(ALTERNATIVE MODEL, CONTROL COIL-B)

Figure 4.2.2.37 Gain-phase diagram of open-loop transfer functions for PD-control, alternative model with control coil position-B

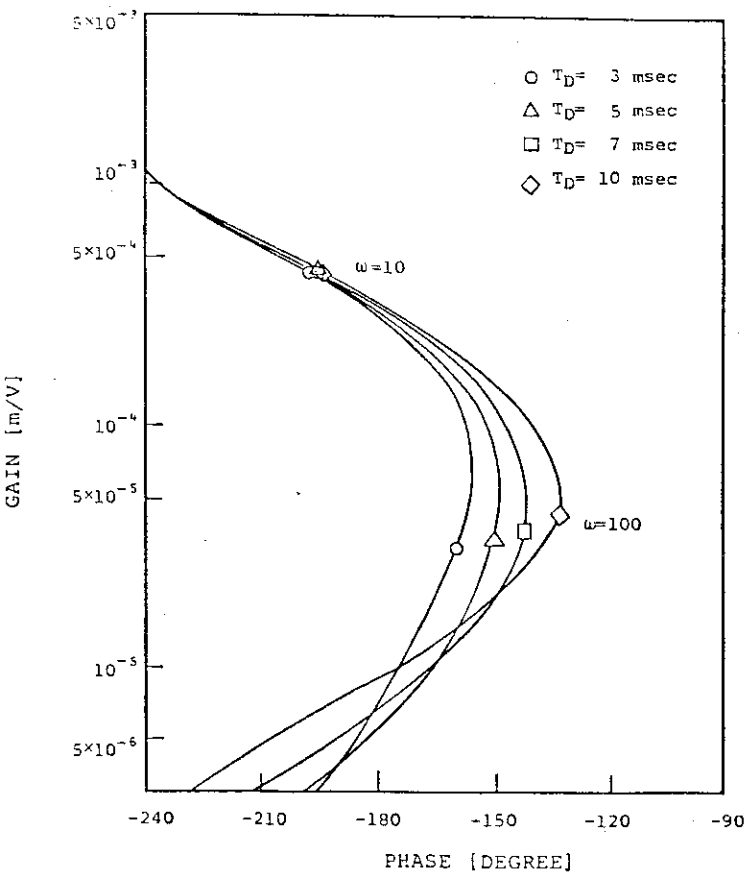

GAIN-PHASE DIAGRAM OF OPEN-LOOP TRANSFER FUNCTIONS
PID-CONTROL, T_I = 200 MSEC
(ALTERNATIVE MODEL, CONTROL COIL-B)

Figure 4.2.2.38 Gain-phase diagram of open-loop transfer functions for PID-control, Ti = 200 msec, alternative model with control coil position-B

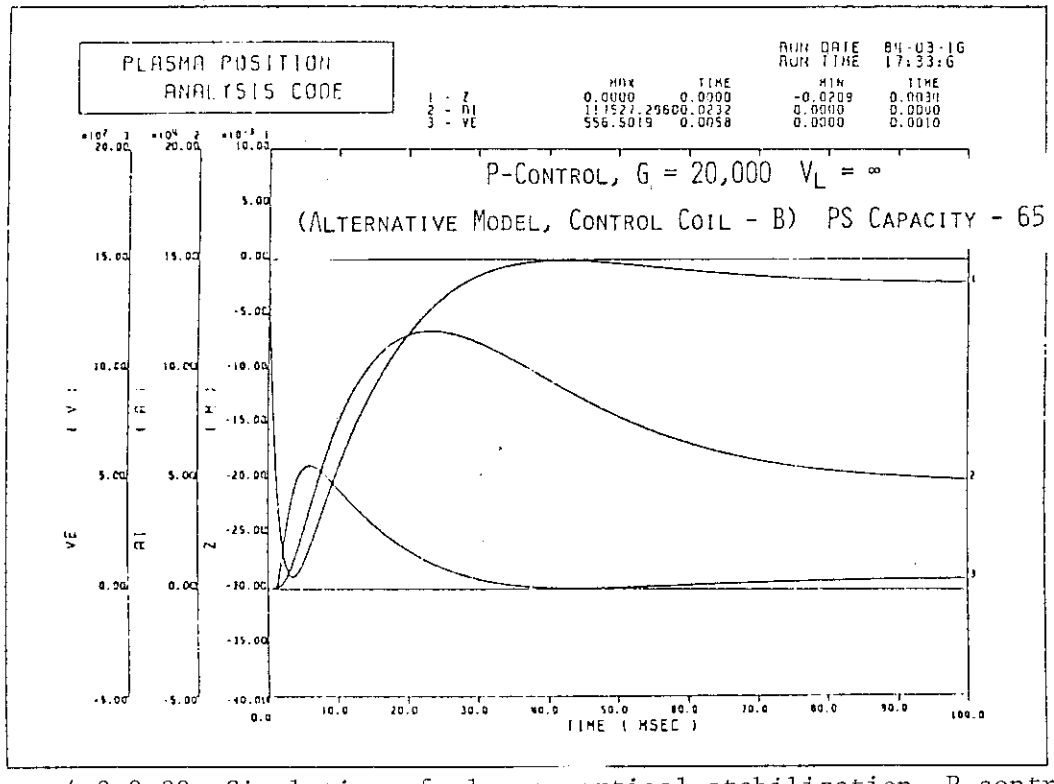

Figure 4.2.2.39 Simulation of plasma vertical stabilization, P-control, G = 20,000, V_l = ∞, alternative model with control coil position-B, required power supply capacity = 65 MVA

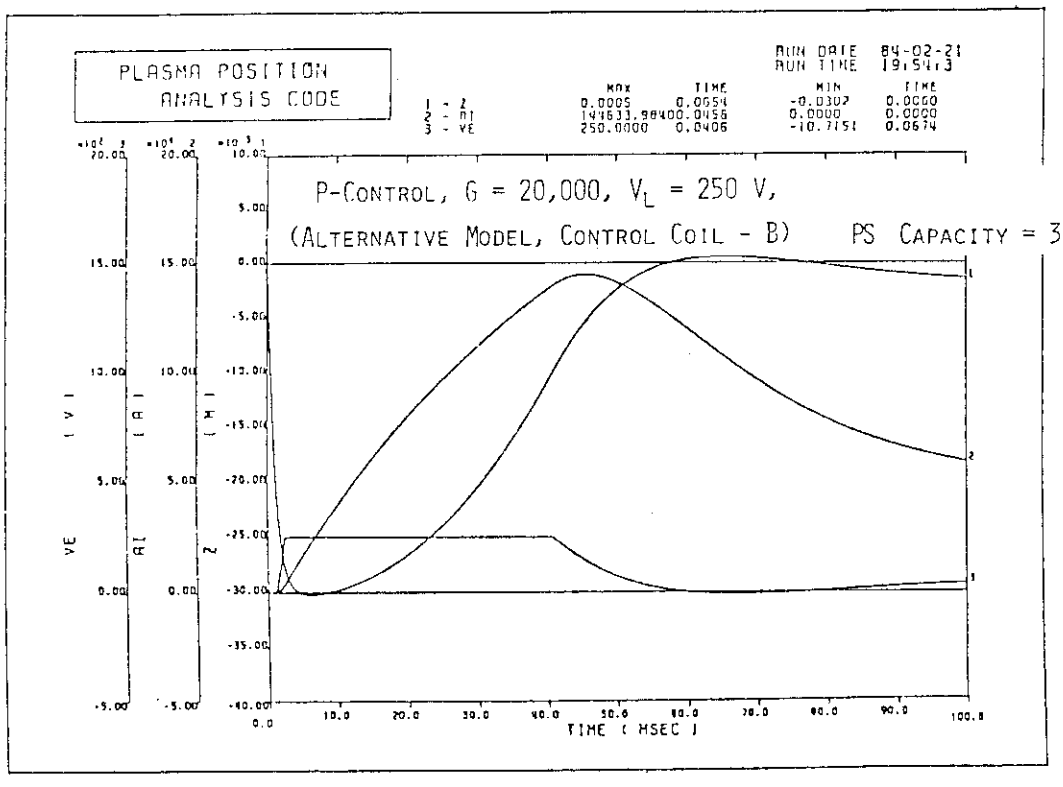

Figure 4.2.2.40 Simulation of plasma vertical stabilization, P-control, G = 20,000, V_l = 250V, alternative model with control coil position-B, required power supply capacity = 36 MVA

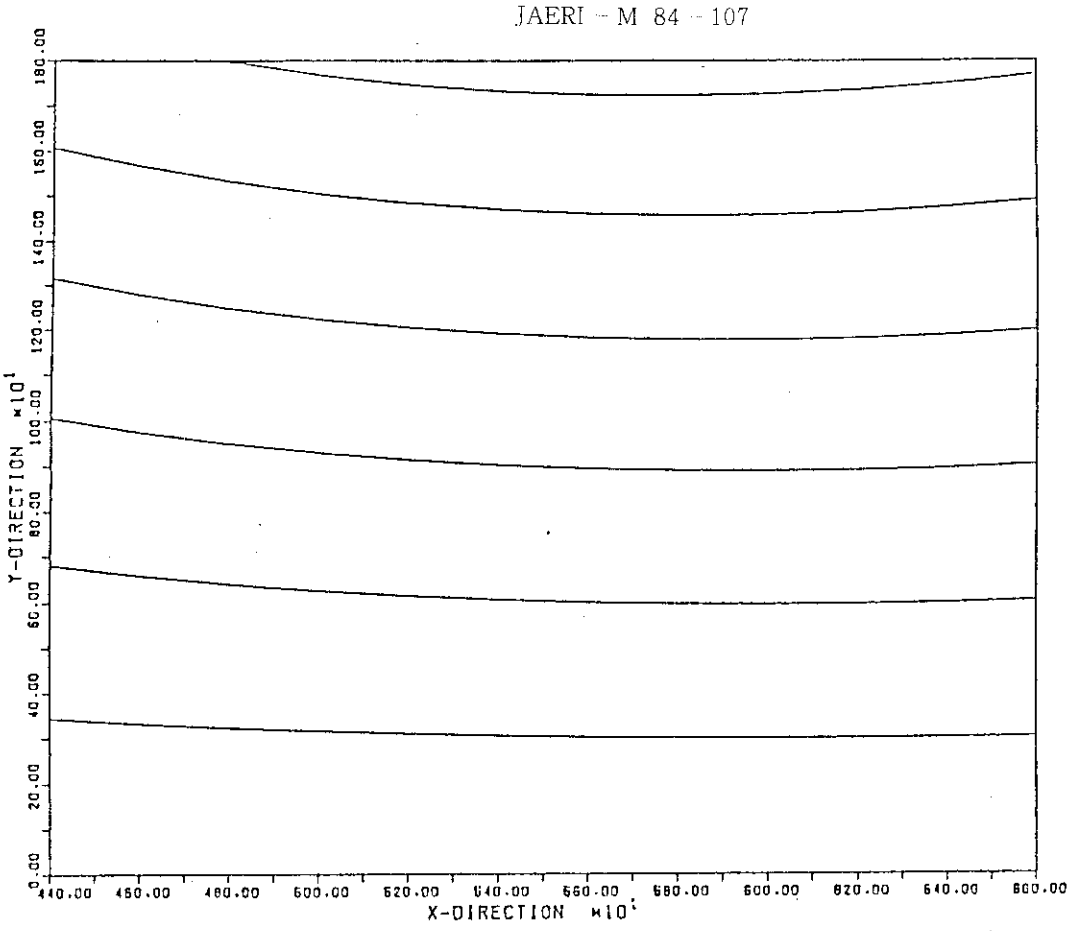

Figure 4.2.2.41 Magnetic flux configuration by control coil position-A

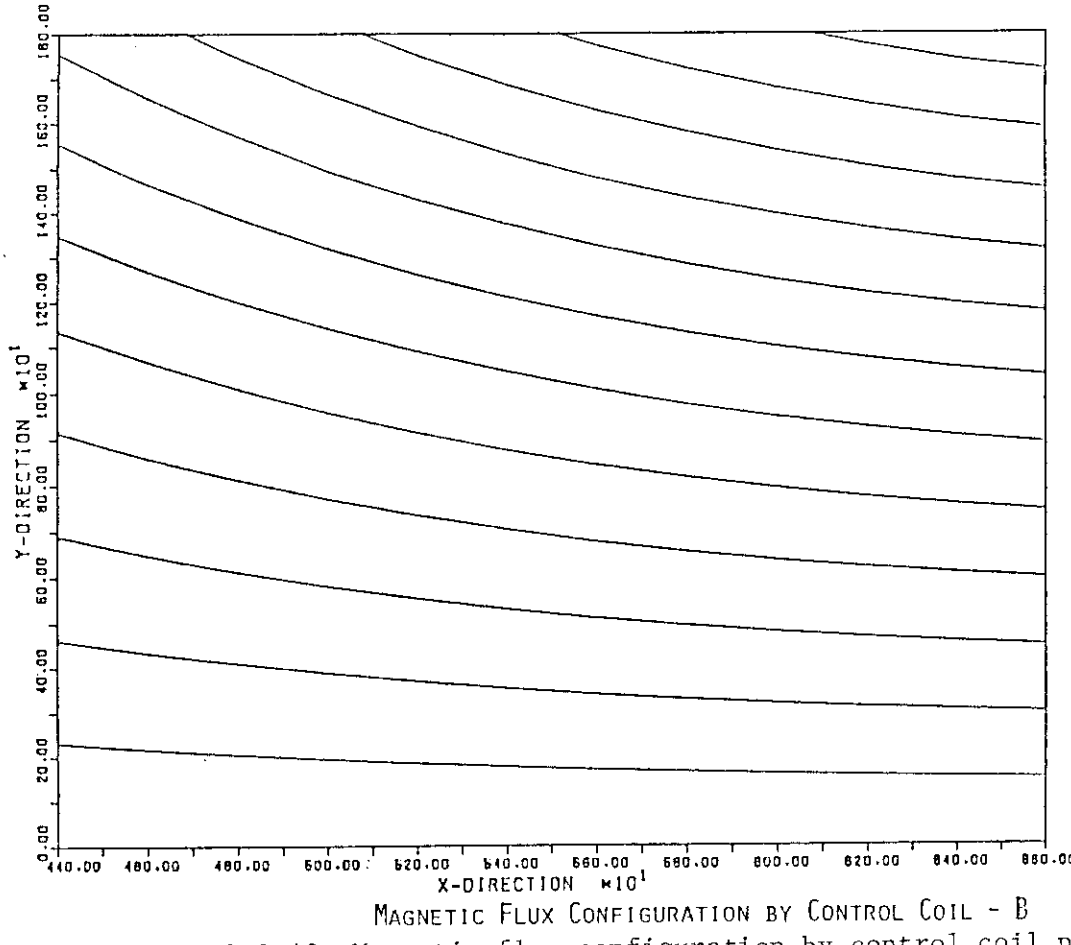

Figure 4.2.2.42 Magnetic flux configuration by control coil position-B

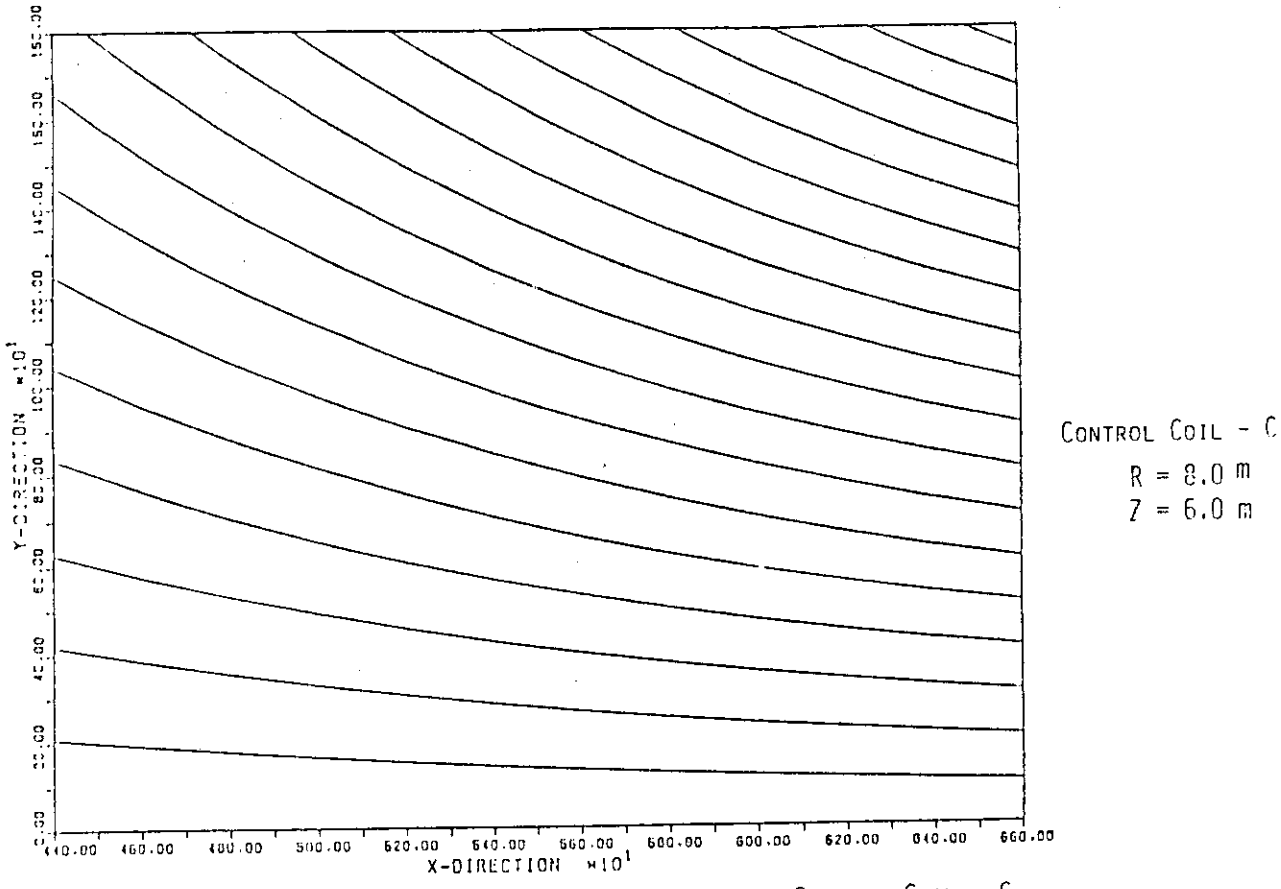

Figure 4.2.2.43 Magnetic flux configuration by control coil position-C

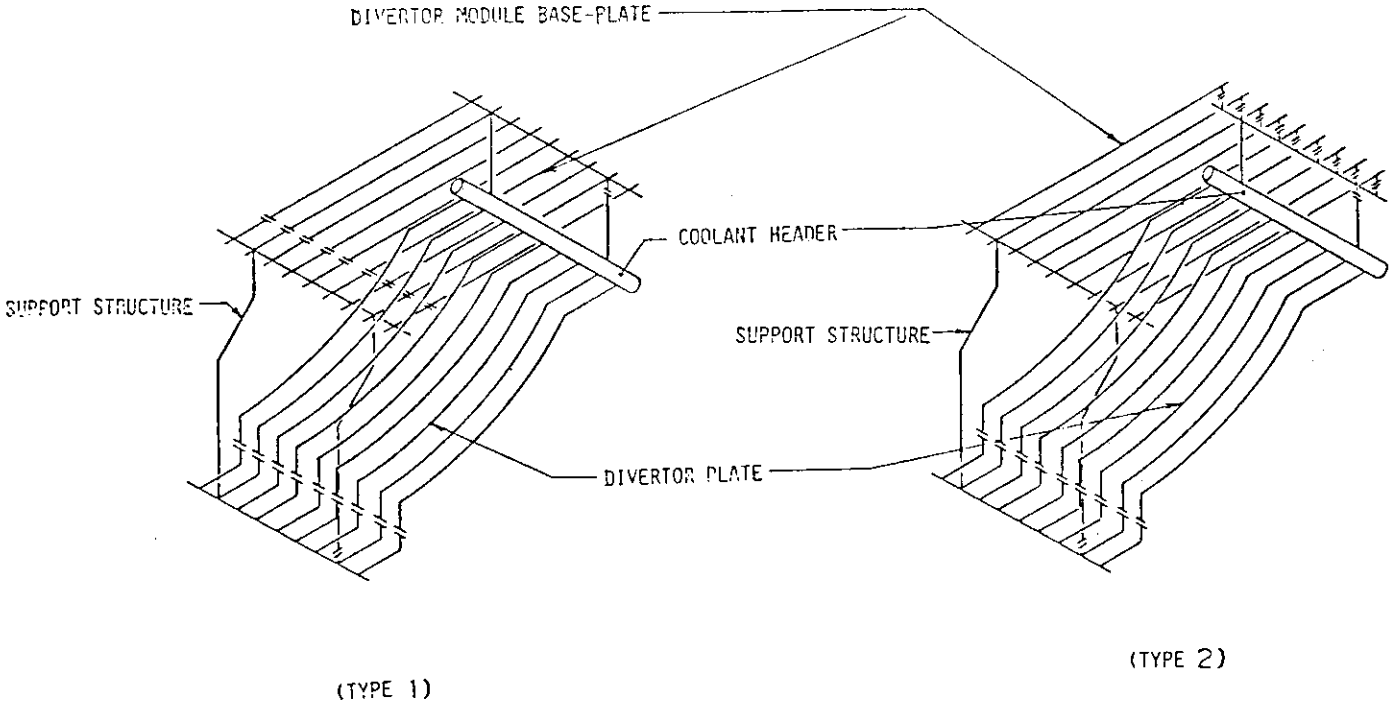

Figure 4.2.2.44 Schematic view of electromagnetic circuit configuration in a divertor module

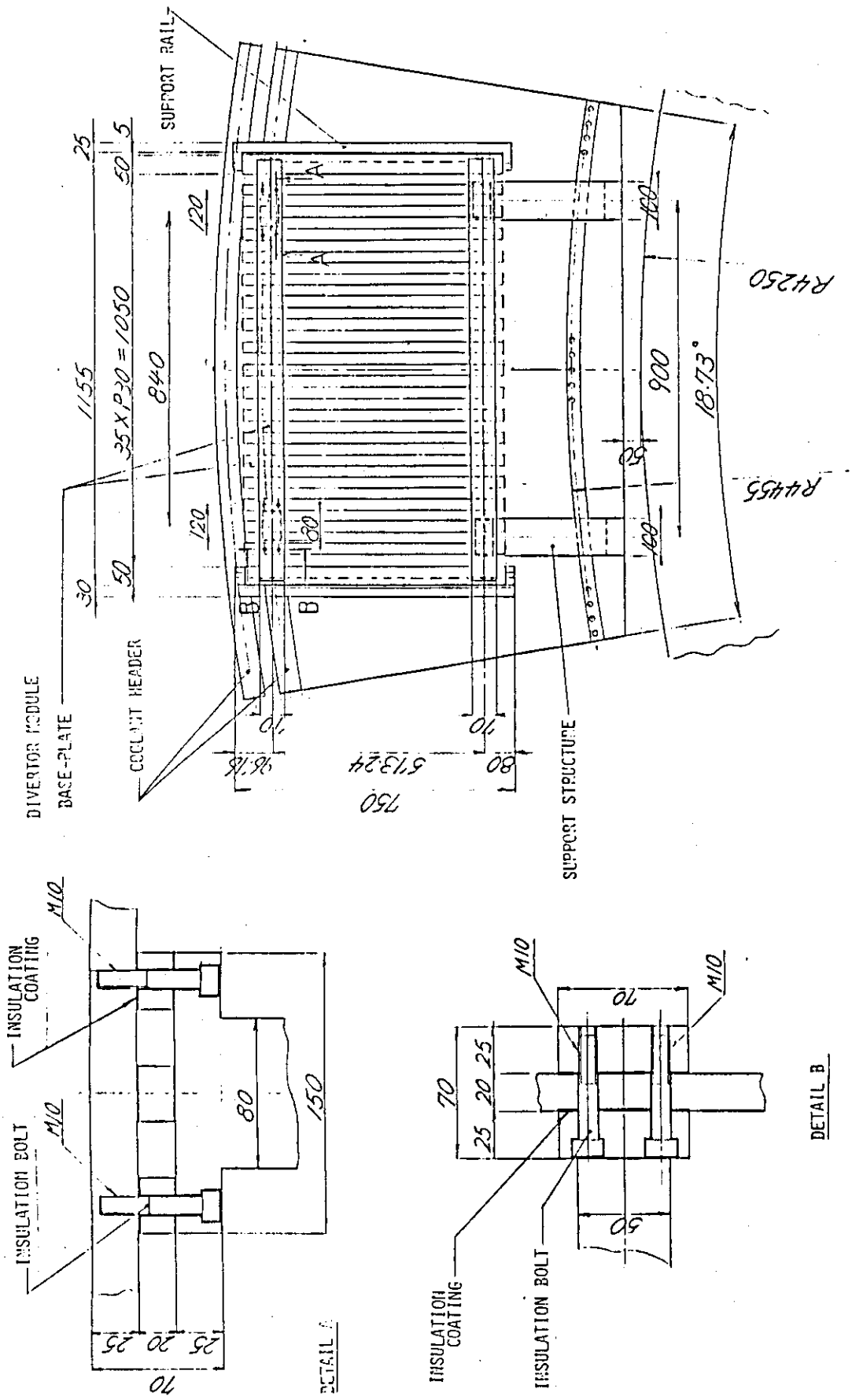

Figure 4.2.2.45 Structure of divertor module

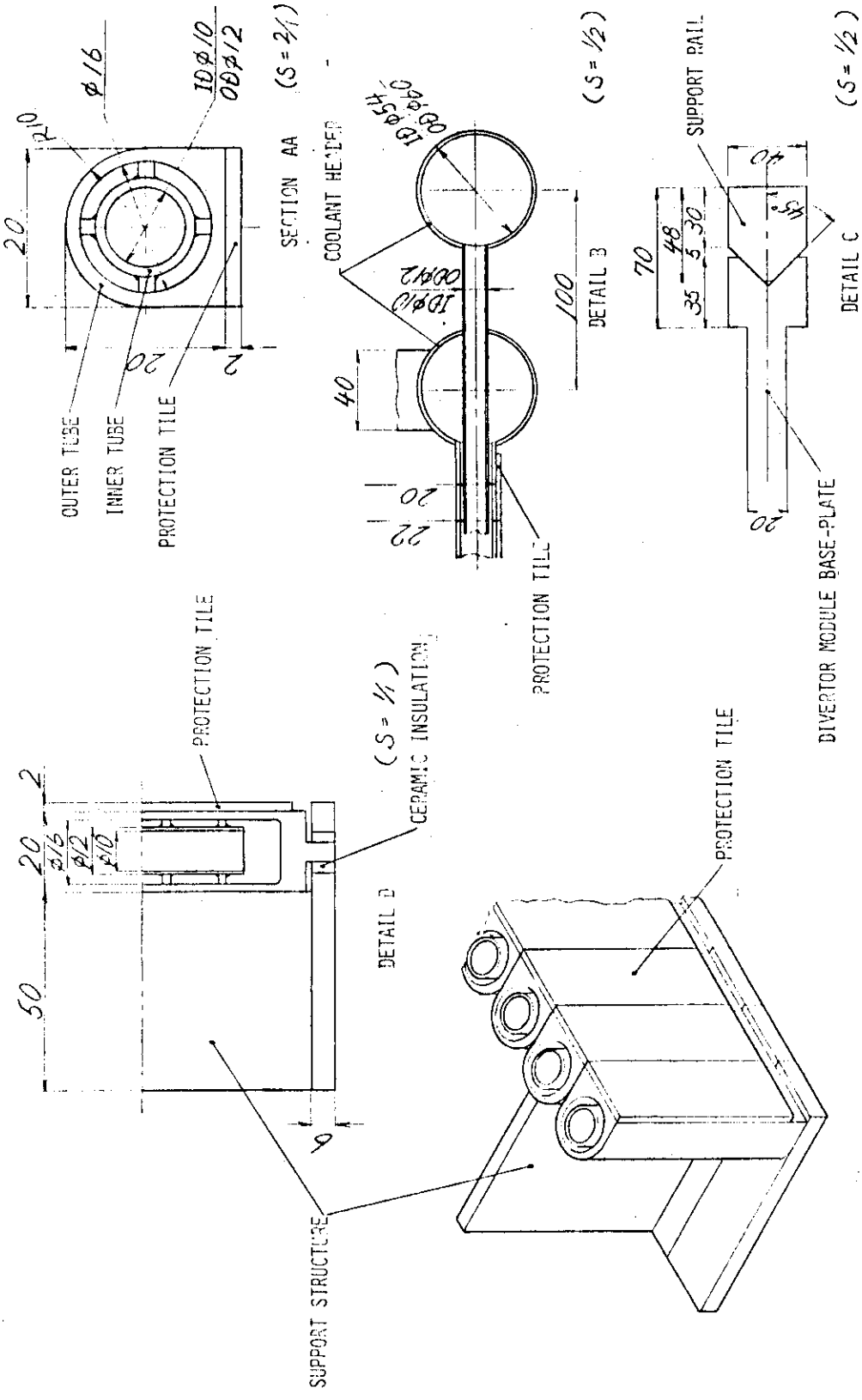

Figure 4.2.2.46 Detail of divertor plate

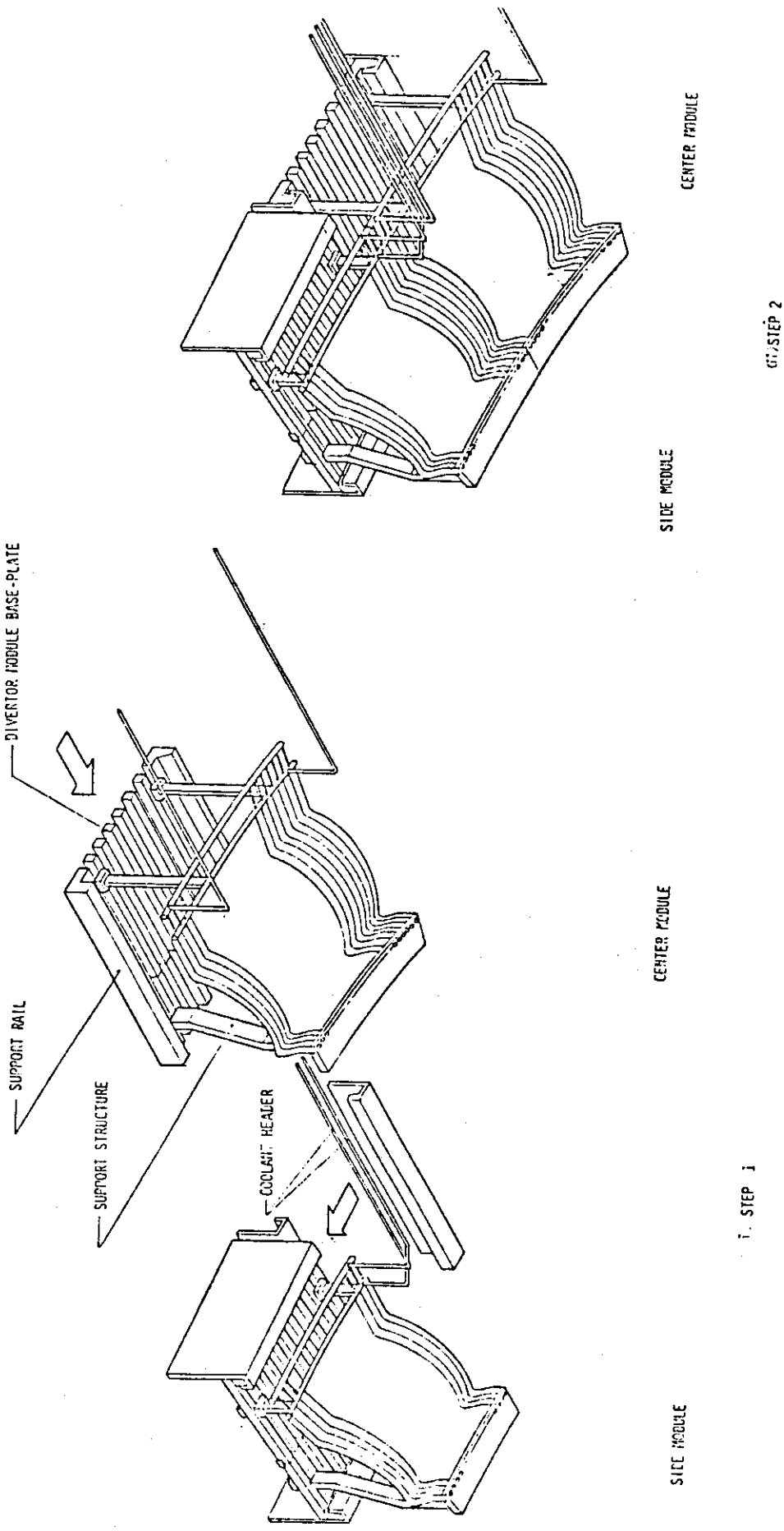

Figure 4.2.2.47 Bird's eye view of divertor and assembling process

4.2.3 A tritium breeding blanket design for FER

Mission of Fusion Experimental Reactor is integral test of technologies concerned with future fusion reactors. Blanket is one of key components in FER and its major functions are tritium production for fuel self-sustaining, removal of fusion power as thermal energy and plasma vertical stabilization. Design of FER blanket has to consistently fulfill the following requirements.

i) Adequate tritium breeding ratio
ii) In-situ continuous tritium recovery
iii) Heat removal
iv) Passive shell effect
v) Structural integrity for cyclic heat loads, internal pressure, electromagnetic forces and intense heat loads during plasma disruption etc.
vi) Maintainability by remote handling
vii) Shielding performance
viii) Safety
ix) Adequate lifetime
x) Simple structure for fabrication
xi) Structure to accommodate to the uncertainties

Key features of presently designed FER blanket are Li_2O breeder in pebble form and beryllium as both neutron multiplier and passive shell conductor Li_2O has relatively good tritium breeding performance and small spherical pebble of breeder gives a solution for serious problems of thermal cracking, mass transfer due to moisture in helium purge gas and decreasing of tritium inventory.

Blanket modulization has been studied on the basis of remote maintenance technique in straight motion. Blankets are removed with outer shield which supports them. (Figs. 4.2.3.1 ∿ 4.2.3.5)

First wall is integrated to the blanket wall from the viewpoint of obtaining relatively high tritium breeding performance and avoiding the complexity of its own support system. The first wall is a bare ribbed-panel type that is fabricated by HIP process. The minimum thickness of the first wall is decided for 1.5 MW-y/m^2 of lifetime considering thermal stress and erosions by physical sputtering and plasma disruption.

(Table 4.2.3.1, Fig. 4.2.3.6, Figs. 4.2.3.10 ∿ 4.2.3.11)

The type of the blanket is tube-in-shell, sometimes called as BOT/NM type. Beryllium neutron multiplier is adopted in this design. And this beryllium acts as passive shell conductor in the outer blanket region. Pressurized light water, H_2O, is selected as the coolants of both of the breeder region and the first wall. Its inlet and outlet temperatures are 60°C and 100°C, respectively. The outlet temperature is low because of no electricity generation. Type 316 stainless steel is selected as the structural material because it provides adequate radiation damage resistance and allowable design stress intensities under the anticipated operating conditions. (Table 4.2.3.2, Figs. 4.2.3.7 ∿ 4.2.3.9)

Net tritium breeding ratio greater than unity (1.05) is obtained by adoption of Li_2O breeder and beryllium neutron multiplier. (Figs. 4.2.3.12 ∿ 4.2.3.14)

Tritium produced in the blanket is continuously carried out and recovered by helium purge gas. Temperature of Li_2O breeder is controlled between 400°C and 1000°C to decrease tritium inventory, promote decomposition of LiOT and reduce mass transfer rate of Li_2O. (Figs. 4.2.3.15 ∿ 4.2.3.18)

Stress analyses show that the integrity of blanket structures is maintained to electromagnetic force during plasma disruption, thermal load during plasma operation and inner pressure of helium purge gas. (Fig. 4.2.3.19)

Performance for plasma vertical stabilization is fulfilled by use of beryllium shell conductor that serves as well neutron multiplier without vicious effects on tritium breeding performance. (Table 4.2.3.3, Figs. 4.2.3.20 ∿ 4.2.3.21)

Fabricability for subassembly process adopted in this design has also been studied (Figs. 4.2.3.22 ∿ 4.2.3.25) and technology issues for future design are identified.

Mission of Fusion Experimental Reactor:

Integral tests of technologies concerned with future fusion reactors

Major Functions of FER Blanket
(Key Component for Fusion Energy Recovery)

- o Tritium production for fuel self-sustaining
  (In-situ continuous tritium recovery)
- o Heat removal from fusion energy
  (Non electricity generation)
- o Passive shell effect for vertical plasma stabilization

Requirements for FER Blanket Design

- o Tritium Breeding $TBR_{net} > 1.0$
- o In-situ continuous tritium recovery
  Low tritium inventory
- o Heat removal
  Low temperature structure
  Temperature control of Li_2O breeder
- o Passive shell effect
- o Structural integrity for cyclic heat loads, internal pressure, electromagnetic forces and intense heat loads during plasma disruptions, etc.
- o Maintainability by remote handling
- o Shielding performance
- o Safety
- o Adequate lifetime
- o Simple structure (Fabricability)
- o Structure to accommodate to the uncertainties

Reactor Concept

Combined vacuum boundary	
Number of sectors	14
Number of blanket units	56 (4units/sector)
Number of modules	42 3 modules/sector 1 center module:2 blanket units 2 side modules :1 blanket units
Module removal	Straight motion
Module support	by shield structure

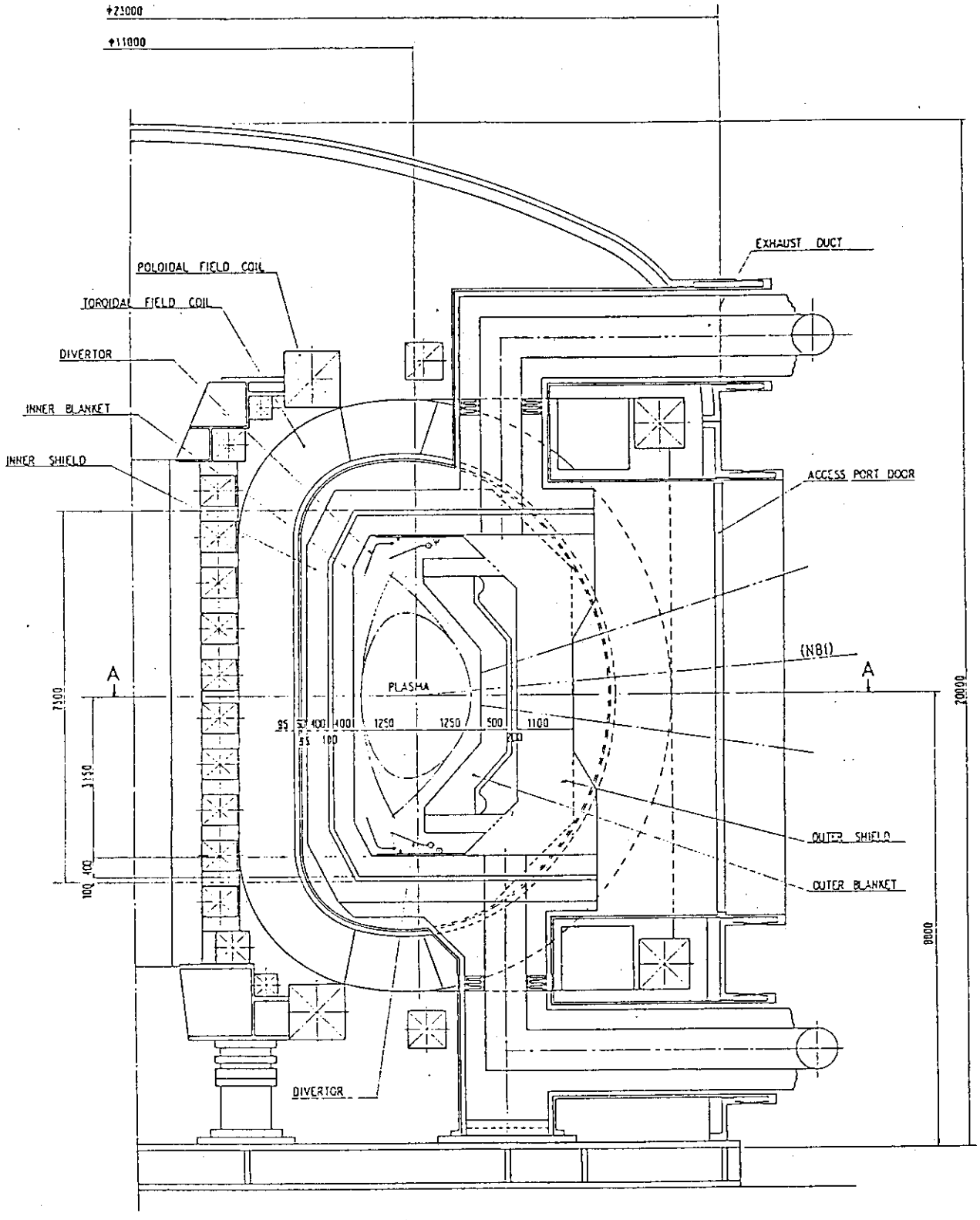

Fig. 4.2.3.1 Elevation view of reactor configuration (Option D)

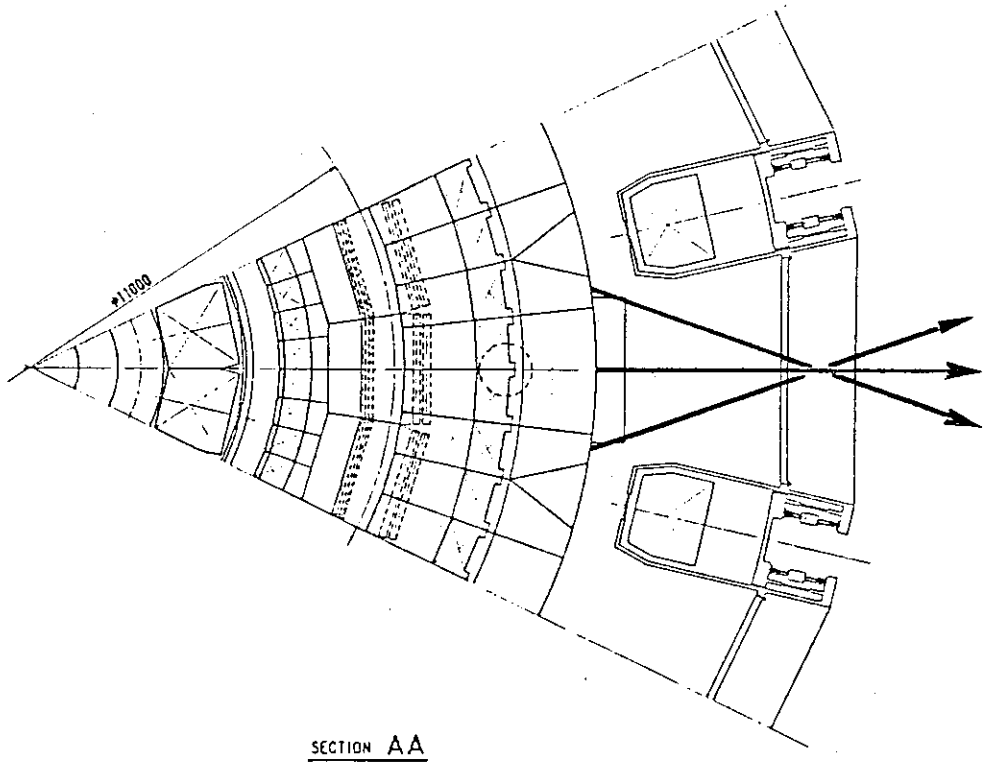

Fig. 4.2.3.2 Plan view of reactor configuration (Option D)

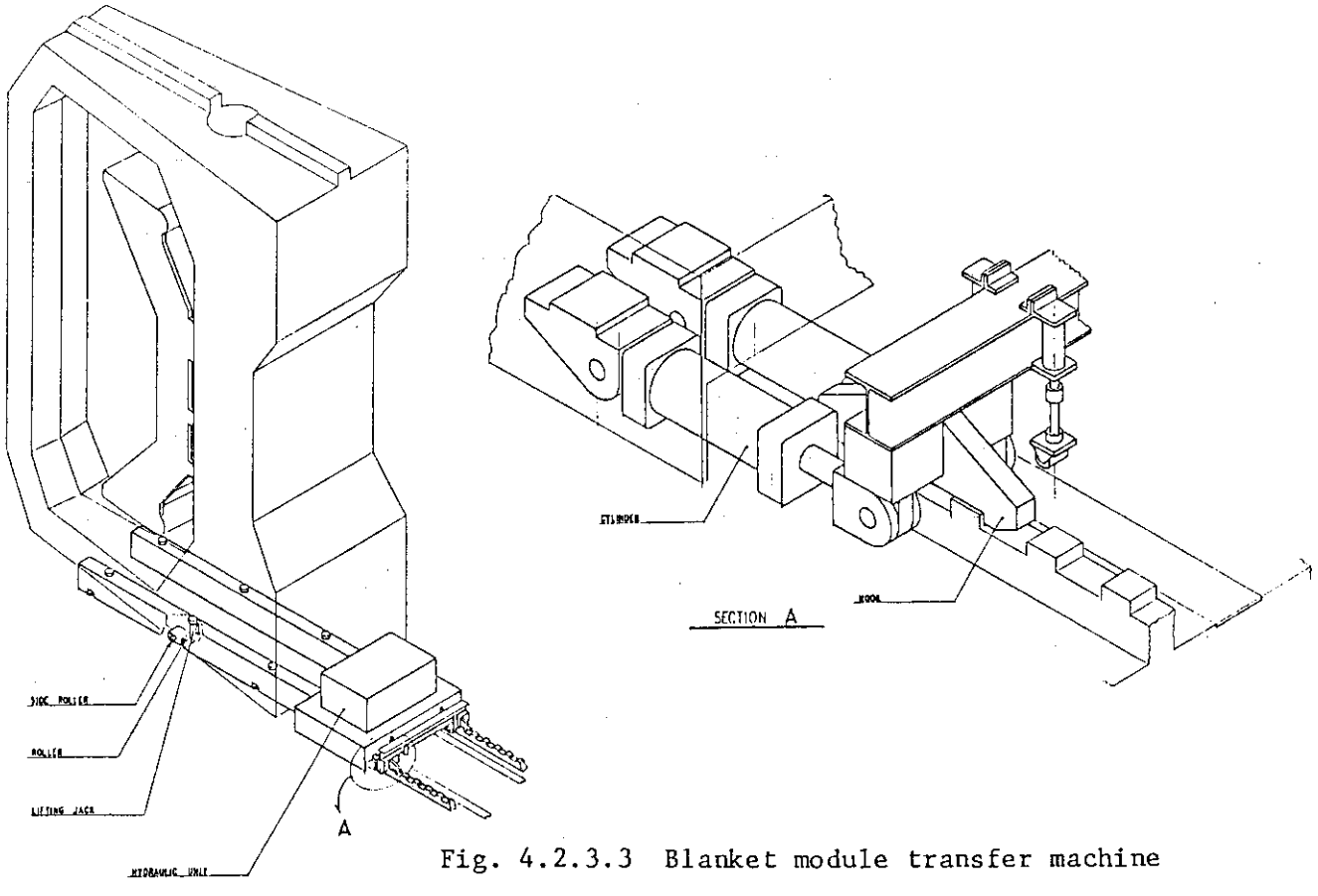

Fig. 4.2.3.3 Blanket module transfer machine

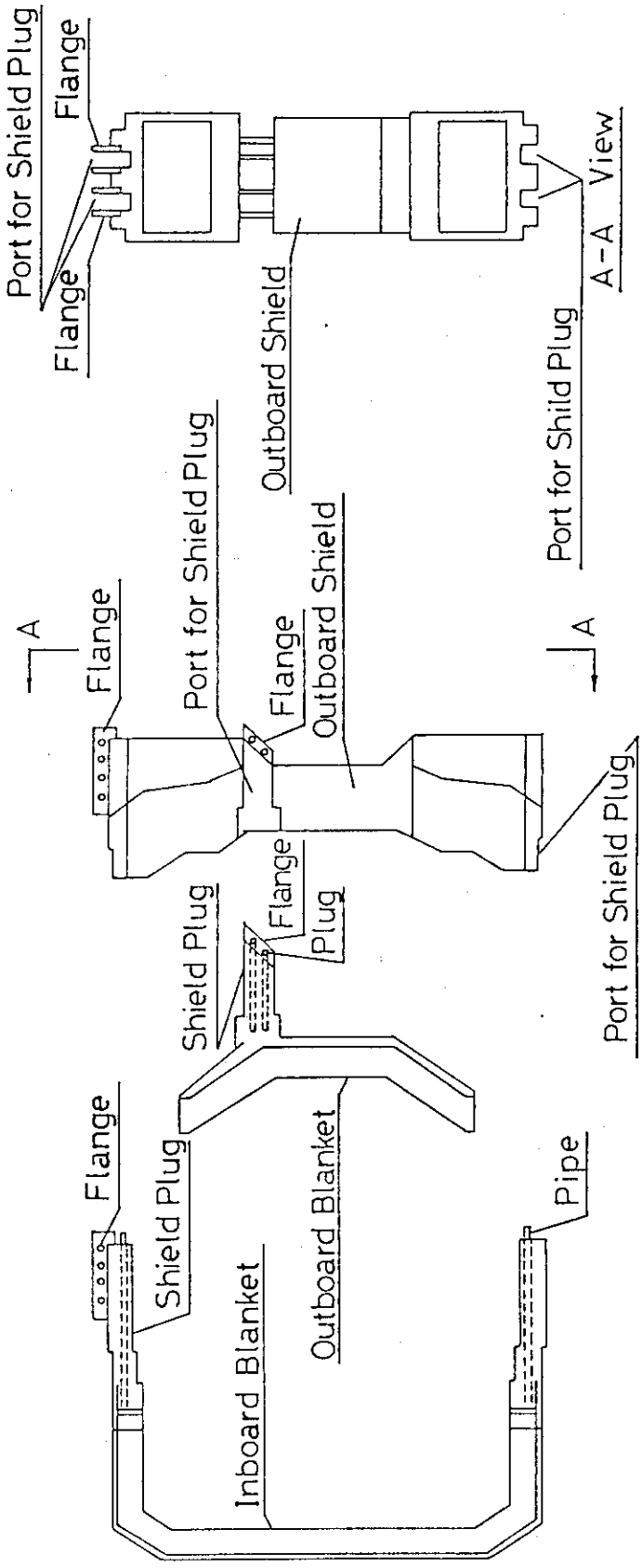

Fig. 4.2.3.4 Support of Blanket Center Module

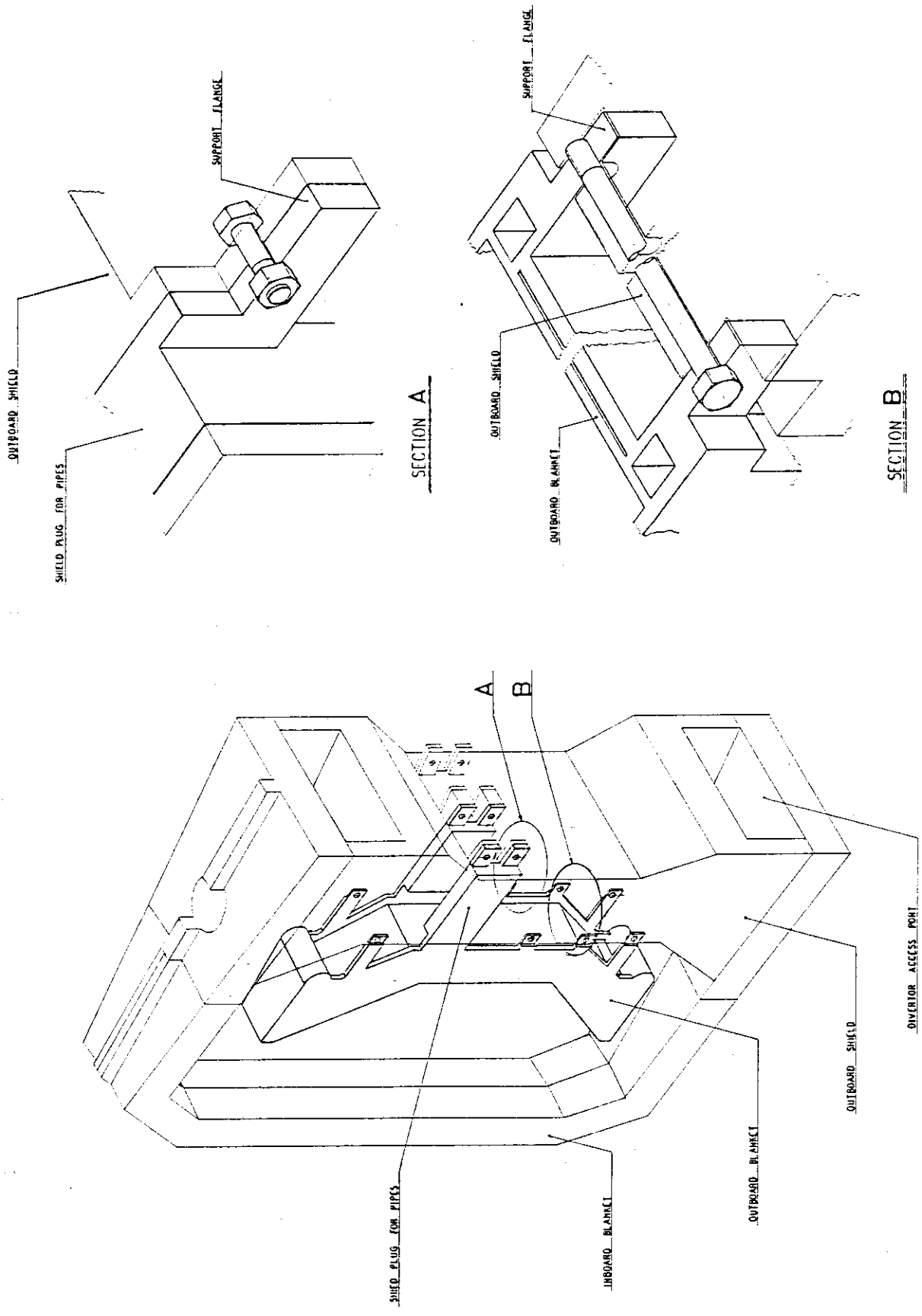

Fig. 4.2.3.5 Support Structure of Outboard Blanket

Blanket Structure

Tube-In-Shell type (BOT/NM)
Integral first wall : Ribbed-panel, lifetime 1.5 MW-y/m^2
Breeder : Li_2O pebble
Breeder temperature control :
Maximum -- Coolant tube arrangement
Minimum -- Helium gap around coolant tube
Neutron multiplier : Be
Shell conductor : Be (in outer blanket design)
Tritium purge : He flow

Table 4.2.3.1 Summary of design parameters for FER first wall

Configuration	Integral with Blanket
Form	Ribbed Panel
Structural Material	Type 316 Stainless steel
Coolant	Pressurized Water(H_2O)
Flow Direction	Toroidal
Inlet Pressure	1.5 MPa
Inlet/Outlet Temperature	60 °C/100 °C
Velocity	1.7 m/s
Pressure Loss	36 kPa
Wall Thickness	
Begining-of-Life	15 mm
End-of-Life(1.5 MW-y/m^2)	10 mm
Coolant Channel	
Size	6 mm^W x 3 mm^h
Pitch	9 mm
Maximum Wall temperature	
during Normal Operation	208 °C
during Neutral Beam Shine-through	219 °C
during Major Plasma Disruption	~1300 °C

Table 4.2.3.2 Summary of design parameters for FER tritium breeding blanket

Blanket Type	Tube-in-Shell Type(BOT/NM)
Thickness(including F/W)	
Inboard	40 cm
Outboard	50 cm
Structure Material	Type 316 Stainless Steel
Breeder	Li_2O(30% ^6Li enrich)
Form	Spherical Pebble
Diameter	1 mm
Theoretical Density	2.0 g/cc
Effective Density	85 %T.D.
Packing Fraction	0.7(bulk)
	0.3(near wall)
Acceptable Temperature Range	400 °C - 1000 °C
Operating Temperature Range	450 °C - 790 °C
Minimum Temperature Control Method	Helium Gas Gap around Coolant Tube
Neutron Multiplier	Beryllium
Shell Conductor	Beryllium
Location	Outboard
Thickness	60 mm
Neutron Moderator	None
Coolant	Pressurized Water(H_2O)
Inlet Pressure	1.5 MPa
Inlet/Outlet Temperature	60 °C/100 °C
Flow Direction	Poloidal
Tube ID/OD	8 mm/10 mm
Velocity	≤1.5 m/s
Pressure Loss	21 kPa
Net Tritium Breeding Ratio	1.05
Tritium Recovery	Continuously by Purge Gas
Purge Gas	Helium
Pressure	0.1 MPa
Flow Rate	200 Nm^3/hr

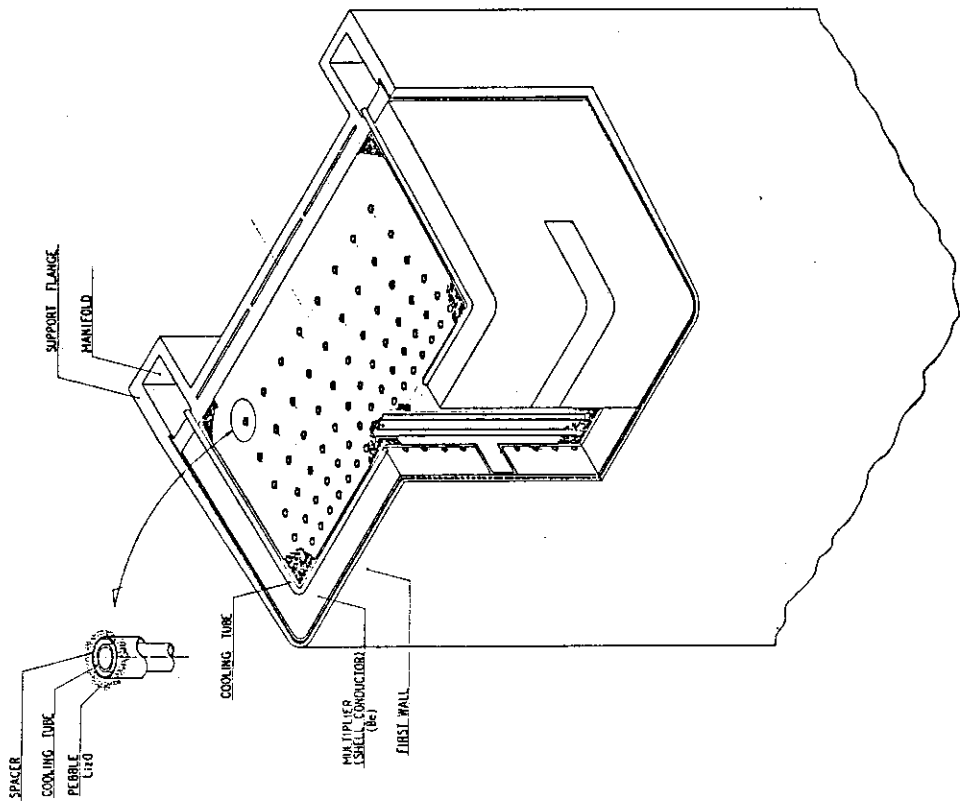

Fig. 4.2.3.7 Concept of tritium breeding blanket

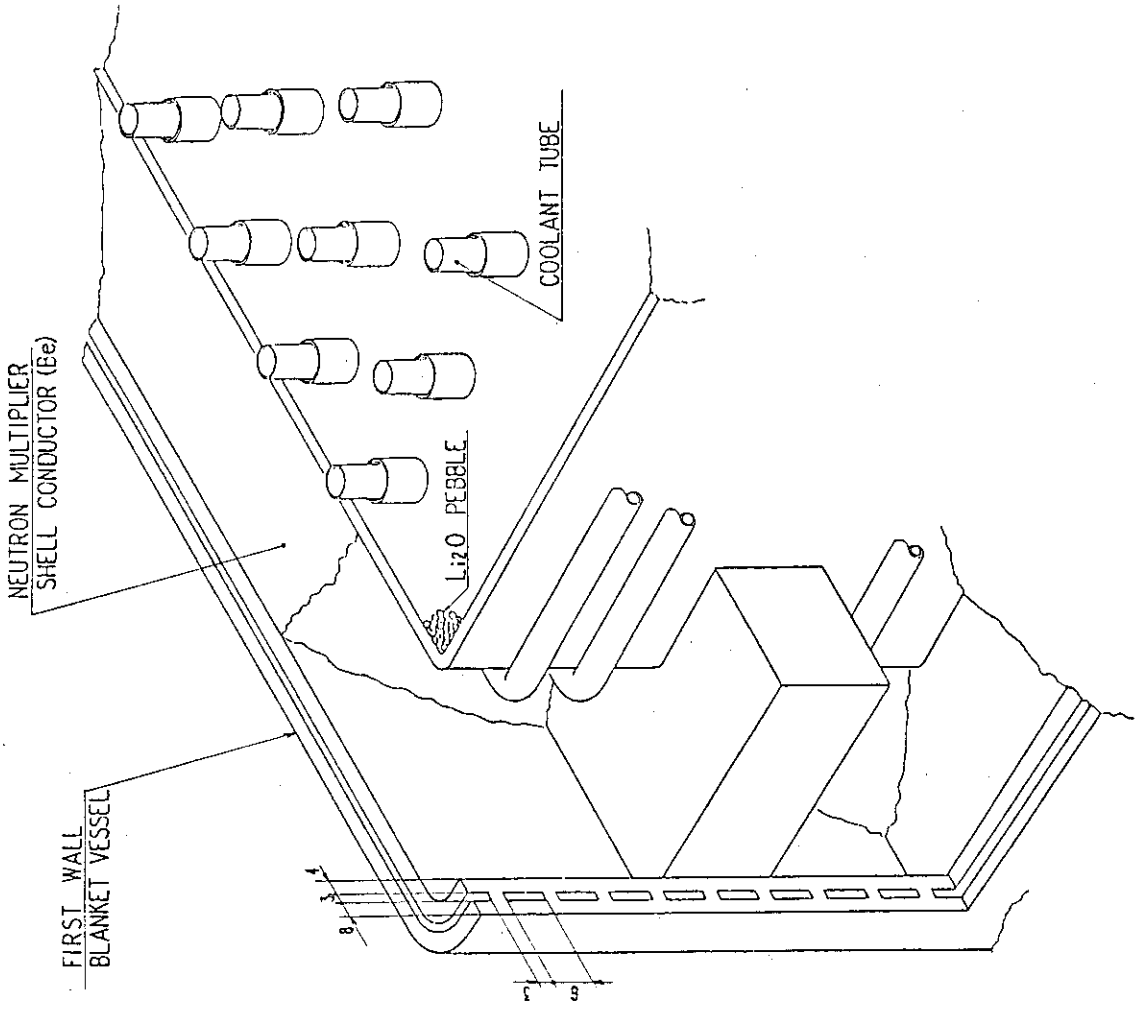

Fig. 4.2.3.6 Concept of first wall

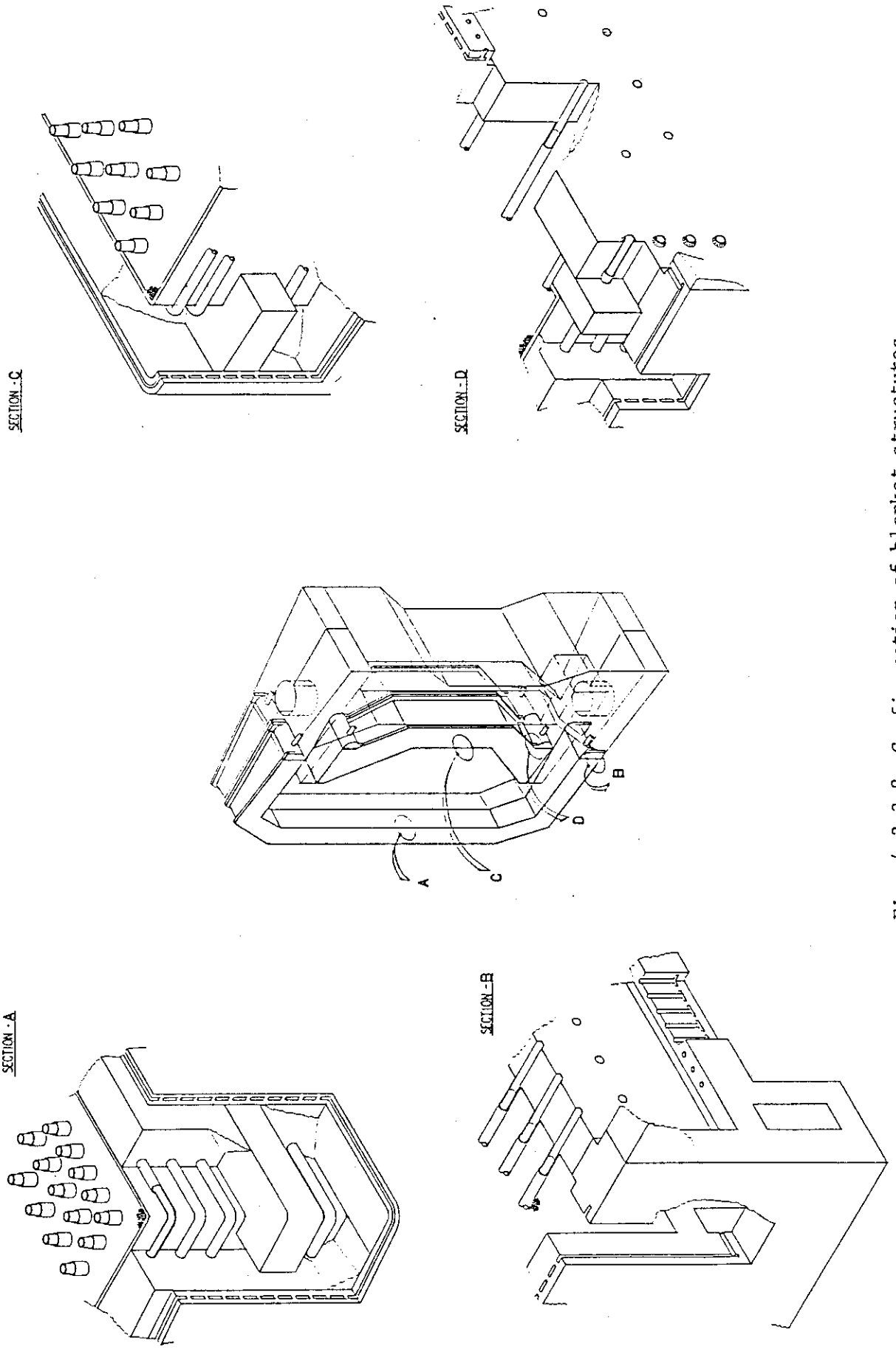

Fig. 4.2.3.8 Configuration of blanket structures

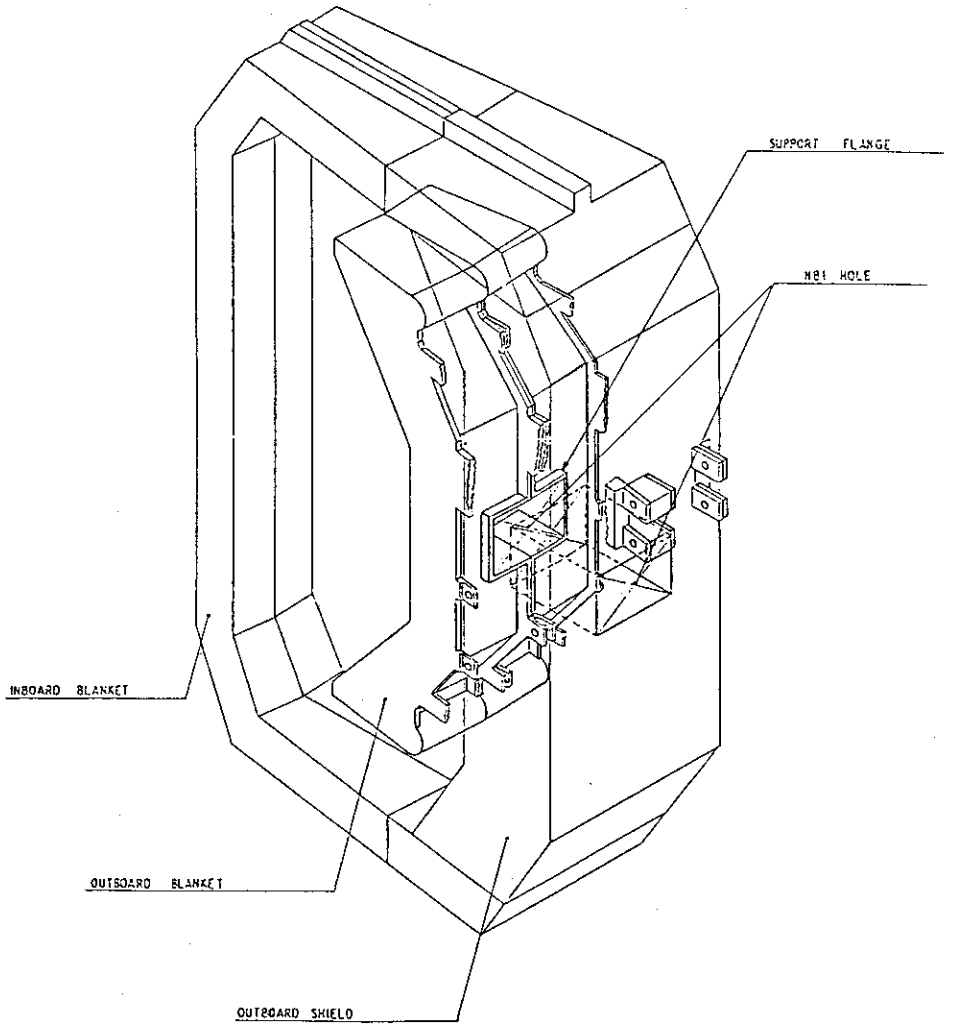

Fig. 4.2.3.9 Schematic drawing of NBI port

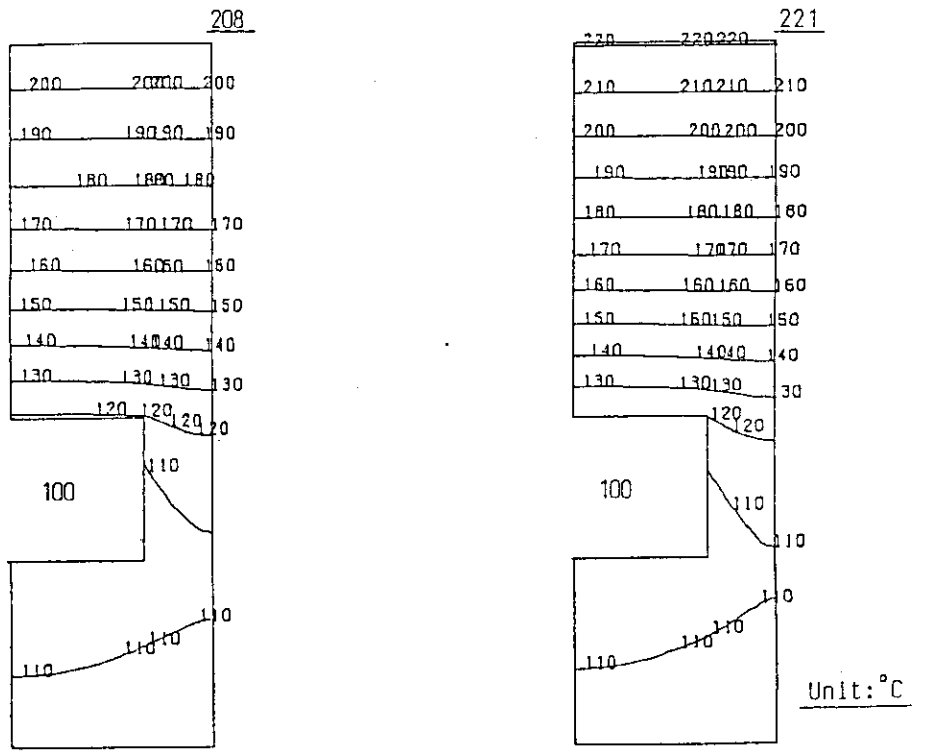

a) Outboard First Wall

b) Inboard First Wall

Fig.4.2.3.10 Temperature profiles in first wall.

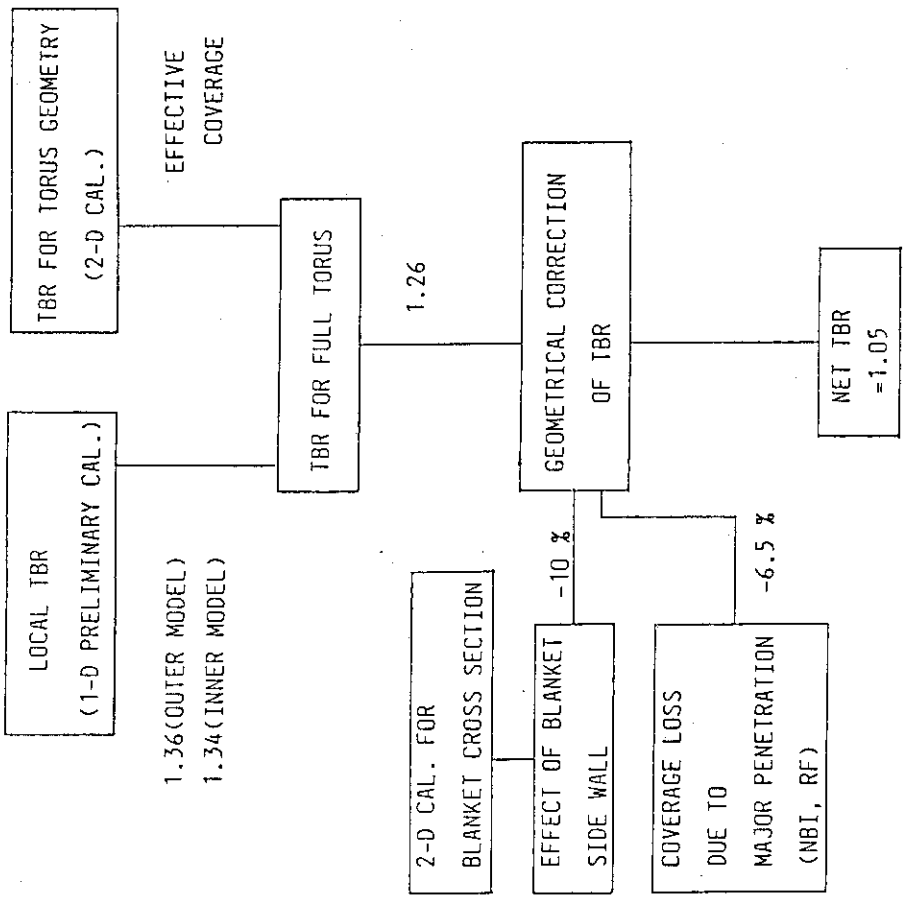

Fig. 4.2.3.12 Calculation Process for Tritium Breeding Ratio

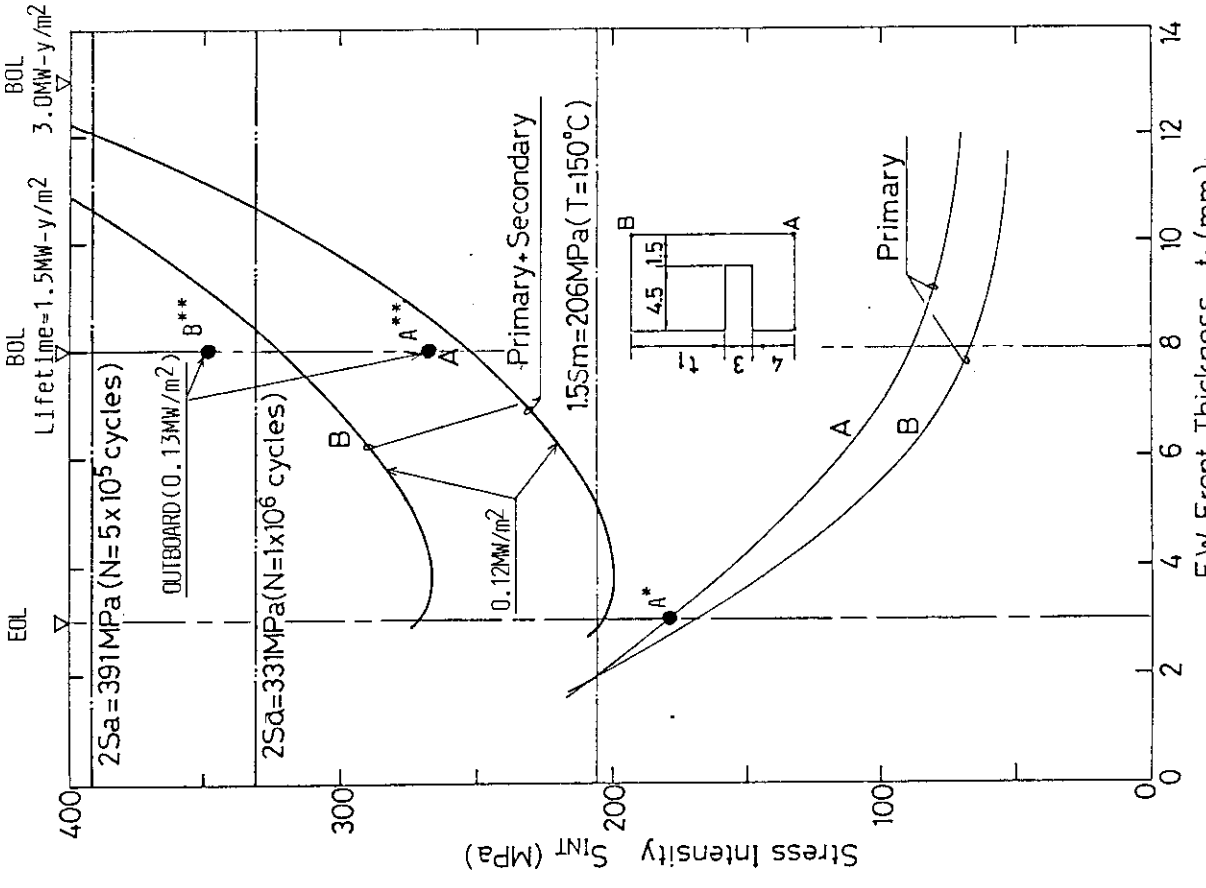

Fig. 4.2.3.11 Stress intensity in first wall

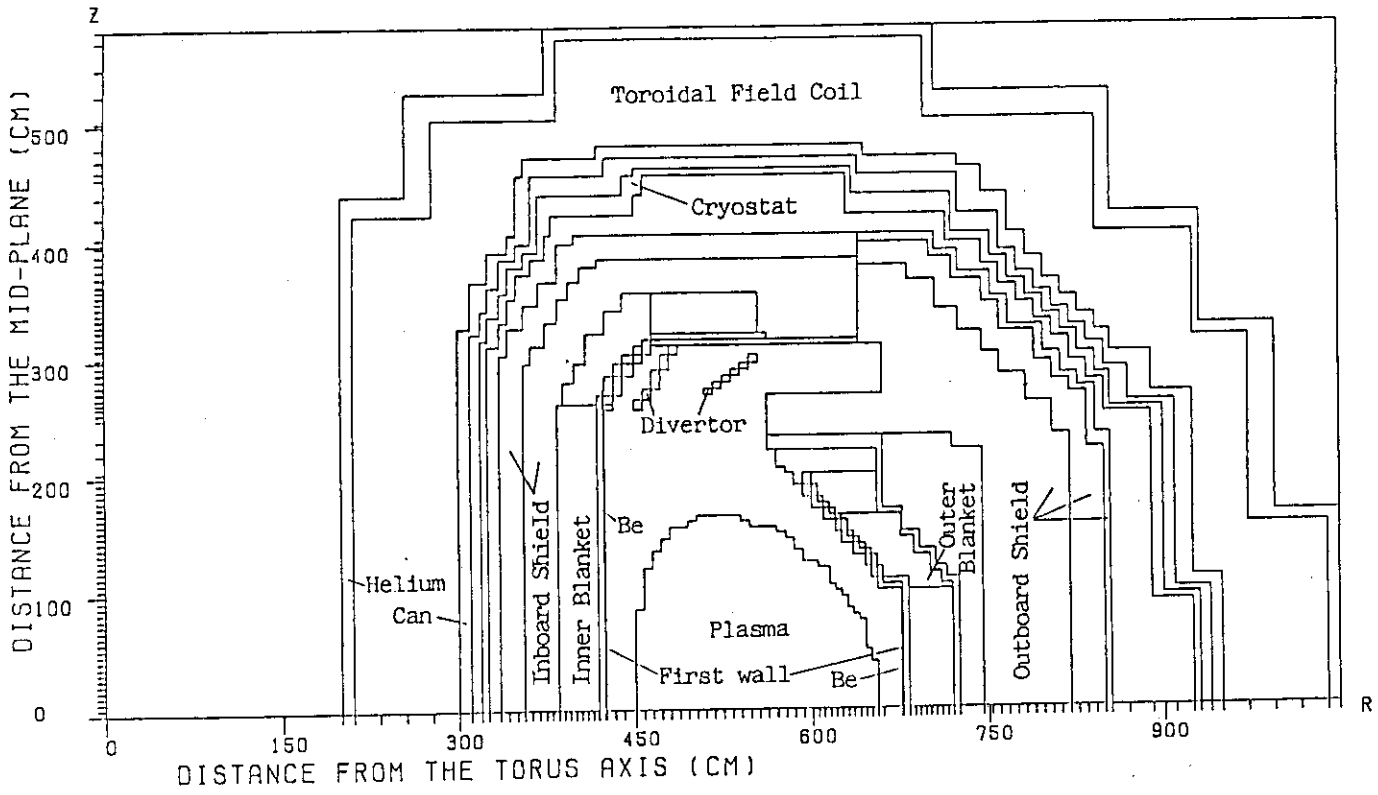

Fig. 4.2.3.13 Analytical model of two-dimensional neutronics analysis for the effect of torus geometry

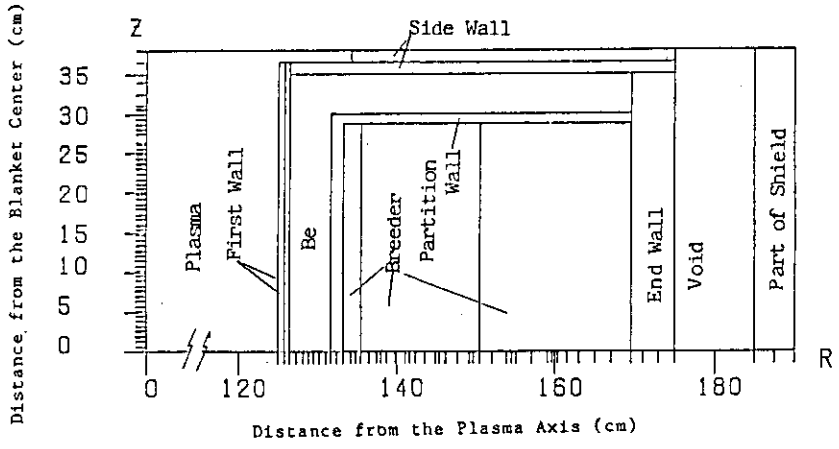

Fig. 4.2.3.14 Analytical model of two-dimensional neutronics analysis for the effect of blanket cross section

Tritium Recovery

o Li_2O pebble (1 mmϕ)

To avoid thermal cracking

Redecomposition of transfered LiOT

Simplicity for blanket fabrication process

Less sensitive to irradiation effects on thermal conductance

o Temperature range of Li_2O breeder for continuous tritium recovery

Lower limit	400 °C	Decomposition of LiOT
		Tritium inventory
Upper limit	1000 °C	Li_2O mass transfer

o Breeder temperature control

Coolant tube arrangement according to heat generation rates

Helium thermal gap between coolant tubes and breeder

o Nominal operating temperature range

450 °C - 790 °C FER reference operation mode

(duty factor 0.5, burn/dwell:100/100 s)

Temperature can be maintained within allowable range

up to duty factor 0.7

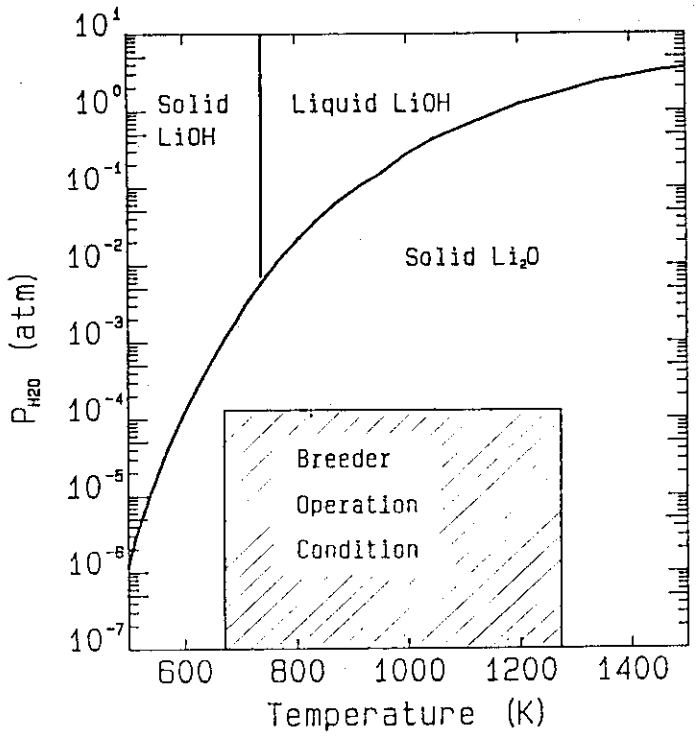

Fig. 4.2.3.15 $Li_2O/LiOH$ Phase equiliblia as a function of P_{H2O} and temperature

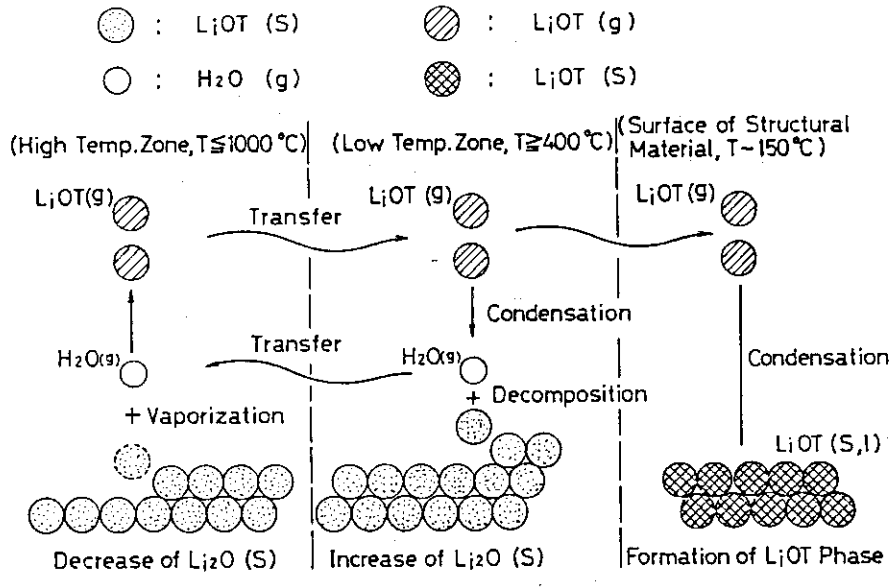

Fig. 4.2.3.16 Concept of Li_2O Transport

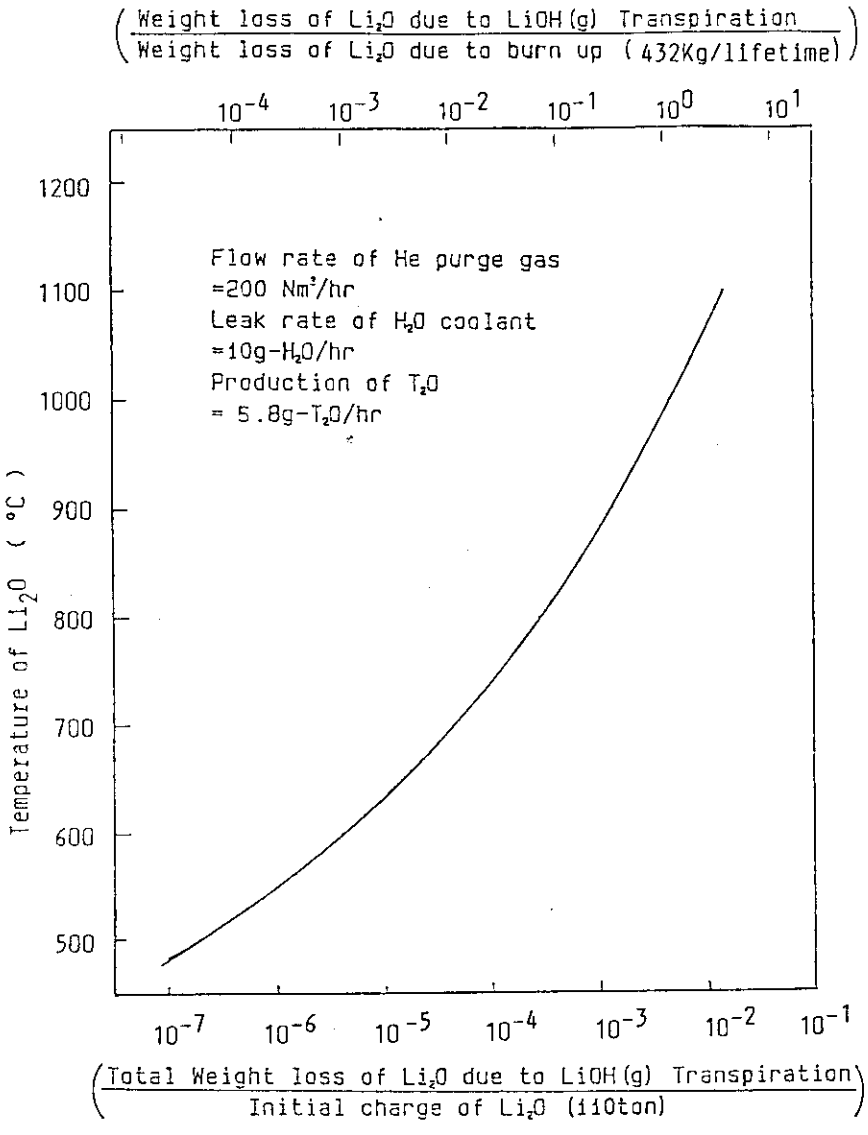

Fig. 4.2.3.17 Relationship between Weight Loss of Li2O and Temperature

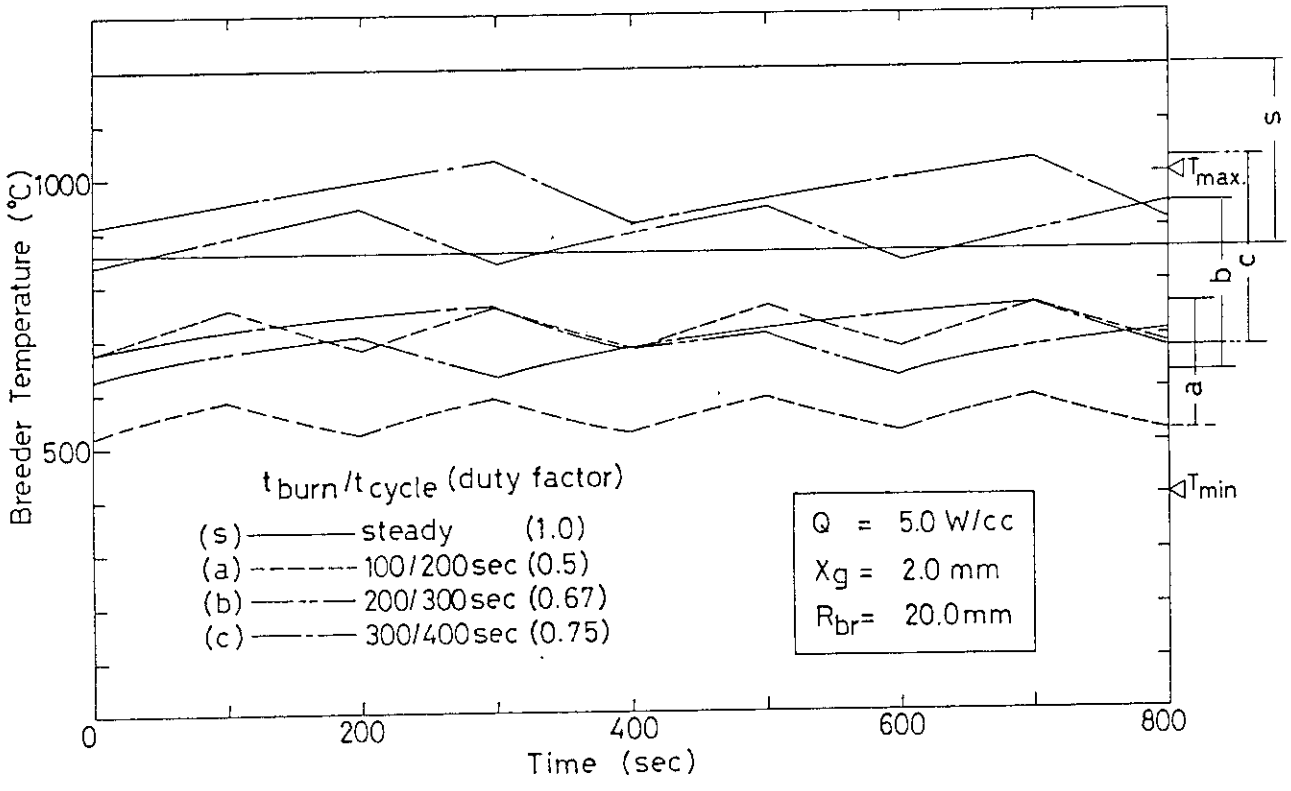

Fig. 4.2.3.18 Temperature Response in Breeder for Pulsed Operation

Analytical Conditions of Blanket and Shield

Analytical Model	1/56 Torus Model		
Structural Material	Type 316 Stainless Steel		
Wall Thickness	FW	SW	EW
Inner Blanket	15	18.75	100
Outer Blanket	15	22.5	55
Shield	50	50	50
		(unit:mm)	
Wall Temperature	FW	SW	EW
Blanket	200	167/133	100
Shield	60	60	60
		(unit:°C)	

Results of 3-D Stress Analysis

Load Case	Maximum Stress Intensity
Internal Pressure	P_{max} 31 MPa
(He pressure 0.1 Mpa)	1.5 S_m 200 MPa
Thermal Load	T_{max} 323 MPa
	2 S_a 380 MPa (5×10^5 cycles)
Electromagnetic Force*	E_{max} 117 MPa
	1.5 S_m 200 MPa

* Imposed electromagnetic force are those at 25 msec after plasma disruption. (obtained from 3-D transient eddy current analysis)

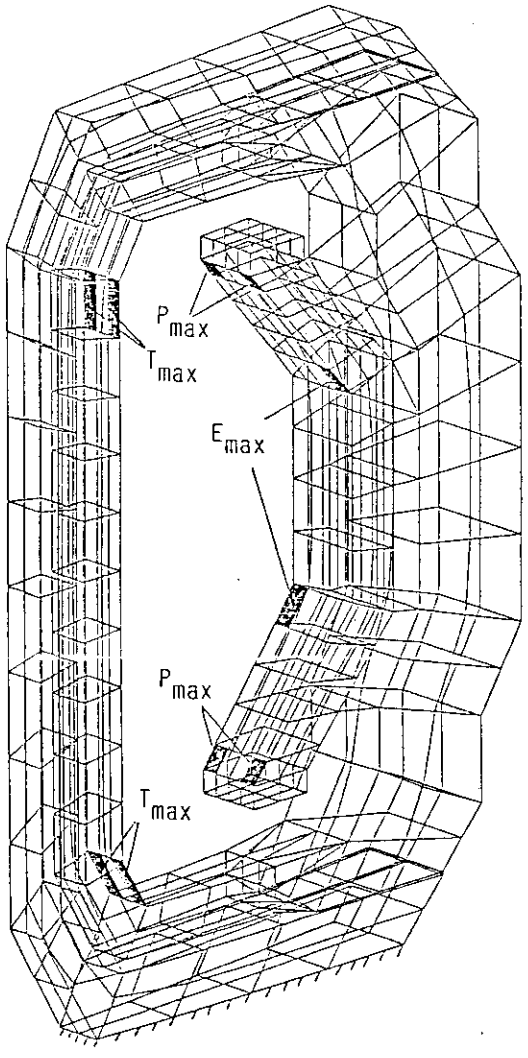

Fig. 4.2.3.19 Model for stress analyses and locations of maximum stress intensities

Passive Shell Structure

Saddle type conductor

-- Consistent to blanket maintenance

-- Installed only in the outer blanket region to avoid the excess electromagnetic force in the inner blanket region

Candidate material : Be 60 mm

Pb high elèctric resistance

Cu,Al low breeding performance

Table 4.2.3.3 Summary of Design Parameters for Passive Shell Conductor

Type	: Rectangular Coil
Location	: Outer Blanket
Number of Conductors	
Center Module	: 14
Side Module	: 28
Material	: Beryllium
Thickness	: 6 cm
Shell Effect (Including Shield and Belljar)	: $N_S \sim 2.635$ $\tau_S \sim$ 30 msec (growth time)
Maximum Temperature of Conductor	: 150°C
Cooling Systems	
Coolant	: Water (H_2O)
Pressure	: 1.5 MPa
Inlet/Outlet Temperature	: 60°C/100°C

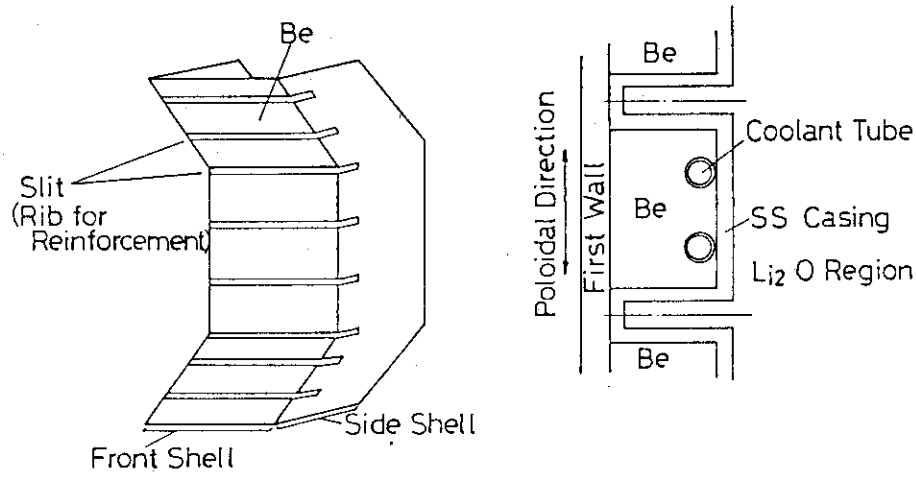

Fig. 4.2.3.20 Concept of Shell Conductor

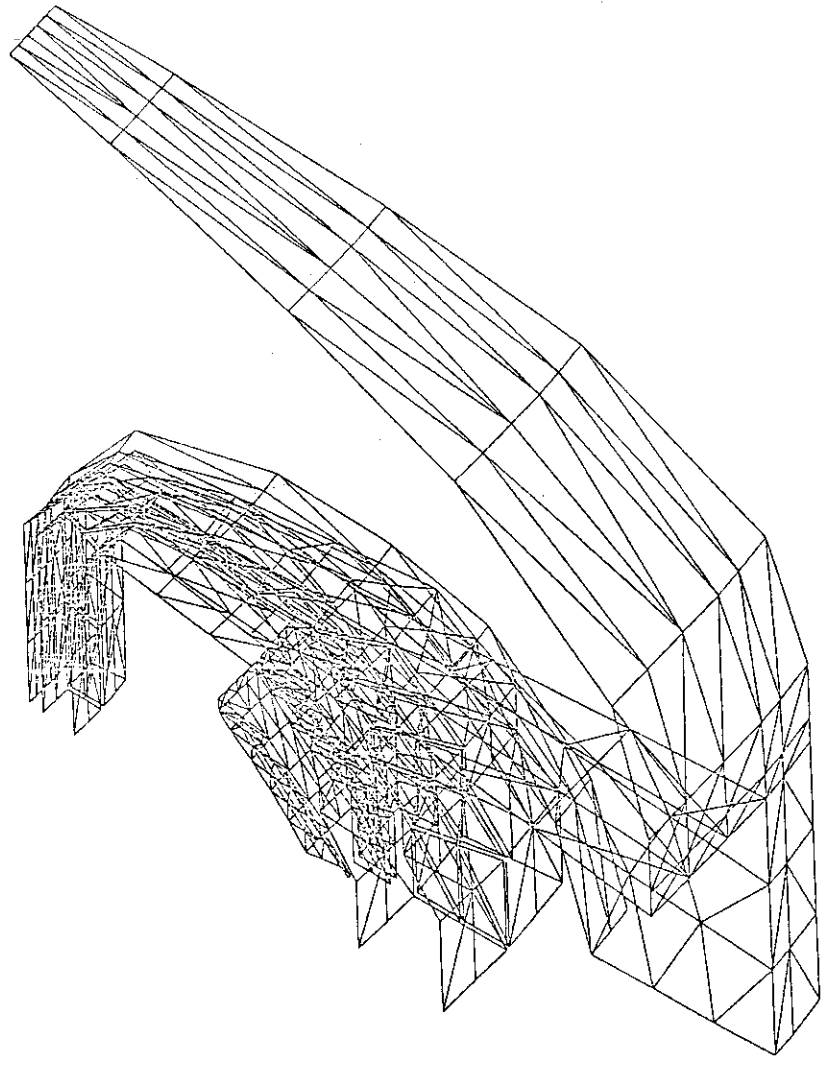

Fig. 4.2.3.21 Model for electromagnetic analyses

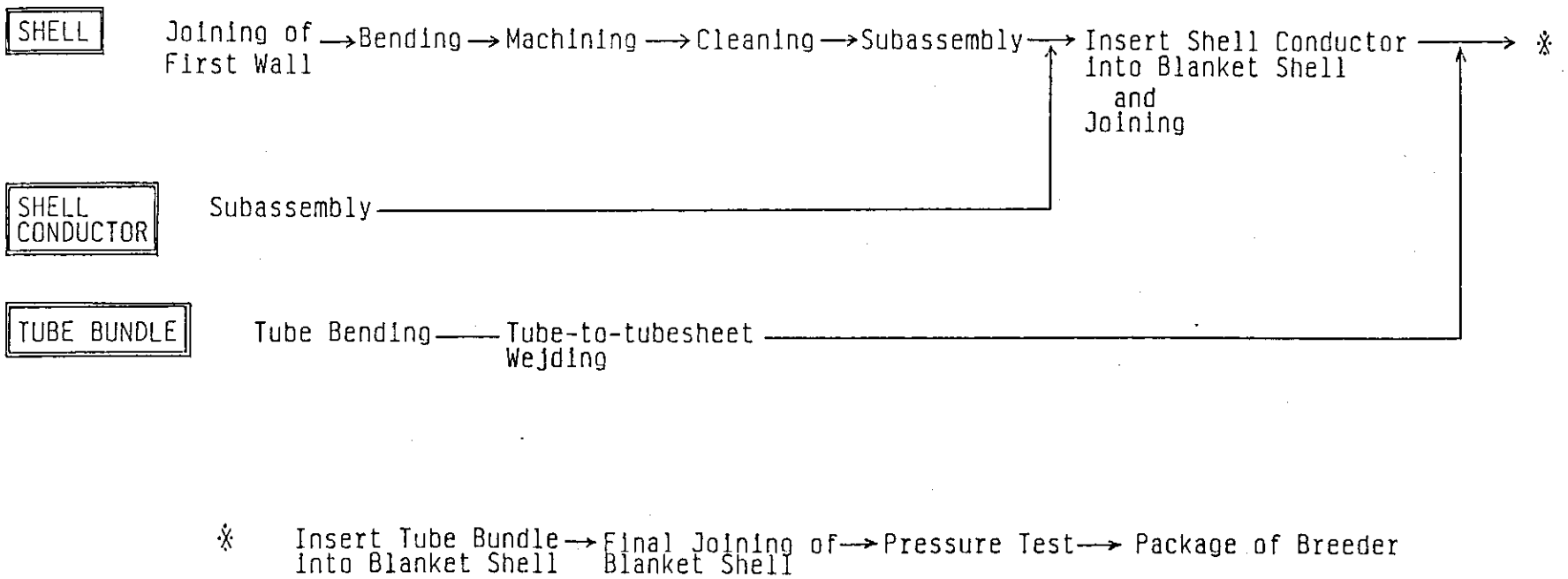

Fig. 4.2.3.22 Blanket fabrication procedure

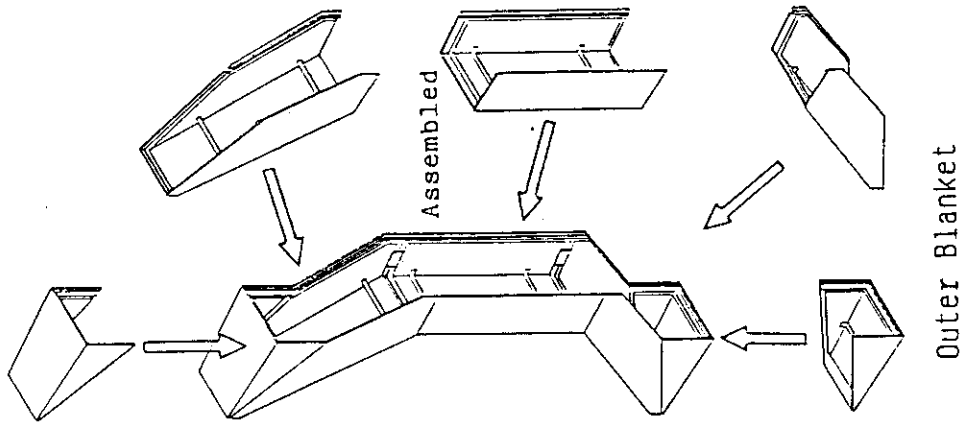

Fig. 4.2.3.23 Blanket Segmentation and Its Assembly (toroidal cooling)

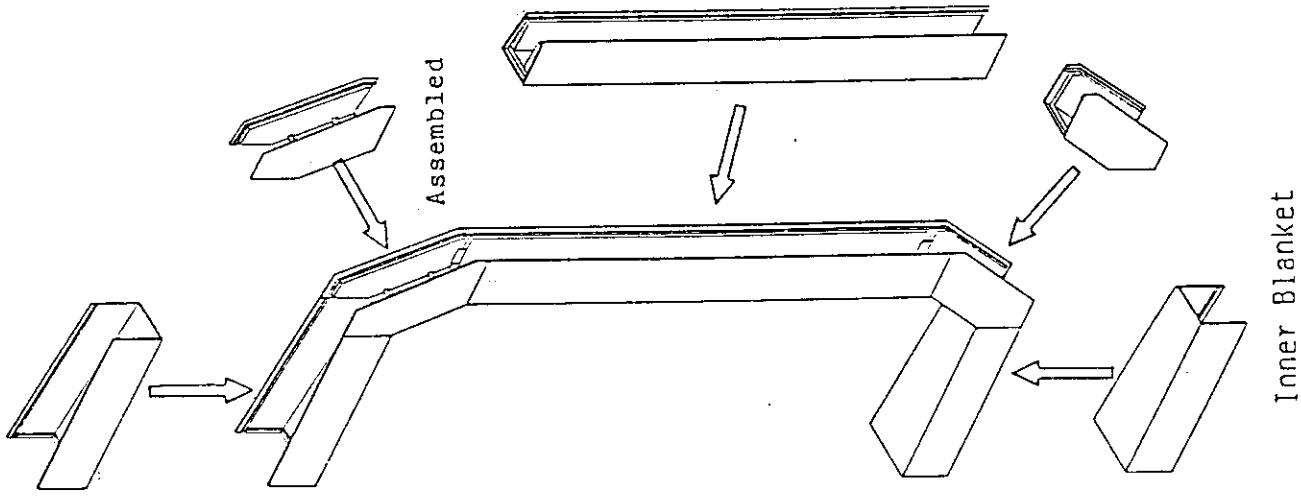

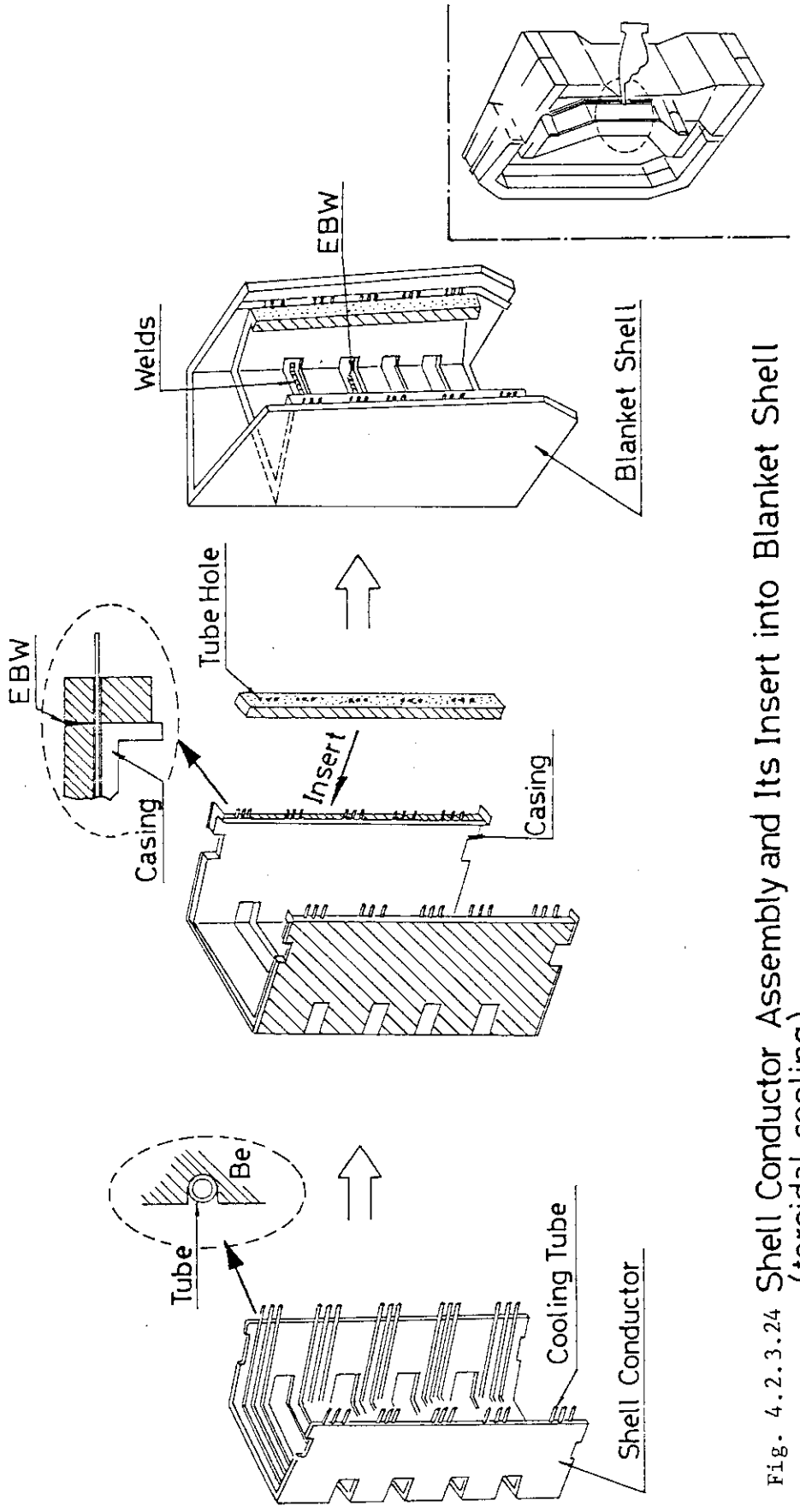

Fig. 4.2.3.24 Shell Conductor Assembly and Its Insert into Blanket Shell (toroidal cooling)

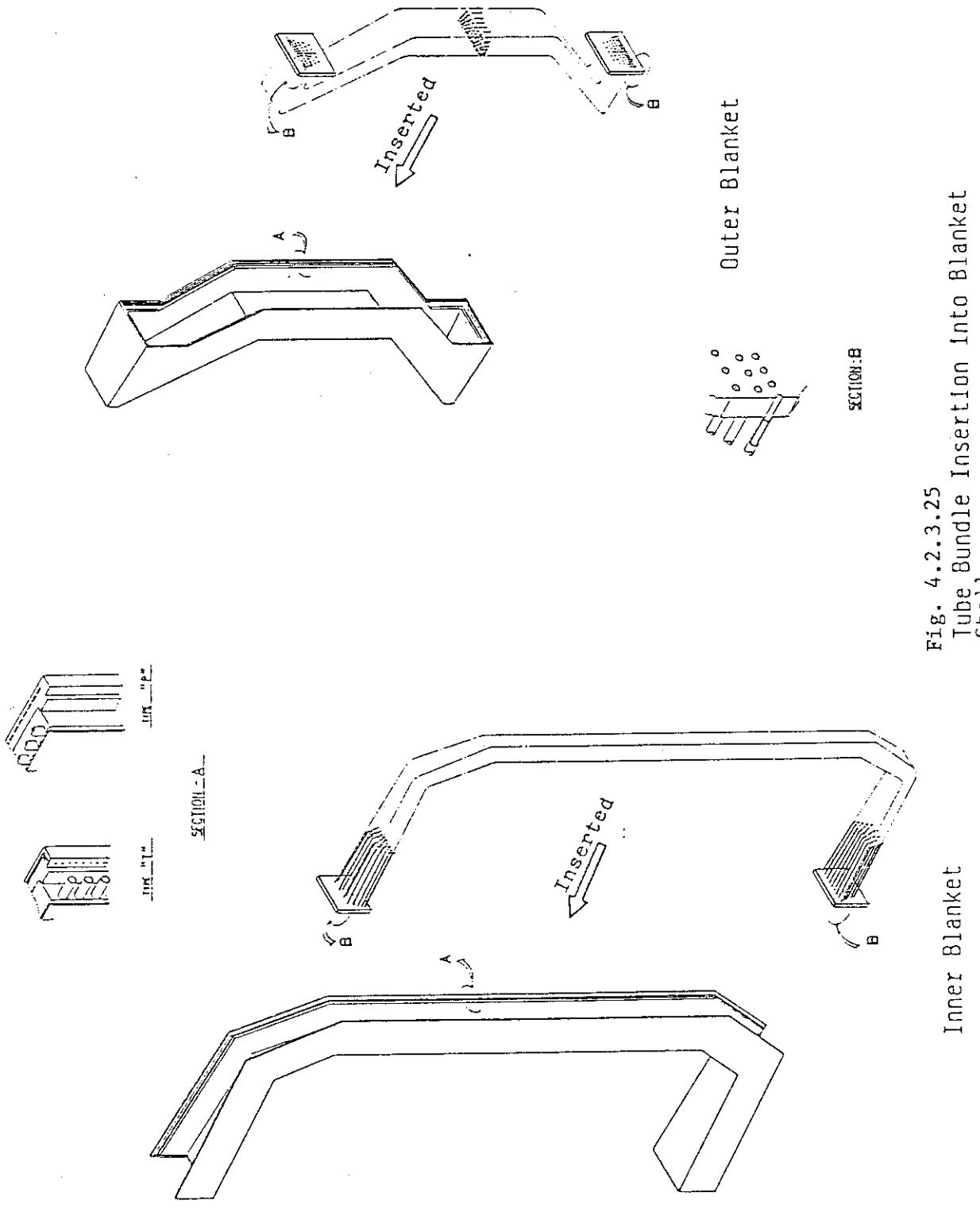

Fig. 4.2.3.25
Tube Bundle Insertion Into Blanket Shell

Technology Issues of the FER Blanket Development

- Material data base
  - Plasma-Wall interaction data
    - Erosion　physical sputtering, chemical sputtering, evaporation by plasma disruption
  - Neutron irradiation data
    - Strength and fatigue data of structural material including welding part
    - Physical properties of breeder, structural and shell materials
- Structural data base
  - First wall structure
    - Structure for erosions
    - Structure for heat removal
    - Structure withstanding cyclic heat load including plasma disruption
  - Temperature control of breeder
    - Effective thermal conductivity of breeder zone
    - Thermal resistance around cooling tubes
    - Spacers for coolant tubes
    - Coolant tube arrangements near headers
    - Uncertainties to be accommodated
  - Structural integrity
    - Thermal expansion
    - Electromagnetic force
    - Detection of coolant leakage
    - Pressure relief for rupture of cooling tube
  - Mechanism for one-turn resistance
  - Mechanism against arcing

Blanket-Tritium Systems

- Fabrication technique of Li_2O pebbles
- Physical and chemical properties of Li_2O breeder
  - Hydrolysis reaction rate and weight loss rate in flowing helium containing moisture
  - Major vapor species over Li_2O and their vaporization pressure in operating temprature range
  - Effective thermal conductivity in helium atmosphere (including Li_2O pebble packing fraction and wall effect)
  - Compatibility with structural material
- Integrity assurance of Li_2O breeder
  - Grain growth, sintering and pore-closure under high temperature and neutron fluence
  - Mechanical integrity of breeder under cyclic thermal condition
- Tritium release rate from Li_2O breeder
  - Effects on tritium release for a number of variables such as chemical composition of breeder, particle and grain size, temperature, and purge gas flow rate.
- Tritium permeation

Fabrication

- Joining
  - Feasibility of first wall fabrication by HIP process
  - Production of large-size HIP machine
  - Feasibility of blanket shell-to-shell joining by EBW
  - Small-size tube-to-tubesheet inner bore welding
  - Feasibility of shell conductor joining
- Non-destructive examination
  - Practical examination of first wall joint by HIP
  - Feasibility of examination of blanket shell joint by EBW
  - Reliable examination of tube-to-tubesheet joint
- Assembly
  - Final assembly of blanket component
- Plastic work
  - Bending first wall and integrity
- Dimension measurement
  - Precise measurement of blanket component
- Mock-up test
  - Corroboration of element techniques through mock-up test

Appendix

Agenda

Japan-US FER/ETR DESIGN WORKSHOP

Fusion Engineering Design Center
March 26-30, 1984

Monday, March 26, 1984

9:00 a.m.	Welcome	O.B. Morgan, Division Director, Fusion Energy Division
	Opening Comments	P.M. Stone, OFE
	Opening Comments	T. Tone, JAERI
	Status of U.S. Program Relative to TFTR/TFCX/ETR Strategy	P.M. Stone, OFE
	Overview of TFCX Design	J. Schmidt, PPPL C. Flanagan, ORNL/W
12:00	LUNCH	
1:30 p.m.	Japanese Program Strategy	T. Tone, JAERI
	Status of JT-60 Construction	T. Tone, JAERI
	Status of FER Design	
	Scope of FER Design Activities	T. Tone, JAERI
	Overview of FER Physics Design	M. Sugihara, JAERI
	Overview of FER Engineering Design	H. Iida, JAERI
4:30 p.m.	Discussion	
5:00 p.m.	Adjourn	

Tuesday, March 27, 1984

RF HEATING & CURRENT DRIVE - PHYSICS

9:00 a.m.	RF Heating Physics Basis	D.L. Hwang, PPPL
	Current Drive Physics Basis	J. Stevens, PPPL
	Plasma Performance & Operating Scenario	Y-K.M. Peng, FEDC
	RF Assisted Plasma Operation Scenario for FER	M. Sugihara, JAERI

12:00	LUNCH	
RF HEATING & CURRENT DRIVE - ENGINEERING		
1:30 p.m.	Introduction	D. Metzler, FEDC/GE
	Plasma Heating Systems for TFCX	D. Metzler, FEDC/GE
	RF Technology Developments for TFCX	W. Becraft, ORNL/GE F. Baity, ORNL D. Hoffman, ORNL
	Current Drive Systems for TFCX	D. Metzler, FEDC/GE
	Engineering Design of an Advanced FER Based on Steady-State Plasma Operation Scenario	T. Kasahara, Hitachi Ltd.
	RF Launcher Designs for FER	K. Kitamura, Toshiba Corp.
4:30 p.m.	Discussion	
5:00 p.m.	Adjourn	
5:00 p.m.	Reception	

Wednesday, March 28, 1984

IMPURITY CONTROL - PHYSICS		
9:00 a.m.	Impurity Control Approaches	J.L. Cecchi, PPPL
	Modeling Plasma Behavior for Impurity Control	D. Post, PPPL
	Physics Design Considerations for Impurity Control by Divertor and Pumped Limiter	M. Sugihara, JAERI
12:00	LUNCH	
IMPURITY CONTROL - ENGINEERING		
1:30 p.m.	Limiter/Divertor Design Issues	R.F. Mattas, ANL
	Limiter/Divertor Design & Analysis	J.R. Haines, FEDC/MDAC
	Comparative Study of Engineering Features for Divertor and Pumped Limiter Reactor Concepts	H. Iida, JAERI
	Engineering Design of Divertor and Pumped Limiter Plates	K. Kitamura, Toshiba Corporation

4:30 p.m.	Discussion	
5:00 p.m.	Adjourn	

Thursday, March 29, 1984

DESIGN INTEGRATION & MAINTENANCE - US

9:00 a.m.	Configuration Engineering; TFCX Configuration Studies	T. Brown, FEDC/GAC
	Maintenance Requirements and Design Guidelines	P. Spampinato, FEDC/GAC
	TFCX Maintenance and Configuration Development	K. Watts, EG&G Idaho
	Specifications and Guidelines for the Reference FER Engineering Design	H. Iida, JAERI
12:00	LUNCH	

DESIGN INTEGRATION & MAINTENANCE - JAPAN

1:30 p.m.	Design Concepts	
	FER Reactor Structure & Maintenance	K. Kitamura, Toshiba Corp.
	A Scenario of FER Electro-magnetics Design	M. Nishikawa Mitsubishi
	A Tritium Breeding Blanket Design for FER	T. Kuroda, Kawasaki
4:30 p.m.	Discussion	
5:00 p.m.	Adjourn	

Friday, March 30, 1984

9:00 a.m.	Discussion on Future Exchanges and Joint Programs	
	Key Technical Issues; Bilateral Work Program; Joint Design Effort	U.S./Japan, Delegates
	Prepare Report	U.S./Japan, Delegates
12:00	LUNCH	
1:30 p.m.	Tour of ORNL Fusion Facilities	
5:00 p.m.	Japanese Delegation Depart	